NEURODEGENERATION AND NEUROPROTECTION IN RETINAL DISEASE

EDITED BY: Giovanni Casini, Peter Koulen and Mohammad Shamsul Ola
PUBLISHED IN: Frontiers in Neuroscience

frontiers Research Topics

frontiers

ISSN 1664-8714
ISBN 978-2-88963-740-9
DOI 10.3389/978-2-88963-740-9

About Frontiers

Frontiers is more than just an open-access publisher of scholarly articles: it is a pioneering approach to the world of academia, radically improving the way scholarly research is managed. The grand vision of Frontiers is a world where all people have an equal opportunity to seek, share and generate knowledge. Frontiers provides immediate and permanent online open access to all its publications, but this alone is not enough to realize our grand goals.

Frontiers Journal Series

The Frontiers Journal Series is a multi-tier and interdisciplinary set of open-access, online journals, promising a paradigm shift from the current review, selection and dissemination processes in academic publishing. All Frontiers journals are driven by researchers for researchers; therefore, they constitute a service to the scholarly community. At the same time, the Frontiers Journal Series operates on a revolutionary invention, the tiered publishing system, initially addressing specific communities of scholars, and gradually climbing up to broader public understanding, thus serving the interests of the lay society, too.

Dedication to Quality

Each Frontiers article is a landmark of the highest quality, thanks to genuinely collaborative interactions between authors and review editors, who include some of the world's best academicians. Research must be certified by peers before entering a stream of knowledge that may eventually reach the public - and shape society; therefore, Frontiers only applies the most rigorous and unbiased reviews.
Frontiers revolutionizes research publishing by freely delivering the most outstanding research, evaluated with no bias from both the academic and social point of view. By applying the most advanced information technologies, Frontiers is catapulting scholarly publishing into a new generation.

What are Frontiers Research Topics?

Frontiers Research Topics are very popular trademarks of the Frontiers Journals Series: they are collections of at least ten articles, all centered on a particular subject. With their unique mix of varied contributions from Original Research to Review Articles, Frontiers Research Topics unify the most influential researchers, the latest key findings and historical advances in a hot research area! Find out more on how to host your own Frontiers Research Topic or contribute to one as an author by contacting the Frontiers Editorial Office: researchtopics@frontiersin.org

NEURODEGENERATION AND NEUROPROTECTION IN RETINAL DISEASE

Topic Editors:
Giovanni Casini, University of Pisa, Italy
Peter Koulen, University of Missouri System, United States
Mohammad Shamsul Ola, King Saud University, Saudi Arabia

Citation: Casini, G., Koulen, P., Ola, M. S., eds. (2020). Neurodegeneration and Neuroprotection in Retinal Disease. Lausanne: Frontiers Media SA.
doi: 10.3389/978-2-88963-740-9

Table of Contents

frontiers in Neuroscience

ORIGINAL RESEARCH
published: 08 March 2019
doi: 10.3389/fnins.2019.00201

Cell Autonomous Neuroprotection by the Mitochondrial Uncoupling Protein 2 in a Mouse Model of Glaucoma

*Daniel T. Hass and Colin J. Barnstable**

Department of Neural and Behavioral Sciences, College of Medicine, The Pennsylvania State University, Hershey, PA, United States

OPEN ACCESS

Edited by:
Peter Koulen, University of Missouri System, United States

Reviewed by:
Raghu Krishnamoorthy, University of North Texas Health Science Center, United States
Rafael Linden, Federal University of Rio de Janeiro, Brazil

***Correspondence:**
Colin J. Barnstable
cbarnstable@psu.edu;
cbarnstable@pennstatehealth.psu.edu

Specialty section:
This article was submitted to Neurodegeneration, a section of the journal Frontiers in Neuroscience

Received: *10 January 2019*
Accepted: *20 February 2019*
Published: *08 March 2019*

Citation:
Hass DT and Barnstable CJ (2019) Cell Autonomous Neuroprotection by the Mitochondrial Uncoupling Protein 2 in a Mouse Model of Glaucoma. Front. Neurosci. 13:201. doi: 10.3389/fnins.2019.00201

Glaucoma is a group of disorders associated with retinal ganglion cell (RGC) degeneration and death. There is a clear contribution of mitochondrial dysfunction and oxidative stress toward glaucomatous RGC death. Mitochondrial uncoupling protein 2 (*Ucp2*) is a well-known regulator of oxidative stress that increases cell survival in acute models of oxidative damage. The impact of *Ucp2* on cell survival during sub-acute and chronic neurodegenerative conditions, however, is not yet clear. Herein, we test the hypothesis that increased *Ucp2* expression will improve RGC survival in a mouse model of glaucoma. We show that increasing RGC but not glial *Ucp2* expression in transgenic animals decreases glaucomatous RGC death, but also that the PPAR-γ agonist rosiglitazone (RSG), an endogenous transcriptional activator of *Ucp2*, does not significantly alter RGC loss during glaucoma. Together, these data support a model whereby increased *Ucp2* expression mediates neuroprotection during a long-term oxidative stressor, but that transcriptional activation alone is insufficient to elicit a neuroprotective effect, motivating further research in to the post-transcriptional regulation of *Ucp2*.

Keywords: retina, RGC, Ucp2, glaucoma, neuroprotection, mitochondria, oxidative stress

INTRODUCTION

Glaucoma is a group of disorders associated with retinal ganglion cell (RGC) degeneration and death (Quigley, 2011) and, after cataracts, is the most frequent cause of blindness worldwide (Resnikoff and Keys, 2012). An increase in intra-ocular pressure (IOP) is a prominent risk factor for glaucoma (Boland and Quigley, 2007), and most therapeutic solutions designed to prevent RGC death in glaucoma share the ability to decrease IOP. However, IOP reduction does not reduce glaucomatous visual field loss in roughly half of patients (Leske et al., 2004), necessitating development of adjuvant therapeutic modalities, including neuroprotective molecules that can protect RGCs.

The molecular mechanisms of glaucoma pathogenesis are multifactorial, but are frequently connected to an increase in damaging free radicals in the eye (Izzotti et al., 2003; Saccà and Izzotti, 2008), retina (Tezel et al., 2005), and optic nerve head (Malone and Hernandez, 2007; Feilchenfeld et al., 2008), herein termed oxidative stress. Ocular hypertension increases RGC oxidative stress (Chidlow et al., 2017), despite anti-oxidative support from endogenous antioxidant proteins (Munemasa et al., 2009) and resident glial cells of the retina, including astrocytes and müller glia (Varela and Hernandez, 1997; Carter-Dawson et al., 1998; Kawasaki et al., 2000; Woldemussie et al., 2004). Exogenous addition of serum antioxidants such as vitamin E is not necessarily protective from the disease (Ramdas et al., 2018), suggesting that current anti-oxidative therapeutics for glaucoma are insufficient. The early transcriptional responses of DBA2/J mouse RGCs to elevated IOP strongly suggest mitochondrial abnormalities in RGCs early in the disease (Williams et al., 2017), which appears to persist in multiple animal models (Coughlin et al., 2015; Takihara et al., 2015; Ito and Di Polo, 2017) as well as in human glaucoma (Abu-Amero et al., 2006; Piotrowska-Nowak et al., 2018).

Mitochondria are a well-known source of cellular free radicals, which during oxidative phosphorylation can leak from multi-protein complexes of the electron transport chain such as NADH:Ubiquinone Oxidoreductase and Coenzyme Q:Cytochrome C Oxidoreductase (St-Pierre et al., 2002). Mitochondrial ROS production is greater at hyperpolarized mitochondrial membrane potentials (Ψ_m), and in isolated mitochondria small decreases in Ψ_m significantly decrease levels of ROS (Korshunov et al., 1997; Miwa et al., 2003). Endogenous uncoupling proteins, particularly the mitochondrial uncoupling protein 2 (UCP2), are able to protect nervous tissue from multiple sources of acute damage (Mattiasson et al., 2003; Andrews et al., 2005; Lapp et al., 2014; Barnstable et al., 2016) by decreasing Ψ_m and presumably ROS (Fleury et al., 1997; Echtay et al., 2001). Lower levels of ROS are protective in most scenarios, but the predicted outcome of a lower Ψ_m is also a decreased mitochondrial drive for ATP synthesis (Klingenberg and Rottenberg, 1977). Therefore, it is unclear whether uncoupling proteins are beneficial for long-term neurodegenerative conditions. As with many neurodegenerative disorders, the clinical course of glaucoma progresses over multiple years. It is therefore essential that model systems of neurodegeneration develop over time and not in reaction to a single damaging insult.

In the microbead model of glaucoma, occlusion of the irido-corneal angle progressively increases damage to RGCs over a sub-acute time frame (Huang et al., 2018). Using this model, we tested whether enhanced *Ucp2* expression in mouse RGCs or in supporting glial cells is protective against injury. We found that increasing levels of *Ucp2* in RGCs, but not in GFAP-expressing glia, were neuroprotective. *Ucp2* levels are under several forms of transcriptional and translational control (Donadelli et al., 2014; Lapp et al., 2014), and our second goal was to determine whether factors that increase *Ucp2* transcription provide protection from cell death. We found that the PPAR-γ agonist rosiglitazone (RSG), a well-known transcriptional activator of Ucp2, does not alter RGC survival during glaucoma, implying an additional need to characterize clinically useful molecules which regulate *Ucp2* at post-transcriptional levels.

MATERIALS AND METHODS

Ethics Statement

This study was carried out in accordance with the National Research Council's Guide for the Care and Use of Laboratory Animals (8th edition). The protocol was approved by the Pennsylvania State University College of Medicine Institutional Animal Care and Use Committee.

Animals

Wild-type (WT) C57BL6/J and transgenic mice were housed in a room with an ambient temperature of 25°C, 30–70% humidity, a 12-h light–dark cycle, and *ad libitum* access to rodent chow. Transgenic mouse strains, B6.Cg-Tg(*GFAP-cre/ER^{T2}*)505Fmv/J (*Gfap-creER^{T2}*, Stock#: 012849) (Ganat et al., 2006) and Tg(*Thy1-cre/ER^{T2}*,-EYFP)HGfng/PyngJ *(Thy1-creER^{T2}*, Stock#: 012708) (Young et al., 2008), were each generated on a WT background and purchased from the Jackson Laboratory (Bar Harbor, ME, United States). *GFAP-creER^{T2}* and *Thy1-creER^{T2}* mice express a fusion product of *cre* recombinase and an estrogen receptor regulatory subunit (*creER^{T2}*) under the control of the *hGFAP* or *Thy1* promoters, respectively. CreER^{T2} activity is regulated by the estrogen receptor modulator and tamoxifen metabolite 4-hydroxytamoxifen (Zhang et al., 1996). Ucp2KI$^{fl/fl}$ mice were derived from Ucp2KOKI$^{fl/fl}$ mice (provided by Sabrina Diano, Ph.D.) and result from multiple back-crosses with WT mice (Toda et al., 2016). In these crosses, mice were selectively bred to retain the Ucp2KI sequence and the WT variant of the *Ucp2* gene. In these mice, a transgene was inserted in to the R26 locus, containing a LoxP-flanked stop codon followed by a copy of the mouse *Ucp2* cDNA and an IRES-EGFP sequence. Following cell-type specific cre-mediated excision of the LoxP-flanked stop codon, these mice express *Ucp2* and EGFP in astrocytes and müller glia (*Ucp2^{KI}; GFAP-creER^{T2}* mice) or in the vast majority of RGCs (*Ucp2^{KI}; Thy1-creER^{T2}* mice*)*. To elicit cre-mediated excision of this stop codon, we injected mice intraperitoneally with 100 mg tamoxifen (Sigma, T5648)/kg mouse/day for 8 days, preceding any experimental manipulations. Same-litter cre recombinase-negative control mice (*Ucp2^{KI}*) were also injected with tamoxifen to control for any potential biological impacts of tamoxifen.

Rosiglitazone was fed to WT mice by grinding 4 mg pills (Avandia, GSK) with a mortar and pestle and mixing them into ground normal mouse chow. We measured daily food consumption and adjusted the amount of RSG used based on food consumption. RSG was fed to mice beginning 2 days prior to microbead injection and does not alter IOP. During this study, we estimate an average RSG consumption of 28.2 mg RSG/kg mouse/day.

Microbead Injection

We modeled glaucoma in mice by elevating IOP. We increased IOP in 2–4 month old mice of both genders as previously described (Cone et al., 2012). At least 24 h prior to bead injection, we took a baseline IOP measurement. Prior to bead injection, IOP is stable and is well represented by a single measurement. Immediately prior to bead injection, we anesthetized mouse corneas topically with proparacaine hydrochloride (0.5%) eyedrops and systemically with an intraperitoneal injection of 100 mg/kg ketamine/10 mg/kg xylazine. While anesthetized, we injected 6 μm (2 μL at 3×10^6 beads/μL; Polysciences, Cat#: 07312-5) and 1 μm (2 μL at 1.5×10^7 beads/μL; Polysciences, Cat#: 07310-15) polystyrene microbeads through a 50–100 μm cannula in the cornea formed by a beveled glass micropipette connected by polyethylene tubing to a Hamilton syringe (Hamilton Company Reno, NV, United States). As an internal control, 4 μL of sterile 1× phosphate buffered saline (PBS) was injected in to the contralateral eye. We measured postoperative IOP every 3 days for 30 days. Following terminal IOP measurements, mice were asphyxiated using a Euthanex SmartBox system, which automatically controls CO_2 dispersion, followed by cervical dislocation.

IOP Measurement

Intra-ocular pressure was measured in mice anesthetized by 1.5% isoflurane in air (v/v) using an Icare® TonoLab (Icare Finland Oy, Espoo, Finland) rebound tonometer, both before and after injection with polystyrene microbeads. Each reported measurement is the average of 18 technical replicates/mouse/eye. Mice were included in this study if their individual IOP was elevated by ≥3 mmHg or if a paired *t*-test of IOP over time between microbead and PBS-injected eyes was statistically significant ($p < 0.05$). Baseline and bead-injected IOPs were compared between mouse strains to confirm the absence of any genotype-dependent differences in IOP increase.

Histology and Immunocytochemistry

Immunolabeling of sectioned retinal tissue was performed as previously described (Pinzon-Guzman et al., 2011). Briefly, whole eyes were fixed in 4% paraformaldehyde (Electron Microscopy Sciences, Hatfield, PA, United States) in 1× PBS overnight at 4°C. The next day, eyes were divided in half with a scalpel blade. One half was frozen and sectioned, while the other was labeled as a whole-mount. Frozen tissues were embedded in a 2:1 mixture of 20% sucrose and OCT (Electron Microscopy Sciences), cooled to −20°C, and cut at a 10 μm thickness. Samples for each experiment were located on the same slide to control for assay variability. Prior to immunohistochemical labeling, we unmasked antigens by exposing them to a 10 mM sodium citrate buffer (pH6.0) for 30 min at 100°C. Subsequent labeling of oxidative protein carbonyls was performed using an OxyIHC kit (EMD-Millipore, Cat#: S7450). Derivatization of protein carbonyl groups and all subsequent steps were performed in accordance with the manufacturer's instructions. Staining intensity was derived using the H-DAB vector of the ImageJ Color Deconvolution tool background was subtracted from each image, resulting in a numerical semiquantitative measure of oxidative tissue stress. Tissue was imaged using an Olympus BX50 microscope. In this and all other experiments, the acquisition parameters for any given label were held constant.

Post-fixation, retinal whole mounts were permeabilized with 0.2% Triton-X-100 in PBS, blocked with 5% non-fat milk, and incubated in rabbit anti-RBPMS antibody (1:500, EMD Millipore) for 6 days at 4°C. Tissue was incubated in secondary antibody and 1 μg/mL Hochest-33258 overnight at 4°C prion to washing and mounting with 0.5% n-propyl gallate in 1:1 glycerol: PBS. Whole-mount tissue was imaged on a Fluoview FV1000 confocal microscope (Olympus).

Retinal Ganglion Cell Counting

Retinal ganglion cells were counted in retinal whole-mounts using the marker RBPMS (Rodriguez et al., 2014) across three to four 317.95 μm × 317.95 μm fields, with each field centered 1000 μm from the optic nerve head. Cell counts were converted to measurements of RGC density, averaged for a single retina, and RGC survival was calculated as a percentage of bead-injected RGC density over contralateral control PBS-injected RGC density. RGC loss or death was 100-mean RGC survival for a given sample. The counter was blinded to the identity of each sample. We did not find a significant effect of retinal quadrant on RGC density normally or with elevated IOP, and our images were therefore taken across all retinal quadrants. The mean±SEM and median $RBPMS^+$ RGC densities in PBS-injected retinas (pooled from WT C57BL6/J and $Ucp2^{KI}$ controls) were 4758±113 and 4738 cells/mm^2, respectively. The mean±SEM and median $RBPMS^+$ RGC densities in bead-injected retinas were 3957±152 and 3858 cells/mm^2, respectively, leading to an average 17% cell loss 30 days following bead injection.

RNA Isolation and Quantitative Real-Time PCR

Flash frozen cells or tissue were lyzed in TRIzol (Thermo-Fischer, Cat#:15596018) and RNA precipitated using the manufacturer's recommended procedure. Final RNA concentration was measured using a NanoDrop ND-1000 Spectrophotometer prior to reverse transcription. We reverse transcribed 300–1000 μg RNA using SuperScript III (Thermo-Fischer, Cat#: 18080093) with random hexamers. cDNA was amplified with iQ SYBR Green Supermix (Bio-Rad, Cat#: 1708882) and amplified on a Bio-Rad iCycler. *Ucp2* primer sequences were F: 5′—GCT CAG AGC ATG CAG GCA TCG—3′ and R: 5′—CGT GCA ATG GTC TTG TAG GCT TCG—3′. TATA-box binding protein (*Tbp)* primer sequences were F: 5′—ACC TTA TGC TCA GGG CTT GGC C—3 R: 5′—GTC CTG TGC CGT AAG GCA TCA TTG—3′. Cq′s from *Ucp2* amplification were normalized against *Tbp* and controls using the $\Delta\Delta C_t$ method. Expression of *Ucp2/Tbp* in DBA2J retinas was analyzed from data deposited in the NCBI Gene Expression Omnibus (Geo) by Howell et al. (2011), under the accession GSE26299.

Primary Astrocyte Culture

Primary mouse cortical astrocytes were isolated from postnatal day 1–4 mice as previously described (Sarafian et al., 2010;

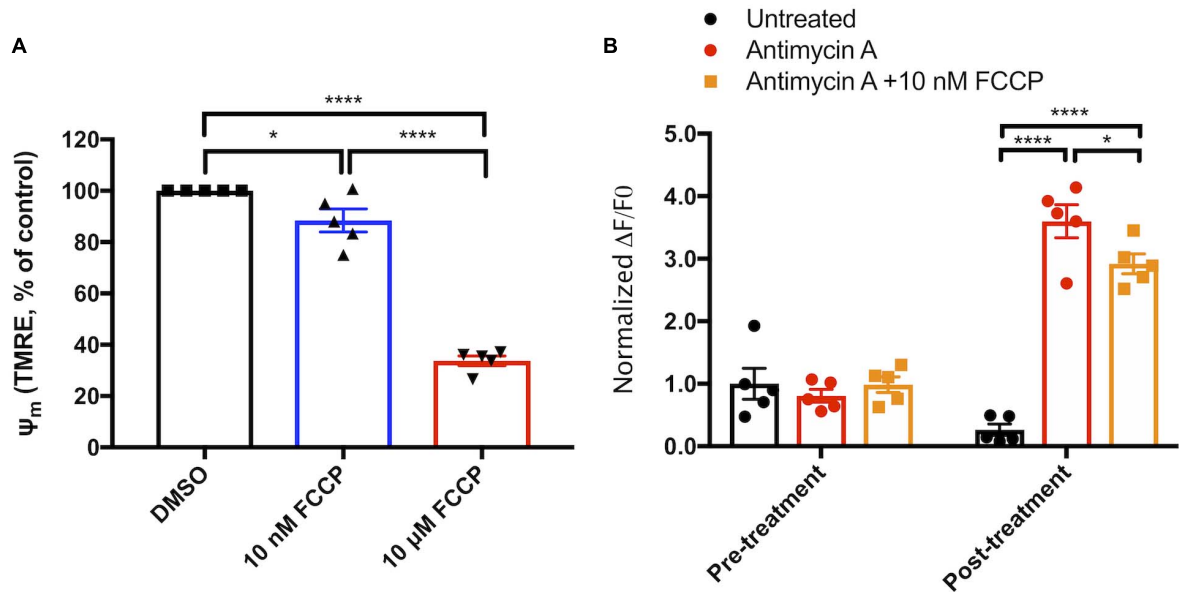

FIGURE 1 | Mitochondrial uncoupling decreases reactive oxygen species production. **(A)** Measurements of TMRE fluorescence as a proxy for mitochondrial membrane potential (Ψ_m) in cells exposed to vehicle, 10 nM FCCP, or 10 μM FCCP ($n = 3$). **(B)** Increase in MitoSox oxidation over a 5-min period prior to and following exposure of primary cortical astrocytes to nothing (black circles), 5 μM antimycin A (red circles), or 5 μM antimycin A and 10 nM FCCP (orange circles, $n = 5$). $^*p < 0.05$, $^{****}p < 0.0001$.

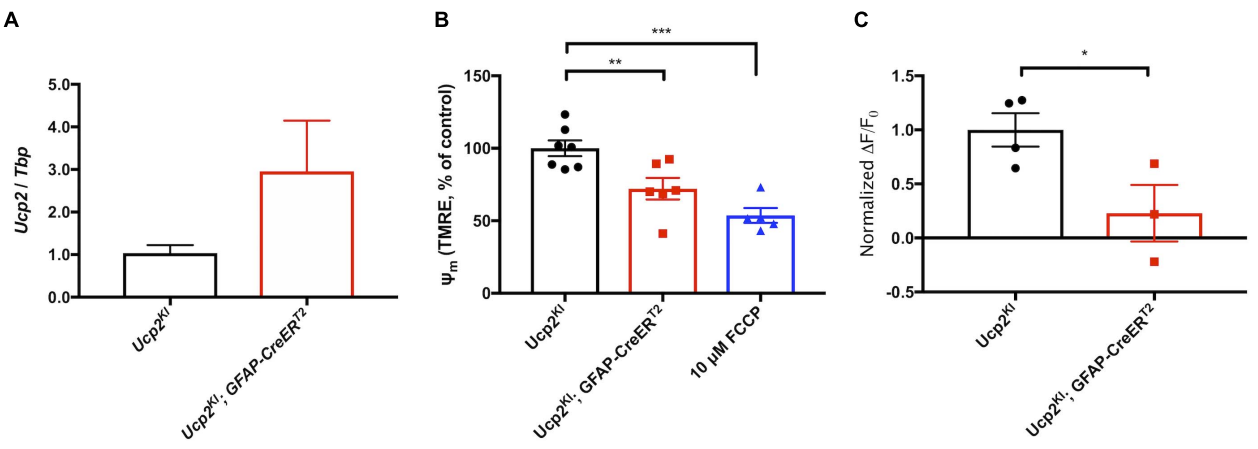

FIGURE 2 | Ucp2 decreases Ψ_m, increasing respiration and decreasing production of ROS. **(A)** Ucp2 gene expression ($n = 3$), **(B)** relative TMRE fluorescence (Ψ_m, $n = 5$–7), and **(C)** the relative rate of increase in MitoSox fluorescence ($n = 3$–4) within primary cortical astrocytes isolated from *Ucp2*^{KI} and *Ucp2*^{KI}*; Gfap-creER*^{T2} mice. $^*p < 0.05$, $^{**}p < 0.01$, $^{***}p < 0.005$.

Lapp et al., 2014). Briefly, mice were decapitated and brains were removed from the skull. In tissue culture medium, a ∼1 cm portion of superior cerebral cortex was pinched off of the brain using curved forceps. Meninges were removed, and the tissue was triturated with a sterile flame-polished glass Pasteur pipette until it formed a single cell suspension, approximately 20×. The suspension was filtered through a 70 μm cell strainer (Corning, Cat#: 352350) to remove larger debris, centrifuged at 500 × *g* and 4°C for 5 min, resuspended in growth medium (Dulbecco's Modified Eagle's Medium/Ham's F12 supplemented with 2 mM L-glutamine, 15 mM HEPES, 10% fetal bovine serum, and 10 ng/mL gentamicin), and plated in a T-25 tissue culture flask. Cells were grown at 37°C in a 5% CO_2/balance air atmosphere. After the cells reached confluence, between 7–14 days *in vitro* (DIV), contaminating cells were shaken off by rotating at 250 RPM overnight. Astrocyte-enriched cultures were plated at 30,000 cells/well on black tissue-culture-treated 96-well plates (Corning, Cat#3603) and used at passage #2 or 3, allowing at least 48 h following medium replacement before experimentation. All cells used in this study were exposed to 1 μM 4-hydroxytamoxifen (Sigma, Cat#: H6278) for 24 h prior to studies of *Ucp2* function.

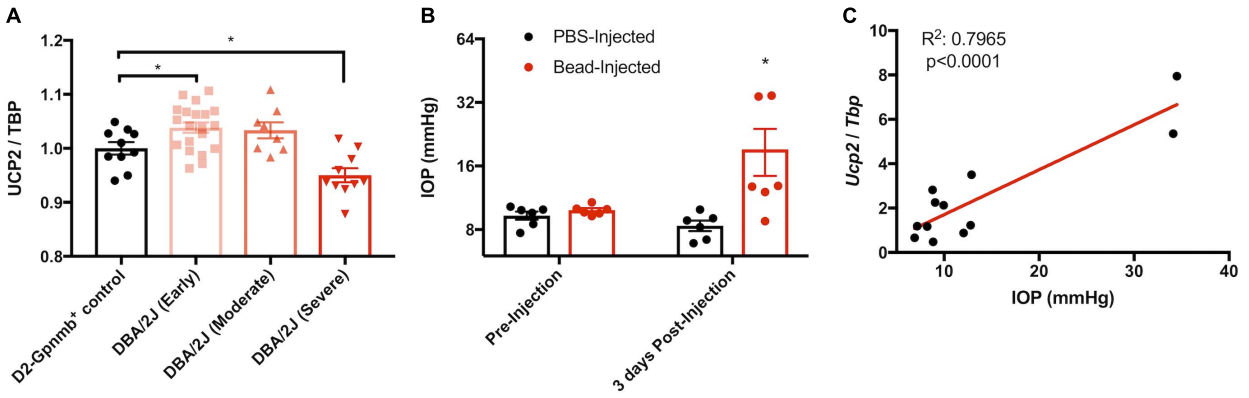

FIGURE 3 | Glaucoma increases *Ucp2* expression. **(A)** *Ucp2* expression in a genome-wide microarray of gene expression in the retinas of DBA/2J mice at various stages of glaucoma (n = 10–20), and DBA/2J-Gpnmb^{+} controls (n = 10; Howell et al., 2011). **(B)** Intra-ocular pressure (IOP) prior to and following microbead injection (n = 6) and **(C)** expression of *Ucp2* in each of the retinas from these mice as a function of IOP, 3 days following bead injection (n = 12). *$p < 0.05$.

Measurement of Mitochondrial Membrane Potential and Oxidative Status

We determined mitochondrial membrane potential (Ψ_m) and oxidative status of primary cortical astrocytes using the mitochondrial membrane potential-sensitive dye TMRE (50 nM, ImmunoChemistry, Cat#: 9103) or the mitochondrial superoxide probe MitoSox (5 μM, Thermo-Fischer, Cat#: M36008), which is selectively targeted to mitochondria. Cells were incubated in either dye in prewarmed assay medium (1× PBS supplemented with 1 mM glucose and 2 mM GlutaMax, Thermo-Fischer, Cat#: 35050-061) for 30 min at 37°C, followed by two washes and imaging. MitoSox fluorescence intensity was measured using the kinetic mode of a microplate reader (BioTek Synergy II), which took serial measurements of MitoSox fluorescence over time. The rate of increase in fluorescence (ΔF) over 10 min was divided by initial fluorescent intensity (F_0) for each well. This rate of increase was normalized to the mean $\Delta F/F_0$ of control cells. We verified the utility of TMRE as an indicator of Ψ_m by simultaneously treating cells with the membrane permeant protonophore carbonyl cyanide-*4*-(trifluoromethoxy) phenylhydrazone (FCCP, 10 μM, Caymen Chemical, Cat#: 15218), which depolarizes Ψ_m. Similarly, we used the mitochondrial complex III inhibitor antimycin A (AA, 5 μM) to stimulate ROS production and confirm the utility of MitoSox as an indicator of ROS.

Statistical Analysis

Quantified data are represented by that group's mean±SEM unless otherwise indicated. We performed all statistical analyses in GraphPad Prism. We determined the statistical effect of one independent variable (such as genetic background) on two groups using a Student's t-test or paired sample t-test in cases where samples were matched (e.g., the control was the contralateral eye of the same animal). We analyzed the effect of one variable on >2 groups (e.g., comparisons of *Ucp2*^{KI} with or without each *cre* variant) using a one-way ANOVA with a Bonferroni *post hoc* analysis. We analyzed the effect of two variables (e.g., the effects AA and FCCP on MitoSox) using a two-way ANOVA with a Bonferroni's *post hoc* analysis. The statistical significance threshold was set at $p < 0.05$ for all tests.

In ANOVAS of unmatched samples, Prism automatically implements a Geisser-Greenhouse correction to improve statistical analysis of non-spherical data sets. In accordance with the Prism Statistics guide, we assumed sphericity in matched data sets (i.e., in bead- vs. PBS-injected eyes, and cells treated with different groups of respiratory chain inhibitors).

RESULTS

Exogenous Uncoupling Agents Decrease the Generation of Mitochondrial ROS

The positive association between mitochondrial membrane potential (Ψ_m) and the production of reactive oxygen species (ROS) has been well characterized in isolated mitochondria, and we tested the hypothesis that mild mitochondrial uncoupling stimulated by an exogenous protonophore will decrease mitochondrial ROS in intact cells. We treated primary cortical astrocytes with FCCP at a low concentration to uncouple mitochondria without completely dissipating the Ψ_m, and found that 10 nM FCCP depolarized the mitochondrial membrane potential (Ψ_m) to 88±4% of control levels, whereas Ψ_m was 34±2% of control in astrocytes treated with 10 μM FCCP, a concentration routinely used to maximally depolarize mitochondria (10 μM; **Figure 1A**); 10 nM FCCP added to MitoSox loaded cells did not significantly alter mitochondrial superoxide generation (data not shown), so we tested the hypothesis that uncoupling will reduce ROS production by dysfunctional mitochondria. To test this hypothesis, we loaded cells with the mitochondrion-targeted superoxide probe MitoSox and treated them with the mitochondrial complex III inhibitor AA (5 μM). AA significantly increased the rate of MitoSox oxidation ($p < 0.001$,

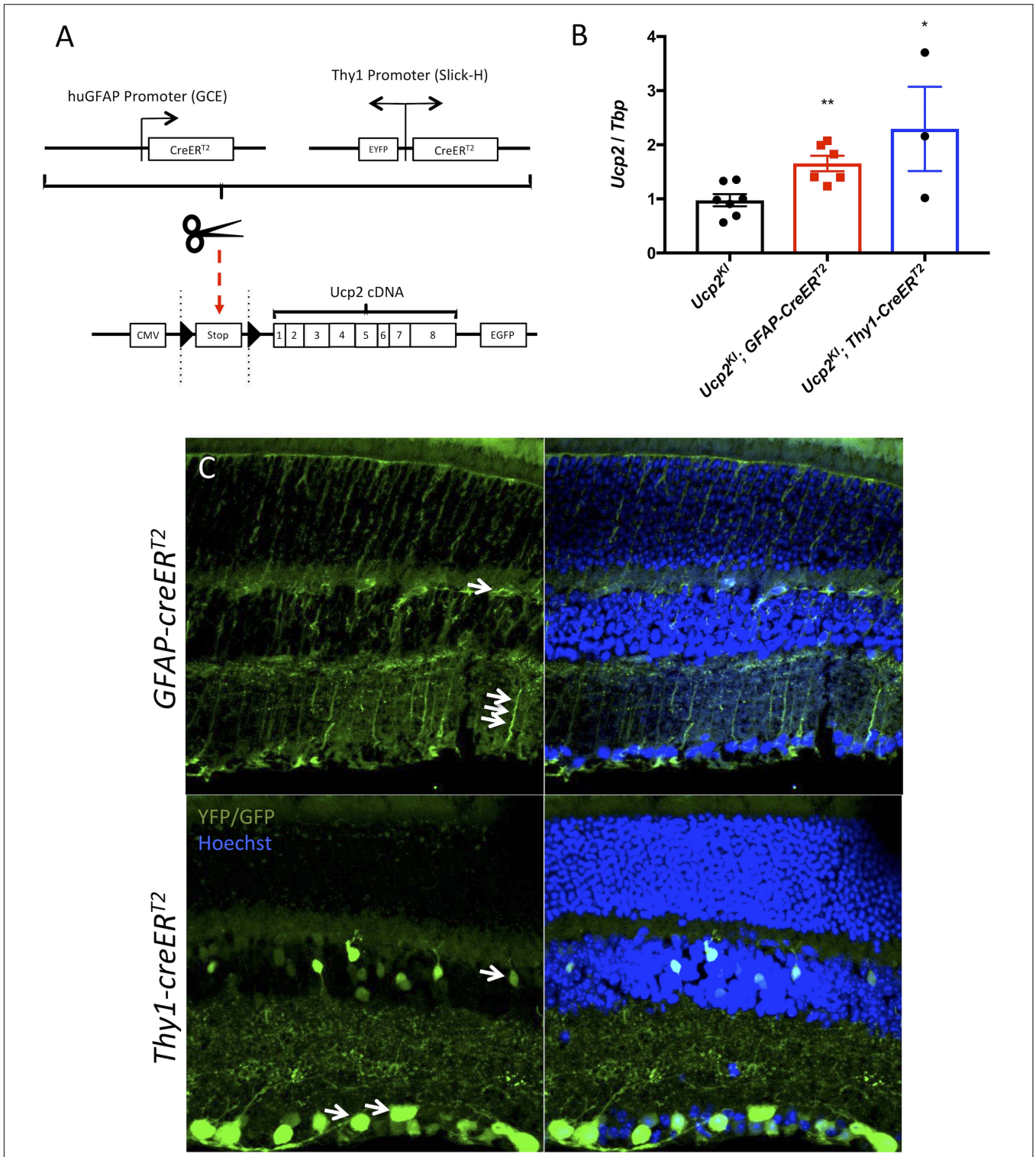

FIGURE 4 | Effects of *Thy1-creER*^{T2} and *Gfap-creER*^{T2} on retinal *Cre* recombinase localization and Ucp2 expression. **(A)** Gene diagram of transgenic *Ucp2* and *cre* recombinase variants used in the present study. **(B)** Expression of *Ucp2* in control and transgenic mice ($n = 3$). **(C)** Hoechst 33258 (blue)-labeled frozen sections of *Ucp2*^{KI}*; GFAP-creER*^{T2} and *Ucp2*^{KI}*; Thy1-creER*^{T2} retinas, showing the endogenous fluorescence of EGFP and YFP, respectively. White arrows point to Muller glia filaments and cell bodies in *GFAP-creER*^{T2} retinas and to RGC soma in *Thy1-creER*^{T2} retinas. *$p < 0.05$, **$p < 0.01$.

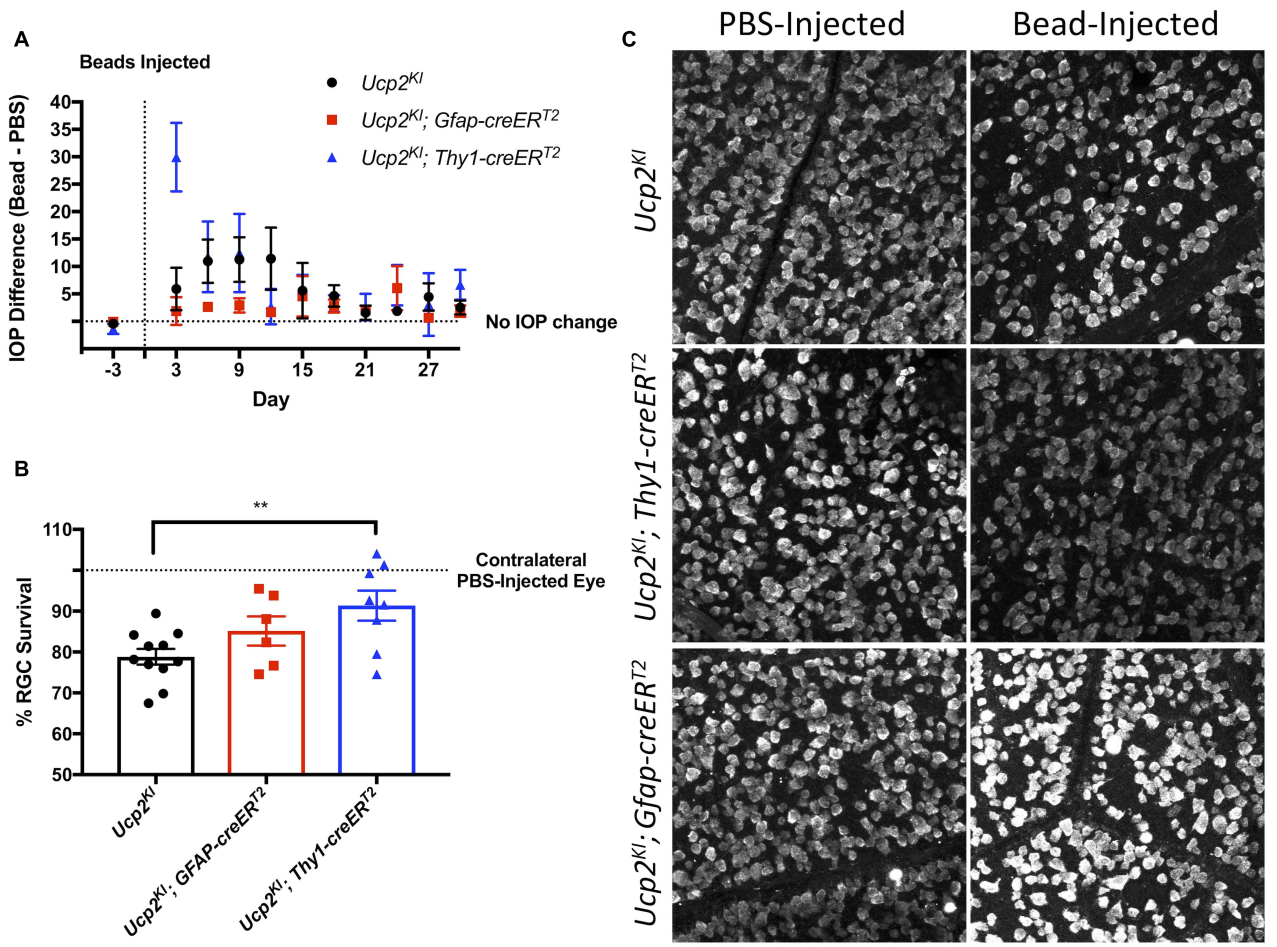

FIGURE 5 | Increased *Ucp2* expression in RGCs but not astrocytes and müller glia decreases retinal ganglion cell loss. **(A)** Difference IOP between bead- and PBS-injected eyes before and following intraocular surgery. Beads injection elevated IOP over a 30-day period in $Ucp2^{KI}$ (n = 11), $Ucp2^{KI}$; *Gfap-creER*^{T2} (n = 6), $Ucp2^{KI}$; *Thy1-creER*^{T2} (n = 9) eyes. **(B)** Percentage RGC survival in retinal whole-mounts from bead-injected eyes, relative to retinas of PBS-injected contralateral control eyes. **(C)** Representative images of retinal whole-mounts labeled for RBPMS, quantified in **B**. $^{**}p < 0.01$.

Figure 1B), but this increase was partially attenuated in cells simultaneously treated with AA and 10 nM FCCP ($p < 0.05$, **Figure 1B**). These data show that uncoupling decreases the generation of ROS by cultured astrocytes with dysfunctional mitochondria.

Uncoupling Protein 2 Decreases Ψ_m and ROS Production

To determine whether mitochondrial uncoupling proteins have the same cellular effects as chemical protonophores on Ψ_m and ROS production, we isolated cortical astrocytes from Ucp2^{KI}; *GFAP-creER*^{T2} mice. *Ucp2* expression is elevated roughly threefold in *GFAP-creER*^{T2} expressing cells of these mice following exposure to 4-hydroxytamoxifen (**Figure 2A**), and we tested the hypothesis that the addition of transgenic *Ucp2* will decrease Ψ_m and the generation of ROS. Our data show that Ucp2 knock-in depolarizes Ψ_m to 72±7% of control levels (p = 0.0095, **Figure 2B**), with 10 μM FCCP decreasing TMRE fluorescence to 54±5% of controls (p = 0.0002). Increasing Ucp2 levels decreased the production of ROS, monitored by the change in MitoSox fluorescence over time and normalized to the mean fluorescent intensity of Ucp2^{KI} control samples (p = 0.043; **Figure 2C**). Together, these data show that increased Ucp2 expression decreases Ψ_m and mitochondrial ROS, which may be similar in mechanism to the protective effects promoted by 10 nM FCCP.

Elevated IOP Increases Ucp2 Expression

To determine whether Ucp2 expression is positively or negatively related to the progression of glaucoma, we analyzed publically available data from a microarray that determined gene expression changes in the retina and optic nerve heads of 10.5 month old DBA/2J mice and DBA/2J; *Gpnmb*$^{+}$ controls (Howell et al., 2014). DBA/2J are genetically predisposed toward glaucoma, and DBA/2J; *Gpnmb*$^{+}$ controls are genetically identical to these mice, except for in the *Gpnmb* gene, for which these control mice express a WT copy. Relative to the housekeeping gene *Tbp*, *Ucp2* expression is elevated

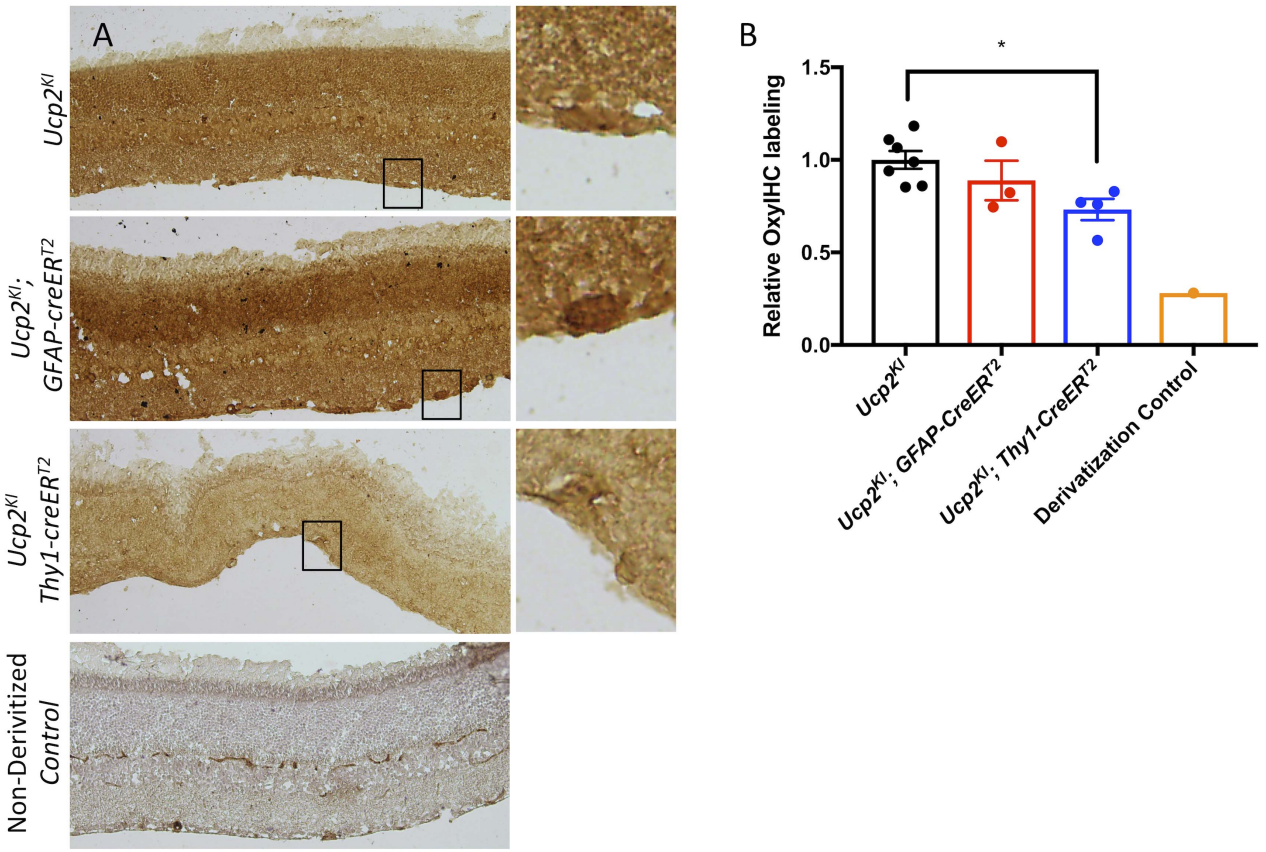

FIGURE 6 | Increased *Ucp2* expression in RGCs but not astrocytes and müller glia decreases oxidative stress. **(A)** Representative labeling of fixed retinas from bead-injected *Ucp2*^{KI} (n = 7), *Ucp2*^{KI}*; Gfap-creER*^{T2} (n = 3), and *Ucp2*^{KI}*; Thy1-creER*^{T2} (n = 4) eyes for oxidative stress-derived protein carbonylation. A single section was labeled without using the 2′,4′-dinitrophenylhydrazine derivitization reagent to confirm the specificity of the primary antibody to toward dinitrophenylhydrazones. **(B)** The intensity of DAB labeling is quantified. *$p < 0.05$.

early in glaucoma, but decreases with increasing disease severity ($p < 0.05$, **Figure 3A**). We confirmed these data in a microbead model of glaucoma, and found that 3 days following microbead injection, IOP is significantly elevated ($p < 0.05$, **Figure 3B**). Following IOP measurement, we determined Ucp2 expression in the retinas of these mice, and found that Ucp2 expression increases proportionally with IOP (r^2=0.8, p = 0.0001 **Figure 3C**). These data suggest that Ucp2 may play a role in the retinal response to IOP elevation.

Elevated Ucp2 Expression in RGCs but Not Astrocytes or Müller Glia Is Protective Against Glaucoma

To determine whether the protective effects of *Ucp2* expression in cells translate to the same *in vivo* system, we used mice in which Ucp2 expression can be increased in *Gfap*- or *Thy1*-expressing cells following exposure to tamoxifen (**Figure 4A**). Following eight consecutive 100 mg/kg/day injections, we found that *GFAP-creER*^{T2} expression increased *Ucp2* transcript levels to 165±14% of control ($p < 0.01$, n = 6), and *Thy1-creER*^{T2} increased Ucp2 to 229±77% of *Ucp2*^{KI} controls ($p < 0.05$, n = 3, **Figure 4B**).

Although *Thy1-creER*^{T2} retinas express YFP both before and following exposure to tamoxifen, *GFAP-creER*^{T2} retinas only express eGFP following LoxP excision. We show that eGFP and YFP are present in the retina, with localizations consistent with Gfap-expressing glia and RGCs, respectively, for the *GFAP-creER*^{T2} and *Thy1-creER*^{T2} transgenes (**Figure 4C**). The white arrows indicate regions of endogenous fluorophore expression, corresponding to müller glia cell bodies and fibers (top image), as well as RGC soma (bottom image) (**Figure 4C**). Notably, *Thy1-creER*^{T2} expression was not limited to the ganglion cell layer, implying cre activity in some inner nuclear layer cells.

We injected microbeads or PBS in to the anterior chambers of these mice, elevating IOP by an average of 5.3 mmHg in *Ucp2*^{KI} control mice (n = 11), 2.4 mmHg in *Ucp2*^{KI}; *GFAP-creER*^{T2} mice (n = 6), and 7.5 mmHg in *Ucp2*^{KI}; *Thy1-creER*^{T2} mice (n = 9, **Figure 5A**). Bead injection in control mice caused a significant loss in RGCs (A 19±3% reduction in RGC density) that was attenuated in mice overexpressing Ucp2 in RGCs (*Ucp2*^{KI}; *Thy1-creER*^{T2}, a 10±4% reduction), but not in *Ucp2*^{KI}; *GFAP-creER*^{T2} mice (a 15±4% reduction,

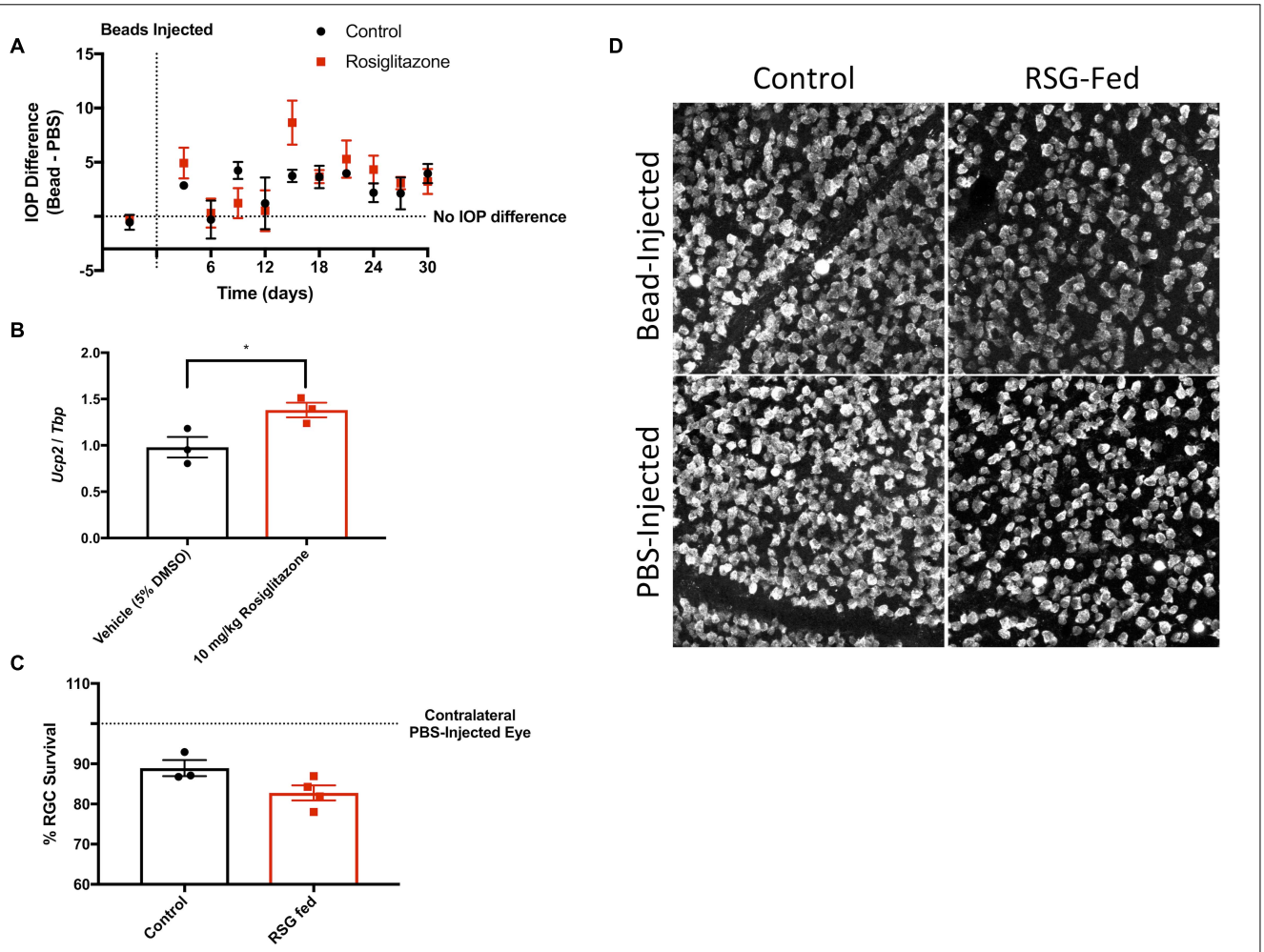

FIGURE 7 | Rosiglitazone increases *Ucp2* transcription but does not alter glaucomatous RGC loss. **(A)** Microbead injection increases IOP to a similar extent in control- and rosiglitazone (RSG)-fed mice. **(B)** Intraperitoneal RSG increases Ucp2 transcript levels in the mouse retina. **(C)** Increased IOP leads to RGC loss (decreased % survival), though dietary RSG does not appear to alter RGC loss. **(D)** Representative RBPMS labeling in whole-mount retinas from PBS- and bead-injected C57BL6J mice. $^*p < 0.05$.

Figures 5C,D). These data demonstrate that Ucp2 decreases RGC loss due to elevated IOP over a sub-acute timeframe, and also that the beneficial effects of Ucp2 are cell autonomous, as Ucp2-overexpression in *GFAP*-positive glia is insufficient to decrease glaucoma-related RGC loss (**Figure 5C**). The protective effects of Ucp2 expression coincided with significant decreases in oxidative protein carbonylation, measured by OxyIHC labeling. Bead-injected retinas from $Ucp2^{KI}$; $Thy1\text{-}creER^{T2}$ mice ($n = 4$) were labeled 27±6% less strongly than corresponding $Ucp2^{KI}$ controls ($p < 0.05$, $n = 7$). In contrast, labeling of $Ucp2^{KI}$; $GFAP\text{-}creER^{T2}$ retinas was non-significantly reduced by 11±11% ($n = 3$, **Figures 6A,B**) relative to controls.

Transcriptional Activation of Ucp2 Is Insufficient to Decrease Microbead-Induced RGC Loss

Past literature suggests that Ucp2 transcription is in part regulated by a PGC1-α/PPAR-γ axis (Chen et al., 2006; Donadelli et al., 2014). RSG is an FDA-approved PPAR-γ agonist. We confirmed that retinal *Ucp2* expression can increase 24 h following exposure to 10 mg/kg RSG (**Figure 7B**), and hypothesized that due to transcriptional activation of Ucp2, dietary RSG confers the same resistance to damage in glaucoma as transgenic Ucp2 overexpression. To test this hypothesis, we increased IOP in control- and RSG-fed WT mice (**Figure 7A**) and measured RGC loss 30 days following bead injection. There was an 11±2% loss in RGC density in bead-injected eyes of WT control mice ($n = 3$), compared to a 17±2% loss in RSG-fed mice ($n = 4$). The degree of cell loss was generally lesser than for $Ucp2^{KI}$ controls, which can be explained by the more advanced age of these mice (3.8 months), which has been demonstrated to reduce the effectiveness of RGC loss following bead injection (Cone et al., 2010). Regardless, the result of this pilot study on the effects of RSG ran contrary to our expectations and did not decrease RGC death, and in fact appeared to non-significantly increase RGC loss (**Figures 7C,D**).

DISCUSSION

Mild levels of ROS are important signals of mitochondrial damage (Frank et al., 2012) among other physiological signals (Angelova and Abramov, 2016). When ROS production exceeds the capacity for detoxification by antioxidants, they damage cellular components in a variety of pathogenic conditions (Elfawy and Das, 2019). More reduced electron transport chain metabolites (NADH, coenzyme Q_{10}) are better able to form ROS. Inhibitors of electrons transport, such as the Coenzyme Q_{10}-cytochrome C Oxidoreductase (complex III) inhibitor AA, increase the accumulation of reduced electron carriers and consequently drive mitochondrial ROS production (Quinlan et al., 2011). However, ROS production is partially dependent on a high Ψ_m (Korshunov et al., 1997; Miwa et al., 2003), which can be depolarized by either an FCCP- or Ucp2-mediated increase in proton conductance (Nègre-Salvayre et al., 1997). These data were mainly gathered in isolated mitochondria. Tissue mitochondrial quantity is too small in the retina and optic nerve, and with our currently available tools, we cannot determine endogenous RGC and optic nerve head astrocyte-specific relations between ROS and Ψ_m, if such relations exist. However, given identical bioenergetic circumstances most cellular mitochondria should react similarly to agents that alter mitochondrial coupling or electron transport. Similarly, our use of transgenic *Ucp2* overexpression is not under the control of endogenous regulatory factors, which are more likely to differ with cell type and condition.

Given the similarity of mitochondrial respiratory chain function across cell types, we used primary cortical astrocytes to demonstrate the concepts that AA-stimulated increases in ROS production that are attenuated by decreases in Ψ_m (**Figure 1**), and that *Ucp2* decreases ROS production (**Figure 2**). While these data lend support to the association between mitochondrial Ψ_m and ROS as well as the control of ROS by *Ucp2*, the most important evidence for their effect on cell and tissue physiology normally and during glaucoma must be determined *in vivo*.

Mitochondria are damaged in both glaucomatous retinal and optic nerve tissue (Coughlin et al., 2015) as well as in systemic circulation of glaucoma patients (Van Bergen et al., 2015). Mitochondria are a major source of ROS, so mitochondrial dysfunction in glaucoma is a likely source of ROS in the same tissues (Feilchenfeld et al., 2008; Chidlow et al., 2017). As with cultured cells, partial dissipation of tissue mitochondrial Ψ_m may decrease the generation of ROS in glaucoma (**Figure 6**).

Ucp2 expression is in fact altered during different stages of glaucoma, and appears to increase with increasing IOP (**Figure 3**). In pilot samples, however, we note that longer periods (30 days) following bead injection result in a depression of Ucp2 expression to roughly 80% of contralateral controls (data not shown). This is consistent with other studies of Ucp2 expression following a damaging insult, wherein tissue Ucp2 expression peaks 3–5 days after an insult (Rupprecht et al., 2012; Dutra et al., 2018). It is likely that over time in glaucoma, *Ucp2* levels may fall, and this may be correlated with RGC loss (Howell et al., 2011). If increased ganglion cell *Ucp2* expression reflects a physiological response to increased ROS early in glaucoma, artificially increasing Ucp2 may increase the ability of that stress response to increase cell survival. We indeed found an increase in retinal *Ucp2* expression following microbead injection (**Figure 5**). The hypothesis that *Ucp2* improves cell survival following a cellular stressor is also strongly supported by previous studies (Diano et al., 2003; Mattiasson et al., 2003; Andrews et al., 2005; Barnstable et al., 2016), but the novelty of our study is that in rodent models of glaucoma, RGC death is progressive over time (Huang et al., 2018), suggesting that Ucp2 is not exclusively protective during acutely stressful conditions, but also during sub-acute neurodegeneration, decreasing the accumulation of oxidative damage (**Figure 6**) and bead-induced RGC loss.

Ucp2-mediated neuroprotection is dependent on cell type, as we show that greater *Ucp2* levels in *Gfap*-expressing glia do not significantly alter RGC loss or oxidative stress-derive protein carbonyls compared to controls (**Figures 5**, **6**). A larger sample size may benefit these studies and be sufficient to demonstrate a glial-derived neuroprotective effect, supported by a trend toward decreased oxidative stress and RGC loss in $Ucp2^{KI}$; $GFAP\text{-}creER^{T2}$ mice, but overall the data argue for much weaker if any *Ucp2*-mediated neuroprotection from glial cells than from RGCs. This seems to suggest that changes in mitochondrial dynamics within *Gfap*-expressing glia of the retina may not be central for the progression of glaucoma, which is unexpected given the many changes they undergo over the course of the disease (Woldemussie et al., 2004) and the protection they give to RGCs (Kawasaki et al., 2000).

Rosiglitazone is a PPAR-γ-dependent transcriptional activator of *Ucp2* (Medvedev et al., 2001; Chen et al., 2006), and increases retinal *Ucp2* expression (**Figure 7**), but does not seem to promote *Ucp2* mediated neuroprotection in the microbead model of glaucoma. PPAR-γ appears to be expressed with high specificity in müller glia cells of the rodent retina (Zhu et al., 2013), and while the failure of RSG to protect RGCs was initially surprising, it likely increases the transcription of glial *Ucp2*. *Ucp2* overexpression in *Gfap*-expressing glia failed to protect RGCs, so our experiments using RSG-fed and $Ucp2^{KI}$; $GFAP\text{-}creER^{T2}$ mice largely support each other. PPAR-γ agonism with pioglitazone is sufficient to decrease RGC loss following optic nerve crush in rats (Zhu et al., 2013) or retinal ischemia/reperfusion injury in mice (Zhang et al., 2017), suggesting that glial *Ucp2* expression may be protective against more acute retinal insults. This protection may also result from the increase in neural PPAR-γ following optic nerve crush (Zhu et al., 2013), which would allow for agonist-stimulated Ucp2 mRNA expression that is likely subject to multiple endogenous regulatory mechanisms (Donadelli et al., 2014), unlike the *Ucp2* derived from our transgenic mice (Toda et al., 2016). Alternatively, PPAR-γ could theoretically promote multiple counteracting effects that render transcriptional stimulation of Ucp2 unimportant in glaucoma. For example, activation of PPAR-γ promotes fatty acid oxidation (Benton et al., 2008), increasing use of a bioenergetic substrate that may directly

increase ROS generation (St-Pierre et al., 2002) and thus mask a Ucp2-dependent anti-oxidative effect. Regardless, a larger study of *Ucp2* and PPAR-γ in retinal disease that uses multiple models and agonists/antagonists may yield a clearer picture that captures the cell type specific dynamics of these factors, and changes during different paradigms of retinal damage.

Overall, our data suggest that the greatest protection against RGC loss can be provided by stimulating Ucp2 expression in RGCs. Expression of this gene in other cell types may not be harmful, but our results suggest that the choice of therapeutic target should be dictated in part by cell type. The expression and activity of this protein is also tightly regulated, so the future studies on *Ucp2*-mediated neuroprotection should also focus on the factors that manipulate *Ucp2* transcription, translation, and functional activity.

DATA AVAILABILITY

The datasets generated for this study are available on request to the corresponding author.

AUTHOR CONTRIBUTIONS

DH performed the experiments, analyzed them, and wrote the first draft of the manuscript. Both DH and CB conceived of the study topic and design, as well as revised the submitted manuscript.

FUNDING

This work was supported by grants from the NIH (Grant No. NS100508-01A1 from the NINDS) and the Macula Vision Research Foundation, and a Summer Student Fellowship from Fight for Sight (Grant No. FFS-SS-18-046).

ACKNOWLEDGMENTS

We thank Sabrina Diano, Ph.D., for generously donating the Ucp2KOKI$^{fl/fl}$ mice that were the progenitors of mice used in this study. We also thank Evgenya Popova, Ph.D., for her thorough discussions on and critical review of this research.

REFERENCES

Abu-Amero, K. K., Morales, J., and Bosley, T. M. (2006). Mitochondrial abnormalities in patients with primary open-angle glaucoma. *Invest. Ophthalmol. Vis. Sci.* 47, 2533–2541. doi: 10.1167/iovs.05-1639

Andrews, Z. B., Horvath, B., Barnstable, C. J., Elsworth, J., Elseworth, J., Yang, L., et al. (2005). Uncoupling protein-2 is critical for nigral dopamine cell survival in a mouse model of Parkinson's disease. *J. Neurosci.* 25, 184–191. doi: 10.1523/JNEUROSCI.4269-04.2005

Angelova, P. R., and Abramov, A. Y. (2016). Functional role of mitochondrial reactive oxygen species in physiology. *Free Radic. Biol. Med.* 100, 81–85. doi: 10.1016/j.freeradbiomed.2016.06.005

Barnstable, C. J., Reddy, R., Li, H., and Horvath, T. L. (2016). Mitochondrial Uncoupling Protein 2 (UCP2) regulates retinal ganglion cell number and survival. *J. Mol. Neurosci.* 58, 461–469. doi: 10.1007/s12031-016-0728-5

Benton, C. R., Holloway, G. P., Campbell, S. E., Yoshida, Y., Tandon, N. N., Glatz, J. F., et al. (2008). Rosiglitazone increases fatty acid oxidation and fatty acid translocase (FAT/CD36) but not carnitine palmitoyltransferase I in rat muscle mitochondria. *J. Physiol.* 586, 1755–1766. doi: 10.1113/jphysiol.2007.146563

Boland, M. V., and Quigley, H. A. (2007). Risk factors and open-angle glaucoma: classification and application. *J. Glaucoma* 16, 406–418. doi: 10.1097/IJG.0b013e31806540a1

Carter-Dawson, L., Shen, F., Harwerth, R. S., Smith, E. L., Crawford, M. L., and Chuang, A. (1998). Glutamine immunoreactivity in Müller cells of monkey eyes with experimental glaucoma. *Exp. Eye Res.* 66, 537–545. doi: 10.1006/exer.1997.0447

Chen, S. D., Wu, H. Y., Yang, D. I., Lee, S. Y., Shaw, F. Z., Lin, T. K., et al. (2006). Effects of rosiglitazone on global ischemia-induced hippocampal injury and expression of mitochondrial uncoupling protein 2. *Biochem. Biophys. Res. Commun.* 351, 198–203. doi: 10.1016/j.bbrc.2006.10.017

Chidlow, G., Wood, J. P. M., and Casson, R. J. (2017). Investigations into hypoxia and oxidative stress at the optic nerve head in a rat model of glaucoma. *Front. Neurosci.* 11:478. doi: 10.3389/fnins.2017.00478

Cone, F. E., Gelman, S. E., Son, J. L., Pease, M. E., and Quigley, H. A. (2010). Differential susceptibility to experimental glaucoma among 3 mouse strains using bead and viscoelastic injection. *Exp. Eye Res.* 91, 415–424. doi: 10.1016/j.exer.2010.06.018

Cone, F. E., Steinhart, M. R., Oglesby, E. N., Kalesnykas, G., Pease, M. E., and Quigley, H. A. (2012). The effects of anesthesia, mouse strain and age on intraocular pressure and an improved murine model of experimental glaucoma. *Exp. Eye Res.* 99, 27–35. doi: 10.1016/j.exer.2012.04.006

Coughlin, L., Morrison, R. S., Horner, P. J., and Inman, D. M. (2015). Mitochondrial morphology differences and mitophagy deficit in murine glaucomatous optic nerve. *Invest. Ophthalmol. Vis. Sci.* 56, 1437–1446. doi: 10.1167/iovs.14-16126

Diano, S., Matthews, R. T., Patrylo, P., Yang, L., Beal, M. F., Barnstable, C. J., et al. (2003). Uncoupling protein 2 prevents neuronal death including that occurring during seizures: a mechanism for preconditioning. *Endocrinology* 144, 5014–5021. doi: 10.1210/en.2003-0667

Donadelli, M., Dando, I., Fiorini, C., and Palmieri, M. (2014). UCP2, a mitochondrial protein regulated at multiple levels. *Cell. Mol. Life Sci.* 71, 1171–1190. doi: 10.1007/s00018-013-1407-0

Dutra, M. R. H., Feliciano, R. D. S., Jacinto, K. R., Gouveia, T. L. F., Brigidio, E., Serra, A. J., et al. (2018). Protective role of UCP2 in oxidative stress and apoptosis during the silent phase of an experimental model of epilepsy induced by pilocarpine. *Oxid. Med. Cell. Longev.* 2018:6736721. doi: 10.1155/2018/6736721

Echtay, K. S., Winkler, E., Frischmuth, K., and Klingenberg, M. (2001). Uncoupling proteins 2 and 3 are highly active H(+) transporters and highly nucleotide sensitive when activated by coenzyme Q (ubiquinone). *Proc. Natl. Acad. Sci. U.S.A.* 98, 1416–1421. doi: 10.1073/pnas.98.4.1416

Elfawy, H. A., and Das, B. (2019). Crosstalk between mitochondrial dysfunction, oxidative stress, and age related neurodegenerative disease: etiologies and therapeutic strategies. *Life Sci.* 218, 165–184. doi: 10.1016/j.lfs.2018.12.029

Feilchenfeld, Z., Yücel, Y. H., and Gupta, N. (2008). Oxidative injury to blood vessels and glia of the pre-laminar optic nerve head in human glaucoma. *Exp. Eye Res.* 87, 409–414. doi: 10.1016/j.exer.2008.07.011

Fleury, C., Neverova, M., Collins, S., Raimbault, S., Champigny, O., Levi-Meyrueis, C., et al. (1997). Uncoupling protein-2: a novel gene linked to obesity and hyperinsulinemia. *Nat. Genet.* 15, 269–272. doi: 10.1038/ng0397-269

Frank, M., Duvezin-Caubet, S., Koob, S., Occhipinti, A., Jagasia, R., Petcherski, A., et al. (2012). Mitophagy is triggered by mild oxidative stress in a mitochondrial fission dependent manner. *Biochim. Biophys. Acta* 1823, 2297–2310. doi: 10.1016/j.bbamcr.2012.08.007

Ganat, Y. M., Silbereis, J., Cave, C., Ngu, H., Anderson, G. M., Ohkubo, Y., et al. (2006). Early postnatal astroglial cells produce multilineage precursors and neural stem cells *in vivo*. *J. Neurosci.* 26, 8609–8621.

Howell, G. R., Macalinao, D. G., Sousa, G. L., Walden, M., Soto, I., Kneeland, S. C., et al. (2011). Molecular clustering identifies complement and endothelin

induction as early events in a mouse model of glaucoma. *J. Clin. Invest.* 121, 1429–1444. doi: 10.1172/JCI44646

Howell, G. R., MacNicoll, K. H., Braine, C. E., Soto, I., Macalinao, D. G., Sousa, G. L., et al. (2014). Combinatorial targeting of early pathways profoundly inhibits neurodegeneration in a mouse model of glaucoma. *Neurobiol. Dis.* 71, 44–52. doi: 10.1016/j.nbd.2014.07.016

Huang, W., Hu, F., Wang, M., Gao, F., Xu, P., Xing, C., et al. (2018). Comparative analysis of retinal ganglion cell damage in three glaucomatous rat models. *Exp. Eye Res.* 172, 112–122. doi: 10.1016/j.exer.2018.03.019

Ito, Y. A., and Di Polo, A. (2017). Mitochondrial dynamics, transport, and quality control: a bottleneck for retinal ganglion cell viability in optic neuropathies. *Mitochondrion* 36, 186–192. doi: 10.1016/j.mito.2017.08.014

Izzotti, A., Saccà, S. C., Cartiglia, C., and De Flora, S. (2003). Oxidative deoxyribonucleic acid damage in the eyes of glaucoma patients. *Am. J. Med.* 114, 638–646. doi: 10.1016/S0002-9343(03)00114-1

Kawasaki, A., Otori, Y., and Barnstable, C. J. (2000). Müller cell protection of rat retinal ganglion cells from glutamate and nitric oxide neurotoxicity. *Invest. Ophthalmol. Vis. Sci.* 41, 3444–3450.

Klingenberg, M., and Rottenberg, H. (1977). Relation between the gradient of the ATP/ADP ratio and the membrane potential across the mitochondrial membrane. *Eur. J. Biochem.* 73, 125–130. doi: 10.1111/j.1432-1033.1977.tb11298.x

Korshunov, S. S., Skulachev, V. P., and Starkov, A. A. (1997). High protonic potential actuates a mechanism of production of reactive oxygen species in mitochondria. *FEBS Lett.* 416, 15–18. doi: 10.1016/S0014-5793(97)01159-9

Lapp, D. W., Zhang, S. S., and Barnstable, C. J. (2014). Stat3 mediates LIF-induced protection of astrocytes against toxic ROS by upregulating the UPC2 mRNA pool. *Glia* 62, 159–170. doi: 10.1002/glia.22594

Leske, M. C., Heijl, A., Hyman, L., Bengtsson, B., and Komaroff, E. (2004). Factors for progression and glaucoma treatment: the early manifest glaucoma trial. *Curr. Opin. Ophthalmol.* 15, 102–106. doi: 10.1097/00055735-200404000-00008

Malone, P. E., and Hernandez, M. R. (2007). 4-Hydroxynonenal, a product of oxidative stress, leads to an antioxidant response in optic nerve head astrocytes. *Exp. Eye Res.* 84, 444–454. doi: 10.1016/j.exer.2006.10.020

Mattiasson, G., Shamloo, M., Gido, G., Mathi, K., Tomasevic, G., Yi, S., et al. (2003). Uncoupling protein-2 prevents neuronal death and diminishes brain dysfunction after stroke and brain trauma. *Nat. Med.* 9, 1062–1068. doi: 10.1038/nm903

Medvedev, A. V., Snedden, S. K., Raimbault, S., Ricquier, D., and Collins, S. (2001). Transcriptional regulation of the mouse uncoupling protein-2 gene. Double E-box motif is required for peroxisome proliferator-activated receptor-gamma-dependent activation. *J. Biol. Chem.* 276, 10817–10823. doi: 10.1074/jbc.M010587200

Miwa, S., St-Pierre, J., Partridge, L., and Brand, M. D. (2003). Superoxide and hydrogen peroxide production by Drosophila mitochondria. *Free Radic. Biol. Med.* 35, 938–948. doi: 10.1016/S0891-5849(03)00464-7

Munemasa, Y., Ahn, J. H., Kwong, J. M., Caprioli, J., and Piri, N. (2009). Redox proteins thioredoxin 1 and thioredoxin 2 support retinal ganglion cell survival in experimental glaucoma. *Gene Ther.* 16, 17–25. doi: 10.1038/gt.2008.126

Nègre-Salvayre, A., Hirtz, C., Carrera, G., Cazenave, R., Troly, M., Salvayre, R., et al. (1997). A role for uncoupling protein-2 as a regulator of mitochondrial hydrogen peroxide generation. *FASEB J.* 11, 809–815. doi: 10.1096/fasebj.11.10.9271366

Pinzon-Guzman, C., Zhang, S. S., and Barnstable, C. J. (2011). Specific protein kinase C isoforms are required for rod photoreceptor differentiation. *J. Neurosci.* 31, 18606–18617. doi: 10.1523/JNEUROSCI.2578-11.2011

Piotrowska-Nowak, A., Kosior-Jarecka, E., Schab, A., Wrobel-Dudzinska, D., Bartnik, E., Zarnowski, T., et al. (2018). Investigation of whole mitochondrial genome variation in normal tension glaucoma. *Exp. Eye Res.* 178, 186–197. doi: 10.1016/j.exer.2018.10.004

Quigley, H. A. (2011). Glaucoma. *Lancet* 377, 1367–1377. doi: 10.1016/S0140-6736(10)61423-7

Quinlan, C. L., Gerencser, A. A., Treberg, J. R., and Brand, M. D. (2011). The mechanism of superoxide production by the antimycin-inhibited mitochondrial Q-cycle. *J. Biol. Chem.* 286, 31361–31372. doi: 10.1074/jbc.M111.267898

Ramdas, W. D., Schouten, J. S. A. G., and Webers, C. A. B. (2018). The effect of vitamins on glaucoma: a systematic review and meta-analysis. *Nutrients* 10:E359. doi: 10.3390/nu10030359

Resnikoff, S., and Keys, T. U. (2012). Future trends in global blindness. *Indian J. Ophthalmol.* 60, 387–395. doi: 10.4103/0301-4738.100532

Rodriguez, A. R., de Sevilla Müller, L. P., and Brecha, N. C. (2014). The RNA binding protein RBPMS is a selective marker of ganglion cells in the mammalian retina. *J. Comp. Neurol.* 522, 1411–1443. doi: 10.1002/cne.23521

Rupprecht, A., Bräuer, A. U., Smorodchenko, A., Goyn, J., Hilse, K. E., Shabalina, I. G., et al. (2012). Quantification of uncoupling protein 2 reveals its main expression in immune cells and selective up-regulation during T-cell proliferation. *PLoS One* 7:e41406. doi: 10.1371/journal.pone.0041406

Saccà, S. C., and Izzotti, A. (2008). Oxidative stress and glaucoma: injury in the anterior segment of the eye. *Prog. Brain Res.* 173, 385–407. doi: 10.1016/S0079-6123(08)01127-8

Sarafian, T. A., Montes, C., Imura, T., Qi, J., Coppola, G., Geschwind, D. H., et al. (2010). Disruption of astrocyte STAT3 signaling decreases mitochondrial function and increases oxidative stress in vitro. *PLoS One* 5:e9532. doi: 10.1371/journal.pone.0009532

St-Pierre, J., Buckingham, J. A., Roebuck, S. J., and Brand, M. D. (2002). Topology of superoxide production from different sites in the mitochondrial electron transport chain. *J. Biol. Chem.* 277, 44784–44790. doi: 10.1074/jbc.M207217200

Takihara, Y., Inatani, M., Eto, K., Inoue, T., Kreymerman, A., Miyake, S., et al. (2015). In vivo imaging of axonal transport of mitochondria in the diseased and aged mammalian CNS. *Proc. Natl. Acad. Sci. U.S.A.* 112, 10515–10520. doi: 10.1073/pnas.1509879112

Tezel, G., Yang, X., and Cai, J. (2005). Proteomic identification of oxidatively modified retinal proteins in a chronic pressure-induced rat model of glaucoma. *Invest. Ophthalmol. Vis. Sci.* 46, 3177–3187. doi: 10.1167/iovs.05-0208

Toda, C., Kim, J. D., Impellizzeri, D., Cuzzocrea, S., Liu, Z. W., and Diano, S. (2016). UCP2 regulates mitochondrial fission and ventromedial nucleus control of glucose responsiveness. *Cell* 164, 872–883. doi: 10.1016/j.cell.2016.02.010

Van Bergen, N. J., Crowston, J. G., Craig, J. E., Burdon, K. P., Kearns, L. S., Sharma, S., et al. (2015). Measurement of systemic mitochondrial function in advanced primary open-angle glaucoma and leber hereditary optic neuropathy. *PLoS One* 10:e0140919. doi: 10.1371/journal.pone.0140919

Varela, H. J., and Hernandez, M. R. (1997). Astrocyte responses in human optic nerve head with primary open-angle glaucoma. *J. Glaucoma* 6, 303–313. doi: 10.1097/00061198-199710000-00007

Williams, P. A., Harder, J. M., Foxworth, N. E., Cochran, K. E., Philip, V. M., Porciatti, V., et al. (2017). Vitamin B3 modulates mitochondrial vulnerability and prevents glaucoma in aged mice. *Science* 355, 756–760. doi: 10.1126/science.aal0092

Woldemussie, E., Wijono, M., and Ruiz, G. (2004). Müller cell response to laser-induced increase in intraocular pressure in rats. *Glia* 47, 109–119. doi: 10.1002/glia.20000

Young, P., Qiu, L., Wang, D., Zhao, S., Gross, J., and Feng, G. (2008). Single-neuron labeling with inducible Cre-mediated knockout in transgenic mice. *Nat. Neurosci.* 11, 721–728. doi: 10.1038/nn.2118

Zhang, Y., Riesterer, C., Ayrall, A. M., Sablitzky, F., Littlewood, T. D., and Reth, M. (1996). Inducible site-directed recombination in mouse embryonic stem cells. *Nucleic Acids Res.* 24, 543–548. doi: 10.1093/nar/24.4.543

Zhang, Y. L., Wang, R. B., Li, W. Y., Xia, F. Z., and Liu, L. (2017). Pioglitazone ameliorates retinal ischemia/reperfusion injury. *Int. J. Ophthalmol.* 10, 1812–1818. doi: 10.18240/ijo.2017.12.04

Zhu, J., Zhang, J., Ji, M., Gu, H., Xu, Y., Chen, C., et al. (2013). The role of peroxisome proliferator-activated receptor and effects of its agonist, pioglitazone, on a rat model of optic nerve crush: PPARγ in retinal neuroprotection. *PLoS One* 8:e68935. doi: 10.1371/journal.pone.0068935

Conflict of Interest Statement: The authors declare that the research was conducted in the absence of any commercial or financial relationships that could be construed as a potential conflict of interest.

frontiers in Neuroscience

ORIGINAL RESEARCH
published: 15 March 2019
doi: 10.3389/fnins.2019.00219

The Susceptibility of Retinal Ganglion Cells to Glutamatergic Excitotoxicity Is Type-Specific

Ian Christensen[2†], Bo Lu[1,2†], Ning Yang[1,2], Kevin Huang[1,2], Ping Wang[1,2] and Ning Tian[1,2]*

[1] VA Salt Lake City Health Care System, Salt Lake City, UT, United States, [2] Department of Ophthalmology & Visual Sciences, University of Utah School of Medicine, Salt Lake City, UT, United States

Retinal ganglion cells (RGCs) are the only output neurons that conduct visual signals from the eyes to the brain. RGC degeneration occurs in many retinal diseases leading to blindness and increasing evidence suggests that RGCs are susceptible to various injuries in a type-specific manner. Glutamate excitotoxicity is the pathological process by which neurons are damaged and killed by excessive stimulation of glutamate receptors and it plays a central role in the death of neurons in many CNS and retinal diseases. The purpose of this study is to characterize the susceptibility of genetically identified RGC types to the excitotoxicity induced by *N*-methyl-D-aspartate (NMDA). We show that the susceptibility of different types of RGCs to NMDA excitotoxicity varies significantly, in which the αRGCs are the most resistant type of RGCs to NMDA excitotoxicity while the J-RGCs are the most sensitive cells to NMDA excitotoxicity. These results strongly suggest that the differences in the genetic background of RGC types might provide valuable insights for understanding the selective susceptibility of RGCs to pathological insults and the development of a strategy to protect RGCs from death in disease conditions. In addition, our results show that RGCs lose dendrites before death and the sequence of the morphological and molecular events during RGC death suggests that the initial insult of NMDA excitotoxicity might set off a cascade of events independent of the primary insults. However, the kinetics of dendritic retraction in RGCs does not directly correlate to the susceptibility of type-specific RGC death.

Keywords: glutamate excitotoxicity, retinal ganglion cell, susceptibility, cell type specific death, retinal diseases

OPEN ACCESS

Edited by:
Peter Koulen,
University of Missouri System,
United States

Reviewed by:
Serge Picaud,
INSERM U968 Institut de la Vision,
France
Colin Barnstable,
Pennsylvania State University,
United States

***Correspondence:**
Ning Tian
ning.tian@hsc.utah.edu

[†]These authors have contributed equally to this work

Specialty section:
This article was submitted to Neurodegeneration, a section of the journal Frontiers in Neuroscience

Received: *24 December 2018*
Accepted: *26 February 2019*
Published: *15 March 2019*

Citation:
Christensen I, Lu B, Yang N, Huang K, Wang P and Tian N (2019) The Susceptibility of Retinal Ganglion Cells to Glutamatergic Excitotoxicity Is Type-Specific. Front. Neurosci. 13:219. doi: 10.3389/fnins.2019.00219

INTRODUCTION

In mammals, retinal ganglion cells (RGCs) are the only output neurons that conduct visual signals from the eyes to the brain and they are classified into at least 40 types using a combination of morphological, functional and genetic features (Badea and Nathans, 2004; Völgyi et al., 2005; Kim et al., 2008; Briggman and Euler, 2011; Briggman et al., 2011; Kay et al., 2011; Sanes and Masland, 2015; Baden et al., 2016; Rheaume et al., 2018). RGC degeneration occurs in many retinal diseases leading to blindness. Increasing evidence suggests that RGCs are susceptible to various injuries in a type-specific manner. For instance, in experimental models of ocular hypertension, OFF RGCs exhibited higher rates of cell death compared to ON RGCs (Della Santina et al., 2013; El-Danaf and Huberman, 2015; Ou et al., 2016), and mono-laminated ON RGCs were found to be more susceptible to elevated IOP than bi-laminated ON-OFF cells (Feng et al., 2013). Similarly, in models

of optic nerve injury, OFF RGCs were found to be more susceptible than ON RGCs, and ON sustained RGCs seem to be more susceptible than ON transient RGCs (Puyang et al., 2017). In addition, αRGCs seem to be the least susceptible RGC type to optic nerve injury in one report (Duan et al., 2015) but more susceptible RGC type in another report (Daniel et al., 2018). Recent studies have suggested that different types of RGCs could have unique gene expression patterns (Siegert et al., 2009; Madisen et al., 2012; Sanes and Masland, 2015) and the same genes expressed by RGCs could protect some type of RGCs but facilitate the death of other types of RGCs (Norsworthy et al., 2017). Thus, an understanding of the type-specific vulnerability of RGCs based on their gene expression may provide insights into the molecular mechanisms of neurodegeneration and suggest novel treatment strategies.

Glutamate excitotoxicity is the pathological process by which neurons are damaged and killed by excessive stimulation of glutamate receptors, such as the *N*-methyl-D-aspartate (NMDA) receptor, and it plays a central role in the death of neurons in many CNS diseases (Camacho and Massieu, 2006; Hulsebosch et al., 2009). Excessive stimulation of NMDA receptors can cause excitotoxicity by allowing high levels of calcium ions (Ca^{2+}) to enter into cells (Manev et al., 1989). Ca^{2+} influx into cells activates a number of enzymes, including phospholipases, endonucleases, and proteases. These enzymes can damage cell structures such as the cytoskeleton, cell membrane, and DNA (Stavrovskaya and Kristal, 2005; Dutta and Trapp, 2011). In addition, a calcium influx through NMDA receptors can cause apoptosis through activation of a cAMP response element binding (CREB) protein shut-off (Hardingham et al., 2002). In the retina, NMDARs are expressed by all RGCs (Fletcher et al., 2000; Zhang and Diamond, 2009) and NMDA excitotoxicity is thought to cause RGC death in several retinal diseases (Kuehn et al., 2005; Kwon et al., 2009; Almasieh et al., 2012; Tezel, 2013; Evangelho et al., 2017). However, to what extent NMDA excitotoxicity causes the death of various types of RGCs has not been systematically investigated. Accordingly, we characterized the type-specific susceptibility of RGCs to NMDA excitotoxicity using several transgenic mouse lines, which express green/yellow fluorescent protein (GFP/YFP) in specific types of RGCs.

Our results show that the susceptibility of RGCs to NMDA excitotoxicity varies significantly among different types of RGCs. Among the RGCs studied, the J-RGCs have the highest susceptibility and the αRGCs have the lowest susceptibility. These results provide for the first time a direct comparison of the susceptibility of genetically identified types of RGCs to NMDA excitotoxicity.

MATERIALS AND METHODS

Animals

The transgenic mouse strains used in this study include B6.Cg-Tg(Thy1-YFP)HJrs/J (Thy1-YFP), Tg(Thy1-EGFP)MJrs/J (Thy1-GFP), B6.129(SJL)-Kcng4$^{tm1.1(cre)Jrs}$/J (Kcng4^{Cre}), FSTL4-CreER (BD-CreER), JamB-CreER, TYW3, Thy1-STOP-loxP-YFP (Thy1-Stop-YFP). The Thy1-YFP, Thy1-GFP, and Kcng4^{Cre} mice were obtained from The Jackson Laboratory (Bar Harbor, ME, United States) (Duan et al., 2015). BD-CreER, JamB-CreER, TYW3, and Thy1-Stop-YFP mice were obtained from Dr. Joshua Sanes' laboratory at Harvard University (Kim et al., 2008, 2010). All transgenic mice used in this study were on C57BL/6 background and were backcrossed with C57BL/6J mice for 4–5 generations in our lab. Then the BD-CreER, JamB-CreER and Kcng4^{Cre} mice were bred into the Thy1-Stop-YFP mice to generate BD-CreER:Thy1-Stop-YFP (BD:YFP), JamB-CreER:Thy1-Stop-YFP (JamB:YFP) and Kcng4^{Cre}:Thy1-Stop-YFP (Kcng4^{Cre}:YFP) double transgenic mice. YFP was expressed specifically in αRGCs without any additional treatment whereas YFP was only expressed specifically in BD-RGCs or J-RGCs upon intraperitoneal (IP) injection of Tamoxifen (150 μg) at the ages of P5-15. All of these mice were viable and no significant defects in general development or overall formation of eye or retina were noticed. All animal procedures used in this study and care were preformed following protocols approved by the IACUC of the University of Utah and the IACUC of VA Salt Lake City Health Care System in compliance with PHS guidelines and with those prescribed by the Association for Research in Vision and Ophthalmology (ARVO).

Intraocular Injection of NMDA

The glutamate receptor agonist, NMDA, was injected intraocularly into the mice to induce *in vivo* glutamate excitotoxicity. The procedure of intraocular injection has been described previously (Xu et al., 2010). The actual dosage of the injected NMDA varied in concentration from 0.375 to 6.25 mmol/L but with a constant volume of 2 μl solution, which equivalent to 0.75–12.5 nmol of NMDA molecules. These amounts of NMDA injected into each eye are similar to those used in previous studies (Bai et al., 2013; Kimura et al., 2015; Jiang et al., 2016; Zhao et al., 2016; Ishimaru et al., 2017; Wang et al., 2018). The distribution of the solution inside the eyes was confirmed by co-injecting NMDA with Alexa Fluor^{TM} 555 conjugated Cholera Toxin Subunit B (CTB, 0.2%, Thermo Fisher Scientific, Eugene, OR, United States) and the retinas were examined by imaging the distribution of the fluorescent signaling (data not shown). To reduce the impact of the variation of YFP expression in some of the transgenic mouse lines, we injected 2 μl NMDA solution into one eye (left) and used the non-injected contralateral eyes (right) as controls to calibrate the cellular survival rate of each mouse. In preparation for intraocular injection, the mice were anesthetized with Isoflurane (1–5% Isoflurane mixed with room air delivered in a rate between 0.8 and 0.9 L/min) through a mouse gas anesthesia head holder (David KOPF Instruments, Tujunga, CA, United States) and local application of 0.5% proparacaine hydrochloride ophthalmic solution on each eye. Glass micropipettes made from borosilicate glass using a Brown-Flaming horizontal puller with fine tip (about 10–15 μM diameter) were used for injection. The glass needle was mounted on a Nano-injection system (Nanoject II, Drummond Scientific Company, Broomall, PA, United States), which could precisely control the amount of injected solution at the nl level. The glass needle was aimed to penetrate the eyeball near its equator under a dissection microscope and a total of 2 μl

solution was slowly injected into each eye. After the injection, the eyes were covered with 0.5% erythromycin ophthalmic ointment and the mice were placed in a clean cage siting on a water blanket. The temperature of the water blanket was set at 33°C. Mice in this cage were continuously monitored until they completely recovered and then they were returned to their original cages. The procedures for anesthesia and intraocular injection fit the procedures approved by the IACUC of the University of Utah and the IACUC of VA Salt Lake City Health Care System.

Primary Antibodies

Rabbit polyclonal antibody against green fluorescent protein (GFP) conjugated with AlexaFluor 488 was purchased from Molecular Probes (Eugene, OR, United States; Catalog No. A21311). This antibody was raised against GFP isolated directly from *Aequorea victoria* and has been previously characterized by immunocytochemistry in granule cells (Overstreet-Wadiche et al., 2006), olfactory sensory neurons (Lèvai and Strotmann, 2003), and hippocampal neurons that express GFP (Huang et al., 2005). Anti-active Caspase-3 antibody (anti-CASP3) was purchased from Abcam (Cambridge, MA, United States; Catalog No. ab2302). This polyclonal antibody was raised in rabbits against synthetic peptide corresponding to the N-terminus adjacent to the cleavage site of human active caspase-3 preferentially recognizes the p17 fragment of the active Caspase-3 and has been characterized by immunocytochemistry and Western blotting. Anti-RBPMS (RNA binding protein with multiple splicing) antibody was purchased from PhosphoSolutions (Aurora, CO, United States; Catalog #: 1832-RBPMS). This polyclonal antibody was raised in guinea pigs against synthetic peptide corresponding to amino acid residues from the N-terminal region of the rat RBPMS sequence conjugated to KLH. This antibody has been characterized by Western blotting and verified with immunocytochemistry on mammalian retinas (Kwong et al., 2010; Rodriguez et al., 2014). The secondary antibodies were purchased from Jackson Immune Research Laboratories (West Grove, PA, United States).

Preparation of Retinal Whole-Mounts for Antibody Staining

Retinal ganglion cells were imaged on whole mount retinal preparation for cell counting and dendritic morphology. The procedures for fluorescent immuno-labeling of YFP-expressing retinal neurons on retinal whole-mounts and slide preparations have been described previously in detail (Xu et al., 2010). In brief, mice were euthanized with 100% CO2 followed by cervical dislocation. Retinas were isolated and fixed in 4% paraformaldehyde (PFA) in 0.01M phosphate-buffered saline (PBS; pH 7.4) for 30 min at room temperature. Fixed retinas were washed 10 min × 3 in 0.01M PBS and incubated in blocking solution (10% normal donkey serum) at 4°C for 2 h. Next, retinas were incubated in a rabbit polyclonal anti-GFP antibody conjugated with Alexa Fluor488 (1:500) for 7 days at 4°C.

In one experiment, the total RGCs were labeled by a guinea pig polyclonal anti-RBPMS antibody (1:500) and the YFP-expressing RGCs were labeled by a rabbit anti-GFP antibody conjugated with AlexaFluor 488. A Cyanine Cy^{TM} 3-conjugated donkey anti-guinea pig (1:400, Jackson ImmunoResearch, West Grove, PA, United States) secondary antibody was used overnight at 4°C to reveal anti-RBPMS antibody staining. In another experiment, a rabbit polyclonal anti-Caspase 3 antibody (1:150) was used to label YFP/GFP expressing RGCs actively undergoing apoptosis. An Alexa 647-conjugated donkey anti-rabbit (1:300, Jackson ImmunoResearch, West Grove, PA, United States) secondary antibody was used overnight at 4°C to reveal anti-Caspase 3 antibody staining. In this experiment, YFP/GFP signals in RGCs were not enhanced by anti-GFP antibody but the YFP/GFP expressing RGCs were still identifiable with confocal imaging. After the antibody incubation, the retinas were washed 3 × 10 min, and flat mounted on Super-Frost slides (Fisher Scientific, Pittsburgh, PA, United States) with Vectashield mounting medium for fluorescence (Vector Laboratories, Burlingame, CA, United States).

Confocal Laser Scanning Microscopy and Image Sampling

Fluorescent images of fixed retinal tissue were collected with a dual-channel Zeiss confocal microscope (Carl Zeiss AG, Germany) with the C-Apochromat 40× 1.2WKorr water immersion lens. Image stacks of YFP expressing RGCs in whole-mount retinas were collected at intervals of 0.5 μm. Imaris software (Bitplane, Inc., Concord, MA, United States) was used to align multi-stacks of images together, quantify the number and dendritic structure of RGCs, and adjust the intensity and contrast of images.

For image sampling, we use two different strategies for retinas with low or high densities of YFP-expressing RGCs to avoid potential bias of data sampling when the persons carrying out the histological analysis were not blinded to the treatment. For Thy1-YFP, BD:YFP and JamB:YFP mice, the YFP is expressed in a relatively low density of RGCs and the expression level varies significantly among mice (from several to several hundreds of YFP-expressing RGCs per retina) but not significantly between left and right eyes (see results in **Figures 1B**, **3B**). Therefore, we imaged the whole retina and counted every YFP-expression RGCs in the GCL layer of these mice. The only case to exclude a mouse from data analysis is when the total number of YFP-expressing RGCs in the whole retina of the control eye is less than 10 to avoid the results to be skewed by mice with extreme low number of YFP-expressing RGCs. For TYW3 and Kcng4^{Cre}:YFP mice, which constitutively express YFP in all W3-RGCs and αRGCs, the density of YFP+ RGCs is very high (several thousands per retina) and the expression level does not very significantly among mice or between left and right eyes (see results in **Figures 3F**, **4A**). We included every mouse assigned to this study for data analysis without exclusion. For image sampling, we scanned 4 squares (304 μm × 304 μm each) at 4 quarters of the retina 600 μm away from the center of optic nerve head (see **Figure 3E** for details). The density of YFP-expressing W3-RGCs and αRGCs of each retina was averaged from the 4 squares.

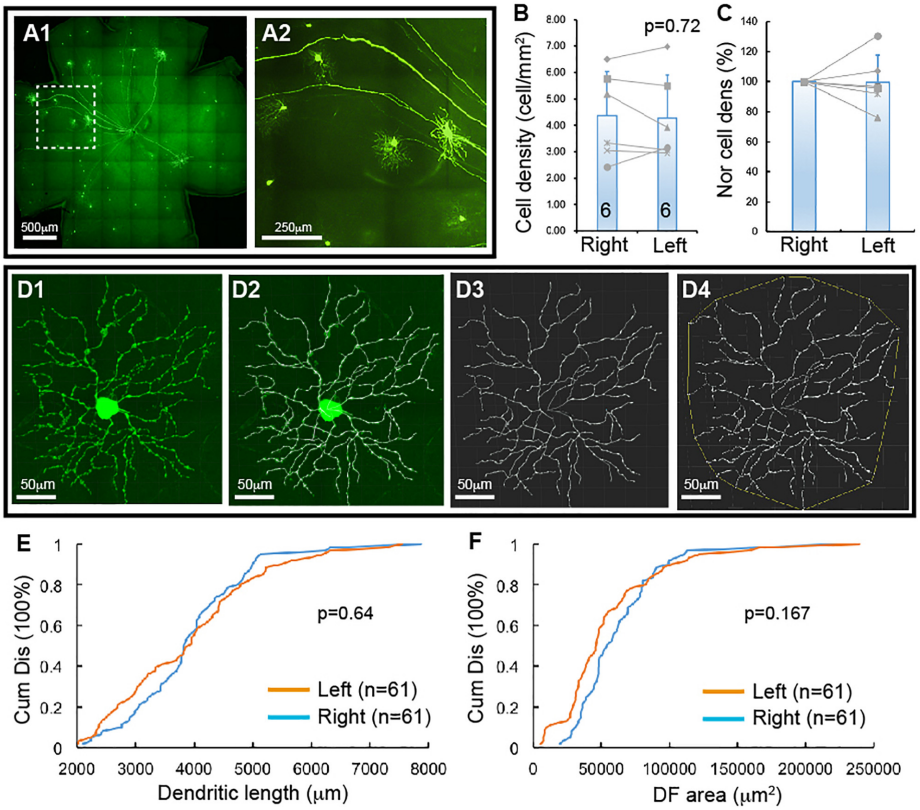

FIGURE 1 | YFP-expressing RGCs of Thy1-YFP mice. The density and dendritic structure of YFP-expressing RGCs of Thy1-YFP mice were quantified and compared between left and right eyes. **(A)** Representative retina image of a Thy1-YFP mouse **(A1)** and a magnified view of the area in the dash-line box of **(A1)** to show the morphology of YFP-positive RGCs **(A2)**. **(B)** Comparison of the average densities of YFP-expressing RGCs of left and right eyes of the same mice [paired *t*-test, $p = 0.72$, number of mice for each group (n) = 6]. The gray lines indicate six pairs of RGC density of left and right eyes. **(C)** Normalized RGC density of the same six mice shown in **(B)**. The RGC density of the left eye of each mouse is normalized to the right eye of the same mouse and the RGC density of right eyes is "self-normalized." The gray lines indicate six pairs of normalized RGC densities. **(D)** A representative image of a YFP-expressing RGC **(D1)**, the overlay of the dendrites and the tracing results **(D2)**, the tracing result **(D3)**, and the measurement of the dendritic field (DF) **(D4)**. **(E)** Paired comparison (K–S test, $p = 0.64$) of the cumulative distribution of the dendritic length of YFP-expressing RGCs of left and right eyes of the same six mice shown in **(B)**. **(F)** Paired comparison (K–S test, $p = 0.167$) of the cumulative distribution of the size of DF of YFP-expressing RGCs of the left and right eyes of the same six mice. n, the number of cells for each group in **(E,F)**.

Preparation of Retinal Whole-Mounts for *ex vivo* Fluorescent Imaging

The time-lapse images of RGCs were taken from whole-mount retina preparations as previously described (Xu et al., 2010). Retinas of Thy1-YFP mice, BD:YFP mice and JamB:YFP mice were used for *ex vivo* imaging of αRGCs, BD-RGCs and J-RGCs, respectively. Retinas were isolated from Thy1-YFP, BD:YFP and JamB:YFP mice in oxygenated extracellular solution that contained (in mmol/L) NaCl 124, KCl 2.5, CaCl2 2, MgCl2 2, NaH2PO4, 1.25, NaHCO3 26, and glucose 22 (pH 7.35 with 95% O2 and 5% CO2), mounted on nitrocellulose filter paper (Millipore Corp), placed in a recording chamber and continuously perfused at 32°C. Image stacks were taken using a two-photon image system (Prairie Technologies, Inc., Middleton, WI, United States) immediately before bath application of NMDA. After 10 min of bath application of 200 nmol/L NMDA, the retinas were continuously perfused with the oxygenated extracellular solution and the cells were imaged every 1 h for 7 h. The dendritic density of imaged cells is measured using a Sholl analysis (Xu et al., 2010) and the dendritic density after NMDA application was normalized to pre-NMDA application (0 h).

Statistical Analysis

Data are all presented as mean ± SE in the text and figures. Student *t*-tests are used to examine the difference between two means, K–S test is used to examine the difference between two cumulative distributions.

RESULTS

RGCs Lose Dendrites Before They Die Due to NMDA Excitotoxicity

Thy1-YFP mice have been used extensively for studying RGC morphology, physiology, development and degeneration. One potential advantage is that YFP is expressed in about 12

morphological types of RGCs in this mouse (Xu et al., 2010). To determine whether this mouse could serve as a model to study type specific RGC death in retinal diseases, we quantified the number and dendritic structure of YFP-expressing RGCs with the approach we previously used in our study (Xu et al., 2010). **Figure 1A** shows a representative image of a flat-mount retina of a Thy1-YFP mouse and a magnified area of the retina. The number and dendritic structure of the YFP-expressing RGCs are readily quantifiable using confocal imaging. **Figure 1B** shows the densities of YFP-expressing RGCs of left and right eyes of 6 Thy1-YFP mice. Although a paired t-test showed that the difference between the densities of YFP-expressing RGCs of left and right eyes is statistically insignificant (paired *t*-test, $p = 0.72$), it seems that the density of YFP-expressing RGCs varies significantly among these mice. To determine the variation of the densities of YFP-expressing RGCs of the left and right eyes of the same mouse, we normalized the density of YFP-expressing RGCs of the left eye to that of the right eye of the same mouse. **Figure 1C** shows the normalized densities of YFP-expressing RGCs of left and right eyes of 6 Thy1-YFP mice. We then quantified the dendritic length and the size of dendritic field (DF) of YFP-expressing RGCs (**Figure 1D**) and found that the distributions of dendritic length and the size of DF of left and right eyes are not statistically different (**Figures 1E,F**, K–S tests, $p = 0.64$ and 0.167, respectively). Therefore, the number and dendritic properties of YFP-expressing RGCs of the left and right eyes are comparable.

Next, we tested whether the Thy1-YFP mice could be used to determine type-specific RGC death under disease conditions. Accordingly, we injected NMDA solution into the left eyes of Thy1-YFP mice and use the non-injected right eyes as controls, quantified the number of YFP-expressing RGCs and their dendritic properties, and compared the results of NMDA treated left eyes to that of non-injected right eyes. **Figure 2A** shows representative images of Thy1-YFP retinas without NMDA injection while **Figure 2B** shows a retina 1 day after NMDA injection. It is evident that many YFP-expressing RGCs died 1 day after NMDA injection and that a significant number of the surviving YFP-expressing RGCs lost dendrites (**Figures 2B2,H3**). Quantitatively, the densities of YFP-expressing RGCs are reduced to 48.1 ± 3.4% (paired *t*-text, $p < 0.001$) and 31.6 ± 2.1% (paired *t*-text, $p < 0.0001$) in retinas with intraocular injection of 2 μL 3.125 mmol/L (6.25 nmol) or 6.25 mmol/L (12.5 nmol) NMDA as compared to the non-injected right eyes (**Figures 2C1,C2**), respectively. More than 60% of the surviving YFP-expressing RGCs completely lost their dendrites with intraocular injection of 2 μL 6.25 mmol/L (12.5 nmol) NMDA (**Figures 2D,E**, K–S test, $p < 0.0001$). In addition, among the surviving YFP-expressing RGCs with dendrites, the total dendritic length and the size of DF are significantly reduced (**Figures 2F,G**, K–S test, $p < 0.0001$ or = 0.008, respectively). These results demonstrate that RGCs lose dendrites before death, which is consistent with previous reports that RGCs significantly lose or re-organize their dendrites under various disease conditions (Kuehn et al., 2005), such as glaucoma (Weber et al., 1998; Shou et al., 2003; Morgan et al., 2006; Williams et al., 2013) and optic nerve crush (ONC) (Leung et al., 2008; Weber et al., 2008).

To further test this idea, we injected NMDA into eyes of Thy1-GFP mice, in which most, if not all, RGCs are GFP-expressing, and labeled NMDA-treated retinas using an anti-CASP3 antibody to identify cells undergoing apoptosis (Pi et al., 2018). The results show that some GFP-positive cells are also CASP3-positive 3 h after NMDA injection (**Figure 2H**), indicating that RGCs actively undergoing apoptosis are still GFP positive, while no CASP3-positive RGCs are found in non-injected eyes (data not shown). We also labeled NMDA-treated retinas of Thy1-YFP mice, in which only a small fraction of RGCs are YFP-expressing, with the anti-CASP3 antibody and found that many YFP-expressing RGCs with no dendrites are still CASP3-negative (**Figure 2H3**). These results further demonstrate that the damaged RGCs lose all dendrites before the beginning of apoptosis. Because the YFP expressed by RGCs are cytosol protein and can fill the fine remnants of dendrites of the injured RGCs (**Figure 2H3**, white arrow in the insert) as well as soma and axon, the changes in YFP-positive dendrites are likely to reflect the changes of dendritic morphology of the RGCs but not the expression level of YFP in responding to NMDA excitotoxicity. Since RGCs lose dendrites prior to death, the Thy1-YFP mice appear to be an unreliable model for studying type-specific RGC death based on dendritic morphology.

Furthermore, to determine whether the death of YFP-expressing RGCs of Thy1-YFP mice could represent the death of total RGCs induced by NMDA excitotoxicity, we compared the survival rate of YFP-expressing RGCs and total RGCs labeled by anti-RBPMS antibody (**Figures 2I1,I2**) of Thy1-YFP mice treated by intraocular injection of 2 μl 3.125 mmol/L (6.25 nmol) NMDA into the left eyes with non-injected right eyes. Our results show that the survival rate of YFP-expressing RGCs (50%) is significantly higher than that of anti-RBPMS antibody labeled RGCs (34.2%) (**Figure 2I3**, paired *t*-test, $p = 0.002$), which is within the range of the results of several previous studies (Bai et al., 2013; Kimura et al., 2015; Jiang et al., 2016; Zhao et al., 2016; Ishimaru et al., 2017; Wang et al., 2018). These results suggest that the susceptibility of YFP-expressing RGCs in this mouse line is lower than the susceptibility of total RGCs. Therefore, Thy1-YFP mice seem to be an unreliable model for studying overall RGC death. Accordingly, we further employed four RGC type-specific transgenic mouse lines to study type-specific RGC death due to NMDA excitotoxicity.

The Dose-Response Relationship of NMDA Excitotoxicity Induced RGC Death

We first quantified cell death as a function of NMDA concentrations using two transgenic mouse lines, in which YFP is expressed by the BD-RGCs or W3-RGCs (Kim et al., 2010). BD:YFP mice express YFP in BD-RGCs and a small fraction of amacrine cells located in INL (Kim et al., 2010) but not displaced amacrine cells in the ganglion cell layer (GCL) (data not shown). In this study, we only included the YFP-expressing cells in the GCL. **Figure 3A** shows a representative image of a BD:YFP retina (A1) and a magnified area to show the dendritic morphology of the BD-RGCs (A2). Similar to Thy1-YFP mice, the density of YFP-expressing BD-RGCs varies significantly among mice.

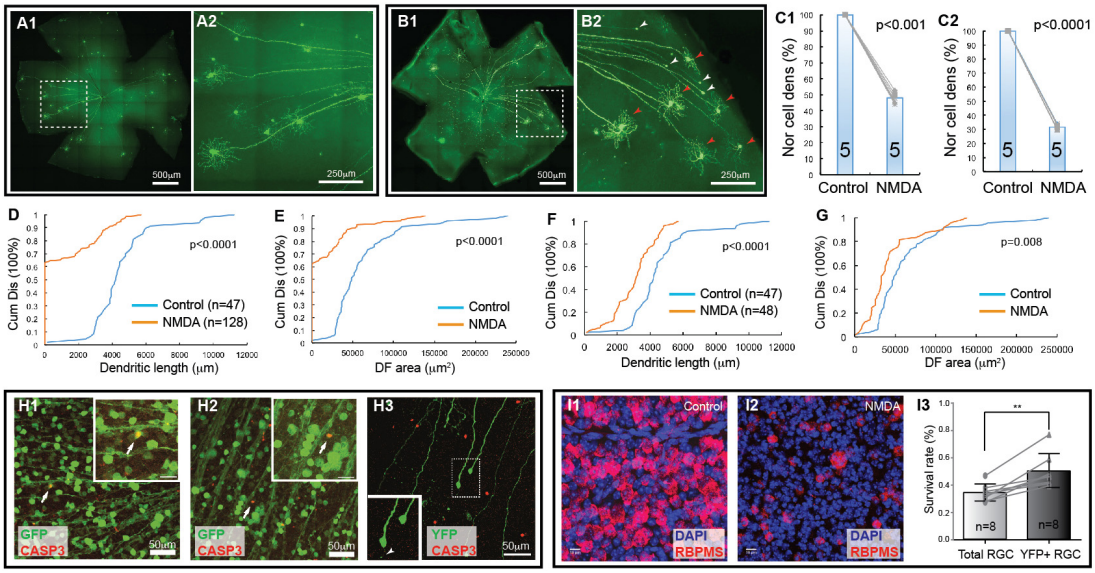

FIGURE 2 | Retinal ganglion cell death in NMDA excitotoxicity of mice. The density and dendritic structure of YFP-expressing RGCs of Thy1-YFP mice with and without NMDA injections were quantified and compared. **(A)** Representative image of a flat mount retina of a Thy1-YFP mouse without NMDA injections **(A1)** and a magnified view of the area in the dash-line box of panel A1 to show the morphology of YFP-positive RGCs **(A2)**. Red arrowheads indicate survival RGCs and white arrowheads indicate remaining axonal segment of RGCs without soma and dendrites. **(B)** Representative image of a flat mount retina of a Thy1-YFP mouse with NMDA injections **(B1)** and a magnified view of the area in the dash-line box of **(B1)** to show death of YFP-positive RGCs **(B2)**. Red arrowheads indicate survival RGCs and white arrowheads indicate remaining axonal segment of RGCs without soma and dendrites. **(C)** Comparison of the normalized density of YFP-expressing RGCs that survived 24 h after 2 μl of 3.125 mmol/L (6.25 nmol, **C1**, paired *t*-test, $p < 0.001$) or 6.25 mmol/L (12.5 nmol, **C2**, paired *t*-test, $p < 0.0001$) NMDA injection to the contralateral control eyes. The numbers in the columns indicate the number of eyes tested. The cell density of the left eye of each mouse is normalized to the right eye of the same mouse. The gray lines indicate six pairs of normalized RGC densities. **(D)** Comparison of the cumulative distributions of the dendritic length of all YFP-expressing RGCs (with and without identifiable dendrites) that survived 24 h after 6.25 mmol/L (12.5 nmol) NMDA injection (left eyes) with the non-injected right eyes of the same mice (5 mice; *n* = number of RGCs for each group) (K–S test, $p < 0.0001$). Because the non-injected eyes have higher density of YFP-expressing RGCs with intact dendritic tree and they overlap more frequently, the number of RGCs can be traced are fewer than that NMDA injected eyes. **(E)** Comparison of the cumulative distributions of the size of the DF of the same two groups of YFP-expressing RGCs as shown in **(D)** (K–S test, $p < 0.0001$). **(F)** Comparison of the cumulative distributions of the dendritic length of the YFP-expressing RGCs with identifiable dendrites after 6.25 mmol/L (12.5 nmol) NMDA injection with the non-injected right eyes of the same mice (the same 5 mice as for data presented in **(D)**; *n* = number of RGCs for each group, K–S test, $p < 0.0001$). **(G)** Comparison of the cumulative distributions of the size of the DF of the same two groups of YFP-expressing RGCs as shown in **(F)** (K–S test, $p = 0.008$). **(H) (H1,H2)** show magnified views of the retinas of Thy1-GFP mice, in which most RGCs are GFP-expressing, treated with NMDA *in vivo* for 3 **(H1)** and 6 **(H2)** hours. The retinas are labeled with anti-GFP (green) and anti-CASP3 (red) antibodies showing some GFP-positive cells are also CASP3-positive. H3 shows a magnified view of the retina of a Thy1-YFP mouse, in which only a small fraction of RGCs are YFP-expressing, treated with NMDA *in vivo* for 6 h and labeled with anti-GFP (green) and anti-CASP3 (red) antibodies. Many YFP-expressing RGCs with no dendrites are still CASP3-negative. Inserts show the enlargement of the cells indicated by the arrows/dash-line box. Insert of **H3** shows two RGCs and one of them completely lost all dendrites but another one has one short dendritic branch remaining (white arrowhead). **(I)** Magnified views of flat mount retinas of Thy1-YFP mice with **(I2)** and without **(I1)** 3.125 mmol/L (6.25 nmol) NMDA injection. The total RGCs were labeled by anti-RBPMS antibody and compared with YFP-expressing RGCs in the same retina (YFP labeling images not shown). Survival rates of total RGCs and YFP-expressing RGCs 24 h after NMDA injection were derived by normalizing the total RGCs and YFP-expressing RGCs of NMDA injected left eyes to the non-injected right eyes of the same mice and compared using a paired *t*-test (**I3**, *n*, number of mice, $p = 0.002$). **indicate $0.05 > p > 0.001$.

However, the densities of YFP-expressing BD-RGCs of the left and right eyes of the same mice are very similar (**Figure 3B**). A paired *t*-test showed that the difference between the densities of YFP-expressing BD-RGCs of left and right eyes of BD:YFP mice is statistically insignificant. Therefore, we treated the left eye with NMDA and compared the cell density with the non-injected right eye of each mouse.

BD-RGCs seem to be very sensitive to NMDA excitotoxicity. **Figure 3C** shows a representative image of a BD:YFP retina 24 h after intraocular injection of 2 μL 0.75 mmol/L (1.5 nmol) NMDA. Clearly, some BD-RGCs completely lose their dendrites and somas but retain axonal remnants 24 h after NMDA injection (C2, white arrows) while a significant fraction of BD-RGCs still retain their dendrites (red arrows). We quantified the survival rates of BD-RGCs to four different NMDA concentrations and found that the density of BD-RGCs was reduced to 39.5 ± 4.3% at 2 μL 0.375 mmol/L (0.75 nmol) to 0% at 2 μL 6.25 mmol/L (12.5 nmol) as compared to the non-injected right eyes (**Figure 3D**). The differences between the RGC densities in all four NMDA treated groups and their respective non-injected controls are statistically significant (paired *t*-test).

Similarly, we quantified the densities of W3-RGCs treated with the same four NMDA concentrations and compared with their respective non-injected controls. In TYW3 mice, YFP is expressed in the W3-RGCs constitutively with a very high density and, therefore, the number of YFP-expressing W3-RGCs does not vary significantly among mice or between the left and right eyes (**Figures 3E,F**, paired *t*-test, $p = 0.466$). Because YFP is also

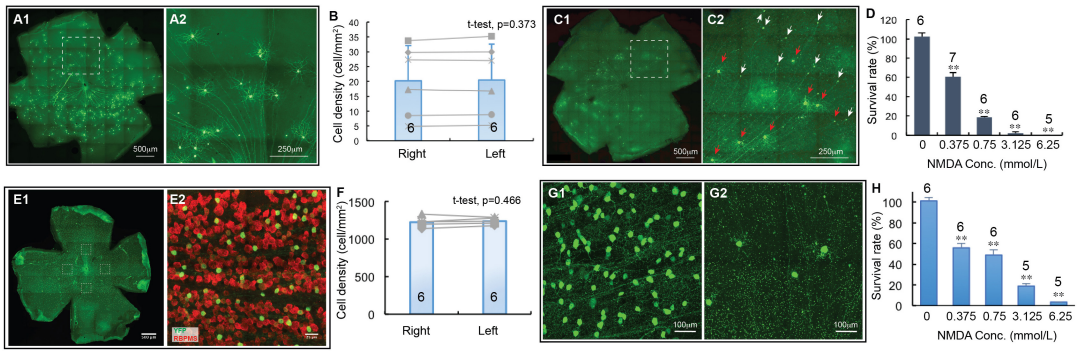

FIGURE 3 | The dose-response relationship of BD-RGCs and W3-RGCs to NMDA excitotoxicity. The density of YFP-expressing RGCs in BD:YFP and TYW3 mice with NMDA injection into left eyes at various concentrations were quantified, normalized to the non-injected right eyes and presented as a function of the concentrations of NMDA injected. **(A)** A representative image of a BD:YFP mouse retina without NMDA injection **(A1)** and a magnified view of the dash-line box of **(A1)** to show the morphology of BD-RGCs **(A2)**. **(B)** Comparison of the density of YFP-expressing BD-RGCs of untreated right and left eyes [number of mice (n) = 6, paired *t*-test, $p = 0.373$]. **(C)** A representative image of a BD:YFP mouse retina 24 h after 2 μl 0.75 mmol/L (1.5 nmol) NMDA injection **(C1)** and a magnified view of the dash-line box of **(C1)** to show the survival BD-RGCs with dendrites (red arrows) and axonal remnants of dead RGCs (white arrows) **(C2)**. **(D)** The survival rates of BD-RGCs treated with four different concentrations of NMDA. The survival rate of each NMDA treated left eye was normalized to the non-injected right eye of the same mouse. The average survival rate of eyes treated by each concentration of NMDA was compared to the untreated contralateral eyes of the same group of mice using paired *t*-test (*n*, number of mice). **(E)** A representative image of a flat-mount TYW3 mouse retina without NMDA injection (**E1**, only showing YFP staining but not anti-RBPMS staining). For RGC counting, we imaged 4 squares (304 μm × 304 μm each) at 4 quarters of the retina 600 μm away from the center of optic nerve head (dash-line boxes). **(E2)** Shows a magnified view of the dash-line box on the right side of **(E1)** to show the anti-RBPMS staining of all RGCs (red) and YFP-expressing W3 RGCs (green). **(F)** Comparison of the density of YFP-expressing W3-RGCs of untreated left and right eyes of TYW3 mice [number of mice (*n*) = 6, paired *t*-test, $p = 0.466$]. **(G)** Magnified views of TYW3 mouse retinas with **(G2)** and without **(G1)** 6.25 mmol/L (12.5 nmol) NMDA injection. **(H)** The survival rates of W3-RGCs treated with four different concentrations of NMDA. The survival rate of each NMDA treated left eye was normalized to the non-injected right eye of the same mouse. The number in each column of **(B,F)** and the number on top of each column of **(D,H)** indicate the number of eyes of each group. In **(D,H)**, **indicates $0.05 > p > 0.001$.

expressed in a very small fraction of amacrine cells located in the INL but not displaced amacrine cells in the GCL in these mice (data not shown), we only included the YFP-expressing cells in the GCL. W3-RGCs were also found to be very sensitive to NMDA excitotoxicity (**Figure 3G**). The density of W3-RGCs was reduced to 55.8 ± 4.3% at 0.375 mmol/L (0.75 nmol) and to 3.5 ± 0.1% at 6.25 mmol/L (12.5 nmol) NMDA in comparison to the non-injected right eyes (**Figure 3H**). The differences between the RGC densities in all four NMDA treated groups and their respective non-injected controls are statistically significant.

αRGCs Are Relatively Resistant to NMDA Excitotoxicity

αRGCs have been reported to be relatively resistant to ONC (Duan et al., 2015). We investigated whether they are also more resistant to NMDA excitotoxicity than BD-RGCs and W3-RGCs. Similar to TYW3 mice, the number of YFP-expressing αRGCs in Kcng4^{Cre}:YFP mice is highly consistency both between mice and between the left and right eyes (**Figure 4A**). In addition to αRGCs, YFP is also expressed in some bipolar cells in Kcng4^{Cre}:YFP mice (Duan et al., 2015). In our study, we only included the YFP-expressing cells in the GCL. Clearly, αRGCs seem to be more resistant to NMDA excitotoxicity than BD-RGCs and W3-RGCs. Many αRGCs were still visible from Kcng4^{Cre}:YFP retina 1 day after 2 μL 6.25 mmol/L (12.5 nmol) NMDA injection (**Figure 4B**). Quantitatively, intraocular injection of 2 μL 3.125 mmol/L (6.25 nmol) or 6.25 mmol/L (12.5 nmol) NMDA reduced the density of αRGCs to 47.4 ± 1.8% and 29.1 ± 3.9% of the non-injected right eyes, respectively (**Figures 4C,D**). The differences between the NMDA injected eyes and the non-injected eyes are statistically significant in both NMDA concentrations (paired *t*-test, $p < 0.001$).

J-RGCs Are Highly Sensitive to NMDA Excitotoxicity

Finally, we examined the susceptibility of J-RGC to NMDA excitotoxicity using JamB:YFP mice. JamB:YFP mice express YFP in two types of J-RGCs with distinctive dendritic morphology, one with an asymmetric DF and another with a more symmetric DF (Kim et al., 2008, 2010). In addition, YFP is also expressed in some amacrine cells located in the INL but not displaced amacrine cells in the GCL (data not shown). In this study, we only count the YFP-expressing cells in the GCL, which includes both types of J-RGCs, but not YFP-expressing cells in the INL. **Figure 4E** shows a representative image of a JamB:YFP retina (E1) and a magnified view to show the dendritic morphology of the two types J-RGCs. J-RGCs seem to be extremely sensitive to NMDA excitotoxicity. **Figure 4F** shows a representative image of a JamB:YFP retina 1 day after intraocular injection of 2 μL 0.75 mmol/L (1.5 nmol) NMDA. In this JamB:YFP retina, the vast majority of J-RGCs lost their dendrites and somas and only retained their axonal processes 1 day after NMDA injection (**Figure 4F2**, indicated by white arrows). Quantitatively, intraocular injection of 2 μL 0.75 mmol/L (1.5 nmol) or 3.125 mmol/L (6.25 nmol) NMDA reduced the densities of J-RGCs to 9.3 ± 0.7% and 2.1 ± 1.2% in comparison with

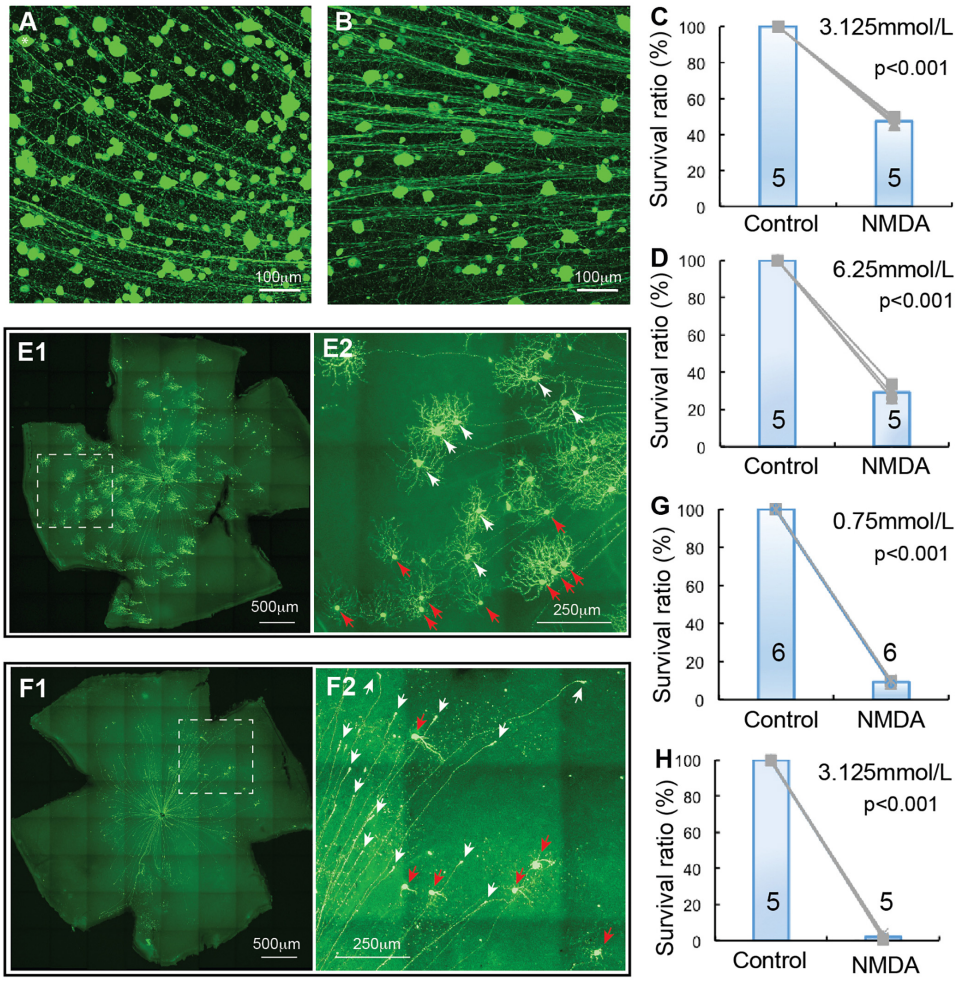

FIGURE 4 | αRGC and J-RGC death in NMDA excitotoxicity. The density YFP-expressing αRGCs and J-RGCs with NMDA injection into left eyes were quantified and normalized to that of non-injected right eyes. **(A)** A magnified view of a Kcng4^{Cre}:YFP mouse retina without NMDA injection to show YFP-expressing αRGCs. **(B)** A magnified view of a Kcng4^{Cre}:YFP mouse retina 24 h after 2 μl 6.25 mmol/L (12.5 nmol) NMDA injection to show the death of αRGCs. **(C)** The normalized survival rates of αRGCs treated with 2 μl 3.125 mmol/L (6.26 nmol) NMDA injection and control eyes. **(D)** The survival rates of αRGCs treated with 6.25 mmol/L (12.5 nmol) NMDA injection and control eyes. **(E)** A representative image of a flat-mount JamB:YFP mouse retina without NMDA injection **(E1)** and a magnified view of the dash-line box of **(E1)** to show the morphology of J-RGCs **(E2)**, in which the J-RGCs with a more symmetric DF are indicated by white arrow-heads and the J-RGCs with an asymmetric DF are indicated by red arrow-heads. **(F)** A representative image of a flat-mount retina of a JamB:YFP mouse 24 h after 0.75 mmol/L (1.5 nmol) NMDA injection **(F1)** and a magnified view of the dash-line box of panel F1 to show the death of J-RGCs **(F2)**, in which survival J-RGCs with dendrites are indicated by red arrows and axonal remnants of dead RGCs are indicated by white arrows. **(G)** The normalized survival rates of J-RGCs treated with 2 μl 0.75 mmol/L (1.5 nmol) NMDA injection and control eyes. **(H)** The survival rates of J-RGCs treated with 2 μl 3.125 mmol/L (6.25 nmol) NMDA injection and control eyes. The numbers in each column of **(C,D,G,H)** indicate the number of eyes of each group.

the non-injected right eyes, respectively (**Figures 4G,H**). The differences between the NMDA injected eyes and the non-injected eyes are highly significant with these two NMDA concentrations (paired *t*-test, $p < 0.001$).

The Susceptibility of RGCs to NMDA Excitotoxicity Is Type-Specific

Overall, we examined the susceptibility of four groups of RGCs to NMDA excitotoxicity and the results showed a clear type-specific pattern of RGC death. Of the tested four groups of RGCs, αRGCs seem to be the most resistant RGCs to NMDA excitotoxicity, while J-RGCs are the most sensitive cells to NMDA excitotoxicity (**Figures 5A,B**). The survival rates of these four groups of RGCs varied from 47.4 ± 1.8% (αRGCs) to 9.3 ± 0.7% (J-RGCs) in response to 2 μL 3.125 mmol/L (6.25 nmol) NMDA. When the results are compared to the collective responses of 12 morphological types of RGCs from the Thy1-YFP mice, the survival rate of αRGCs is very close to that of 12 morphological types of YFP-positive RGCs of Thy1-YFP mice (**Figure 5A**). Paired tests show that the differences in RGC survival rates between the four groups of NMDA treated RGCs to their non-injected contralateral eyes are statistically significant (paired *t*-tests).

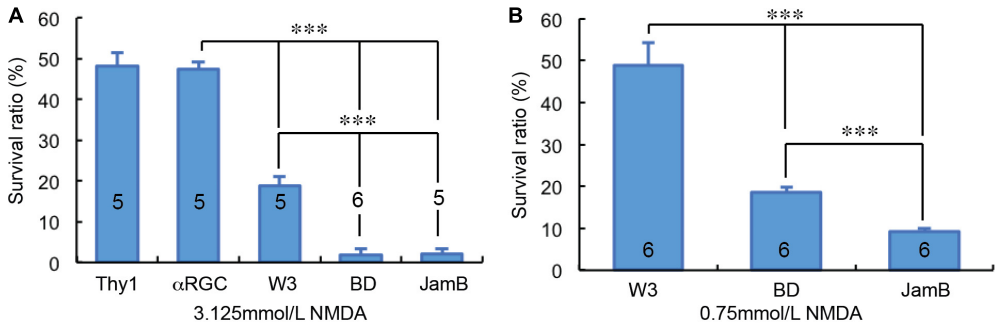

FIGURE 5 | RGC type-specific susceptibility to NMDA excitotoxicity. The survival rates of YFP-expressing RGCs in Thy1-YFP mice, Kcng4^{Cre}:YFP mice, TYW3 mice, BD:YFP and JamB:YFP mice 24 h after intraocular injection of 2 μl 3.125 mmol/L (6.25 nmol) NMDA **(A)** or 2 μl 0.75 mmol/L (1.5 nmol) NMDA **(B)** were compared to the contralateral control eyes. The number in each column indicates the number of eyes of the group. *** indicates $0.001 > p$.

The Kinetics of Dendritic Retraction of RGCs in NMDA Excitotoxicity

It has been postulated that RGCs lose synaptic connections and dendritic processes before death in glaucoma and ONC models (Weber et al., 1998; Shou et al., 2003; Kuehn et al., 2005; Morgan et al., 2006; Leung et al., 2008; Weber et al., 2008; Liu et al., 2011; Della Santina et al., 2013; Feng et al., 2013; Ou et al., 2016). To test whether the extent of RGC dendritic retraction is correlated to the death rate of RGCs in a type-specific manner, we examined the kinetics of dendritic retraction of αRGCs, BD-RGCs and J-RGCs in response to NMDA excitotoxicity using time lapse imaging on an *ex vivo* retinal preparation (Xu et al., 2010). αRGCs can be easily recognized based on their dendritic pattern in Thy1-YFP mice (Xu et al., 2010). BD-RGCs and J-RGCs are recognized in BD:YFP and JamB:YFP retinas based on their YFP signaling and dendritic pattern (**Figure 6A**). Our results showed that J-RGCs lost 67% of their dendrites 1 h after 200 nmol/L NMDA application and completely lost all dendrites 2 h after NMDA application for 10 min (**Figure 6B**). The αRGCs, on the other hand, only lost 38% of their dendrites 1 h after NMDA application for 10 min but still lost all dendrites 7 h after NMDA application. Most noticeably, BD-RGCs lost 36% of their dendrites 1 h after NMDA application for 10 min but still maintained 18% of their dendrites 7 h after NMDA application (**Figure 6B**). Taken together with the results shown in **Figure 5**, these results demonstrate that the kinetics of dendritic retraction of RGCs does not correlate to the susceptibility of RGC death due to NMDA excitotoxicity.

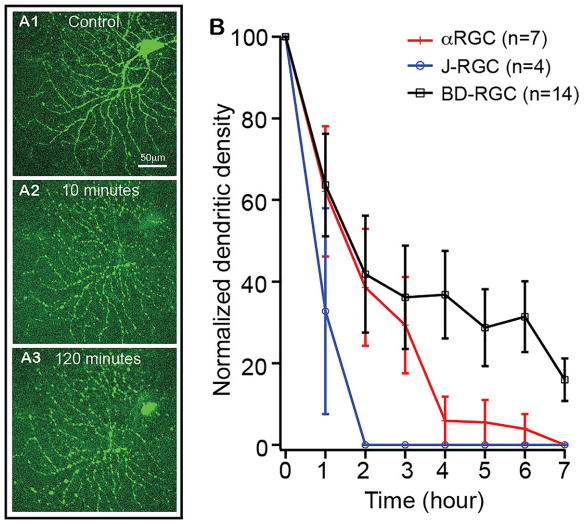

FIGURE 6 | The kinetics of dendritic retraction of RGCs induced by NMDA excitotoxicity. The kinetics of dendritic retraction of αRGCs in Thy1-YFP retinas, BD-RGCs in BD:YFP retinas, and J-RGCs in JamB:YFP retinas were quantified using time lapse imaging on an *ex vivo* retinal preparation. **(A)** Images of an αRGC of a Thy1-YFP retina before **(A1)**, 10 min **(A2)** and 120 min **(A3)** after 10 min of 200 nmol/L NMDA perfusion. **(B)** Average dendritic density of αRGCs, BD-RGCs and J-RGCs as a function of time after bath application of 10 min of 200 nmol/L NMDA. Dendritic density was measured using a Sholl analysis (Xu et al., 2010) and was normalized to pre-NMDA application (0 h). The numbers of "*n*" indicate the number of cells analyzed for each type of RGCs.

DISCUSSION

Our results show that the susceptibility of different types of genetically identified RGCs to NMDA excitotoxicity varies significantly. The αRGCs are the most resistant RGCs to NMDA excitotoxicity while the J-RGCs are the most sensitive RGCs to NMDA excitotoxicity. These results strongly suggest that the differences in the genetic background of RGC types might provide valuable insights for the understanding of the selective vulnerability of RGCs to pathological insults and could assist in the development of strategies for protecting RGCs under disease conditions. In addition, the sequence of the morphological and molecular events during RGC death suggests that the initial insult of NMDA excitotoxicity might set off a cascade of events that is subsequently independent of the primary insults.

Classification of RGC Types

Morphologically, RGCs are classified into about 20 types (Badea and Nathans, 2004; Völgyi et al., 2005; Kim et al., 2008;

Kay et al., 2011), which is closely correlated to the function of RGCs (Cleland et al., 1975). For instance, based on RGC dendritic ramification in the IPL, RGCs are functionally divided into ON, OFF and ON-OFF types. Recent advances in optical imaging methods have provided an efficient way to record RGC light responses for functional classification of RGCs (Briggman and Euler, 2011; Briggman et al., 2011; Baden et al., 2016). More recently, RGCs have been classified into at least 40 types by combining morphological, functional and genetic features (Sanes and Masland, 2015; Rheaume et al., 2018).

This study includes four groups of RGCs with unique structural, functional and genetic features. The BD-RGCs are a type of ON-OFF direction-selective RGCs (DS-RGCs). In mouse retinas, there are four types of ON-OFF DS-RGCs, tuned to motion in ventral, dorsal, nasal, and temporal. BD-RGCs are sensitive to ventral motion (Kim et al., 2010; Trenholm et al., 2011). W3-RGCs are the smallest in size and the most numerous RGCs (Kim et al., 2010). There are at least two types of W3-RGCs: W3B, which are motion sensitive, and W3D, which remain physiologically uncharacterized (Zhang et al., 2012; Kim and Kerschensteiner, 2017). There are at least three types of αRGCs in mouse retinas (Pang et al., 2003; Estevez et al., 2012). Kcng4^{Cre}:YFP mice express YFP in all three types of αRGCs, and some subsets of bipolar cells (Duan et al., 2015). There are three types of JamB expressing RGCs in mouse retina, which differ in dendritic tree morphology (Kim et al., 2008, 2010; Sanes and Masland, 2015). The JamB:YFP mice express YFP in two types of JamB expressing RGCs (J-RGCs). One type of J-RGCs orients its dendrites toward ventrally to form a polarized DF and is sensitive to directional movement, color-opponent responses, and orientation selective response (Kim et al., 2008, 2010; Joesch and Meister, 2016; Nath and Schwartz, 2017). The second type of J-RGCs has a symmetric DF and the function of them is not well characterized (Kim et al., 2008). In addition, YFP is expressed in about 12 morphological types of RGCs in the Thy1-YFP mice (Xu et al., 2010). Altogether, these transgenic mice provide a total of 8 RGC types individually or in small groups, including 1 DS-RGCs, 2 W3-RGCs, 3 αRGCs, 2 J-RGCs, and a mouse strain for a group of 12 types of RGCs.

NMDA Excitotoxicity in Retinal Diseases

Glutamate excitotoxicity is thought to play a critical role in RGC death in many retinal diseases, such as glaucoma, diabetic retinopathy, optic nerve injury and retinal ischemia (Kuehn et al., 2005; Kwon et al., 2009; Tezel, 2013). Glaucoma is a chronic optic neuropathy characterized by progressive RGC axon degeneration and cell death. One proposed mechanism for glaucomatous damage describes increased pressure in the eye leading to glutamate-induced excitotoxicity. Consistently, elevated IOP increases the expression of NMDARs in DBA/2J mice (Dong et al., 2013) and the numbers of NMDAR positive RGCs are reduced parallel to the loss of RGC in a chronic elevated IOP model (Luo et al., 2009). In addition, a NMDA antagonist, memantine, significantly reduces RGC loss and the expression of NMDARs (WoldeMussie et al., 2002; Sánchez-López et al., 2018), suggesting that NMDARs are involved in the RGC death in glaucoma. Furthermore, elevated IOP activates NMDARs, which triggers mitochondria-mediated apoptosis through releasing of optic atrophy 1 (OPA1) (Ju et al., 2008). Blockade of glutamate receptor inhibits OPA1 release, increases Bcl-2 expression, decreases Bax expression, and block apoptosis in glaucomatous mouse retina (Ju et al., 2009).

There is an emerging body of evidence that suggests neurodegeneration is a key initial process in the development of diabetic retinopathy (DR) and RGC injury occurs prior to microvascular damage via multiple potential mechanisms including overstimulation of the NMDAR (Smith, 2002; Barber, 2003; Araszkiewicz and Zozulinska-Ziolkiewicz, 2016). For instance, there is an elevated aqueous/vitreous glutamate level in DR animal models and DR patients (Ambati et al., 1997; Kowluru et al., 2001). The immunoreactivities of NR1 and GluR2/3 are upregulated in RGCs of both patients with diabetes and experimental DR animals (Ng et al., 2004; Santiago et al., 2008). In addition, blocking of NMDAR protects RGCs against neurodegeneration in DR rats (Kusari et al., 2007).

In ONC models, the NMDA antagonists, memantine and MK-801, protect RGCs from death (Yoles et al., 1997; WoldeMussie et al., 2002). In addition, the AMPA-KA antagonist, DNQX, also protects RGCs after ONC (Schuettauf et al., 2000). Furthermore, MK-801 and other NMDAR antagonists also prevent RGC death by retinal ischemia, reduces the expression of the pro-degeneration gene Bad and significantly increases the pro-survival activity of the PI3K/Akt pathway in the retina (Russo et al., 2008). Therefore, NMDA excitotoxicity seems to participate in RGC death induced by both optic nerve injury and retinal ischemia.

RGC Type-Specific Susceptibility to Retinal Diseases

The type-specific susceptibility of RGCs has been proposed as a factor in several retinal diseases. It has been proposed that the susceptibility of RGCs to glutamate excitotoxicity depends on soma size and retinal eccentricity. Larger RGCs at peripheral retina are more sensitive to kainate excitotoxicity while smaller RGCs at central retina are more sensitive to NMDA excitotoxicity (Vorwerk et al., 1999). In addition, intrinsically photosensitive melanopsin-expressing RGCs (ipRGCs) are also resistant to NMDA excitotoxicity (DeParis et al., 2012; Wang et al., 2018). In animal models of glaucoma, RGCs with large somata or big axon are more vulnerable to elevated IOP (Quigley et al., 1988; Glovinsky et al., 1991). Functionally, OFF RGCs appear to be more vulnerable to elevated IOP by reducing the strength of light responses and decreasing the size of the OFF receptive field (Della Santina and Ou, 2017; Sabharwal et al., 2017). OFF RGCs also exhibited higher rates of cell death and a more rapid decline in both structural and functional organizations compared to ON RGCs (Della Santina et al., 2013; El-Danaf and Huberman, 2015; Ou et al., 2016), but ON RGCs were more susceptible to elevated IOP than ON-OFF RGCs (Feng et al., 2013). In addition,

the transient OFF αRGCs exhibited higher rate of cell death, while neither sustained OFF αRGCs nor sustained ON αRGCs have reduced synaptic activity due to elevated IOP (Ou et al., 2016). Similar to models with elevated IOP, OFF RGCs were more susceptible than ON RGCs to ONC, and ON sustained RGCs seem to be more susceptible than ON transient RGCs to ONC (Puyang et al., 2017). Among αRGCs, ipRGCs, DSRGCs and W3-RGCs, αRGCs seem to be the least susceptible type to ONC (Duan et al., 2015). These results are consistent with our observation in this study and support the notion that glutamate excitotoxicity could play critical roles in RGC death of optic nerve injury.

Inconsistent with some previous reports, our results do not provide a clear correlation between RGC morphology and susceptibility to NMDA excitotoxicity. Among the 4 groups of genetically identified RGCs tested in this study, their susceptibility to NMDA excitotoxicity seems not directly correlate to the size of their soma and DF. This is evident that both BD-RGCs and J-RGCs have much higher susceptibility to NMDA excitotoxicity than αRGCs, which are known to have the biggest size of soma and DF, and W3-RGCs, which are the RGCs with the smallest size of soma and DF (Kim et al., 2010). This is opposite to the observations by several previous studies (Quigley et al., 1988; Glovinsky et al., 1991; Vorwerk et al., 1999). It was also reported that OFF RGCs appear to be more vulnerable to elevated IOP and ONC than ON RGCs (Della Santina et al., 2013; El-Danaf and Huberman, 2015; Ou et al., 2016; Della Santina and Ou, 2017; Puyang et al., 2017; Sabharwal et al., 2017), while ON RGCs are more susceptible to elevated IOP than ON-OFF RGCs (Feng et al., 2013). However, the ON and OFF inputs seem not play a critical role in NMDA-induced RGC death to BD-RGCs, which are ON-OFF RGCs (Kim et al., 2010; Trenholm et al., 2011), and J-RGCs, which are OFF-RGCs (Kim et al., 2008, 2010; Joesch and Meister, 2016; Nath and Schwartz, 2017).

An important question is what the underlying reasons contribute to these inconsistent observations. At least two important factors might play significant roles to this RGC type-specific susceptibility: the way how the RGC types are determined and the types of pathological insults. RGCs have been classified into types based on morphological, functional and genetic properties (Cleland et al., 1975; Badea and Nathans, 2004; Völgyi et al., 2005; Kim et al., 2008; Briggman and Euler, 2011; Briggman et al., 2011; Kay et al., 2011; Sanes and Masland, 2015; Baden et al., 2016; Rheaume et al., 2018). Most previous studies of RGC type-specific susceptibility are based on morphological and functional classification (Quigley et al., 1988; Glovinsky et al., 1991; Vorwerk et al., 1999; Della Santina et al., 2013; Feng et al., 2013; El-Danaf and Huberman, 2015; Ou et al., 2016; Della Santina and Ou, 2017; Puyang et al., 2017; Sabharwal et al., 2017). Because these morphologically and functionally classified RGC types are likely to have heterogeneous gene expression profiles and, if the gene expression profiles of RGCs contribute to the type-specific susceptibility, how the RGCs are grouped into types could have significant influence on the observed susceptibility.

Although very few studies have directly compared the susceptibility of the same type of RGCs to different pathological insults, it is plausible to assume that the underlying molecular mechanisms of RGC death induced by different pathological insults might be different due to the nature of insults, such as NMDA excitotoxicity elevates intracellular calcium while ONC reduces axonal transportation. Therefore, the susceptibility of the same type of RGCs might vary significantly to different types of pathological insults. Consistent with this idea, our unpublished data of an ongoing study demonstrate that the susceptibility of the four types RGCs tested in this study varies dramatically with types of injuries. In responding to ONC, BD-RGCs have the lowest susceptibility while W3-RGCs have the highest susceptibility, which is opposite to the ranking of susceptibility to NMDA excitotoxicity. Therefore, we propose that the susceptibility of different types of RGCs is likely to be determined by an interaction between the pathological insults and cell intrinsic response mechanisms. Different types of injuries might trigger different intrinsic response mechanisms in different types of RGCs, which might have different efficacy in activation of the cell death processes in different types of RGCs. If this is a general rule for type-specific RGC death in retinal diseases, it may not be reliable to predict the pattern of RGC death in one disease based on patterns of other diseases.

The Sequence of RGC Degeneration

Retinal ganglion cells lose synapses prior to a reduction in synaptic activity, leading to dendritic shrinkage and eventually cell death in glaucoma models of primates, cats, rats and human patients and animal models of ONC (Weber et al., 1998; Shou et al., 2003; Kuehn et al., 2005; Morgan et al., 2006; Leung et al., 2008; Weber et al., 2008; Liu et al., 2011; Della Santina et al., 2013; Feng et al., 2013; Ou et al., 2016). Carefully studying the sequence of structural, functional and molecular changes of injured RGCs could provide critical insights into the underlying mechanisms of RGC death and shed light on potential treatments aimed at reversing or slowing RGC degeneration. The present study demonstrates that many RGCs that lost all of their dendrites remained CASP3-negative while hardly any RGCs expressed CASP3 before completely losing their dendrites. The sequence of these morphological and molecular events suggests that the initial insult of NMDA excitotoxicity might only induce the loss of RGC dendrites through altering of the synaptic activity. Because this sequence of events seems to be consistent across several different experimental disease models, the initial insult in retinal diseases may set off a cascade of events that is subsequently independent of the primary insults. Regardless the underlying mechanisms, the kinetics of dendritic retraction of RGCs does not directly correlate to the susceptibility of type-specific RGC death. Because RGCs lose dendrites prior to cell death, using the dendritic morphology, the ramification patterns of RGC dendrites or patterns of light responses of RGCs to identify types of the cells under disease conditions might be misleading. The use of genetic markers provides a more reliable approach to identify

the types of RGC under disease conditions. Therefore, our results provide valuable insights into the type-specific susceptibility of RGCs to NMDA excitotoxicity.

DATA AVAILABILITY

All datasets generated for this study are included in the manuscript and/or the supplementary files.

AUTHOR CONTRIBUTIONS

IC and NY collected and analyzed the data and prepared the manuscript. BL and KH collected and analyzed the data. PW contributed the animal preparation and resource management. NT designed the experiments, analyzed the data, prepared the manuscript, and managed the research fund.

FUNDING

This work was supported by the Department Veterans Affair (1 I01BX002412-01A2), the National Eye Institute (R01EY012345 and EY014800), and Research to Prevent Blindness (RPB). This work was also supported by the National Institutes of Health under Ruth L. Kirschstein National Research Service Award (T35EY026511) from the National Eye Institute and a Medical Student Summer Research Scholarship from American Academy of Neurology.

REFERENCES

Almasieh, M., Wilson, A. M., Morquette, B., Cueva Vargas, J. L., and Di Polo, A. (2012). The molecular basis of retinal ganglion cell death in glaucoma. *Prog. Retin. Eye Res.* 31, 152–181. doi: 10.1016/j.preteyeres.2011.11.002

Ambati, J., Chalam, K. V., Chawla, D. K., D'Angio, C. T., Guillet, E. G., Rose, S. J., et al. (1997). Elevated gamma-aminobutyric acid, glutamate, and vascular endothelial growth factor levels in the vitreous of patients with proliferative diabetic retinopathy. *Arch. Ophthalmol.* 115, 1161–1166. doi: 10.1001/archopht.1997.01100160331011

Araszkiewicz, A., and Zozulinska-Ziolkiewicz, D. (2016). Retinal neurodegeneration in the course of diabetes-pathogenesis and clinical perspective. *Curr. Neuropharmacol.* 14, 805–809. doi: 10.2174/1570159X14666160225154536

Badea, T. C., and Nathans, J. (2004). Quantitative analysis of neuronal morphologies in the mouse retina visualized by using a genetically directed reporter. *J. Comp. Neurol.* 480, 331–351. doi: 10.1002/cne.20304

Baden, T., Berens, P., Franke, K., Román Rosón, M., Bethge, M., and Euler, T. (2016). The functional diversity of retinal ganglion cells in the mouse. *Nature* 529, 345–350. doi: 10.1038/nature16468

Bai, N., Aida, T., Yanagisawa, M., Katou, S., Sakimura, K., Mishina, M., et al. (2013). NMDA receptor subunits have different roles in NMDA-induced neurotoxicity in the retina. *Mol. Brain* 6:34. doi: 10.1186/1756-6606-6-34

Barber, A. J. (2003). A new view of diabetic retinopathy: a neurodegenerative disease of the eye. *Prog. Neuropsychopharmacol. Biol. Psychiatry* 27, 283–290.

Briggman, K. L., and Euler, T. (2011). Bulk electroporation and population calcium imaging in the adult mammalian retina. *J. Neurophysiol.* 105, 2601–2609. doi: 10.1152/jn.00722.2010

Briggman, K. L., Helmstaedter, M., and Denk, W. (2011). Wiring specificity in the direction-selectivity circuit of the retina. *Nature* 471, 183–188. doi: 10.1038/nature09818

Camacho, A., and Massieu, L. (2006). Role of glutamate transporters in the clearance and release of glutamate during ischemia and its relation to neuronal death. *Arch. Med. Res.* 37, 11–18. doi: 10.1016/j.arcmed.2005.05.014

Cleland, B. G., Levick, W. R., and Wässle, H. (1975). Physiological identification of a morphological class of cat retinal ganglion cells. *J. Physiol.* 248, 151–171. doi: 10.1113/jphysiol.1975.sp010967

Daniel, S., Clark, A. F., and McDowell, C. M. (2018). Subtype-specific response of retinal ganglion cells to optic nerve crush. *Cell Death Discov.* 4:67. doi: 10.1038/s41420-018-0069-y

Della Santina, L., Inman, D. M., Lupien, C. B., Horner, P. J., and Wong, R. O. (2013). Differential progression of structural and functional alterations in distinct retinal ganglion cell types in a mouse model of glaucoma. *J. Neurosci.* 33, 17444–17457. doi: 10.1523/JNEUROSCI.5461-12.2013

Della Santina, L., and Ou, Y. (2017). Who's lost first? Susceptibility of retinal ganglion cell types in experimental glaucoma. *Exp. Eye Res.* 158, 43–50. doi: 10.1016/j.exer.2016.06.006

DeParis, S., Caprara, C., and Grimm, C. (2012). Intrinsically photosensitive retinal ganglion cells are resistant to N-methyl-D-aspartic acid excitotoxicity. *Mol. Vis.* 18, 2814–2827.

Dong, L. D., Chen, J., Li, F., Gao, F., Wu, J., Miao, Y., et al. (2013). Enhanced expression of NR2B subunits of NMDA receptors in the inherited glaucomatous DBA/2J mouse retina. *Neural Plast.* 2013:670254. doi: 10.1155/2013/670254

Duan, X., Qiao, M., Bei, F., Kim, I. J., He, Z., and Sanes, J. R. (2015). Subtype-specific regeneration of retinal ganglion cells following axotomy: effects of osteopontin and mTOR signaling. *Neuron* 85, 1244–1256. doi: 10.1016/j.neuron.2015.02.017

Dutta, R., and Trapp, B. D. (2011). Mechanisms of neuronal dysfunction and degeneration in multiple sclerosis. *Prog. Neurobiol.* 93, 1–12. doi: 10.1016/j.pneurobio.2010.09.005

El-Danaf, R. N., and Huberman, A. D. (2015). Characteristic patterns of dendritic remodeling in early-stage glaucoma: evidence from genetically identified retinal ganglion cell types. *J. Neurosci.* 35, 2329–2343. doi: 10.1523/JNEUROSCI.1419-14.2015

Estevez, M. E., Fogerson, P. M., Ilardi, M. C., Borghuis, B. G., Chan, E., Weng, S., et al. (2012). Form and function of the M4 cell, an intrinsically photosensitive retinal ganglion cell type contributing to geniculocortical vision. *J. Neurosci.* 32, 13608–13620. doi: 10.1523/JNEUROSCI.1422-12.2012

Evangelho, K., Mogilevskaya, M., Losada-Barragan, M., and Vargas-Sanchez, J. K. (2017). Pathophysiology of primary open-angle glaucoma from a neuroinflammatory and neurotoxicity perspective: a review of the literature. *Int. Ophthalmol.* doi: 10.1007/s10792-017-0795-9 [Epub ahead of print].

Feng, L., Zhao, Y., Yoshida, M., Chen, H., Yang, J. F., Kim, T. S., et al. (2013). Sustained ocular hypertension induces dendritic degeneration of mouse retinal ganglion cells that depends on cell type and location. *Invest. Ophthalmol. Vis. Sci.* 54, 1106–1117. doi: 10.1167/iovs.12-10791

Fletcher, E. L., Hack, I., Brandstatter, J. H., and Wassle, H. (2000). Synaptic localization of NMDA receptor subunits in the rat retina. *J. Comp. Neurol.* 420, 98–112. doi: 10.1002/(SICI)1096-9861(20000424)420:1<98::AID-CNE7>3.0.CO;2-U

Glovinsky, Y., Quigley, H. A., and Dunkelberger, G. R. (1991). Retinal ganglion cell loss is size dependent in experimental glaucoma. *Invest. Ophthalmol. Vis. Sci.* 32, 484–491.

Hardingham, G. E., Fukunaga, Y., and Bading, H. (2002). Extrasynaptic NMDARs oppose synaptic NMDARs by triggering CREB shut-off and cell death pathways. *Nat. Neurosci.* 5, 405–414. doi: 10.1038/nn835

Huang, Z., Zang, K., and Reichardt, L. F. (2005). The origin recognition core complex regulates dendrite and spine development in postmitotic neurons. *J. Cell Biol.* 170, 527–535. doi: 10.1083/jcb.200505075

Hulsebosch, C. E., Hains, B. C., Crown, E. D., and Carlton, S. M. (2009). Mechanisms of chronic central neuropathic pain after spinal cord injury. *Brain Res. Rev.* 60, 202–213. doi: 10.1016/j.brainresrev.2008.12.010

Ishimaru, Y., Sumino, A., Kajioka, D., Shibagaki, F., Yamamuro, A., Yoshioka, Y., et al. (2017). Apelin protects against NMDA-induced retinal neuronal death via an APJ receptor by activating Akt and ERK1/2, and suppressing TNF-α

expression in mice. *J. Pharmacol. Sci.* 133, 34–41. doi: 10.1016/j.jphs.2016.12.002

Jiang, H., Wang, X., Zhang, H., Chang, Y., Feng, M., and Wu, S. (2016). Loss-of-function mutation of serine racemase attenuates excitotoxicity by intravitreal injection of N-methyl-D-aspartate. *J. Neurochem.* 136, 186–193. doi: 10.1111/jnc.13400

Joesch, M., and Meister, M. (2016). A neuronal circuit for colour vision based on rod-cone opponency. *Nature* 532, 236–239. doi: 10.1038/nature17158

Ju, W. K., Kim, K. Y., Angert, M., Duong-Polk, K. X., Lindsey, J. D., Ellisman, M. H., et al. (2009). Memantine blocks mitochondrial OPA1 and cytochrome c release and subsequent apoptotic cell death in glaucomatous retina. *Invest. Ophthalmol. Vis. Sci.* 50, 707–716. doi: 10.1167/iovs.08-2499

Ju, W. K., Lindsey, J. D., Angert, M., Patel, A., and Weinreb, R. N. (2008). Glutamate receptor activation triggers OPA1 release and induces apoptotic cell death in ischemic rat retina. *Mol. Vis.* 14, 2629–2638.

Kay, J. N., De la Huerta, I., Kim, I. J., Zhang, Y., Yamagata, M., Chu, M. W., et al. (2011). Retinal ganglion cells with distinct directional preferences differ in molecular identity, structure, and central projections. *J. Neurosci.* 31, 7753–7762. doi: 10.1523/JNEUROSCI.0907-11.2011

Kim, I. J., Zhang, Y., Meister, M., and Sanes, J. R. (2010). Laminar restriction of retinal ganglion cell dendrites and axons: subtype-specific developmental patterns revealed with transgenic markers. *J. Neurosci.* 30, 1452–1462. doi: 10.1523/JNEUROSCI.4779-09.2010

Kim, I. J., Zhang, Y., Yamagata, M., Meister, M., and Sanes, J. R. (2008). Molecular identification of a retinal cell type that responds to upward motion. *Nature* 452, 478–482. doi: 10.1038/nature06739

Kim, T., and Kerschensteiner, D. (2017). Inhibitory control of feature selectivity in an object motion sensitive circuit of the retina. *Cell Rep.* 19, 1343–1350. doi: 10.1016/j.celrep.2017.04.060

Kimura, A., Namekata, K., Guo, X., Noro, T., Harada, C., and Harada, T. (2015). Valproic acid prevents NMDA-induced retinal ganglion cell death via stimulation of neuronal TrkB receptor signaling. *Am. J. Pathol.* 185, 756–764. doi: 10.1016/j.ajpath.2014.11.005

Kowluru, R. A., Engerman, R. L., Case, G. L., and Kern, T. S. (2001). Retinal glutamate in diabetes and effect of antioxidants. *Neurochem. Int.* 38, 385–390. doi: 10.1016/S0197-0186(00)00112-1

Kuehn, M. H., Fingert, J. H., and Kwon, Y. H. (2005). Retinal ganglion cell death in glaucoma: mechanisms and neuroprotective strategies. *Ophthalmol. Clin. N. Am.* 18, 383–395. doi: 10.1016/j.ohc.2005.04.002

Kusari, J., Zhou, S., Padillo, E., Clarke, K. G., and Gil, D. W. (2007). Effect of memantine on neuroretinal function and retinal vascular changes of streptozotocin-induced diabetic rats. *Invest. Ophthalmol. Vis. Sci.* 48, 5152–5159. doi: 10.1167/iovs.07-0427

Kwon, Y. H., Fingert, J. H., Kuehn, M. H., and Alward, W. L. (2009). Primary open-angle glaucoma. *N. Engl. J. Med.* 360, 1113–1124. doi: 10.1056/NEJMra0804630

Kwong, J. M., Caprioli, J., and Piri, N. (2010). RNA binding protein with multiple splicing: a new marker for retinal ganglion cells. *Invest. Ophthalmol. Vis. Sci.* 51, 1052–1058. doi: 10.1167/iovs.09-4098

Leung, C. K., Lindsey, J. D., Crowston, J. G., Lijia, C., Chiang, S., and Weinreb, R. N. (2008). Longitudinal profile of retinal ganglion cell damage after optic nerve crush with blue-light confocal scanning laser ophthalmoscopy. *Invest. Ophthalmol. Vis. Sci.* 49, 4898–4902. doi: 10.1167/iovs.07-1447

Lèvai, O., and Strotmann, J. (2003). Projection pattern of nerve fibers from the septal organ: DiI-tracing studies with transgenic OMP mice. *Histochem. Cell Biol.* 120, 483–492. doi: 10.1007/s00418-003-0594-4

Liu, M., Duggan, J., Salt, T. E., and Cordeiro, M. F. (2011). Dendritic changes in visual pathways in glaucoma and other neurodegenerative conditions. *Exp. Eye Res.* 92, 244–250. doi: 10.1016/j.exer.2011.01.014

Luo, X. G., Chiu, K., Lau, F. H., Lee, V. W., Yung, K. K., and So, K. F. (2009). The selective vulnerability of retinal ganglion cells in rat chronic ocular hypertension model at early phase. *Cell. Mol. Neurobiol.* 29, 1143–1151. doi: 10.1007/s10571-009-9407-1

Madisen, L., Mao, T., Koch, H., Zhuo, J. M., Berenyi, A., Fujisawa, S., et al. (2012). A toolbox of Cre-dependent optogenetic transgenic mice for light-induced activation and silencing. *Nat. Neurosci.* 15, 793–802. doi: 10.1038/nn.3078

Manev, H., Favaron, M., Guidotti, A., and Costa, E. (1989). Delayed increase of Ca2+ influx elicited by glutamate: role in neuronal death. *Mol. Pharmacol.* 36, 106–112.

Morgan, J. E., Datta, A. V., Erichsen, J. T., Albon, J., and Boulton, M. E. (2006). Retinal ganglion cell remodelling in experimental glaucoma. *Adv. Exp. Med. Biol.* 572, 397–402. doi: 10.1007/0-387-32442-9_56

Nath, A., and Schwartz, G. W. (2017). Electrical synapses convey orientation selectivity in the mouse retina. *Nat. Commun.* 8:2025. doi: 10.1038/s41467-017-01980-9

Ng, Y. K., Zeng, X. X., and Ling, E. A. (2004). Expression of glutamate receptors and calcium-binding proteins in the retina of streptozotocin-induced diabetic rats. *Brain Res.* 1018, 66–72. doi: 10.1016/j.brainres.2004.05.055

Norsworthy, M. W., Bei, F., Kawaguchi, R., Wang, Q., Tran, N. M., Li, Y., et al. (2017). Sox11 expression promotes regeneration of some retinal ganglion cell types but kills others. *Neuron* 94, 1112–1120. doi: 10.1016/j.neuron.2017.05.035

Ou, Y., Jo, R. E., Ullian, E. M., Wong, R. O., and Della Santina, L. (2016). Selective vulnerability of specific retinal ganglion cell types and synapses after transient ocular hypertension. *J. Neurosci.* 36, 9240–9252. doi: 10.1523/JNEUROSCI.0940-16.2016

Overstreet-Wadiche, L. S., Bromberg, D. A., Bensen, A. L., and Westbrook, G. L. (2006). Seizures accelerate functional integration of adult-generated granule cells. *J. Neurosci.* 26, 4095–4103. doi: 10.1523/JNEUROSCI.5508-05.2006

Pang, J. J., Gao, F., and Wu, S. M. (2003). Light-evoked excitatory and inhibitory synaptic inputs to ON and OFF alpha ganglion cells in the mouse retina. *J. Neurosci.* 23, 6063–6073. doi: 10.1523/JNEUROSCI.23-14-06063.2003

Pi, Z., Lin, H., and Yang, J. (2018). Isoflurane reduces pain and inhibits apoptosis of myocardial cells through the phosphoinositide 3-kinase/protein kinase B signaling pathway in mice during cardiac surgery. *Mol. Med. Rep.* 17, 6497–6505. doi: 10.3892/mmr.2018.8642

Puyang, Z., Gong, H. Q., He, S. G., Troy, J. B., Liu, X., and Liang, P. J. (2017). Different functional susceptibilities of mouse retinal ganglion cell subtypes to optic nerve crush injury. *Exp. Eye Res.* 162, 97–103. doi: 10.1016/j.exer.2017.06.014

Quigley, H. A., Dunkelberger, G. R., and Green, W. R. (1988). Chronic human glaucoma causing selectively greater loss of large optic nerve fibers. *Ophthalmology* 95, 357–363. doi: 10.1016/S0161-6420(88)33176-3

Rheaume, B. A., Jereen, A., Bolisetty, M., Sajid, M. S., Yang, Y., Renna, K., et al. (2018). Single cell transcriptome profiling of retinal ganglion cells identifies cellular subtypes. *Nat. Commun.* 9:2759. doi: 10.1038/s41467-018-05134-3

Rodriguez, A. R., de Sevilla Müller, L. P., and Brecha, N. C. (2014). The RNA binding protein RBPMS is a selective marker of ganglion cells in the mammalian retina. *J. Comp. Neurol.* 522, 1411–1443. doi: 10.1002/cne.23521

Russo, R., Cavaliere, F., Berliocchi, L., Nucci, C., Gliozzi, M., Mazzei, C., et al. (2008). Modulation of pro-survival and death-associated pathways under retinal ischemia/reperfusion: effects of NMDA receptor blockade. *J. Neurochem.* 107, 1347–1357. doi: 10.1111/j.1471-4159.2008.05694.x

Sabharwal, J., Seilheimer, R. L., Tao, X., Cowan, C. S., Frankfort, B. J., and Wu, S. M. (2017). Elevated IOP alters the space-time profiles in the center and surround of both ON and OFF RGCs in mouse. *Proc. Natl. Acad. Sci. U.S.A.* 114, 8859–8864. doi: 10.1073/pnas.1706994114

Sánchez-López, E., Egea, M. A., Davis, B. M., Guo, L., Espina, M., and Silva, A. M. (2018). Memantine-loaded PEGylated biodegradable nanoparticles for the treatment of glaucoma. *Small* 14:1701808. doi: 10.1002/smll.201701808

Sanes, J. R., and Masland, R. H. (2015). The types of retinal ganglion cells: current status and implications for neuronal classification. *Annu. Rev. Neurosci.* 38, 221–246. doi: 10.1146/annurev-neuro-071714-034120

Santiago, A. R., Hughes, J. M., Kamphuis, W., Schlingemann, R. O., and Ambrósio, A. F. (2008). Diabetes changes ionotropic glutamate receptor subunit expression level in the human retina. *Brain Res.* 1198, 153–159. doi: 10.1016/j.brainres.2007.12.030

Schuettauf, F., Naskar, R., Vorwerk, C. K., Zurakowski, D., and Dreyer, E. B. (2000). Ganglion cell loss after optic nerve crush mediated through AMPA-kainate and NMDA receptors. *Invest. Ophthalmol. Vis. Sci.* 41, 4313–4316.

Shou, T., Liu, J., Wang, W., Zhou, Y., and Zhao, K. (2003). Differential dendritic shrinkage of alpha and beta retinal ganglion cells in cats with chronic glaucoma. *Invest. Ophthalmol. Vis. Sci.* 44, 3005–3010. doi: 10.1167/iovs.02-0620

Siegert, S., Scherf, B. G., Del Punta, K., Didkovsky, N., Heintz, N., and Roska, B. (2009). Genetic address book for retinal cell types. *Nat. Neurosci.* 12, 1197–1204. doi: 10.1038/nn.2370

Smith, S. B. (2002). Diabetic Retinopathy and the NMDA Receptor. *Drug News Perspect.* 15, 226–232. doi: 10.1358/dnp.2002.15.4.840055

Stavrovskaya, I. G., and Kristal, B. S. (2005). The powerhouse takes control of the cell: is the mitochondrial permeability transition a viable therapeutic target against neuronal dysfunction and death? *Free Radic. Biol. Med.* 38, 687–697.

Tezel, G. (2013). Immune regulation toward immunomodulation for neuroprotection in glaucoma. *Curr. Opin. Pharmacol.* 13, 23–31. doi: 10.1016/j.coph.2012.09.013

Trenholm, S., Johnson, K., Li, X., Smith, R. G., and Awatramani, G. B. (2011). Parallel mechanisms encode direction in the retina. *Neuron* 71, 683–694. doi: 10.1016/j.neuron.2011.06.020

Völgyi, B., Abrams, J., Paul, D. L., and Bloomfield, S. A. (2005). Morphology and tracer coupling pattern of alpha ganglion cells in the mouse retina. *J. Comp. Neurol.* 492, 66–77. doi: 10.1002/cne.20700

Vorwerk, C. K., Kreutz, M. R., Böckers, T. M., Brosz, M., Dreyer, E. B., and Sabel, B. A. (1999). Susceptibility of retinal ganglion cells to excitotoxicity depends on soma size and retinal eccentricity. *Curr. Eye Res.* 19, 59–65. doi: 10.1076/ceyr.19.1.59.5336

Wang, S., Gu, D., Zhang, P., Chen, J., Li, Y., Xiao, H., et al. (2018). Melanopsin-expressing retinal ganglion cells are relatively resistant to excitotoxicity induced by N-methyl-d-aspartate. *Neurosci. Lett.* 662, 368–373. doi: 10.1016/j.neulet.2017.10.055

Weber, A. J., Harman, C. D., and Viswanathan, S. (2008). Effects of optic nerve injury, glaucoma, and neuroprotection on the survival, structure, and function of ganglion cells in the mammalian retina. *J. Physiol.* 586, 4393–4400. doi: 10.1113/jphysiol.2008.156729

Weber, A. J., Kaufman, P. L., and Hubbard, W. C. (1998). Morphology of single ganglion cells in the glaucomatous primate retina. *Invest. Ophthalmol. Vis. Sci.* 39, 2304–2320.

Williams, P. A., Howell, G. R., Barbay, J. M., Braine, C. E., Sousa, G. L., and John, S. W. (2013). Retinal ganglion cell dendritic atrophy in DBA/2J glaucoma. *PLoS One* 8:e72282. doi: 10.1371/journal.pone.0072282

WoldeMussie, E., Yoles, E., Schwartz, M., Ruiz, G., and Wheeler, L. A. (2002). Neuroprotective effect of memantine in different retinal injury models in rats. *J. Glaucoma* 11, 474–480. doi: 10.1097/00061198-200212000-00003

Xu, H. P., Chen, H., Ding, Q., Xie, Z. H., Chen, L., Diao, L., et al. (2010). The immune protein CD3ζ is required for normal development of neural circuits in the retina. *Neuron* 65, 503–515. doi: 10.1016/j.neuron.2010.01.035

Yoles, E., Muller, S., and Schwartz, M. (1997). NMDA-receptor antagonist protects neurons from secondary degeneration after partial optic nerve crush. *J. Neurotrauma* 14, 665–675. doi: 10.1089/neu.1997.14.665

Zhang, J., and Diamond, J. S. (2009). Subunit- and pathway-specific localization of NMDA receptors and scaffolding proteins at ganglion cell synapses in rat retina. *J. Neurosci.* 29, 4274–4286. doi: 10.1523/JNEUROSCI.5602-08.2009

Zhang, Y., Kim, I. J., Sanesk, J. R., and Meister, M. (2012). The most numerous ganglion cell type of the mouse retina is a selective feature detector. *Proc. Natl. Acad. Sci. U.S.A.* 109, E2391–E2398. doi: 10.1073/pnas.1211547109

Zhao, J., Mysona, B. A., Qureshi, A., Kim, L., Fields, T., Gonsalvez, G. B., et al. (2016). (+)-pentazocine reduces NMDA-induced murine retinal ganglion cell death through a σR1-dependent mechanism. *Invest. Ophthalmol. Vis. Sci.* 57, 453–461. doi: 10.1167/iovs.15-18565

Conflict of Interest Statement: The authors declare that the research was conducted in the absence of any commercial or financial relationships that could be construed as a potential conflict of interest.

frontiers in Neuroscience

REVIEW
published: 02 September 2019
doi: 10.3389/fnins.2019.00931

Immune Mediated Degeneration and Possible Protection in Glaucoma

*Teresa Tsai†, Sabrina Reinehr†, Ana M. Maliha and Stephanie C. Joachim**

Experimental Eye Research, University Eye Hospital, Ruhr-University Bochum, Bochum, Germany

The underlying pathomechanisms for glaucoma, one of the most common causes of blindness worldwide, are still not identified. In addition to increased intraocular pressure (IOP), oxidative stress, excitotoxicity, and immunological processes seem to play a role. Several pharmacological or molecular/genetic methods are currently investigated as treatment options for this disease. Altered autoantibody levels were detected in serum, aqueous humor, and tissue sections of glaucoma patients. To further analyze the role of the immune system, an IOP-independent, experimental autoimmune glaucoma (EAG) animal model was developed. In this model, immunization with ocular antigens leads to antibody depositions, misdirected T-cells, retinal ganglion cell death and degeneration of the optic nerve, similar to glaucomatous degeneration in patients. Moreover, an activation of the complement system and microglia alterations were identified in the EAG as well as in ocular hypertension models. The inhibition of these factors can alleviate degeneration in glaucoma models with and without high IOP. Currently, several neuroprotective approaches are tested in distinct models. It is necessary to have systems that cover underlying pathomechanisms, but also allow for the screening of new drugs. *In vitro* models are commonly used, including single cell lines, mixed-cultures, and even organoids. In *ex vivo* organ cultures, pathomechanisms as well as therapeutics can be investigated in the whole retina. Furthermore, animal models reveal insights in the *in vivo* situation. With all these models, several possible new drugs and therapy strategies were tested in the last years. For example, hypothermia treatment, neurotrophic factors or the blockage of excitotoxity. However, further studies are required to reveal the pressure independent pathomechanisms behind glaucoma. There is still an open issue whether immune mechanisms directly or indirectly trigger cell death pathways. Hence, it might be an imbalance between protective and destructive immune mechanisms. Moreover, identified therapy options have to be evaluated in more detail, since deeper insights could lead to better treatment options for glaucoma patients.

Keywords: glaucoma, complement system, autoantibody, organ culture, porcine, neuroprotection

OPEN ACCESS

Edited by:
Mohammad Shamsul Ola, King Saud University, Saudi Arabia

Reviewed by:
Ana Raquel Santiago, University of Coimbra, Portugal
Dong Feng Chen, Schepens Eye Research Institute, United States

****Correspondence:***
Stephanie C. Joachim
stephanie.joachim@rub.de

† These authors have contributed equally to this work

Specialty section:
This article was submitted to Neurodegeneration, a section of the journal Frontiers in Neuroscience

Received: *13 June 2019*
Accepted: *19 August 2019*
Published: *02 September 2019*

Citation:
Tsai T, Reinehr S, Maliha AM and Joachim SC (2019) Immune Mediated Degeneration and Possible Protection in Glaucoma. Front. Neurosci. 13:931. doi: 10.3389/fnins.2019.00931

Abbreviations: $CoCl_2$, cobalt-chloride; EAG, experimental autoimmune glaucoma animal; H_2O_2, hydrogen peroxide; HSP, heat shock protein; IL, interleukin; IOP, intraocular pressure; L, long; M, middle; MASP1 and 2, the mannose-associated-serine-proteases 1 and 2; MAC, membrane attack complex; MBL, mannose binding lectin; NFκB, nucleus factor-kappa-light-chain enhancer of activated B cells; NTG, normal-tension glaucoma; OHT, ocular hypertension; ONA, optic nerve antigen homogenate; POAG, primary open-angle glaucoma; RGC, retinal ganglion cells; RPE, retinal pigment epithelium; S, short.

INTRODUCTION

Glaucoma is a multifactorial and neurodegenerative disease, which is characterized by a chronic loss of retinal ganglion cells (RGCs) and their axons (Casson et al., 2012; EGS, 2017). Patients suffer from irreversible visual field loss, which ultimately leads to blindness (Stevens et al., 2013). As a result, glaucoma is one of the most common causes of blindness worldwide, affecting approximately 79.6 million people by 2020 (Quigley and Broman, 2006; EGS, 2017). As society ages, there will be an additional increase in severe visual impairment and blindness and by the year 2030 nearly 13% of these patients will be affected by glaucoma (Finger et al., 2011; Lang, 2014).

Glaucoma can be differentiated into several types, which makes diagnosis difficult. Hence, in most western countries around 50% of patients with manifest glaucoma are unaware of their disease (Tielsch et al., 1991; Mitchell et al., 1996; Grodum et al., 2002; Quigley and Jampel, 2003; EGS, 2017). Additionally, in most cases, glaucoma is diagnosed too late (Martus et al., 2005), since it might be clinically not detectable until 20–40% of RGCs are lost, resulting in a potential 10 year delay in diagnosis (Zeyen, 1999; Kerrigan-Baumrind et al., 2000). In general, glaucoma can be subdivided into primary and secondary forms. The latter usually occurs as a result of an already existing (eye) disease or as an undesirable side effect of drugs, after a medical procedure, as well as after traumatic injury. The most common form of primary glaucoma is the primary open-angle glaucoma (POAG). POAG is generally characterized by a clinical triad of elevated intraocular pressure (IOP), the appearance of optic atrophy, and a progressive loss of peripheral visual sensitivity in the early stages of the disease, which may ultimately progress and then impair visual acuity (Quigley, 1993). But in about 30% of all cases, glaucomatous damage is developed IOP-independently (Sommer et al., 1991). This form is known as normal-tension glaucoma (NTG). It is a controversial issue if the separation of POAG and NTG is artificial and both diseases trace back to the same pathogenic mechanisms.

The underlying pathomechanisms for glaucoma are still not fully identified. High IOP remains the main risk factor. In addition, age, myopia, gender, and ethnicity seem to play an important role in the development of glaucoma (Coleman and Miglior, 2008; Chen et al., 2012; McMonnies, 2017). For example, people of African descent are more likely to develop POAG than Caucasians, and Asians are particularly prone to NTG (McMonnies, 2017). Although the exact pathomechanisms of glaucoma are still unclear, several possible factors that likely contribute to the onset of glaucoma are discussed. In addition to mechanical processes, circulatory disorders, excitotoxicity, and immunological reactions are also considered contribute to the pathogenesis of glaucoma (Joachim et al., 2005; Casson, 2006; Tezel et al., 2010; Evangelho et al., 2019). Moreover, hypoxic processes as well as oxidative stress are involved in the early disease progression (Zanon-Moreno et al., 2008; Greco et al., 2016).

Currently, an elevated IOP is considered the main risk factor and can be treated medically or surgically. Therefore, IOP lowering is the main treatment option and known to slow down or even stop progressive vision loss in patients (Vass et al., 2007). Although the IOP in NTG is not significantly increased, lowering pressure is the common therapy. For every glaucoma patient, an individual desired IOP is determined, depending on individual disease factors. Unfortunately, in many cases, despite medical or surgical IOP lowering therapy, optic nerve and RGC degeneration as well as visual field loss continue on a long-term basis (Chang and Goldberg, 2012; Pascale et al., 2012). Thus, it would be tremendously beneficial to develop treatment options that protect RGCs and preserve visual function through mechanisms other than IOP reduction. In the last years, researchers have searched for pharmacological or molecular genetic methods to protect retinal neurons or nerve fibers and thus prevent cell death. The list of neuroprotective substances studied so far is long. Unfortunately, a big breakthrough has not yet been achieved. Recent research approaches, however, give hope and point to new and promising therapeutic strategies.

IMMUNE RESPONSE IN GLAUCOMA PATIENTS

In recent years, possible pathogenic factors, such as oxidative stress (Tezel et al., 2010; Tezel, 2011), ischemic events (Almasieh et al., 2012; Schmid et al., 2014), or increased glutamate levels (Dreyer et al., 1996; Neufeld et al., 1997; Kuehn et al., 2017b), were implicated to contribute to glaucoma. Furthermore, a possible involvement of the immune system moved more and more into the focus (Tezel and Wax, 2004; Grus et al., 2008; Wax, 2011). In patients with POAG as well as with NTG, changes in the antibody profile were found in serum and aqueous humor (Grus et al., 2004; Joachim et al., 2007; Boehm et al., 2012). One of the first antibodies identified was against heat shock protein (HSP) 60 and small HSPs (Wax et al., 1994). Further studies revealed complex altered antibody responses in patients. Some of these antibodies were upregulated, such as HSP27 (Tezel et al., 1998), HSP70 (Joachim et al., 2007), γ-enolase (Maruyama et al., 2000), α-fodrin (Grus et al., 2006), or myelin basic protein (Joachim et al., 2008). Further analysis of the increased antibody titers showed that the direct administration of small HSPs to retinal tissue or cells can induce cell death through apoptotic mechanisms. Thus, increased titers of circulating antibodies HSPs, like HSP27, may appear pathogenic in some patients (Tezel et al., 1998). However, a downregulation of antibodies, like GFAP, vimentin, β-crystallin, or 14-3-3 was also detected (Joachim et al., 2007, 2008; Bell et al., 2015). Since some autoantibodies have neuroprotective potential on neuronal cells, the reduction of GFAP and 14-3-3 appears to be an indication of the loss of naturally occurring protective autoimmunity (Bell et al., 2013). Similar antibody changes were noted in other neurodegenerative diseases, such as Alzheimer's disease and multiple sclerosis (Krumbholz et al., 2012; Liao et al., 2013). Patients with Alzheimer's disease for example exhibited a reduced level of their protective autoantibodies against amyloid-β (Dodel et al., 2011) whereas patients with multiple sclerosis showed an upregulation of demyelinating autoantibodies (Elliott et al., 2012).

Furthermore, depositions of IgG antibodies were found in the retinae of glaucomatous eyes (Wax et al., 1998; Gramlich et al., 2013). Antibodies are usually able to activate the complement system, a part of the innate immune response. This could also be the case in glaucoma. Here, elevated complement proteins, such as C3 or lectin pathway associated proteins, were noted in the sera and retinae of POAG patients (Boehm et al., 2010; Tezel et al., 2010). Also, evidences showed altered macroglia reactions as well as contributions of activated microglia cells (Yuan and Neufeld, 2001; Wang et al., 2002). Recently, Chen et al. reported that an IOP elevation can induce infiltration of autoreactive T-cells into the retina, which cause neurodegeneration by cross-reacting with HSP-expressing RGCs. Furthermore, they noted that both POAG and NTG patients also have an increase of HSP27- and HSP60-specific T-cells, indicating that these findings are likely to be of relevance for glaucoma patients (Chen et al., 2018).

FINDINGS FROM GLAUCOMA ANIMAL MODELS

Immune Response in Glaucoma Models

In order to analyze the altered immune response found in human glaucoma patients more precisely, an experimental autoimmune glaucoma (EAG) model was developed (Wax et al., 2008). This model should help to shed light on the question if the immune system alterations are cause or consequence of the disease. Glaucomatous-like damage in this model is induced by immunization with ocular antigens without altering IOP. The immunization with antigens, like HSP27, HSP60, or S100B protein lead to RGC loss and optic nerve degeneration after 28 days (Wax et al., 2008; Casola et al., 2015; Noristani et al., 2016; Reinehr et al., 2018a). Also, immunization with an optic nerve antigen homogenate (ONA) provoked glaucoma-like damage in the animals (Laspas et al., 2011; Noristani et al., 2016). However, prior to the loss of RGCs in this model, it was possible to detect antibody deposits in the retina, similar to those seen in tissue from glaucoma patients (Joachim et al., 2012). IgM deposits were already detected after 7 days, while IgG deposits could be detected in the ganglion cell layer of immunized animals after 14 days. These deposits were often co-localized with apoptotic RGCs (Joachim et al., 2014). In an intermittent ocular hypertension (OHT) animal model, IgG autoantibody deposits and microglia activation were also notable. Furthermore, elevated serum autoantibody immunoreactivities were detected, for example against glutathione-S-transferase and transferrin (Gramlich et al., 2016).

The findings of the antibodies raised the question, how they are contributing to glaucomatous cell death. It is possible that antibodies activate certain pathways, like the complement system. It is known that IgGs are able to initiate the complement cascade (Sontheimer et al., 2005; Ehrnthaller et al., 2011). In the EAG model, an activation of the complement system was noted via the lectin pathway in the retina and the optic nerve at the early stage of the disease, already 2 weeks after the immunization. The number of RGCs was still unchanged at this time (Reinehr et al., 2016a). Interestingly, in addition to the upregulation of complement factors, an increased number and activation of microglial cells could be observed in the EAG model at this early stage (Noristani et al., 2016).

Activation of the Complement System

The complement system is part of the innate immune response and consists of a large number of different plasma proteins that interact to opsonize pathogens and to induce a series of inflammatory responses. It is also a bridge between the innate and the adaptive immunity. The proteins are mostly synthesized in the liver and exist in the plasma or on cell surfaces as inactive precursors, called zymogens (Nesargikar et al., 2012). The activation is initiated through a triggered enzyme cascade. A key site for the activation processes is the pathogen surface and there are three distinct pathways leading to complement activation, the classical, the lectin, and the alternative pathway (**Figure 1**). The classical pathway plays a role in both innate and adaptive immune response. The first component, C1q, can bind either to antibodies complexed with antigens or to naturally produced antibodies. The lectin pathway can be induced through the mannose binding lectin (MBL). It binds specifically to sugar residues, which are present on many pathogen surfaces. MBL forms a complex with the mannose-associated-serine-proteases 1 and 2 (MASP1- and 2), which then activate the further complement cascade. The third pathway, the alternative one, is activated spontaneously via hydrolysis of C3 into C3b (Murphy and Walport, 2008). Finally, the membrane attack complex (MAC) is formed. MAC has a hydrophobic external face and a hydrophilic internal channel. The disruption of the lipid bilayer leads to the loss of cellular homeostasis, which results in the lysis of the target cell (Fosbrink et al., 2005; Murphy and Walport, 2008).

As already described in glaucoma patients, also in animal models a dysregulation of the complement system seems to be involved in disease development. Significantly more complement depositions were described in various OHT studies. For example, C3 and MAC depositions were found in rat retinae 14 and 28 days after OHT induction (Kuehn et al., 2006). Increased C3 and MAC levels were also observed 6 weeks after IOP elevation through laser treatment (Jha et al., 2011). In addition, even a moderate increased IOP, of about 19%, leads to an enhancement of the complement factors C3 and MAC in the retinae of rats (Becker et al., 2015). To investigate the contribution of the complement system in glaucoma independent from IOP, studies on the EAG model were carried out. It is known that a loss of RGCs is observable 28 days, but not 14 days after immunization with ONA (Laspas et al., 2011; Noristani et al., 2016; Reinehr et al., 2016b). Hence, the question arises whether an activation of the complement cascade is detectable even before cell death. Significantly more C3 depositions were noted in retinae and optic nerves of ONA immunized animals after 7 days. Furthermore, the terminal pathway of the complement system, MAC, was also activated at these points in time. Due to previous findings of IgG antibodies in human (Gramlich et al., 2013) and animal glaucomatous eyes (Joachim et al., 2014), activation of the complement cascade via C1q seemed likely. Interestingly, this was not the case. In human glaucoma as well as in OHT

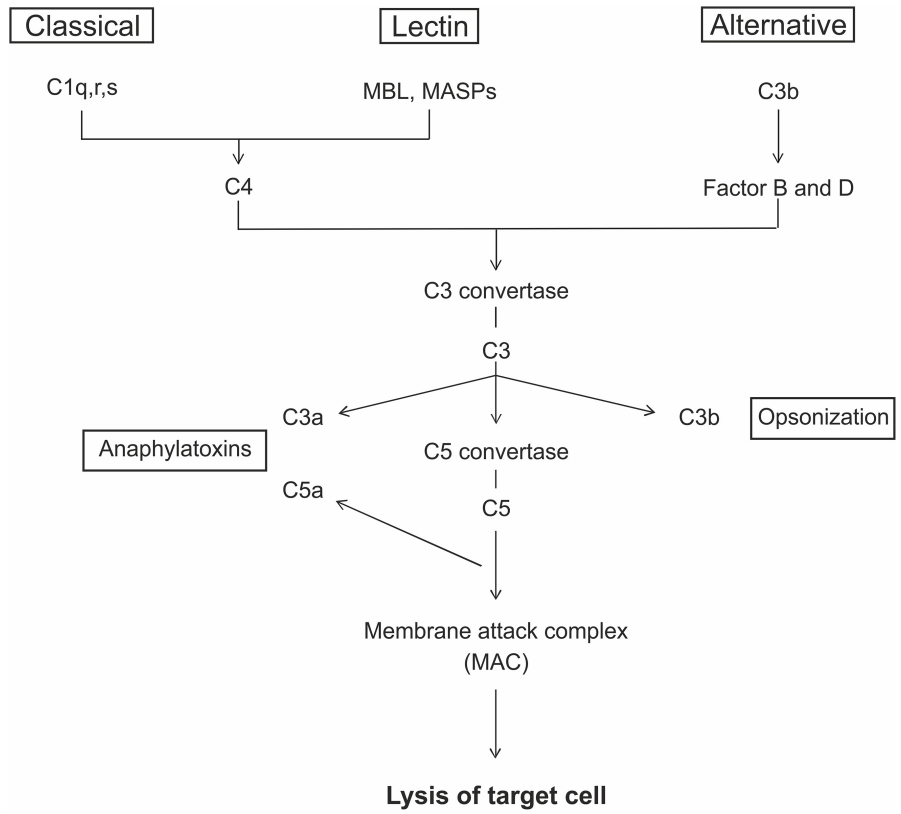

FIGURE 1 | The complement system can be activated via three different pathways. The classical pathway is initiated by antibody complexes binding to C1q. The mannose binding lectin (MBL) and the mannose-associated-serine-proteases (MASPs) bind to specific carbohydrate structures leading to the activation via the lectin pathway. The alternative pathway is spontaneously activated through the cleavage of C3 to C3b. All three pathways lead to the generation of C3 convertases that cleaves the C3 protein into C3a and C3b. C3b acts in the opsonization of target cells and additionally form the C5 convertase, which cleaves C5 to C5a and C5b. C5a and C3a act as anaphylatoxins. At the end, the interaction of C5b with C6, C7, C8, and C9 lead to the formation of C5b-9, the membrane attack complex (MAC). MAC is the terminal pathway, which can cause lysis of the target cells due to a formation of a pore.

models, on the other hand, elevated C1q levels were identified (Kuehn et al., 2006; Stasi et al., 2006; Howell et al., 2011). Also, an inhibition of C1q seems to be protective against dendritic and synaptic degeneration (Williams et al., 2016). In previous studies using the EAG model, depositions of IgG were noted at 14 days, but not at 8 days after immunization (Joachim et al., 2014). Hence, it is possible that C1q is expressed at later points in time in this model. Interestingly, a simultaneous activation of components of the lectin pathway in retinae and optic nerves was observed. The lectin pathway cannot only be initiated through mannose residues on pathogen surfaces, but also through apoptotic and necrotic cells (Ogden et al., 2001; Nauta et al., 2003; Stuart et al., 2005). It is also known that hypoxia induces restructuring of the endothelial cell surface, resulting in an activation of the complement system via the lectin pathway (Collard et al., 1999). As stated above, in glaucoma human donor eyes, proteomic analysis revealed an upregulation of proteins linked to the lectin pathway, such as MASP1 and MASP2 (Tezel et al., 2010). It is known that MASP2 cleaves C4 and C2 to form the C3 convertase. MASP1 alone is insufficient to activate the lectin pathway, but the activation of both MASPs ultimately initiates the complement cascade (Matsushita et al., 2000; Takahashi et al., 2008). After immunization with the glia protein S100B, an activation of the lectin pathway occurred. Here, MBL was upregulated in the S100B retinae after 3 days, and after 7 and 14 days in optic nerves as well (Reinehr et al., 2018b).

Role of Microglia in Glaucoma Models

The observations of complement proteins in glaucomatous retinae and optic nerves raise the question how these components could enter the eye. Although the blood-retina-barrier is not impenetrable, most proteins cannot invade the eye. Therefore, local synthesis by resident cells in the retina is necessary. It seems likely that glia cells are the source of complement components. Microglia are the resident immune cells in the central nervous system and therefore also in the retina (Kettenmann et al., 2011; Karlstetter et al., 2015). In the retina, they are mainly located in the ganglion cell layer or in the inner plexiform layer. In the optic nerve, activated microglia are first localized in the optic nerve head (Bosco et al., 2011). Microglia are linked to many neurodegenerative diseases, such as multiple sclerosis (Ajami et al., 2011), Alzheimer's disease (Fuhrmann et al., 2010), and Parkinson's disease (Ouchi et al., 2005). Activated microglia are

also a hallmark in retinal diseases, including diabetic retinopathy (Zeng et al., 2008) or uveitis (Rao et al., 2003; Kerr et al., 2008). When neurons are damaged, microglia respond by adopting an activated phenotype (Kreutzberg, 1995; Graeber and Streit, 2010; Ramirez et al., 2017). Additionally, they can change the expression of different enzymes, receptors, cytokines, and growth factors (Rojas et al., 2014). In the EAG model, a significantly higher number of microglia was seen in the retina after 14 and 28 days when immunizating with different ocular antigens (Casola et al., 2016; Noristani et al., 2016). But not only the number of these cells was increased. In addition, more activated cells were observed in these animals, especially 14 days after immunization. However, no alterations could be detected anymore at 28 days (Noristani et al., 2016). These results are in accordance with OHT studies, where a microglia activation was noted prior to RGC loss (Ebneter et al., 2010; Bosco et al., 2011). In a laser induced OHT model, a non-proliferative microglia activation was detected already after 24 h (de Hoz et al., 2018). Also, after an intravitreal application of S100B, an increase in the microglia cell number was accompanied with a loss of RGCs after 14 days (Kuehn et al., 2018).

It is known that the transcription factor nucleus factor-kappa-light-chain enhancer of activated B cells (NFκB) controls the migration of microglia to the site of injury due to expression of β-integrin CD11a. In rats, which were systemically immunized with S100B, an increase of NFκB could be observed in retinae after 7 and 14 days. Furthermore, enhanced levels of the pro-inflammatory cytokine IL-1β were observed in aqueous humor of S100B animals at day 7 (Reinehr et al., 2018b). Yoneda et al. noted that IL-1β plays an important role in mediating ischemic and excitotoxic damage in glaucomatous retina (Yoneda et al., 2001). Several studies claim that IL-1β is secreted by microglia after photo-oxidative damage (Hu et al., 2015; Jiao et al., 2015; Natoli et al., 2017), in neovascular age-related macular degeneration (Lavalette et al., 2011), in retinitis pigmentosa (Zhao et al., 2015), and after retinal detachment (Kataoka et al., 2015). Besides microglia/macrophages, also NFκB was reported to induce transcription of the IL-1β gene (Cogswell et al., 1994).

The Immune System as Therapeutic Target in Glaucoma

Several findings demonstrate a contribution of the immune system in glaucoma pathogenesis. Since lowering the IOP is the common treatment approach for glaucoma to date, new therapeutic solutions are needed. As noted, previous studies in glaucoma models discuss the role of the complement system for glaucoma pathology. Therefore, the inhibition of it could be a potential therapeutic target. In an OHT model, it could demonstrate that the cobra venom factor (CVF) depleted the complement system and led to a reduced loss of RGCs due to inhibition of intrinsic and extrinsic apoptotic pathways. Furthermore, the treatment with CVF resulted in a diminution of MAC depositions (Jha et al., 2011). Additionally, C5 deficient glaucomatous DBA/2J mice exhibited reduced neurodegeneration in comparison to C5-sufficient animals. Inhibition of complement activation was accompanied by reduced MAC deposition and RGC loss (Howell et al., 2013). Recently, Bosco et al. published a retinal gene therapy approach, where they injected the C3 inhibitor CR2-Crry intravitreally in DBA2/J mice. They revealed a reduction of C3d in RGCs and the inner retinal layers leading to a preservation of RGC somata and axons (Bosco et al., 2018). These results demonstrate the possibility of a complement inhibition for glaucoma treatment.

In terms of microglial inhibition, several studies investigated how minocycline effects microglia in glaucoma models. This semi-synthetic tetracycline can cross the brain-blood-barrier, respectively, the retina-blood-barrier. In neurodegenerative conditions accompanied with neuroinflammation, such as multiple sclerosis or Parkinson's disease, remarkable neuroprotective effects were noted (Kim and Suh, 2009; Russo et al., 2016). In a study, where rats received an intravitreal injection of S100B and were additionally treated with minocycline, loss of RGCs was diminished and a preservation of the optic nerve structure was demonstrated (Kuehn et al., 2018). In OHT models it has been observed that after treatment with either minocycline or a high dose of irradiation, microglia activation was significantly reduced and hence less RGC death was noted (Levkovitch-Verbin et al., 2006; Bosco et al., 2008; Bosco et al., 2012). Minocycline not only prevented the increase of $Iba1^+$ microglia, but also decreased the $GFAP^+$ area and preserved the anterograde transport after OHT (Bordone et al., 2017).

All these promising results underline a contribution of the immune system in glaucoma disease. Nevertheless, more studies are needed to bring these aspects from bench to bedside.

DIFFERENT MODELS FOR SCREENING OF NEUROPROTECTIVE AGENTS

In the following section, we will discuss and elaborate different existing models that are suitable to investigate neuroprotective agents. To this end, this section deals with the pros and contras of different *in vitro* cell lines, primary cells, co-culture systems, as well as organoids. Also, different *in vivo* animal models will be discussed. In addition, an alternative model, namely explanted and cultured retinas of different animals, like pigs and cows, will be introduced (**Figure 2**).

Findings From *in vitro* Cell Culture Studies

Since the underlying molecular pathomechanisms occurring in glaucoma are not fully understood yet, standard therapeutic interventions deal with the deceleration of disease progression and target the main risk factor, namely the elevated IOP. The most common medical therapy for glaucoma are IOP lowering eye drops, which include prostaglandin analogs, beta-blockers, diuretics, cholinergic agonists, and alpha agonists (Narayanaswamy et al., 2007; Conlon et al., 2017). The mechanism of action of those classes of eye drops are different. The most commonly used classes are prostaglandin analogs. An increase of the aqueous humor outflow results in a decreased IOP (Gaton et al., 2001). Since the medical therapy does not always

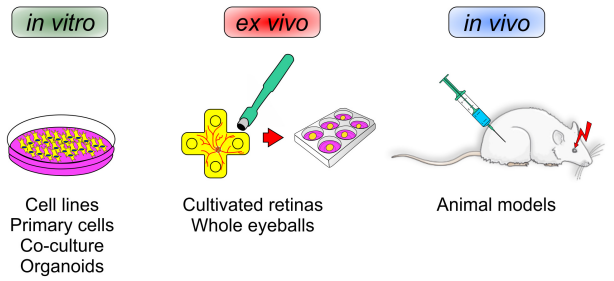

FIGURE 2 | Various mechanisms can influence a loss of retinal ganglion cells. To identify novel neuroprotective treatments for glaucoma, different experimental setups are currently used. *In vitro* analyses reveal the function of new therapeutics on single cells, mixed cultures, or organoids. *Ex vivo* experiments can provide insights into the whole retina, e.g., in cultured porcine/bovine retina. *In vivo* investigations in animals have the advantage to provide a closer look at local and systemic mechanisms and possible side effects.

reduce the IOP sufficiently, other therapy options such as laser treatments and surgical interventions are performed to lower IOP. Laser treatments aim to reduce the IOP in a less invasive manner than e.g., trabeculectomy or drainage implants (Latina et al., 1998; Conlon et al., 2017).

For the evaluation of novel therapies, it is inevitable to have models that on the one hand cover underlying pathomechanisms and on the other hand allow the screening of new therapeutic approaches. Monoclonal *in vivo* cultured cells or cell-lines are, in general, commonly used models for research of several pathomechanisms involved in eye diseases. There are many cell-lines obtained from retinal tissue, like retinal pigment epithelium cells (Liu et al., 2016), retinal microvascular endothelial cells (Xie et al., 2017) and retinal cone photoreceptor cells (Sanchez-Bretano et al., 2017). For example, with the help of the human retinal pigment epithelial cell line ARPE-19, it has recently been shown that baicalin, a flavonoid extract from *Scutellaria baicalensis*, protects against high glucose-induced cell injury such as it occurs in diabetic retinopathy (Dai et al., 2019). Also, cobalt-chloride ($CoCl_2$) damaged ARPE-19-cells were protected by betulinic acid, a pentacyclic triterpenoid with anti-oxidative effects (Cheng et al., 2019). On the other hand, several studies investigate the protective, therapeutic effect of RNA-modulation on degenerative RGCs (Nickells et al., 2017; Yu et al., 2019).

Due to the structure of the retina, which consists of different cell-enriched layers and layers with synaptic connections, homeostasis and interactions of retinal cells are crucial for its integrity and visual signal transduction (Hoon et al., 2014; Grossniklaus et al., 2015). Cell-lines as well as primary monoclonal cultured cells, consisting of only one retinal cell type, are not able to mimic the *in vivo* situation of the retina at all. Furthermore, cell-lines are immortalized which on the one hand simplifies the handling but on the other hand requires manipulated/modified DNA. Modifications of DNA can often be accompanied by further unintended gene alterations. A very prominent example for a cell-line with undefined DNA modifications are RGC-5 cells. RGC-5 cells have been used for researches on RGCs and were introduced as a cell-line derived from rat RGCs (Krishnamoorthy et al., 2001). The expression of RGC-characteristic proteins like Brn-3a or Thy1 was given, but over time many concerns of several laboratories raised, since it was noted that the cells seem to be of murine origin and expressions of several not-RGC-characteristic proteins were observed (Wood et al., 2010; Sippl and Tamm, 2014). The ambiguity of the RGC-5 cell-line as well as the fact that the visual system benefits from the interaction of several retinal cell types, indicates that this cell-line is possibly not the best model for glaucoma research.

Besides, there are several available *in vitro* models of primary mixed cultures of retinal tissue. Li et al. (2015) established a co-culture system of Sprague-Dawley rat retinas together with microglia and Müller cells to evaluate the effect of interactions between microglia and Müller cells on the photoreceptor cell survival. Another model used for investigations on retina are retinal organoids. In those models the goal of research is more the improvement of co-culture systems to investigate retina-RPE dynamics during retinal development. A study by Akhtar et al. (2019) noted that the co-culture of different staged murine RPE cells accelerated photoreceptor differentiation of retinal organoids derived from human-induced pluripotent stem cells. Newly developed mouse multipotent retinal stem cell-derived RGCs, which expresses characteristic RGC-genes, are a suitable model to investigate RGC-aimed gene delivery systems for neuroprotective agents, such as non-viral neurotrophic factor gene therapy (Chen et al., 2019).

Treatment Screening in *in vivo* Models

Most frequently used models for research in general, as well as for ophthalmic research, including glaucoma, are animal models. The first form of retinal degeneration inherited in a mouse model was reported around 90 years ago (Keeler, 1924). Since then, the usage of mouse models for retinal degeneration by genetic modifications increased (Dalke and Graw, 2005; Baehr and Frederick, 2009). Genetics in vertebrates are highly correlated. Especially retinal structure and function of rodents are very similar to those of human: the neuronal cells of the retina and the cell body as well as the synapse distribution and connectivity is comparable in all vertebrate retinae (Hoon et al., 2014). Due to those facts and the short life cycle of rodents, especially mice, make them suitable and very common models for ophthalmic research. Furthermore, the modifications of several genes, to obtain knock-in or knock-out-based diseases, is easy to manage and enables a wide area for diverse research. Inbreeding of animals prevents genetic variability within the mouse strain, which guarantees an equal genetic background of the animals during experiments. Based on this, glaucomatous models, such as the DBA/2J mouse, are used to test new therapeutic approaches such as the flavonoid fisetin. This treatment results in retention of retinal function by suppressing inflammatory response (Li et al., 2019).

Besides the high effort for the bureaucracy, breeding and housing of animals involve higher costs than cell cultures. Despite the genetic similarities within the retina of vertebrates, there are broad disparities between the structure of human and rodent eyes

(Zhou et al., 2007). Not only the size of the eyes differs strongly, also the anatomy of the retina varies. Due to the highest density of cone photoreceptors the fovea centralis, which is located in the center of the macula, is responsible for sharp central vision in humans (Curcio et al., 1990). Rodents, on the other hand, do not have a macula, which makes the research of e.g., age-related macular degeneration much more complicated (Volland et al., 2015). Also, the distribution of rods and cones in the mice retina differs from the human retina. A further difference between the anatomy of rodent and human eyeballs in general is that rodents do not have a real vitreous body: the primary vitreous body recedes completely on postnatal day 30, whereas the secondary vitreous body develops on postnatal day four (Tkatchenko et al., 2010). The lens of rodents is, in comparison to that of humans, much bigger since it fills the whole eye to stabilize it.

In the last few years, many theories for different pathomechanisms leading to glaucoma were discussed. Several rat glaucoma models indicate that the shortage of neurotrophic factors, like BDNF or NGF, in the optic nerve might contribute to the progression of glaucomatous optic nerve degradation (Song et al., 2015). Studies in regard to neurotrophic factors indicate that this might be of interest for glaucoma treatment. The injection as well as the pre-treatment with BDNF lowered RGC loss and suppressed axon loss of glaucomatous rats (Ko et al., 2001; Martin et al., 2003). Another pathomechanism, which seems to be involved in glaucoma disease, is excitotoxicity (Song et al., 2015). To this end, the blockage of excitotoxicity might also be of interest for glaucoma treatment. A well-researched NMDA-receptor antagonist is MK801, which was shown to lower RGC death rate in different glaucoma rat models (Chaudhary et al., 1998; Nucci et al., 2005).

Looking for alternative models, where no classical animal experiments are needed, but similarities to human tissue are still given, it becomes clear that porcine or bovine tissue might serve as a good option.

Ex vivo Organ Culture Models

Due to the high similarities between bovine or porcine and human vision as well as their retinal structure, these retinae seem to be a very promising alternative to animal experiments in ophthalmologic research. An advantage of these eyes is that they are more similar to human eyes than those of rodents. Not only the size is comparable between porcine/bovine and human eyeballs, also the vision, especially of pigs, is more likely to the vision of humans. Humans are trichromats and their cones contain of three different subtypes due to their activation through different wavelengths: they are divided into the short (S)-, the middle (M)-, and the long (L)-cones, depending on the wavelength-sensitivity of the opsins (Nathans et al., 1986). Mice, in contrast, contain of a dichromatic vision, expressing M-cones and ultraviolet-cones (Jacobs et al., 1991). As mice, pigs also have a dichromatic vision, but still the porcine retina and therefore the vision is more like the human vision: porcine cone photoreceptors contain of two opsins, the S- and the M-cones, (Szel et al., 1988; Li et al., 1998; Hendrickson and Hicks, 2002). Even though pigs do not have a real macula, they still have a part in the retina which is very similar to the human macula. This area is called visual streak and is located above the optic disc extending from nasal to the almost temporal edge (Hendrickson and Hicks, 2002). In contrast to classical animal testing, the bureaucracy to use porcine or bovine eyes is much less. In addition, the costs are lower, because porcine and bovine eyes can be obtained from local slaughterhouse, where they are a waste product of the food industry.

Another important advantage of the usage of porcine or bovine retina is, that in contrast to conventional cell culture models, the retina itself can be cultivated for a certain time. The retinal organ culture allows the maintenance of interactions and connections of neurons within the retina. Of course, cultivating retinal organ explants has a time limitation, since the retina, due to the axotomy and the removal of retinal pigment epithelium, cannot be kept alive for a long period *ex vivo*. Nevertheless, during cultivation the nutrient supply can be maintained chemically to alleviate degeneration processes.

Glaucoma is a multifactorial disease where the exact pathomechanisms are not fully understood yet, but it is known that also hypoxic processes as well as oxidative stress are involved in the early progression (Zanon-Moreno et al., 2008; Greco et al., 2016). Chemical substances, such as hydrogen peroxide (H_2O_2) and $CoCl_2$ can be used *in vitro* to simulate this oxidative stress or hypoxic processes (Hurst et al., 2017; Kuehn et al., 2017a). The combination of porcine retina organ culture and chemical simulation of degenerative pathomechanisms *in vitro* is a very well-suited alternative model for ophthalmic research. A commonly used substance, as mentioned above, to mimic oxidative stress, not only in retinal tissue, is $CoCl_2$. It is used for the investigation of the mentioned pathomechanisms as well as possible treatments against it by using several cells of different origin like mesenchymal cells (Yoo et al., 2016), PC12 cells (Hartwig et al., 2014), RPE cells (Li et al., 2013; Cheng et al., 2019), as well as in retinal organ culture (Kuehn et al., 2017a; Maliha et al., 2019). A substance which is frequently used to induce oxidative stress is H_2O_2. This allows the investigation of underlying pathomechanisms and possible neuroprotective substances for various disorders, such as retinal diseases (Cui et al., 2017; Du et al., 2018; Zhao et al., 2019). As shown in previous studies of our group, the addition of H_2O_2 as well as $CoCl_2$ leads to strong neurodegenerative effects in the inner retinal layers of porcine retinae (Hurst et al., 2017; Kuehn et al., 2017a).

For the preparation of a porcine retina organ culture, as mentioned above, porcine eyes are obtained from the local slaughterhouse. Surrounding tissue as well as anterior parts of the eye, are separated from the posterior part of the eye, including the retina. Using a dermal punch, retinal explants are punched out and placed, with the ganglion cell layer facing up, on a millicell insert. The retina is than placed in a 6-well-plate and can be cultivated for up to eight days (**Figure 3A**; Hurst et al., 2017; Kuehn et al., 2017a; Maliha et al., 2019). Simulation of oxidative stress in porcine retina organ culture can be achieved through the addition of H_2O_2 for 3 h at the first day of cultivation (**Figure 3B**). Hypoxic processes, however, can be simulated in porcine retinae, by adding $CoCl_2$ to the medium for 48 h, from day one to day three of

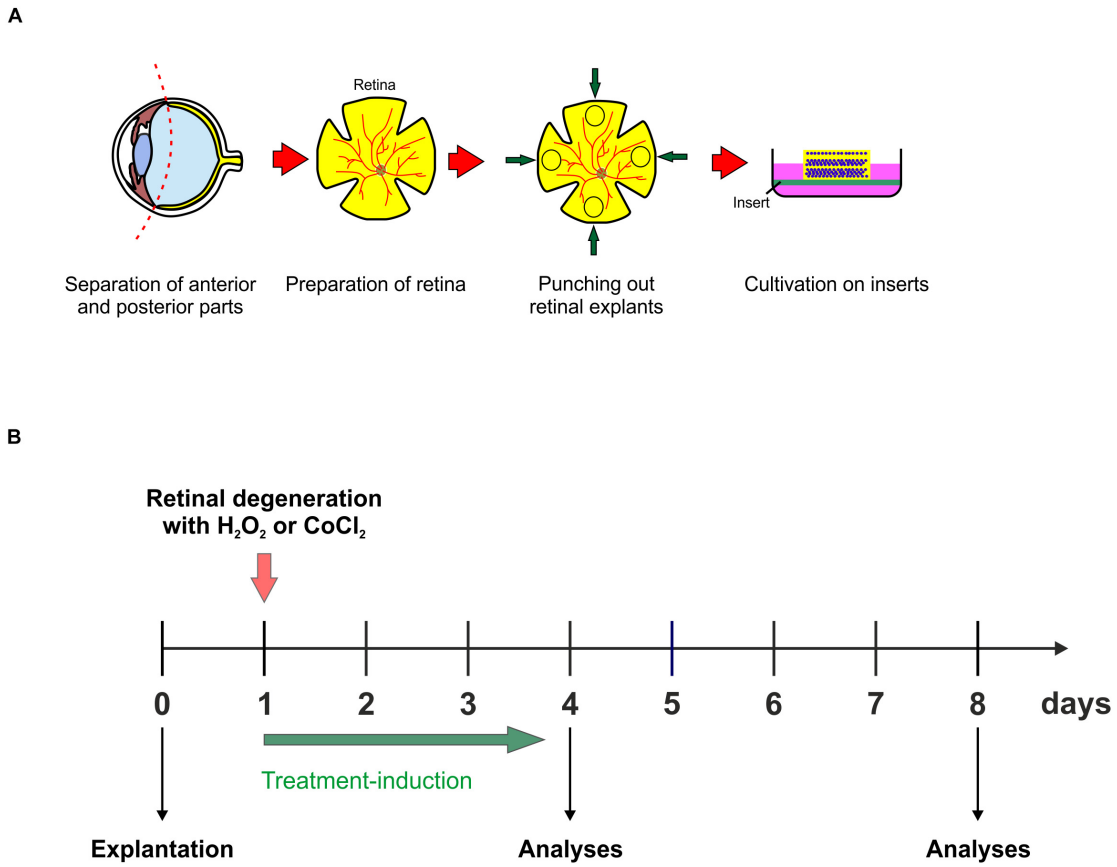

FIGURE 3 | (A) Schematic illustration of the explantation process. Porcine eyes were obtained from the local slaughterhouse. Anterior parts of the eyeball were separated from the posterior, retina containing part of the eye. A dermal punch was used to punch out four retinal explants per eye and cultivated on an insert the ganglion cell layer facing up. **(B)** Retinal explants were cultivated in 6-well plates for up to eight days at 37°C and 5% CO_2. There are two possibilities to induce different pathomechanisms in the retina, which lead to a degeneration of the inner layers. Either with 300 μM H_2O_2 for 3 h to induce oxidative stress on day one of cultivation or with 300 μM $CoCl_2$ for 48 h, starting on day one, to induce hypoxic processes. The best point in time to start therapeutic treatment is at day one, simultaneously to the degeneration via H_2O_2 or $CoCl_2$. The treatment-duration varies, depending on the substance. In the end of the cultivation, retinal explants can be prepared for e.g., immunohistological and qPCR-analyses.

cultivation (**Figure 3B**). $CoCl_2$ as well as H_2O_2 induce strong degenerative effects in retinal tissue, however, both substances have different effects. $CoCl_2$ leads to an early loss of RGCs, which is accompanied by a highly increased apoptosis rate (Kuehn et al., 2017a). Furthermore, $CoCl_2$ enhances the expression of several cellular stress markers like, HIF-1α, HSP70, and iNOS (Maliha et al., 2019). Interestingly, cells of the inner nuclear layers, like amacrine and bipolar cells, are damaged in a later point in time by $CoCl_2$-induced hypoxia. A further pathway which is strongly induced by $CoCl_2$ is apoptosis. Not only the cell cycle arrest gene p21, also caspase 8 and 3, and highly upregulated after the $CoCl_2$-treatment (Maliha et al., 2019). A further cell type which is also affected by $CoCl_2$, are microglia. $CoCl_2$ seems to have toxic effects on microglia, since the attendance of $CoCl_2$ induces a prominent loss of them (Kuehn et al., 2017a). Damaging effects through H_2O_2 on retinal tissue are similar to those seen after $CoCl_2$. The induction of oxidative stress due to H_2O_2 led to a strong loss of RGCs, which was associated with higher RGC apoptosis rate. Cells located in the inner nuclear layer, namely bipolar and amacrine cells, were tendentially decreased after oxidative stress. Interestingly, in contrast to the treatment with $CoCl_2$, H_2O_2 led to a significantly increased microglia cell number as well as induced the activation of these cells. Also, proinflammatory cytokines, such as TNF-α as well as IL-1β, were strongly increased through oxidative stress in retinal organ cultures (Hurst et al., 2017).

The commonly used method for the application of drugs to the eyes are intravitreal injections. Many barriers in the eye itself, like the vitreous body, complicate or even prevent the reaching of the drug to the retina. Here, *ex vivo* bovine eyes can be used to improve or investigate possible enhancements, like nanoparticles, for the drug to reach the retina (Huang et al., 2017; Peynshaert et al., 2017).

Due to the *ex vivo* cultivation, where the retina is separated from the optical nerve and therefore the natural nutrient supply is not taking place anymore, of course, animal experiments cannot be replaced totally by the organ culture. However, the organ culture model in combination with chemical substances, as used

in previous studies by our group and others, seems to be a very promising alternative model for analyzing new therapeutic approaches for ophthalmology and might help to reduce the number of animal experiments. Nevertheless, *in vivo* models will still be necessary for the ophthalmic research, not only for investigations of underlying pathomechanisms in several neuroretinal diseases, but also for the proof of principle of newly tested therapeutics. However, the use of *ex vivo* retina organ culture models is increasing, not only used for treatment screening, but also e.g., to study complement involvement in retinal degeneration (Mohlin et al., 2018). In regard to research on new therapeutics, it was shown that autoantibodies, which are downregulated in the vitreous humor of glaucoma patients, seem to have neuroprotective effects on damaged porcine retinae (Bell et al., 2016). In a study by Maliha et al. (2019) it was described that hypoxic processes due to $CoCl_2$ can be inhibited by mild hypothermia. Cell-stress level as well as apoptotic mechanisms were strongly diminished after hypothermia treatment, leading to a prominent protection of retinal cells. Even toxic effects of $CoCl_2$ on microglia were counteracted by hypothermia. Most interestingly, RGCs, which are affected in glaucoma, were protected by a mild hypothermia due to a significantly decreased apoptosis rate (Maliha et al., 2019).

Taken together, porcine organ culture models seem to be a very promising alternative to conventional animal experiments in the glaucoma research. They are very suitable for the screening of new therapeutic approaches, and therefore can help to reduce the number of animals in the ophthalmic research.

CONCLUSION

The results of all these studies undermine that analyzes in different model systems are necessary in order to decode glaucoma pathogenesis in the near future and thus to develop new therapeutic approaches.

Given the high cost of animal testing and their numerous ethical and legal barriers, alternative approaches are becoming increasingly important. Due to the widespread establishment of various organ cultures, *ex vivo* culture systems are presently available also for glaucoma research, since they can be obtained as by-products of the food industry. *Ex vivo* organ cultures, e.g., from porcine retinae, are also quite suitable for therapy testing. Recently, it was shown that a hypothermic treatment protects RGCs from oxidative stress.

Nonetheless, ophthalmic research will continue to require *in vivo* models, not only to investigate the pathomechanisms, but above all to test new therapeutics. It is of enormous importance that the used *in vivo* model reflects the patient's situation as faithfully as possible. Thus, with regard to glaucoma, it is essential that the various forms of the disease are represented. In the last years, the EAG model was in used to identify mechanisms related to immunological alterations in IOP-independent glaucoma. These animals have a loss of RGCs and optic nerve degeneration plus an enhanced activation of glia cells and complement system proteins. Results point toward the importance especially of the complement system in glaucoma. Immune dysregulation appears to be an important factor for the disease development and progression. Complement and microglia inhibition in the OHT models underlined their potential as future therapeutic approaches. Nevertheless, deeper insights into these mechanisms will lead to better treatment options for glaucoma patients.

AUTHOR CONTRIBUTIONS

All authors wrote sections of the manuscript, read and approved the submitted and revised version of the manuscript.

FUNDING

The studies were supported in part by the Deutsche Forschungsgemeinschaft (DFG, Grant JO-886/1-3), FoRUM (Ruhr-University Bochum), and SET Stiftung.

ACKNOWLEDGMENTS

We are grateful to our collaborators who have contributed to our studies over the years.

REFERENCES

Ajami, B., Bennett, J. L., Krieger, C., Mcnagny, K. M., and Rossi, F. M. (2011). Infiltrating monocytes trigger EAE progression, but do not contribute to the resident microglia pool. *Nat. Neurosci.* 14, 1142–1149. doi: 10.1038/nn.2887

Akhtar, T., Xie, H., Khan, M. I., Zhao, H., Bao, J., Zhang, M., et al. (2019). Accelerated photoreceptor differentiation of hiPSC-derived retinal organoids by contact co-culture with retinal pigment epithelium. *Stem Cell Res.* 39:101491. doi: 10.1016/j.scr.2019.101491

Almasieh, M., Wilson, A. M., Morquette, B., Cueva Vargas, J. L., and Di Polo, A. (2012). The molecular basis of retinal ganglion cell death in glaucoma. *Prog. Retin. Eye Res.* 31, 152–181. doi: 10.1016/j.preteyeres.2011.11.002

Baehr, W., and Frederick, J. M. (2009). Naturally occurring animal models with outer retina phenotypes. *Vision Res.* 49, 2636–2652. doi: 10.1016/j.visres.2009.04.008

Becker, S., Reinehr, S., Burkhard Dick, H., and Joachim, S. C. (2015). [Complement activation after induction of ocular hypertension in an animal model]. *Ophthalmologe* 112, 41–48. doi: 10.1007/s00347-014-3100-6

Bell, K., Gramlich, O. W., Von Thun Und Hohenstein-Blaul, N., Beck, S., Funke, S., Wilding, C., et al. (2013). Does autoimmunity play a part in the pathogenesis of glaucoma? *Prog. Retin. Eye Res.* 36, 199–216. doi: 10.1016/j.preteyeres.2013.02.003

Bell, K., Wilding, C., Funke, S., Perumal, N., Beck, S., Wolters, D., et al. (2016). Neuroprotective effects of antibodies on retinal ganglion cells in an adolescent retina organ culture. *J. Neurochem.* 139, 256–269. doi: 10.1111/jnc.13765

Bell, K., Wilding, C., Funke, S., Pfeiffer, N., and Grus, F. H. (2015). Protective effect of 14-3-3 antibodies on stressed neuroretinal cells via the mitochondrial apoptosis pathway. *BMC Ophthalmol.* 15:64. doi: 10.1186/s12886-015-0044-9

Boehm, N., Beck, S., Lossbrand, U., Pfeiffer, N., and Grus, F. H. (2010). Analysis of complement proteins in retina and sera of glaucoma patients. *Invest. Ophthalmol. Vis. Sci.* 51:5221. doi: 10.1371/journal.pone.0057557

Boehm, N., Wolters, D., Thiel, U., Lossbrand, U., Wiegel, N., Pfeiffer, N., et al. (2012). New insights into autoantibody profiles from immune privileged sites in the eye: a glaucoma study. *Brain Behav. Immun.* 26, 96–102. doi: 10.1016/j.bbi.2011.07.241

Bordone, M. P., Gonzalez Fleitas, M. F., Pasquini, L. A., Bosco, A., Sande, P. H., Rosenstein, R. E., et al. (2017). Involvement of microglia in early axoglial alterations of the optic nerve induced by experimental glaucoma. *J. Neurochem.* 142, 323–337. doi: 10.1111/jnc.14070

Bosco, A., Anderson, S. R., Breen, K. T., Romero, C. O., Steele, M. R., Chiodo, V. A., et al. (2018). Complement C3-targeted gene therapy restricts onset and progression of neurodegeneration in chronic mouse glaucoma. *Mol. Ther.* 26, 2379–2396. doi: 10.1016/j.ymthe.2018.08.017

Bosco, A., Crish, S. D., Steele, M. R., Romero, C. O., Inman, D. M., Horner, P. J., et al. (2012). Early reduction of microglia activation by irradiation in a model of chronic glaucoma. *PLoS One* 7:e43602. doi: 10.1371/journal.pone.0043602

Bosco, A., Inman, D. M., Steele, M. R., Wu, G., Soto, I., Marsh-Armstrong, N., et al. (2008). Reduced retina microglial activation and improved optic nerve integrity with minocycline treatment in the DBA/2J mouse model of glaucoma. *Invest. Ophthalmol. Vis. Sci.* 49, 1437–1446. doi: 10.1167/iovs.07-1337

Bosco, A., Steele, M. R., and Vetter, M. L. (2011). Early microglia activation in a mouse model of chronic glaucoma. *J. Comp. Neurol.* 519, 599–620. doi: 10.1002/cne.22516

Casola, C., Reinehr, S., Kuehn, S., Stute, G., Spiess, B. M., Dick, H. B., et al. (2016). Specific inner retinal layer cell damage in an autoimmune glaucoma model is induced by GDNF with or without HSP27. *Invest. Ophthalmol. Vis. Sci.* 57, 3626–3639. doi: 10.1167/iovs.15-18999R2

Casola, C., Schiwek, J. E., Reinehr, S., Kuehn, S., Grus, F. H., Kramer, M., et al. (2015). S100 alone has the same destructive effect on retinal ganglion cells as in combination with HSP 27 in an autoimmune glaucoma model. *J. Mol. Neurosci.* 56, 228–236. doi: 10.1007/s12031-014-0485-2

Casson, R. J. (2006). Possible role of excitotoxicity in the pathogenesis of glaucoma. *Clin. Exp. Ophthalmol.* 34, 54–63. doi: 10.1111/j.1442-9071.2006.01146.x

Casson, R. J., Chidlow, G., Wood, J. P., Crowston, J. G., and Goldberg, I. (2012). Definition of glaucoma: clinical and experimental concepts. *Clin. Exp. Ophthalmol.* 40, 341–349. doi: 10.1111/j.1442-9071.2012.02773.x

Chang, E. E., and Goldberg, J. L. (2012). Glaucoma 2.0: neuroprotection, neuroregeneration, neuroenhancement. *Ophthalmology* 119, 979–986. doi: 10.1016/j.ophtha.2011.11.003

Chaudhary, P., Ahmed, F., and Sharma, S. C. (1998). MK801-a neuroprotectant in rat hypertensive eyes. *Brain Res.* 792, 154–158. doi: 10.1016/s0006-8993(98)00212-1

Chen, D. W., Narsineni, L., and Foldvari, M. (2019). Multipotent stem cell-derived retinal ganglion cells in 3D culture as tools for neurotrophic factor gene delivery system development. *Nanomedicine* 21:102045. doi: 10.1016/j.nano.2019.102045

Chen, H., Cho, K. S., Vu, T. H. K., Shen, C. H., Kaur, M., Chen, G., et al. (2018). Commensal microflora-induced T cell responses mediate progressive neurodegeneration in glaucoma. *Nat. Commun.* 9:3209. doi: 10.1038/s41467-018-05681-9

Chen, S. J., Lu, P., Zhang, W. F., and Lu, J. H. (2012). High myopia as a risk factor in primary open angle glaucoma. *Int. J. Ophthalmol.* 5, 750–753. doi: 10.3980/j.issn.2222-3959.2012.06.18

Cheng, Z., Yao, W., Zheng, J., Ding, W., Wang, Y., Zhang, T., et al. (2019). A derivative of betulinic acid protects human Retinal Pigment Epithelial (RPE) cells from cobalt chloride-induced acute hypoxic stress. *Exp. Eye Res.* 180, 92–101. doi: 10.1016/j.exer.2018.12.011

Cogswell, J. P., Godlevski, M. M., Wisely, G. B., Clay, W. C., Leesnitzer, L. M., Ways, J. P., et al. (1994). NF-kappa B regulates IL-1 beta transcription through a consensus NF-kappa B binding site and a nonconsensus CRE-like site. *J. Immunol.* 153, 712–723.

Coleman, A. L., and Miglior, S. (2008). Risk factors for glaucoma onset and progression. *Surv. Ophthalmol.* 53(Suppl. 1), S3–S10. doi: 10.1016/j.survophthal.2008.08.006

Collard, C. D., Lekowski, R., Jordan, J. E., Agah, A., and Stahl, G. L. (1999). Complement activation following oxidative stress. *Mol. Immunol.* 36, 941–948. doi: 10.1016/s0161-5890(99)00116-9

Conlon, R., Saheb, H., and Ahmed, I. I. (2017). Glaucoma treatment trends: a review. *Can. J. Ophthalmol.* 52, 114–124. doi: 10.1016/j.jcjo.2016.07.013

Cui, Y., Xu, N., Xu, W., and Xu, G. (2017). Mesenchymal stem cells attenuate hydrogen peroxide-induced oxidative stress and enhance neuroprotective effects in retinal ganglion cells. *In Vitro Cell. Dev. Biol. Anim.* 53, 328–335. doi: 10.1007/s11626-016-0115-0

Curcio, C. A., Sloan, K. R., Kalina, R. E., and Hendrickson, A. E. (1990). Human photoreceptor topography. *J. Comp. Neurol.* 292, 497–523. doi: 10.1002/cne.902920402

Dai, C., Jiang, S., Chu, C., Xin, M., Song, X., and Zhao, B. (2019). Baicalin protects human retinal pigment epithelial cell lines against high glucose-induced cell injury by up-regulation of microRNA-145. *Exp. Mol. Pathol.* 106, 123–130. doi: 10.1016/j.yexmp.2019.01.002

Dalke, C., and Graw, J. (2005). Mouse mutants as models for congenital retinal disorders. *Exp. Eye Res.* 81, 503–512. doi: 10.1016/j.exer.2005.06.004

de Hoz, R., Ramirez, A. I., Gonzalez-Martin, R., Ajoy, D., Rojas, B., Salobrar-Garcia, E., et al. (2018). Bilateral early activation of retinal microglial cells in a mouse model of unilateral laser-induced experimental ocular hypertension. *Exp. Eye Res.* 171, 12–29. doi: 10.1016/j.exer.2018.03.006

Dodel, R., Balakrishnan, K., Keyvani, K., Deuster, O., Neff, F., Andrei-Selmer, L. C., et al. (2011). Naturally occurring autoantibodies against beta-amyloid: investigating their role in transgenic animal and in vitro models of Alzheimer's disease. *J. Neurosci.* 31, 5847–5854. doi: 10.1523/JNEUROSCI.4401-10.2011

Dreyer, E. B., Zurakowski, D., Schumer, R. A., Podos, S. M., and Lipton, S. A. (1996). Elevated glutamate levels in the vitreous body of humans and monkeys with glaucoma. *Arch. Ophthalmol.* 114, 299–305.

Du, W., An, Y., He, X., Zhang, D., and He, W. (2018). Protection of kaempferol on oxidative stress-induced retinal pigment epithelial cell damage. *Oxid. Med. Cell. Longev.* 2018:1610751. doi: 10.1155/2018/1610751

Ebneter, A., Casson, R. J., Wood, J. P., and Chidlow, G. (2010). Microglial activation in the visual pathway in experimental glaucoma: spatiotemporal characterization and correlation with axonal injury. *Invest. Ophthalmol. Vis. Sci.* 51, 6448–6460. doi: 10.1167/iovs.10-5284

EGS (2017). European glaucoma society terminology and guidelines for glaucoma, 4th edition - chapter 2: classification and terminology. *Br. J. Ophthalmol.* 101, 73–127. doi: 10.1136/bjophthalmol-2016-egsguideline.002

Ehrnthaller, C., Ignatius, A., Gebhard, F., and Huber-Lang, M. (2011). New insights of an old defense system: structure, function, and clinical relevance of the complement system. *Mol. Med.* 17, 317–329. doi: 10.2119/molmed.2010.00149

Elliott, C., Lindner, M., Arthur, A., Brennan, K., Jarius, S., Hussey, J., et al. (2012). Functional identification of pathogenic autoantibody responses in patients with multiple sclerosis. *Brain* 135, 1819–1833. doi: 10.1093/brain/aws105

Evangelho, K., Mogilevskaya, M., Losada-Barragan, M., and Vargas-Sanchez, J. K. (2019). Pathophysiology of primary open-angle glaucoma from a neuroinflammatory and neurotoxicity perspective: a review of the literature. *Int. Ophthalmol.* 39, 259–271. doi: 10.1007/s10792-017-0795-9

Finger, R. P., Fimmers, R., Holz, F. G., and Scholl, H. P. (2011). Incidence of blindness and severe visual impairment in Germany: projections for 2030. *Invest. Ophthalmol. Vis. Sci.* 52, 4381–4389. doi: 10.1167/iovs.10-6987

Fosbrink, M., Niculescu, F., and Rus, H. (2005). The role of c5b-9 terminal complement complex in activation of the cell cycle and transcription. *Immunol. Res.* 31, 37–46. doi: 10.1385/ir:31:1:37

Fuhrmann, M., Bittner, T., Jung, C. K., Burgold, S., Page, R. M., Mitteregger, G., et al. (2010). Microglial Cx3cr1 knockout prevents neuron loss in a mouse model of Alzheimer's disease. *Nat. Neurosci.* 13, 411–413. doi: 10.1038/nn.2511

Gaton, D. D., Sagara, T., Lindsey, J. D., Gabelt, B. T., Kaufman, P. L., and Weinreb, R. N. (2001). Increased matrix metalloproteinases 1, 2, and 3 in the monkey uveoscleral outflow pathway after topical prostaglandin F(2 alpha)-isopropyl ester treatment. *Arch. Ophthalmol.* 119, 1165–1170.

Graeber, M. B., and Streit, W. J. (2010). Microglia: biology and pathology. *Acta Neuropathol.* 119, 89–105. doi: 10.1007/s00401-009-0622-0

Gramlich, O. W., Beck, S., Von Thun Und Hohenstein-Blaul, N., Boehm, N., Ziegler, A., Vetter, J. M., et al. (2013). Enhanced insight into the autoimmune component of glaucoma: IgG autoantibody accumulation and pro-inflammatory conditions in human glaucomatous retina. *PLoS One* 8:e57557. doi: 10.1371/journal.pone.0057557

Gramlich, O. W., Teister, J., Neumann, M., Tao, X., Beck, S., Von Pein, H. D., et al. (2016). Immune response after intermittent minimally invasive intraocular pressure elevations in an experimental animal model of glaucoma. *J. Neuroinflammation* 13:82. doi: 10.1186/s12974-016-0542-6

Greco, A., Rizzo, M. I., De Virgilio, A., Gallo, A., Fusconi, M., and De Vincentiis, M. (2016). Emerging concepts in glaucoma and review of the literature. *Am. J. Med.* 129, 1000.e7–1000.e13. doi: 10.1016/j.amjmed.2016.03.038

Grodum, K., Heijl, A., and Bengtsson, B. (2002). A comparison of glaucoma patients identified through mass screening and in routine clinical practice. *Acta Ophthalmol. Scand.* 80, 627–631. doi: 10.1034/j.1600-0420.2002.800613.x

Grossniklaus, H. E., Geisert, E. E., and Nickerson, J. M. (2015). Introduction to the retina. *Prog. Mol. Biol. Transl. Sci.* 134, 383–396. doi: 10.1016/bs.pmbts.2015.06.001

Grus, F. H., Joachim, S. C., Bruns, K., Lackner, K. J., Pfeiffer, N., and Wax, M. B. (2006). Serum autoantibodies to alpha-fodrin are present in glaucoma patients from Germany and the United States. *Invest. Ophthalmol. Vis. Sci.* 47, 968–976.

Grus, F. H., Joachim, S. C., Hoffmann, E. M., and Pfeiffer, N. (2004). Complex autoantibody repertoires in patients with glaucoma. *Mol. Vis.* 10, 132–137.

Grus, F. H., Joachim, S. C., Wuenschig, D., Rieck, J., and Pfeiffer, N. (2008). Autoimmunity and glaucoma. *J. Glaucoma* 17, 79–84. doi: 10.1097/ijg.0b013e318156a592

Hartwig, K., Fackler, V., Jaksch-Bogensperger, H., Winter, S., Furtner, T., Couillard-Despres, S., et al. (2014). Cerebrolysin protects PC12 cells from CoCl2-induced hypoxia employing GSK3beta signaling. *Int. J. Dev. Neurosci.* 38, 52–58. doi: 10.1016/j.ijdevneu.2014.07.005

Hendrickson, A., and Hicks, D. (2002). Distribution and density of medium- and short-wavelength selective cones in the domestic pig retina. *Exp. Eye Res.* 74, 435–444. doi: 10.1006/exer.2002.1181

Hoon, M., Okawa, H., Della Santina, L., and Wong, R. O. (2014). Functional architecture of the retina: development and disease. *Prog. Retin. Eye Res.* 42, 44–84. doi: 10.1016/j.preteyeres.2014.06.003

Howell, G. R., Macalinao, D. G., Sousa, G. L., Walden, M., Soto, I., Kneeland, S. C., et al. (2011). Molecular clustering identifies complement and endothelin induction as early events in a mouse model of glaucoma. *J. Clin. Invest.* 121, 1429–1444. doi: 10.1172/JCI44646

Howell, G. R., Soto, I., Ryan, M., Graham, L. C., Smith, R. S., and John, S. W. (2013). Deficiency of complement component 5 ameliorates glaucoma in DBA/2J mice. *J. Neuroinflammation* 10:76. doi: 10.1186/1742-2094-10-76

Hu, S. J., Calippe, B., Lavalette, S., Roubeix, C., Montassar, F., Housset, M., et al. (2015). Upregulation of P2RX7 in Cx3cr1-deficient mononuclear phagocytes leads to increased interleukin-1beta secretion and photoreceptor neurodegeneration. *J. Neurosci.* 35, 6987–6996. doi: 10.1523/JNEUROSCI.3955-14.2015

Huang, D., Chen, Y. S., Thakur, S. S., and Rupenthal, I. D. (2017). Ultrasound-mediated nanoparticle delivery across ex vivo bovine retina after intravitreal injection. *Eur. J. Pharm. Biopharm.* 119, 125–136. doi: 10.1016/j.ejpb.2017.06.009

Hurst, J., Kuehn, S., Jashari, A., Tsai, T., Bartz-Schmidt, K. U., Schnichels, S., et al. (2017). A novel porcine ex vivo retina culture model for oxidative stress induced by H(2)O(2). *Altern. Lab. Anim.* 45, 11–25. doi: 10.1177/026119291704500105

Jacobs, G. H., Neitz, J., and Deegan, J. F. II (1991). Retinal receptors in rodents maximally sensitive to ultraviolet light. *Nature* 353, 655–656. doi: 10.1038/353655a0

Jha, P., Banda, H., Tytarenko, R., Bora, P. S., and Bora, N. S. (2011). Complement mediated apoptosis leads to the loss of retinal ganglion cells in animal model of glaucoma. *Mol. Immunol.* 48, 2151–2158. doi: 10.1016/j.molimm.2011.07.012

Jiao, H., Natoli, R., Valter, K., Provis, J. M., and Rutar, M. (2015). Spatiotemporal cadence of macrophage polarisation in a model of light-induced retinal degeneration. *PLoS One* 10:e0143952. doi: 10.1371/journal.pone.0143952

Joachim, S. C., Bruns, K., Lackner, K. J., Pfeiffer, N., and Grus, F. H. (2007). Antibodies to alpha B-crystallin, vimentin, and heat shock protein 70 in aqueous humor of patients with normal tension glaucoma and IgG antibody patterns against retinal antigen in aqueous humor. *Curr. Eye Res.* 32, 501–509. doi: 10.1080/02713680701375183

Joachim, S. C., Gramlich, O. W., Laspas, P., Schmid, H., Beck, S., Von Pein, H. D., et al. (2012). Retinal ganglion cell loss is accompanied by antibody depositions and increased levels of microglia after immunization with retinal antigens. *PLoS One* 7:e40616. doi: 10.1371/journal.pone.0040616

Joachim, S. C., Mondon, C., Gramlich, O. W., Grus, F. H., and Dick, H. B. (2014). Apoptotic retinal ganglion cell death in an autoimmune glaucoma model is accompanied by antibody depositions. *J. Mol. Neurosci.* 52, 216–224. doi: 10.1007/s12031-013-0125-2

Joachim, S. C., Pfeiffer, N., and Grus, F. H. (2005). Autoantibodies in patients with glaucoma: a comparison of IgG serum antibodies against retinal, optic nerve, and optic nerve head antigens. *Graefes Arch. Clin. Exp. Ophthalmol.* 243, 817–823. doi: 10.1007/s00417-004-1094-5

Joachim, S. C., Reichelt, J., Berneiser, S., Pfeiffer, N., and Grus, F. H. (2008). Sera of glaucoma patients show autoantibodies against myelin basic protein and complex autoantibody profiles against human optic nerve antigens. *Graefes Arch. Clin. Exp. Ophthalmol.* 246, 573–580. doi: 10.1007/s00417-007-0737-8

Karlstetter, M., Scholz, R., Rutar, M., Wong, W. T., Provis, J. M., and Langmann, T. (2015). Retinal microglia: just bystander or target for therapy? *Prog. Retin. Eye Res.* 45, 30–57. doi: 10.1016/j.preteyeres.2014.11.004

Kataoka, K., Matsumoto, H., Kaneko, H., Notomi, S., Takeuchi, K., Sweigard, J. H., et al. (2015). Macrophage- and RIP3-dependent inflammasome activation exacerbates retinal detachment-induced photoreceptor cell death. *Cell Death Dis.* 6:e1731. doi: 10.1038/cddis.2015.73

Keeler, C. E. (1924). The inheritance of a retinal abnormality in white mice. *Proc. Natl. Acad. Sci. U.S.A.* 10, 329–333. doi: 10.1073/pnas.10.7.329

Kerr, E. C., Copland, D. A., Dick, A. D., and Nicholson, L. B. (2008). The dynamics of leukocyte infiltration in experimental autoimmune uveoretinitis. *Prog. Retin. Eye Res.* 27, 527–535. doi: 10.1016/j.preteyeres.2008.07.001

Kerrigan-Baumrind, L. A., Quigley, H. A., Pease, M. E., Kerrigan, D. F., and Mitchell, R. S. (2000). Number of ganglion cells in glaucoma eyes compared with threshold visual field tests in the same persons. *Invest. Ophthalmol. Vis. Sci.* 41, 741–748.

Kettenmann, H., Hanisch, U. K., Noda, M., and Verkhratsky, A. (2011). Physiology of microglia. *Physiol. Rev.* 91, 461–553. doi: 10.1152/physrev.00011.2010

Kim, H. S., and Suh, Y. H. (2009). Minocycline and neurodegenerative diseases. *Behav. Brain Res.* 196, 168–179. doi: 10.1016/j.bbr.2008.09.040

Ko, M. L., Hu, D. N., Ritch, R., Sharma, S. C., and Chen, C. F. (2001). Patterns of retinal ganglion cell survival after brain-derived neurotrophic factor administration in hypertensive eyes of rats. *Neurosci. Lett.* 305, 139–142. doi: 10.1016/s0304-3940(01)01830-4

Kreutzberg, G. W. (1995). Microglia, the first line of defence in brain pathologies. *Arzneimittelforschung* 45, 357–360.

Krishnamoorthy, R. R., Agarwal, P., Prasanna, G., Vopat, K., Lambert, W., Sheedlo, H. J., et al. (2001). Characterization of a transformed rat retinal ganglion cell line. *Brain Res. Mol. Brain Res.* 86, 1–12. doi: 10.1016/s0169-328x(00)00224-2

Krumbholz, M., Derfuss, T., Hohlfeld, R., and Meinl, E. (2012). B cells and antibodies in multiple sclerosis pathogenesis and therapy. *Nat. Rev. Neurol.* 8, 613–623. doi: 10.1038/nrneurol.2012.203

Kuehn, M. H., Kim, C. Y., Ostojic, J., Bellin, M., Alward, W. L., Stone, E. M., et al. (2006). Retinal synthesis and deposition of complement components induced by ocular hypertension. *Exp. Eye Res.* 83, 620–628. doi: 10.1016/j.exer.2006.03.002

Kuehn, S., Grotegut, P., Smit, A., Stute, G., Dick, H. B., and Joachim, S. C. (2018). Important role of microglia in a novel S100B based retina degeneration model. *Invest. Ophthalmol. Vis. Sci.* 59:4500.

Kuehn, S., Hurst, J., Rensinghoff, F., Tsai, T., Grauthoff, S., Satgunarajah, Y., et al. (2017a). Degenerative effects of cobalt-chloride treatment on neurons and microglia in a porcine retina organ culture model. *Exp. Eye Res.* 155, 107–120. doi: 10.1016/j.exer.2017.01.003

Kuehn, S., Rodust, C., Stute, G., Grotegut, P., Meissner, W., Reinehr, S., et al. (2017b). Concentration-dependent inner retina layer damage and optic nerve degeneration in a NMDA model. *J. Mol. Neurosci.* 63, 283–299. doi: 10.1007/s12031-017-0978-x

Lang, G. K. (2014). *Augenheilkunde*. Stuttgart: Thieme.

Laspas, P., Gramlich, O. W., Muller, H. D., Cuny, C. S., Gottschling, P. F., Pfeiffer, N., et al. (2011). Autoreactive antibodies and loss of retinal ganglion cells in rats induced by immunization with ocular antigens. *Invest. Ophthalmol. Vis. Sci.* 52, 8835–8848. doi: 10.1167/iovs.10-6889

Latina, M. A., Sibayan, S. A., Shin, D. H., Noecker, R. J., and Marcellino, G. (1998). Q-switched 532-nm Nd:YAG laser trabeculoplasty (selective laser trabeculoplasty): a multicenter, pilot, clinical study. *Ophthalmology* 105, 2082–2088; discussion 2089–2090.

Lavalette, S., Raoul, W., Houssier, M., Camelo, S., Levy, O., Calippe, B., et al. (2011). Interleukin-1beta inhibition prevents choroidal neovascularization and does not exacerbate photoreceptor degeneration. *Am. J. Pathol.* 178, 2416–2423. doi: 10.1016/j.ajpath.2011.01.013

Levkovitch-Verbin, H., Kalev-Landoy, M., Habot-Wilner, Z., and Melamed, S. (2006). Minocycline delays death of retinal ganglion cells in experimental glaucoma and after optic nerve transection. *Arch. Ophthalmol.* 124, 520–526.

Li, K. R., Zhang, Z. Q., Yao, J., Zhao, Y. X., Duan, J., Cao, C., et al. (2013). Ginsenoside Rg-1 protects retinal pigment epithelium (RPE) cells from cobalt chloride (CoCl2) and hypoxia assaults. *PLoS One* 8:e84171. doi: 10.1371/journal.pone.0084171

Li, L., Qin, J., Fu, T., and Shen, J. (2019). Fisetin rescues retinal functions by suppressing inflammatory response in a DBA/2J mouse model of glaucoma. *Doc. Ophthalmol.* 138, 125–135. doi: 10.1007/s10633-019-09676-9

Li, L., Qu, C., and Wang, F. (2015). A novel method for co-culture with Muller cells and microglia in rat retina in vitro. *Biomed. Rep.* 3, 25–27. doi: 10.3892/br.2014.370

Li, Z. Y., Wong, F., Chang, J. H., Possin, D. E., Hao, Y., Petters, R. M., et al. (1998). Rhodopsin transgenic pigs as a model for human retinitis pigmentosa. *Invest. Ophthalmol. Vis. Sci.* 39, 808–819.

Liao, K. P., Kurreeman, F., Li, G., Duclos, G., Murphy, S., Guzman, R., et al. (2013). Associations of autoantibodies, autoimmune risk alleles, and clinical diagnoses from the electronic medical records in rheumatoid arthritis cases and non-rheumatoid arthritis controls. *Arthritis Rheum.* 65, 571–581. doi: 10.1002/art.37801

Liu, X., Xie, J., Liu, Z., Gong, Q., Tian, R., and Su, G. (2016). Identification and validation of reference genes for quantitative RT-PCR analysis of retinal pigment epithelium cells under hypoxia and/or hyperglycemia. *Gene* 580, 41–46. doi: 10.1016/j.gene.2016.01.001

Maliha, A. M., Kuehn, S., Hurst, J., Herms, F., Fehr, M., Bartz-Schmidt, K. U., et al. (2019). Diminished apoptosis in hypoxic porcine retina explant cultures through hypothermia. *Sci. Rep.* 9:4898. doi: 10.1038/s41598-019-41113-4

Martin, K. R., Quigley, H. A., Zack, D. J., Levkovitch-Verbin, H., Kielczewski, J., Valenta, D., et al. (2003). Gene therapy with brain-derived neurotrophic factor as a protection: retinal ganglion cells in a rat glaucoma model. *Invest. Ophthalmol. Vis. Sci.* 44, 4357–4365.

Martus, P., Stroux, A., Budde, W. M., Mardin, C. Y., Korth, M., and Jonas, J. B. (2005). Predictive factors for progressive optic nerve damage in various types of chronic open-angle glaucoma. *Am. J. Ophthalmol.* 139, 999–1009. doi: 10.1016/j.ajo.2004.12.056

Maruyama, I., Ohguro, H., and Ikeda, Y. (2000). Retinal ganglion cells recognized by serum autoantibody against gamma-enolase found in glaucoma patients. *Invest. Ophthalmol. Vis. Sci.* 41, 1657–1665.

Matsushita, M., Thiel, S., Jensenius, J. C., Terai, I., and Fujita, T. (2000). Proteolytic activities of two types of mannose-binding lectin-associated serine protease. *J. Immunol.* 165, 2637–2642. doi: 10.4049/jimmunol.165.5.2637

McMonnies, C. W. (2017). Glaucoma history and risk factors. *J. Optom.* 10, 71–78.

Mitchell, P., Smith, W., Attebo, K., and Healey, P. R. (1996). Prevalence of open-angle glaucoma in Australia. The blue mountains eye study. *Ophthalmology* 103, 1661–1669. doi: 10.1016/s0161-6420(96)30449-1

Mohlin, C., Sandholm, K., Kvanta, A., Ekdahl, K. N., and Johansson, K. (2018). A model to study complement involvement in experimental retinal degeneration. *Ups. J. Med. Sci.* 123, 28–42. doi: 10.1080/03009734.2018.1431744

Murphy, K. T., and Walport, M. (2008). *Janeway's Immunobiology*. Milton Park: Taylor & Francis Ltd.

Narayanaswamy, A., Neog, A., Baskaran, M., George, R., Lingam, V., Desai, C., et al. (2007). A randomized, crossover, open label pilot study to evaluate the efficacy and safety of Xalatan in comparison with generic Latanoprost (Latoprost) in subjects with primary open angle glaucoma or ocular hypertension. *Indian J. Ophthalmol.* 55, 127–131.

Nathans, J., Thomas, D., and Hogness, D. S. (1986). Molecular genetics of human color vision: the genes encoding blue, green, and red pigments. *Science* 232, 193–202. doi: 10.1126/science.2937147

Natoli, R., Fernando, N., Madigan, M., Chu-Tan, J. A., Valter, K., Provis, J., et al. (2017). Microglia-derived IL-1beta promotes chemokine expression by Muller cells and RPE in focal retinal degeneration. *Mol. Neurodegener.* 12:31. doi: 10.1186/s13024-017-0175-y

Nauta, A. J., Raaschou-Jensen, N., Roos, A., Daha, M. R., Madsen, H. O., Borrias-Essers, M. C., et al. (2003). Mannose-binding lectin engagement with late apoptotic and necrotic cells. *Eur. J. Immunol.* 33, 2853–2863. doi: 10.1002/eji.200323888

Nesargikar, P. N., Spiller, B., and Chavez, R. (2012). The complement system: history, pathways, cascade and inhibitors. *Eur. J. Microbiol. Immunol.* 2, 103–111. doi: 10.1556/EuJMI.2.2012.2.2

Neufeld, A. H., Hernandez, M. R., and Gonzalez, M. (1997). Nitric oxide synthase in the human glaucomatous optic nerve head. *Arch. Ophthalmol.* 115, 497–503.

Nickells, R. W., Schmitt, H. M., Maes, M. E., and Schlamp, C. L. (2017). AAV2-mediated transduction of the mouse retina after optic nerve injury. *Invest. Ophthalmol. Vis. Sci.* 58, 6091–6104. doi: 10.1167/iovs.17-22634

Noristani, R., Kuehn, S., Stute, G., Reinehr, S., Stellbogen, M., Dick, H. B., et al. (2016). Retinal and optic nerve damage is associated with early glial responses in an experimental autoimmune glaucoma model. *J. Mol. Neurosci.* 58, 470–482. doi: 10.1007/s12031-015-0707-2

Nucci, C., Tartaglione, R., Rombola, L., Morrone, L. A., Fazzi, E., and Bagetta, G. (2005). Neurochemical evidence to implicate elevated glutamate in the mechanisms of high intraocular pressure (IOP)-induced retinal ganglion cell death in rat. *Neurotoxicology* 26, 935–941. doi: 10.1016/j.neuro.2005.06.002

Ogden, C. A., Decathelineau, A., Hoffmann, P. R., Bratton, D., Ghebrehiwet, B., Fadok, V. A., et al. (2001). C1q and mannose binding lectin engagement of cell surface calreticulin and CD91 initiates macropinocytosis and uptake of apoptotic cells. *J. Exp. Med.* 194, 781–795.

Ouchi, Y., Yoshikawa, E., Sekine, Y., Futatsubashi, M., Kanno, T., Ogusu, T., et al. (2005). Microglial activation and dopamine terminal loss in early Parkinson's disease. *Ann. Neurol.* 57, 168–175. doi: 10.1002/ana.20338

Pascale, A., Drago, F., and Govoni, S. (2012). Protecting the retinal neurons from glaucoma: lowering ocular pressure is not enough. *Pharmacol. Res.* 66, 19–32. doi: 10.1016/j.phrs.2012.03.002

Peynshaert, K., Devoldere, J., Forster, V., Picaud, S., Vanhove, C., De Smedt, S. C., et al. (2017). Toward smart design of retinal drug carriers: a novel bovine retinal explant model to study the barrier role of the vitreoretinal interface. *Drug Deliv.* 24, 1384–1394. doi: 10.1080/10717544.2017.1375578

Quigley, H. A. (1993). Open-angle glaucoma. *N. Engl. J. Med.* 328, 1097–1106.

Quigley, H. A., and Broman, A. T. (2006). The number of people with glaucoma worldwide in 2010 and 2020. *Br. J. Ophthalmol.* 90, 262–267. doi: 10.1136/bjo.2005.081224

Quigley, H. A., and Jampel, H. D. (2003). How are glaucoma patients identified? *J. Glaucoma* 12, 451–455. doi: 10.1097/00061198-200312000-00001

Ramirez, A. I., De Hoz, R., Salobrar-Garcia, E., Salazar, J. J., Rojas, B., Ajoy, D., et al. (2017). The role of microglia in retinal neurodegeneration: Alzheimer's disease, Parkinson, and glaucoma. *Front. Aging Neurosci.* 9:214. doi: 10.3389/fnagi.2017.00214

Rao, N. A., Kimoto, T., Zamir, E., Giri, R., Wang, R., Ito, S., et al. (2003). Pathogenic role of retinal microglia in experimental uveoretinitis. *Invest. Ophthalmol. Vis. Sci.* 44, 22–31.

Reinehr, S., Kuehn, S., Casola, C., Koch, D., Stute, G., Grotegut, P., et al. (2018a). HSP27 immunization reinforces AII amacrine cell and synapse damage induced by S100 in an autoimmune glaucoma model. *Cell Tissue Res.* 371, 237–249. doi: 10.1007/s00441-017-2710-0

Reinehr, S., Reinhard, J., Gandej, M., Gottschalk, I., Stute, G., Faissner, A., et al. (2018b). S100B immunization triggers NFκB and complement activation in an autoimmune glaucoma model. *Sci. Rep.* 8:9821. doi: 10.1038/s41598-018-28183-6

Reinehr, S., Reinhard, J., Gandej, M., Kuehn, S., Noristani, R., Faissner, A., et al. (2016a). Simultaneous complement response via lectin pathway in retina and optic nerve in an experimental autoimmune glaucoma model. *Front. Cell. Neurosci.* 10:140. doi: 10.3389/fncel.2016.00140

Reinehr, S., Reinhard, J., Wiemann, S., Stute, G., Kuehn, S., Woestmann, J., et al. (2016b). Early remodelling of the extracellular matrix proteins tenascin-C and phosphacan in retina and optic nerve of an experimental autoimmune glaucoma model. *J. Cell. Mol. Med.* 20, 2122–2137. doi: 10.1111/jcmm.12909

Rojas, B., Gallego, B. I., Ramirez, A. I., Salazar, J. J., De Hoz, R., Valiente-Soriano, F. J., et al. (2014). Microglia in mouse retina contralateral to experimental glaucoma exhibit multiple signs of activation in all retinal layers. *J. Neuroinflammation* 11:133. doi: 10.1186/1742-2094-11-133

Russo, R., Varano, G. P., Adornetto, A., Nucci, C., Corasaniti, M. T., Bagetta, G., et al. (2016). Retinal ganglion cell death in glaucoma: exploring the role of neuroinflammation. *Eur. J. Pharmacol.* 787, 134–142. doi: 10.1016/j.ejphar.2016.03.064

Sanchez-Bretano, A., Baba, K., Janjua, U., Piano, I., Gargini, C., and Tosini, G. (2017). Melatonin partially protects 661W cells from H_2O_2-induced death by inhibiting Fas/FasL-caspase-3. *Mol. Vis.* 23, 844–852.

Schmid, H., Renner, M., Dick, H. B., and Joachim, S. C. (2014). Loss of inner retinal neurons after retinal ischemia in rats. *Invest. Ophthalmol. Vis. Sci.* 55, 2777–2787. doi: 10.1167/iovs.13-13372

Sippl, C., and Tamm, E. R. (2014). What is the nature of the RGC-5 cell line? *Adv. Exp. Med. Biol.* 801, 145–154. doi: 10.1007/978-1-4614-3209-8_19

Sommer, A., Tielsch, J. M., Katz, J., Quigley, H. A., Gottsch, J. D., Javitt, J., et al. (1991). Relationship between intraocular pressure and primary open angle glaucoma among white and black Americans. The Baltimore eye survey. *Arch. Ophthalmol.* 109, 1090–1095.

Song, W., Huang, P., and Zhang, C. (2015). Neuroprotective therapies for glaucoma. *Drug Des. Devel. Ther.* 9, 1469–1479. doi: 10.2147/DDDT.S80594

Sontheimer, R. D., Racila, E., and Racila, D. M. (2005). C1q: its functions within the innate and adaptive immune responses and its role in lupus autoimmunity. *J. Invest. Dermatol.* 125, 14–23. doi: 10.1111/j.0022-202x.2005.23673.x

Stasi, K., Nagel, D., Yang, X., Wang, R. F., Ren, L., Podos, S. M., et al. (2006). Complement component 1Q (C1Q) upregulation in retina of murine, primate, and human glaucomatous eyes. *Invest. Ophthalmol. Vis. Sci.* 47, 1024–1029.

Stevens, G. A., White, R. A., Flaxman, S. R., Price, H., Jonas, J. B., Keeffe, J., et al. (2013). Global prevalence of vision impairment and blindness: magnitude and temporal trends, 1990-2010. *Ophthalmology* 120, 2377–2384.

Stuart, L. M., Takahashi, K., Shi, L., Savill, J., and Ezekowitz, R. A. (2005). Mannose-binding lectin-deficient mice display defective apoptotic cell clearance but no autoimmune phenotype. *J. Immunol.* 174, 3220–3226. doi: 10.4049/jimmunol.174.6.3220

Szel, A., Diamantstein, T., and Rohlich, P. (1988). Identification of the blue-sensitive cones in the mammalian retina by anti-visual pigment antibody. *J. Comp. Neurol.* 273, 593–602. doi: 10.1002/cne.902730413

Takahashi, M., Iwaki, D., Kanno, K., Ishida, Y., Xiong, J., Matsushita, M., et al. (2008). Mannose-binding lectin (MBL)-associated serine protease (MASP)-1 contributes to activation of the lectin complement pathway. *J. Immunol.* 180, 6132–6138. doi: 10.4049/jimmunol.180.9.6132

Tezel, G. (2011). The immune response in glaucoma: a perspective on the roles of oxidative stress. *Exp. Eye Res.* 93, 178–186. doi: 10.1016/j.exer.2010.07.009

Tezel, G., Seigel, G. M., and Wax, M. B. (1998). Autoantibodies to small heat shock proteins in glaucoma. *Invest. Ophthalmol. Vis. Sci.* 39, 2277–2287.

Tezel, G., and Wax, M. B. (2004). The immune system and glaucoma. *Curr. Opin. Ophthalmol.* 15, 80–84. doi: 10.1097/00055735-200404000-00003

Tezel, G., Yang, X., Luo, C., Kain, A. D., Powell, D. W., Kuehn, M. H., et al. (2010). Oxidative stress and the regulation of complement activation in human glaucoma. *Invest. Ophthalmol. Vis. Sci.* 51, 5071–5082. doi: 10.1167/iovs.10-5289

Tielsch, J. M., Sommer, A., Katz, J., Royall, R. M., Quigley, H. A., and Javitt, J. (1991). Racial variations in the prevalence of primary open-angle glaucoma. The Baltimore eye survey. *JAMA* 266, 369–374. doi: 10.1001/jama.266.3.369

Tkatchenko, T. V., Shen, Y., and Tkatchenko, A. V. (2010). Analysis of postnatal eye development in the mouse with high-resolution small animal magnetic resonance imaging. *Invest. Ophthalmol. Vis. Sci.* 51, 21–27. doi: 10.1167/iovs.08-2767

Vass, C., Hirn, C., Sycha, T., Findl, O., Bauer, P., and Schmetterer, L. (2007). Medical interventions for primary open angle glaucoma and ocular hypertension. *Cochrane Database Syst. Rev.* 4:CD003167.

Volland, S., Esteve-Rudd, J., Hoo, J., Yee, C., and Williams, D. S. (2015). A comparison of some organizational characteristics of the mouse central retina and the human macula. *PLoS One* 10:e0125631. doi: 10.1371/journal.pone.0125631

Wang, L., Cioffi, G. A., Cull, G., Dong, J., and Fortune, B. (2002). Immunohistologic evidence for retinal glial cell changes in human glaucoma. *Invest. Ophthalmol. Vis. Sci.* 43, 1088–1094.

Wax, M. B. (2011). The case for autoimmunity in glaucoma. *Exp. Eye Res.* 93, 187–190. doi: 10.1016/j.exer.2010.08.016

Wax, M. B., Barrett, D. A., and Pestronk, A. (1994). Increased incidence of paraproteinemia and autoantibodies in patients with normal-pressure glaucoma. *Am. J. Ophthalmol.* 117, 561–568. doi: 10.1016/s0002-9394(14)70059-5

Wax, M. B., Tezel, G., and Edward, P. D. (1998). Clinical and ocular histopathological findings in a patient with normal-pressure glaucoma. *Arch. Ophthalmol.* 116, 993–1001. doi: 10.1001/archopht.116.8.993

Wax, M. B., Tezel, G., Yang, J., Peng, G., Patil, R. V., Agarwal, N., et al. (2008). Induced autoimmunity to heat shock proteins elicits glaucomatous loss of retinal ganglion cell neurons via activated T-cell-derived fas-ligand. *J. Neurosci.* 28, 12085–12096. doi: 10.1523/JNEUROSCI.3200-08.2008

Williams, P. A., Tribble, J. R., Pepper, K. W., Cross, S. D., Morgan, B. P., Morgan, J. E., et al. (2016). Inhibition of the classical pathway of the complement cascade prevents early dendritic and synaptic degeneration in glaucoma. *Mol. Neurodegener.* 11:26. doi: 10.1186/s13024-016-0091-6

Wood, J. P., Chidlow, G., Tran, T., Crowston, J. G., and Casson, R. J. (2010). A comparison of differentiation protocols for RGC-5 cells. *Invest. Ophthalmol. Vis. Sci.* 51, 3774–3783. doi: 10.1167/iovs.09-4305

Xie, J., Gong, Q., Liu, X., Liu, Z., Tian, R., Cheng, Y., et al. (2017). Transcription factor SP1 mediates hyperglycemia-induced upregulation of roundabout4 in retinal microvascular endothelial cells. *Gene* 616, 31–40. doi: 10.1016/j.gene.2017.03.027

Yoneda, S., Tanihara, H., Kido, N., Honda, Y., Goto, W., Hara, H., et al. (2001). Interleukin-1beta mediates ischemic injury in the rat retina. *Exp. Eye Res.* 73, 661–667. doi: 10.1006/exer.2001.1072

Yoo, H. I., Moon, Y. H., and Kim, M. S. (2016). Effects of CoCl2 on multi-lineage differentiation of C3H/10T1/2 mesenchymal stem cells. *Korean J. Physiol. Pharmacol.* 20, 53–62. doi: 10.4196/kjpp.2016.20.1.53

Yu, J., Sun, W., Song, Y., Liu, J., Xue, F., Gong, K., et al. (2019). SIRT6 protects retinal ganglion cells against hydrogen peroxide-induced apoptosis and oxidative stress by promoting Nrf2/ARE signaling via inhibition of Bach1. *Chem. Biol. Interact.* 300, 151–158. doi: 10.1016/j.cbi.2019.01.018

Yuan, L., and Neufeld, A. H. (2001). Activated microglia in the human glaucomatous optic nerve head. *J. Neurosci. Res.* 64, 523–532. doi: 10.1002/jnr.1104

Zanon-Moreno, V., Marco-Ventura, P., Lleo-Perez, A., Pons-Vazquez, S., Garcia-Medina, J. J., Vinuesa-Silva, I., et al. (2008). Oxidative stress in primary open-angle glaucoma. *J. Glaucoma* 17, 263–268. doi: 10.1097/IJG.0b013e31815c3a7f

Zeng, H. Y., Green, W. R., and Tso, M. O. (2008). Microglial activation in human diabetic retinopathy. *Arch. Ophthalmol.* 126, 227–232. doi: 10.1001/archophthalmol.2007.65

Zeyen, T. (1999). Target pressures in glaucoma. *Bull. Soc. Belge Ophtalmol.* 274, 61–65.

Zhao, H., Wang, R., Ye, M., and Zhang, L. (2019). Genipin protects against H_2O_2-induced oxidative damage in retinal pigment epithelial cells by promoting Nrf2 signaling. *Int. J. Mol. Med.* 43, 936–944. doi: 10.3892/ijmm.2018.4027

Zhao, L., Zabel, M. K., Wang, X., Ma, W., Shah, P., Fariss, R. N., et al. (2015). Microglial phagocytosis of living photoreceptors contributes to inherited retinal degeneration. *EMBO Mol. Med.* 7, 1179–1197. doi: 10.15252/emmm.201505298

Zhou, X., Wang, W., Lu, F., Hu, S., Jiang, L., Yan, D., et al. (2007). A comparative gene expression profile of the whole eye from human, mouse, and guinea pig. *Mol. Vis.* 13, 2214–2221.

Conflict of Interest Statement: The authors declare that the research was conducted in the absence of any commercial or financial relationships that could be construed as a potential conflict of interest.

frontiers in Neuroscience

BRIEF RESEARCH REPORT
published: 16 September 2019
doi: 10.3389/fnins.2019.00983

Adult Goat Retinal Neuronal Culture: Applications in Modeling Hyperglycemia

*Sapana Sharma†, Harshini Chakravarthy†, Gowthaman Suresh and Vasudharani Devanathan**

Department of Biology, Indian Institute of Science Education and Research (IISER), Tirupati, India

Culture of adult neurons of the central nervous system (CNS) can provide a unique model system to explore neurodegenerative diseases. The CNS includes neurons and glia of the brain, spinal cord and retina. Neurons in the retina have the advantage of being the most accessible cells of the CNS, and can serve as a reliable mirror to the brain. Typically, primary cultures utilize fetal rodent neurons, but very rarely adult neurons from larger mammals. Here, we cultured primary retinal neurons isolated from adult goat up to 10 days, and established an *in vitro* model of hyperglycemia for performing morphological and molecular characterization studies. Immunofluorescence staining revealed that approximately 30–40% of cultured cells expressed neuronal markers. Next, we examined the relative expression of cell adhesion molecules (CAMs) in adult goat brain and retina. We also studied the effect of different glucose concentrations and media composition on the growth and expression of CAMs in cultured retinal neurons. Hyperglycemia significantly enhances neurite outgrowth in adult retinal neurons in culture. Expression of CAMs such as Caspr1, Contactin1 and Prion is downregulated in the presence of high glucose. Hyperglycemia downregulates the expression of the transcription factor CCAAT/enhancer binding protein (C/EBP α), predicted to bind CAM gene promoters. Collectively, our study demonstrates that metabolic environment markedly affects transcriptional regulation of CAMs in adult retinal neurons in culture. The effect of hyperglycemia on CAM interactions, as well as related changes in intracellular signaling pathways in adult retinal neurons warrants further investigation.

Keywords: neurodegeneration, hyperglycemia, retinal neurons, CCAAT-enhancer-binding protein, adult neurons, cell adhesion molecules, neurite extension

OPEN ACCESS

Edited by:
Peter Koulen,
University of Missouri System,
United States

Reviewed by:
Elisa L. Hill-Yardin,
RMIT University, Australia
Suzanne Hosie,
RMIT University, Australia,
in collaboration with reviewer EH-Y
Jeffrey Dupree,
Virginia Commonwealth University,
United States

****Correspondence:***
Vasudharani Devanathan
vasudharani@iisertirupati.ac.in

† These authors have contributed equally to this work

Specialty section:
This article was submitted to Neurodegeneration, a section of the journal Frontiers in Neuroscience

Received: *31 May 2019*
Accepted: *02 September 2019*
Published: *16 September 2019*

Citation:
Sharma S, Chakravarthy H, Suresh G and Devanathan V (2019) Adult Goat Retinal Neuronal Culture: Applications in Modeling Hyperglycemia. Front. Neurosci. 13:983. doi: 10.3389/fnins.2019.00983

INTRODUCTION

In vitro study of adult neurons is a fundamental and indispensable tool for understanding the precise contribution of neuronal genes and proteins toward the pathophysiology of neurodegenerative diseases. Analysis of neurons cultured in isolation over time facilitates perturbation of neuron-specific signaling pathways by exposing them to chemical agents, and manipulation of neuronal genes using knock-down or overexpression studies. Traditionally, neurons are studied by *in vitro* culturing of cells obtained not from adult, but from embryonic tissue or young pups within 1–10 days of birth (Tabata et al., 2000; Liu et al., 2013; Gao et al., 2016), since adult tissue consists of mature neurons which do not undergo cell division. The culture

of early postnatal neurons from embryonic or immature tissue has enabled crucial advances in our understanding of molecular pathways involved in development or differentiation (Watanabe and Raff, 1990; Waid and McLoon, 1998; Reese, 2011). However, these cultures are of limited value in studying neurodegenerative disease which primarily affects mature and aged neuronal tissue. Study of hyperglycemia-associated neuronal damage in adult tissues isolated from higher mammals may provide clinically-relevant data applicable to adult-onset diabetes which currently affects nearly half a billion people worldwide. Although fully post-mitotic, terminally differentiated adult neurons retain the ability regenerate their neurites when maintained in culture and hence may be more useful as an *in vitro* model system for investigating neuroprotection, neurite regeneration and pathogenic mechanisms of neurodegenerative disease (Brewer et al., 2005; Ghosh et al., 2012; Salvadores et al., 2017).

Similar to the brain, retinal neurons and Müller glia are derived from the neuroepithelium in two temporal phases during embryonic development (Centanin and Wittbrodt, 2014). In recent years, several studies have demonstrated significant correlations between retinal pathology and neurodegeneration in the brain (Ciudin et al., 2017; Ramirez et al., 2017; Mutlu et al., 2018; Sundstrom et al., 2018). Proteomic analysis of post-mortem diabetic human retinas shows activation of the same pathogenic mediators which are involved in neurodegenerative brain diseases (Sundstrom et al., 2018). Retinal microperimetry demonstrates that retinal sensitivity in diabetic patients correlates significantly with brain neurodegeneration (Ciudin et al., 2017). β-amyloid plaques and phosphorylated tau have recently been detected in retinas of Alzheimer's disease (AD) patients (den Haan et al., 2018), while α-synuclein aggregates have been detected in retinas of Parkinson's disease patients (Veys et al., 2019). An ongoing clinical trial (NCT02360527) is currently examining the feasibility of using diabetic retinal neurodegeneration as a biomarker for AD. Such correlations are not surprising, since the neural retina is a brain-derived tissue and shares striking molecular parallels with the brain and spinal cord (Byerly and Blackshaw, 2009). Developmentally and anatomically the retina is an extension of the CNS, and consists of five distinct types of neurons forming a complex neural circuitry that transmits visual signals to the brain. Several features of neurodegeneration reported in the brain have been detected in retinal diseases. Amyloid-beta deposition is found in drusen, the hallmark of age-related macular degeneration, and in glaucoma (Dentchev et al., 2003; Yan et al., 2017). Neuroinflammatory markers are associated with onset of AD as well as diabetic retinopathy (Heppner et al., 2015; Chakravarthy and Devanathan, 2018).

Most experiments in neurobiology are conducted using neurons isolated from rodents; however, mouse models often fall short of recapitulating human pathophysiology. In this study we utilized goat retina as our model system; we postulate that *in vitro* studies in goat could facilitate identification of novel pathways in higher mammals which may not be revealed by rodent-derived cells. Here, we examined the relative expression of neuron-specific cell adhesion molecules (CAMs) in adult goat brain and retina. Further, we cultured primary neurons from the retina isolated from adult goat. We also studied the effect of different glucose concentrations and media compositions on neurite outgrowth and expression of CAMs in cultured adult neurons. Our studies reveal that hyperglycemia significantly enhances neurite extension in cultured retinal neurons, while downregulating expression of specific neuronal CAMs. We further propose that the expression of these CAMs is transcriptionally regulated by CCAAT/enhancer binding proteins (CEBP) α and β which have predicted binding sites upstream of goat CAM gene promoters.

MATERIALS AND METHODS

Isolation of Retina and Brain From Adult Goat and Mouse

Eyes were isolated from adult goat (*Capra hircus*), 2–3 months of age from the local abattoir in Tirupati, India. As per institutional guidelines, we obtained written informed consent from the abattoir owner for participation of animals in this study. After euthanasia, brain and eyeballs were carefully removed and transported to the lab in sterile HBSS (Gibco) on ice. In the biosafety cabinet, the eyeball was immersed in 70% ethanol for 2 min. The eyeball was punctured posterior to the limbus, cut around the circumference of the limbus, and cornea, lens, and sclera were removed. The vitreous was extracted, and retina was detached gently from eye cup, by gently dissociating from the retinal pigmented epithelium. A cut was made at the center of the retina to detach it from the optic nerve head. The dissection was done under sterile conditions in HBSS solution (**Supplementary Figure S1**). The brain was also dissected under sterile conditions to isolate cerebrum, cerebellum and brain stem. 8-week old male BALB/c mice were euthanized, enucleated, and retina isolated as described above. All procedures involving mice were approved by the Institutional Animal Ethics Committee (IAEC number: IAEC/56/SRU/624/2018).

Establishment of an Adult Retinal Neuron Model of Hyperglycemia

In this study, retinal cells were cultured in normoglycemia (5 mM glucose) or hyperglycemia (25 mM glucose). A previous study has shown that changes in glucose concentrations during culture preparation significantly affects neuronal viability (Kleman et al., 2008). Hence, retinal tissue was processed, washed, triturated and counted in 5 mM or 25 mM glucose-containing buffer/media, depending on the final glucose concentration used. DMEM (Dulbecco's Modified Eagle Medium) is a widely used basal medium for maintaining mammalian cell types in culture such as fibroblasts, glia, neurons, and cell lines. DMEM is typically supplemented with 10% fetal bovine serum (FBS). Neurobasal-A medium is a basal medium specifically designed for maintenance of adult neurons without the need for an astrocyte feeder layer, when used with serum-free B-27 supplement (Brewer et al., 1993). A major difference between the two media is their osmolarity: DMEM is 335mOsm, while Neurobasal-A is 260mOsm. We compared the growth of adult goat neurons in

both DMEM and Neurobasal-A media. We used five goats to establish the consistency of the culture system. From one adult goat, retina isolated from both eyes were used for primary culture.

The isolated retina was immersed in 5 mM or 25 mM glucose-containing HBSS, cut into small pieces (1–2 mm size), and digested with 0.05% trypsin (Gibco) for 15 min, at 37°C. The reaction was terminated by adding DMEM complete medium: 5 mM or 25 mM glucose DMEM (Gibco) respectively, containing 10% FBS (Gibco), 0.06 g/L L-glutamine, and 1% Penicillin/Streptomycin (Sigma). The resultant suspension was filtered through a 40 μm nylon mesh, centrifuged at 200 g for 5 min, and resuspended in DMEM complete medium (**Supplementary Figure S2**). Immunopanning was done to remove fibroblast and glial cells: Culture dishes were coated with anti-vimentin antibody (1:50) prepared in 50 mM Tris–HCl. Anti-vimentin-coated dishes were incubated overnight at 4°C. Immediately before use, dishes were rinsed with PBS three times. Retinal cell suspension was incubated in panning dishes for 60 min, and non-adherent cells were collected. Cells were quantified, and viability assessed after staining with Trypan blue, and viewed under an inverted light microscope (Thermo Fisher Scientific). 1.3×10^6cells/well were added to poly-L-Lysine-coated 6-well plates containing 12 × 12 mm coverslips. After 24 h, media was changed to 5 mM or 25 mM glucose DMEM complete medium, or 25 mM glucose Neurobasal-A medium containing 2% B-27 supplement, 1% Penicillin/Streptomycin, 10% FBS and 0.06 g/L L-glutamine. Half medium was renewed every 1–2 days. Cells were observed daily to evaluate morphology, length of neurites, and adherence as described previously (Perry et al., 1997). Cell counts per field, for 6–10 random fields under 10× magnification were recorded every 2 days up to 10 days.

MTT Assay for Cytotoxicity Evaluation

Cells were seeded into a 24-well plate at a density of 0.05 million cells/well. Cells were grown in 5 mM glucose and 25 mM glucose-containing DMEM medium, and in Neurobasal-A medium (25 mM glucose). Media was changed every alternate day. After 6 days, 50 μl of MTT solution (0.5 mg/ml) was added and plate incubated at 37°C. After 4 h, cells were treated with 500 μl of isopropanol for 20 min at RT. Absorbance at 570 nm was recorded using a microplate reader (Biotek). The experiment was performed in triplicate.

Antibodies Used

Contactin-1(1:100), Caspr-2(1:200), PrP(1:200) from Sigma, NCAM-1(1:50), Synaptophysin(1:250), GFAP(1:100), Caspr-1(1:200) from Novus, NeuN(1:100) from Abcam.

Immunocytochemistry

Immunofluorescence staining was performed as described previously (Sytnyk et al., 2002). Cells cultured for 10 days on coverslips were washed in PBS and fixed in 4% formaldehyde for 15 min at 4°C. Cells were washed three times with PBS, blocked in 1% BSA in PBS, and incubated with primary antibodies for 60 min at RT. Corresponding fluorescent labeled secondary antibodies (Alexa Flour 488 and 594, Invitrogen) staining was done for 60 min at RT. Stained cells were mounted using Fluoromount mounting medium containing nuclear stain DAPI (Sigma). Images were acquired using a fluorescence microscope (Olympus).

Identification of Neurons and Glial Cells

Cells cultured were stained for neuronal (NeuN, Synaptophysin) and glial (GFAP) markers. 6–10 random fields were examined under 10× magnification. Number of neurons and glia were calculated using the formula: percentage of neurons (%) = number of neurons/total number of cells in the field × 100.

Quantitative Real-Time PCR

Tissue homogenates of retinas and brain were prepared at 4°C using a Potter Elvehjem homogenizer (Biolab Instruments) in lysis buffer (50 mM HEPES, 1 mM EGTA, 1.5 mM $MgCl_2$, 150 mM NaCl, 10% glycerol, 1% Triton ×-100) at pH 7.4, containing protease inhibitor (Roche). After 30 min of mild shaking at 4°C, homogenate was centrifuged at 15000 g for 15 min at 4°C. Supernatant containing protein was flash-frozen and stored in −80°C.

RNA was extracted from cell lysates and tissue homogenates using TRIzol (Invitrogen). RNA was quantified using Nanodrop2000 spectrophotometer (Thermo Fisher Scientific) and reverse-transcribed using iScript cDNA synthesis kit (Bio-Rad). Goat and mouse primers were used for checking expression of specific genes by performing quantitative RT-PCR using iTaq Universal SYBR Green supermix (Bio-Rad). Results were normalized to GAPDH or β-actin. Primers used are given in **Supplementary Table S1**.

Neurite Outgrowth Assay

Cultured cells maintained for 10 days were fixed with 4% formaldehyde and immunostained with neuronal marker, NeuN (green). To quantify neurite outgrowth, neurons were visualized under 10× magnification and total length of all neurites were determined by neurite tracing using ImageJ, as described previously (Ng et al., 2003). Neurite length measurements from at least 100 cells per dish were recorded from randomly chosen fields. Each experiment was repeated three times.

Prediction of C/EBP Binding Sites in CAM Gene Promoters

C/EBP binds to an extensive range of DNA sequences. Several C/EBP-α binding sites were predicted within 600 bp upstream of goat CAM promoters (Caspr1, Caspr2, Prion and Contactin1), using Alibaba2 program, Version 2.1, Germany. Alibaba2 software predicts binding sites of transcription factors in a DNA sequence, available on http://gene-regulation.com/pub/programs/alibaba2/index.html (Grabe, 2002). By convention, numbering of nucleotides on the gene sequence begins with "1" at **A** of ATG start codon, while nucleotides upstream (5'UTR) of ATG-translation initiation codon are marked with a "−" (minus) sign, and are numbered −1, −2, −3, etc. going further upstream from ATG.

Statistical Analysis

Data are presented as mean ± SEM. Results were analyzed for statistical significance by Student's *t*-test or one-way ANOVA followed by Tukey's *post hoc* test (Prism 8, GraphPad Prism).

RESULTS

Growth and Morphology of Retinal Neurons in Primary Culture

We successfully isolated retinal neurons from adult goat retina, identified by expression of neuronal markers like Synaptophysin, NCAM1 and NeuN (**Figure 2**). Mammalian neuronal cultures are typically grown in high glucose-containing media based on DMEM or Neurobasal, with addition of supplements to optimize neuronal survival (Tabata et al., 2000; Liu et al., 2013). To study the effect of different glucose concentrations and media compositions on adult neurons, we cultured them in 5 mM and 25 mM glucose-containing DMEM and Neurobasal-A medium (25 mM glucose). High glucose DMEM and Neurobasal-A media differ primarily in osmolarity, and in the addition of serum for DMEM versus serum-free supplements for Neurobasal-A. After 1–2 days, some cells (between 0.9 ± 1.7 and 3.6 ± 2.7 cells per field) were observed adhering to the plate surface, and cell body was predominantly small and round (**Figure 1A** and **Supplementary Table S2**). After 3–4 days, cells displayed axon-like projections. The projection-forming process was hastened in cells cultured in hyperglycemic conditions as compared to cells in normoglycemic conditions (**Figure 1B**). After 5–6 days, projections increased in length, and were on average about 1-2 folds longer than cell body (**Figure 1C**). At 7–8 days, retinal cells continue to grow in culture (**Figure 1D**). After 10–11 days, axon-like projections were prominent in length, gradually forming complex networks (**Figure 1E**).

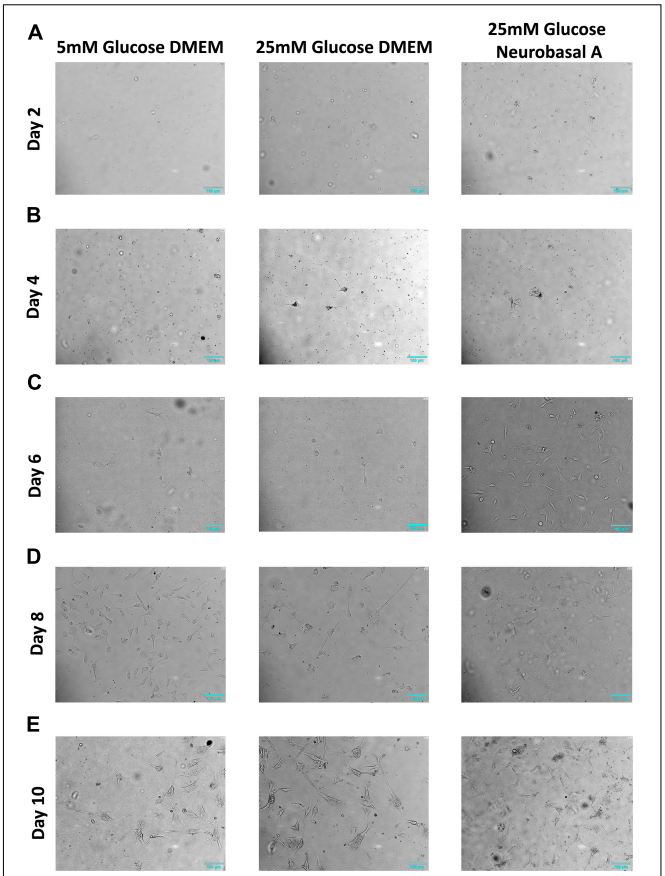

FIGURE 1 | Morphology of retinal neurons cultured in 5 mM glucose DMEM, 25 mM glucose DMEM, or 25 mM glucose Neurobasal A medium. **(A)** On Day 2, adherent cells are few in number in all three media conditions. **(B)** On Day 4, more cells start to attach to the cell culture dish in 25 mM glucose-containing DMEM and Neurobasal A medium, whereas fewer cells are adherent in 5 mM glucose containing DMEM. **(C)** On Day 6, more cells start to adhere to the culture dish, especially in high glucose-containing Neurobasal A medium. **(D)** Day 8 adherent cells continue to grow in culture. **(E)** On Day 10 post primary culture initiation, axon-like projections were prominent in length, gradually forming complex networks. *N* = 5.

Hyperglycemia Does Not Affect Neuronal Viability

A greater number of adherent cells per field were observed in cells cultured in hyperglycemic conditions, as compared to normoglycemic conditions between 4 and 8 days in culture. However, 10 days post primary culture initiation, neuronal cell count appeared to decrease under hyperglycemic conditions (**Supplementary Table S2**). In order to evaluate possible cytotoxic effects of hyperglycemia, MTT assay was performed. Results of this assay clearly indicate that hyperglycemia does not affect neuronal viability ($P > 0.05$ for 5 mM vs. 25 mM glucose DMEM and Neurobasal-A, **Supplementary Figure S3**).

Retinal Neurons Express Cell Adhesion Molecules Expressed in Brain

Immunofluorescence staining was performed to estimate the percentage of cells expressing neuronal and glial markers. Expression of CAMs was examined by staining with primary antibodies against specific CAMs. Retinal cells cultured for 10 days showed 46% of cells expressing neuronal markers like Synaptophysin and NeuN (**Figures 2Ab,c**). Expression of neuronal CAMs like NCAM1, Contactin1, Prion, Caspr1, and Caspr2 was also observed (**Figures 2Aa,Ba–d**). Glial marker GFAP was expressed by 15% of cultured cells (**Figure 2Ad**). The percentage of neurons and glial cells are representative of cells cultured in Neurobasal-A medium containing 25 mM glucose; the numbers did not vary significantly with different media or glycemic conditions.

Hyperglycemia Increases Neurite Length in Retinal Neurons

Next, we studied the effect of different glucose concentrations and media compositions on neurite outgrowth. Under hyperglycemic conditions, retinal neurons had longer neurite outgrowth (DMEM 18.5 ± 0.63 μm; Neurobasal-A 18 ± 0.45 μm) compared to those cultured in normoglycemic conditions (12.6 ± 0.99 μm) (**Figure 2**). This suggests that glucose aids

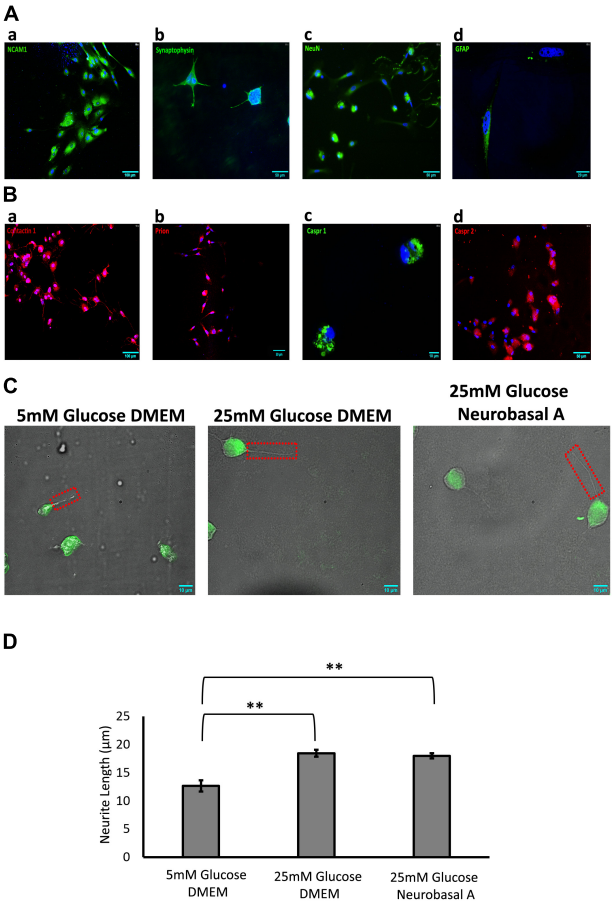

FIGURE 2 | (A) Identification of adult retinal neurons and glia in culture by immunofluorescence staining. **(a)** NCAM1 (green), expressed by all retinal neurons and glia; **(b)** Synaptophysin (green), expressed by neurons in the plexiform layers of the retina; **(c)** NeuN (green), expressed by neuronal nuclei; **(d)** GFAP (green), expressed by retinal glia. **(B)** Expression of cell adhesion molecules (CAMs) in adult retinal neurons and glial culture by immunofluorescence staining: **(a)** Contactin1, red **(b)** Prion, red **(c)** Caspr1, green **(d)** Caspr2, red. **(C)** Representative 60× DIC combined with NeuN (green) immunostained images showing length of neurite outgrowth (red box) in retinal neurons cultured in 5 mM glucose DMEM, 25 mM glucose DMEM, or 25 mM glucose Neurobasal A medium. **(D)** Quantification shows a significant increase in neurite length in 25 mM glucose-containing DMEM and Neurobasal A medium, as compared to 5 mM glucose DMEM (**$p < 0.01$). Neurite outgrowth was measured in 50–100 cells per slide, and experiment repeated in triplicate. $N = 5$.

neurite extension/growth ($P < 0.01$ for 5 mM vs. 25 mM glucose-containing media, **Figure 2D**). Our studies reveal that hyperglycemia significantly enhances neurite extension in primary cultures of adult retinal neurons.

Expression Patterns of Cell Adhesion Molecules in Retina and Brain

Since most studies in neurobiology utilize early postnatal neurons isolated from rodents, we examined the relative expression of CAMs in goat and mouse retina. Further, neuronal CAMs are more widely studied in the brain; hence we compared the relative expression of CAMs in different regions of goat brain (cerebrum, cerebellum and brain stem) with their expression in retina. Results of RT-PCR show similar expression levels of Caspr1, Caspr2, Contactin1, and Prion in retina compared with expression of these proteins in brain regions like cerebrum, cerebellum and brain stem ($P > 0.05$ for all CAMs, **Figure 3A**). In goat and mouse retinal tissues similar levels of Caspr2 and Prion were expressed. However, expression of Caspr1 and Contactin1 was significantly higher in goat retina relative to mouse retina ($P < 0.001$ for Caspr1 and Contactin1, **Figure 3B**).

Hyperglycemia Affects Expression and Transcriptional Regulation of Cell Adhesion Molecules

We studied the effect of different glucose concentrations and media compositions on expression of CAMs. Results of RT-PCR show that expression of Prion and Contactin1 is significantly downregulated under hyperglycemia ($P < 0.05$ for Contactin1 and Prion). Caspr1 expression shows a clear trend toward downregulation in hyperglycemia, while Caspr2 expression was low in normoglycemia and did not change significantly under hyperglycemic conditions. Media composition did not have any significant effect on expression of neuronal CAMs (**Figure 4A**).

We also explored the contribution of glucose homeostasis-sensitive transcription factors, CCAAT/enhancer binding protein isoforms C/EBP-α and C/EBP-β toward regulation of neuronal CAM expression. Using Alibaba2 program, we predicted that C/EBP-α and C/EBP-β have binding sites in goat neuronal CAM genes (Caspr1, Caspr2, Contactin1 and Prion) within −600 bp proximal to the promoter region (**Supplementary Table S3**). "Start" and "Stop" columns indicate specific locations of putative binding sites for C/EBP-α and C/EBP-β upstream of ATG-translation initiation codon. We studied the effect of hyperglycemia on expression of C/EBP-α and C/EBP-β. RT-PCR indicated that hyperglycemia significantly downregulates expression of C/EBP-α, while expression of C/EBP-β remains unchanged ($P = 0.002$ for C/EBP-α, **Figure 4B**).

DISCUSSION

Much is known about individual disease states such as diabetes, metabolic syndrome, and dementia; nevertheless, there is a need to identify where and how their pathophysiology intersects. Our study evaluates effects of hyperglycemia on expression and transcriptional regulation of CAMs in retinal neurons cultured from adult goat. We show for the first time that hyperglycemia significantly enhances neurite outgrowth, with downregulation of CAMs in cultured retinal neurons (**Figures 2C,D**, **4A**). Neuronal CAMs have been well-characterized in the brain for their role in regulating neurite outgrowth (Santuccione et al., 2005; Devanathan et al., 2010) and in the nodal/paranodal domain organization of myelinated axons (Peles and Salzer, 2000). However, the function of CAMs has not been elucidated in the retina, which consists of non-myelinated neurons. Here, we demonstrate that specific CAMs (Caspr1, Caspr2, Contactin1 and Prion) are expressed in the retinal tissue at levels comparable

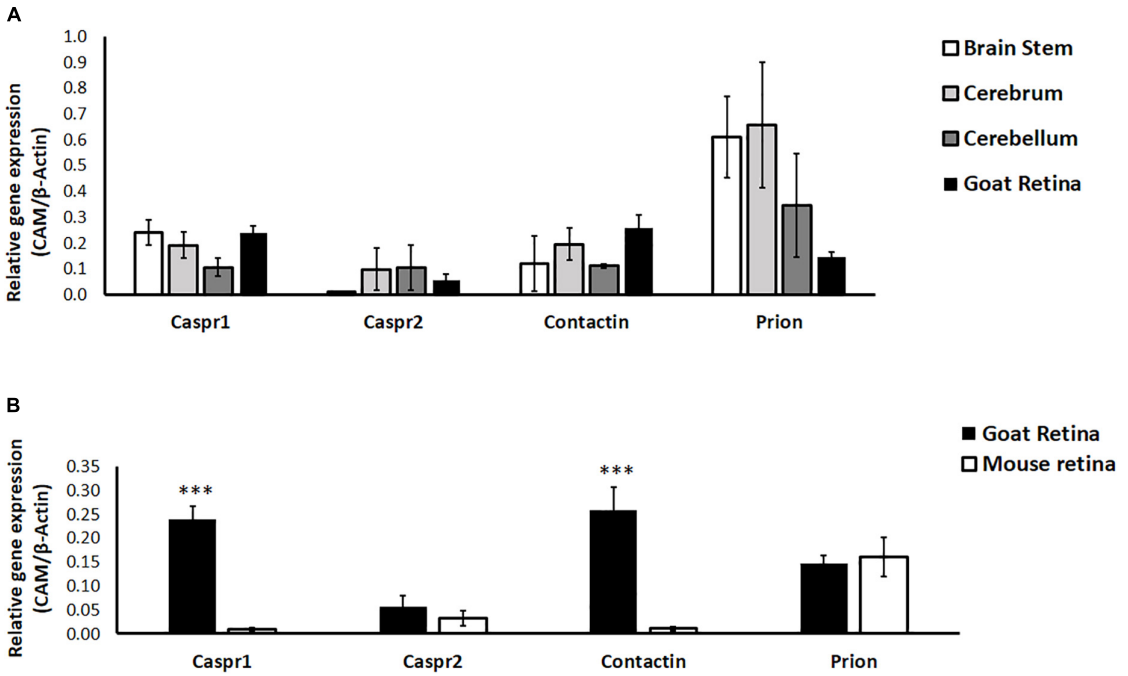

FIGURE 3 | (A) Relative expression of specific cell adhesion molecules (Caspr1, Caspr2, Prion, Contactin1) in goat retina and different parts of the brain (cerebrum, cerebellum and brain stem) was quantified by RT-PCR. *N* = 3–4. **(B)** Relative expression of specific cell adhesion molecules (Caspr1, Caspr2, Prion, Contactin1) in goat and BALB/c mouse retina was quantified by RT-PCR. Similar expression levels of Caspr2 and Prion were observed in goat and mouse retina, whereas levels of Caspr1 and Contactin1 were significantly high in goat retina (***$p < 0.001$ for goat retinal Caspr1 and Contactin1 compared to mouse retina). *N* = 4–5.

to their expression in brain (**Figure 3A**), and that their expression is downregulated under hyperglycemic conditions (**Figure 4A**).

Caspr1 and Contactin1 typically form a complex at the paranodal junction of myelinated neurons in the CNS. The absence of Caspr1 leads to mislocalization of Contactin1 and its exclusion from the paranodes (Bhat et al., 2001), while the absence of Contactin1 prevents delivery of Caspr1 to the axonal membrane (Boyle et al., 2001). We have previously demonstrated that Prion protein directly binds to Caspr1, protecting it from proteolysis. Deficiency of Prion results in reduced levels of Caspr at the neuronal membrane and enhanced neurite extension *in vitro* (Devanathan et al., 2010). In our current study we go one step further, and show that hyperglycemia leads to a significant reduction in levels of specific neuronal CAMs, while enhancing neurite length (**Figures 2C,D**, **4A**). Neurite extension in adult neurons is also believed to be enhanced by an IL-1β-dependent pathway (Saleh et al., 2013). Since hyperglycemia is known to increase levels of pro-inflammatory cytokines such as IL-1β and TNF-α in the diabetic retina (Busik et al., 2008; Chakravarthy et al., 2016), these factors presumably exert their effect on neuritogenesis as observed in our study (**Figures 2C,D**).

Neuronal CAM expression can be modulated in different ways including transcriptional regulation. The C/EBP constitute a family of transcription factors sensitive to changes in glucose homeostasis (Matsusue et al., 2004; Schroeder-Gloeckler et al., 2007). Among six C/EBP isoforms, C/EBP-α, β and δ are enriched in CNS neurons, and have been implicated in neuronal development, survival and neurogenesis (Ménard et al., 2002; Ramji and Foka, 2002; Paquin et al., 2005). C/EBP-α expression is downregulated, while C/EBP-β is upregulated in animal models of diabetes (Arizmendi et al., 1999). In our study, we observe a similar downregulation of C/EBP-α expression in cultured retinal cells under hyperglycemic conditions (**Figure 4B**). We also identified binding sites for C/EBP-α and β upstream of the promoter in goat neuronal CAM genes, Contactin1, Caspr1, Caspr2 and Prion (**Supplementary Table S3**). C/EBPs act as transcriptional enhancers or repressors depending on the C/EBP isoform, target gene and cell-type. We propose that hyperglycemia represses expression of C/EBP α, thereby diminishing its transcription-activating effect on CAMs, which in turn leads to downregulation of CAM expression in retinal neurons (**Supplementary Figure S4**).

A unique advantage of studying neurodegenerative changes in adult retina is easier accessibility to CNS neurons, and rapid detection of neuronal abnormalities in animal models using non-invasive techniques such as multifocal electroretinography, ultra-widefield fundus imaging, and spectral-domain OCT (Cheung et al., 2017; Chakravarthy and Devanathan, 2018). Moreover, administration of experimental drugs to the retina in animal models is relatively easier, making it a robust tool for preclinical studies (Edelhauser et al., 2010). Retinal and brain neurodegenerative diseases although affecting different parts of the CNS, appear to involve similar pathogenic mechanisms like oxidative stress, low-grade chronic neuroinflammation, disruption of blood-brain or blood-retinal barrier, and vascular abnormalities (London et al., 2013; Colligris et al., 2018).

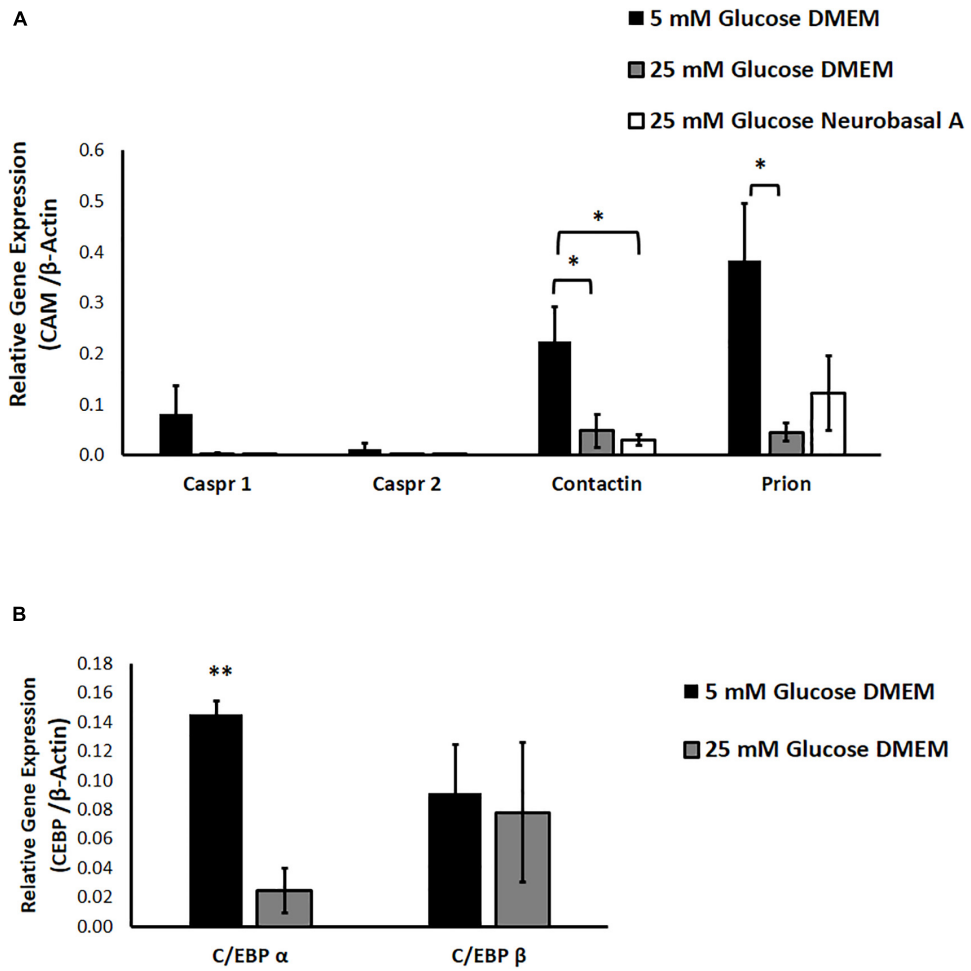

FIGURE 4 | (A) The effect of hyperglycemia and media composition on expression of specific cell adhesion molecules in cultured retinal cells was quantified by RT-PCR. In 25 mM glucose DMEM and Neurobasal A medium, Contactin1 expression was significantly downregulated. In 25 mM DMEM, Prion expression was significantly downregulated. *$p < 0.05$ compared to 5 mM glucose medium. $N = 4–5$. **(B)** The effect of hyperglycemia on expression of transcription factors C/EBP α and C/EBP β in cultured retinal cells was quantified by RT-PCR. In 25 mM glucose medium, expression of C/EBP α was significantly downregulated. **$p < 0.01$ compared to 5 mM glucose medium. $N = 3$.

Increasing clinical and preclinical evidence points to associations between metabolic dysregulation and neurodegenerative brain disease (Weinstein et al., 2015; Arnold et al., 2018; Ogama et al., 2018).

Culture of primary neurons is an indispensable method to study pathological responses of CNS neurons to metabolic conditions or inflammatory environments associated with neurodegenerative diseases. However, most *in vitro* experiments in neurobiology employ neurons isolated from rodents because of advantages such as ease of availability, well-characterized genetics, and availability of tissue from transgenic animals. Moreover, primary retinal cultures are typically generated from early postnatal rat or mouse pups. There are several disadvantages to using rodent tissue for cell culture. Cell yields from multiple animals typically permit a single experiment, or may be used in studies involving single cell electrophysiology. Compared to studies in rodents which yield lower retinal cell numbers, we successfully obtained 20 million cells from retina isolated from one goat eye which is suitable for several experiments over 3–10 days, and greatly reduces the number of animals needed. Once cultured, adult retinal neurons can be subjected to genetic manipulation, or physiological, biochemical and pharmacological procedures for functional characterization experiments. An additional advantage is that these animals were not sacrificed exclusively for the purpose of isolating CNS neurons, since animal parts were subsequently sold at the abattoir for other purposes.

Another important concern is that although mouse and human genomes are 85% similar, mouse models often do not accurately predict human pathophysiology leading to failure of clinical trials based on preclinical validation in mice, especially in the field of neurodegenerative diseases (Gordon et al., 2007; Duyckaerts et al., 2008; Dawson et al., 2010). Goats and cattle are considered phylogenetically distant from humans and rodents (Kim et al., 2017); however, elevated rate of evolution in rodents relative to other mammals is believed to result in higher amino

acid sequence identity between human and ruminant proteins as compared to human and rodent proteins (Bovine Genome Sequencing and Analysis Consortium et al., 2009). Indeed, a basic sequence comparison among orthologous CAMs across species using Clustal Omega demonstrates higher sequence similarity between goat and human relative to rodent proteins, as observed in previous studies (Bovine Genome Sequencing and Analysis Consortium et al., 2009). Thus, *in vitro* studies of protein interactions and signaling in cells cultured from goat or cow could facilitate identification of novel functionally important pathways in higher mammals.

CONCLUSION

To the best of our knowledge, no other study has been conducted using a similar approach to culture retinal neurons from adult goat. Higher mammals such as pigs have similar vasculature and retinal structures as humans, while dogs develop morphological lesions most similar to diabetic human retina (Lai and Lo, 2013). While the neural retina in all mammals contains distinct classes of interneurons, species-specific functional differences have been found in overtly similar cell types (Dacey et al., 2003; Dhande et al., 2019). Further, traditional laboratory-bred animals have a limited number of alleles which does not reflect the genetic diversity and natural variation found in human populations. Therefore, *in vitro* models using higher mammals can provide an important platform for investigating neuronal responses that may not be revealed by rodent-derived cells. Additionally, exploring metabolic and signaling mechanisms in adult retinal neurons may provide vital insights that can be translated to neurodegenerative processes in the entire CNS. The unique model of adult goat retinal culture described in our study can be used to perform detailed investigations into effects of hyperglycemia on interactions between specific CAMs expressed on distinct retinal neuronal types, as well as related changes in downstream signaling to elucidate functions of CAMs in adult retina.

DATA AVAILABILITY

All datasets generated for this study are included in the manuscript and/or the **Supplementary Files**.

ETHICS STATEMENT

The animal study was reviewed and approved by Institutional Animal Ethics Committee (IAEC), Sri Ramachandra Medical College and Research Institute. Written informed consent was obtained from the owners for the participation of their animals in this study.

AUTHOR CONTRIBUTIONS

SS and HC performed the research, analyzed the data, and wrote the manuscript. GS performed the research and analyzed the data. VD designed the research, contributed reagents and analytic tools, wrote the manuscript, and had full access to all data in the study. All authors took responsibility for the integrity of the data and accuracy of data analysis.

FUNDING

VD is a recipient of Early Career Research Award from SERB, Department of Science and Technology (Grant Number: ECR/2016/001124/LS). HC is a recipient of Women Scientist Scheme-A (WOS-A), Department of Science and Technology (Grant Number: SR/WOS-A/LS-327/2018). VD would like to thank DST, Government of India and IISER Tirupati for research support. HC and SS thank DST and IISER Tirupati for their research fellowships.

ACKNOWLEDGMENTS

We thank Dr. B. J. Rao and Dr. Ambrish Saxena for their critical comments on the manuscript. We also thank Dr. Pakala Suresh Babu for his valuable suggestions which helped us to elaborate on our research ideas.

SUPPLEMENTARY MATERIAL

The Supplementary Material for this article can be found online at: https://www.frontiersin.org/articles/10.3389/fnins.2019.00983/full#supplementary-material

REFERENCES

Arizmendi, C., Liu, S., Croniger, C., Poli, V., and Friedman, J. E. (1999). The transcription factor CCAAT/enhancer-binding protein beta regulates gluconeogenesis and phosphoenolpyruvate carboxykinase (GTP) gene transcription during diabetes. *J. Biol. Chem.* 274, 13033–13040. doi: 10.1074/jbc.274.19.13033

Arnold, S. E., Arvanitakis, Z., Macauley-Rambach, S. L., Koenig, A. M., Wang, H.-Y., Ahima, R. S., et al. (2018). Brain insulin resistance in type 2 diabetes and Alzheimer disease: concepts and conundrums. *Nat. Rev. Neurol.* 14, 168–181. doi: 10.1038/nrneurol.2017.185

Bhat, M. A., Rios, J. C., Lu, Y., Garcia-Fresco, G. P., Ching, W., St Martin, M., et al. (2001). Axon-glia interactions and the domain organization of myelinated axons requires neurexin IV/Caspr/Paranodin. *Neuron* 30, 369–383. doi: 10.1016/s0896-6273(01)00294-x

Bovine Genome Sequencing and Analysis Consortium, C. G., Tellam, R. L., Worley, K. C., Gibbs, R. A., Muzny, D. M., et al. (2009). The genome sequence of taurine cattle: a window to ruminant biology and evolution. *Science* 324, 522–528. doi: 10.1126/science.1169588

Boyle, M. E., Berglund, E. O., Murai, K. K., Weber, L., Peles, E., and Ranscht, B. (2001). Contactin orchestrates assembly of the septate-like junctions at the paranode in myelinated peripheral nerve. *Neuron* 30, 385–397. doi: 10.1016/s0896-6273(01)00296-3

Brewer, G. J., Lim, A., Capps, N. G., and Torricelli, J. R. (2005). Age-related calcium changes, oxyradical damage, caspase activation and nuclear condensation

in hippocampal neurons in response to glutamate and beta-amyloid. *Exp. Gerontol.* 40, 426–437. doi: 10.1016/j.exger.2005.03.007

Brewer, G. J., Torricelli, J. R., Evege, E. K., and Price, P. J. (1993). Optimized survival of hippocampal neurons in B27-supplemented neurobasal, a new serum-free medium combination. *J. Neurosci. Res.* 35, 567–576. doi: 10.1002/jnr.490350513

Busik, J. V., Mohr, S., and Grant, M. B. (2008). Hyperglycemia-induced reactive oxygen species toxicity to endothelial cells is dependent on paracrine mediators. *Diabetes* 57, 1952–1965. doi: 10.2337/db07-1520

Byerly, M. S., and Blackshaw, S. (2009). Vertebrate retina and hypothalamus development. *Wiley Interdiscip. Rev. Syst. Biol. Med.* 1, 380–389. doi: 10.1002/wsbm.22

Centanin, L., and Wittbrodt, J. (2014). Retinal neurogenesis. *Dev. Camb. Engl.* 141, 241–244. doi: 10.1242/dev.083642

Chakravarthy, H., Beli, E., Navitskaya, S., O'Reilly, S., Wang, Q., Kady, N., et al. (2016). Imbalances in mobilization and activation of pro-inflammatory and vascular reparative bone marrow-derived cells in diabetic retinopathy. *PloS One* 11:e0146829. doi: 10.1371/journal.pone.0146829

Chakravarthy, H., and Devanathan, V. (2018). Molecular mechanisms mediating diabetic retinal neurodegeneration: potential research avenues and therapeutic targets. *J. Mol. Neurosci. MN* 66, 445–461. doi: 10.1007/s12031-018-1188-x

Cheung, C. Y.-L., Ikram, M. K., Chen, C., and Wong, T. Y. (2017). Imaging retina to study dementia and stroke. *Prog. Retin. Eye Res.* 57, 89–107. doi: 10.1016/j.preteyeres.2017.01.001

Ciudin, A., Simó-Servat, O., Hernández, C., Arcos, G., Diego, S., Sanabria, Á, et al. (2017). Retinal microperimetry: a new tool for identifying patients with type 2 diabetes at risk for developing Alzheimer Disease. *Diabetes* 66, 3098–3104. doi: 10.2337/db17-0382

Colligris, P., Perez de Lara, M. J., Colligris, B., and Pintor, J. (2018). Ocular manifestations of Alzheimer's and other Neurodegenerative diseases: the prospect of the eye as a tool for the early diagnosis of Alzheimer's Disease. *J. Ophthalmol.* 2018:8538573. doi: 10.1155/2018/8538573

Dacey, D. M., Peterson, B. B., Robinson, F. R., and Gamlin, P. D. (2003). Fireworks in the primate retina: in vitro photodynamics reveals diverse LGN-projecting ganglion cell types. *Neuron* 37, 15–27. doi: 10.1016/s0896-6273(02)01143-1

Dawson, T. M., Ko, H. S., and Dawson, V. L. (2010). Genetic animal models of Parkinson's disease. *Neuron* 66, 646–661. doi: 10.1016/j.neuron.2010.04.034

den Haan, J., Morrema, T. H. J., Verbraak, F. D., de Boer, J. F., Scheltens, P., Rozemuller, A. J., et al. (2018). Amyloid-beta and phosphorylated tau in post-mortem Alzheimer's disease retinas. *Acta Neuropathol. Commun.* 6:147. doi: 10.1186/s40478-018-0650-x

Dentchev, T., Milam, A. H., Lee, V. M.-Y., Trojanowski, J. Q., and Dunaief, J. L. (2003). Amyloid-beta is found in drusen from some age-related macular degeneration retinas, but not in drusen from normal retinas. *Mol. Vis.* 9, 184–190.

Devanathan, V., Jakovcevski, I., Santuccione, A., Li, S., Lee, H. J., Peles, E., et al. (2010). Cellular form of prion protein inhibits reelin-mediated shedding of caspr from the neuronal cell surface to potentiate caspr-mediated inhibition of neurite outgrowth. *J. Neurosci. Off. J. Soc. Neurosci.* 30, 9292–9305. doi: 10.1523/JNEUROSCI.5657-09.2010

Dhande, O. S., Stafford, B. K., Franke, K., El-Danaf, R., Percival, K. A., Phan, A. H., et al. (2019). Molecular fingerprinting of On-off direction-selective retinal ganglion cells across species and relevance to primate visual circuits. *J. Neurosci. Off. J. Soc. Neurosci.* 39, 78–95. doi: 10.1523/JNEUROSCI.1784-18.2018

Duyckaerts, C., Potier, M.-C., and Delatour, B. (2008). Alzheimer disease models and human neuropathology: similarities and differences. *Acta Neuropathol.* 115, 5–38. doi: 10.1007/s00401-007-0312-8

Edelhauser, H. F., Rowe-Rendleman, C. L., Robinson, M. R., Dawson, D. G., Chader, G. J., Grossniklaus, H. E., et al. (2010). Ophthalmic drug delivery systems for the treatment of retinal diseases: basic research to clinical applications. *Invest. Ophthalmol. Vis. Sci.* 51, 5403–5420. doi: 10.1167/iovs.10-5392

Gao, F., Li, T., Hu, J., Zhou, X., Wu, J., and Wu, Q. (2016). Comparative analysis of three purification protocols for retinal ganglion cells from rat. *Mol. Vis.* 22, 387–400.

Ghosh, D., LeVault, K. R., Barnett, A. J., and Brewer, G. J. (2012). A reversible early oxidized redox state that precedes macromolecular ROS damage in aging nontransgenic and 3xTg-AD mouse neurons. *J. Neurosci. Off. J. Soc. Neurosci.* 32, 5821–5832. doi: 10.1523/JNEUROSCI.6192-11.2012

Gordon, P. H., Moore, D. H., Miller, R. G., Florence, J. M., Verheijde, J. L., Doorish, C., et al. (2007). Efficacy of minocycline in patients with amyotrophic lateral sclerosis: a phase III randomised trial. *Lancet Neurol.* 6, 1045–1053. doi: 10.1016/S1474-4422(07)70270-3

Grabe, N. (2002). AliBaba2: context specific identification of transcription factor binding sites. *In Silico Biol.* 2, S1–S15.

Heppner, F. L., Ransohoff, R. M., and Becher, B. (2015). Immune attack: the role of inflammation in Alzheimer disease. *Nat. Rev. Neurosci.* 16, 358–372. doi: 10.1038/nrn3880

Kim, J., Farré, M., Auvil, L., Capitanu, B., Larkin, D. M., Ma, J., et al. (2017). Reconstruction and evolutionary history of eutherian chromosomes. *Proc. Natl. Acad. Sci. U.S.A.* 114, E5379–E5388. doi: 10.1073/pnas.1702012114

Kleman, A. M., Yuan, J. Y., Aja, S., Ronnett, G. V., and Landree, L. E. (2008). Physiological glucose is critical for optimized neuronal viability and AMPK responsiveness in vitro. *J. Neurosci. Methods* 167, 292–301. doi: 10.1016/j.jneumeth.2007.08.028

Lai, A. K. W., and Lo, A. C. Y. (2013). Animal models of diabetic retinopathy: summary and comparison. *J. Diabetes Res.* 2013:106594. doi: 10.1155/2013/106594

Liu, Y., Xu, X., Tang, R., Chen, G., Lei, X., Gao, L., et al. (2013). Viability of primary cultured retinal neurons in a hyperglycemic condition. *Neural Regen. Res.* 8, 410–419. doi: 10.3969/j.issn.1673-5374.2013.05.004

London, A., Benhar, I., and Schwartz, M. (2013). The retina as a window to the brain-from eye research to CNS disorders. *Nat. Rev. Neurol.* 9, 44–53. doi: 10.1038/nrneurol.2012.227

Matsusue, K., Gavrilova, O., Lambert, G., Brewer, H. B., Ward, J. M., Inoue, Y., et al. (2004). Hepatic CCAAT/enhancer binding protein alpha mediates induction of lipogenesis and regulation of glucose homeostasis in leptin-deficient mice. *Mol. Endocrinol. Baltim. Md* 18, 2751–2764. doi: 10.1210/me.2004-0213

Ménard, C., Hein, P., Paquin, A., Savelson, A., Yang, X. M., Lederfein, D., et al. (2002). An essential role for a MEK-C/EBP pathway during growth factor-regulated cortical neurogenesis. *Neuron* 36, 597–610. doi: 10.1016/s0896-6273(02)01026-7

Mutlu, U., Colijn, J. M., Ikram, M. A., Bonnemaijer, P. W. M., Licher, S., Wolters, F. J., et al. (2018). Association of retinal neurodegeneration on optical coherence tomography with dementia: a population-based study. *JAMA Neurol.* 75, 1256–1263. doi: 10.1001/jamaneurol.2018.1563

Ng, Y. P., He, W., and Ip, N. Y. (2003). Leukemia inhibitory factor receptor signaling negatively modulates nerve growth factor-induced neurite outgrowth in PC12 cells and sympathetic neurons. *J. Biol. Chem.* 278, 38731–38739. doi: 10.1074/jbc.M304623200

Ogama, N., Sakurai, T., Kawashima, S., Tanikawa, T., Tokuda, H., Satake, S., et al. (2018). Postprandial hyperglycemia is associated with white matter hyperintensity and brain atrophy in older patients with type 2 diabetes mellitus. *Front. Aging Neurosci.* 10:273. doi: 10.3389/fnagi.2018.00273

Paquin, A., Barnabé-Heider, F., Kageyama, R., and Miller, F. D. (2005). CCAAT/enhancer-binding protein phosphorylation biases cortical precursors to generate neurons rather than astrocytes in vivo. *J. Neurosci. Off. J. Soc. Neurosci.* 25, 10747–10758. doi: 10.1523/JNEUROSCI.2662-05.2005

Peles, E., and Salzer, J. L. (2000). Molecular domains of myelinated axons. *Curr. Opin. Neurobiol.* 10, 558–565. doi: 10.1016/s0959-4388(00)00122-7

Perry, S. W., Epstein, L. G., and Gelbard, H. A. (1997). In situ trypan blue staining of monolayer cell cultures for permanent fixation and mounting. *BioTechniques* 22, 1024–1021. doi: 10.2144/97226bm01

Ramirez, A. I., de Hoz, R., Salobrar-Garcia, E., Salazar, J. J., Rojas, B., Ajoy, D., et al. (2017). The Role of Microglia in Retinal Neurodegeneration: Alzheimer's Disease, parkinson, and glaucoma. *Front. Aging Neurosci.* 9:214. doi: 10.3389/fnagi.2017.00214

Ramji, D. P., and Foka, P. (2002). CCAAT/enhancer-binding proteins: structure, function and regulation. *Biochem. J.* 365, 561–575. doi: 10.1042/BJ20020508

Reese, B. E. (2011). Development of the retina and optic pathway. *Vision Res.* 51, 613–632. doi: 10.1016/j.visres.2010.07.010

Saleh, A., Chowdhury, S. K. R., Smith, D. R., Balakrishnan, S., Tessler, L., Schartner, E., et al. (2013). Diabetes impairs an interleukin-1β-dependent pathway that enhances neurite outgrowth through JAK/STAT3 modulation of mitochondrial

bioenergetics in adult sensory neurons. *Mol. Brain* 6:45. doi: 10.1186/1756-6606-6-45

Salvadores, N., Sanhueza, M., Manque, P., and Court, F. A. (2017). Axonal degeneration during aging and its functional role in neurodegenerative disorders. *Front. Neurosci.* 11:451. doi: 10.3389/fnins.2017.00451

Santuccione, A., Sytnyk, V., Leshchyns'ka, I., and Schachner, M. (2005). Prion protein recruits its neuronal receptor NCAM to lipid rafts to activate p59fyn and to enhance neurite outgrowth. *J. Cell Biol.* 169, 341–354. doi: 10.1083/jcb.200409127

Schroeder-Gloeckler, J. M., Rahman, S. M., Janssen, R. C., Qiao, L., Shao, J., Roper, M., et al. (2007). CCAAT/enhancer-binding protein beta deletion reduces adiposity, hepatic steatosis, and diabetes in Lepr(db/db) mice. *J. Biol. Chem.* 282, 15717–15729. doi: 10.1074/jbc.M701329200

Sundstrom, J. M., Hernández, C., Weber, S. R., Zhao, Y., Dunklebarger, M., Tiberti, N., et al. (2018). Proteomic analysis of early diabetic retinopathy reveals mediators of neurodegenerative brain diseases. *Invest. Ophthalmol. Vis. Sci.* 59, 2264–2274. doi: 10.1167/iovs.17-23678

Sytnyk, V., Leshchyns'ka, I., Delling, M., Dityateva, G., Dityatev, A., and Schachner, M. (2002). Neural cell adhesion molecule promotes accumulation of TGN organelles at sites of neuron-to-neuron contacts. *J. Cell Biol.* 159, 649–661. doi: 10.1083/jcb.200205098

Tabata, T., Sawada, S., Araki, K., Bono, Y., Furuya, S., and Kano, M. (2000). A reliable method for culture of dissociated mouse cerebellar cells enriched for Purkinje neurons. *J. Neurosci. Methods* 104, 45–53. doi: 10.1016/s0165-0270(00)00323-x

Veys, L., Vandenabeele, M., Ortuño-Lizarán, I., Baekelandt, V., Cuenca, N., Moons, L., et al. (2019). Retinal α-synuclein deposits in Parkinson's disease patients and animal models. *Acta Neuropathol.* 137, 379–395. doi: 10.1007/s00401-018-01956-z

Waid, D. K., and McLoon, S. C. (1998). Ganglion cells influence the fate of dividing retinal cells in culture. *Dev. Camb. Engl.* 125, 1059–1066.

Watanabe, T., and Raff, M. C. (1990). Rod photoreceptor development in vitro: intrinsic properties of proliferating neuroepithelial cells change as development proceeds in the rat retina. *Neuron* 4, 461–467. doi: 10.1016/0896-6273(90)90058-n

Weinstein, G., Maillard, P., Himali, J. J., Beiser, A. S., Au, R., Wolf, P. A., et al. (2015). Glucose indices are associated with cognitive and structural brain measures in young adults. *Neurology* 84, 2329–2337. doi: 10.1212/WNL.0000000000001655

Yan, Z., Liao, H., Chen, H., Deng, S., Jia, Y., Deng, C., et al. (2017). Elevated intraocular pressure induces amyloid-β deposition and tauopathy in the lateral geniculate nucleus in a monkey model of glaucoma. *Invest. Ophthalmol. Vis. Sci.* 58, 5434–5443. doi: 10.1167/iovs.17-22312

Conflict of Interest Statement: The authors declare that the research was conducted in the absence of any commercial or financial relationships that could be construed as a potential conflict of interest.

frontiers in Neuroscience

ORIGINAL RESEARCH
published: 19 September 2019
doi: 10.3389/fnins.2019.00991

Retinal Phenotype in the rd9 Mutant Mouse, a Model of X-Linked RP

*Antonio Falasconi[1,2], Martina Biagioni[1], Elena Novelli[1], Ilaria Piano[3], Claudia Gargini[3] and Enrica Strettoi[1]**

[1] *Institute of Neuroscience, National Research Council (CNR), Pisa, Italy,* [2] *Sant'Anna School of Advanced Studies, Pisa, Italy,* [3] *Department of Pharmacy, University of Pisa, Pisa, Italy*

Retinal degeneration 9 (rd9) mice carry a mutation in the retina specific "Retinitis Pigmentosa GTPase Regulator (RPGR)" Open Reading Frame (ORF) 15 gene, located on the X chromosome and represent a rare model of X-linked Retinitis Pigmentosa (XLRP), a common and severe form of retinal degeneration (Wright et al., 2010; Tsang and Sharma, 2018). The rd9 RPGR-ORF15 mutation in mice causes lack of the protein in photoreceptors and a slow degeneration of these cells with consequent decrease in Outer Nuclear Layer (ONL) thickness and amplitude of ERG responses, as previously described (Thompson et al., 2012). However, relative rates of rod and cone photoreceptor loss, as well as secondary alterations occurring in neuronal and non-neuronal retinal cell types of rd9 mutants remain to be assessed. Aim of this study is to extend phenotype analysis of the rd9 mouse retina focusing on changes occurring in cells directly interacting with photoreceptors. To this purpose, first we estimated rod and cone survival and its degree of intraretinal variation over time; then, we studied the morphology of horizontal and bipolar cells and of the retinal pigment epithelium (RPE), extending our observations to glial cell reactivity. We found that in rd9 retinas rod (but not cone) death is the main cause of decrease in ONL thickness and that degeneration shows a high degree of intraretinal variation. Rod loss drives remodeling in the outer retina, with sprouting of second-order neurons of the rod-pathway and relative sparing of cone pathway elements. Remarkably, despite cone survival, functional defects can be clearly detected in ERG recordings in both scotopic and photopic conditions. Moderate levels of Muller cells and microglial reactivity are sided by striking attenuation of staining for RPE tight junctions, suggesting altered integrity of the outer Blood Retina Barrier (BRB). Because of many features resembling slowly progressing photoreceptor degeneration paradigms or early stages of more aggressive forms of RP, the rd9 mouse model can be considered a rare and useful tool to investigate retinal changes associated to a process of photoreceptor death sustained throughout life and to reveal disease biomarkers (e.g., BRB alterations) of human XLRP.

Keywords: Retinitis Pigmentosa, sprouting, remodeling, retinal pigment epithelium, cone photoreceptor(s), bipolar cell, horizontal cell

OPEN ACCESS

Edited by:
Peter Koulen,
University of Missouri System, United States

Reviewed by:
Wolfgang Baehr,
The University of Utah, United States
Nicolás Cuenca,
University of Alicante, Spain

****Correspondence:***
Enrica Strettoi
enrica.strettoi@in.cnr.it

Specialty section:
This article was submitted to Neurodegeneration, a section of the journal Frontiers in Neuroscience

Received: *09 July 2019*
Accepted: *03 September 2019*
Published: *19 September 2019*

Citation:
Falasconi A, Biagioni M, Novelli E, Piano I, Gargini C and Strettoi E (2019) Retinal Phenotype in the rd9 Mutant Mouse, a Model of X-Linked RP. Front. Neurosci. 13:991. doi: 10.3389/fnins.2019.00991

INTRODUCTION

Retinitis pigmentosa (RP) is a family of clinically analogous disorders, featuring photoreceptor degeneration and alterations in retinal pigment epithelium (RPE), in most cases leading to blindness (Hartong et al., 2006). Etiology is linked to a plethora of mutations affecting more than 70 genes, involving virtually all aspects of photoreceptor structure and function (Daiger et al., 2007; Wright et al., 2010). These extremely specialized cells have a high metabolic demand, require a complex gene network and rely on a fully functional RPE to sustain the energetic and physiological burden of phototransduction, outer segment renewal and continuous communication with inner retinal neurons (Wright et al., 2010). While the outer segment of photoreceptors is tightly packed with membranes and proteins necessary to phototransduction, the inner segment acts as biosynthetic factory to produce needed proteins and fatty acids. The continuous flow of these fundamental factors to the outer segments relies on a highly specialized connecting cilium (Besharse et al., 1977; Wolfrum and Schmitt, 2000; Burgoyne et al., 2015; Chadha et al., 2019) and it is not surprising that almost one quarter of known photoreceptor degeneration-causing genes are involved in the function of this organelle (RetNet, the Retinal Information Network)[1]. The Retinitis Pigmentosa GTPase Regulator (RPGR) is located on the X chromosome and, together with its interactome (Zhang et al., 2019), plays a critical role for connecting cilium function (Megaw et al., 2015). Mutations in RPGR account for 10–20% of all RP cases and 70–80% of all cases of X-linked RP (Huang et al., 2012; Megaw et al., 2015; Tsang and Sharma, 2018) with different mutations corresponding to different retinal phenotypes (Megaw et al., 2015; Charng et al., 2016; Lyraki et al., 2016). RPGR exists in two different isoforms: one is expressed throughout the body, while the other is retina-specific. The retinal-specific form is composed of 15 exons, the first 14 of which shared with the non-retinal isoform. Exon 15 or Open Reading Frame 15 (ORF15) is solely present in retinal RPGR and constitutes a mutational hotspot in the gene (Megaw et al., 2015; Lyraki et al., 2016; Rao et al., 2016).

The rd9 mouse model carries a 32 bp duplication in ORF15 with a premature stop-codon, causing absence of the protein and a slowly progressing loss of photoreceptors (Thompson et al., 2012). The main features of this rare model of X-linked RP have been described in previous studies. Nonetheless, the relative rate of degeneration of rods and cones, as well as possible remodeling of inner retinal neurons and RPE following the slow pattern of photoreceptor death typical of this model, remain unknown. Yet, evaluation of retinal effects beyond photoreceptors are of utmost importance, especially in view of newly developed potential therapeutic strategies, such as gene-therapy or epiretinal prostheses, which rely considerably upon preservation of retinal architecture.

In this study, we provide a secondary retinal characterization of the rd9 mouse model, focusing on cells directly interacting with photoreceptors, and namely bipolar and horizontal cells, as well as on non-neuronal retinal cell types (Muller cells, microglia/macrophages and the, RPE), describing their morphological changes in parallel to photoreceptor loss and to functional abnormalities detected by ERG recordings.

[1]https://sph.uth.edu/retnet/

MATERIALS AND METHODS

Mouse Lines and Animals Used

Animals were treated in accordance to Italian and European institutional guidelines, following experimental protocols approved by the Italian Ministry of Health (Protocol #17/E-2017, Authorization 599 2017-PR, CNR Neuroscience Institute, Pisa; Protocol #DGSAF0001996/2014, Authorization 653/2017-PR, Department of Pharmacy, University of Pisa) and by the Ethical Committees of both Institutions. Protocols adhere to the Association for Research in Vision and Ophthalmology (ARVO) statement for the use of animals in research.

Male rd9/Y, female rd9/X and WT mice were used for this study. Rd9 mice are naturally occurring mutants, identified by the Jackson Laboratories (Chang et al., 2002), and have a C57Bl6/J background. All mice were originally from Jackson (Bar Harbor, Maine, United States). Groups of $n = 4$ mice were used for studies carried on at specific ages (12 months for WT mice, 12 and 18 months for rd9 mice) for both quantitative and qualitative analysis. Additional rd9/Y male mice ($n = 4$) were used for pilot experiments. A total of 16 rd9 and 8 WT mice were used for morphological studies only. A group of 12-months old male rd9/Y and female rd9/X mice ($n = 9$) and 12 months old WT ($n = 5$) were used for ERG recordings and their retinas further studied by morphological methods.

Tissue Preparation, Histology and Immunocytochemistry (ICCH)

Mice were anesthetized with intraperitoneal injections of 3-bromo-ethanol in 1% tert-amyl alcohol (Avertin, 0.1 ml/5 g body weight), their eyes enucleated. Animals were killed by cervical dislocation or intracardiac Avertin injection. Eyes were dorsally labeled and eye cups were obtained by removing anterior segments and lens and fixed in 4% paraformaldehyde (PFA) in 0.1 M phosphate buffer, PB, pH7.4, for 1 h, at room temperature. Afterward, they were washed four times (15' intervals) in PB and infiltrated in 30% sucrose in PB overnight. Eye cups were then frozen in Tissue-Tek O.C.T. compound (4583, Sakura Olympus, Italy) using cold isopentane (−80°C) and keeping a reference on the dorsal pole. Cryostat sections (12 μm thick) were collected on Super Frost slides and used for immunocytochemistry (ICCH). Some eyes were used to prepare retinal whole mounts, in which the retina was separated from the RPE and flattened by making four radial cuts toward the head of the optic nerve. For some eyes, the RPE was also used for ICCH as described below. ICCH on retinal sections, whole mounts and RPE was performed following (Barone et al., 2012), by incubation in (i) blocking solution with 0.3% Triton-X 100, 5% of the serum of the species in which the secondary antibody was generated and 0.01 M Phosphate Buffer Saline (PBS); incubation time was 2 h for the sections and overnight for whole mounts and

RPEs; (ii) primary antibody (Ab), diluted in PBS, 0.1% Triton-X 100 and 1% serum; incubation time was overnight for the sections and 3 days for whole mounts and RPEs; (iii) fluorescent secondary Ab, diluted as the primary Ab; incubation time was 2–3 h for the sections and 2 days for whole mounts and RPEs. Incubations steps were done at 4°C. Mouse monoclonal, primary Abs used for retinal sections were against: Neurofilament 200 (13552 AbCam, Cambridge United Kingdom; diluted 1:400), Ctbp2/Ribeye (BD Transduction Laboratories, Milan, Italy; diluted 1:500), Post-Synaptic Density 95 (13552 AbCam, Cambridge United Kingdom; diluted 1:500); Light Sensitive Channel (kindly donated by Robert Molday, University of British Columbia, Vancouver, Canada), diluted 1:1000); Protein Kinase Cα (PKCα; P5704, Sigma-Aldrich, Italy; diluted 1:800), Synaptotagmin 2 (ZNP-1) (Zebrafish International Resource Center, Eugene, OR, United States; diluted 1:500). Rabbit polyclonal, primary Abs were: Cone Arrestin (AB15282, Merck-Millipore, Italy; diluted 1:5000); Calbindin D (CB38a, Swant Ltd., Switzerland, diluted 1:500); Protein Kinase Cα (PKCα; P4334, Sigma-Aldrich, Italy; diluted 1:800); Glial Fibrillary Acidic Protein (GFAP; G9269, Sigma-Aldrich, Italy; diluted 1:1000), Iba1 (019-19741, Wako, United States; diluted 1:500), Zonula Occludens 1 (ZO-1) (ZYMED Laboratories 40_2300, diluted 1:100). Sheep (polyclonal or monoclonal) primary Abs were: Secretagogin (SCGN) (BioVendor, GmbH, Germany, diluted 1:2000). Abs against Cone Arrestin were also used in whole mount preparations, at 10x the concentrations used for sections. Secondary antibodies were: donkey anti-mouse Alexa Fluor 488 (A-21202, Life Technologies, Italy); donkey anti-rabbit Rhodamine Red X (715296151); Donkey Anti-Sheep (713-546-147), all from Jackson ImmunoResearch laboratories, United States; these were diluted 1:1000 for retinal sections and for whole mount preparations. For nuclear counterstaining, retinal sections were incubated for 2 min in Hoechst (33342), from Life technologies, Italy, diluted 1:1000. After rinsing in PBS, specimens were mounted in Vectashield (H-1000; Vector Laboratories, Burlingame, CA, United States) and coverslipped.

RPE Preparation

After separation of the retina from the outer eye (RPE and sclera), the sclera was carefully made clear of all muscle insertions. The outer ocular layers were then radially cut with 4 to 12 incisions toward the head of the optic nerve and incubated (RPE side up) in small plastic wells, processed for ICCH as described above and mounted flat on glass slides.

Imaging

Images of retinal preparations were obtained with a Zeiss Imager.Z2 microscope equipped with an Apotome2 device (Zeiss, Milan, Italy), using a Plan Neofluar 40x/1.25 and a Plan Neofluar 63x/1.25 oil objectives. Images were saved as tiff files; brightness and contrast were adjusted with the Zeiss software ZEN®PRO 2012 or with Adobe Photoshop. Retinal whole mounts were also imaged with the Imager.Z2 microscope using EC Plan-Neofluar 5x/0.16 M27, 10x/0.3 M27 and 20x/0.50 M27 objectives; images were tiled with ZEN module "Tiles & Positions" software to reconstruct the entire retinal surface when needed.

Outer Nuclear Layer (ONL) Measurements on Retinal Sections

Three equatorial retinal sections (including the optic nerve head) were obtained from eyes of different mice at each age point; after nuclear staining, 4 *z*-stack images (6 μm thickness, 0.6 μm intervals) at different eccentricities (peripheral ventral, central ventral, peripheral dorsal, central dorsal) were acquired from each section. Using the count tool of Adobe Photoshop, the number of ONL rows were counted in each image and the results were averaged to obtain the mean number (and standard error) of ONL rows per group (WT 12 months, rd9 12 months and rd9 18 months). The coefficient of variation (standard deviation/mean) was calculated for each eccentricity in each retina and results were averaged to obtain the mean Coefficient of Variation per experimental group (WT 12 months, rd9 12 months, and rd9 18 months).

Cone Counts in Retinal Whole Mounts

Whole-mount retinas were stained for cone Arrestin. To assess total cone numbers taking into account local anisotropies in retinal degeneration patterns and center-to-periphery changes in cell density, cells were counted in 16 fields regularly spaced along the two main (horizontal and vertical) retinal meridians (8 fields along the dorso-ventral axis and 8 along the naso-temporal axis, respectively), covering the retina from the far periphery to the proximity of the optic nerve head. Counting fields were $223.8 \times 167.6\ \mu m^2$ fields within which z-stacks of 3 focal planes at 0.6 μm intervals, (1.8 μm total thickness) encompassing cone inner segments were obtained. Maximum projections of *z*-stacks were used for further analysis.

Manual Counting

The average number of cones per image was assessed as described before (Barone et al., 2012). The number of cones/mm^2 in each retina was then estimated. The Adobe Photoshop Measure tool was used to measure the area of each retina using low-magnification images of whole mounts. Then, the number of cones per retina were estimated and averaged to obtain the mean number of cones per retina in each experimental group. Coefficient of variation (standard deviation/mean) was calculated for each eccentricity level in each retina for all experimental groups.

Automated Counting

Images used for manual counting were also used to test a method for automated counting of cones developed *ad hoc*. Through a custom-made MATLAB® (Mathworks, United States) script, images were binarized; connected components in the image were identified and those with an area smaller than 2% of the average cone's area were not considered for further analysis. The image was then down sampled with a factor 0.3 and watershed segmentation was applied to ensure appropriate counting of touching components. As in the manual counting, all components intersecting the right or bottom borders were not included in the counts. After obtaining the number of cones in each acquired image, the number of cones per retina, the mean number of cones per retina in each experimental group as well as

the individual and mean value of the coefficient of variation were calculated as for the manual counting protocol.

Parameters for area filtering (2%) and down-sampling (0.3) were identified empirically based on accuracy of the algorithm on test images. Performance assessment of the algorithm was carried out by Pearson correlation analysis between manual and automated counting in single images and through analysis of the error (*Manual result − Automated Result)/ Manual result*) distribution. Results are shown in **Supplementary Figure S1**. The automated method was found to have an accuracy of 95% and allowed much faster counting of elements in each image.

ZO-1 Staining Intensity Quantification in RPE

Each whole-mount RPE was stained for ZO-1 and revealed with a secondary antibody conjugated with Alexa Fluor 488. *z*-stack images (2.5 μm thickness) were acquired with the Zeiss Imager.Z2 microscope equipped with an Apotome2 device, using both the green and red filters, which made numerous autofluorescent bodies visible in the *cytoplasm* of RPE cells (**Supplementary Figure S2**), as previously reported (Marmorstein et al., 2002). Acquisition parameters were set for the first rd9 12 months old sample and then kept consistent for images from all different preparations.

To understand whether *cytosolic* fluorescence (**Supplementary Figure S2**) had to be attributed to non-specific secondary antibody binding or to effective presence of ZO-1 (revealed by Alexa Fluor 488-s) we performed spectral profiling of RPE cells using a lambda scan routine of a Leica TCS SL confocal microscope (Leica Microsystems, Milan, Italy) equipped with an argon and a helium/neon laser, using a 40x/1.25 HCX PL APO oil objective. Emission spectra with an excitation wavelength of 488 nm allowed univocal differentiation of specific and non-specific staining (**Supplementary Figure S2**), confirming that cytosolic labeling, observed with both green and red filters through the standard fluorescence microscope, corresponded to autofluorescent material, well different from Alexa Fluor 488-conjugated secondary Ab in terms of emission spectra. Based on these findings, fluorescence intensity in the green channel (containing ZO-1 positive elements) was quantified with the aid of a custom-made MATLAB script, discarding pixels with a fluorescence intensity higher than 8 arbitrary units in the red channel, allowing customized denoising of the pictures. Nonetheless, consistent parameters used during acquisition caused saturation of the ZO-1 signal in the WT, biasing downward fluorescence intensity measurement of WT ZO-1. This fact makes our quantification indicative and not absolute.

ERG Recordings

ERGs were recorded from dark-adapted mice by standard methods (Gargini et al., 2007). Briefly, coiled gold electrodes were placed in contact with the cornea moisturized by a thin layer of gel. Pupils were fully dilated by application of a drop of 1% atropine (Farmigea, Pisa, Italy). Scotopic ERG recordings were average responses (n = 5) to flashes of increasing intensity (1.7×10^{-5} to 377.2 cd*s/m^2, 0.6 log units steps) presented with an inter-stimulus interval ranging from 20 s for dim flashes to 1 min for the brightest flashes. Cone (photopic) components were isolated by superimposing the test flashes (0.016 to 377.2 cd*s/m^2, 0.6 log units steps) on a steady background of saturating intensity for rods (30 cd/m^2), after at least 15 min from background onset. Amplitude of the a-wave was measured at 7 ms after the onset of light stimulus; amplitude of the b-wave was measured from the peak of the a-wave to the peak of the b-wave. Oscillatory potentials (OPs) were also measured in both scotopic and photopic conditions. OPs were extracted digitally by using a fifth-order Butterworth filter as previously described (Hancock and Kraft, 2004; Lei et al., 2006). Peak amplitude of each OP (OP1–OP4) was measured (Piano et al., 2016). ERG data were collected from 5 WT and 8 rd9 mice, respectively.

Statistics and Data Analysis

Statistical comparisons were run on GraphPad Prism v6 (GraphPad Software, San Diego, CA, United States) after ensuring the data passed a normality distribution test. Comparisons were made using a double-tailed t-test analysis, with a confidence interval (CI) of 95%. Statistical significance was assessed through p-values reported as asterisks in graphs (*** for $p \leq 0.001$, ** for $p \leq 0.01$, * for $p \leq 0.05$). All results are shown as mean ± standard error of the mean, unless otherwise specified.

RESULTS

Photoreceptor Degeneration

Global photoreceptor loss in rd9 mice was assessed through counting ONL rows of nuclei in vertical retinal sections (**Figure 1**) and counting cones in whole-mount retinas stained for cone arrestin, to confirm and extend previous analysis of ONL thickness in this mutant (Thompson et al., 2012).

ONL rows are slightly but clearly diminished in rd9 12 months old mice (from now on referred to as "rd9 12 months") (8.6 ± 0.2 rows) compared to age matched WT (11.2 ± 0.3 rows) (p = 0.003); photoreceptor loss continues in rd9 18 months old mice (from now on referred to as "rd9 18 months") (7.4 ± 0.2 rows) with respect to rd9 12 months (p = 0.03) (**Figures 1A,B**), confirming previous findings (Thompson et al., 2012). We could not detect a visible topographical pattern in the loss of photoreceptors, which, however, upon quantitative analysis, exhibits a "patchy" distribution with some, apparently random, areas displaying fewer photoreceptors than others. We measured the extent of irregularity in the process of rod degeneration by measuring the coefficient of variation (standard deviation/mean) of ONL rows (**Figure 1C**). Indeed, rd9 12 months showed a significantly higher coefficient of variation in ONL rows (11.6 ± 0.5) compared to WT controls (8.51 ± 0.2) (p = 0.0008), and the pattern become even more irregular in rd9 18 months (16.84 ± 0.9) ($p < 0.0001$). An indication of ON irregularity can be obtained by **Figure 9B** (arrows).

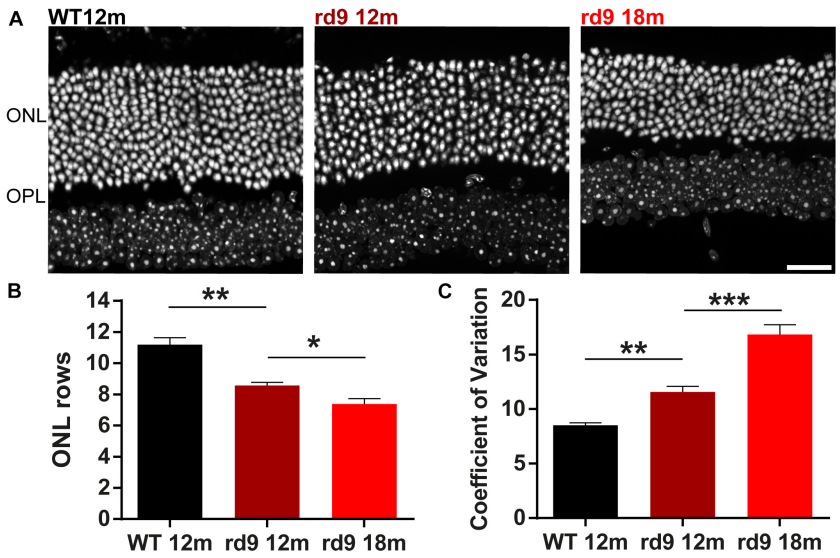

FIGURE 1 | Outer nuclear layer (ONL) in rd9 mutants. **(A)** Representative images of vertical retinal sections with nuclear staining in WT 12 months old, rd9 12 months old and rd9 18 months old mice. Scale bar is 20 μm. **(B)** Quantification [mean ± standard error (se)] of ONL rows in WT 12 months old, rd9 12 months old and rd9 18 months old mice. **(C)** Quantification (mean ± se) of Coefficient of variation in ONL rows (Coefficient of Variation) in WT 12 months old, rd9 12 months old and rd9 18 months old mice. ***for $p < 0.0001$, **for $p < 0.005$, *for $p < 0.05$.

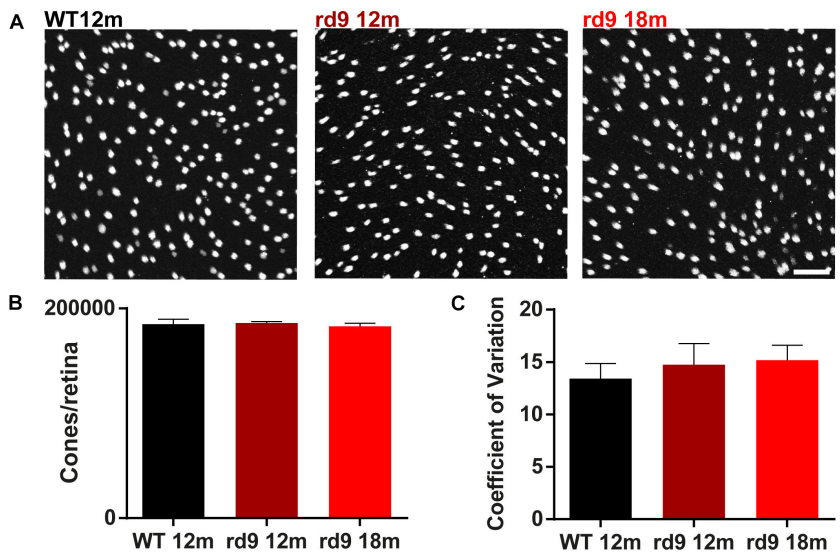

FIGURE 2 | Cone loss in retinal whole mounts. **(A)** Representative images of whole mount ICCH with cone Arrestin antibodies from WT 12 months old, rd9 12 months old and rd9 18 months old mice. Scale bar is 20 μm. **(B)** Quantification (mean ± se) of cones/retina in WT 12 months old, rd9 12 months old and rd9 18 months old mice. **(C)** Quantification (mean ± se) of Coefficient of Variation in cones/retina (Coefficient of Variation) in WT 12 months old, rd9 12 months old and rd9 18 months old mice. Scale bar is 20 μm.

To assess whether the degeneration process affected rods and cone equally, we counted the number of cones/retina using whole mount preparations and also determining the coefficient of variation of these data (**Figure 2**). Results show no significant loss of cone photoreceptors in both rd9 12 months (186,129.9 ± 1,260.4 cones/retina) and rd9 18 months (182,865.2 ± 2,992.9 cones/retina) compared to WT 12 months ((184,921.5 ± 4687.4 cones/retina) (**Figures 2A,B**). Consistently with the absence of numerical alterations in cone numbers, the coefficient of variation does not vary either between the analyzed experimental groups (WT12 months, 13.4 ± 1.45; rd9 12 months, 14.7 ± 2.0; rd9 18 months 15.2 ± 1.4) (**Figure 2C**).

Besides complete survival of cones, we excluded the occurrence of major morphological alterations in this photoreceptor type (**Figure 3**), confirming previous data

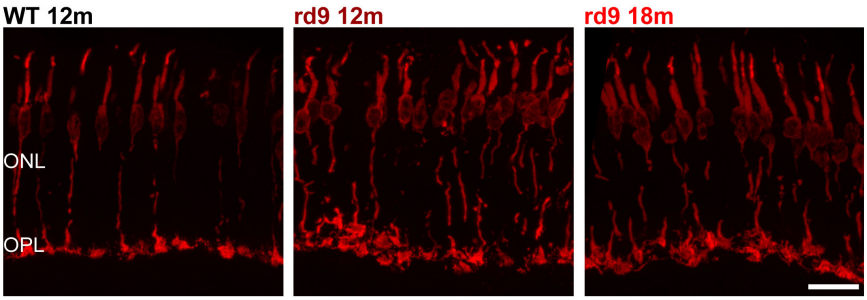

FIGURE 3 | Cone morphology. Representative images of vertical retinal sections stained with anti-cone Arrestin antibodies from WT 12 months old, rd9 12 months old and rd9 18 months old mice. Scale bar is 20 μm. Note the enlargement and slight misalignment of cone pedicles in rd9 compared to WT mice. ONL, Outer Nuclear Layer; OPL, Outer Plexiform Layer.

(Thompson et al., 2012). However, an enlargement of cone pedicles and a distribution along a more irregular plane were observed (**Figure 3**), likely attributable to loss of synaptic spherules and OPL rearrangement following degeneration of rods. Yet, cone pedicles were never observed outside the boundaries of the OPL.

Altogether, our quantitative analysis shows that photoreceptor loss in rd9 mice is mainly due to rod degeneration, while cone number and architecture are mostly preserved, and is associated to intraretinal variation, in agreement with previous findings in humans and murine models of RPGR related disease (Charng et al., 2016). Yet, ERG data (see below) indicate the occurrence of functional abnormalities preceding any morphological alteration in cone cells.

If not otherwise specified, histological images shown to illustrate inner retinal changes were obtained from areas of maximum ONL thinning.

Remodeling of Horizontal Cells

Horizontal cells in the mouse retina are a homogenous axon-bearing population. They receive glutamatergic input from photoreceptors, with dendrites being postsynaptic to cones and axonal arbors receiving synaptic inputs from rods. We studied the morphology of these two specific horizontal cell compartments by means of anti-Calbindin D (**Figures 4A,C**) and anti-Neurofilament 200 antibodies (**Figures 4B,C**) labeling the entire horizontal cell and its axonal compartment (González-soriano, 1994), respectively.

Siding the slow loss of rods, horizontal cells in rd9 retinas sprout profusely with visible remodeling affecting the axonal, rod-connected, components (**Figures 4A–C**, arrows). Thick sprouts can be followed in the outer retina of rd9 12 months with their thin, apical portions ending deeply in the outer half of the ONL (**Figures 4B,C**). Progressing from rd9 12 months to rd9 18 months, an increase in length of dendrites of horizontal cells was also observed, with fine processes penetrating the outer retina and becoming less orderly stratified as the degeneration proceeds (**Figures 4A,C**).

Changes in the axonal compartment of horizontal cells likely reflect the loss of rods, while the subsequent dendritic sprouting suggests abnormalities also in cone-horizontal cell interactions.

Remodeling of Bipolar Cells

Bipolar cells morphology can be studied with specific antibodies, while co-staining of photoreceptor synaptic contacts provides information of remodeling in the OPL.

To study rod bipolar cells, we used anti-PKCα antibodies while labeling photoreceptor ribbon synapses with anti Ctbp1 (Ribeye) antibodies (**Figure 5**). Consistently with rod photoreceptor loss, we observed dendritic sprouting of rod bipolar cells in rd9 12 months, with sprouts virtually always abutting ribeye-positive rod synaptic terminals (**Figure 5**). Fine dendrites of rod bipolar cells elongate toward the ONL, following putative retraction of rod synaptic terminals, and these changes become more evident as the disease progresses (rd9 18 months) and more precisely as rod degeneration continues (**Figure 5**). The inner aspect of rod bipolar cells (axon and axonal arborizations) appeared identical to the WT counterparts (**Figure 5A**).

With similar methods, we assessed putative remodeling of cone to cone bipolar cell synapses (**Figure 6**). Some subtypes of cone bipolar cells (type 2, 3, 4, 5, 6) were stained through anti-secretagogin (SCGN) antibodies (Kim et al., 2008; Puthussery et al., 2010) and their morphology studied, while photoreceptors synaptic contacts were identified by anti-PostSynaptic Density 95 (PSD95) to investigate the presence of paired remodeling, as done for rod bipolar cells (**Figures 6A,B**). SCGN positive cone bipolar cells did not show dendritic sprouting or abnormality of any kind (**Figures 6A,C**) and maintained a morphology undistinguishable from that of WT counterparts. Conversely, rod photoreceptor synaptic terminals, labeled by PSD95 antibodies, confirm retraction in the ONL and irregular arrangement in the OPL (**Figures 6B,C**). Confirming these results, synaptotagmin-2 (ZNP-1) positive cells, which include cone bipolar cell types 2 and 6 (Berntson and Morgans, 2005; Wassle et al., 2009) retained unaltered morphologies in both dendritic and axonal compartments (**Figure 7**).

Altogether, these observations indicate the occurrence of rod degeneration, moderate remodeling of rod-connected neurons, with sparing of the cone-pathway as the degeneration proceeds.

Retinal Physiology

Functional analysis of one-year-old rd9 animals showed a reduction of retinal light responses compared to age-matched

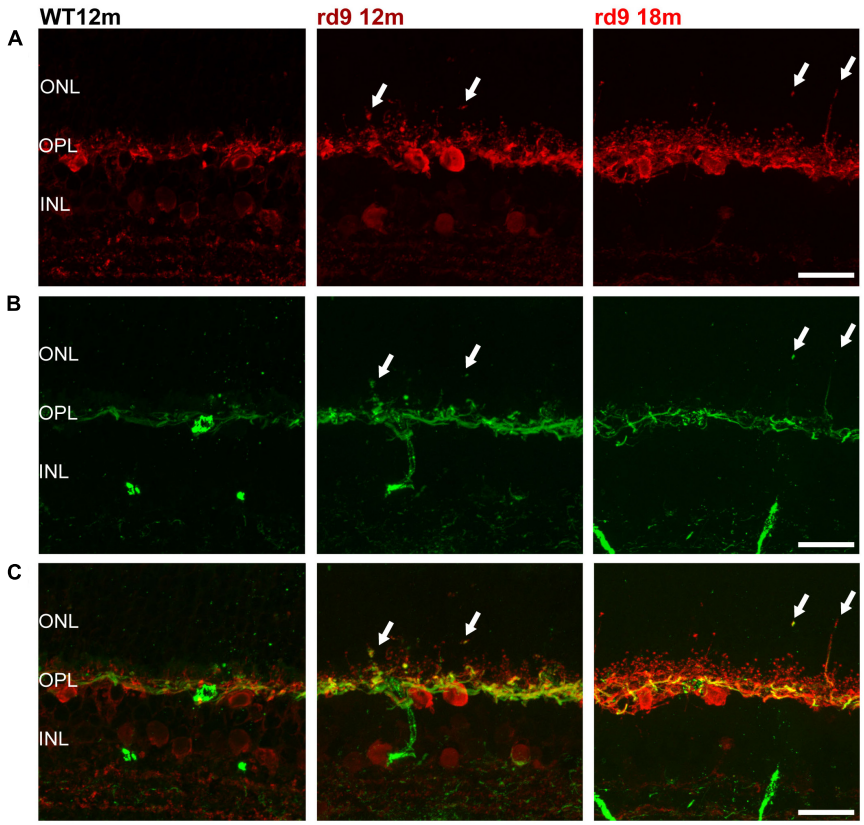

FIGURE 4 | Horizontal cell axonal and dendritic remodeling. **(A)** Representative images of vertical retinal sections stained with anti-Calbindin (red) antibodies from WT 12 months old, rd9 12 months old and rd9 18 months old mice. Scale bar is 20 μm. **(B)** Same fields as above stained with anti-Neurofilament 200 (green) antibodies. Scale bar is 20 μm. **(C)** Merge of **(A)** and **(B)**. Scale bar is 20 μm. Arrows indicate sprouting of the horizontal cell's rod-connected axonal compartment. ONL, Outer Nuclear Layer; OPL, Outer Plexiform Layer; INL, Inner Nuclear Layer.

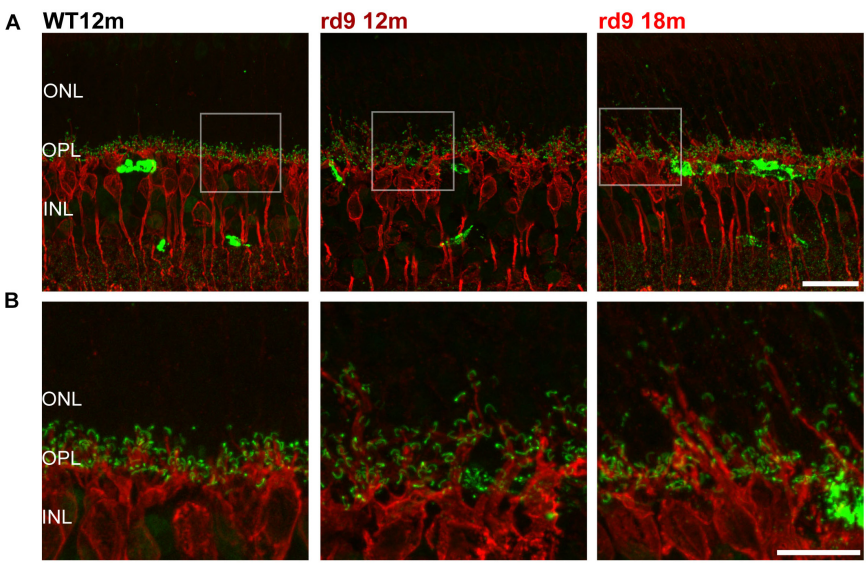

FIGURE 5 | Rod Bipolar cell dendritic remodeling. **(A)** Representative images of vertical retinal sections stained with anti-PKCα (red) and anti-Ribeye (green) antibodies from WT 12 months old, rd9 12 months old and rd9 18 months old mice. Scale bar is 20 μm. **(B)** Details from images in A. Scale bar is 20 μm. Note the extension of bipolar cell dendrites beyond the OPL toward photoreceptor nuclei. ONL, Outer Nuclear Layer; OPL, Outer Plexiform Layer; INL, Inner Nuclear Layer.

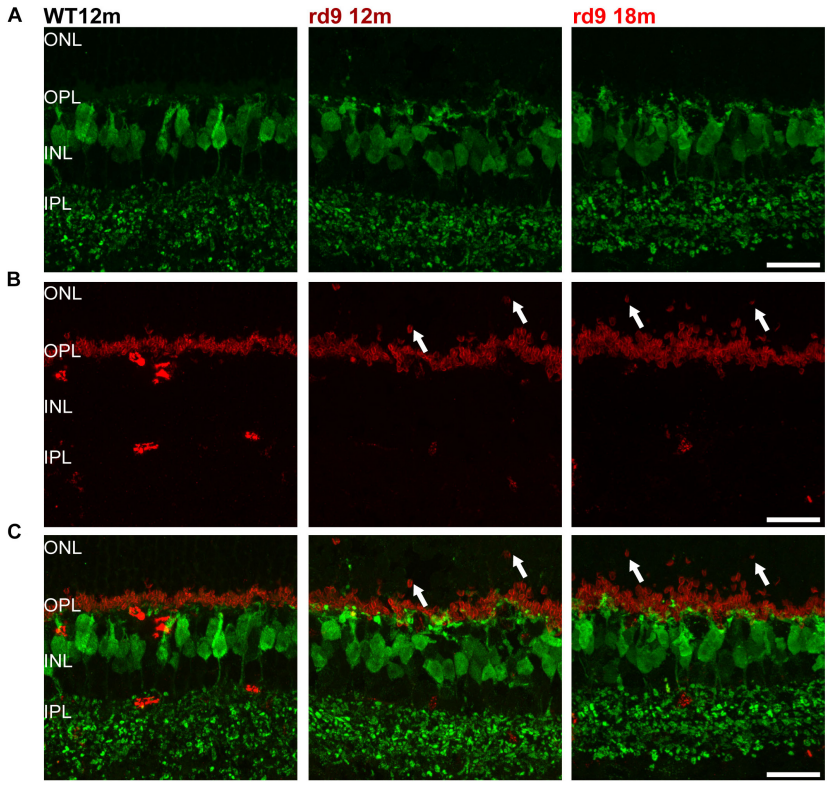

FIGURE 6 | Cone Bipolar cell morphology. **(A)** Representative images of vertical retinal sections stained with anti-Secretagogin (green) antibodies from WT 12 months old, rd9 12 months old and rd9 18 months old mice. Scale bar is 20 μm. **(B)** Same retinal fields as above after staining with Post Synaptic Density 95 (PSD95) (red) antibodies. Scale bar is 20 μm. **(C)** Merge of **(A)** and **(B)**. Scale bar is 20 μm. Note lack of correspondence between displaced rod presynaptic terminals (PSD95 positive) and dendrites of cone bipolar cells (SCGN) (arrows).

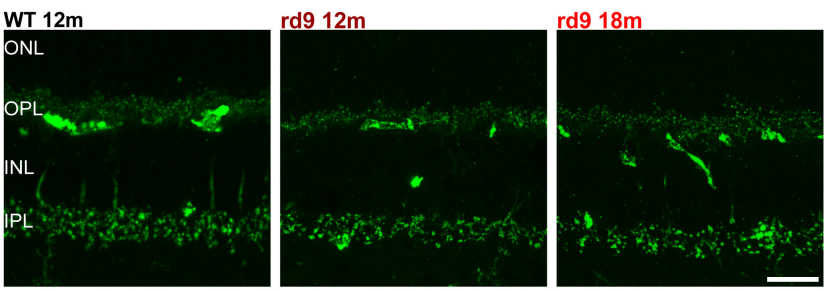

FIGURE 7 | Cone Bipolar cell synaptic contacts. Representative images of vertical retinal sections stained with anti-Synaptotagmin 2 antibodies from WT 12 months old, rd9 12 months old and rd9 18 months old mice. Scale bar is 20 μm. Regular alignment of dendrites in the OPL and axonal arbors in the IPL are evident. ONL, Outer Nuclear Layer; OPL, Outer Plexiform Layer; INL, Inner Nuclear Layer; IPL, Inner Plexiform Layer.

WT controls mice (**Figure 8**), confirming previous results in this mouse model (Thompson et al., 2012). The amplitude of the a-wave of the scotopic ERG measured 7 ms after stimulus onset (and directly correlated with the dark current of the photoreceptors) was significantly reduced in rd9 mice; the b-wave amplitude, an indicator of bipolar cell function, also showed a significant decrement. ERG responses following photopic stimulation also showed a significantly reduction in amplitude as well. The kinetic of the response is also slower in rd9 respect to the control mice in both types of ERG protocol used (**Table 1**). The OPs, extrapolated from both ERG protocols, show a significant reduction in amplitude (**Figures 8C,F**), demonstrating that not only photoreceptors (OP1) but also neurons of the inner retina (OP2-OP4) are compromised by the degenerative processes.

Activation of Muller Glia, Astrocytes and Microglia/Macrophages

Recent data indicate pathological glial cell phenotypes actively contributing to disease progression in the retina

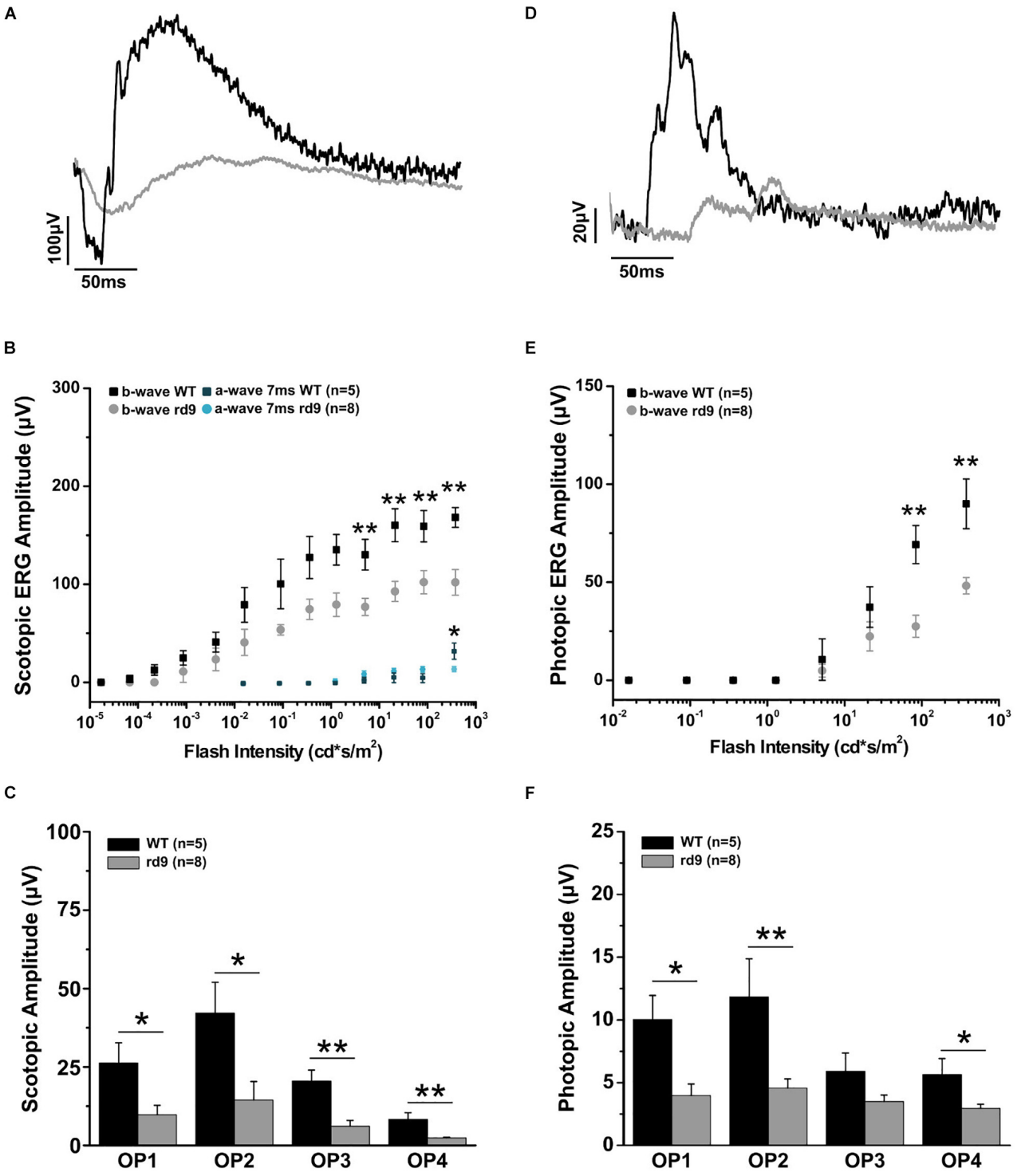

FIGURE 8 | Impairment of scotopic and photopic retinal function. **(A)** Representative scotopic flash ERG recordings from WT and rd9 mice in response to a flash intensity of 377.2 cd*s/m^2, the highest used for all experiments. **(B)** Scotopic a-wave and b-wave amplitude as a function of flash intensity from WT and rd9 mice. Both a-wave and b-wave amplitudes are significantly reduced in rd9 mutants. **(C)** Scotopic oscillatory potentials amplitude (OP1-OP4) extracted from ERG response to the bright test flash (377 cd*s/m^2). **(D)** Representative photopic flash ERG recordings from WT and rd9 mice in response to a flash intensity of 377 cd*s/m^2 superimposed on steady background of 30 cd/m^2. **(E)** Photopic b-wave amplitude as a function of flash intensity. Cone function is significantly reduced in rd9 mice. The graph shows all the luminances used in the photopic ERG protocol, corresponding to medium and high intensity luminances also used in the scotopic ERG, but superimposed on fixed background of 30cd/m^2. **(F)** Photopic oscillatory potentials (OP1-OP4) extracted from the ERG response to the bright test flash (377 cd*s/m^2). OPs show significantly lower amplitudes in rd9 mutants compared to WT mice. **for $p < 0.005$, *for $p < 0.05$.

TABLE 1 | Peak time values of scotopic and photopic ERG.

Flash intensity (cd*s/m2)	WT 12 months Peak time (mean ± SD)	rd9 12 months Peak time (mean ± SD)	*p*-value
Scotopic ERG			
0.09	0.11965 ± 0.00617	0.15947 ± 0.01076	0.013*
0.36	0.09604 ± 0.00618	0.14027 ± 0.01637	0.023*
1.29	0.08884 ± 0.0053	0.12677 ± 0.0149	0.026*
5.12	0.07607 ± 0.00565	0.11507 ± 0.01131	0.013*
21.2	0.07196 ± 0.00424	0.14187 ± 0.02364	0.0085**
83.7	0.0786 ± 0.00773	0.1106 ± 0.01481	N/A
377	0.07734 ± 0.00384	0.13607 ± 0.01625	0.004**
Photopic ERG			
5.12	0.10535 ± 0.02259	0.15227 ± 0.01785	N/A
21.2	0.06381 ± 0.0163	0.09563 ± 0.01441	N/A
83.7	0.05719 ± 0.00903	0.08011 ± 0.01451	N/A
377	0.06359 ± 0.00697	0.0898 ± 0.0143	N/A

***for $p < 0.001$, *for $p < 0.05$.*

(Fletcher et al., 2007; Zhao et al., 2015; Silverman and Wong, 2018; Guadagni et al., 2019) and, more in general, in the CNS (Liddelow et al., 2017; Deczkowska et al., 2018). We examined the morphology of the main glial cell types in the retina of the rd9 mutant, focusing on astrocyte and Muller cell reactivity as assessed by GFAP staining, and on the morphology and distribution of microglia/macrophages.

We found that Muller cells processes exhibit only a moderate GFAP upregulation (with radial processes more intensely immunoreactive) in rd9 12 months compared to WT controls (**Figure 9**). Such reactivity becomes slightly more diffused across the retina in rd9 18 months compared to rd9 12 months (**Figure 9**) but never extends to astrocytes in the time span considered in this study (**Figure 9**).

Putative microglia/macrophages were studied through anti-Iba1 antibodies; double immunostaining for the light-sensitive channel (LSC) of rods allowed visualization of the spatial relationship between microglia and outer segments of degenerating photoreceptors (**Figure 10**). In normal conditions, the ONL is completely void of microglia/macrophages, being resident microglia normally distributed in the two plexiform layers (**Figure 10**). Rd9 mice showed a remarkable increase in the number of microglial cells/macrophages located at the outer retinal level, in close proximity to rod outer segments (**Figure 10** and **Supplementary Figures S3A,B**). These Iba-1 positive cells had ameboid morphologies (**Figures 10B,C**), indicative of activated proinflammatory state (Langmann, 2007; Li et al., 2015), and were also observed to contain LSC-positive vacuoles, strongly suggesting their active phagocytosis of dying rod outer segments (**Figure 10** and **Supplementary Figure S3B**). The inner plexus of microglia displayed a complex and ramified morphology (**Figure 10**), typical of the physiological microglial condition, reinforcing the notion that degeneration in the rd9 mouse model is mostly a process confined to the outer retina.

Interestingly, the presence of microglia/macrophages at the outer retinal level suggests recruitment from the blood vessels, indicative of a generalized inflammatory/immune reaction.

Retinal Pigment Epithelium (RPE) Alterations

The RPE tight junction network is a key component of the outer BRB, while retinal capillary endothelial cells contribute to the inner BRB (Cunha-Vaz et al., 2011; Campbell et al., 2018). Tight junctions are made up of intracellular, transmembrane and extracellular proteins that allow intercellular contacts and relative intracellular signaling: Zonula Occludens 1 (ZO-1) is an intracellular tight junction scaffolding protein, regulating RPE proliferation, patterning and homeostasis in physiological and pathological conditions (Itoh et al., 1999; González-Mariscal et al., 2003; Georgiadis et al., 2010; Campbell et al., 2018).

We investigated RPE morphology through ZO-1 immunostaining (**Figure 11**). Qualitative exploratory analysis disclosed a critical decrement of the intensity of ZO-1 staining in rd9 mice with respect to WT controls (**Figure 11A**). Quantification confirmed the almost 4-fold, decrease in ZO-1 immunofluorescence in rd9 12 months [5.2 ± 0.3 arbitrary units (a.u.)] compared to their WT counterpart (17.14 ± 2.4 a.u.) ($p = 0.003$), with changes being maintained also in rd9 18 months (4.4 ± 1.5 a.u.) (**Figure 11B**).

These findings suggest that RPE integrity is critically altered in rd9 mutants, pinpointing at a non-linearity in the RPE changes with respect to photoreceptor loss.

DISCUSSION

In this study, we provide the secondary characterization of the retinal phenotype of the rd9 mouse model of XLRP, originally described by Thompson et al. (2012), carrying a mutation in the RPGR-ORF15 gene.

Even though both rods and cones carry the mutation, degeneration in this mouse model is mainly driven by rod death, with survival of 65% of all photoreceptors and 100% of cones at 1 year of age compared to WT mice. Degeneration occurs in a patchy fashion with a measurable intraretinal variation. This feature could not be clearly ascribed to a topographical pattern of photoreceptor loss, nonetheless, together with cone preservation, it is a recurrent finding in XLRP patients (Charng et al., 2016).

The slow but continuous process of rod loss entails an expected remodeling in post synaptic neurons, with thickening and extension toward the outer retina in horizontal cells axonal arborizations and major dendritic sprouting of rod bipolar cells. Sprouting is paired by dislocation of rod spherules (but not cone pedicles) in the outer retina, where they are found at different depths throughout the ONL. Hence, it appears that synaptic connections of rods and their partners in the OPL are maintained, albeit spatially rearranged. These changes might be due to excessive and

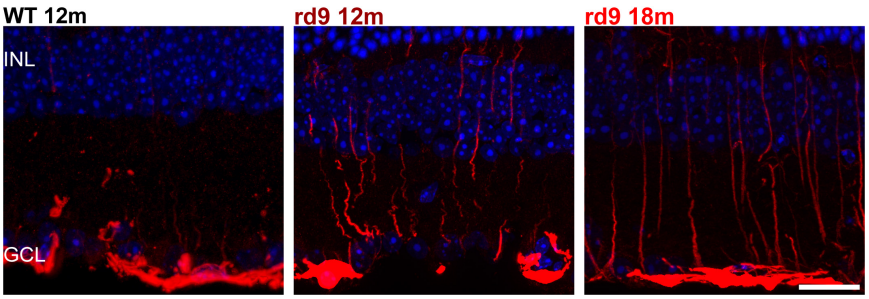

FIGURE 9 | Astrocytes and Muller cells. Representative images of vertical retinal sections labeled with anti-GFAP antibodies (red) and counterstained with DAPI (blue) from WT 12 months old, rd9 12 months old and rd9 18 months old mice. Scale bar is 20 μm. Highly reactive Muller cells' processes are visible at in rd912 months and rd9 18 months. INL, Inner Nuclear Layer; GCL, Ganglion cell layer.

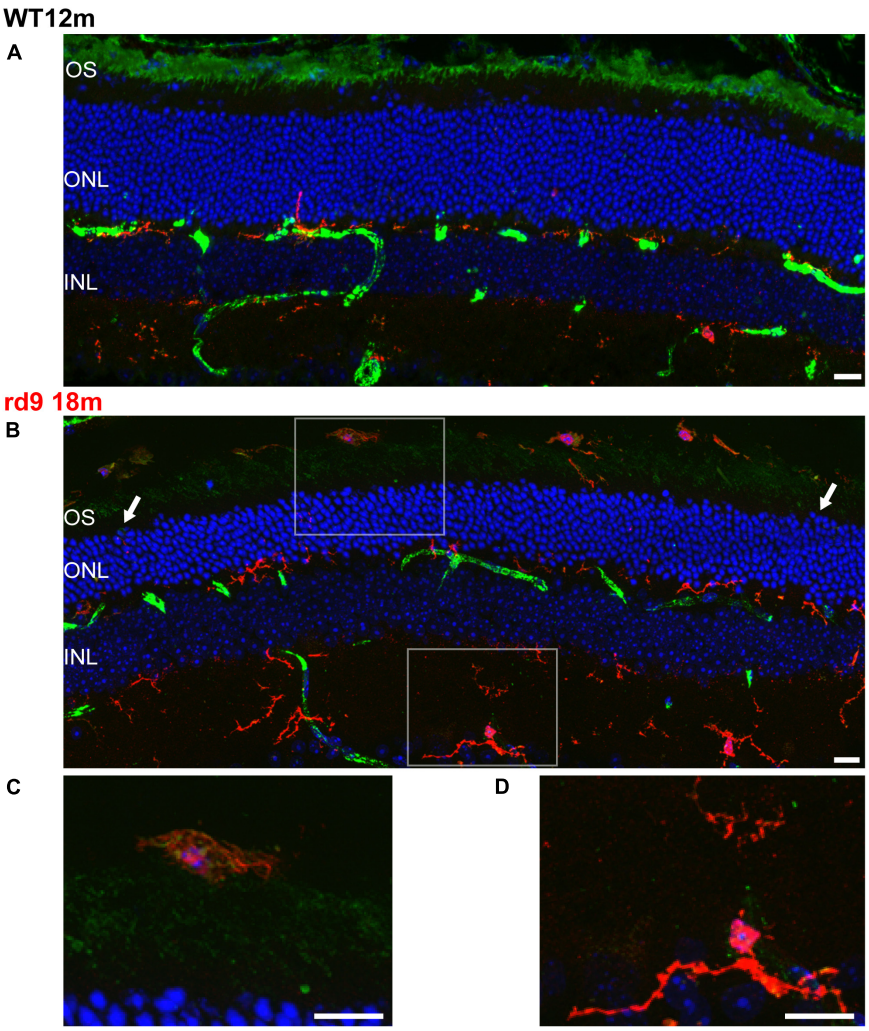

FIGURE 10 | Rod Outer Segments and Microglial reactivity in the outer retina. **(A,B)** Representative image of vertical retinal sections stained with anti-Light Sensitive Channel (green), anti-Iba1 (red) antibodies and Dapi (blue). A: WT 12 months old mouse; B: rd9 18 months old mouse. Arrows point to the left and right sides of the section, where the numbers of ONL rows of nuclei are visibly different, indicating local variability in rod degeneration. Scale bar is 20 μm. **(C)** Detail from **(B)**. Note ameboid morphology of microglia in the subretinal space and the presence of LSC positive residues in intracellular inclusions. Scale bar is 10 μm. **(D)** Detail from **(B)**. Note ramified morphology of microglia in the inner retina. Scale bar is 10 μm. OS, Outer Segments; ONL; Outer Nuclear Layer; OPL; Outer Plexiform Layer.

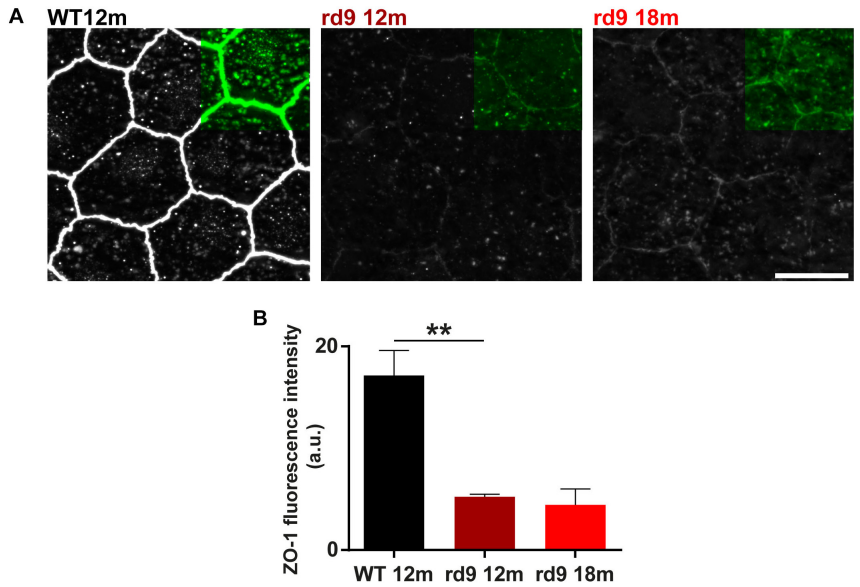

FIGURE 11 | RPE remodeling. **(A)** Representative images of RPE whole mount ICCH with anti-Zonula Occludens 1 (ZO-1) antibodies from WT 12 months old, rd9 12 months old and rd9 18 months old mice. Scale bar is 10 μm. **(B)** Quantification (mean ± se) of Fluorescence intensity (a.u.) in WT 12 months old, rd9 12 months old and rd9 18 months old mice. **for $p < 0.005$.

TABLE 2 | Remodeling of retinal cell types at early stages of degeneration in different mouse models.

	Horizontal cells	Rod bipolars	Cone bipolars	Muller cells	Microglia
rd9 mouse (12/18 months)	Dendritic and axonal sprouting toward the ONL	Dendritic sprouting toward the ONL	Preserved morphology and synaptic architecture	Slightly abnormal GFAP expression and reactivity	Migration in the outer retina and transition to activated ameboid morphology in the outer retina
XLPRA2-affected dogs (< 42 weeks)	Decreased complexity of thin synaptic endings and following dendritic retraction	Dendritic retraction	Preserved morphology and synaptic architecture	Abnormal GFAP expression and reactivity	N/A
rd10 mouse (< P45)	Decreased complexity of thin synaptic endings and following dendritic retraction	Dendritic retraction and mislocalization of metabotropic glutamate receptors	Preserved morphology and synaptic architecture followed by dendritic retraction	Abnormal GFAP expression and reactivity	Migration in the outer retina and transition to activated ameboid morphology
$Crx^{-/-}$ mouse (5–8 months)	Axonal sprouting toward the INL	Dendritic retraction and mislocalization of metabotropic glutamate receptors	Preserved morphology and synaptic architecture followed by dendritic retraction	N/A	N/A
Tvrm4 (7 days post-induction)	Dendritic retraction and axonal arbor thickening	Dendritic retraction and mislocalization of metabotropic glutamate receptors	Dendritic retraction	Abnormal GFAP expression and reactivity	Migration in the outer retina and transition to activated ameboid morphology
P23H transgenic rat (< P40)	Decreased complexity of thin synaptic endings and following dendritic retraction	Dendritic retraction and mislocalization of metabotropic glutamate receptors	Preserved morphology and synaptic architecture followed by dendritic retraction	Abnormal GFAP expression and reactivity	Migration in the outer retina and transition to activated ameboid morphology

References are: XLPRA2 affected dogs (Beltran et al., 2006); rd10 mouse (Gargini et al., 2007; Zabel et al., 2016); $Crx^{-/-}$ (Pignatelli et al., 2004); Tvrm4 mouse (Gargini et al., 2017); P23H rat (Cuenca et al., 2004; Fernández-Sánchez et al., 2015; Noailles et al., 2016). N/A, not available.

dysregulated release of neurotransmitter during rod death, working as a growth signal for second-order neurons (McKinney et al., 2002). Dendritic retraction of second order neurons, typically observed in faster forms of retinal degeneration (Jones et al., 2003; Marc et al., 2003; Gargini et al., 2007; Strettoi, 2015), is never observed in rd9 mutants, reinforcing the notion that only major photoreceptor death can drive synaptic deafferentation in the outer retina and major regressive

remodeling of inner retinal neurons and suggesting the existence of a photoreceptor loss threshold for initiating this remodeling.

Cone pedicles maintain their spatial location but undergo slight enlargement, paralleled by remodeling of horizontal cells dendrites. In the face of these changes, cone bipolar cells are spared, as assessed by morphological examination of types 2, 3, 4, 5, 6 cone bipolar cells. The complete survival of cones and their minor changes at the synaptic level despite the mutation suggests that these cells are less metabolically vulnerable than rods, perhaps as a consequence of the slower or absent renewal of outer segments (Young, 1971; Hogan et al., 1974; Anderson et al., 1980). Secondly, remaining rods may maintain a relatively normal outer retinal microenvironment halting the death of even vulnerable cones (Aït-Ali et al., 2015). Furthermore, cone conservation might partly be responsible for the overall preservation of retinal architecture (Jones et al., 2016). In agreement with morphological data, the scotopic ERG records a reduction of both the a-wave measured 7 ms post stimulus and of the b-wave, confirming the loss of rod photoreceptors and a malfunctioning of the synapses with rod bipolar cells. Despite the considerable maintenance of cone morphological integrity and number, ERG data demonstrate abnormalities in the physiology of the cone system, indicated by the reduction of photopic b-wave as well as by the decrement in OPs. The latter are indicative of a worsening of the transfer of information from photoreceptors to inner retinal neurons. ERG data, also showing delayed kinetics of both scotopic and photopic responses, confirm and extend previous studies on the same animal model (Thompson et al., 2012) and correlate with existing literature on other paradigms of retinal degeneration (Gargini et al., 2007; Piano et al., 2016; Tanabu et al., 2019) all demonstrating that alterations of retinal physiology can be detected before any major morphological change besides rod loss.

The overall process of glial activation and GFAP upregulation typical of RP (Marc et al., 2003; Gargini et al., 2007; Jones et al., 2016) appears limited in the rd9 phenotype, with mild activation of Muller cell processes and presence of infiltrating and/or migrating microglia/macrophages in the outer retina and mostly at the subretinal space. Compared to mutants where the degeneration takes place in few weeks, this phenotype is sensibly milder (Gargini et al., 2007; Zhao et al., 2015; Guadagni et al., 2019). Despite relatively moderate changes in other retinal cell types, RPE cells visibly down-regulate ZO-1, a scaffolding protein, physiologically responsible of epithelium proliferation control and BRB permeability (Itoh et al., 1999; González-Mariscal et al., 2003; Georgiadis et al., 2010). Changes in the RPE junctional architecture have been previously characterized in other models of retinal degeneration (Campbell et al., 2006; Chrenek et al., 2012), nonetheless, to our knowledge, this is the first report of a decrease of ZO-1 immunostaining in an RP model, suggesting an increase of BRB permeability. Indeed, increases in BRB permeability are common in RP patients (Mallick et al., 1984; van Dorp et al., 1992) and also in diabetic retinopathy and Age-related Macular Degeneration (AMD) (Cunha-Vaz et al., 2011; Cunha-Vaz, 2017). Their role in RP progression remains unknown and worth investigating. This suggests that the rd9 mutant can be used to reveal abnormalities of the outer BRB and to study their possible pathological role, in the presence of relatively conserved retinal architecture, mirroring early stages of disease or slowly progressing phenotypes. Generalization of these findings to other mouse models of RP would support the search of mutation-independent biomarkers of early stage disease and motivate development of new therapeutic strategies to halt BRB changes.

Altogether, observed changes occurring in rd9 retinas recapitulate very early stages of degeneration in other mouse models of RP and in RP patients (Strettoi and Pignatelli, 2000; Strettoi et al., 2002, 2003; Marc et al., 2003; Pignatelli et al., 2004; Gargini et al., 2007; Strettoi, 2015; Jones et al., 2016). Indeed, increased or misplaced wiring of inner retinal neurons has been observed in human retinal degeneration and in mouse models at very early stages of the disease. In most cases, it is quickly followed by dendritic retraction and regressive remodeling of second orderd retinal neurons (**Table 2**; Milam et al., 1998; Fariss et al., 2000; Strettoi et al., 2002; Jones et al., 2003, 2016; Marc et al., 2003; Pignatelli et al., 2004). This regressive remodeling is predicted to take place only around 30 months of age in rd9 mice, when ONL thickness is relevantly reduced (Chang et al., 2002). This highlights the potential of the rd9 mouse model as a tool to study early phases of retinal degeneration in a slow-progressing phenotype, with the aim of searching for disease biomarkers (e.g., BRB alterations or opsin mislocalization (Chang et al., 2002; Thompson et al., 2012). This could accelerate diagnosis in human patients and develop treatments to be used in contexts where retinal architecture is largely conserved, like targeted gene therapy, indeed a planned treatment for X-linked RP (Boye et al., 2013; Aguirre, 2017; DiCarlo et al., 2018; Trapani and Auricchio, 2018).

DATA AVAILABILITY

Protocols and analytic methods are given in the text. The datasets generated are available upon request to the corresponding author.

ETHICS STATEMENT

The animal study was reviewed and approved by the CNR Neuroscience Institute, Pisa, Animal Welfare Ethical Committee; and Italian Ministry of Health Protocol #17/E-2017, Authorization 599 2017-PR (for CNR Neuroscience Institute, Pisa) and by the Ethical Committee for Animal Welfare, University of Pisa; and Italian Ministry of Health, Protocol DGSAF0001996/2014, Authorization 653/2017-PR (Department of Pharmacy, University of Pisa).

AUTHOR CONTRIBUTIONS

All authors conceived the study. AF, MB, and EN performed the histological experiments and collected the data. MB conducted the first original observations on RPE abnormalities. AF and ES performed the data analysis. CG and IP performed the electroretinogram recordings, and collected and analyzed the data. AF, CG, and ES wrote the manuscript.

FUNDING

This study was supported by Fondazione Roma, Italy (Retinitis Pigmentosa call).

ACKNOWLEDGMENTS

We thank Dr. Antonia Stefanov for valuable help in tissue preparation; Francesca Biondi and Renzo Direnzo for expert technical assistance. We also thank the BioEnable project, Tuscany region, action POR FESR.

SUPPLEMENTARY MATERIAL

The Supplementary Material for this article can be found online at: https://www.frontiersin.org/articles/10.3389/fnins.2019.00991/full#supplementary-material

REFERENCES

Aguirre, G. D. (2017). Concepts and strategies in retinal gene therapy. *Investig. Ophthalmol. Vis. Sci.* 58, 5399–5411. doi: 10.1167/iovs.17-22978

Aït-Ali, N., Fridlich, R., Millet-Puel, G., Clérin, E., Delalande, F., Jaillard, C., et al. (2015). Rod-derived cone viability factor promotes cone survival by stimulating aerobic glycolysis. *Cell* 161, 817–832. doi: 10.1016/j.cell.2015.03.023

Anderson, D. H., Fisher, S. K., Erickson, P. A., and Tabor, G. A. (1980). Rod and cone disc shedding in the rhesus monkey retina: a quantitative study. *Exp. Eye Res.* 30, 559–574. doi: 10.1016/0014-4835(80)90040-8

Barone, I., Novelli, E., Piano, I., Gargini, C., and Strettoi, E. (2012). environmental enrichment extends photoreceptor survival and visual function in a mouse model of Retinitis Pigmentosa. *PLoS One* 7:e50726. doi: 10.1371/journal.pone.0050726

Beltran, W. A., Hammond, P., Acland, G. M., and Aguirre, G. D. (2006). A Frameshift Mutation in RPGR Exon ORF15 causes photoreceptor degeneration and inner retina remodeling in a model of X-Linked Retinitis Pigmentosa. *Invest. Ophthalmol. Vis. Sci.* 47, 1669–1681. doi: 10.1167/iovs.05-0845

Berntson, A. K., and Morgans, C. W. (2005). Distribution of the presynaptic calcium sensors, synaptotagmin I/II and synaptotagmin III, in the goldfish and rodent retinas. *J. Vis.* 3, 274–280. doi: 10.1167/3.4.3

Besharse, J. C., Hollyfield, J. G., and Rayborn, M. E. (1977). Turnover of rod photoreceptor outer segments: II. membrane addition and loss in relationship to light. *J. Cell Biol.* 75, 507–527. doi: 10.1083/jcb.75.2.507

Boye, S. E., Boye, S. L., Lewin, A. S., and Hauswirth, W. W. (2013). A comprehensive review of retinal gene therapy. *Mol. Ther.* 21, 509–519. doi: 10.1038/mt.2012.280

Burgoyne, T., Meschede, I. P., Burden, J. J., Bailly, M., Seabra, M. C., and Futter, C. E. (2015). Rod disc renewal occurs by evagination of the ciliary plasma membrane that makes cadherin-based contacts with the inner segment. *Proc. Natl. Acad. Sci. U.S.A.* 112, 15922–15927. doi: 10.1073/pnas.1509285113

Campbell, M., Cassidy, P. S., O'Callaghan, J., Crosbie, D. E., and Humphries, P. (2018). Manipulating ocular endothelial tight junctions: applications in treatment of retinal disease pathology and ocular hypertension. *Prog. Retin. Eye Res.* 62, 120–133. doi: 10.1016/j.preteyeres.2017.09.003

Campbell, M., Humphries, M., Kennan, A., Kenna, P., Humphries, P., and Brankin, B. (2006). Aberrant retinal tight junction and adherens junction protein expression in an animal model of autosomal dominant Retinitis pigmentosa: the Rho(−/−) mouse. *Exp. Eye Res.* 83, 484–492. doi: 10.1016/j.exer.2006.01.032

Chadha, A., Volland, S., Baliaouri, N. V., Tran, E. M., and Williams, D. S. (2019). The route of the visual receptor rhodopsin along the cilium. *J. Cell Sci.* 132:jcs229526. doi: 10.1242/jcs.229526

Chang, B., Hawes, N. L., Hurd, R. E., Davisson, M. T., Nusinowitz, S., and Heckenlively, J. R. (2002). Retinal degeneration mutants in the mouse. *Vis. Res.* 42, 517–525. doi: 10.1016/S0042-6989(01)00146-8

Charng, J., Cideciyan, A. V., Jacobson, S. G., Sumaroka, A., Schwartz, S. B., Swider, M., et al. (2016). Variegated yet non-random rod and cone photoreceptor disease patterns in RPGR-ORF15-associated retinal degeneration. *Hum. Mol. Genet.* 25, 5444–5459. doi: 10.1093/hmg/ddw361

Chrenek, M. A., Dalal, N., Gardner, C., Grossniklaus, H., Jiang, Y., Boatright, J. H., et al. (2012). Analysis of the RPE sheet in the rd10 retinal degeneration model. *Adv. Exp. Med. Biol.* 723, 641–647. doi: 10.1007/978-1-4614-0631-0_81

Cuenca, N., Pinilla, I., Sauvé, Y., Lu, B., Wang, S., and Lund, R. D. (2004). Regressive and reactive changes in the connectivity patterns of rod and cone pathways of P23H transgenic rat retina. *Neuroscience* 127, 301–317. doi: 10.1016/j.neuroscience.2004.04.042

Cunha-Vaz, J. (2017). The blood-retinal barrier in the management of retinal disease: EURETINA award lecture. *Ophthalmologica* 237, 1–10. doi: 10.1159/000455809

Cunha-Vaz, J., Bernardes, R., and Lobo, C. (2011). Blood-retinal barrier. *Eur. J. Ophthalmol.* 21, 3–9. doi: 10.5301/EJO.2010.6049

Daiger, S. P., Bowne, S. J., and Sullivan, L. S. (2007). Perspective on genes and mutations causing retinitis pigmentosa. *Arch. Ophthalmol.* 125, 151–158. doi: 10.1001/archopht.125.2.151

Deczkowska, A., Amit, I., and Schwartz, M. (2018). Microglial immune checkpoint mechanisms. *Nat. Neurosci.* 21, 779–786. doi: 10.1038/s41593-018-0145-x

DiCarlo, J. E., Mahajan, V. B., and Tsang, S. H. (2018). Gene therapy and genome surgery in the retina. *J. Clin. Invest.* 128, 2177–2188. doi: 10.1172/JCI120429

Fariss, R. N., Li, Z. Y., and Milam, A. H. (2000). Abnormalities in rod photoreceptors, amacrine cells, and horizontal cells in human retinas with retinitis pigmentosa. *Am. J. Ophthalmol.* 129, 215–223. doi: 10.1016/S0002-9394(99)00401-8

Fernández-Sánchez, L., Lax, P., Campello, L., Pinilla, I., and Cuenca, N. (2015). Astrocytes and müller cell alterations during retinal degeneration in a transgenic rat model of Retinitis Pigmentosa. *Front. Cell. Neurosci.* 9:484. doi: 10.3389/fncel.2015.00484

Fletcher, E., Phipps, J., Ward, M., Puthussery, T., and Wilkinson-Berka, J. (2007). Neuronal and glial cell abnormality as predictors of progression of diabetic retinopathy. *Curr. Pharm. Des.* 13, 2699–2712. doi: 10.2174/138161207781662920

Gargini, C., Novelli, E., Piano, I., Biagioni, M., and Strettoi, E. (2017). Pattern of retinal morphological and functional decay in a light-inducible, rhodopsin mutant mouse. *Sci. Rep.* 7:5730. doi: 10.1038/s41598-017-06045-x

Gargini, C., Terzibasi, E., Mazzoni, F., and Strettoi, E. (2007). Retinal organization in the retinal degeneration 10 (rd10) mutant mouse: a morphological and ERG study. *J. Comp. Neurol.* 500, 222–238. doi: 10.1002/cne.21144

Georgiadis, A., Tschernutter, M., Bainbridge, J. W. B., Balaggan, K. S., Mowat, F., West, E. L., et al. (2010). The tight junction associated signalling proteins ZO-1 and ZONAB regulate retinal pigment epithelium homeostasis in mice. *PLoS One* 5:e15730. doi: 10.1371/journal.pone.0015730

González-Mariscal, L., Betanzos, A., Nava, P., and Jaramillo, B. E. (2003). Tight junction proteins. *Prog. Biophys. Mol. Biol.* 81, 1–44. doi: 10.1016/S0079-6107(02)00037-8

González-soriano, J. (1994). Morphological types of horizontal cell in rodent retinae: a comparison of rat, mouse, gerbil, and guinea pig. *Vis. Neurosci.* 11, 501–517. doi: 10.1017/S0952523800 00242X

Guadagni, V., Biagioni, M., Novelli, E., Aretini, P., Mazzanti, C. M., and Strettoi, E. (2019). Rescuing cones and daylight vision in retinitis pigmentosa mice. *FASEB J.* 33, 10177–10192. doi: 10.1096/fj.201900414R

Hancock, H. A., and Kraft, T. W. (2004). Oscillatory potential analysis and ERGs of normal and diabetic rats. *Investig. Ophthalmol. Vis. Sci.* 45, 1002–1008. doi: 10.1167/iovs.03-1080

Hartong, D. T., Berson, E. L., and Dryja, T. P. (2006). Retinitis pigmentosa. *Lancet* 368, 1795–1809. doi: 10.1016/S0140-6736(06)69740-7

Hogan, M. J., Wood, I., and Steinberg, R. H. (1974). Phagocytosis by pigment epithelium of human retinal cones. *Nature* 252, 305–307. doi: 10.1038/252305a0

Huang, W. C., Wright, A. F., Roman, A. J., Cideciyan, A. V., Manson, F. D., Gewaily, D. Y., et al. (2012). RPGR-associated retinal degeneration in human X-linked RP and a murine model. *Investig. Ophthalmol. Vis. Sci.* 53, 5594–5608. doi: 10.1167/iovs.12-10070

Itoh, M., Furuse, M., Morita, K., Kubota, K., Saitou, M., and Tsukita, S. (1999). Direct binding of three tight junction-associated MAGUKs, ZO-1, ZO-2, and ZO-3, with the COOH termini of claudins. *J. Cell Biol.* 147, 1351–1363. doi: 10.1083/jcb.147.6.1351

Jones, B. W., Pfeiffer, R. L., Ferrell, W. D., Watt, C. B., Marmor, M., and Marc, R. E. (2016). Retinal remodeling in human retinitis pigmentosa. *Exp. Eye Res.* 150, 149–165. doi: 10.1016/j.exer.2016.03.018

Jones, B. W., Watt, C. B., Frederick, J. M., Baehr, W., Chen, C. K., Levine, E. M., et al. (2003). Retinal remodeling triggered by photoreceptor degenerations. *J. Comp. Neurol.* 464, 1–16. doi: 10.1002/cne.10703

Kim, D. S., Ross, S. E., Trimarchi, J. M., Aach, J., Greenberg, M. E., and Cepko, C. L. (2008). Identification of molecular markers of bipolar cells in the murine retina. *J. Comp. Neurol.* 507, 1795–1810. doi: 10.1002/cne.21639

Langmann, T. (2007). Microglia activation in retinal degeneration. *J. Leukoc. Biol.* 81, 1345–1351. doi: 10.1189/jlb.0207114

Lei, B., Yao, G., Zhang, K., Hofeldt, K. J., and Chang, B. (2006). Study of rod- and cone-driven oscillatory potentials in mice. *Investig. Ophthalmol. Vis. Sci.* 47, 2732–2738. doi: 10.1167/iovs.05-1461

Li, L., Eter, N., and Heiduschka, P. (2015). The microglia in healthy and diseased retina. *Exp. Eye Res.* 136, 116–130. doi: 10.1016/j.exer.2015.04.020

Liddelow, S. A., Guttenplan, K. A., Clarke, L. E., Bennett, F. C., Bohlen, C. J., Schirmer, L., et al. (2017). Neurotoxic reactive astrocytes are induced by activated microglia. *Nature* 541, 481–487. doi: 10.1038/nature21029

Lyraki, R., Megaw, R., and Hurd, T. (2016). Disease mechanisms of X-linked retinitis pigmentosa due to RP2 and RPGR mutations. *Biochem. Soc. Trans.* 44, 1235–1244. doi: 10.1042/bst20160148

Mallick, K. S., Zeimer, R. C., Fishman, G. A., Blair, N. P., and Anderson, R. J. (1984). Transport of fluorescein in the ocular posterior segment in Retinitis Pigmentosa. *Arch. Ophthalmol.* 102, 691–696. doi: 10.1001/archopht.1984.01040030547013

Marc, R. E., Jones, B. W., Watt, C. B., and Strettoi, E. (2003). Neural remodeling in retinal degeneration. *Prog. Retin. Eye Res.* 22, 607–655. doi: 10.1016/S1350-9462(03)00039-9

Marmorstein, A. D., Marmorstein, L. Y., Sakaguchi, H., and Hollyfield, J. G. (2002). Spectral profiling of autofluorescence associated with lipofuscin, Bruch's membrane, and sub-RPE deposits in normal and AMD eyes. *Investig. Ophthalmol. Vis. Sci.* 43, 2435–2441.

McKinney, R. A., Luthi, A., Bandtlow, C. E., Gahwiler, B. H., and Thompson, S. M. (2002). Selective glutamate receptor antagonists can induce or prevent axonal sprouting in rat hippocampal slice cultures. *Proc. Natl. Acad. Sci. U.S.A.* 96, 11631–11636. doi: 10.1073/pnas.96.20.11631

Megaw, R. D., Soares, D. C., and Wright, A. F. (2015). RPGR: its role in photoreceptor physiology, human disease, and future therapies. *Exp. Eye Res.* 138, 32–41. doi: 10.1016/j.exer.2015.06.007

Milam, A. H., Li, Z. Y., and Fariss, R. N. (1998). Histopathology of the human retina in retinitis pigmentosa. *Prog. Retin. Eye Res.* 17, 175–205. doi: 10.1016/S1350-9462(97)00012-8

Noailles, A., Maneu, V., Campello, L., Gómez-Vicente, V., Lax, P., and Cuenca, N. (2016). Persistent inflammatory state after photoreceptor loss in an animal model of retinal degeneration. *Sci. Rep.* 6:33356. doi: 10.1038/srep33356

Piano, I., Novelli, E., Della Santina, L., Strettoi, E., Cervetto, L., and Gargini, C. (2016). Involvement of autophagic pathway in the progression of retinal degeneration in a mouse model of diabetes. *Front. Cell. Neurosci.* 10:42. doi: 10.3389/fncel.2016.00042

Pignatelli, V., Cepko, C. L., and Strettoi, E. (2004). Inner retinal abnormalities in a mouse model of Leber's Congenital Amaurosis. *J. Comp. Neurol.* 469, 351–359. doi: 10.1002/cne.11019

Puthussery, T., Gayet-Primo, J., and Taylor, W. R. (2010). Localization of the calcium-binding protein secretagogin in cone bipolar cells of the mammalian retina. *J. Comp. Neurol.* 518, 513–525. doi: 10.1002/cne.22234

Rao, K. N., Anand, M., and Khanna, H. (2016). The carboxyl terminal mutational hotspot of the ciliary disease protein RPGR ORF15 (retinitis pigmentosa GTPase regulator) is glutamylated in vivo. *Biol. Open* 5, 424–428. doi: 10.1242/bio.016816

Silverman, S. M., and Wong, W. T. (2018). Microglia in the retina: roles in development, maturity, and disease. *Annu. Rev. Vis. Sci.* 4, 45–77. doi: 10.1146/annurev-vision-091517-034425

Strettoi, E. (2015). A survey of retinal remodeling. *Front. Cell. Neurosci.* 9:494. doi: 10.3389/fncel.2015.00494

Strettoi, E., and Pignatelli, V. (2000). Modifications of retinal neurons in a mouse model of retinitis pigmentosa. *Proc. Natl. Acad. Sci. U.S.A.* 97, 11020–11025. doi: 10.1073/pnas.190291097

Strettoi, E., Pignatelli, V., Rossi, C., Porciatti, V., and Falsini, B. (2003). Remodeling of second-order neurons in the retina of rd/rd mutant mice. *Vis. Res.* 43, 867–877. doi: 10.1016/S0042-6989(02)00594-1

Strettoi, E., Porciatti, V., Falsini, B., Pignatelli, V., and Rossi, C. (2002). Morphological and functional abnormalities in the inner retina of the rd/rd mouse. *J. Neurosci.* 22, 5492–5504. doi: 10.1523/jneurosci.22-13-05492.2002

Tanabu, R., Sato, K., Monai, N., Yamauchi, K., Gonome, T., Xie, Y., et al. (2019). The findings of optical coherence tomography of retinal degeneration in relation to the morphological and electroretinographic features in RPE65 -/- mice. *PLoS One* 14:e0210439. doi: 10.1371/journal.pone.0210439

Thompson, D. A., Khan, N. W., Othman, M. I., Chang, B., Jia, L., Grahek, G., et al. (2012). Rd9 is a naturally occurring mouse model of a common form of retinitis pigmentosa caused by mutations in RPGR-ORF15. *PLoS One* 7:e35865. doi: 10.1371/journal.pone.0035865

Trapani, I., and Auricchio, A. (2018). Seeing the light after 25 Years of retinal gene therapy. *Trends Mol. Med.* 24, 669–681. doi: 10.1016/j.molmed.2018.06.006

Tsang, S. H., and Sharma, T. (2018). X-linked retinitis pigmentosa. *Adv. Exp. Med. Biol.* 1085, 31–35. doi: 10.1007/978-3-319-95046-4_8

van Dorp, D. B., Wright, A. F., Carothers, A. D., and Bleeker-Wagemakers, E. M. (1992). A family with RP3 type of X-linked retinitis pigmentosa: an association with ciliary abnormalities. *Hum. Genet.* 88, 331–334. doi: 10.1007/BF00197269

Wassle, H., Puller, C., Muller, F., and Haverkamp, S. (2009). Cone contacts, mosaics, and territories of bipolar cells in the mouse retina. *J. Neurosci.* 29, 106–117. doi: 10.1523/jneurosci.4442-08.2009

Wolfrum, U., and Schmitt, A. (2000). Rhodopsin transport in the membrane of the connecting cilium of mammalian photoreceptor cells. *Cell Motil. Cytoskeleton* 46, 95–107. doi: 10.1002/1097-0169(200006)46:2<95::AID-CM2<3.0.CO;2-Q

Wright, A. F., Chakarova, C. F., Abd El-Aziz, M. M., and Bhattacharya, S. S. (2010). Photoreceptor degeneration: genetic and mechanistic dissection of a complex trait. *Nat. Rev. Genet.* 11, 273–284. doi: 10.1038/nrg2717

Young, R. W. (1971). The renewal of rod and cone outer segments in the rhesus monkey. *J. Cell Biol.* 49, 303–318. doi: 10.1083/jcb.49.2.303

Zabel, M. K., Zhao, L., Zhang, Y., Gonzalez, S. R., Ma, W., Wang, X., et al. (2016). Microglial phagocytosis and activation underlying photoreceptor degeneration is regulated by CX3CL1-CX3CR1 signaling in a mouse

model of retinitis pigmentosa. *Glia* 64, 1479–1491. doi: 10.1002/glia.23016

Zhang, Q., Giacalone, J. C., Searby, C., Stone, E. M., Tucker, B. A., and Sheffield, V. C. (2019). Disruption of RPGR protein interaction network is the common feature of RPGR missense variations that cause XLRP. *Proc. Natl. Acad. Sci. U.S.A.* 116, 1353–1360. doi: 10.1073/pnas.1817639116

Zhao, L., Zabel, M. K., Wang, X., Ma, W., Shah, P., Fariss, R. N., et al. (2015). Microglial phagocytosis of living photoreceptors contributes to inherited retinal degeneration. *EMBO Mol. Med.* 7, 1179–1197. doi: 10.15252/emmm.201505298

Conflict of Interest Statement: The authors declare that the research was conducted in the absence of any commercial or financial relationships that could be construed as a potential conflict of interest.

frontiers in Neuroscience

REVIEW
published: 09 October 2019
doi: 10.3389/fnins.2019.01031

Neuroprotective Potential of Pituitary Adenylate Cyclase Activating Polypeptide in Retinal Degenerations of Metabolic Origin

Robert Gábriel[1,2]*, *Etelka Pöstyéni*[1] and *Viktória Dénes*[1]

[1] Department of Experimental Zoology and Neurobiology, University of Pécs, Pécs, Hungary, [2] János Szentágothai Research Centre, University of Pécs, Pécs, Hungary

OPEN ACCESS

Edited by:
Giovanni Casini,
University of Pisa, Italy

Reviewed by:
Claudio Bucolo,
University of Catania, Italy
Ilaria Piano,
University of Pisa, Italy
Hirokazu Ohtaki,
Showa University, Japan

***Correspondence:**
Robert Gábriel
gabriel@gamma.ttk.pte.hu

Specialty section:
This article was submitted to Neurodegeneration, a section of the journal Frontiers in Neuroscience

Received: 26 June 2019
Accepted: 12 September 2019
Published: 09 October 2019

Citation:
Gábriel R, Pöstyéni E and Dénes V (2019) Neuroprotective Potential of Pituitary Adenylate Cyclase Activating Polypeptide in Retinal Degenerations of Metabolic Origin. Front. Neurosci. 13:1031. doi: 10.3389/fnins.2019.01031

Pituitary adenylate cyclase-activating polypeptide (PACAP1-38) is a highly conserved member of the secretin/glucagon/VIP family. The repressive effect of PACAP1-38 on the apoptotic machinery has been an area of active research conferring a significant neuroprotective potential onto this peptide. A remarkable number of studies suggest its importance in the etiology of neurodegenerative disorders, particularly in relation to retinal metabolic disorders. In our review, we provide short descriptions of various pathological conditions (diabetic retinopathy, excitotoxic retinal injury and ischemic retinal lesion) in which the remedial effect of PACAP has been well demonstrated in various animal models. Of all the pathological conditions, diabetic retinopathy seems to be the most intriguing as it develops in 75% of patients with type 1 and 50% of patients with type 2 diabetes, with concomitant progression to legal blindness in about 5%. Several animal models have been developed in recent years to study retinal degenerations and out of these glaucoma and age-related retina degeneration models bear human recapitulations. PACAP neuroprotection is thought to operate through enhanced cAMP production upon binding to PAC1-R. However, the underlying signaling network that leads to neuroprotection is not fully understood. We observed that (i) PACAP is not equally efficient in the above conditions; (ii) in some cases more than one signaling pathways are activated; (iii) the coupling of PAC1-R and signaling is stage dependent; and (iv) PAC1-R is not the only receptor that must be considered to interpret the effects in our experiments. These observations point to a complex signaling mechanism, that involves alternative routes besides the classical cAMP/protein kinase A pathway to evoke the outstanding neuroprotective action. Consequently, the possible contribution of the other two main receptors (VPAC1-R and VPAC2-R) will also be discussed. Finally, the potential

medical use of PACAP in some retinal and ocular disorders will also be reviewed. By taking advantage of, low-cost synthesis technologies today, PACAP may serve as an alternative to the expensive treatment modelities currently available in ocular or retinal conditions.

Keywords: PACAP, signaling, retina degeneration, metabolic origin, neuroprotection

INTRODUCTION

Neuropeptides have a fundamental role in the maturation of the nervous system and their functional consequences appear in countless biological mechanisms, both in physiological and in pathological conditions. Peptides may act as neurotransmitters, neuromodulators or neurohormones, therefore their function in neuronal development/regeneration may confer crucial protective roles during pathological conditions (Strand, 2003; Casini, 2005; Cervia and Casini, 2013).

Pituitary adenylate cyclase-activating polypeptide (PACAP) was first isolated from ovine hypothalamic extract as a 38 amino acid long peptide (PACAP1-38) in 1989 (Miyata et al., 1989). It belongs to the vasoactive intestinal peptide (VIP)/secretin/glucagon peptide family members and has another isoform eleven amino acids shorter (PACAP1-27) which is less dominant in vertebrates (Arimura and Shioda, 1995; Vaudry et al., 2009). Unless stated otherwise, we refer PACAP1-38 as PACAP throughout this paper.

The biological effects of PACAP are mediated by three types of G-protein coupled receptors which have seven transmembrane domains (PAC1-R, VPAC1-R, VPAC2-R, see below). PACAP binds to pituitary adenylate cyclase-activating polypeptide type I receptor (PAC1-R) with approximately 100x higher affinity than VIP while both peptides have similar affinities for VPAC1-R and VPAC2-R. These receptors are widely distributed in the central and peripheral nervous system (Vaudry et al., 2000; Laburthe et al., 2007). The variable effects of PACAP are due to the activation of diverse signal transduction pathways and their outcomes depend on which receptor types have been activated. AC, PLC and Ca^{2+} are main effectors during the signal transduction mechanisms of PACAP (Spengler et al., 1993; Pisegna and Wank, 1996). PAC1R and VPAC1R are coupled to AC, which leads to cyclic adenosine 3′,5′-monophosphate (cAMP) level elevations and the subsequent activation of PKA, which in turn could activate the MAPK pathway. Both receptor types are coupled to PLC as well, which leads to the stimulation of Ca^{2+} mobilization and the activation of the protein kinase C (PKC) pathway. VPAC2R subtype also seems to activate the AC signaling pathway. Beyond the receptor types, activation of different pathways depends on the ligands, the tissue type, and the stage of the development (Filipsson et al., 1998; Basille et al., 2000; Vaudry et al., 2000).

PACAP and its receptors are present in the CNS and in peripheral organs of mammals (Arimura and Shioda, 1995; Vaudry et al., 2009). In the CNS it behaves as a neurotransmitter or neurotrophic factor and is expressed in the hippocampus, cerebellum, hypothalamus and in several brainstem nuclei (Hannibal, 2002; Lee and Seo, 2014). Several studies discussed its neuroprotective effects in neurodegenerative diseases such as in stroke, brain ischemic injuries, Alzheimer's diseases and in Parkinsonism (Wang et al., 2008; Atlasz et al., 2010; Han et al., 2014; Matsumoto et al., 2016). Studies have revealed the expression of PAC1-R in the conjunctiva while PACAP/PAC1-R show higher expression in the lacrimal glands, in the cornea and in the retina (Wang et al., 1995; Elsas et al., 1996). In the retina, the nerve cell bodies in the GCL, some amacrine cells and horizontal cells show PACAP immunopositivity (Izumi et al., 2000; Denes et al., 2014). PAC1-R is strongly expressed in the GCL, in the INL and shows lower expression in the outer and inner plexiform layers (OPL, IPL) as well as in the ONL (Seki et al., 1997). To date, several studies have described the significant neuroprotective potential and neurotrophic effects of PACAP in relation to retinal metabolic disorders. Although its physiological action is incompletely elucidated, this peptide exerts neuroprotective and trophic actions by regulating cell survival and death, not only during the development and maturation of the nervous system but also in pathological conditions. Although pivotal roles in retinal metabolic disorders have been extensively investigated, the mechanisms are still not well understood and further signal transduction pathways may await to be revealed.

The primary aims of the present review are to summarize our knowledge about PACAP action in the retina in various physiological and pathological conditions (diabetic retinopathy, excitotoxic retinal injury and ischemic retinal lesion) and to discuss the potential signal transduction pathways in the context

Abbreviations: AC, adenylate cyclase; Akt, protein kinase B; ATP, adenosine triphosphate; BCCAO, bilateral carotid artery occlusion; Bcl-2, B-cell lymphoma 2 protein; BDNF, brain-derived neurotrophic factor; cAMP, cyclic adenosine 3′,5′-monophosphate; CNS, central nervous system; CNTF, ciliary neurotrophic factor; CRE, cAMP response element; CREB, cAMP response element-binding protein; DAG, diacylglycerol; DR, diabetic retinopathy; ERK 1/2, extracellular signal-regulated-kinase 1/2; Gα/β/γ, G protein alpha/beta/gamma subunit; GCL, ganglion cell layer; GFAP, glial fibrillary acidic protein; GSK, glycogen syntase kinase-3; HIF1α, hypoxia-inducible factor 1 α; HRE, hypoxia response element; IL6, interleukin6; INL, inner nuclear layer; IP3, inositol trisphosphate; IPL, inner plexiform layer; JNK, jun N-terminal protein kinase; LPS, lipopolysaccharide; MAPK, mitogen activated protein kinase; MAPK, mitogen-activated protein kinase; MGS, monosodium glutamate; mRNA, messenger RNA; NaAsO2, sodium arsenite; NFκB, nuclear factor κB; NR2B, *N*-methyl D-aspartate receptor subtype 2B; OCTR, ocreotide; ONL, outer nuclear layer; OPL, outer plexiform layer; PAC1-R, pituitary adenylate cyclase-activating polypeptide type I receptor; PACAP, pituitary adenylate cyclase-activating polypeptide; PARP, poly ADP ribose polymerase; phospho-CaMKII, calcium/calmodulin-dependent protein kinase II; PI3K, phoshoinositide 3-kinase; PIP2, phosphatidylinositol 4,5-bisphosphate; PKA, protein kinase A; PKCα, protein kinase C alpha; PKC, protein kinase C; PLC, phospholipase C; PLC, phospholipase C; ROS, reactive oxygen species; RPE, retinal pigment epithelium; SST, somatostatin; STZ, streptozotocin; TNFα, tumor necrosis factor alpha; VEGF, vascular endothelial growth factor; VEGF-R, VEGF- receptor; VIP, mitogen activated protein kinase; VPAC1-R, vasoactive intestinal polypeptide receptor 1; VPAC2-R, vasoactive intestinal polypeptide receptor 2.

of its protective action. Particularly, we pay special attention to (i) the lack of PACAP in the retina and supplementation of PACAP during early postnatal development; (ii) PAC1-R subtypes in the retina and their possible involvement in the neuroprotective events; and (iii) role of PACAP in mobilizing the immune system, both white blood cells and chemical messengers, to achieve retinal neuroprotection. Finally, we summarize the synergistic and diverging pathways through which PACAP acts and achieves functional improvement in concerted action with other neuropeptides.

PACAP CONTRA RETINAL DEGENERATION WITH METABOLIC ORIGINS

As we mentioned above, the physiological role of PACAP in the adult retina is not well established. Clearly, an emerging theory is that the lack of endogenous PACAP would accelerate age-related degeneration (Reglodi et al., 2018). PACAP deficiency mimics aspects of age-related pathophysiological changes including increased neuronal vulnerability and systemic degeneration accompanied by increased apoptosis, oxidative stress, and inflammation thus mimicking early aging. In support of this theory, it has been proven recently that endogenous PACAP has a protective effect during retinal inflammation. Experiments with PACAP KO mice revealed that intraperitoneal injection of LPS induced markedly more seriously eye-inflammation in PACAP KO mice than in the wild type group. During the process of inflammation, protein kinase B (pAkt) and glycogen synthase kinase-3 (pGSK) levels decreased in PACAP KO mice while cytokines (sICAM-1, JE, TIMP-1) were elevated (Vaczy et al., 2018).

INVOLVEMENT OF PACAP IN RETINAL CELL DEVELOPMENT AND AGING

In the CNS numerous extrinsic and intrinsic factors contribute to the formation of mature tissue by the precise regulation of the appropriate number and distribution of neurons. Neuropeptides influence many developmental processes of the CNS in a regulated way (Casini, 2005). In the developing retina, progenitor cells proliferate and differentiate into various retinal cell types as a result of numerous regulated cell cycle processes and develop into the final multi-layered structure of the retina. In postnatal (P6, P9) rat retinas PACAP treatment modulates cell death by activation of cAMP-PKA pathways (Silveira et al., 2002). Njaine et al. (2010) have investigated the exact timing and role of PACAP and its receptors in the cell generation of the developing rat retina. PAC1-R is expressed as early as E16 during development while VPAC1-R and VPAC2-R are expressed later, but then are present at all other stages. PACAP treatment resulted in an anti-proliferative effect by phosphorylation of CREB in cyclin D1 expressing retinal progenitor cells after PACAP receptor activation. Conversely, PACAP receptor activation led to a decreased level of cyclin D1 mRNA and further decreased by a combined treatment with PACAP and the cAMP degradation inhibitor IBMX. These findings have shown that PACAP has control over a subpopulation of progenitor cells and modulate cell proliferation in the developing retinal tissues (Njaine et al., 2010). Interestingly, PACAP shows both pro- and anti-apoptotic effects on postnatal retinal development in rat models. Caspase activity analysis has shown dose- and stage-dependent effects of PACAP on developmental apoptosis in rat retinas. Intravitreal injection of PACAP from postnatal day 1 (P1) to P7 induces apoptosis during the early stage of the retinogenesis. When 100 pmol PACAP was injected, it increased caspase 3/7 activity at P1, P3, and P5, but had no effect at P7. At P3, treatment repressed caspase 3/7 activity 18 h after the intravitreal injection, however, their levels increased 24 h post-injection. Apparently, PACAP treatment did not exert anti-apoptotic effects at P1, P5, and P7 rat retinas (Nyisztor et al., 2018). These findings warn us to re-evaluate PACAP action cautiously, always taking the timing and concentrations into account, especially in development. Unfortunately, not much is known about the functions of this peptide in mature retinas. Aging experienced as loss of function is accompanied by functional and morphological changes in retinal tissues (Gao and Hollyfield, 1992; Curcio and Drucker, 1993; Ramirez et al., 2001; Kovacs-Valasek et al., 2017). PACAP KO mice show accelerated age-related changes compared to wild type retinas. Altered structural changes included enhanced loss of ganglion cells and spouting of rod bipolar cell dendrites into the ONL in aging PACAP KO mice. Protein kinase C (PKC) α level in rod bipolar cells has been reduced in this condition. In contrast, GFAP levels have increased with an absence of endogenous PACAP. At the same time, PAC1-R has been upregulated in PACAP deficient young adult mice retinas. Surprisingly, the authors did not find differences in the histological structure of young adult PACAP KO and wild type mice (Kovacs-Valasek et al., 2017). These results suggest that PACAP contributes to maintaining the biochemical balance within neurons and glial cells. Thus, in the absence of this peptide, aging processes (e.g., reactive oxygen species formation) may gain strength earlier than in animals with normal PACAP levels.

PACAP RECEPTOR TYPES EXPRESSED IN RETINA

In the retina, the presence of four PAC1-R isoforms has been verified during postnatal development. The Null isoform showed no impressive changes at early stages (P1 to P5), but then manifested a decline from P5 to P15. Null message levels fell almost to zero in early adult ages. The Hip isoform had a similar expression pattern. The Hiphop1 isoform showed one prominent peak at P10. The Hop1 splice variant did not change much between P1 and P5, but thereafter it showed a significant increase at P10, P15, and P20. This seems to be the major isoform during adult life. Depending on the type of the PAC1-R isoform, PACAP can induce precursor cells to exit the cell cycle (through activation of the Null isoform (Lu and DiCicco-Bloom, 1997) or can promote proliferation in neuroblasts (if they express the Hop isoform (Lu et al., 1998). Interestingly, expression of both

Hip and Hop1 isoforms displays a sudden increase at P10 prior to eye opening. Due to technical difficulties, PAC1-R bearing retinal cells could not be sorted by their respective isoforms (isoform-specific antibodies are not available currently).

Based on these experimental results, a subsequent study has investigated the exact time period of isoform shift from postnatal day 5–10. The transcript level of Hip mRNA decreased from P6 through P9, while Hop1 expression level did not display any changes until P10. Consequently, a Hip/Hop1 isoform shift occurs between P6 and P8, which could alter PACAP functions in the postnatal rat retina (Denes et al., 2014). In contrast to the PAC1-R expression levels of the VPAC1-R receptor did not change during postnatal retinal development, though both the mRNA and protein could be detected in all selected time points. A similar scenario has been found in the case of VPAC2-R. Therefore, these receptors appear to be expressed in the newborn as well as in the adult retina, with similar intensity both at message and protein level (Lakk et al., 2012).

RETINAL PATHOLOGIES AND PACAP

Retinal diseases fall into two main categories: inherited disorders and problems of metabolic origin. Both conditions have attracted substantial research interest. According to our PubMed survey, approximately 4,000 papers have been published in the last 10 years dealing with the former and about 3,000 with the latter. Approximately half of the papers deal either with diagnostic advances or treatment options. Below we shall summarize some of the experimental results regarding the three most common conditions: diabetic retinopathy, excitotoxic retinal injury and ischemic retinal conditions.

Diabetic Retinopathy and PACAP

Diabetes is a multifactorial, metabolic disorder which appears to be the result of several pathological metabolic processes with increased morbidity statistics worldwide. In 2017, 425 million adults lived with diabetes and the size of the affected population will rise to 629 million until 2045 (International Diabetes Federation, 2017)[1]. DR is a microvascular complication of diabetes and the leading cause of vision loss (Cheung et al., 2010; Antonetti et al., 2012). DR is also considered as a chronic inflammatory disorder; low-grade inflammation has been observed in the retinas of both diabetic animals and human patients (Krady et al., 2005; Kern, 2007; Zeng et al., 2008). Patients with 1 type diabetes have a higher risk of DR than with the type 2 disease (Yau et al., 2012). DR has two distinguishable stages depending on the presence of neovascularization: an earlier non-proliferative phase characterized by abnormalities in the microvasculature, which could progress into a proliferative phase with macular neovascularization (Cheung et al., 2010).

The pathogenesis of DR includes increased polyol and hexosamine pathway activation, higher advanced glycation end-products production and the activation of PKC pathways. These altered signaling mechanisms could result in oxidative stress and chronic inflammation. Retinal microglial cells become activated and migrate in the subretinal space in several retinopathies, including DR (Zeng et al., 2000, 2008). The activation of microglia induced by hyperglycemia has been associated with the early development of DR, and occurs as early as electroretinographic modifications (Gaucher et al., 2007; Kern, 2007). Cytokines, released by activated microglia, were shown to contribute to neuronal cell death (Krady et al., 2005). They stimulate the production of cytotoxic substances, such as TNFα and ROS, proteases and even excitatory amino acids, which may induce neuronal degeneration. Leukocyte-mediated retinal cell apoptosis is among the earliest pathological manifestations of DR and results in the formation of a cellular-occluded capillaries, microaneurysms, and vascular basement membrane thickening (Kern and Engerman, 1995). Macrophages have long been known to play a major role in the pathogenesis of proliferative vitreoretinal disorders. In human DR, all types of macrophages could be detected regardless of clinical history and duration of the disease (Esser et al., 1993). Consequences of vascular occlusions contribute to neurodegeneration and dysfunction of the retina (Frank, 2004; Cheung et al., 2010; Giacco and Brownlee, 2010). Neuroprotective effects of PACAP in this pathological condition are complex because they have both structural, physiological and synaptic aspects as evidenced by many papers in this field (**Table 1**). In a rat model, intravitreal injection of PACAP ameliorated the structural changes of the retina in streptozotocin-induced DR. This treatment attenuates neuronal cell loss in the GCL, reduces cone cell degeneration and shows normal dopaminergic amacrine cell number compared to untreated diabetic retinas. These findings have demonstrated the significant neuroprotective effect of PACAP and its therapeutic potential in DR (Szabadfi et al., 2012). In their latest study, Maugeri et al. (2019) have provided evidence that PACAP1-38 protects not only neurons, but also the retinal pigmented epithelium both *in vivo* and *in vitro*. In another study, the intraocular PACAP injection attenuated the retinal injury by increasing the anti-apoptotic p-Akt, extracellular signal-regulated-kinase (p-ERK1/2), PKC and B-cell lymphoma 2 (Bcl-2) proteins levels, meanwhile the pro-apoptotic phosphorylated p38MAPK and activated caspase -3,-8, and -12 levels were decreased. As a result PACAP treatment significantly decreased apoptotic cell numbers compared to untreated diabetic rats and attracted a number of unidentified immune cells into the retina through the inner limiting membrane (Szabadfi et al., 2014). At the same time, electron microscopic analysis found altered synaptic structures in the diabetic retinas, in contrast to PACAP-treated diabetic groups, where more bipolar ribbon synapses appeared in the inner plexiform layer indicating higher levels of synapse-retention (Szabadfi et al., 2016). Giunta and his colleagues have described that MAPK transcripts levels were modified in the retina of diabetic rats during the early stages and the levels of PACAP, VIP and their receptors were all significantly downregulated as compared to non-diabetic rats (Giunta et al., 2012). At the same time, PACAP treatment has increased the PAC1-R expression in the retina, sometimes even in cells where PAC1-Rs are normally not present (Szabadfi et al., 2012).

[1] http://www.diabetesatlas.org

TABLE 1 | *In vivo* and *in vitro* experiments with PACAP application in DR (rat retina).

	References	Study aim	Findings
In vivo	Giunta et al., 2012	PACAP, VIP and their receptors expression change in retina of streptozotocin-induced diabetic rats.	The expression of peptides and their receptors were decreased after induction of diabetes. PACAP38 intravitreal injection restored diabetic changes in Bcl-2 and p53 expression to non-diabetic levels.
	Szabadfi et al., 2012	Highlights the protective effects of PACAP in diabetic retinopathy	PACAP ameliorated structural changes in DR, attenuated neuronal cell loss and increased the levels of PAC1-receptor and tyrosine-hydroxylase.
	D'Amico et al., 2015	The effects of PACAP in hyperglycemic retina is mediated by modulation of HIFs' expression in retina.	In diabetic rats HIF-1α and HIF-2α expression decreased after PACAP intraocular administration while HIF-3α downregulated in retinas of STZ injected rats and increased after PACAP treatment.
	Szabadfi et al., 2016	Analyze the synaptic structure and proteins of PACAP-treated diabetic retinas after intravitreal PACAP administration.	In the PACAP-treated diabetic retinas more bipolar ribbon synapses were found intact in the inner plexiform layer than in DR animals. Degeneration of bipolar and ganglion cells could be ameliorated by PACAP treatment.
	D'Amico et al., 2017	Protective role of PACAP through IL1β and VEGF expression in rat diabetic retinopathy	PACAP reduced the IL-1β expression and downregulates VEGF, VEGFRs in STZ-treated animals.
	Maugeri et al., 2019	Effect of PACAP-38 against high glucose damage is mediated by EGFR phosphorylation in retina.	PACAP-38 induced p-EGFR over-expression in diabetic rats retina.
In vitro	Maugeri et al., 2019	Effect of PACAP-38 on ARPE-19 cells exposed to hyperglycemic/hypoxic insult	PACAP-38 treatment improved cell viability.

Unfortunately, there is no data available regarding VPAC1-R and VPAC2-R involvement in the PACAP response in the retina. However, VIP and PACAP have been shown to cooperate in functional studies by using other disease models (Schratzberger et al., 1998; Ganea and Delgado, 2003; Abad et al., 2016).

Excitotoxic Retinal Injury and PACAP

Excitotoxic retinal injury in animal models mimics the changes associated with elevated intraocular pressure in human that causes glaucoma. Several studies have examined the neuroprotective effect of PACAP in excitotoxic retinal injuries. In normal conditions, glutamate is a neurotransmitter molecule in the retina, however, in high concentration it causes excessive stimulation of glutamate receptors and leads to excitotoxicity. In animal models of excitotoxic retinal injury, monosodium-glutamate treatment is used *in vivo* to model this pathological condition.

Monosodium glutamate (MSG) injection treatment has caused severe degenerations in neonatal rat retinas (Tamas et al., 2004; Atlasz et al., 2009). If prior to MSG treatment PACAP was injected unilaterally into the vitreous body of neonatal rat eyes, the MSG-induced degeneration became less pronounced. PACAP was applied in two different concentrations (1 and 100 pmol) to examine the dose-dependency of PACAP treatment in excitotoxic retinal injury. After MSG treatment the thickness of the entire retina was reduced by more than half and the reduction was especially due to the degeneration of the inner layers. Retinas of rats treated with 100 pmol PACAP showed significantly less damage than the retinas of animals treated with 1 pmol PACAP. These findings have described how PACAP could significantly attenuate the degeneration of the retina and underlined the importance of the dose-dependent effects of PACAP (Tamas et al., 2004). In another study, two different forms of PACAP (PACAP1-27, PACAP1-38) and their antagonists (PACAP6-38, PACAP6-27) have been tested in excitotoxic injury. The thickness of the retina has been significantly reduced, much of the IPL disappeared, the GCL and the INL cells intermingled and the ONL cells were swollen. During the investigation, PACAP1-38 and PACAP1-27 treated groups have shown retained retinal structure and the INL and GCL remained well separated. The two isoforms of PACAP have shown the same degree of neuroprotection after MSG treatments. The application of two PACAP antagonists after MSG injection did not ameliorate the MSG-induced retinal degenerations and led to a pronounced degeneration in the rat retina (Atlasz et al., 2009). During these experiments, the degenerations of the inner retinal layers were ameliorated by PACAP treatment. Note that PAC1-R distribution in the retina corresponds to the location of the protective effect because it shows the highest expression in the INL and in the GCL, and the lowest in the ONL and OPL (Seki et al., 2000). Another study examined the molecular background of signal transduction pathways underlying the neuroprotective effect of PACAP in MSG-induced retinal injury. The authors found that MSG inhibits the production of the anti-apoptotic molecules (phospho-PKA, phospho-Bad, Bcl-xL and 14-3-3 proteins) using rat models. PACAP treatment attenuates these effects by inducing the activation of the anti-apoptotic pathway by phosphorylation of PKA and Bad molecules and increasing the levels of Bcl-xL, and 14-3-3 proteins (Racz et al., 2007). These results highlighted that PACAP has a retinoprotective effect in glutamate induced injuries by reducing the pro-apoptotic pathways, while inducing anti-apoptotic signaling.

Interestingly, an enriched environment surrounding the experimental animals has also been shown to provide strong protective effect. A combination of enriched environment and PACAP treatment, however, did not further improve the protective effect, suggesting that these two treatments may utilize the same pathway for protection (Kiss et al., 2011).

Retinal Ischemic Conditions and PACAP

Retinal ischemia, as well as ischemia-reperfusion, causes inflammation which leads to injury progression, though inflammation usually helps in neuronal repair. These conditions contribute to excess ROS production, increase intracellular

calcium levels and initiate mitochondrial damage. In addition, MAPKs, nuclear factor κB (NFκB) and hypoxia-inducible factor 1α (HIF1α) are also activated when ischemic conditions elicit inflammation (Rayner et al., 2006; Wang et al., 2014; Kovacs et al., 2019). In the BCCAO model, PACAP activated one of the most important cytoprotective pathways, the PI3K-Akt, and suppressed the p38 MAPK and JNK pathways (Szabo et al., 2012) just like PARP inhibitors (Mester et al., 2009). Furthermore, a neurotrophic agent with a similar mode of action, CNTF, a member of the IL6 family (Wen et al., 2012), has also been tested in the form of intravitreal injection in preclinical studies. Using 12 animal models from 4 different species, researchers described a strong neuroprotective effect on photoreceptors and ganglion cells in the retina (Tao et al., 2002; Pease et al., 2009; Flachsbarth et al., 2014; Lipinski et al., 2015).

The effect of PACAP fragments has also been tested extensively in this model (Werling et al., 2014). The rationale for this study was that bioavailability and fast degradation of PACAP limit its therapeutic use and therefore scientific attention has been drawn to shorter fragments, especially the ones where C-terminus is truncated (Bourgault et al., 2009; Bourgault et al., 2011; Dejda et al., 2011). Therefore, it was necessary to test whether shorter PACAP fragments (4–13, 4–22, 6–10, 6–15, 11–15, and 20–31) have any effect on retinal lesions caused by chronic retinal hypoperfusion. Since the N-terminal fragments show a high similarity with the structure of VIP, and the 4-13 domain shows high selectivity to the PAC1-R, the prospect of creating a short and effective peptide fragment with a similar neuroprotective potential to PACAP seemed very promising. However, the authors came to the conclusion that the natural form of the peptide, PACAP1-38, is the most effective in retinal ischemia, and the 38 amino acid form of the peptide cannot be replaced by another fragment or another member of the peptide family (Werling et al., 2014). It has also been shown that PACAP mediates functional recovery after 14 days of intraocular treatment (Danyadi et al., 2014), probably through downregulation of VEGF production and glutamate release (D'Alessandro et al., 2014).

COMMON, SYNERGISTIC AND DIVERGING PATHWAYS OF PACAP SIGNALING TO ACHIEVE FUNCTIONAL IMPROVEMENT

In the next few paragraphs, we aim to summarize the pathways activated, directly or indirectly by PACAP receptors (**Figure 1**). Unfortunately, most studies do not provide evidence which PACAP receptors are involved in the processes described below. Nevertheless, all the available data point to a critical function of PACAP in neuroprotection.

Downregulation of Vascular Endothelial Growth Factor (VEGF)

Vascular endothelial growth factor, a dimeric glycoprotein functions as a mitogen by stimulating proliferation and migration of endothelial cells. It is also responsible for formation of new blood vessels (Ferrari and Scagliotti, 1996). The receptors of this signal molecule (VEGF- receptor 1, VEGF-R1 and VEGF- receptor 2, VEGF-R2) have tyrosine kinase domains and contribute to angiogenesis (Yancopoulos et al., 2000; Rahimi, 2006).

Among retinal cell types, mainly astrocytes, Müller glia cells, retinal pigment epithelium (RPE) and pericytes produce VEGF (Chalam et al., 2014). VEGF expression level is increased under low-oxygen concentrations through the induction of hypoxia-inducible factor 1 (HIF-1) expression. Hypoxia inducible factors (HIFs, see later) are modulators in hypoxia and cause endothelial cell transmigration across the RPE in the eye. These endothelial cells contribute to new vessel formation under VEGF control (Wang et al., 1995; Kaur et al., 2008; Skeie and Mullins, 2009). Elevated VEGF production leads to angiogenesis in order to supply tissues in hypoxic conditions (Kim et al., 2015). However, the newly generated blood vessels scatter light, and thus, instead of contributing to a better vision, they actually deteriorate visual acuity.

Studies have described diverse effects of PACAP on VEGF expression levels. Both PACAP and VIP are able to modulate HIF and VEGF expression during diabetic macular edema. VEGF expression is increased during hyperglycemic insult compared to control conditions. This effect can be ameliorated by PACAP or VIP treatment which could reduce the expression of VEGF and its receptors (Maugeri et al., 2017). Conversely, in another study, unrelated to diabetes, intravitreal treatment with PACAP has increased VEGF expression levels in rats after bilateral common carotid artery occlusion (Szabo et al., 2012). Although the results appear contradictory at first, at biological level the finding further demonstrates how profoundly protective PACAP is. In the extreme hypoxia at carotid artery occlusion the only survival strategy is more capillaries, that PACAP can also provide by an adaptive switch in its signaling bias. Nevertheless, the anti-VEGF effects of PACAP are clearly beneficial in patients suffering from DR conditions (Gabriel, 2013).

Upregulation of HIF1alpha

HIFs are important transcriptional regulators under hypoxic circumstances targeting quite a few genes including VEGF (Hu et al., 2003). Under reduced oxygen conditions, these factors could modulate the cellular response to hypoxia (Loboda et al., 2010; Manalo et al., 2011). The HIF1 protein has two types of subunits (i.e., HIF1-α and HIF1-β) that show oxygen-dependent expression; while HIF1-β constitutively expressed, HIF1-α expression is increased under reduced oxygen concentrations (Jiang et al., 1996). During hypoxia, HIF1-α forms dimers with HIF1-β and the dimer binds to the HRE. This complex is able to regulate transcription of genes, which contribute to angiogenesis. One of them is the VEGF gene (Pugh and Ratcliffe, 2003). It has been previously shown that PACAP is able to modulate expression of HIFs in streptozotocin (STZ) induced diabetic retinas. After 3 weeks, HIF-1 alpha and HIF-2 alpha levels increased in diabetic groups and significantly decreased as a result of PACAP treatment. Conversely, HIF-3α was downregulated in diabetic

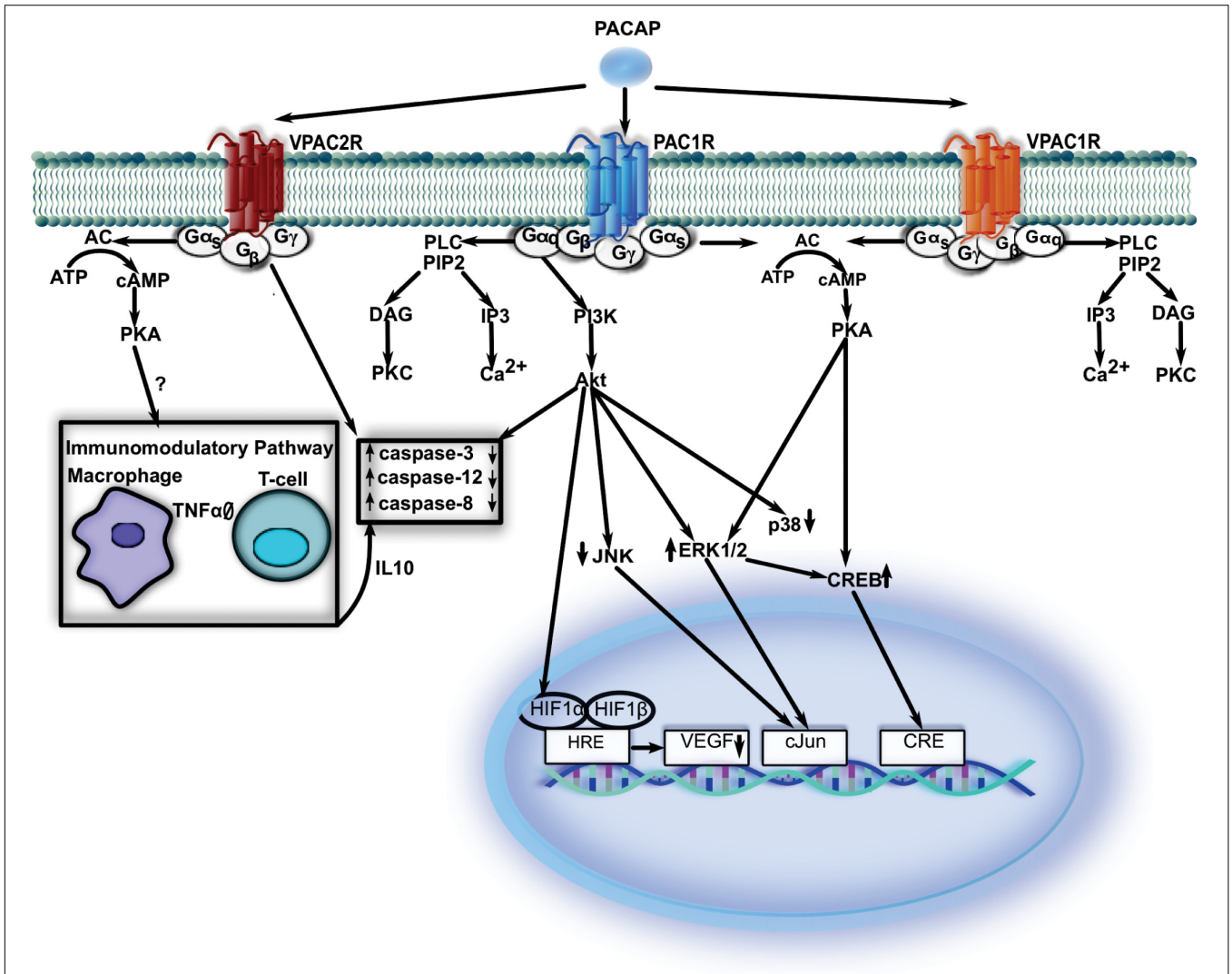

FIGURE 1 | While PAC1-R-mediated signaling is at least partially synergistic with that of VPAC1-R, VPAC2-R that is inducible in some immune elements and utilizes additional signal molecules to restore normal function. VPAC1-R, vasoactive intestinal polypeptide receptor 1; VPAC2-R, vasoactive intestinal polypeptide receptor 2; PAC1-R, pituitary adenylate cyclase-activating polypeptide type I receptor; cAMP, cyclic adenosine3′,5′-monophosphate; AC, adenylate cyclase; PKA, protein kinase A; ATP, adenosine triphosphate; Gα/β/γ, G protein alpha/beta/gamma subunit; IL, interleukin; TNFα, tumor necrosis factor alpha; PLC, phospholipase C; PIP2, phosphatidylinositol 4,5-bisphosphate; DAG, diacylglycerol; IP3, inositol trisphosphate; PI3K, phoshoinositide 3-kinase; JNK, jun N-terminal protein kinase; ERK 1/2, extracellular signal-regulated-kinase 1/2; Akt, protein kinase; CREB, cAMP response element-binding protein; VEGF, vascular endothelial growth factor; HRE, hypoxia response element; HIF1α, hypoxia-inducible factor 1 α; HIF1β, hypoxia-inducible factor 1 β.

rats and enhanced after intraocular administration of PACAP (D'Amico et al., 2015). In normal conditions, HIF1α level is reduced while HIF3α level increases, unlike in hypoxia or hyperglycemia, where their expression patterns are reversed. Treatments with VIP or PACAP reduce HIF1α levels and increase HIF3α levels in ARPE-19 cells under hyperglycemic conditions (Maugeri et al., 2017).

Downregulation of c-Jun and p38 Kinases

c-Jun N-terminal protein kinase (JNK) and p38 kinase are members of the MAPK superfamily and they regulate apoptotic signaling pathways in cells (Estus et al., 1994; Ham et al., 1995; Mesner et al., 1995). JNK can have both pro- and anti-apoptotic effects (Ham et al., 1995; Xia et al., 1995; Lenczowski et al., 1997). In experiments using sodium arsenite ($NaAsO_2$) to trigger neuronal apoptosis, both p38 kinase and JNK3 were upregulated and c-Jun phosphorylation was induced. The results showed that p38 kinase and JNK inhibitors attenuated apoptosis in cortical neurons and established the differences between JNK isoforms which differently contributed to the apoptotic processes (Namgung and Xia, 2000). It has also been described that intravitreal PACAP treatment decreased JNK, p38 activation and the activation of ERK1/2, AKT in hypoperfused

rat retinas (Szabo et al., 2012). In MSG-induced retinal degeneration, PACAP treatment attenuated the activation of JNK and caspase 3 and increased the level of phospho-Bad (Racz et al., 2006). On the contrary, the same group demonstrated that PACAP treatment decreased the expression and activation of pro-apoptotic p38 in diabetic rat retinas (Szabadfi et al., 2014).

Synergism With Other Peptidergic Mechanisms

The therapeutic potentials of different neuropeptides have been confirmed by numerous animal models of human diseases. These substances deserve prominent attention in the development of peptide-based therapeutic strategies of vision-threatening diseases.

The effectiveness of SST neuropeptide has been described in various pathological conditions of the retina. SST is an important neuromodulator and its immunoreactivity occurs mainly in the GABAergic amacrine cells in the retina (Feigenspan and Bormann, 1994; van Hagen et al., 2000). SST levels are downregulated at the early stage of DR (Carrasco et al., 2007). Topical administration of SST and its analogs have a preventive effect in retinal neurodegeneration in STZ-induced diabetes. It has been established that SST treatment inhibits extracellular glutamate accumulation, glial activation, ERG abnormalities and it modulates the proapoptotic/survival signaling pathways in experimental diabetes (Hernandez et al., 2013). Octreotide (OCTR) is a synthetic SST analog which, for example, in an ischemia/reperfusion injury study reduced cell loss, retinal thickness changes, ROS formation and inhibited NF-κB p65 activation. These findings demonstrated that OCTR application has a neuroprotective and antioxidant effect on ischemic injury in the retina (Wang et al., 2015). In another investigation, OCTR reduced hypoxia induced activation of STAT3 and HIF1 levels in retinal explants (Mei et al., 2012). OCTR and another SST analog (Woc4D) decreased neovascularization in the mouse model of oxygen-induced retinopathy (Higgins et al., 2002). A metabolomic analysis revealed the roles of PACAP, SP, and OCTR in *ex vivo* mouse models of retinal ischemia. These *ex vivo* results show a synergistic action of the above mentioned peptides. All treatments reduce VEGF overexpression, cell death and glutamate release and modulate pro-survival pathways by restoring IP3 signaling, cAMP levels and PIP2/PIP3 ratio in ischemia-induced retinal damages. It has also been demonstrated in ischemia related oxidative stress that PACAP and SP treatments help to cope with this condition and OCTR also contributes to the preventive effect in pathological processes (D'Alessandro et al., 2014).

Takuma et al. have investigated the effect of an enriched environment on memory impairments in PACAP deficient-mice. This environment ameliorates the memory impairments in knockout mice after 4 weeks and the beneficial effects of it were also observed if mice were returned to a standard environment after 2 weeks. The results showed that the levels of BDNF, phospho-ERK, phospho-CaMKII and *N*-methyl D-aspartate receptor subtype 2B (NR2B) in the hippocampus increased in an enriched environment and these factors are responsible for the ameliorating effect of the this environment on memory dysfunction. In PACAP −/− mice, however, these increased expression levels disappeared after 2 weeks when they were returned to standard housing, so in the lack of PACAP the long-lasting ameliorating effects of the enriched environment could not be verified (Takuma et al., 2014). An *in vitro* examination by Ogata and his colleagues have compared morphological effects of PACAP and BDNF on primary cultures of hippocampal neurons. Both PACAP and BDNF increased neurite length and numbers at a similar level, while PACAP increased the axon length only, but not the branching. Interestingly, the use of PACAP6-38 antagonist blocked both PACAP and BDNF-induced increases in axon length, suggesting that these two peptides may act through the same intracellular signal transduction machinery and that PACAP antagonists can interfere effectively with BDNF signaling (Ogata et al., 2015).

Divergence in PACAP Receptor Signaling – How Immune Elements Are Recruited to Damaged Tissue Sites?

It has been demonstrated that immune cells express functional PACAP receptors. However, PAC1-R has minor roles in the immune response whereas VPAC1-R and VPAC2-R signaling evoke diverging effects. The former is constitutively expressed on macrophages, while the latter is inducible and particularly strongly effected by LPS (Abad et al., 2016). While VPAC1-R is thought to act mainly as an inhibitor of the immune response, VPAC2-R is able to accelerate inflammatory processes by initiating the production of several cytokines, most prominently IL-6 and IL-10. Additionally, D'Amico et al. (2017) have provided evidence that both IL1ß and VEGF levels are modified in diabetic rat retinas after PACAP administration. In peripheral organs PACAP also activates T-lymphocytes. In PACAP KO mice, however, PACAP treatment failed to reduce neutrophil infiltration into organs indicating that other indirect downstream PACAP signaling is also essential in this system (Martinez et al., 2005). VPAC1 and VPAC2 receptors, but not PAC1-R mRNA levels, were transiently induced in retinas 1 week following diabetes induction (Giunta et al., 2012). In the same diabetic condition, immune cells were attracted to the retina through the inner limiting membrane and resulted in strengthening of IL-6 but not tumor-necrosis factor (TNF) α-immunoreactivity in retinal ganglion cells. The reason for this difference is currently unknown and research is needed to clarify the underlying signaling routes. It is even more interesting that TNFα is dramatically increased in glaucoma and ischemia (Martinez et al., 2005). Therefore, it seems evident that not all of the microcircuitry-related disorders have identical immune cell recruitment pathways. This immune response may enhance the degeneration of the damaged cells. That, however, may be beneficial science when a protective signal like PACAP appears, it may be hasten the clearance of the dying elements, help to rearrange the neural connections and maintain the integrity of the remaining cells, to restore function as quickly as possible.

DISCUSSION

Our review highlights the importance of PACAP and, some other neuropeptides in retinal degenerative diseases with metabolic origins. Neuropeptides with their wide range of signaling potential could modulate the pathological pathways of retinal diseases through converging signal pathways. The question arises why these potentials are neglected in drug development and subsequent clinical trials. One of the difficulties of using natural peptides as protective agents is their relatively short half-life (in some cases it can be shorter than 1 min). The solution for this problem is to modify these peptides at their N and/or C termini in order to prevent degradation (acetylation, cyclization, N and/or C termini modification, PEGylation, D-amino acid substitution, etc.). In the case of PACAP, half-life can be longer than 4 h after some modifications (Mathur et al., 2016). Another potential problem using peptides as therapeutic agents is their limited passage through the blood brain barrier (Banks et al., 1993; Banks and Kastin, 1996). In the case of the retina there is no need for systemic administration since the peptides can injected into the vitreus body and must pass through the retinal inner limited membrane. Indeed it has been shown in the case of PACAP that it reaches the inner retinal layers after intravitreal injection (Werling et al., 2017).

At the same time, one of the mobilized downstream signals in the pathogenesis, VEGF is intensively targeted by different anti-VEGF therapies (Gabriel, 2013). While anti-VEGF therapies are expensive, synthesis and modification of peptides like PACAP are cost effective, so they may provide alternatives to the treatments available today in various retinal conditions, particularly in the case of DR. It would also be reasonable to consider the combination of modified neuropeptides, which can effectively counteract pathological retinal metabolic conditions. As discussed above, there are a number of candidates to be included in this mixture. In order to effectively protect every retinal cell type and layer we suggest trying the combination of modified BDNF, CNTF, OCTR, and PACAP. These substances together satisfy the following criteria (i) under normal conditions their native form is present in the retina in low concentration; (ii) each retinal cell type has a receptor for at least one of the four peptides; (iii) the signal transduction pathways behind the retinal receptors of these substances do not ameliorate or cross each other's action; and (iv) none of them causes unwanted side effects even if they are given in higher concentrations. Considering that anti-VEGF drugs cost over 500 million pounds in Great Britain alone in 2015 (Hollingworth et al., 2017), alternatives are definitely needed, especially in low and medium income countries (Shanmugam, 2014). Clinical trials with the combinations of the above substances could be envisioned based on the results achieved on animal models in research laboratories.

AUTHOR CONTRIBUTIONS

All authors read and approved the final manuscript. RG wrote the manuscript and supervised the manuscript production. EP wrote the manuscript. VD gave expert advice and provided critical feedback.

FUNDING

Funding was provided by the Hungarian Scientific Research Fund (NKFIH) (Grant No. 119289) and EFOP-3.6.2-16-2017-00008.

ACKNOWLEDGMENTS

We would like to express our special thanks to Peter Geck for language editing. We also thank Alina Bolboaca for special assistance with editing the manuscript.

REFERENCES

Abad, C., Jayaram, B., Becquet, L., Wang, Y., O'Dorisio, M. S., Waschek, J. A., et al. (2016). VPAC1 receptor (Vipr1)-deficient mice exhibit ameliorated experimental autoimmune encephalomyelitis, with specific deficits in the effector stage. *J. Neuroinflammation* 13:169. doi: 10.1186/s12974-016-0626-3

Antonetti, D. A., Klein, R., and Gardner, T. W. (2012). Diabetic retinopathy. *N. Engl. J. Med.* 366, 1227–1239. doi: 10.1056/NEJMra1005073

Arimura, A., and Shioda, S. (1995). Pituitary adenylate cyclase activating polypeptide (PACAP) and its receptors: neuroendocrine and endocrine interaction. *Front. Neuroendocrinol.* 16:53–88. doi: 10.1006/frne.1995.1003

Atlasz, T., Szabadfi, K., Kiss, P., Racz, B., Gallyas, F., Tamas, A., et al. (2010). Pituitary adenylate cyclase activating polypeptide in the retina: focus on the retinoprotective effects. *Ann. N. Y. Acad. Sci.* 1200, 128–139. doi: 10.1111/j.1749-6632.2010.05512.x

Atlasz, T., Szabadfi, K., Reglodi, D., Kiss, P., Tamas, A., Toth, G., et al. (2009). Effects of pituitary adenylate cyclase activating polypeptide and its fragments on retinal degeneration induced by neonatal monosodium glutamate treatment. *Ann. N. Y. Acad. Sci.* 1163, 348–352. doi: 10.1111/j.1749-6632.2008.03650.x

Banks, W. A., and Kastin, A. J. (1996). Passage of peptides across the blood-brain barrier: pathophysiological perspectives. *Life Sci.* 59, 1923–1943. doi: 10.1016/s0024-3205(96)00380-3

Banks, W. A., Kastin, A. J., Komaki, G., and Arimura, A. (1993). Passage of pituitary adenylate cyclase activating polypeptide1-27 and pituitary adenylate cyclaseactivating polypeptide1-38 across the blood-brain barrier. *J. Pharmacol. Exp. Ther.* 267, 690–696.

Basille, M., Vaudry, D., Coulouarn, Y., Jegou, S., Lihrmann, I., Fournier, A., et al. (2000). Comparative distribution of pituitary adenylate cyclase-activating polypeptide (PACAP) binding sites and PACAP receptor mRNAs in the rat brain during development. *J. Comp. Neurol.* 425, 495–509. doi: 10.1002/1096-9861(20001002)425:4<495::aid-cne3>3.3.co;2-1

Bourgault, S., Chatenet, D., Wurtz, O., Doan, N. D., Leprince, J., Vaudry, H., et al. (2011). Strategies to convert PACAP from a hypophysiotropic neurohormone into a neuroprotective drug. *Curr. Pharm. Des.* 17, 1002–1024. doi: 10.2174/138161211795589337

Bourgault, S., Vaudry, D., Dejda, A., Doan, N. D., Vaudry, H., and Fournier, A. (2009). Pituitary adenylate cyclase-activating polypeptide: focus on structure-activity relationships of a neuroprotective Peptide. *Curr. Med. Chem.* 16, 4462–4480. doi: 10.2174/092986709789712899

Carrasco, E., Hernandez, C., Miralles, A., Huguet, P., Farres, J., and Simo, R. (2007). Lower somatostatin expression is an early event in diabetic retinopathy and is associated with retinal neurodegeneration. *Diabetes Care* 30, 2902–2908. doi: 10.2337/dc07-0332

Casini, G. (2005). Neuropeptides and retinal development. *Arch. Ital. Biol.* 143, 191–198.

Cervia, D., and Casini, G. (2013). The neuropeptide systems and their potential role in the treatment of mammalian retinal ischemia: a developing story. *Curr. Neuropharmacol.* 11, 95–101. doi: 10.2174/157015913804999423

Chalam, K. V., Brar, V. S., and Murthy, R. K. (2014). Human ciliary epithelium as a source of synthesis and secretion of vascular endothelial growth factor in neovascular glaucoma. *JAMA Ophthalmol.* 132, 1350–1354. doi: 10.1001/jamaophthalmol.2014.2356

Cheung, N., Mitchell, P., and Wong, T. Y. (2010). Diabetic retinopathy. *Lancet* 376, 124–136. doi: 10.1016/S0140-6736(09)62124-3

Curcio, C. A., and Drucker, D. N. (1993). Retinal ganglion cells in Alzheimer's disease and aging. *Ann. Neurol.* 33, 248–257. doi: 10.1002/ana.410330305

D'Alessandro, A., Cervia, D., Catalani, E., Gevi, F., Zolla, L., and Casini, G. (2014). Protective effects of the neuropeptides PACAP, substance P and the somatostatin analogue octreotide in retinal ischemia: a metabolomic analysis. *Mol. Biosyst.* 10, 1290–1304. doi: 10.1039/c3mb70362b

D'Amico, A. G., Maugeri, G., Rasà, D. M., Bucolo, C., Saccone, S., Federico, C., et al. (2017). Modulation of IL-1β and VEGF expression in rat diabetic retinopathy after PACAP administration. *Peptides* 97, 64–69. doi: 10.1016/j.peptides

D'Amico, A. G., Maugeri, G., Reitano, R., Bucolo, C., Saccone, S., Drago, F., et al. (2015). PACAP Modulates expression of hypoxia-inducible factors in streptozotocin-induced diabetic rat retina. *J. Mol. Neurosci.* 57, 501–509. doi: 10.1007/s12031-015-0621-7

Danyadi, B., Szabadfi, K., Reglodi, D., Mihalik, A., Danyadi, T., Kovacs, Z., et al. (2014). PACAP application improves functional outcome of chronic retinal ischemic injury in rats-evidence from electroretinographic measurements. *J. Mol. Neurosci.* 54, 293–299. doi: 10.1007/s12031-014-0296-5

Dejda, A., Bourgault, S., Doan, N. D., Letourneau, M., Couvineau, A., Vaudry, H., et al. (2011). Identification by photoaffinity labeling of the extracellular N-terminal domain of PAC1 receptor as the major binding site for PACAP. *Biochimie* 93, 669–677. doi: 10.1016/j.biochi.2010.12.010

Denes, V., Czotter, N., Lakk, M., Berta, G., and Gabriel, R. (2014). PAC1-expressing structures of neural retina alter their PAC1 isoform splicing during postnatal development. *Cell Tissue Res.* 355, 279–288. doi: 10.1007/s00441-013-1761-0

Elsas, T., Uddman, R., and Sundler, F. (1996). Pituitary adenylate cyclase-activating peptide-immunoreactive nerve fibers in the cat eye. *Graefes Arch. Clin. Exp. Ophthalmol.* 234, 573–580. doi: 10.1007/bf00448802

Esser, P., Heimann, K., and Wiedemann, P. (1993). Macrophages in proliferative vitreoretinopathy and proliferative diabetic retinopathy: differentiation of subpopulations. *Br. J. Ophthalmol.* 77, 731–733. doi: 10.1136/bjo.77.11.731

Estus, S., Zaks, W. J., Freeman, R. S., Gruda, M., Bravo, R., Johnson, E. M. Jr., et al. (1994). Altered gene expression in neurons during programmed cell death: identification of c-jun as necessary for neuronal apoptosis. *J. Cell Biol.* 127(6 Pt 1), 1717–1727. doi: 10.1083/jcb.127.6.1717

Feigenspan, A., and Bormann, J. (1994). Facilitation of GABAergic signaling in the retina by receptors stimulating adenylate cyclase. *Proc. Natl. Acad. Sci. U.S.A.* 91, 10893–10897. doi: 10.1073/pnas.91.23.10893

Ferrari, G., and Scagliotti, G. V. (1996). Serum and urinary vascular endothelial growth factor levels in non-small cell lung cancer patients. *Eur. J. Cancer* 32A, 2368–2369. doi: 10.1016/s0959-8049(96)00272-9

Filipsson, K., Sundler, F., Hannibal, J., and Ahren, B. (1998). PACAP and PACAP receptors in insulin producing tissues: localization and effects. *Regul. Pept.* 74, 167–175. doi: 10.1016/s0167-0115(98)00037-8

Flachsbarth, K., Kruszewski, K., Jung, G., Jankowiak, W., Riecken, K., Wagenfeld, L., et al. (2014). Neural stem cell-based intraocular administration of ciliary neurotrophic factor attenuates the loss of axotomized ganglion cells in adult mice. *Invest. Ophthalmol. Vis. Sci.* 55, 7029–7039. doi: 10.1167/iovs.14-15266

Frank, R. N. (2004). Diabetic retinopathy. *N. Engl. J. Med.* 350, 48–58. doi: 10.1056/NEJMra021678

Gabriel, R. (2013). Neuropeptides and diabetic retinopathy. *Br. J. Clin. Pharmacol.* 75, 1189–1201. doi: 10.1111/bcp.12003

Ganea, D., and Delgado, M. (2003). The neuropeptides VIP/PACAP and T cells: inhibitors or activators? *Curr. Pharm. Des.* 9, 997–1004. doi: 10.2174/1381612033455116

Gao, H., and Hollyfield, J. G. (1992). Aging of the human retina. Differential loss of neurons and retinal pigment epithelial cells. *Invest. Ophthalmol. Vis. Sci.* 33, 1–17.

Gaucher, D., Chiappore, J. A., Paques, M., Simonutti, M., Boitard, C., Sahel, J. A., et al. (2007). Microglial changes occur without neural cell death in diabetic retinopathy. *Vision Res.* 47, 612–623. doi: 10.1016/j.visres.2006.11.017

Giacco, F., and Brownlee, M. (2010). Oxidative stress and diabetic complications. *Circ. Res.* 107, 1058–1070. doi: 10.1161/CIRCRESAHA.110.223545

Giunta, S., Castorina, A., Bucolo, C., Magro, G., Drago, F., and D'Agata, V. (2012). Early changes in pituitary adenylate cyclase-activating peptide, vasoactive intestinal peptide and related receptors expression in retina of streptozotocin-induced diabetic rats. *Peptides* 37, 32–39. doi: 10.1016/j.peptides.2012.06.004

Ham, J., Babij, C., Whitfield, J., Pfarr, C. M., Lallemand, D., Yaniv, M., et al. (1995). A c-Jun dominant negative mutant protects sympathetic neurons against programmed cell death. *Neuron* 14, 927–939. doi: 10.1016/0896-6273(95)90331-3

Han, P., Liang, W., Baxter, L. C., Yin, J., Tang, Z., Beach, T. G., et al. (2014). Pituitary adenylate cyclase-activating polypeptide is reduced in Alzheimer disease. *Neurology* 82, 1724–1728. doi: 10.1212/WNL.0000000000000417

Hannibal, J. (2002). Pituitary adenylate cyclase-activating peptide in the rat central nervous system: an immunohistochemical and in situ hybridization study. *J. Comp. Neurol.* 453, 389–417. doi: 10.1002/cne.10418

Hernandez, C., Garcia-Ramirez, M., Corraliza, L., Fernandez-Carneado, J., Farrera-Sinfreu, J., Ponsati, B., et al. (2013). Topical administration of somatostatin prevents retinal neurodegeneration in experimental diabetes. *Diabetes Metab. Res. Rev.* 62, 2569–2578. doi: 10.2337/db12-0926

Higgins, R. D., Yan, Y., and Schrier, B. K. (2002). Somatostatin analogs inhibit neonatal retinal neovascularization. *Exp. Eye Res.* 74, 553–559. doi: 10.1006/exer.2001.1147

Hollingworth, W., Jones, T., Reeves, B. C., and Peto, T. (2017). A longitudinal study to assess the frequency and cost of antivascular endothelial therapy, and inequalities in access, in England between 2005 and 2015. *BMJ Open.* 7:e018289. doi: 10.1136/bmjopen-2017-018289

Hu, C. J., Wang, L. Y., Chodosh, L. A., Keith, B., and Simon, M. C. (2003). Differential roles of hypoxia-inducible factor 1alpha (HIF-1alpha) and HIF-2alpha in hypoxic gene regulation. *Mol. Cell. Biol.* 23, 9361–9374. doi: 10.1128/mcb.23.24.9361-9374.2003

Izumi, S., Seki, T., Shioda, S., Zhou, C. J., Arimura, A., and Koide, R. (2000). Ultrastructural localization of PACAP immunoreactivity in the rat retina. *Ann. N. Y. Acad. Sci.* 921, 317–320. doi: 10.1111/j.1749-6632.2000.tb06985.x

Jiang, B. H., Semenza, G. L., Bauer, C., and Marti, H. H. (1996). Hypoxia-inducible factor 1 levels vary exponentially over a physiologically relevant range of O2 tension. *Am. J. Physiol.* 271(4 Pt 1), C1172–C1180. doi: 10.1152/ajpcell.1996.271.4.C1172

Kaur, C., Foulds, W. S., and Ling, E. A. (2008). Hypoxia-ischemia and retinal ganglion cell damage. *Clin. Ophthalmol.* 2, 879–889. doi: 10.2147/opth.s3361

Kern, T. S. (2007). Contributions of inflammatory processes to the development of the early stages of diabetic retinopathy. *Exp. Diabetes Res.* 2007:95103. doi: 10.1155/2007/95103

Kern, T. S., and Engerman, R. L. (1995). Galactose-induced retinal microangiopathy in rats. *Invest. Ophthalmol. Vis. Sci.* 36, 490–496.

Kim, M., Lee, C., Payne, R., Yue, B. Y., Chang, J. H., and Ying, H. (2015). Angiogenesis in glaucoma filtration surgery and neovascular glaucoma: a review. *Surv. Ophthalmol.* 60, 524–535. doi: 10.1016/j.survophthal.2015.04.003

Kiss, P., Atlasz, T., Szabadfi, K., Horvath, G., Griecs, M., Farkas, J., et al. (2011). Comparison between PACAP- and enriched environment-induced retinal protection in MSG-treated newborn rats. *Neurosci. Lett.* 487, 400–405. doi: 10.1016/j.neulet.2010.10.065

Kovacs, K., Vaczy, A., Fekete, K., Kovari, P., Atlasz, T., Reglodi, D., et al. (2019). PARP inhibitor protects against chronic hypoxia/reoxygenation-induced retinal injury by regulation of MAPKs, HIF1alpha, Nrf2, and NFkappaB. *Invest. Ophthalmol. Vis. Sci.* 60, 1478–1490. doi: 10.1167/iovs.18-25936

Kovacs-Valasek, A., Szabadfi, K., Denes, V., Szalontai, B., Tamas, A., Kiss, P., et al. (2017). Accelerated retinal aging in PACAP knock-out mice. *Neuroscience* 348, 1–10. doi: 10.1016/j.neuroscience.2017.02.003

Krady, J. K., Basu, A., Allen, C. M., Xu, Y., LaNoue, K. F., Gardner, T. W., et al. (2005). Minocycline reduces proinflammatory cytokine expression, microglial activation, and caspase-3 activation in a rodent model of diabetic retinopathy. *Diabetes Metab. Res. Rev.* 54, 1559–1565. doi: 10.2337/diabetes.54.5.1559

Laburthe, M., Couvineau, A., and Tan, V. (2007). Class II G protein-coupled receptors for VIP and PACAP: structure, models of activation and pharmacology. *Peptides* 28, 1631–1639. doi: 10.1016/j.peptides.2007.04.026

Lakk, M., Szabo, B., Volgyi, B., Gabriel, R., and Denes, V. (2012). Development-related splicing regulates pituitary adenylate cyclase-activating polypeptide (PACAP) receptors in the retina. *Invest. Ophthalmol. Vis. Sci.* 53, 7825–7832. doi: 10.1167/iovs.12-10417

Lee, E. H., and Seo, S. R. (2014). Neuroprotective roles of pituitary adenylate cyclase-activating polypeptide in neurodegenerative diseases. *BMB Rep.* 47, 369–375. doi: 10.5483/bmbrep.2014.47.7.086

Lenczowski, J. M., Dominguez, L., Eder, A. M., King, L. B., Zacharchuk, C. M., and Ashwell, J. D. (1997). Lack of a role for Jun kinase and AP-1 in Fas-induced apoptosis. *Mol. Cell. Biol.* 17, 170–181. doi: 10.1128/mcb.17.1.170

Lipinski, D. M., Barnard, A. R., Singh, M. S., Martin, C., Lee, E. J., Davies, W. I. L., et al. (2015). CNTF gene therapy confers lifelong neuroprotection in a mouse model of human retinitis pigmentosa. *Mol. Ther.* 23, 1308–1319. doi: 10.1038/mt.2015.68

Loboda, A., Jozkowicz, A., and Dulak, J. (2010). HIF-1 and HIF-2 transcription factors–similar but not identical. *Mol. Cells* 29, 435–442. doi: 10.1007/s10059-010-0067-2

Lu, N., and DiCicco-Bloom, E. (1997). Pituitary adenylate cyclase-activating polypeptide is an autocrine inhibitor of mitosis in cultured cortical precursor cells. *Proc. Natl. Acad. Sci. U.S.A.* 94, 3357–3362. doi: 10.1073/pnas.94.7.3357

Lu, N., Zhou, R., and DiCicco-Bloom, E. (1998). Opposing mitogenic regulation by PACAP in sympathetic and cerebral cortical precursors correlates with differential expression of PACAP receptor (PAC1-R) isoforms. *J. Neurosci. Res.* 53, 651–662. doi: 10.1002/(sici)1097-4547(19980915)53:6<651::aid-jnr3>3.0.co;2-4

Manalo, K. B., Choong, P. F., and Dass, C. R. (2011). Pigment epithelium-derived factor as an impending therapeutic agent against vascular epithelial growth factor-driven tumor-angiogenesis. *Mol. Carcinog.* 50, 67–72. doi: 10.1002/mc.20711

Martinez, C., Juarranz, Y., Abad, C., Arranz, A., Miguel, B. G., Rosignoli, F., et al. (2005). Analysis of the role of the PAC1 receptor in neutrophil recruitment, acute-phase response, and nitric oxide production in septic shock. *J. Leukoc. Biol.* 77, 729–738. doi: 10.1189/jlb.0704432

Mathur, D., Prakash, S., Anand, P., Kaur, H., Agrawal, P., Mehta, A., et al. (2016). PEPlife: a repository of the half-life of peptides. *Sci Rep.* 6:36617. doi: 10.1038/srep36617

Matsumoto, M., Nakamachi, T., Watanabe, J., Sugiyama, K., Ohtaki, H., Murai, N., et al. (2016). Pituitary adenylate cyclase-activating polypeptide (PACAP) is involved in adult mouse hippocampal neurogenesis after stroke. *J. Mol. Neurosci.* 59, 270–279. doi: 10.1007/s12031-016-0731-x

Maugeri, G., D'Amico, A. G., Bucolo, C., and D'Agata, V. (2019). Protective effect of PACAP-38 on retinal pigmented epithelium in an in vitro and in vivo model of diabetic retinopathy through EGFR-dependent mechanism. *Peptides* 119:170108. doi: 10.1016/j.peptides

Maugeri, G., D'Amico, A. G., Saccone, S., Federico, C., Cavallaro, S., and D'Agata, V. (2017). PACAP and VIP inhibit HIF-1alpha-mediated VEGF expression in a model of diabetic macular edema. *J. Cell. Physiol.* 232, 1209–1215. doi: 10.1002/jcp.25616

Mei, S., Cammalleri, M., Azara, D., Casini, G., Bagnoli, P., and Dal Monte, M. (2012). Mechanisms underlying somatostatin receptor 2 down-regulation of vascular endothelial growth factor expression in response to hypoxia in mouse retinal explants. *J. Pathol.* 226, 519–533. doi: 10.1002/path.3006

Mesner, P. W., Epting, C. L., Hegarty, J. L., and Green, S. H. (1995). A timetable of events during programmed cell death induced by trophic factor withdrawal from neuronal PC12 cells. *J. Neurosci.* 15, 7357–7366. doi: 10.1523/jneurosci.15-11-07357.1995

Mester, L., Szabo, A., Atlasz, T., Szabadfi, K., Reglodi, D., Kiss, P., et al. (2009). Protection against chronic hypoperfusion-induced retinal neurodegeneration by PARP inhibition via activation of PI-3-kinase Akt pathway and suppression of JNK and p38 MAP kinases. *Neurotox. Res.* 16, 68–76. doi: 10.1007/s12640-009-9049-6

Miyata, A., Arimura, A., Dahl, R. R., Minamino, N., Uehara, A., Jiang, L., et al. (1989). Isolation of a novel 38 residue-hypothalamic polypeptide which stimulates adenylate cyclase in pituitary cells. *Biochem. Biophys. Res. Commun.* 164, 567–574. doi: 10.1016/0006-291x(89)91757-9

Namgung, U., and Xia, Z. (2000). Arsenite-induced apoptosis in cortical neurons is mediated by c-Jun N-terminal protein kinase 3 and p38 mitogen-activated protein kinase. *J. Neurosci.* 20, 6442–6451. doi: 10.1523/jneurosci.20-17-06442.2000

Njaine, B., Martins, R. A., Santiago, M. F., Linden, R., and Silveira, M. S. (2010). Pituitary adenylyl cyclase-activating polypeptide controls the proliferation of retinal progenitor cells through downregulation of cyclin D1. *Eur. J. Neurosci.* 32, 311–321. doi: 10.1111/j.1460-9568.2010.07286.x

Nyisztor, Z., Denes, V., Kovacs-Valasek, A., Hideg, O., Berta, G., and Gabriel, R. (2018). Pituitary adenylate cyclase activating polypeptide (PACAP1-38) exerts both pro and anti-apoptotic effects on postnatal retinal development in rat. *Neuroscience* 385, 59–66. doi: 10.1016/j.neuroscience.2018.06.008

Ogata, K., Shintani, N., Hayata-Takano, A., Kamo, T., Higashi, S., Seiriki, K., et al. (2015). PACAP enhances axon outgrowth in cultured hippocampal neurons to a comparable extent as BDNF. *PLoS One* 10:e0120526. doi: 10.1371/journal.pone.0120526

Pease, M. E., Zack, D. J., Berlinicke, C., Bloom, K., Cone, F., Wang, Y., et al. (2009). Effect of CNTF on retinal ganglion cell survival in experimental glaucoma. *Invest. Ophthalmol. Vis. Sci.* 50, 2194–2200. doi: 10.1167/iovs.08-3013

Pisegna, J. R., and Wank, S. A. (1996). Cloning and characterization of the signal transduction of four splice variants of the human pituitary adenylate cyclase activating polypeptide receptor. Evidence for dual coupling to adenylate cyclase and phospholipase C. *J. Biol. Chem.* 271, 17267–17274. doi: 10.1074/jbc.271.29.17267

Pugh, C. W., and Ratcliffe, P. J. (2003). Regulation of angiogenesis by hypoxia: role of the HIF system. *Nat. Med.* 9, 677–684. doi: 10.1038/nm0603-677

Racz, B., Gallyas, F. Jr., Kiss, P., Tamas, A., Lubics, A., Lengvari, I., et al. (2007). Effects of pituitary adenylate cyclase activating polypeptide (PACAP) on the PKA-Bad-14-3-3 signaling pathway in glutamate-induced retinal injury in neonatal rats. *Neurotox. Res.* 12, 95–104. doi: 10.1007/bf03033918

Racz, B., Gallyas, F. Jr., Kiss, P., Toth, G., Hegyi, O., Gasz, B., et al. (2006). The neuroprotective effects of PACAP in monosodium glutamate-induced retinal lesion involve inhibition of proapoptotic signaling pathways. *Regul. Pept.* 137, 20–26. doi: 10.1016/j.regpep.2006.02.009

Rahimi, N. (2006). Vascular endothelial growth factor receptors: molecular mechanisms of activation and therapeutic potentials. *Exp. Eye Res.* 83, 1005–1016. doi: 10.1016/j.exer.2006.03.019

Ramirez, J. M., Ramirez, A. I., Salazar, J. J., de Hoz, R., and Trivino, A. (2001). Changes of astrocytes in retinal ageing and age-related macular degeneration. *Exp. Eye Res.* 73, 601–615. doi: 10.1006/exer.2001.1061

Rayner, B. S., Duong, T. T., Myers, S. J., and Witting, P. K. (2006). Protective effect of a synthetic anti-oxidant on neuronal cell apoptosis resulting from experimental hypoxia re-oxygenation injury. *J. Neurochem.* 97, 211–221. doi: 10.1111/j.1471-4159.2006.03726.x

Reglodi, D., Atlasz, T., Szabo, E., Jungling, A., Tamas, A., Juhasz, T., et al. (2018). PACAP deficiency as a model of aging. *Geroscience* 40, 437–452. doi: 10.1007/s11357-018-0045-8

Schratzberger, P., Geiseler, A., Dunzendorfer, S., Reinisch, N., Kahler, C. M., and Wiedermann, C. J. (1998). Similar involvement of VIP receptor type I and type II in lymphocyte chemotaxis. *J. Neuroimmunol.* 87, 73–81. doi: 10.1016/s0165-5728(98)00043-5

Seki, T., Shioda, S., Izumi, S., Arimura, A., and Koide, R. (2000). Electron microscopic observation of pituitary adenylate cyclase-activating polypeptide (PACAP)-containing neurons in the rat retina. *Peptides* 21, 109–113. doi: 10.1016/s0196-9781(99)00180-1

Seki, T., Shioda, S., Ogino, D., Nakai, Y., Arimura, A., and Koide, R. (1997). Distribution and ultrastructural localization of a receptor for pituitary adenylate cyclase activating polypeptide and its mRNA in the rat retina. *Neurosci. Lett.* 238, 127–130. doi: 10.1016/s0304-3940(97)00869-0

Shanmugam, P. M. (2014). Changing paradigms of anti-VEGF in the Indian scenario. *Indian J. Ophthalmol.* 62, 88–92. doi: 10.4103/0301-4738.126189

Silveira, M. S., Costa, M. R., Bozza, M., and Linden, R. (2002). Pituitary adenylyl cyclase-activating polypeptide prevents induced cell death in retinal tissue through activation of cyclic AMP-dependent protein kinase. *J. Biol. Chem.* 277, 16075–16080. doi: 10.1074/jbc.M110106200

Skeie, J. M., and Mullins, R. F. (2009). Macrophages in neovascular age-related macular degeneration: friends or foes? *Eye* 23, 747–755. doi: 10.1038/eye.2008.206

Spengler, D., Waeber, C., Pantaloni, C., Holsboer, F., Bockaert, J., Seeburg, P. H., et al. (1993). Differential signal transduction by five splice variants of the PACAP receptor. *Nature* 365, 170–175. doi: 10.1038/365170a0

Strand, F. L. (2003). Neuropeptides: general characteristics and neuropharmaceutical potential in treating CNS disorders. *Prog. Drug Res.* 61, 1–37. doi: 10.1007/978-3-0348-8049-7_1

Szabadfi, K., Atlasz, T., Kiss, P., Reglodi, D., Szabo, A., Kovacs, K., et al. (2012). Protective effects of the neuropeptide PACAP in diabetic retinopathy. *Cell Tissue Res.* 348, 37–46. doi: 10.1007/s00441-012-1349-0

Szabadfi, K., Reglodi, D., Szabo, A., Szalontai, B., Valasek, A., Setalo, G., et al. (2016). Pituitary adenylate cyclase activating polypeptide, a potential therapeutic agent for diabetic retinopathy in rats: focus on the vertical information processing pathway. *Neurotox. Res.* 29, 432–446. doi: 10.1007/s12640-015-9593-1

Szabadfi, K., Szabo, A., Kiss, P., Reglodi, D., Setalo, G. Jr., Kovacs, K., et al. (2014). PACAP promotes neuron survival in early experimental diabetic retinopathy. *Neurochem. Int.* 64, 84–91. doi: 10.1016/j.neuint.2013.11.005

Szabo, A., Danyadi, B., Bognar, E., Szabadfi, K., Fabian, E., Kiss, P., et al. (2012). Effect of PACAP on MAP kinases, Akt and cytokine expressions in rat retinal hypoperfusion. *Neurosci. Lett.* 523, 93–98. doi: 10.1016/j.neulet.2012.06.044

Takuma, K., Maeda, Y., Ago, Y., Ishihama, T., Takemoto, K., Nakagawa, A., et al. (2014). An enriched environment ameliorates memory impairments in PACAP-deficient mice. *Behav. Brain Res.* 272, 269–278. doi: 10.1016/j.bbr.2014.07.005

Tamas, A., Gabriel, R., Racz, B., Denes, V., Kiss, P., Lubics, A., et al. (2004). Effects of pituitary adenylate cyclase activating polypeptide in retinal degeneration induced by monosodium-glutamate. *Neurosci. Lett.* 372, 110–113. doi: 10.1016/j.neulet.2004.09.021

Tao, W., Wen, R., Goddard, M. B., Sherman, S. D., O'Rourke, P. J., Stabila, P. F., et al. (2002). Encapsulated cell-based delivery of CNTF reduces photoreceptor degeneration in animal models of retinitis pigmentosa. *Invest. Ophthalmol. Vis. Sci.* 43, 3292–3298.

Vaczy, A., Kovari, P., Kovacs, K., Farkas, K., Szabo, E., Kvarik, T., et al. (2018). Protective role of endogenous PACAP in inflammation-induced retinal degeneration. *Curr. Pharm. Des.* 24, 3534–3542. doi: 10.2174/1381612824666180924141407

van Hagen, P. M., Baarsma, G. S., Mooy, C. M., Ercoskan, E. M., ter Averst, E., Hofland, L. J., et al. (2000). Somatostatin and somatostatin receptors in retinal diseases. *Eur. J. Endocrinol.* 143(Suppl. 1), S43–S51.

Vaudry, D., Falluel-Morel, A., Bourgault, S., Basille, M., Burel, D., Wurtz, O., et al. (2009). Pituitary adenylate cyclase-activating polypeptide and its receptors: 20 years after the discovery. *Pharmacol. Rev.* 61, 283–357. doi: 10.1124/pr.109.001370

Vaudry, D., Gonzalez, B. J., Basille, M., Yon, L., Fournier, A., and Vaudry, H. (2000). Pituitary adenylate cyclase-activating polypeptide and its receptors: from structure to functions. *Pharmacol. Rev.* 52, 269–324.

Wang, G., Pan, J., Tan, Y. Y., Sun, X. K., Zhang, Y. F., Zhou, H. Y., et al. (2008). Neuroprotective effects of PACAP27 in mice model of Parkinson's disease involved in the modulation of K(ATP) subunits and D2 receptors in the striatum. *Neuropeptides* 42, 267–276. doi: 10.1016/j.npep.2008.03.002

Wang, J., Sun, Z., Shen, J., Wu, D., Liu, F., Yang, R., et al. (2015). Octreotide protects the mouse retina against ischemic reperfusion injury through regulation of antioxidation and activation of NF-kappaB. *Oxid. Med. Cell. Longev.* 2015:970156. doi: 10.1155/2015/970156

Wang, Z., Han, X., Cui, M., Fang, K., Lu, Z., and Dong, Q. (2014). Tissue kallikrein protects rat hippocampal CA1 neurons against cerebral ischemia/reperfusion-induced injury through the B2R-Raf-MEK1/2-ERK1/2 pathway. *J. Neurosci. Res.* 92, 651–657. doi: 10.1002/jnr.23325

Wang, Z. Y., Alm, P., and Hakanson, R. (1995). Distribution and effects of pituitary adenylate cyclase-activating peptide in the rabbit eye. *Neuroscience* 69, 297–308. doi: 10.1016/0306-4522(95)00258-k

Wen, R., Tao, W., Li, Y., and Sieving, P. A. (2012). CNTF and retina. *Prog. Retin. Eye Res.* 31, 136–151. doi: 10.1016/j.preteyeres.2011.11.005

Werling, D., Banks, W. A., Salameh, T. S., Kvarik, T., Kovacs, L. A., Vaczy, A., et al. (2017).). Passage through the ocular barriers and beneficial effects in retinal ischemia of topical application of PACAP1-38 in rodents. *Int. J. Mol. Sci.* 18:E675. doi: 10.3390/ijms18030675

Werling, D., Reglodi, D., Kiss, P., Toth, G., Szabadfi, K., Tamas, A., et al. (2014). Investigation of PACAP fragments and related peptides in chronic retinal hypoperfusion. *J. Ophthalmol.* 2014:563812. doi: 10.1155/2014/563812

Xia, Z., Dickens, M., Raingeaud, J., Davis, R. J., and Greenberg, M. E. (1995). Opposing effects of ERK and JNK-p38 MAP kinases on apoptosis. *Science* 270, 1326–1331. doi: 10.1126/science.270.5240.1326

Yancopoulos, G. D., Davis, S., Gale, N. W., Rudge, J. S., Wiegand, S. J., and Holash, J. (2000). Vascular-specific growth factors and blood vessel formation. *Nature* 407, 242–248. doi: 10.1038/35025215

Yau, J. W., Rogers, S. L., Kawasaki, R., Lamoureux, E. L., Kowalski, J. W., Bek, T., et al. (2012). Global prevalence and major risk factors of diabetic retinopathy. *Diabetes Care* 35, 556–564. doi: 10.2337/dc11-1909

Zeng, H. Y., Green, W. R., and Tso, M. O. (2008). Microglial activation in human diabetic retinopathy. *Arch. Ophthalmol.* 126, 227–232. doi: 10.1001/archophthalmol.2007.65

Zeng, X. X., Ng, Y. K., and Ling, E. A. (2000). Neuronal and microglial response in the retina of streptozotocin-induced diabetic rats. *Vis. Neurosci.* 17, 463–471. doi: 10.1017/s0952523800173122

Conflict of Interest: The authors declare that the research was conducted in the absence of any commercial or financial relationships that could be construed as a potential conflict of interest.

frontiers in Neuroscience

ORIGINAL RESEARCH
published: 10 October 2019
doi: 10.3389/fnins.2019.01065

Auranofin Mediates Mitochondrial Dysregulation and Inflammatory Cell Death in Human Retinal Pigment Epithelial Cells: Implications of Retinal Neurodegenerative Diseases

*Thangal Yumnamcha, Takhellembam Swornalata Devi and Lalit Pukhrambam Singh**

Department of Ophthalmology, Visual and Anatomical Sciences (OVAS), Wayne State University School of Medicine, Detroit, MI, United States

Purpose: Photoreceptor degeneration occurs in various retinal diseases including age-related macular degeneration (AMD), Retinitis pigmentosa (RP), and diabetic retinopathy (DR). However, molecular mechanisms are not fully understood yet. The retinal pigment epithelium (RPE) forms the outer blood retinal barrier (oBRB) and supplies glucose, oxygen and nutrients from the fenestrated choriocapillaris to photoreceptors for visual function. Therefore, RPE dysfunction leads to photoreceptor injury/death and progression of blinding eye diseases. This study aims to understand the role of the thioredoxin (Trx) and its reductase (TrxR) redox signaling in human RPE dysfunction and cell death mechanism(s) in an *in vitro* system.

Methods: A human RPE cell line (APRE-19) was cultured in DMEM/F12 medium and treated with auranofin (AF – 4 μM, an inhibitor of TrxR) for 4 and 24 h. Mitochondrial and lysosomal function, cellular oxidative stress and NLRP3 inflammasome activity were measured using cell assays, Western blotting, and confocal microscopy. Antioxidants and anti-inflammatory compounds were tested for blocking AF effects on RPE damage. Cell death mechanisms (LDH release to culture media) were determined using necroptosis, ferroptosis and pyroptosis inhibitors. $P < 0.05$ was considered significant in statistical analysis.

Results: Auranofin causes mitochondrial dysfunction ($\Delta\psi m\downarrow$ and ATP↓), oxidative stress ($H_2O_2\uparrow$) and mitophagic flux to lysosomes. Furthermore, the lysosomal enzyme (cathepsin L) activity is reduced while that of pro-inflammatory caspase-1 (NLRP3 inflammasome) is enhanced in ARPE-19. These effects of AF on ARPE-19 are inhibited by antioxidant N-acetylcysteine (5 mM, NAC) and significantly by a combination of SS31 (mitochondrial antioxidant) and anti-inflammatory drugs (amlexanox and tranilast). AF also causes cell death as measured by cytosolic LDH release/leakage, which is not inhibited by either ferrostatin-1 or necrostatin-1 (ferroptosis and necroptosis inhibitors, respectively). Conversely, AF-induced LDH release is significantly reduced by MCC950 and Ac-YVAD-cmk (NLRP3 and Caspase-1 inhibitors, respectively), suggesting a pro-inflammatory cell death by pyroptosis.

OPEN ACCESS

Edited by:
Mohammad Shamsul Ola, King Saud University, Saudi Arabia

Reviewed by:
Ilaria Piano, University of Pisa, Italy
Ilaria Bellezza, University of Perugia, Italy

****Correspondence:***
Lalit Pukhrambam Singh
ak1157@wayne.edu;
plsingh@med.wayne.edu

Specialty section:
This article was submitted to Neurodegeneration, a section of the journal Frontiers in Neuroscience

Received: *31 July 2019*
Accepted: *24 September 2019*
Published: *10 October 2019*

Citation:
Yumnamcha T, Devi TS and Singh LP (2019) Auranofin Mediates Mitochondrial Dysregulation and Inflammatory Cell Death in Human Retinal Pigment Epithelial Cells: Implications of Retinal Neurodegenerative Diseases. Front. Neurosci. 13:1065. doi: 10.3389/fnins.2019.01065

Conclusion: The Trx/TrxR redox system is critical for RPE function and viability. We previously showed that thioredoxin-interacting protein (TXNIP) is strongly induced in DR inhibiting the Trx/TrxR system and RPE dysfunction. Therefore, our results suggest that the TXNIP-Trx-TrxR redox pathway may participate in RPE dysfunction in DR and other retinal neurodegenerative diseases.

Keywords: neurodegeneration, mitophagy, auranofin, Trx-TrxR, pyroptosis, inflammation, RPE

INTRODUCTION

Retina is a window to the brain (Chiquita et al., 2019). Being a part of the central nervous system, the retina consumes large amounts of glucose and oxygen for its bioenergetics (ATP production), light perception, and visual processing (Country, 2017). The retina also has tight blood-retinal barriers (BRB) and protects the neuroretina from the circulating immune cells and plasma components (Cunha-Vaz et al., 2011). The inner BRB consists of tight junctions of endothelial cells in the blood vessel while the outer BRB consists of a single layer of retinal pigmented epithelium (RPE) and its tight junction proteins. RPE separates the fenestrated choriocapillaris from the neuroretina and functions to transport glucose, oxygen, and nutrients to the retinal outer segments consisting of rod and cone photoreceptors (Campbell and Humphries, 2012; Ivanova et al., 2019). Breakdown of the outer BRB and RPE dysfunction is associated with age-related macular degeneration (AMD) (Handa et al., 2019; Jun et al., 2019) while gene mutation in RPE and photoreceptor cause photoreceptor degeneration and blindness including retinitis pigmentosa (RP) (Dias et al., 2018; Shu and Dunaief, 2018). In these various retinal diseases, RPE dysfunction, photoreceptor injury/death and retinal neurodegeneration leads to blindness. In addition to nutrient exchange, RPE also involves in recycling of the visual pigment (retinoid) to photoreceptors, daily phagocytosis of the photoreceptor outer segment, and synthesis of melanosome (melanin) to absorb excess light in the retina (Biesemeier et al., 2015; Spencer et al., 2019).

On the other hand, breakdown of the inner BRB and formation of new fragile/leaky blood vessels are associated in proliferative diabetic retinopathy (PDR) leading to blindness as well as visual distortion in diabetic macular edema (DME) (Graham et al., 2018; Bapputty et al., 2019). Recent studies have further demonstrated that photoreceptor oxidative stress and dysfunction may occur early in diabetics prior to vessel histopathology (Fu et al., 2018; Liu et al., 2019). However, the study of the role of RPE in photoreceptor dysfunction in DR is still limited (Xia and Rizzolo, 2017; Tarchick et al., 2019). Diabetic retinopathy (DR) is the most devastating disease of diabetes mellitus affecting millions of people among the working adult life in the US and around the globe (Cheloni et al., 2019). As the number of people living with diabetes particularly of obesity and type 2 diabetes increases, the incident of DR will escalate several folds in coming decades (Caspard et al., 2018). DR is generally defined by microvascular complications of capillary endothelium and pericytes leading to microaneurysm, iBRB leakage, and fragile new blood vessel formation (neovascularization). Most patients with Type 1 or Type 2 diabetes will develop some forms of DR, beginning with non-proliferative DR (NPDR) then progress to a severe form of proliferative DR (PDR) causing blindness (Xia and Rizzolo, 2017; Fu et al., 2018). Yet, the molecular basis of the pathogenesis is not fully understood and, therefore, no known cure or effective treatment options are available still today.

The retina consumes large amounts of glucose and oxygen to generate energy (ATP) for its visual function via the mitochondrial electron transport chain (ETC) in inner membranes (Country, 2017). During this process, electrons leak out from the ETC, which are captured by molecular oxygen generating reactive oxygen radicals/species (ROS), which damage mitochondrial membrane lipid, proteins, and mtDNA. Damaged mitochondrial are inefficient in ATP but produces more ROS. Mitochondrial ROS and oxidized mtDNA, when released into the cytosol, are recognized as damaged-associated molecular patterns (DAMPs) by cytosolic pattern recognition receptors (PRRs) including toll-like receptors TLR4, TLR9, and the NLRP3 inflammasome. These inflammatory receptors produce and activate inflammatory pro-IL-1β and pro-caspase-1. An assembled NLRP3 inflammasome forms the platform for pro-caspase-1 processing and activation, which in turn is responsible for processing pro-inflammatory IL-1 β and active IL-1 β. Caspase-1 also induces pro-inflammatory cell death by pyroptosis, which involves release of the N-terminal part of gasdermin D (Dubois et al., 2019). The cleaved N-terminus portion of gasdermin D is then inserted into the plasma membrane forming pores resulting in plasma membrane permeabilization. Therefore, removal of the damaged mitochondrial by mitophagy, an autophagic process of degrading damaged mitochondria by lysosomes, is critical for maintaining mitochondria health, bioenergetics, and cell survival (Devi et al., 2019). In addition, the RPE phagocytes the damaged photoreceptor outer segment daily and recycle visual pigment retinol for photoreceptor function. Therefore, the mitochondrial-lysosomal axis in RPE and maintaining its function may play a critical role in photoreceptor function in DR. Hence, enhancing the antioxidant capacity while reducing inflammation at initial stages of the disease may constitute potential therapies (Lin and Beal, 2006; Di Carlo et al., 2012; Stephenson et al., 2018; Bapputty et al., 2019).

One of the genes strongly induced by diabetes and aging in retinal cells and neurons is the thioredoxin-interacting/inhibiting protein (TXNIP) (Perrone et al., 2010; Devi et al., 2012, 2013, 2019; Singh and Perrone, 2013). TXNIP's actions include binding to and inhibition of the anti-oxidant and thiol reducing capacity of thioredoxin (Trx), thereby, causing cellular oxidative stress,

inflammation, and premature cell death (Stephenson et al., 2018). Trx1 and its reductase TrxR1 are present in the cytosol and nucleus while Trx2/TrxR2 redox system is in the mitochondrion. Therefore, Trx/TrxR redox system plays an important role in scavenging reactive oxygen species (ROS) and maintaining reduced state of proteins in their functionally active sites and cell survival (Devi et al., 2017; Stephenson et al., 2018; Booty et al., 2019). Thus, TXNIP inhibition of the Trx/TrxR system causes oxidative stress, mitochondrial dysfunction, and retinal cell death in diabetes (Perrone et al., 2010; Singh and Perrone, 2013). Nonetheless, TXNIP is a multifunctional protein and is also considered as a scaffold protein of the α-arrestin type (Stephenson et al., 2018). Therefore, TXNIP is also involved in interactions with other proteins including glucose transporter 1 and 4, REDD1 (regulated in development and DNA damage responses 1), VEGF-R (vascular endothelial growth factor receptor), and other nuclear proteins that are involved in cell cycle regulation (Devi et al., 2012; Stephenson et al., 2018). Therefore, to further understand a direct effect of the Trx/TrxR redox system in RPE and retinal neurodegenerative diseases, we used in this study, auranofin, a gold compound, which specifically inhibits redox proteins TrxR1 and TrxR2 (Yoshihara et al., 2014). We demonstrate that auranofin causes mitochondrial dysfunction, mitophagic flux and inflammatory pyroptotic cell death in RPE cells in culture. These findings may be relevant to various retinal neurodegenerative diseases where RPE dysfunction plays a causative role in disease progression.

MATERIALS AND METHODS

Tissue Culture Media

DMEM medium was purchased from (Mediatech Inc., Cat #10-014-CM, Manassas, VA, United States) while Ham's F12 was from Hyclone (Cat # SH30025.01, Logan, UT, United States). Antibiotics and trypsin were also purchased from Hyclone, whereas fetal bovine serum was obstained (Corning, Cat # MT35010CV). Details of other chemicals used in this study are provided in **Supplementary Table S1**.

Cell Culture

A human retinal pigment epithelial cell line (ARPE-19), purchased from ATCC (Cat# 2302), was maintained in DMEM/F12 medium (1:1 ratio) containing LG (low glucose, 5.5 mM), 5% fetal bovine serum (FBS), 2% penicillin, and 1% antimycotic in a humidified incubator with 5% CO_2 at 37°C as described previously (Devi et al., 2013). After reaching ∼80% confluence, the medium was changed to 1% serum overnight. Initially, a concentration and time dependent effect of auranofin (AF) on ARPE-19 function was tested; and subsequently we selected 4 μM and 4–24 h as optimal concentration and time period for the current study. Then, ARPE-19 cells were maintained with or without AF (4 μM) for 4 and 24 h, respectively. Because we observed cell death at 24 h but not at 4 h of AF treatment, we decided to investigate early molecular defects that might lead to demise and determine potential rescue mechanisms. Before treatment with 4 μM AF, we pre-incubated ARPE-19 cells with different concentration of drugs targeting mitochondria and NLRP3 inflammasome for 2 h and they were present throughout the period of incubation.

Measurement of Mitochondrial Membrane Potential

The mitochondrial membrane potential in ARPE-19 cells was measured using MitoProbeTM JC-1 Assay Kit (Cat# M34152, Life Technologies, Eugene, OR, United States) (Devi et al., 2012, 2013). JC1 dye penetrates the cell and exhibits potential-dependent accumulation in mitochondria. After treatment, ARPE 19 cells were washed with 1× phosphate-buffered saline (PBS). Then, the cells were incubated with 200 μl of 2 μM JC1 dye for 10 min in a 48-well cell culture plate. After incubation, the cells were washed thrice with 1× PBS. The relative fluorescence was measured at Ex529/Em590 nm using (SpectraMax Gemini EM Microplate Reader, Molecular Devices) as per manufacturer's instructions.

Measurement of Intracellular ATP

Cellular ATP concentration in ARPE-19 cells was measured using a ATP determination kit from Life Technologies (Cat # A22066, Life Technologies, Eugene, OR, United States) (Devi et al., 2012, 2013). After treatment, ARPE-19 cells were washed twice with 1× PBS. Then, 250 μl of 1× TE Buffer (Tris EDTA, 1× solution, pH 8.0, Cat #BP24731, Thermo Fisher Scientific) was added to each well of a 48-well cell culture plate containing the ARPE-19 cells. The cells were scrapped out and transferred to a 1.5 ml Eppendorf tube. The samples were boiled for 5 min in a water bath. After keeping on ice for 3 min, the samples were centrifuged at 12000 rpm for 10 min at 4°C. Ninety μl of the ATP reaction solution and 10 μl of the sample were mixed and kept protected from light. Relative fluorescence units (RFUs) were measured using luminometer plate reader (SpectraMax L Microplate Reader, Molecular Devices).

Measurement of Intracellular Reactive Oxygen Species (ROS)

Cellular ROS production in ARPE-19 cells was measured using the CM-H2DCFDA probe (Cat # 6827, Life Technologies, Eugene, OR, United States) as per company's instructions. After different treatments, ARPE-19 cells were washed twice with 1× PBS and incubated with 200 μl of 10 μM CM-H2DCFDA dye for 30 min at 37°C on 24-well cell culture plate. Following incubation, ARPE-19 cells were washed once in 1× PBS. The fluorescence intensity of CM-H2DXFDA was measured at Ex495/Em517 nm in 1× PBS buffer using a Fluorescence Plate Reader (SpectraMax Gemini EM Microplate Reader, Molecular Devices).

Assessment of Cathepsin-L Activity

Cathepsin-L activity in ARPE-19 cells was measured using a Magic Red Cathepsin-L detection Kit (Cat #941, Immunochemistry Technologies, Bloomington, MN, United States) as described recently (Devi et al., 2013). Briefly, ARPE-19 cells were incubated with 20 μl Magic Red

Cathepsin-L reagent and 480 μl of cell culture media for 1 h. The cells were then washed twice with 1× PBS. The fluorescence intensity of dye was measured at Ex592/Em628 nm using a Fluorescence Plate Reader (SpectraMax Gemini EM Microplate Reader, Molecular Devices).

Assessment of Caspase-1 Activity

Caspase-1 activity in ARPE-19 cells was measured using a FAM-FLICA Caspase-1 detection kit (Cat #97, Immunochemistry Technologies, Bloomington, MN, United States) in a 24-well cell culture plate as described before (Devi et al., 2013). After treatment with various reagents for a stipulated time period, ARPE-19 cells were washed with wash buffer. Then, the cells were incubated with 10 μl of FLICA solution and 300 μl of freshly replaced 1% serum media for 1 h. Following incubation, the cells were washed twice with 1× PBS. The fluorescence intensity was measured at Ex492/Em520 nm using a Fluorescence Plate Reader (SpectraMax Gemini EM Microplate Reader, Molecular Devices).

Measurement of Lactate Dehydrogenase Activity (LDH)

Lactate dehydrogenase activity in ARPE-19 cells was measured using Pierce TM LDH cytotoxicity Assay Kit (Cat# 88954, Thermo Fisher scientific). After treatment, 50 μl of the Sample's cell culture media were mixed with 50 μl of reaction mixture in a 96-well plate and incubated at room temperature for 30 min. The absorbance was measured at 490 nm and 680 nm using SpectraMax plus 384 Microplate Reader (Molecular Devices), as per company's instructions. The amount of LDH release in the media was calculated by difference in absorbance of 490–680 nm, according to manufacturer's instructions.

Western Blotting and Mitophagic Flux

These procedures, both Western blotting and mitophagy analysis, were performed similar to those described (Devi et al., 2017, 2019). Cytosol, mitochondria and nuclear fractions were fractionated using a kit as described before (Devi et al., 2012, 2013). Briefly, for Western blots, 20–30 μg protein extracts were loaded on SDS-PAGE, and proteins were separated, trans-blotted and incubated with appropriate primary antibodies. After overnight incubation with primary antibodies at 40_c with shaking, HRP conjugate secondary antibodies were added for 2 h. ECL detected the reactive bands in a FluorChem E Western blot imaging instrument (ProteinSimple, San Jose, California). ImageJ (NIH) was used to quantitate the blots. The source of primary and secondary antibodies and their dilution used are shown in **Supplementary Tables S2A,B**, respectively.

For mitophagy, Ad-CMV-mt-Keima was expressed in the mitochondrial matrix by transduction for 3 days; then treated with AF with or without inhibitors. Mt-Keima emits a green light (neutral or alkaline pH > 7.0) in mitochondria while, in lysosomes after mitophagic flux, it emits red light at acidic pH (<5.0). Therefore, the same mt-Keima can detect mitophagic flux by a change in color from green to red in living cells. A Zeiss LMS 780 Confocal Microscope captured multiple images from triplicate samples. Similarly, a CMV-LAMP1-mCherry carrying adenovirus was transduced in ARPE-19 cells to examine lysosomal morphology and distribution after the AF treatment.

Statistical Analysis

Results are represented by means ± SEM of the indicated number of experiments. One-way ANOVA and Bonferroni *post hoc* test determined differences among means in multiple sets of experiments. On the other hand, a comparison between two sets of experiments was analyzed by unpaired two-tailed *t*-test. A p-value of <0.05 was considered to be statistically significant.

RESULTS

Auranofin Causes Mitochondria-Lysosome Dysfunction and Inflammatory Responses in ARPE-19 Cells

Treatment of APRE-19 with AF (4 μM) for 4 h reduces significantly the mitochondrial ATP level as well as mediates mitochondrial membrane depolarization as measured by a reduction in JC1 (**Figures 1A,B**, respectively). In addition, there is an increase in the cellular ROS level as determined by H_2DCFDA probe (**Figure 1C**). These results suggest that AF induces mitochondrial dysfunction and cellular oxidative stress in ARPE-19. To further investigate if lysosomal function is also altered due to mitochondrial defects as the mitochondria-lysosome function are closely related, we measured the activity of lysosomal acid hydrolase, cathepsin L. Indeed, we observed that cathepsin L activity is significantly reduced by AF (**Figure 1D**) and also increases the activity of pro-inflammatory caspase-1 (**Figure 1E**) suggesting inflammasome activation by the AF treatment. Furthermore, we show that lysosome destabilization by lysosomotropic agent LLME (LeuLeuOMe) also causes a reduction in ATP level along with activation of caspase 1 and inhibition of the cathepsin L activity, which are similar to that observed with AF further supporting that the mitochondria and lysosomal injury in AF action on ARPE-19 cells (**Figure 2**). Nonetheless, AF does not alter levels of TrxR1 and TrxR2 significantly and similarly no significant change is observed with Trx1 and Trx2, although Trx2 is marginally reduced (**Figure 3**).

Auranofin Does Not Evoke mtUPR but Mediates Mitophagic Flux in ARPE-19 Cells

The mitochondrion responses to oxidative stress (i) by increasing the expression of nuclear-encoded mitochondria-targeted chaperones and proteases to counter its oxidative protein stress and misfolding known as the mitochondrial unfolded protein response (mtUPR) (Harper, 2019). (ii) Another mitochondrial stress response is segregation of the damaged part of the mitochondrion by fission involving Drp1 (dynamin related protein 1), then engulfment within a double-membrane autophagosome, which is further targeted to lysosomes for degradation, a process known as

mitophagy – autophagy of damaged mitochondria (Pareek and Pallanck, 2018). Nonetheless, we did not observe significant changes in the expression of mitochondrial proteases (LonP and YMEIL1) and chaperones (Tid1/mtHSP40 and PDIA, protein disulfide isomerase A) by AF. Conversely, during the same period of AF treatment, autophagic/mitophagic markers, such as microtubule light-chain LC3BII and adaptors optineurin and p62/Sequestosome1, are reduced within minutes to hours (**Supplementary Figure S1**), suggesting a mitophagy induction.

Subsequently, we examined AF-induced mitophagic flux in ARPE-19 cells using a mito-probe known as mt-Keima (Devi et al., 2013), which emits green light in mitochondria at neutral or alkaline pH (>7.0) whereas it emits red light after mitophagic flux to lysosomes at acidic pH (<5.0). Using confocal live cell imaging of ARPE-19 after mt-Keima transduction and treatment with AF, we observed mt-Keima in control cells as green filaments of mitochondria, and a lesser amount of the red mt-Keima (**Figure 4A**, first panel). Conversely, AF treatment increases the level of red mt-Keima in ARPE-19, indicating a mitophagy flux to acidic lysosomes (**Figure 4A**, second panel). Next, we tested effectiveness of several inhibitors in combination targeting different steps in the mitochondria-lysosome pathway (**Supplementary Figures S2, S3**).

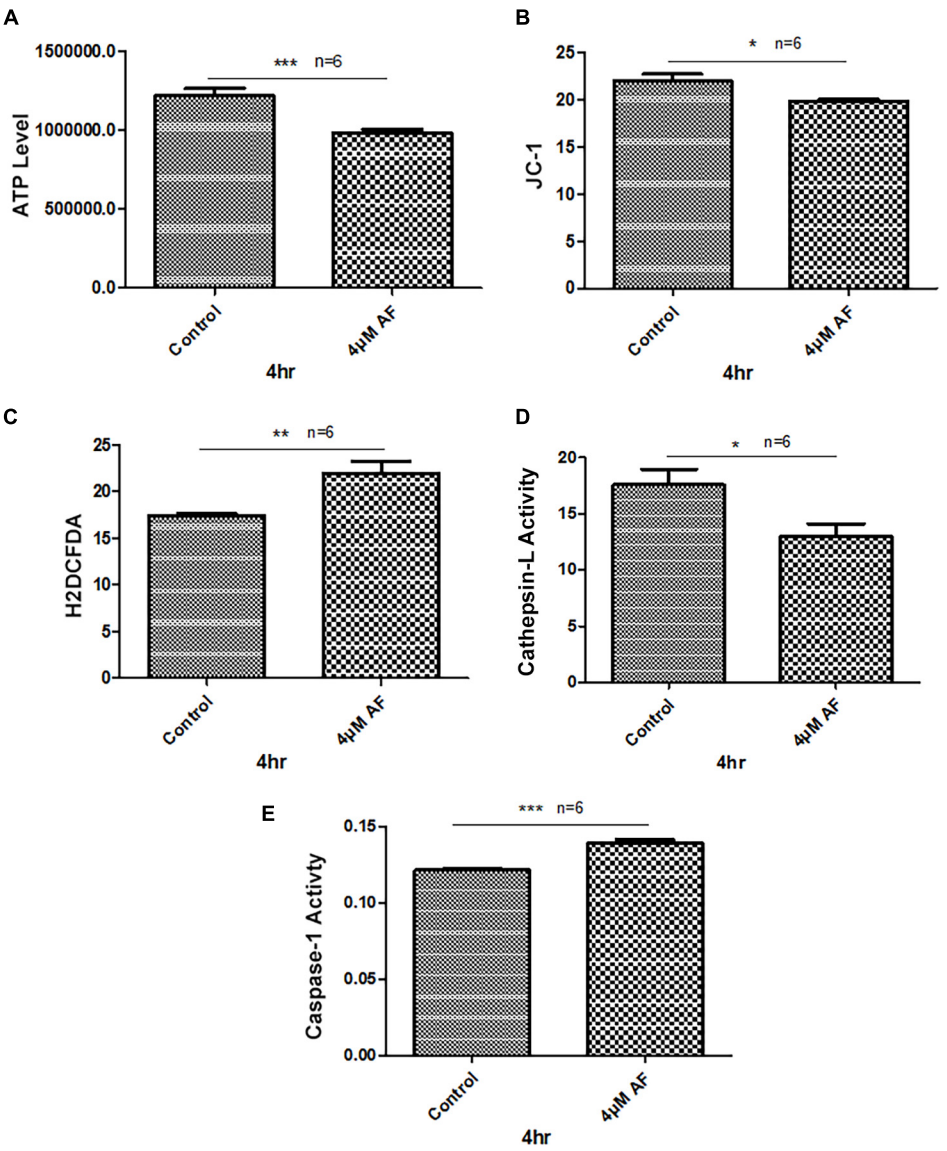

FIGURE 1 | Auranofin causes mitochondrial dysfunction and lysosomal enzyme inactivation in ARPE-19 cells. **(A)** AF treatment (4 μM, 4 h) of ARPE-19 cells reduces cellular ATP level and **(B)** causes mitochondrial membrane depolarization as measured by a reduction in JC1. **(C)** In addition, AF increases cellular ROS levels and **(D)** reduces lysosomal cathepsin L activity. These changes in mitochondrial and lysosomal function are associated with an increase in the activity of proinflammatory enzyme, caspase-1 **(E)**. Significant changes are indicated by *p* values of * <0.05; ** <0.001; and *** <0.0001; *n* = 6.

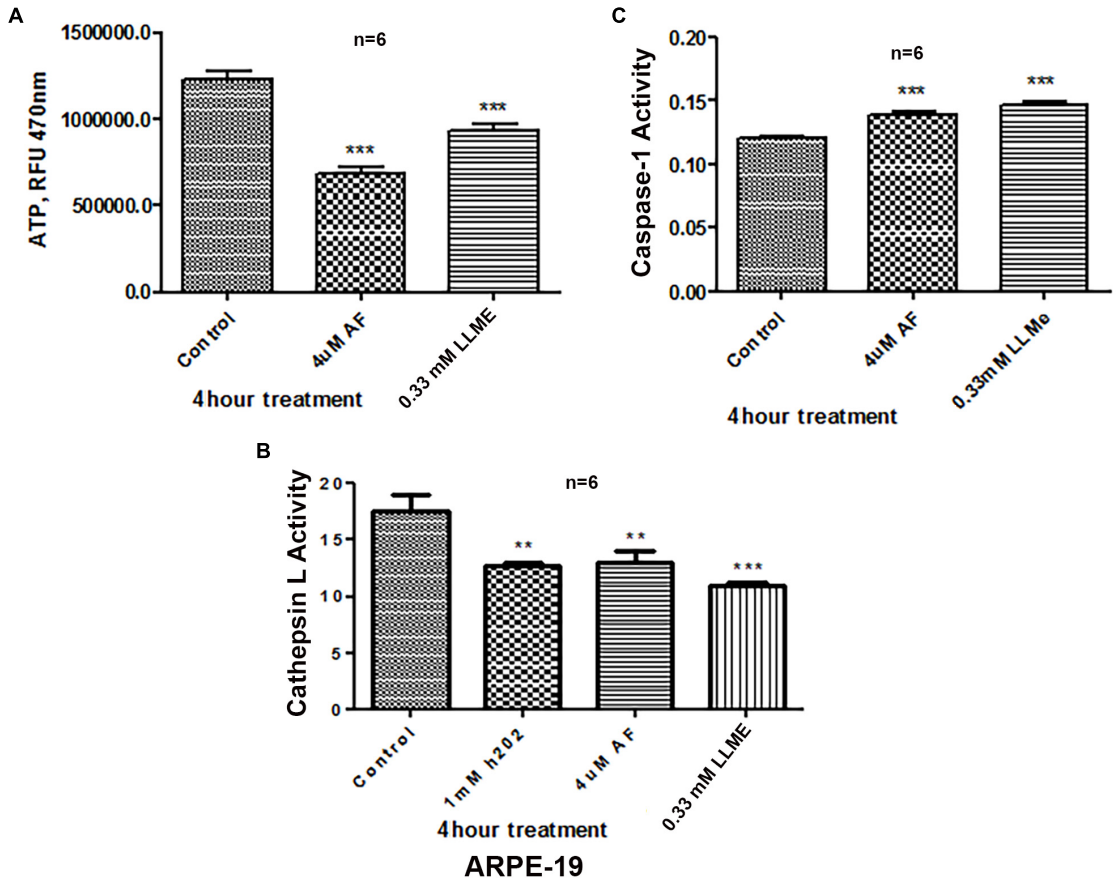

FIGURE 2 | Lysosomal damage reduces ATP levels and activates Caspase-1 activity in ARPE-19 cells. **(A,B)** Treatment with auranofin (AF, 4 μM, 4 h) or lysosomal membrane iononophore (LLMe, 0.33 mM, 4 h) significantly reduces ATP levels and cathepsin L activity. In addition, H_2O_2 also reduces cathepsin L activity significantly suggesting a role for oxidative stress. **(C)** Conversely, both AF and LLMe increase pro-inflammatory caspase1 activity in ARPE-19 cells. Significant changes in figures are indicated by *p* values of symbols ** <0.001 and *** <0.0001; *n* = 6 for each experiment.

These include SS31 – mitochondrial antioxidant (Fivenson et al., 2017), Mdiv-1 – Drp1 fission inhibitor (Campbell et al., 2019), amlexanox – TBK1 and Optineurin/p62 inhibition (Devi et al., 2013; Manczak et al., 2019) and tranilast – NLRP3 inhibitor (Oral et al., 2017). As shown in **Figure 4A** (last 2 panels), we observe that the presence of Mdiv-1 reduces the level of red mt-Keima of AF but produces vesiculated mitochondria, indicating a prevention of the mitophagic flux and an accumulation of damaged mitochondria. However, a combination of SS31 + Amlexanox + Tranilast prevents AF-induced mitophagic flux as the level of green mt-Keima is maintained and the mitochondria are seen as filamentous networks. In support, the level of autophagic/mitophagic markers, LC3BII and Optineurin proteins, are increased in the present of Mdiv-1 suggesting mitophagy inhibition and reduced lysosomal degradation, which is not observed with SS31 + Amlexanox + Tranilast (**Supplementary Figure S4**). Furthermore, this later three drug combination normalizes mitochondrial ATP level, which is also seen with anti-oxidant NAC (N-acetylcysteine) (**Figure 5**), again suggesting a role for oxidative stress in mitochondrial dysregulation in ARPE-19. Therefore, this drug combination may have potential therapeutic benefits in neurodegenerative diseases.

AF Causes Nuclear Deformation and Transcription Factor EB Translocation in ARPE-19 Cells

An interesting observation with AF treatment in ARPE-19 is that the perinuclear DNA shrinks and deform when compared with the control suggesting nuclear stress (shown in **Figure 4B**). However, AF effects on nuclear deformation are restored by combination treatment with SS31 + Amlexanox + Tranilast, but not in the presence of Mdiv-1 (**Figures 4B,C**). Furthermore, AF treatment causes lysosomal destabilization shown by peripheral LAMP1-mCherry expression and membrane exocytosis in ARPE-19 cells (**Supplementary Figure S5**). Subsequently, one of the lysosomal membrane-associated transcription factors, TFEB, migrates from the lysosome to the nucleus as a mitophagy-lysosomal stress response (**Figures 6A–C**). In fact, the combination treatment with SS31 + Amlexanox + Tranilast also restores AF-induced TFEB

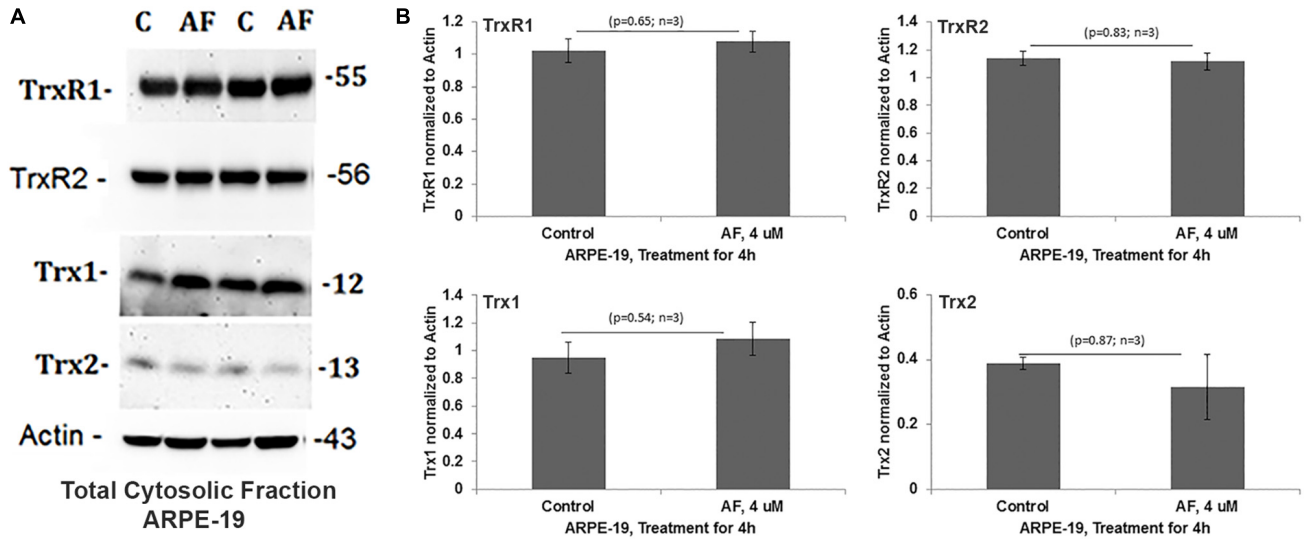

FIGURE 3 | Auranofin does not change the level of redox proteins significantly in ARPE-19 cells. **(A,B)** On Western blots, auranofin treatment does not cause a significant change in protein levels of TrxR1, TrxR2, Trx1, or Trx2 when normalized to actin ($p > 0.05$; $n = 3$).

nuclear translocation (**Supplementary Figure S6**), suggesting lysosomal stabilization. TFEB is involved in the synthesis of lysosomal and autophagy genes within a gene network known as the coordinated lysosomal expression and autophagy regulation (CLEAR) (Huang et al., 2018; Pan et al., 2019). On the other hand, p53 also known to response to DNA damage and cellular stress is not altered by AF treatment. However, AF treatment significantly reduces the level of nuclear actin (**Figures 6A,B**). Nuclear actin filaments together with lamins form the peripheral nuclear skeletal network; therefore, this observation may be related to nuclear DNA deformation or shrinkage as described above (**Figure 4B**) and may affect transcriptional network of TFEB.

AF Induces Pro-inflammatory Pyroptotic Cell Death in ARPE-19 Cells

To examine further that AF causes ARPE-19 cells death, we used the release of cytosolic LDH to the culture media upon plasma membrane leakage. We did not observe ARPE-19 cell death at 4 h although mitochondrial dysregulation occurs as demonstrated above. However, as shown in **Figures 6A**, **7A** AF increases LDH release at 24 h indicating ARPE-19 demise, which is significantly reduced by 2 h pre-incubation of a combination of SS31 + Amlexanox + Tranilast before auranofin. However, the AF-mediated LDH release is not prevented by ferrostatin 1, an inhibition of ferroptosis (Settembre and Medina, 2015), while NAC prevents cell death indicating oxidative stress mechanisms (**Figure 7B**). Ferroptosis is a newly identified cell death mechanism due to iron-accumulation and lipid peroxidation and inactivation of glutathione peroxidase 4 (GPX4), which detoxifies membrane lipid peroxidation (Yoshida et al., 2019). Similarly, necrostatin 1, an inhibitor of necroptosis (Forcina and Dixon, 2019), has no effect on AF-mediated ARPE-19 death (**Figure 7C**). On the other hand, inhibition of NLRP3 inflammasome and caspase-1 together (MCC950 and Ac-YVAD-cmk, respectively) reduces AF-mediated LDH leakage significantly in ARPE-19 (**Figure 7D**), indicating an inflammatory cell death mediated by caspase-1 known as pyroptosis (Hanus et al., 2016). Because mitochondria are critical for iron metabolism and its TCA cycle enzymes and ETC complexes contain iron-sulfur complexes (Pronin et al., 2019), when fluxed to lysosomes via mitophagy, there may be iron accumulation and ferroptosis. Therefore, to ensure that AF-induced ARPE-19 demise is indeed due to pyroptosis, but not by ferroptosis under the experimental conditions, we again treated ARPE-19 cells with RSL3, an inducer of ferroptosis (Lill et al., 2012). Indeed RSL3 induces LDH release in ARPE-19, which is prevented by ferrostatin 1 (**Figure 7E**), indicating that ferroptosis occurs in RPE cells. Furthermore, AF increases the level of gasdermin D (a pyroptosis marker) in ARPE-19 at 4 h significantly ($p < 0.05$ vs. control, 0 time), then returns to the basal level at 24 h (**Supplementary Figure S7**). Cytosolic gasdermin D is cleaved by activated caspase-1 and then inserts into the plasma membrane to form pores and leakage (Dubois et al., 2019). Thus, the results here suggest that AF causes cellular oxidative stress, mitochondria-lysosome dysregulation, and inflammatory pyroptotic cell death in ARPE-19.

DISCUSSION

The current study identifies that the Trx redox system is critical for RPE function and an inhibition of the Trx/TrxR thiol redox by AF leads to cellular oxidative stress, mitochondrial damage, lysosomal dysfunction, and pro-inflammatory cell death as summarized in **Figure 8**. Furthermore, we recently published that hyperglycemia-induced TXNIP upregulation in RPE cells where Trx1 and Trx2 are inhibited causes mitochondrial damage, mitophagic flux to lysosomes and lysosomal enlargement in human RPE cells under diabetic conditions (Devi et al., 2019).

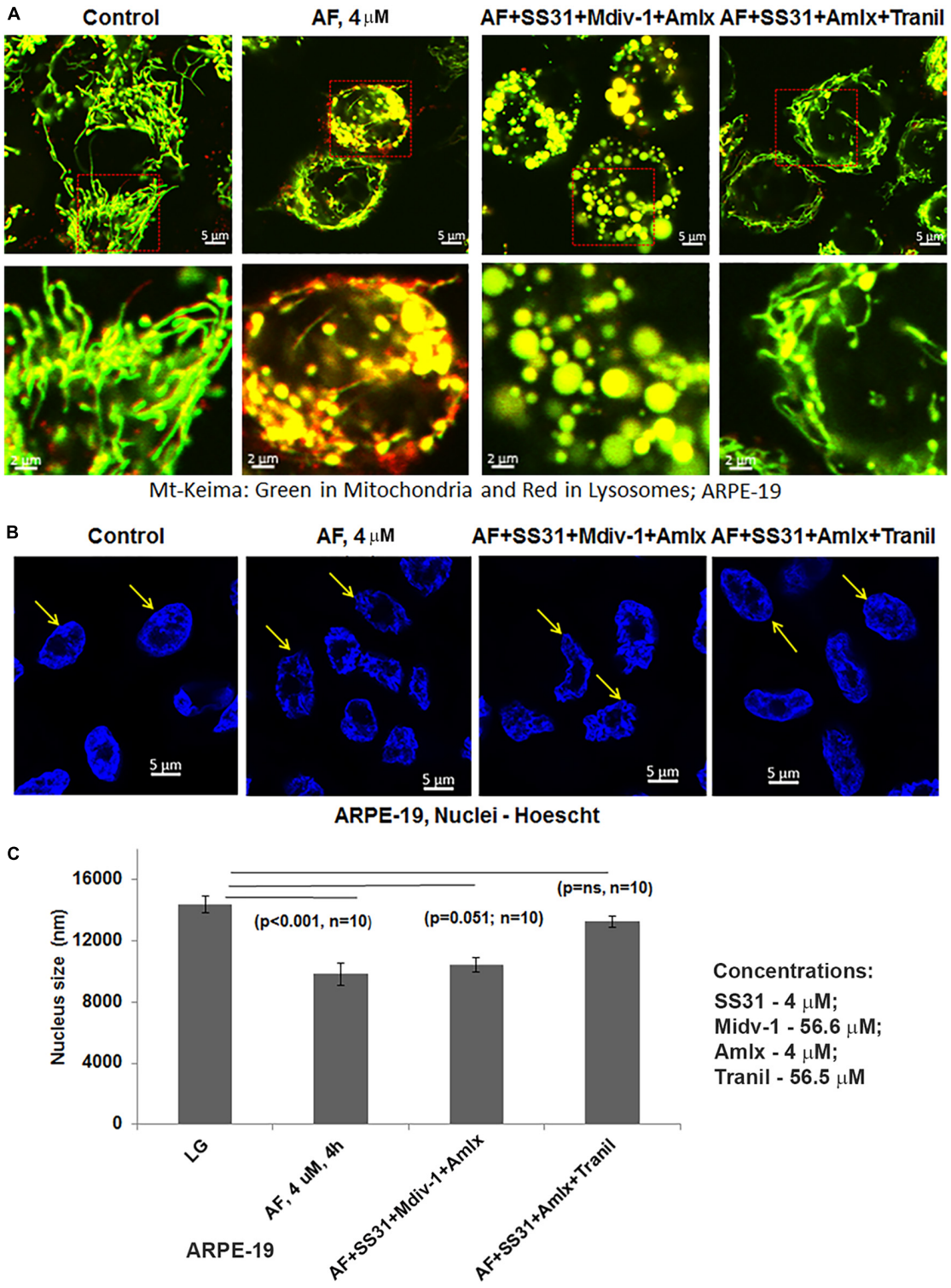

FIGURE 4 | Auranofin causes mitophagic flux and nuclear deformation in ARPE-19 cells. **(A)** AF treatment (4 μM, 4 h) increases the level of red mt-Keima in ARPE-19 cells when compared to the control where green mt-Keima is predominantly observed. Combination treatment of ARPE-19 cells with SS31 + Midiv-1 + Amlexanox (added 2 h before AF) reduces red mt-Keima; however, the treatment also results in the formation of vesiculated (round and enlarged) mitochondria. Conversely, pretreatment with SS31 + Amlexanox + Tranilast prevents AF-induced mitophagy (reduced red mt-Keima); also seen as filamentous green network. A representative of $n = 3$ is shown here at mag. 630×. **(B,C)** AF causes nuclear deformation or chromatin shrinkage as shown by DAPI staining and reduced nuclear diameter compared to the control ARPE-19 (significant decrease, $p < 0.001$ AF vs. Control; $n = 10$ nuclei). Such nuclear changes are prevented by pre-treatment with a combination of SS31 + Amlexanox + Tranilast (p = ns vs. LG, control) but not with SS31 + Midiv-1 + Amlexanox ($p = 0.051$; $n = 10$ vs. LG, control).

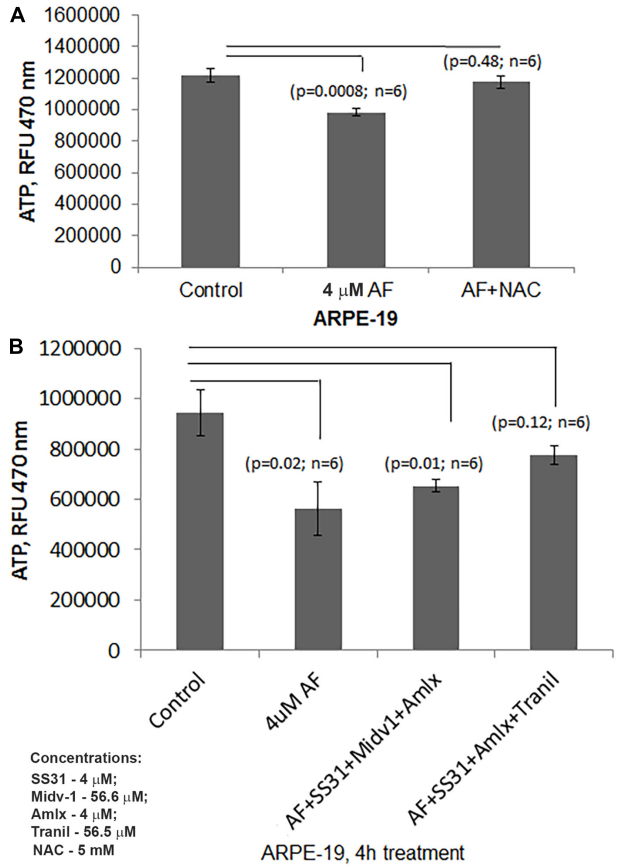

FIGURE 5 | AF reduced ATP levels are restored by combination treatment with SS31 + Amlexanox + Tranilast in ARPE-19 cells. **(A)** Here, AF (4 μM, 4 h) reduces cellular ATP levels significantly in ARPE-19 cells ($p = 0.0008$; $n = 6$), which is nullified by NAC (5 mM) suggesting a role of ROS stress. **(B)** AF mediated ATP reduction in ARPE-19 ($p = 0.02$; $n = 6$) is restored by pre-treatment with SS31 + Amlexanox + Tranilast ($p = 0.12$; $n = 6$ vs. LG, control) but not with SS31 + Midiv1 + Amlexanox ($p = 0.01$; $n = 6$ vs. LG, control).

Therefore, the AF effect on ARPE-19 observed here may also be similar to defects in TXNIP and Trx-thiol redox signaling defects in DR to an extent (Di Carlo et al., 2012; Devi et al., 2013; Stephenson et al., 2018). RPE oxidative stress and mitochondrial dysfunction are also seen in AMD and RP, serious blinding retinal neurodegenerative diseases (Kaarniranta et al., 2019; Zhou et al., 2019). RPE is a fully differentiated cell; therefore, they cannot dilute or distribute damaged mitochondria to daughter cells. Therefore, an efficient removal of the damage mitochondria by mitophagy and biosynthesis of new mitochondria (mitogenesis) to maintain number and bioenergetics is critically important. In addition, lysosomal function needs to be preserve for its POS phagocytosis and visual pigment recycling. Mitophagy is a protective and survival mechanism for cell viability (Pareek and Pallanck, 2018); however, too much of a mitophagic flux could lead to lysosomal overloading, enlargement, and reduced capacity to digest proteolipids causing accumulation of undigested lipofuscin and drusens in Bruch's membrane in AMD (Dias et al., 2018; Zhou et al., 2019). Similarly, the pathogenesis of genetic neurodegenerative diseases including RP also involves RPE mitochondrial dysfunction and photoreceptor demise. As mentioned before, photoreceptors are very active neurons, which maintain a large number of mitochondria for its bioenergetics (Shu and Dunaief, 2018; Kaarniranta et al., 2019). Therefore, not only in RPE cells, mitophagy defects, and bioenergetics failure in photoreceptors may also be involved in RP etiology. Nonetheless, the role of redox imbalance and mitophagy dysfunction in RP is yet to be fully understood.

Mitochondria are the powerhouse of the cell; therefore, their dysregulation leads to excess ROS production while ATP synthesis is blunted causing bioenergetics failure in neurodegeneration (Moreno et al., 2018). In addition, damaged mitochondria release their components into the cytosol, such as mtROS and oxidized mtDNA, which are recognized as DAMPs (damage associated molecular patterns) by the cytosolic PRRs including TLRs (Toll-like receptors) and NOD-like NLRP3 inflammasomes (Zhao et al., 2019). Indeed, we demonstrate in this study that AF increases caspase-1 activity while that of the lysosomal enzyme cathepsin L is reduced, indicating an autophagic/mitophagic flux to lysosome and its destabilization (Devi et al., 2013). Cathepsins and other lysosomal acid hydrolases are important for proper digestion of the ingested cargos and recycling (exocytosis of) the digested material as nutrients (Wilkins et al., 2017). Therefore, the removal of damaged mitochondria by mitophagy is critically important to reduce cellular ROS, inflammation and premature cell demise.

Two important cellular anti-oxidant systems are the Trxs and glutathione (Samie and Xu, 2014). The Trx/TrxR works with NADPH and peroxiredoxin 3 (Prx3) to scavenge hydrogen peroxide in mitochondria and to maintain a reduced state of cysteines in a protein (Ren et al., 2017). The GSH/GPX (particularly the mtGPX4 and cytosolic GPX4) are the sole enzymes to detoxify membrane lipid peroxidation and damage (Forred et al., 2017). Therefore, these two systems work together to maintain mitochondrial health and cellular function and, therefore, a defect in one of the two systems will lead to overburden and depletion of the anti-oxidant system in mitochondria, bioenergetics failure, and mitophagy-lysosome pathway dysregulation leading to demise (Samie and Xu, 2014). Indeed, we show in this study that AF induces caspase-1 activation and cell death by pyroptosis in APRE-19 as NLRP3 and caspase-1 inhibitors prevent AF-mediated cell death. In support, we also observed an increase in gasdermin D levels by AF. Caspase-1 cleaves a 50-kD gasdermin D to a 29-kD pore forming N-terminus fragment, which is inserted into the plasma membrane causing membrane leakage and cell death by pyroptosis (Dubois et al., 2019). Recently, a role for gasdermine E in pyroptosis was implicated (Jiang et al., 2019); therefore, we will perform further studies on the role of caspase-1 and gasdermin isoforms in pyroptosis.

Furthermore, necrostatin 1 (necroptosis inhibitor) and ferrostatin 1 (ferroptosis inhibitor) are ineffective in blocking the AF-induced cell death in ARPE-19. Mitochondrial involvement

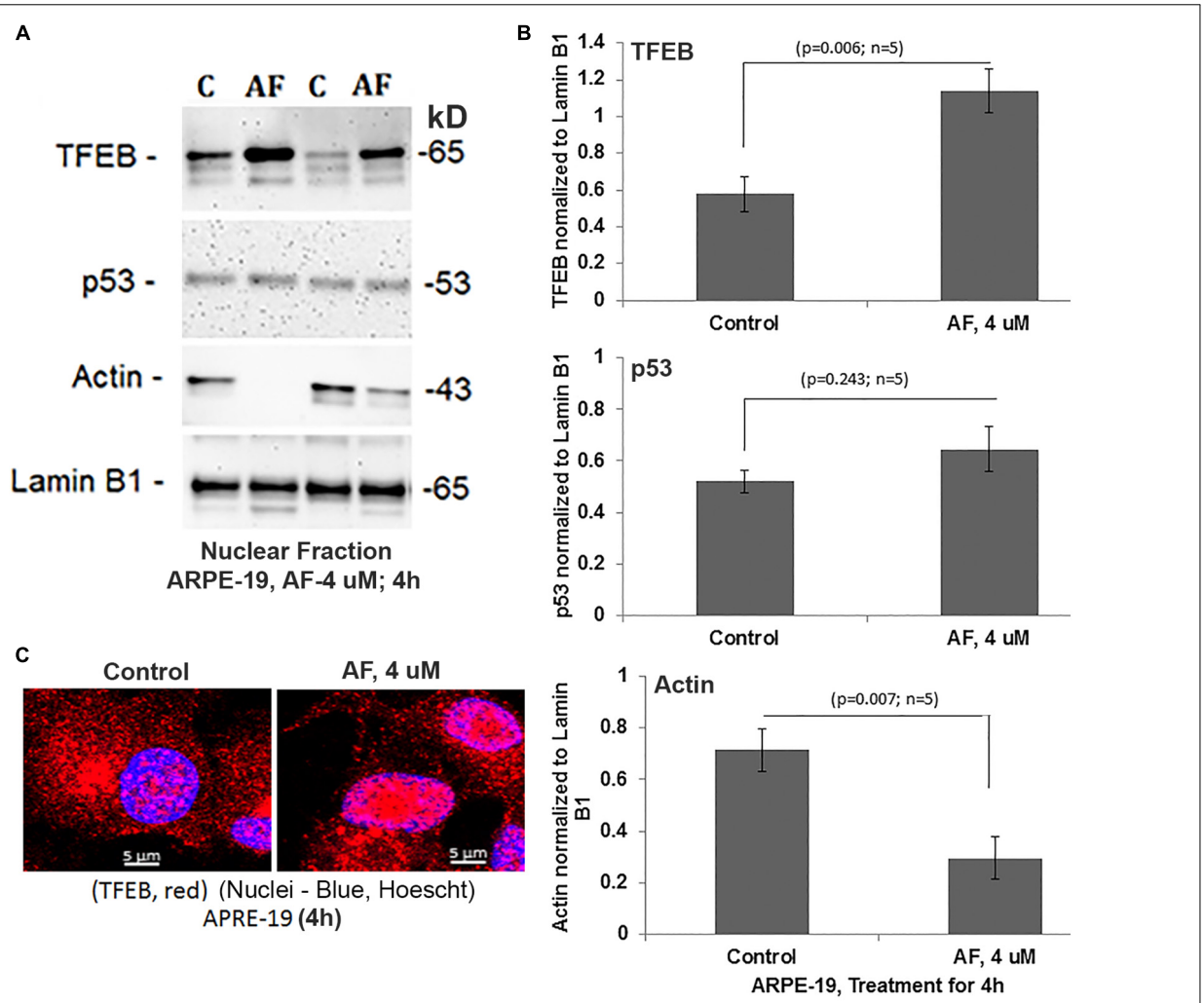

FIGURE 6 | AF increases nuclear TFEB level and reduces actin in ARPE-19. **(A,B)** AF treatment (4 μM, 4 h) of ARPE-19 induces nuclear translocation of transcription factor TFEB significantly than in controls ($p = 0.006$; $n = 5$) on Western blots while that of the p53 is unchanged ($p = 0.245$; $n = 5$). Interestingly, the level of nuclear actin is significantly reduced ($p = 0.007$; $n = 5$) than in controls. All proteins were normalized to nuclear lamin B1. **(C)** Similarly, nuclear translocation of TFEB after treatment with AF (4 μM, 4 h) is also seen when examined by confocal microscopy. A representative of $n = 3$ is shown; mag. 630×.

in this ARPE-19 death is also evident by inhibition of the mitochondrial dysfunction and cell death by a combination of SS31 (mitochondrial antioxidant), Amlexanox (inhibits TBK1 and normalize mitophagic flux) and tranilast (which inhibits NLRP3). Therefore, these three drug combinations may be useful in the treatment of mitochondria-associated neurodegenerative diseases particularly in DR as well as in AMD and PR.

One of the important factors in the mitochondrial quality control is coordinated regulation of mitophagy (removal of damaged parts of mitochondria by autophagy as mentioned earlier) and mitogenesis (synthesis of new mitochondrial and fusion with existing mitochondria) to maintain an optimal mitochondrial number and efficient bioenergetics (Maiorino et al., 2018). One transcription factor that is critical for lysosome and autophagy gene expression is TFEB (Huang et al., 2018). TFEB is also involved in the mitochondrial biogenesis via induction of PGC1α, another important transcription factor for nuclear-encoded mitochondrial gene expression (Ni et al., 2015; Pan et al., 2019). The fact that we observe TFEB translocation to the nucleus upon AF addition to ARPE-19 indicates lysosomal destabilization. Interestingly, the nuclear actin is downregulated suggesting nuclear chromatin organization may be disturbed and, therefore, transcriptional activity may be altered (Salma et al., 2015; Lammerding and Wolf, 2016). Further studies are needed to clarify this observation. TFEB is phosphorylated at multiple sites, including Ser122, Ser142, and Ser211, by mTORC1 at the lysosomal membrane and traps TEFB in the cytosol via an interaction with 14-3-3 scaffold proteins (Hatch and Hetzer, 2016). Conversely, TFEB nuclear translocation is regulated by mucolipin 1/TRPML1, a lysosomal calcium and divalent metal ion channel (Napolitano et al., 2018). Transient release of lysosomal calcium locally by TRPML1 activates calcineurin, a protein phosphatase, which dephosphorylates TFEB sites targeted by mTORC1 and releases from 14-3-3,

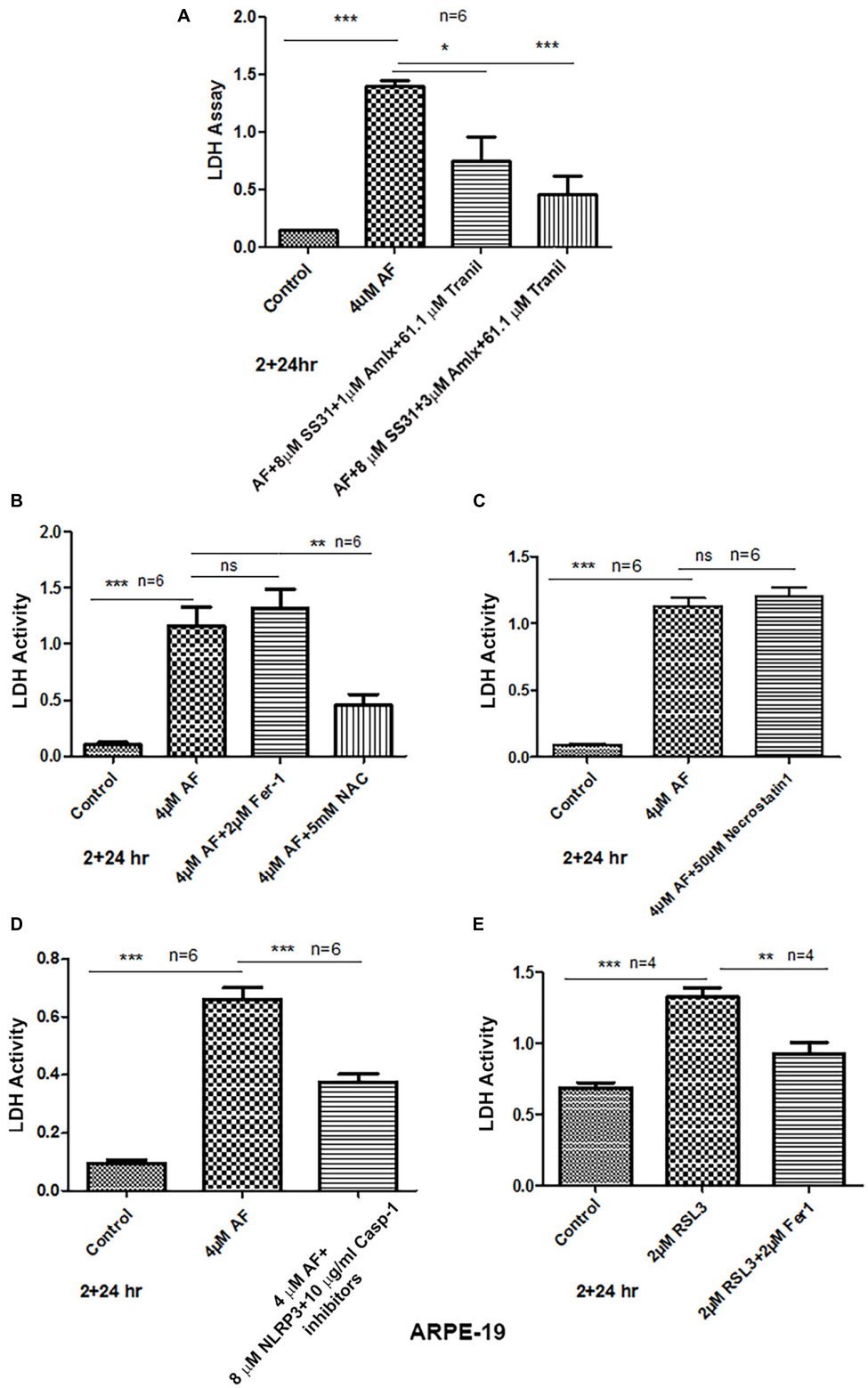

FIGURE 7 | AF induces ARPE-19 death by pyroptosis. **(A)** AF (4 μM, 24 h) treatment of ARPE-19 cells induces cell death as measured by cytosolic LDH release in the culture media. AF effect is significantly countered by addition (2 h before AF) of three drugs combination SS31 + Amlexanox + Tranilast. **(B)** AF-induced LDH release is not reduced by ferrostatin-1 (inhibitor of ferroptosis, an iron-dependent cell death) but with NAC (N-acetylcysteine), suggesting the role of anti-oxidants. **(C)** Similarly, necrostatin-1 (an inhibitor of necroptosis) was without an effect on AF-mediated LDH release. **(D)** Conversely, AF-mediated LDH release is significantly

(Continued)

FIGURE 7 | Continued
reduced by a combination of NLRP3 (MCC950, 8 μM) and caspase-1 (Ac-YVAD-cmk, 10 μg/ml) inhibitors (pyroptosis inhibitors). Symbols, *$p < 0.05$; **$p < 0.001$; ***$p < 0.0001$; $n = 6$ for all experiments. **(E)** Lastly, ferroptosis inducer RSL3 (an inhibitor GPX4) causes LDH release (ferroptotic cell death), which is significantly reduced by ferrostatin-1, further indicating that AF-mediated ARPE-19 cell death is due to inflammatory pyroptosis.

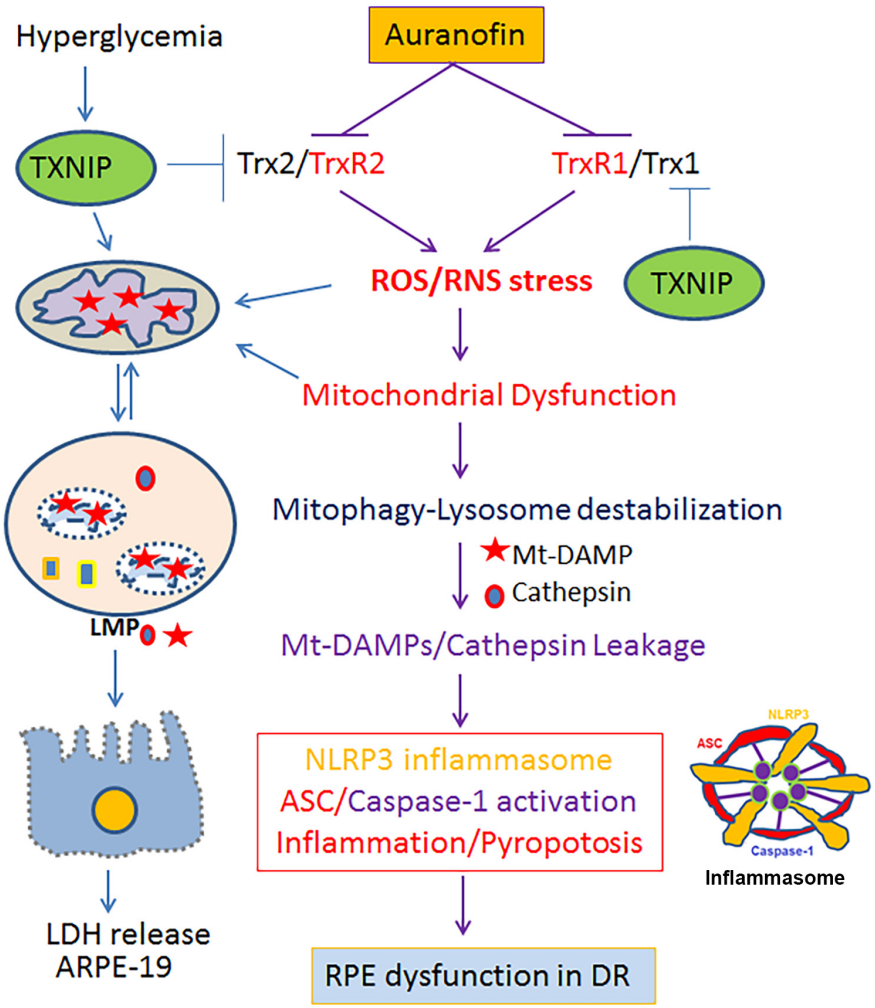

FIGURE 8 | A schematic diagram depicting a potential role for the Trx/TrxR redox pathway in oxidative stress and mitochondria-lysosome axis dysfunction in RPE. Inhibition of the Trx/TrxR pathway either by auranofin on TrxR or by TXNIP on Trx under hyperglycemia (Devi et al., 2019) may lead to cellular oxidative stress, mitochondrial dysfunction, altered mitophagic flux, lysosomal damage and pro-inflammatory cell death in DR as well as in other chronic retinal neurodegenerative diseases such as AMD and RP. A combination therapy strengthening the Trx/TrxR redox system and normalizing the mitochondrial-lysosomal axis may be a potential therapeutic approach to prevent progression of various neurodegenerative diseases.

thereby translocating to the nucleus (Napolitano et al., 2018). Nonetheless, TRPML1 is also regulated by PI3,5 bisphosphate in the lysosomal membrane, which is synthesized by PIKFYVE kinase (Di Paola and Medina, 2019). Therefore, these kinases and phosphatases may also involve in the regulation of lysosomal function, autophagy/mitophagy flux, exocytosis, and mitochondrial biogenesis. Indeed, we observe that apilimod (Medina et al., 2015), an inhibitor of PIKFYVE, causes lysosomal enlargement and cathepsin L downregulation, while ML-SA1 (Medina et al., 2015), an activator of TRPML1, causes lysosome biogenesis and increase cathepsin L level (unpublished data). To what extent the Trx-TrxR and redox signaling regulates these kinases and phosphatases are yet to be determined in RPE and retinal neurodegenerative diseases. Nonetheless, most chronic neurodegenerative diseases involve dysregulation of mitochondrial function and lysosomal defects leading to bioenergetics failure and accumulation of undigested materials inside cells as well as extracellularly, particularly for RPE cells because they are involved in the degradation of melanosomes and phagocytosis of photoreceptor outer segments (POS) daily (Isobe et al., 2019). Thus, an accumulation of undigested oxidized lipoproteins with lysosomes will reduce lysosomal

enzyme activities and enhance exocytosis of undigested material to the Bruch's membrane (a combined basement membrane of the RPE and endothelium of the choriocapillaris), which form Drusens, yellow deposits under the retina (Isobe et al., 2019). Such an event may cause RPE dysregulation and photoreceptor dysfunction in chronic retinal neurodegenerative diseases.

CONCLUSION

The present findings suggest that the Trx/TrxR redox system is critical for reducing oxidative stress, normalizing mitophagic flux, lysosome function, and prevention of pyroptotic cell death in the RPE, and therefore, in preventing retinal neurodegenerative diseases. Furthermore, the effectiveness of the therapy with three drug combinations targeting the mitochondrial ROS, mitophagic flux and NLRP3 inflammasome (SS31 + Amlexanox + Tranilast, respectively) needs to be tested in retinal neurodegenerative diseases of animal models particularly in DR. This three drugs combination may also be beneficial in the treatment and prevention of retinal neurodegenerative diseases such as AMD and RP as they also encounter mitochondrial and lysosomal dysregulation in the etiology of the diseases (Warburton et al., 2007; Bergen et al., 2019). The present study was presented as a poster at the annual meeting of the ARVO April 28, 2019 – May 02, 2019 at Vancouver, Canada.

DATA AVAILABILITY STATEMENT

All materials and data developed in this study will be made available upon request.

AUTHOR CONTRIBUTIONS

TY performed the cell assays, developed the methodologies, and wrote the Materials and Methods section and reviewed the manuscript. TD performed the Western blotting and immunohistochemistry. LS developed the concept, provided the guidance, and wrote the manuscript.

FUNDING

This work was supported by the grants EY023992 (LS), Research to Prevent Blindness (RPB to OVAS), and Core Grant P30 EY004068 (OVAS).

SUPPLEMENTARY MATERIAL

The Supplementary Material for this article can be found online at: https://www.frontiersin.org/articles/10.3389/fnins.2019.01065/full#supplementary-material

REFERENCES

Bapputty, R., Talahalli, R., Zarini, S., Samuels, I., Murphy, R., and Gubitosi-Klug, R. (2019). Montelukast prevents early diabetic retinopathy in mice. *Diabetes* 68, 2004–2015. doi: 10.2337/db19-0026

Bergen, A. A., Arya, S., Koster, C., Pilgrim, M. G., Wiatrek-Moumoulidis, D., van der Spek, P. J., et al. (2019). On the origin of proteins in human drusen: the meet, greet and stick hypothesis. *Prog. Retin. Eye Res.* 70, 55–84. doi: 10.1016/j.preteyeres.2018.12.003

Biesemeier, A., Yoeruek, E., Eibl, O., and Schraermeyer, U. (2015). Iron accumulation in Bruch's membrane and melanosomes of donor eyes with age-related macular degeneration. *Exp. Eye Res.* 137, 39–49. doi: 10.1016/j.exer.2015.05.019

Booty, L. M., Gawel, J. M., Cvetko, F., Caldwell, S. T., Hall, A. R., Mulvey, J. F., et al. (2019). Selective disruption of mitochondrial thiol redox state in cells and in vivo. *Cell Chem. Biol.* 26, 449–461. doi: 10.1016/j.chembiol.2018.12.002

Campbell, M. I, and Humphries, P. (2012). The blood-retina barrier: tight junctions and barrier modulation. *Adv. Exp. Med. Biol.* 763, 70–84. doi: 10.1007/978-1-4614-4711-5_3

Campbell, M. D., Duan, J., Samuelson, A. T., Gaffrey, M. J., Merrihew, G. E., Egertson, J. D., et al. (2019). Improving mitochondrial function with SS-31 reverses age-related redox stress and improves exercise tolerance in aged mice. *Free Radic. Biol. Med.* 134, 268–281. doi: 10.1016/j.freeradbiomed.2018.12.031

Caspard, H., Jabbour, S., Hammar, N., Fenici, P., Sheehan, J. J., and Kosiborod, M. (2018). Recent trends in the prevalence of type 2 diabetes and the association with abdominal obesity lead to growing health disparities in the USA: an analysis of the NHANES surveys from 1999 to 2014. *Diabetes Obes. Metab.* 20, 667–671. doi: 10.1111/dom.13143

Cheloni, R., Gandolfi, S. A., Signorelli, C., and Odone, A. (2019). Global prevalence of diabetic retinopathy: protocol for a systematic review and meta-analysis. *BMJ Open* 9:e022188. doi: 10.1136/bmjopen-2018-022188

Chiquita, S., Rodrigues-Neves, A. C., Baptista, F. I., Carecho, R., Moreira, P. I., Castelo-Branco, M., et al. (2019). The retina as a window or mirror of the brain changes detected in Alzheimer's disease: critical aspects to unravel. *Mol. Neurobiol.* 56, 5416–5435. doi: 10.1007/s12035-018-1461-6

Country, M. W. (2017). Retinal metabolism: a comparative look at energetics in the retina. *Brain Res.* 1672, 50–57. doi: 10.1016/j.brainres.2017.07.025

Cunha-Vaz, J., Bernardes, R., and Lobo, C. (2011). Blood-retinal barrier. *Eur. J. Ophthalmol.* 21(Suppl. 6), S3–S9. doi: 10.5301/EJO.2010.6049

Devi, T. S., Hosoya, K., Terasaki, T., and Singh, L. P. (2013). Critical role of TXNIP in oxidative stress, DNA damage and retinal pericyte apoptosis under high glucose: implications for diabetic retinopathy. *Exp. Cell Res.* 319, 1001–1012. doi: 10.1016/j.yexcr.2013.01.012

Devi, T. S., Lee, I., Hüttemann, M., Kumar, A., Nantwi, K. D., and Singh, L. P. (2012). TXNIP links innate host defense mechanisms to oxidative stress and inflammation in retinal müller glia under chronic hyperglycemia: implications for diabetic retinopathy. *Exp Diabetes Res.* 2012:438238.

Devi, T. S., Somayajulu, M., Kowluru, R. A., and Singh, L. P. (2017). TXNIP regulates mitophagy in retinal Müller cells under high-glucose conditions: implications for diabetic retinopathy. *Cell Death Dis.* 8:e2777. doi: 10.1038/cddis.2017.190

Devi, T. S., Yumnamcha, T., Yao, F., Somayajulu, M., Kowluru, R. A., and Singh, L. P. (2019). TXNIP mediates high glucose-induced mitophagic flux and lysosome enlargement in human retinal pigment epithelial cells. *Biol Open* 8:bio038521. doi: 10.1242/bio.038521

Di Carlo, M I, Giacomazza, D., Picone, P., Nuzzo, D., and San, Biagio PL (2012). Are oxidative stress and mitochondrial dysfunction the key players in the neurodegenerative diseases? *Free Radic. Res.* 46, 1327–1338. doi: 10.3109/10715762.2012.714466

Di Paola, S., and Medina, D. L. (2019). TRPML1-/TFEB-dependent regulation of lysosomal exocytosis. *Methods Mol. Biol.* 1925, 143–144. doi: 10.1007/978-1-4939-9018-4_12

Dias, M. F., Joo, K., Kemp, J. A., Fialho, S. L., da Silva Cunha, A. Jr., Woo, S. J., et al. (2018). Molecular genetics and emerging therapies for retinitis pigmentosa: basic research and clinical perspectives. *Prog. Retin. Eye Res.* 63, 107–131. doi: 10.1016/j.preteyeres.2017.10.004

Dubois, H., Sorgeloos, F., Sarvestani, S. T., Martens, L., Saeys, Y., Mackenzie, J. M., et al. (2019). Nlrp3 inflammasome activation and gasdermin D-driven pyroptosis are immunopathogenic upon gastrointestinal norovirus infection. *PLoS Pathog* 15:e1007709. doi: 10.1371/journal.ppat.1007709

Fivenson, E. M., Lautrup, S., Sun, N., Scheibye-Knudsen, M., Stevnsner, T., Nilsen, H., et al. (2017). Mitophagy in neurodegeneration and aging. *Neurochem. Int.* 109, 202–209. doi: 10.1016/j.neuint.2017.02.007

Forcina, G. C., and Dixon, S. J. (2019). GPX4 at the crossroads of lipid homeostasis and ferroptosis. *Proteomics* 19:e1800311. doi: 10.1002/pmic.201800311

Forred, B. J., Daugaard, D. R., Titus, B. K., Wood, R. R., Floen, M. J., Booze, M. L., et al. (2017). Detoxification of mitochondrial oxidants and apoptotic signaling are facilitated by thioredoxin-2 and peroxiredoxin-3 during hyperoxic injury. *PLoS One* 12:e0168777. doi: 10.1371/journal.pone.0168777

Fu, Z., Löfqvist, C. A., Liegl, R., Wang, Z., Sun, Y., Gong, Y., et al. (2018). Photoreceptor glucose metabolism determines normal retinal vascular growth. *EMBO Mol. Med.* 10, 76–90. doi: 10.15252/emmm.201707966

Graham, P. S., Kaidonis, G., Abhary, S., Gillies, M. C., Daniell, M., Essex, R. W., et al. (2018). Genome-wide association studies for diabetic macular edema and proliferative diabetic retinopathy. *BMC Med. Genet.* 19:71. doi: 10.1186/s12881-018-0587-8

Handa, J. T., Bowes Rickman, C., Dick, A. D., Gorin, M. B., Miller, J. W., Toth, C. A., et al. (2019). A systems biology approach towards understanding and treating non-neovascular age-related macular degeneration. *Nat. Commun.* 10:3347. doi: 10.1038/s41467-019-11262-1

Hanus, J., Anderson, C., Sarraf, D., Ma, J., and Wang, S. (2016). Retinal pigment epithelial cell necroptosis in response to sodium iodate. *Cell Death Discov.* 2:16054. doi: 10.1038/cddiscovery.2016.54

Harper, M. T. (2019). Auranofin, a thioredoxin reductase inhibitor, causes platelet death through calcium overload. *Platelets* 30, 98–104. doi: 10.1080/09537104.2017.1378809

Hatch, E. M., and Hetzer, M. W. (2016). Nuclear envelope rupture is induced by actin-based nucleus confinement. *J. Cell Biol.* 215, 27–36. doi: 10.1083/jcb.201603053

Huang, Y., Jiang, H., Chen, Y., Wang, X., Yang, Y., Tao, J., et al. (2018). Tranilast directly targets NLRP3 to treat inflammasome-driven diseases. *EMBO Mol. Med.* 10:e8689. doi: 10.15252/emmm.201708689

Isobe, Y., Nigorikawa, K., Tsurumi, G., Takemasu, S., Takasuga, S., Kofuji, S., et al. (2019). PIKfyve accelerates phagosome acidification through activation of TRPML1 while arrests aberrant vacuolation independent of the Ca^{2+} channel. *J. Biochem.* 165, 75–84. doi: 10.1093/jb/mvy084

Ivanova, E., Alam, N. M., Prusky, G. T., and Sagdullaev, B. T. (2019). Blood-retina barrier failure and vision loss in neuron-specific degeneration. *JCI Insight* 5:126747. doi: 10.1172/jci.insight.126747

Jiang, S., Gu, H., Zhao, Y., and Sun, L. (2019). Teleost gasdermin E Is cleaved by caspase 1, 3, and 7 and induces pyroptosis. *J. Immunol.* 203, 1369–1382. doi: 10.4049/jimmunol.1900383

Jun, S., Datta, S., Wang, L., Pegany, R., Cano, M., and Handa, J. T. (2019). The impact of lipids, lipid oxidation, and inflammation on AMD, and the potential role of miRNAs on lipid metabolism in the RPE. *Exp. Eye Res.* 181, 346–355. doi: 10.1016/j.exer.2018.09.023

Kaarniranta, K., Pawlowska, E., Szczepanska, J., Jablkowska, A., and Blasiak, J. (2019). Role of mitochondrial DNA damage in ROS-mediated pathogenesis of age-related macular degeneration (AMD). *Int. J. Mol. Sci.* 20:E2374. doi: 10.3390/ijms20102374

Lammerding, J., and Wolf, K. (2016). Nuclear envelope rupture: actin fibers are putting the squeeze on the nucleus. *J. Cell Biol.* 215, 5–8. doi: 10.1083/jcb.201609102

Lill, R., Hoffmann, B., Molik, S., Pierik, A. J., Rietzschel, N., Stehling, O., et al. (2012). The role of mitochondria in cellular iron-sulfur protein biogenesis and iron metabolism. *Biochim. Biophys. Acta* 1823, 1491–1508. doi: 10.1016/j.bbamcr.2012.05.009

Lin, M. T., and Beal, M. F. (2006). Mitochondrial dysfunction and oxidative stress in neurodegenerative diseases. *Nature* 443, 787–795. doi: 10.1038/nature05292

Liu, H., Tang, J., Du, Y., Saadane, A., Samuels, I., Veenstra, A., et al. (2019). Transducin1, phototransduction and the development of early diabetic retinopathy. *Invest. Ophthalmol. Vis. Sci.* 60, 1538–1546. doi: 10.1167/iovs.18-26433

Maiorino, M., Conrad, M., and Ursini, F. (2018). GPx4, lipid peroxidation, and cell death: discoveries, rediscoveries, and open issues. *Antioxid. Redox. Signal.* 29, 61–74. doi: 10.1089/ars.2017.7115

Manczak, M., Kandimalla, R., Yin, X., and Reddy, P. H. (2019). Mitochondrial division inhibitor 1 reduces dynamin-related protein 1 and mitochondrial fission activity. *Hum. Mol. Genet.* 28, 177–199. doi: 10.1093/hmg/ddy335

Medina, D. L., Di Paola, S., Peluso, I., Armani, A., De Stefani, D., Venditti, R., et al. (2015). Lysosomal calcium signalling regulates autophagy through calcineurin and TFEB. *Nat. Cell Biol.* 17, 288–299. doi: 10.1038/ncb3114

Moreno, M. L., Mérida, S., Bosch-Morell, F., Miranda, M., and Villar, V. M. (2018). Autophagy dysfunction and oxidative stress, two related mechanisms implicated in retinitis pigmentosa. *Front. Physiol.* 9:1008. doi: 10.3389/fphys.2018.01008

Napolitano, G., Esposito, A., Choi, H., Matarese, M., Benedetti, V., Di Malta, C., et al. (2018). mTOR-dependent phosphorylation controls TFEB nuclear export. *Nat. Commun.* 9:3312. doi: 10.1038/s41467-018-05862-6

Ni, H. M., Williams, J. A., and Ding, W. X. (2015). Mitochondrial dynamics and mitochondrial quality control. *Redox. Biol.* 2015, 6–13. doi: 10.1016/j.redox.2014.11.006

Oral, E. A., Reilly, S. M., Gomez, A. V., Meral, R., Butz, L., Ajluni, N., et al. (2017). Inhibition of IKKε and TBK1 improves glucose control in a subset of patients with type 2 diabetes. *Cell Metab.* 26, 157.e7–170.e7. doi: 10.1016/j.cmet.2017.06.006

Pan, H. Y., Alamri, A. H., and Valapala, M. (2019). Nutrient deprivation and lysosomal stress induce activation of TFEB in retinal pigment epithelial cells. *Cell Mol. Biol. Lett.* 24:33. doi: 10.1186/s11658-019-0159-8

Pareek, G., and Pallanck, L. J. (2018). Inactivation of lon protease reveals a link between mitochondrial unfolded protein stress and mitochondrial translation inhibition. *Cell Death Dis.* 9:1168. doi: 10.1038/s41419-018-1213-6

Perrone, L., Devi, T. S., Hosoya, K. I., Terasaki, T., and Singh, L. P. (2010). Inhibition of TXNIP expression in vivo blocks early pathologies of diabetic retinopathy. *Cell Death Dis.* 1:E65. doi: 10.1038/cddis.2010.42

Pronin, A., Pham, D., An, W., Dvoriantchikova, G., Reshetnikova, G., Qiao, J., et al. (2019). Inflammasome activation induces pyroptosis in the retina exposed to ocular hypertension injury. *Front. Mol. Neurosci.* 12:3. doi: 10.3389/fnmol.2019.00036

Ren, X., Zou, L., Zhang, X., Branco, V., Wang, J., Carvalho, C., et al. (2017). Redox signaling mediated by thioredoxin and glutathione systems in the central nervous system. *Antioxid. Redox. Signal.* 27, 989–1010. doi: 10.1089/ars.2016.6925

Salma, N., Song, J. S., Arany, Z., and Fisher, D. E. (2015). Transcription factor Tfe3 directly regulates Pgc-1alpha in muscle. *J. Cell. Physiol.* 230, 2330–2336. doi: 10.1002/jcp.24978

Samie, M. A., and Xu, H. (2014). Lysosomal exocytosis and lipid storage disorders. *J. Lipid Res.* 55, 995–1009. doi: 10.1194/jlr.R046896

Settembre, C., and Medina, D. L. (2015). TFEB and the CLEAR network. *Methods Cell Biol.* 126, 45–62. doi: 10.1016/bs.mcb.2014.11.011

Shu, W., and Dunaief, J. L. (2018). Potential treatment of retinal diseases with iron chelators. *Pharmaceuticals* 11:E112. doi: 10.3390/ph11040112

Singh, L. P., and Perrone, L. (2013). Thioredoxin interacting protein (TXNIP) and pathogenesis of diabetic retinopathy. *J. Clin. Exp. Ophthalmol.* 4:287.

Spencer, W. J., Ding, J. D., Lewis, T. R., Yu, C., Phan, S., Pearring, J. N., et al. (2019). PRCD is essential for high-fidelity photoreceptor disc formation. *Proc. Natl. Acad. Sci. U.S.A.* 116, 13087–13096. doi: 10.1073/pnas.1906421116

Stephenson, J., Nutma, E., van der Valk, P., and Amor, S. (2018). Inflammation in CNS neurodegenerative diseases. *Immunology* 154, 204–219. doi: 10.1111/imm.12922

Tarchick, M. J., Cutler, A. H., Trobenter, T. D., Kozlowski, M. R., Makowski, E. R., Holoman, N., et al. (2019). Endogenous insulin signaling in the RPE contributes to the maintenance of rod photoreceptor function in diabetes. *Exp. Eye Res.* 180, 63–74. doi: 10.1016/j.exer.2018.11.020

Warburton, S., Davis, W. E., Southwick, K., Xin, H., Woolley, A. T., Burton, G. F., et al. (2007). Proteomic and phototoxic characterization of melanolipofuscin: correlation to disease and model for its origin. *Mol. Vis.* 13, 318–329.

Wilkins, H. M., Weidling, I. W., Ji, Y., and Swerdlow, R. H. (2017). Mitochondria-derived damage-associated molecular patterns in neurodegeneration. *Front. Immunol.* 8:508. doi: 10.3389/fimmu.2017.00508

Xia, T., and Rizzolo, L. J. (2017). Effects of diabetic retinopathy on the barrier functions of the retinal pigment epithelium. *Vis. Res.* 139, 72–81. doi: 10.1016/j.visres.2017.02.006

Yoshida, M., Minagawa, S., Araya, J., Sakamoto, T., Hara, H., Tsubouchi, K., et al. (2019). Involvement of cigarette smoke-induced epithelial cell ferroptosis in COPD pathogenesis. *Nat. Commun.* 10:3145. doi: 10.1038/s41467-019-10991-7

Yoshihara, E., Masaki, S., Matsuo, Y., Chen, Z., Tian, H., and Yodoi, J. (2014). Thioredoxin/Txnip: redoxisome, as a redox switch for the pathogenesis of diseases. *Front. Immunol.* 4:514. doi: 10.3389/fimmu.2013.00514

Zhao, Y., Sun, X., Hu, D., Prosdocimo, D. A., Hoppel, C., Jain, M. K., et al. (2019). ATAD3A oligomerization causes neurodegeneration by coupling mitochondrial fragmentation and bioenergetics defects. *Nat. Commun.* 10:1371. doi: 10.1038/s41467-019-09291-x

Zhou, B. I, Liu, J. II, Kang, R. III, Klionsky, D. J. IV, Kroemer, G. V, and Tang, D. VI (2019). Ferroptosis is a type of autophagy-dependent cell death. *Semin. Cancer Biol.* . doi: 10.1016/j.semcancer.2019.03.002 [Epub ahead of print].

Conflict of Interest: The authors declare that the research was conducted in the absence of any commercial or financial relationships that could be construed as a potential conflict of interest.

frontiers in Neuroscience

ORIGINAL RESEARCH
published: 15 October 2019
doi: 10.3389/fnins.2019.01096

Systemic and Intravitreal Antagonism of the TNFR1 Signaling Pathway Delays Axotomy-Induced Retinal Ganglion Cell Loss

Fernando Lucas-Ruiz[1,2], *Caridad Galindo-Romero*[1,2†], *Manuel Salinas-Navarro*[1,2†], *María Josefa González-Riquelme*[1,2], *Manuel Vidal-Sanz*[1,2] *and Marta Agudo Barriuso*[1,2*]

[1] Grupo de Oftalmología Experimental, Instituto Murciano de Investigación Biosanitaria Virgen de la Arrixaca (IMIB-Arrixaca), Murcia, Spain, [2] Departamento de Oftalmología, Facultad de Medicina, Universidad de Murcia, Murcia, Spain

Here, we have blocked the signaling pathway of tumor necrosis factor α (TNFα) in a mouse model of traumatic neuropathy using a small cell permeable molecule (R7050) that inhibits TNFα/TNF receptor 1 (TNFR1) complex internalization. Adult pigmented mice were subjected to intraorbital optic nerve crush (ONC). Animals received daily intraperitoneal injections of R7050, and/or a single intravitreal administration the day of the surgery. Some animals received a combinatorial treatment with R7050 (systemic or local) and a single intravitreal injection of brain derived neurotrophic factor (BDNF). As controls, untreated animals were used. Retinas were analyzed for RGC survival 5 and 14 days after the lesion i.e., during the quick and slow phase of axotomy-induced RGC death. qPCR analyses were done to verify that *Tnfr1* and *TNFα* were up-regulated after ONC. At 5 days post-lesion, R7050 intravitreal or systemic treatment neuroprotected RGCs as much as BDNF alone. At 14 days, RGC rescue by systemic or intravitreal administration of R7050 was similar. At this time point, intravitreal treatment with BDNF was significantly better than intravitreal R7050. Combinatory treatment was not better than BDNF alone, although at both time points, the mean number of surviving RGCs was higher. In conclusion, antagonism of the extrinsic pathway of apoptosis rescues axotomized RGCs as it does the activation of survival pathways by BDNF. However, manipulation of both pathways at the same time, does not improve RGC survival.

Keywords: optic nerve crush, retinal ganglion cells, R7050, BDNF, combinatory therapy, neuroprotection

OPEN ACCESS

Edited by:
Mohammad Shamsul Ola,
King Saud University, Saudi Arabia

Reviewed by:
Yang Hu,
Stanford University, United States
Michael B. Powner,
City University of London,
United Kingdom

***Correspondence:**
Marta Agudo Barriuso
martabar@um.es

†*Joint second authors*

Specialty section:
This article was submitted to Neurodegeneration, a section of the journal Frontiers in Neuroscience

Received: *29 July 2019*
Accepted: *30 September 2019*
Published: *15 October 2019*

Citation:
Lucas-Ruiz F, Galindo-Romero C, Salinas-Navarro M, González-Riquelme MJ, Vidal-Sanz M and Agudo Barriuso M (2019) Systemic and Intravitreal Antagonism of the TNFR1 Signaling Pathway Delays Axotomy-Induced Retinal Ganglion Cell Loss. Front. Neurosci. 13:1096. doi: 10.3389/fnins.2019.01096

INTRODUCTION

The link between tumor necrosis factor-α (TNFα) and retinal ganglion cell (RGC) loss in glaucoma and traumatic optic neuropathies has been extensively investigated in humans (Yuan and Neufeld, 2000; Tezel et al., 2001) and animal models (Agudo et al., 2008; Tezel, 2008; Roh et al., 2012; Cueva Vargas et al., 2015; Tse et al., 2018; Wei et al., 2019).

TNFα is a multi-functional cytokine that promotes inflammation and mediates cell death through the binding to TNF receptor 1 (TNFR1), a death receptor that triggers the extrinsic pathway of apoptosis (Lorz and Mehmet, 2009; Cabal-Hierro and Lazo, 2012; Sedger and McDermott, 2014). In the retina, TNFα is expressed by microglial cells (Yuan and Neufeld, 2000; Roh et al., 2012), and TNFR1 by RGCs (Tezel et al., 2001; Agudo et al., 2008).

TNFα induced cell death does not occur in healthy cells, but in stressed or metabolically imbalanced ones (reviewed in Sedger and McDermott, 2014). Thus, TNFα/TNFR1 signaling depends on the cellular context and can lead to proliferation, apoptosis, or necroptosis. TNFα binding to TNFR1 causes the formation of two multiprotein complexes. Complex I prevents apoptosis, while complex II induces cell death. Complex I is membrane bound, and complex II is activated after being endocytosed and released from the cytoplasmic membrane (reviewed in Cabal-Hierro and Lazo, 2012).

In pre-clinical models of ocular hypertension, the main risk factor of glaucoma, or of traumatic optic nerve injury (optic nerve crush or transection) both, the blockade of TNFα using decoy-receptors (Roh et al., 2012; Tse et al., 2018) or natural anti-TNFα compounds (Kyung et al., 2015), and the deletion of TNFR1 (Tezel et al., 2004) have neuroprotective properties on the injured RGCs.

Anti-TNFα therapies based on decoy-receptors or anti-TNF antibodies have some intrinsic problems such as availability, potential antigenicity, and tissue distribution.

R7050 is a small cell permeable triazoloquinoxaline that blocks TNFα signaling through the inhibition of the ligand-induced TNFR1 endocytosis (Gururaja et al., 2007), impairing the association of TNFR1 with the intracellular adaptor molecules that form the multi-protein complexes. Thus, R7050 is a selective antagonist of the TNFα/TNFR1 pathway. Importantly, R7050 crosses the blood brain barrier and it has been shown that attenuates neurovascular injury and improves neurological behavior in an animal model of intra-cerebral hemorrhage (King et al., 2013).

Here we have tested the neuroprotective potential of R7050 on axotomized RGCs. Because single therapies are not sufficient to stop RGC degeneration (Harvey, 2007) we assayed the TNFR1 antagonist alone or in combination with brain derived neurotrophic factor (BDNF), to date the best administered neuroprotectant for injured RGCs (Mansour-Robaey et al., 1994; Peinado-Ramon et al., 1996; Di Polo et al., 1998; Pernet and Di, 2006; Parrilla-Reverter et al., 2009; Sanchez-Migallon et al., 2011, 2016; Galindo-Romero et al., 2013b; Valiente-Soriano et al., 2015; Feng et al., 2016, 2017; Osborne et al., 2018). BDNF activates survival pathways [PI_3K/Akt and ERK; (Isenmann et al., 1998; Klocker et al., 2000; Nakazawa et al., 2002)] and TNFR1 antagonism inhibits apoptosis. Thus, the combinatory treatment directed to increase pro-survival pathways and to decrease apoptotic ones would, ideally, have a synergistic effect.

We have used the well-characterized model of optic nerve crush (ONC) in mice (Galindo-Romero et al., 2011, 2013b; Sanchez-Migallon et al., 2016, 2018). The course of RGC death induced by ONC in mice occurs in two phases, a quick one that lasts 7–9 days during which ∼85% of RGCs die, and a second slower one thereafter. In this model, 50% of RGCs are lost at day 5 post-lesion (reviewed in Vidal-Sanz et al., 2017). Here we have administered R7050 intravitreally and/or intraperitoneally, and BDNF intravitreally, and analyzed RGC survival at 5 or 14 days post-ONC, i.e., during the quick and the slow phase of death.

MATERIALS AND METHODS

Animal Handling

Adult pigmented C57Bl/6 male mice (25 g) were obtained from the University of Murcia breeding colony. All animals were treated in compliance with the European Union guidelines for Animal Care and Use for Scientific Purpose (Directive 2010/63/EU) and the guidelines from the Association for Research in Vision and Ophthalmology (ARVO) Statement for the Use of Animals in Ophthalmic and Vision Research. All procedures were approved by the Ethical and Animal Studies Committee of the University of Murcia, Spain (number: A1320140704).

Animals undergoing surgery were anesthetized by intraperitoneal injection of a mixture of ketamine (60 mg/kg; ketolar, Pfizer, Alcobendas, Madrid, Spain) and xylazine (10 mg/kg; Rompum, Bayer, Kiel, Germany). Analgesia was provided by subcutaneous administration of buprenorphine (0.1 mg/kg; Buprex, Buprenorphine 0.3 mg/mL; Schering-Plow, Madrid, Spain). During and after surgery, the eyes were covered with an ointment (Tobrex; Alcon S.A., Barcelona, Spain) to prevent corneal desiccation. Animals were sacrificed with an intraperitoneal injection of an overdose of sodium pentobarbital (Dolethal, Vetoquinol; Especialidades Veterinarias, S.A., Alcobendas, Madrid, Spain).

Animal Groups

Animal groups are detailed in **Figure 1**. The number of retinas per group and time point was 4–6 for anatomical analysis (see **Table 1** for a detailed n), and 4 for qPCR.

Surgery

The left optic nerve was crushed at 0.5 mm from the optic disc following previously described methods (Galindo-Romero et al., 2011; Sanchez-Migallon et al., 2016). In brief, to access the optic nerve at the back of the eye, an incision was made in the skin overlying the superior orbital rim, the supero-external orbital contents were dissected, and the superior and external rectus muscles were sectioned. Then, the optic nerve was crushed at 0.5 mm from the optic disc for 10 s using watchmaker's forceps. Before and after the procedure, the eye fundus was observed through the operating microscope to assess the integrity of the retinal blood flow.

Intravitreal and Intraperitoneal Treatments

Intravitreal injections were all done in a final volume of 2.5 μl, following previously published methods (Galindo-Romero et al., 2013b; Sanchez-Migallon et al., 2016). Animals were treated with single or combinatory intravitreal treatments of R7050 (0.2 or 1 mM, in 1 and 5% of DMSO-saline, respectively. Tocris Bioscience; Bio-Techne R&D Systems. Madrid, Spain) and/or BDNF (2.5 μg in 1% bovine serum albumin-PBS, PreproTech, London, UK).

Systemic treatment with R7050 (12 mg/kg i.p.) was done daily for 7 or 14 days. Some animals received a combinatorial therapy of intravitreal and intraperitoneal treatments. All groups are detailed in **Figure 1**.

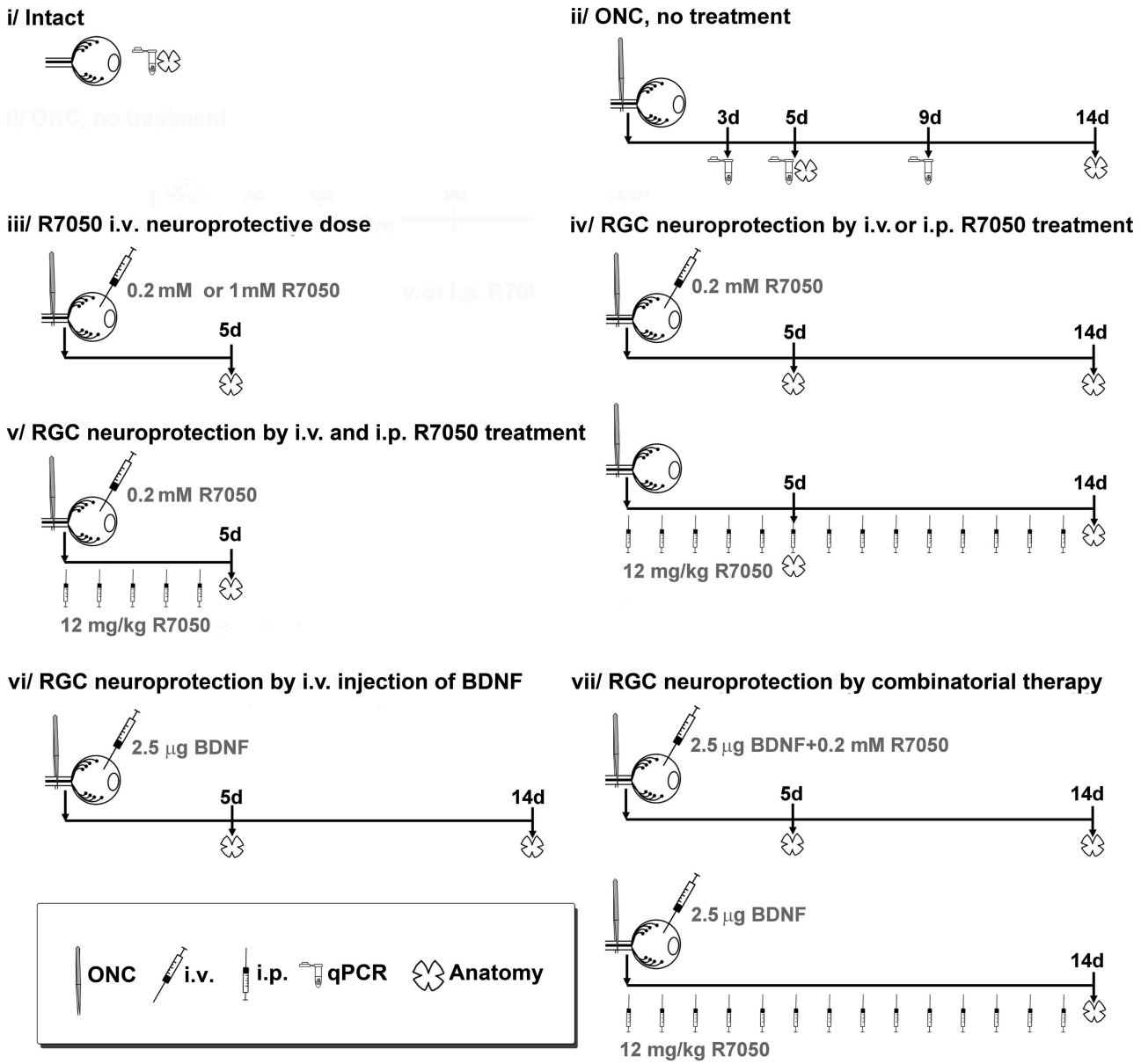

FIGURE 1 | Experimental design and animal groups. R7050 toxicity was studied at 0.2 mM in intact retinas, which were analyzed 5 days after administration. As vehicle control groups, we assayed R7050 1 mM vehicle (5% DMSO in saline) since it has been published that at this concentration is toxic for neurons (Galvao et al., 2014). Two groups were done, intact + i.v. of 5% DMSO and ONC + i.v. of DMSO analyzed 5 days later. To reduce the number of animals, control groups for 1% DMSO (R7050 0.2 mM vehicle) were not done since in our conditions neither the population of RGCs nor their loss after axotomy was affected by an i.v. injection of 5% DMSO. Likewise, intraperitoneal vehicle of R7050 and intravitreal vehicle of BDNF groups were not done because we have already shown that those vehicle formulations and administration routes do not have a negative effect in the retina (Galindo-Romero et al., 2013b; Di Pierdomenico et al., 2018). i.v, intravitreal injection; i.p., intraperitoneal injection.

Immunodetection

Animals were perfused transcardially with 0.9% saline solution followed by 4% paraformaldehyde in 0.1 M phosphate buffer. Retinas were prepared as flat mounts, or eyes were cryo-sectioned. In all experimental groups, RGCs were immunodetected in whole-mounts as reported (Galindo-Romero et al., 2011; Sanchez-Migallon et al., 2016) using mouse α-Brn3a primary antibody (1:500; MAB1585, Merck Millipore; Madrid, Spain). Secondary detection was carried out with donkey α-mouse IgG1-Alexa fluor 594 (1:500; Molecular Probes; Thermo Fisher Scientific, Madrid, Spain). In brief, flat mounted retinas were permeabilized in PBS 0.5% Triton by freezing them for 15 min at −70°C, rinsed in new PBS 0.5% Triton, and incubated overnight at 4°C with the primary antibody diluted in

blocking buffer (phosphate buffer saline (PBS) with 2% donkey normal serum and 2% Triton). Then, the retinas were washed three times in PBS and incubated for 2 h at room temperature with the secondary antibody. Finally, they were thoroughly washed in PBS, mounted vitreous side up and covered with antifading solution (Vectashield, Vector laboratories, Palex Medical, Barcelona, Spain).

In retinal cross sections from intact animals or animals processed 5 days after ONC, Tnfr1 (1:100, ab19139 Abcam, Cambridge, UK) and Brn3a (MAB1585, 1:500) were double immunodetected. Secondary antibodies were donkey α-mouse IgG1-Alexa fluor 488 or α-rabbit-Alexa fluor 594 (1:500; Molecular Probes). Briefly, sections were incubated overnight a 4°C with the primary antibodies diluted in blocking buffer. Secondary detection was carried out as in flat-mounts.

Image Acquisition and Analysis

Images were acquired using an epifluorescence microscope (Axioscop 2 Plus; Zeiss Mikroskopie, Jena, Germany) equipped with a computer-driven motorized stage (ProScan H128 Series; Prior Scientific Instruments, Cambridge, UK) controlled by image analysis software (Image-Pro Plus, IPP 5.1 for Windows; Media Cybernetics, Silver Spring, MD).

Retinal photomontages of Brn3a$^+$RGCs were reconstructed from 154 (11 × 14) individual images (Galindo-Romero et al., 2011). The whole population of Brn3a$^+$RGCs was quantified automatically and their distribution assessed by neighbor maps using previously reported methods (Galindo-Romero et al., 2013a). Briefly for each RGC its center mass position coordinates (x, y) were measured using the IPP macro language and the data were exported to a spreadsheet (Office Excel 2000; Microsoft Corp., Redmond, WA). Next, the Java (Oracle Corporation, Redwood Shores, California, USA) application described previously (Galindo-Romero et al., 2013a) was used to calculate the number of neighbors around each cell by measuring their euclidean distance to the rest of cells. Those cells closer than the fixed radius (0.22 mm) were counted. Finally, spatial study was used to spatially plot every RGC, and the number of neighbors served to color each one with a color scale representing the number of neighbors for each one. All maps were plotted using SigmaPlot (SigmaPlot 9.0 for Windows; Systat Software, Inc., Richmond, CA, USA).

qPCR

Fresh dissected retinas were immediately frozen on dry ice ($n = 4$ per group and time point). Total RNA was extracted using Trizol reagent (Thermo Fisher Scientific) and the RNA samples were dissolved in 20 μL Milli-Q water. Total RNA concentration was determined using SimpliNanoTM (GE Healthcare Life Sciences, Madrid, Spain). Complementary DNA amplification was performed according to the instructions provided by the manufacturer SuperScript^{TM} IV VILO^{TM} Master Mix, Thermo Fisher Scientific) using 1 μg total RNA.

Mouse pre-designed SYBR green primers (pair 1) for *Tnfrs1*, *Tnfα*, and *Hrpt* (housekeeping) were purchased from Sigma Aldrich.

SYBR Premix Ex Taq II (Tli RNaseH Plus, TaKara; Thermo Fisher Scientific) based qPCR was carried out by the Genomic Platform at the IMIB-Arrixaca in a final volume of 5 μl with a primer concentration of 450 nM using the QuantStudio 5 (Applied Biosystems; Thermo Fisher Scientific). Technical triplicates were done for each sample. The Ct values were converted to relative quantification using the $2^{\Delta\Delta Ct}$ method (Livak and Schmittgen, 2001).

Statistics

Data were analyzed and plotted with GraphPad Prism v.7 (GraphPad San Diego, USA). Anatomical data are presented as mean ± standard deviation (SD), and qPCR data as mean ± standard error of the mean (SEM). Differences were considered significant when $p < 0.05$. Tests are detailed in results.

RESULTS

TNFR1 Expression in Intact and Injured Retinas

In intact retinas, TNFR1 is expressed in the inner nuclear layer (INL) and in the ganglion cell layer (GCL) (**Figure 2A**). TNFR1$^+$ cells in the GCL do not express Brn3a, and most possibly are displaced amacrine cells, since they are 50% of the cells in the GCL (Pérez De Sevilla Müller et al., 2007; Nadal-Nicolás et al., 2015). Five days after ONC, TNFR1 is expressed more brightly and by more cells than in intact retinas. In the GCL many RGCs are TNFR1 positive (**Figure 2B**, yellow arrows). Interestingly, TNFR1 expression is observed in those RGCs with a lower signal of Brn3a, as we observed before for those RGCs expressing the cleaved form of caspase 3 (Sanchez-Migallon et al., 2016).

qPCR analyses support the anatomical data, and at 3, 5, and 9 days after ONC there is a 2–3-fold increase of *Tnfr1* mRNA compared to intact retinas (**Figure 2C**, left graph). Furthermore, after ONC there is as well a significant increase of the *Tnfr1* ligand, *TNFα* (**Figure 2C**, right graph), in agreement with previous reports (Tse et al., 2018).

Intraperitoneal and Intravitreal Antagonism of TNFR1 Rescues RGCs From Optic Nerve Crush

To evaluate if a systemic treatment with R7050 protects axotomized RGCs, we performed ONC and animals were treated daily with an intraperitoneal injection of 12 mg/kg of R7050. This dose was chosen based on a previous work where this antagonist was used to treat the brain (King et al., 2013).

Five and fourteen days after the lesion, when without treatment 50 and 92%, respectively, of the RGCs have died, the number of RGCs is significantly higher in the treated than in the untreated groups (**Table 1**; **Figures 3**, **4**).

Next, we wondered whether a single intravitreal treatment would improve this outcome. We tested two different concentrations (0.2 and 1 mM) because this is the first time this route is used for this drug. Since R7050 is dissolved in DMSO, which has been reported toxic for RGCs after intravitreal

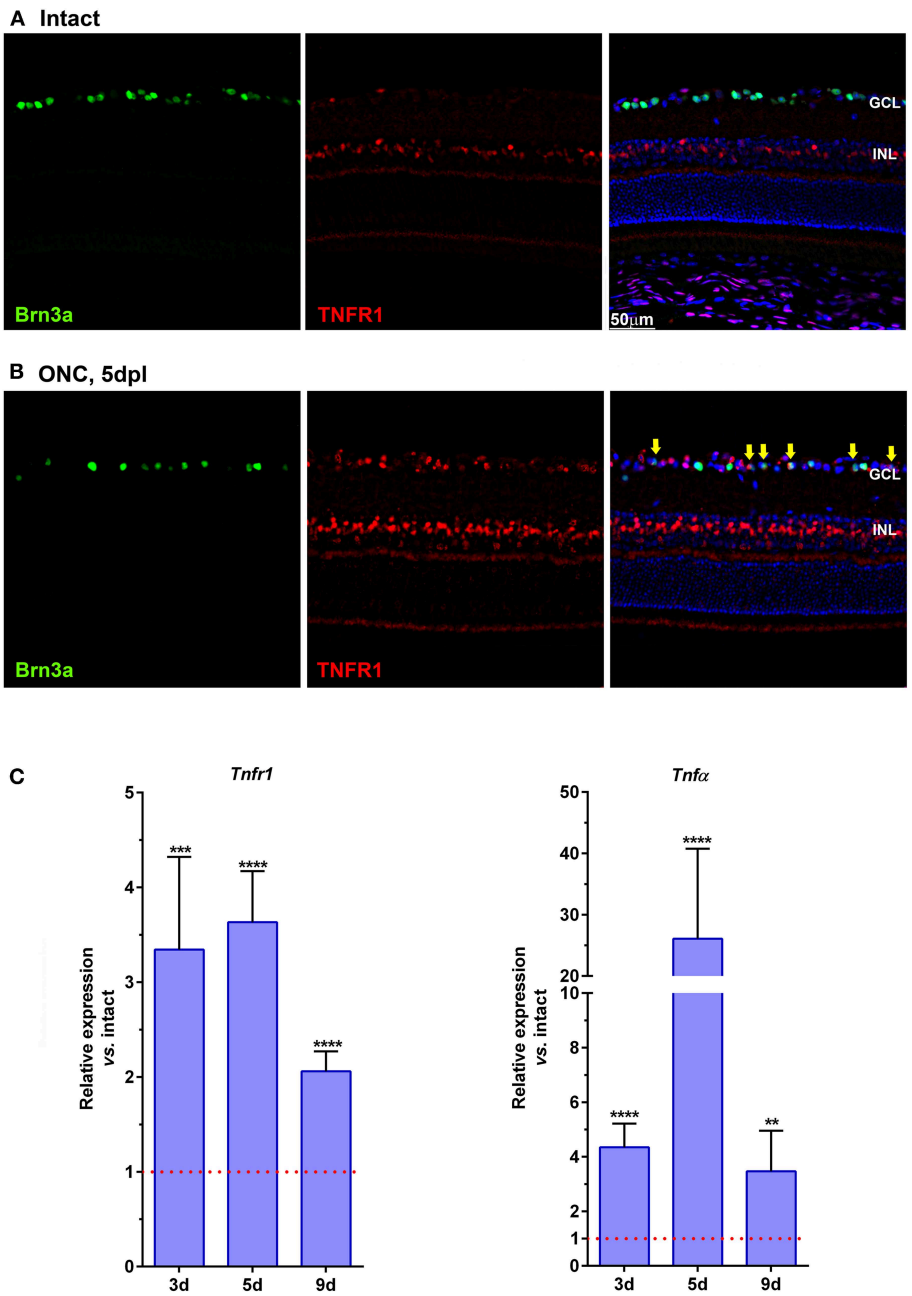

FIGURE 2 | TNFR1 is over-expressed in the retina after ONC. **(A,B)** Magnifications from retinal cross-sections showing the double immunodetection of Brn3a (green), TNFR1 (red), and the merged image with DAPI. In intact retinas **(A)** TNFR1 expression is observed mainly in the inner nuclear layer (INL), and in few Brn3a negative cells in the ganglion cell layer (GCL). Five days after ONC **(B)** many cells in the GCL, including RGCs (yellow arrows) express TNFR1. **(C)** Graph bars showing the fold change ± SEM of *Tnfr1* and *TNFα* mRNA levels in ONC-injured retinas relative to intact retinas (value 1, red dotted line; $^{**}p < 0.01$; $^{***}p < 0.001$; $^{****}p < 0.0001$, *T*-test vs. naive). d, days post-lesion.

administration (Galvao et al., 2014), we injected 5% DMSO in PBS (the maximum concentration used here) in intact retinas and after ONC, and both groups were analyzed 5 days later. Our data show that in intact retinas 5% DMSO does not cause RGC loss, and it does not increase the loss of RGCs after ONC (**Table 1**).

Five days after the lesion, R7050 intravitreal treatment increases significantly the number of surviving RGCs compared to untreated retinas. With the 0.2 mM intravitreal injection, the elicited neuroprotection was significantly higher than after intraperitoneal treatment (**Table 1**; **Figure 3**).

TABLE 1 | Total number of RGCs.

		Intact	ONC	
			5d	14d
No treatment	Mean	43,609	22,832	3,782
	SD	1,237	2,362	585
	n	6	6	5
i.p. R7050	Mean		25,802*	6,993**†
	SD		1,002	1,064
	n		5	5
i.v. 5% DMSO	Mean	43,935	23,374	
	SD	773	252	
	n	4	4	
i.v. 0.2 mM R7050	Mean	43,683	28,911$^{***\#\#}$	5,371*†
	SD	1,355	1604	942
	n	4	5	5
i.v. 1 mM R7050	Mean		28,207***	
	SD		2,313	
	n		4	
i.v. 0.2 mM + i.p. R7050	Mean		29,710$^{***\#}$	
	SD		1,827	
	n		5	
i.v. 2.5 μg BDNF	Mean		27,201**	10,222***‡
	SD		2,275	2,187
	n		5	4
i.v. 2.5 μg BDNF + i.v. 0.2 mM R7050	Mean		29,351***	11,392***
	SD		1,812	4,023
	n		5	5
i.v. 2.5 μg BDNF + i.p. R7050	Mean			12,109***
	SD			1,926
	n			5

Intact retinas treated with 5% DMSO or with 0.2 mM of R7050 were analyzed 5 days after the injection. SD, standard deviation; i.v., intravitreal injection; i.p., intraperitoneal injection; *Statistically different from ONC alone within the same time point ($^{*}p < 0.05$; $^{**}p < 0.01$; $^{***}p < 0.001$). $^{\#}$Statistical difference with i.p. treatment ($^{\#\#}p < 0.001$; $^{\#}p < 0.01$). †Significantly different compared to combinatorial treatments ($p < 0.05$). ‡Significantly different compared to i.v. R7050 treatment ($p < 0.05$). At all time post-lesions and irrespectively of the treatment, the loss of RGCs was significant compared to intact retinas ($p < 0.01$). T-test to compare two treatments. ANOVA Kruskal-Wallis test with Dunn's multiple comparisons post-hoc test, to analyze the effect of a treatment along time.

Both intravitreal doses achieved a similar RGC rescue and we chose the lower one for subsequent experiments. To verify that the treatment itself was not toxic for RGCs, 0.2 mM R7050 was intravitreally injected in intact retinas. As observed in **Table 1**, at this dose there was no RGC loss 5 days post-injection. Because the 1 mM dose was not used further and to save animals, we did not test its toxicity.

At 14 days, the intravitreal treatment still protects RGCs (**Table 1**; **Figure 4**), but the mean number of surviving RGCs is smaller than with the intraperitoneal treatment, although this difference does not reach statistical significance.

Finally, we combined both routes and treated animals with a single intravitreal injection and a daily intraperitoneal one. This posology does not improve the neuroprotection observed by intravitreal injection alone at 5 days post-lesion, therefore we did not assayed this combination at 14 days (**Table 1**; **Figure 3**).

The study of RGC topography by neighbor maps, shows in agreement with previous works, that RGC loss by axotomy affects the whole retina (Galindo-Romero et al., 2011; Nadal-Nicolás et al., 2015; Sanchez-Migallon et al., 2016, 2018). In addition, here we show that the intraperitonal and intravitreal administration of R7050 protects RGCs across the whole retina (**Figures 3B**, **4B**).

In conclusion, at 5 days the percent of surviving RGCs in R7050-treated retinas is 13% (intraperitoneal), 26% (intravitreal, 0.2 mM), 23% (intravitreal, 1 mM), and 30% (intraperitoneal+intravitreal) higher than after ONC alone. Neuroprotection by R7050 is relatively better at 14 than at 5 days: at 14 days there are 54% (intraperitoneal) and 42% (intravitreal) more RGCs than in untreated retinas.

Combinatorial Treatment: TNFR1 Antagonism and BDNF

BDNF is, excluding knocking out pro-apoptotic proteins or transfecting anti-apoptotic ones (Malik et al., 2005; Nickells et al., 2008), the best neuroprotectant for axotomized RGCs. Thus, we decided to test whether a combinatory therapy with BDNF and R7050 was better than each one alone.

At 5 days after ONC, a single intravitreal injection of BDNF rescues as many RGCs as the intravitreal or intraperitoneal treatment with R7050 (**Table 1**; **Figure 3**). An intravitreal injection of BDNF and 0.2 mM of R7050 increases the mean number of surviving RGCs, but no significantly so compared to either treatment alone. To save animals, we did not combine BDNF with systemic R7050, because R7050 administered intravitreally gives better results at this time point.

At 14 days post-injury, RGC neuroprotection by BDNF alone was significantly higher than R7050 administered intravitreally and better, but no significantly, than intraperitoneal R7050. Combination of BDNF and R7050 administered intravitreally or systemically, does not increase significantly the number of surviving RGCs compared to BDNF treatment alone. Even so, and as it occurs at 5 days, the mean number of RGCs is higher in the combinatory experiment (**Table 1**; **Figure 4**).

Again, and as observed for the single therapy with R7050, RGC neuroprotection by the combinatory treatments expands the whole retina (**Figures 3B**, **4B**).

In summary, while none of the treatments rescued the whole population of RGCs (see **Table 1**, intact retinas and neighbor map from an intact retina in **Figure 3B**), they elicited significant neuroprotection: at 5 days and compared to ONC alone, the percent of surviving RGCs in the treated retinas is 19% (BDNF), and 28% (BDNF + intravitreal R7050) higher. Again neuroprotection is relatively better at 14 than at 5 days: at 14 days there are 270% (BDNF), 301% (BDNF + intravitreal R7050), and 320% (BDNF + intraperitoneal R7050) more RGCs than in untreated retinas.

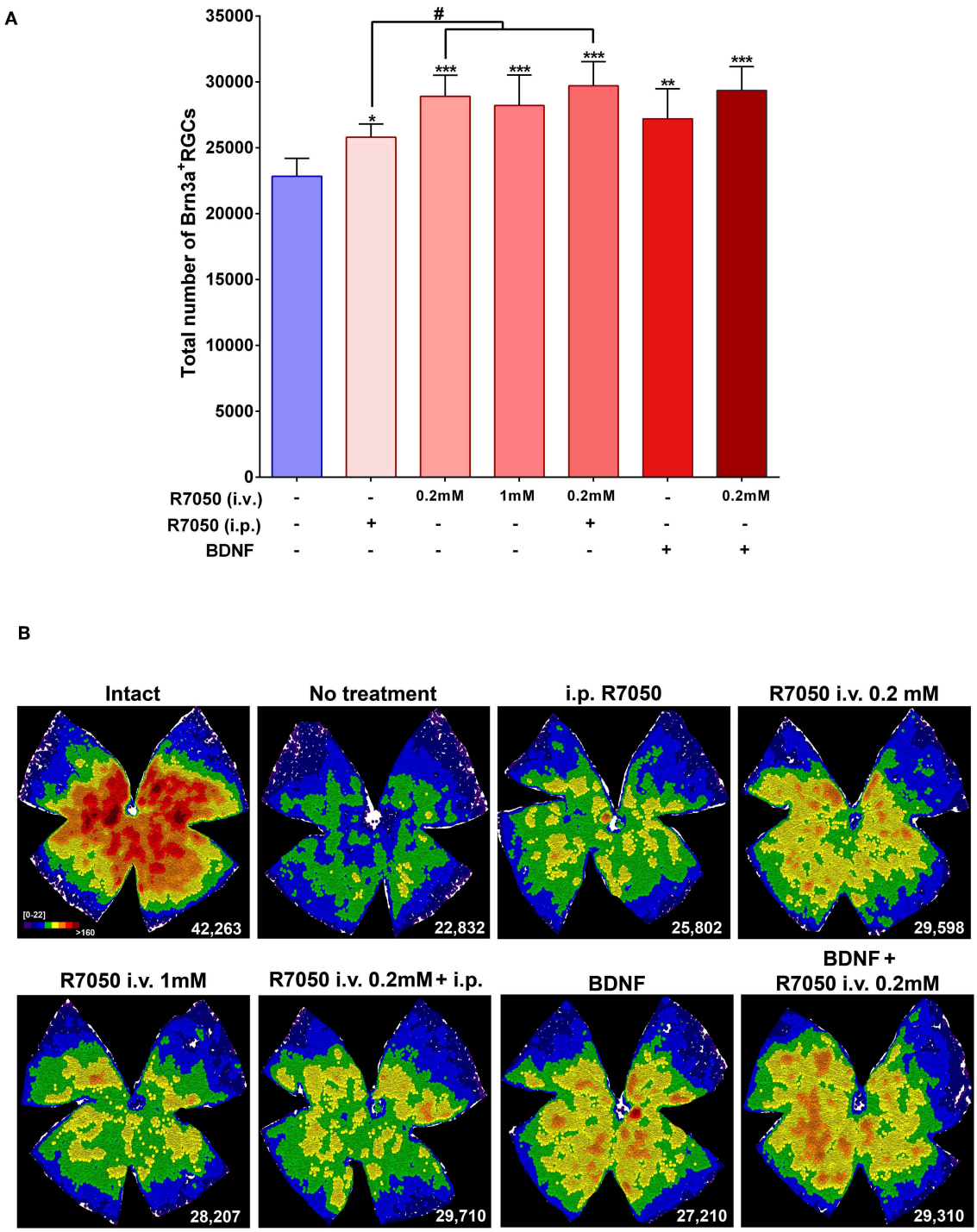

FIGURE 3 | Systemic and intravitreal treatment with R7050 alone or in combination with BDNF rescues RGCs during the quick phase of death after optic nerve axotomy. **(A)** Column bar graph showing the total mean number ± standard deviation of RGCs quantified in the different animal groups analyzed 5 days after ONC. *Statistically different from ONC alone (*$p < 0.05$; **$p < 0.01$; ***$p < 0.001$. ANOVA, Kruskal-Wallis. Dunn's *post-hoc* test). $^{\#}p < 0.01$ (*T*-test). For detailed statistics see **Table 1**. **(B)** Neighbor maps showing the distribution of RGCs in a representative retina from each group and treatment. These maps illustrate the number of RGCs around a given RGC in a radius of 0.200 mm with a color scale (top left panel) from 0 to 22 neighbors (purple) to >160 neighbors (dark red). At the bottom left of each map is shown the number of RGCs counted in the original retina.

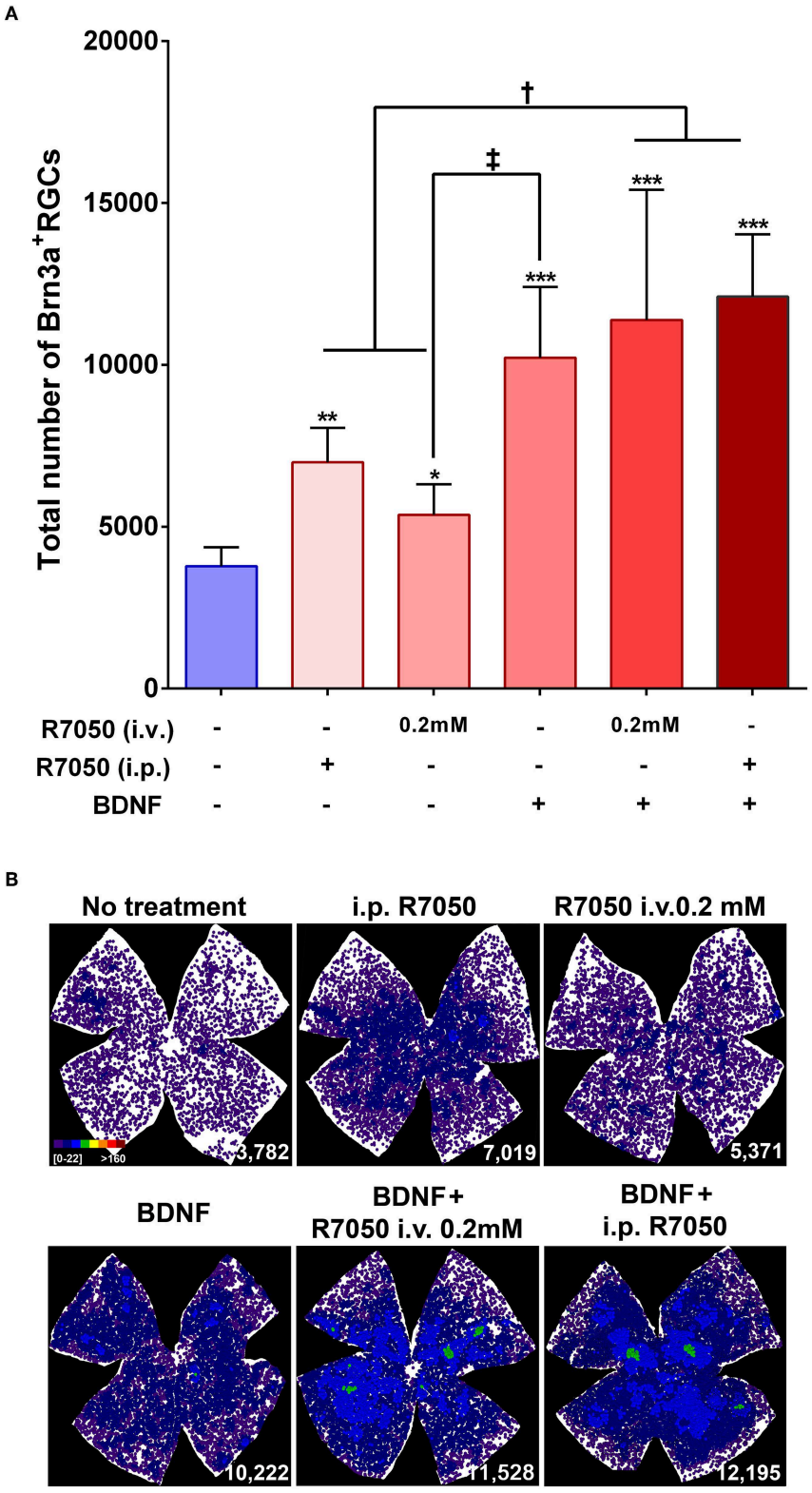

FIGURE 4 | Systemic and intravitreal treatment with R7050 alone or in combination with BDNF rescues RGCs during the slow phase of death after optic nerve axotomy. **(A)** Column bar graph showing the total mean number ± standard deviation of RGCs quantified in the different animal groups analyzed 14 days after ONC.

(Continued)

FIGURE 4 | *Statistically different from ONC alone (*$p < 0.05$; **$p < 0.01$; ***$p < 0.001$). †$p < 0.01$; ‡$p < 0.05$ (ANOVA, Kruskal-Wallis. Dunn's *post-hoc* test). See **Table 1** for more details. **(B)** Neighbor maps showing the distribution of RGCs in a representative retina from each group and treatment. These maps illustrate the number of RGCs around a given RGC in a radius of 0.220 mm with a color scale (top left panel) from 0 to 22 neighbors (purple) to >160 neighbors (dark red). At the bottom left of each map is shown the number of RGCs counted in the original retina.

DISCUSSION

The role of TNFα in neurodegeneration has been widely reported, not only in the retina (Yuan and Neufeld, 2000; Tezel et al., 2001; Kitaoka et al., 2006; Agudo et al., 2008; Tezel, 2008; Cueva Vargas et al., 2015; De Groef et al., 2015) but also in neurodegenerative diseases such as Alzheimer's or Parkinson's (Mogi et al., 1994; Cheng et al., 2010).

Our results confirm and extend those previous reports connecting axonal damage, RGC loss and TNFα. Our strategy differs from previous works targeting TNFα (Roh et al., 2012; Tse et al., 2018; Park et al., 2019) in that instead of blocking TNFα using decoy-receptors, we have used an antagonist of the TNFα/TNFR1 signaling pathway. R7050 inhibits the endocytosis of the TNF-α/TNFR1 multiprotein complex (Gururaja et al., 2007), thus blocking the extrinsic pathway of apoptosis. This antagonist is a small cell permeable molecule that crosses the blood brain barrier, allowing a systemic administration to treat the central nervous system (King et al., 2013). TNFα decoy receptors are also administered systemically, however because they are proteins they come with inherent problems such as bioavailability, tissue distribution and most importantly, antigenicity.

Our data show that R7050 administered locally or systemically, rescues axotomized RGCs. Intravitreal treatment elicits a better neuroprotection at 5 days than the intraperitoneal route. At long time post-lesions, intraperitoneal and intravitreal administration render similar results. Nevertheless, we should not forget that here we performed a single intravitreal injection, while the systemic dose was administered daily.

Neuroprotection by R7050 14 days after ONC is higher (54–42%) than that shown in a previous work where TNFα was intercepted with etanercept, a decoy-receptor (Tse et al., 2018). Tse et al. reported an increase of ∼24% of RGC survival. These differences could mean that R7050 is a better inhibitor of the TNFα apoptotic signaling. Alternatively, the differences could be due to the different route (subcutaneous) or methodology, as they sample the retinas and present RGC densities, while here we quantify the total population of RGCs.

Another strategy to study the implication of a given protein in axotomy-induced RGC death is the use of knockout mice. In a time course study using TNFR1$^{-/-}$ mice, Tezel et al. (2004) analyzed the retinas from 1 to 6 weeks after ONC and observed, in agreement with our data that compared to wild type animals, RGC neuroprotection in the deficient mice was higher at longer times post-lesion.

RGC loss by axotomy triggers a myriad of signals, encompassing multiple pro-death, and pro-survival pathways (Agudo et al., 2008, 2009; Agudo-Barriuso et al., 2013), and this is believed to be one of the reasons why single treatments are not enough (Harvey, 2007). Thus, combinatory therapies are needed to increase neuroprotection not only in number of neurons, but also in time. Here we combined BDNF, whose neuroprotective potential has been widely studied (Mansour-Robaey et al., 1994; Peinado-Ramon et al., 1996; Di Polo et al., 1998; Pernet and Di, 2006; Parrilla-Reverter et al., 2009; Sanchez-Migallon et al., 2011, 2016; Galindo-Romero et al., 2013b; Valiente-Soriano et al., 2015; Feng et al., 2016, 2017; Osborne et al., 2018) with R7050. We hypothesized that activating pro-survival pathways while inhibiting pro-apoptotic ones would increase RGC survival. However, our data show that the combined rescue of R7050 and BDNF is not summative. This suggest that either both pathways share a common denominator, and/or that the activation of the survival pathways by BDNF blocks the apoptotic signals thus effectively overriding the effect of R7050. Further experiments are needed to assess whether a sequential treatment first with BDNF and then with R7050 (or vice versa) would be more effective.

In conclusion, here we show for the first time that local and systemic treatment with the small inhibitor of the TNFR1 signaling, R7050, protects RGCs from axotomy-induced degeneration. While knockout or transgenic animals are very useful to assign specific functions to specific proteins, this strategy cannot (yet) be used in human patients. Given that to date there are no therapies to overcome neuronal death, proof of concept pre-clinical studies are needed to expand the possible therapeutic avenues to treat not only traumatic neuropathies, but also neurodegenerative diseases.

DATA AVAILABILITY STATEMENT

All datasets generated for this study are included in the manuscript/supplementary files.

ETHICS STATEMENT

The animal study was reviewed and approved by the Ethical and Animal Studies Committee of the University of Murcia, Spain (number: A1320140704).

AUTHOR CONTRIBUTIONS

FL-R, CG-R, MS-N, MG-R: methodology, data analysis and representation, and review and editing. MV-S: writing, review and editing, and funding acquisition. MA: conceptualization,

supervision, data analysis and representation, writing, review and editing, and funding acquisition.

FUNDING

This study was supported the Spanish Ministry of Economy and Competitiveness, Instituto de Salud Carlos III, Fondo Europeo de Desarrollo Regional Una manera de hacer Europa (PI16/00031, SAF2015-67643-P, RD16/0008/0026, and RD16/0008/0016), and by the Fundación Séneca, Agencia de Ciencia y Tecnología Región de Murcia (19881/GERM/15).

ACKNOWLEDGMENTS

The authors want to thank the Genomic Platform of the IMIB-Arrixaca.

REFERENCES

Agudo, M., Perez-Marin, M. C., Lonngren, U., Sobrado, P., Conesa, A., Canovas, I., et al. (2008). Time course profiling of the retinal transcriptome after optic nerve transection and optic nerve crush. *Mol. Vis*. 14, 1050–1063.

Agudo, M., Perez-Marin, M. C., Sobrado-Calvo, P., Lonngren, U., Salinas-Navarro, M., Canovas, I., et al. (2009). Immediate upregulation of proteins belonging to different branches of the apoptotic cascade in the retina after optic nerve transection and optic nerve crush. *Invest. Ophthalmol. Vis. Sci.* 50, 424–431. doi: 10.1167/iovs.08-2404

Agudo-Barriuso, M., Lahoz, A., Nadal-Nicolas, F. M., Sobrado-Calvo, P., Piquer-Gil, M., Diaz-Llopis, M., et al. (2013). Metabolomic changes in the rat retina after optic nerve crush. *Invest. Ophthalmol. Vis. Sci.* 54, 4249–4259. doi: 10.1167/iovs.12-11451

Cabal-Hierro, L., and Lazo, P. S. (2012). Signal transduction by tumor necrosis factor receptors. *Cell Signal*. 24, 1297–1305. doi: 10.1016/j.cellsig.2012.02.006

Cheng, X., Yang, L., He, P., Li, R., and Shen, Y. (2010). Differential activation of tumor necrosis factor receptors distinguishes between brains from Alzheimer's disease and non-demented patients. *J. Alzheimers Dis*. 19, 621–630. doi: 10.3233/JAD-2010-1253

Cueva Vargas, J. L., Osswald, I. K., Unsain, N., Aurousseau, M. R., Barker, P. A., Bowie, D., et al. (2015). Soluble tumor necrosis factor alpha promotes retinal ganglion cell death in glaucoma via calcium-permeable ampa receptor activation. *J. Neurosci.* 35, 12088–12102. doi: 10.1523/JNEUROSCI.1273-15.2015

De Groef, L., Salinas-Navarro, M., Van Imschoot, G., Libert, C., Vandenbroucke, R. E., and Moons, L. (2015). Decreased TNF levels and improved retinal ganglion cell survival in MMP-2 null mice suggest a role for MMP-2 as TNF sheddase. *Mediators Inflamm*. 2015:108617. doi: 10.1155/2015/108617

Di Pierdomenico, J., Scholz, R., Valiente-Soriano, F. J., Sánchez-Migallón, M. C., Vidal-Sanz, M., Langmann, T., et al. (2018). Neuroprotective effects of FGF2 and minocycline in two animal models of inherited retinal degeneration. *Invest. Ophthalmol. Vis. Sci*. 59, 4392–4403. doi: 10.1167/iovs.18-24621

Di Polo, A., Aigner, L. J., Dunn, R. J., Bray, G. M., and Aguayo, A. J. (1998). Prolonged delivery of brain-derived neurotrophic factor by adenovirus-infected Muller cells temporarily rescues injured retinal ganglion cells. *Proc. Natl. Acad. Sci. U.S.A*. 95, 3978–3983. doi: 10.1073/pnas.95.7.3978

Feng, L., Chen, H., Yi, J., Troy, J. B., Zhang, H. F., and Liu, X. (2016). Long-term protection of retinal ganglion cells and visual function by brain-derived neurotrophic factor in mice with ocular hypertension. *Invest. Ophthalmol. Vis. Sci.* 57, 3793–3802. doi: 10.1167/iovs.16-19825

Feng, L., Puyang, Z., Chen, H., Liang, P., Troy, J. B., and Liu, X. (2017). Overexpression of brain-derived neurotrophic factor protects large retinal ganglion cells after optic nerve crush in mice. *eNeuro*. 4:ENEURO.0331-16.2016. doi: 10.1523/ENEURO.0331-16.2016

Galindo-Romero, C., Aviles-Trigueros, M., Jimenez-Lopez, M., Valiente-Soriano, F. J., Salinas-Navarro, M., Nadal-Nicolas, F., et al. (2011). Axotomy-induced retinal ganglion cell death in adult mice: quantitative and topographic time course analyses. *Exp. Eye Res*. 92, 377–387. doi: 10.1016/j.exer.2011.02.008

Galindo-Romero, C., Jimenez-Lopez, M., Garcia-Ayuso, D., Salinas-Navarro, M., Nadal-Nicolas, F. M., Agudo-Barriuso, M., et al. (2013a). Number and spatial distribution of intrinsically photosensitive retinal ganglion cells in the adult albino rat. *Exp. Eye Res*. 108, 84–93. doi: 10.1016/j.exer.2012.12.010

Galindo-Romero, C., Valiente-Soriano, F. J., Jimenez-Lopez, M., Garcia-Ayuso, D., Villegas-Perez, M. P., Vidal-Sanz, M., et al. (2013b). Effect of brain-derived neurotrophic factor on mouse axotomized retinal ganglion cells and phagocytic microglia. *Invest. Ophthalmol. Vis. Sci.* 54, 974–985. doi: 10.1167/iovs.12-11207

Galvao, J., Davis, B., Tilley, M., Normando, E., Duchen, M. R., and Cordeiro, M. F. (2014). Unexpected low-dose toxicity of the universal solvent DMSO. *FASEB J.* 28, 1317–1330. doi: 10.1096/fj.13-235440

Gururaja, T. L., Yung, S., Ding, R., Huang, J., Zhou, X., McLaughlin, J., et al. (2007). A class of small molecules that inhibit TNFalpha-induced survival and death pathways via prevention of interactions between TNFalphaRI, TRADD, and RIP1. *Chem. Biol*. 14, 1105–1118. doi: 10.1016/j.chembiol.2007.08.012

Harvey, A. R. (2007). Combined therapies in the treatment of neurotrauma: polymers, bridges and gene therapy in visual system repair. *Neurodegener. Dis*. 4, 300–305. doi: 10.1159/000101886

Isenmann, S., Klocker, N., Gravel, C., and Bahr, M. (1998). Short communication: protection of axotomized retinal ganglion cells by adenovirally delivered BDNF *in vivo*. *Eur. J. Neurosci*. 10, 2751–2756. doi: 10.1046/j.1460-9568.1998.00325.x

King, M. D., Alleyne, C. H. Jr., and Dhandapani, K. M. (2013). TNF-alpha receptor antagonist, R-7050, improves neurological outcomes following intracerebral hemorrhage in mice. *Neurosci. Lett*. 542, 92–96. doi: 10.1016/j.neulet.2013.02.051

Kitaoka, Y., Kitaoka, Y., Kwong, J. M., Ross-Cisneros, F. N., Wang, J., Tsai, R. K., et al. (2006). TNF-alpha-induced optic nerve degeneration and nuclear factor-kappaB p65. *Invest. Ophthalmol. Vis. Sci.* 47, 1448–1457. doi: 10.1167/iovs.05-0299

Klocker, N., Kermer, P., Weishaupt, J. H., Labes, M., Ankerhold, R., and Bahr, M. (2000). Brain-derived neurotrophic factor-mediated neuroprotection of adult rat retinal ganglion cells *in vivo* does not exclusively depend on phosphatidyl-inositol-3'-kinase/protein kinase B signaling. *J. Neurosci*. 20, 6962–6967. doi: 10.1523/JNEUROSCI.20-18-06962.2000

Kyung, H., Kwong, J. M., Bekerman, V., Gu, L., Yadegari, D., Caprioli, J., et al. (2015). Celastrol supports survival of retinal ganglion cells injured by optic nerve crush. *Brain Res*. 1609, 21–30. doi: 10.1016/j.brainres.2015.03.032

Livak, K. J., and Schmittgen, T. D. (2001). Analysis of relative gene expression data using real-time quantitative PCR and the 2 (-Delta Delta C (T) method. *Methods* 25, 402–408. doi: 10.1006/meth.2001.1262

Lorz, C., and Mehmet, H. (2009). The role of death receptors in neural injury. *Front Biosci*. 14, 583–595. doi: 10.2741/3265

Malik, J. M., Shevtsova, Z., Bahr, M., and Kugler, S. (2005). Long-term *in vivo* inhibition of CNS neurodegeneration by Bcl-XL gene transfer. *Mol. Ther*. 11, 373–381. doi: 10.1016/j.ymthe.2004.11.014

Mansour-Robaey, S., Clarke, D. B., Wang, Y. C., Bray, G. M., and Aguayo, A. J. (1994). Effects of ocular injury and administration of brain-derived neurotrophic factor on survival and regrowth of axotomized retinal ganglion cells. *Proc. Natl. Acad. Sci. U.S.A.* 91, 1632–1636. doi: 10.1073/pnas.91.5.1632

Mogi, M., Harada, M., Riederer, P., Narabayashi, H., Fujita, K., and Nagatsu, T. (1994). Tumor necrosis factor-alpha (TNF-alpha) increases both in the brain and in the cerebrospinal fluid from parkinsonian patients. *Neurosci. Lett*. 165, 208–210. doi: 10.1016/0304-3940(94)90746-3

Nadal-Nicolás, F. M., Sobrado-Calvo, P., Jiménez-López, M., Vidal-Sanz, M., and Agudo-Barriuso, M. (2015). Long-term effect of optic nerve axotomy on the retinal ganglion cell layer. *Invest. Ophthalmol. Vis. Sci*. 56, 6095–6112. doi: 10.1167/iovs.15-17195

Nakazawa, T., Tamai, M., and Mori, N. (2002). Brain-derived neurotrophic factor prevents axotomized retinal ganglion cell death through MAPK and PI3K signaling pathways. *Invest. Ophthalmol. Vis. Sci.* 43, 3319–3326.

Nickells, R. W., Semaan, S. J., and Schlamp, C. L. (2008). Involvement of the Bcl2 gene family in the signaling and control of retinal ganglion cell death. *Prog. Brain Res*. 173, 423–435. doi: 10.1016/S0079-6123(08)01129-1

Osborne, A., Khatib, T. Z., Songra, L., Barber, A. C., Hall, K., Kong, G. Y. X., et al. (2018). Neuroprotection of retinal ganglion cells by a novel gene therapy construct that achieves sustained enhancement of brain-derived neurotrophic factor/tropomyosin-related kinase receptor-B signaling. *Cell Death. Dis*. 9:1007. doi: 10.1038/s41419-018-1041-8

Park, J., Lee, S. Y., Shon, J., Kim, K., Lee, H. J., Kim, K. A., et al. (2019). Adalimumab improves cognitive impairment, exerts neuroprotective effects and attenuates neuroinflammation in an Abeta1-40-injected mouse model of Alzheimer's disease. *Cytotherapy*. 21, 671–682. doi: 10.1016/j.jcyt.2019.04.054

Parrilla-Reverter, G., Agudo, M., Sobrado-Calvo, P., Salinas-Navarro, M., Villegas-Perez, M. P., and Vidal-Sanz, M. (2009). Effects of different neurotrophic factors on the survival of retinal ganglion cells after a complete intraorbital nerve crush injury: a quantitative *in vivo* study. *Exp. Eye Res*. 89, 32–41. doi: 10.1016/j.exer.2009.02.015

Peinado-Ramon, P., Salvador, M., Villegas-Perez, M. P., and Vidal-Sanz, M. (1996). Effects of axotomy and intraocular administration of NT-4, NT-3, and brain-derived neurotrophic factor on the survival of adult rat retinal ganglion cells. A quantitative *in vivo* study. *Invest. Ophthalmol. Vis. Sci.* 37, 489–500.

Pérez De Sevilla Müller, L., Shelley, J., and Weiler, R. (2007). Displaced amacrine cells of the mouse retina. *J Comp Neurol*. 505, 177–89. doi: 10.1002/cne.21487

Pernet, V., and Di, P. A. (2006). Synergistic action of brain-derived neurotrophic factor and lens injury promotes retinal ganglion cell survival, but leads to optic nerve dystrophy *in vivo*. *Brain* 129, 1014–1026. doi: 10.1093/brain/awl015

Roh, M., Zhang, Y., Murakami, Y., Thanos, A., Lee, S. C., Vavvas, D. G., et al. (2012). Etanercept, a widely used inhibitor of tumor necrosis factor-alpha (TNF-alpha), prevents retinal ganglion cell loss in a rat model of glaucoma. *PLoS. ONE*. 7:e40065. doi: 10.1371/journal.pone.0040065

Sanchez-Migallon, M. C., Nadal-Nicolas, F. M., Jimenez-Lopez, M., Sobrado-Calvo, P., Vidal-Sanz, M., and Agudo-Barriuso, M. (2011). Brain derived neurotrophic factor maintains Brn3a expression in axotomized rat retinal ganglion cells. *Exp. Eye Res*. 92, 260–267. doi: 10.1016/j.exer.2011.02.001

Sanchez-Migallon, M. C., Valiente-Soriano, F. J., Nadal-Nicolas, F. M., Vidal-Sanz, M., and Agudo-Barriuso, M. (2016). Apoptotic retinal ganglion cell death after optic nerve transection or crush in mice: delayed RGC loss with BDNF or a caspase 3 inhibitor. *Invest. Ophthalmol. Vis. Sci.* 57, 81–93. doi: 10.1167/iovs.15-17841

Sanchez-Migallon, M. C., Valiente-Soriano, F. J., Salinas-Navarro, M., Nadal-Nicolas, F. M., Jimenez-Lopez, M., Vidal-Sanz, M., et al. (2018). Nerve fibre layer degeneration and retinal ganglion cell loss long term after optic nerve crush or transection in adult mice. *Exp. Eye Res*. 170, 40–50. doi: 10.1016/j.exer.2018.02.010

Sedger, L. M., and McDermott, M. F. (2014). TNF and TNF-receptors: from mediators of cell death and inflammation to therapeutic giants - past, present and future. *Cytokine Growth Factor Rev*. 25, 453–472. doi: 10.1016/j.cytogfr.2014.07.016

Tezel, G. (2008). TNF-alpha signaling in glaucomatous neurodegeneration. *Prog. Brain Res*. 173, 409–421. doi: 10.1016/S0079-6123(08)01128-X

Tezel, G., Li, L. Y., Patil, R. V., and Wax, M. B. (2001). TNF-alpha and TNF-alpha receptor-1 in the retina of normal and glaucomatous eyes. *Invest. Ophthalmol. Vis. Sci.* 42, 1787–1794.

Tezel, G., Yang, X., Yang, J., and Wax, M. B. (2004). Role of tumor necrosis factor receptor-1 in the death of retinal ganglion cells following optic nerve crush injury in mice. *Brain Res*. 996, 202–212. doi: 10.1016/j.brainres.2003.10.029

Tse, B. C., Dvoriantchikova, G., Tao, W., Gallo, R. A., Lee, J. Y., Pappas, S., et al. (2018). Tumor necrosis factor inhibition in the acute management of traumatic optic neuropathy. *Invest. Ophthalmol. Vis. Sci.* 59, 2905–2912. doi: 10.1167/iovs.18-24431

Valiente-Soriano, F. J., Nadal-Nicolas, F. M., Salinas-Navarro, M., Jimenez-Lopez, M., Bernal-Garro, J. M., Villegas-Perez, M. P., et al. (2015). BDNF rescues RGCs but not intrinsically photosensitive RGCs in ocular hypertensive albino rat retinas. *Invest. Ophthalmol. Vis. Sci.* 56, 1924–1936. doi: 10.1167/iovs.15-16454

Vidal-Sanz, M., Galindo-Romero, C., Valiente-Soriano, F. J., Nadal-Nicolas, F. M., Ortin-Martinez, A., Rovere, G., et al. (2017). Shared and differential retinal responses against optic nerve injury and ocular hypertension. *Front. Neurosci*. 11:235. doi: 10.3389/fnins.2017.00235

Wei, X., Cho, K. S., Thee, E. F., Jager, M. J., and Chen, D. F. (2019). Neuroinflammation and microglia in glaucoma: time for a paradigm shift. *J. Neurosci. Res*. 97, 70–76. doi: 10.1002/jnr.24256

Yuan, L., and Neufeld, A. H. (2000). Tumor necrosis factor-alpha: a potentially neurodestructive cytokine produced by glia in the human glaucomatous optic nerve head. *Glia* 32, 42–50. doi: 10.1002/1098-1136(200010)32:13.3.CO;2-V

Conflict of Interest: The authors declare that the research was conducted in the absence of any commercial or financial relationships that could be construed as a potential conflict of interest.

frontiers in Neuroscience

REVIEW
published: 08 November 2019
doi: 10.3389/fnins.2019.01172

Relationships Between Neurodegeneration and Vascular Damage in Diabetic Retinopathy

Maria Grazia Rossino[1], *Massimo Dal Monte*[1,2]* *and Giovanni Casini*[1,2]*

[1] Department of Biology, University of Pisa, Pisa, Italy, [2] Interdepartmental Research Center Nutrafood "Nutraceuticals and Food for Health", University of Pisa, Pisa, Italy

Diabetic retinopathy (DR) is a common complication of diabetes and constitutes a major cause of vision impairment and blindness in the world. DR has long been described exclusively as a microvascular disease of the eye. However, in recent years, a growing interest has been focused on the contribution of neuroretinal degeneration to the pathogenesis of the disease, and there are observations suggesting that neuronal death in the early phases of DR may favor the development of microvascular abnormalities, followed by the full manifestation of the disease. However, the mediators that are involved in the crosslink between neurodegeneration and vascular changes have not yet been identified. According to our hypothesis, vascular endothelial growth factor (VEGF) could probably be the most important connecting link between the death of retinal neurons and the occurrence of microvascular lesions. Indeed, VEGF is known to play important neuroprotective actions; therefore, in the early phases of DR, it may be released in response to neuronal suffering, and it would act as a double-edged weapon inducing both neuroprotective and vasoactive effects. If this hypothesis is correct, then any retinal stress causing neuronal damage should be accompanied by VEGF upregulation and by vascular changes. Similarly, any compound with neuroprotective properties should also induce VEGF downregulation and amelioration of the vascular lesions. In this review, we searched for a correlation between neurodegeneration and vasculopathy in animal models of retinal diseases, examining the effects of different neuroprotective substances, ranging from nutraceuticals to antioxidants to neuropeptides and others and showing that reducing neuronal suffering also prevents overexpression of VEGF and vascular complications. Taken together, the reviewed evidence highlights the crucial role played by mediators such as VEGF in the relationship between retinal neuronal damage and vascular alterations and suggests that the use of neuroprotective substances could be an efficient strategy to prevent the onset or to retard the development of DR.

Keywords: nutraceuticals, antioxidants, neuropeptides, vascular endothelial growth factor, blood-retina barrier

OPEN ACCESS

Edited by:
Abel Santamaria, National Institute of Neurology and Neurosurgery (INNN), Mexico

Reviewed by:
Nataliya G. Kolosova, Institute of Cytology and Genetics (RAS), Russia
José Carlos Rivera, Université de Montréal, Canada

***Correspondence:**
Massimo Dal Monte
massimo.dalmonte@unipi.it
Giovanni Casini
giovanni.casini@unipi.it

Specialty section:
This article was submitted to Neurodegeneration, a section of the journal Frontiers in Neuroscience

Received: *23 August 2019*
Accepted: *16 October 2019*
Published: *08 November 2019*

Citation:
Rossino MG, Dal Monte M and Casini G (2019) Relationships Between Neurodegeneration and Vascular Damage in Diabetic Retinopathy. Front. Neurosci. 13:1172. doi: 10.3389/fnins.2019.01172

INTRODUCTION

Diabetes is a disease affecting a growing number of people worldwide. It is expected to increase to a little <700 million by 2045, with almost half of diabetics suffering from the slowly progressive type 2 diabetes, which in many cases remains undiagnosed (Cho et al., 2018). Type 2 diabetes is the main cause of diabetes in the population aged 40–74 years, although there is an increasing number

of people aged <40 suffering from this form of the disease (Pantalone et al., 2015). Untreated or poorly controlled diabetes may lead to the appearance of serious complications, including diabetic retinopathy (DR). DR is the most common complication of diabetes and the leading cause of preventable visual impairment in the working age population in developed countries. It is also one of the main causes of blindness worldwide. In 2010, it has been estimated that about 95 million people suffered from a form of DR (Leasher et al., 2016). Due to the increasing number of diabetic people and the increased life expectancy, these numbers are expected to rise in the near future.

DR is a multifactorial progressive disease characterized by an extremely complex pathogenesis involving different factors and a variety of pathophysiologic mechanisms. Hyperglycemia represents a link between diabetes and DR complications. Indeed, prolonged high glucose levels damage the retina, inducing metabolic changes that result in dysregulation of a number of mediators, including growth factors, neurotrophic factors, cytokines/chemokines, vasoactive agents, and inflammatory and adhesion molecules. The altered retinal microenvironment is responsible for the appearance and the progression of extended vascular lesions and cell death (Qian and Ripps, 2011; Ola et al., 2012; Tarr et al., 2013; Abcouwer and Gardner, 2014).

DR has often been regarded as a purely vascular disorder of the retina. Clinically, it is classified as non-proliferative, characterized by microvascular damage, including blood-retina barrier (BRB) breakdown, basement membrane thickening, leukocyte adhesion, occurrence of acellular capillaries, capillary degeneration, pericyte loss; or proliferative, where neoangiogenesis phenomena are observed and new blood vessels are formed. These neovessels may generate a mechanic traction, causing retinal detachment and consequent blindness (Stitt et al., 2013). The key factor involved in pathologic vascular changes, from microvascular damage to neoangiogenesis, is vascular endothelial growth factor (VEGF). Consequently, DR treatments are mainly based on intraocular delivery of anti-VEGF molecules; however, the intravitreal administration of anti-VEGF drugs has several drawbacks, not the least of which is the fact that, due to the short half-life of the drug, frequent intraocular injections are necessary, generating different side effects, such as endophthalmitis and cataracts (Simo et al., 2014; Duh et al., 2017; Zhao and Singh, 2018). In addition, anti-VEGF drugs are used in mid to late stages of DR—when the vascular phenotype becomes evident, the disease is well-established, and vision has been significantly affected. Therefore, new alternative approaches to the current standard are urgently required to develop effective and early treatment options that may counteract the progression of DR at stages preceding the appearance of an evident vessel damage or vessel proliferation.

In addition to, and in contrast with, the view of DR as a purely vascular pathology, several investigations have studied the involvement and the role of retinal neurons in the disease. Indeed, since neurons are the most fragile and demanding cellular elements in the retina, it is conceivable that they are the first to be affected by damage when the microenvironment composition is drastically changed. Consistent with this hypothesis, a large amount of data has been collected in recent years, confirming that considerable damage of retinal neurons is present in early stages of DR (Antonetti et al., 2006; Hernandez and Simo, 2012; Zhang et al., 2013; Jindal, 2015; Simo and Hernandez, 2015; Hernandez et al., 2016b) and that DR may be considered a neurodegenerative disease of the retina (Barber, 2003).

Summarizing the evidence, one can say that both retinal neurons and vessels are affected in DR; therefore, the question is what kind of relationship, if any, exists between neuronal and vascular damage in DR. A first possibility is that there is no relationship and that neurons on one side and vascular elements on the other independently respond to the alterations caused by high glucose. Only at late stages of the disease, when proliferating vessels cause retinal detachment, the vascular pathology would affect neuronal function and survival. This hypothesis seems unlikely because neuronal, glial, and vascular cells are known to be intimately connected in the neurovascular unit, and recently reviewed evidence indicates that glial, neural, and microvascular dysfunctions are interdependent and intimately involved in the development of DR (Hammes, 2018; Simo et al., 2018). In this line, the American Diabetes Association has defined DR as a tissue-specific neurovascular complication involving progressive disruption of the interdependence between multiple cell types in the retina (Solomon et al., 2017; Simo et al., 2018). In particular, the function of the neurovascular unit is precociously affected in DR often before microvascular complications can be appreciated (see Simo and Hernandez, 2015, for references). Therefore, we favor the hypothesis that in DR, retinal neurons are primarily affected and their reaction to stress induces the vascular complications. Supporting this hypothesis, there are observations suggesting that brain damage, together with the activation of death pathways, also stimulates protective mechanisms mediated by chemical signals derived from the injured brain itself (Iadecola and Anrather, 2011). In the case of DR, one of these signals is likely to be represented by VEGF, which would be released by the retina in the early phases of the disease as an immediate response to neuronal stress. Indeed, this growth factor not only is a powerful inducer of vascular responses but is also known to exert important neuroprotective actions in the retina (Azzouz et al., 2004; Saint-Geniez et al., 2008; Romano et al., 2012;

Abbreviations: ACE, Angiotensin-converting enzyme; ADNP, Activity-dependent neurotrophic protein; AGE, Advanced glycation end products; AngI, Angiotensin I; AngII, Angiotensin II; AT1R, Angiotensin type 1 receptor; AT2R, Angiotensin type 2 receptor; BRB, Blood-retina barrier; CaD, Calcium dobesilate; DNMT, DNA methyltransferase; DPP4, Dipeptidyl peptidase 4; DR, Diabetic retinopathy; EPO, Erythropoietin; ERG, Electroretinogram; ET, Endothelin; ETRA, ET type A receptor; ETRB, ET type B receptor; GLP-1, Glucagon-like peptide-1; HIF, Hypoxia-inducible factor; HIF-1α, α subunit of HIF-1; ICAM-1, Intercellular adhesion molecule-1; IL-1β, Interleukin-1β; IL-6, Interleukin-6; NF-κB, Nuclear factor kappa-light-chain-enhancer of activated B cells; Nrf2, Nuclear factor erythroid-2-related factor 2; PACAP, Pituitary adenylate cyclase-activating polypeptide; PAC1, PACAP receptor 1; PPARα, Peroxisome proliferator-activated receptor α; RAS, Renin-angiotensin system; SRIF, Somatotropin release inhibiting factor (or somatostatin); sst, Somatostatin receptor subtype; STZ, Streptozotocin; TNFα, Tumor necrosis factor α; uPA, Urokinase-type plasminogen activator; uPAR, Urokinase-type plasminogen activator receptor; VEGF, Vascular endothelial growth factor; VIP, Vasoactive intestinal peptide; VPAC1, Vasoactive intestinal peptide type 1 receptor; VPAC2, Vasoactive intestinal peptide type 2 receptor; α-MSH, α-Melanocyte-stimulating hormone.

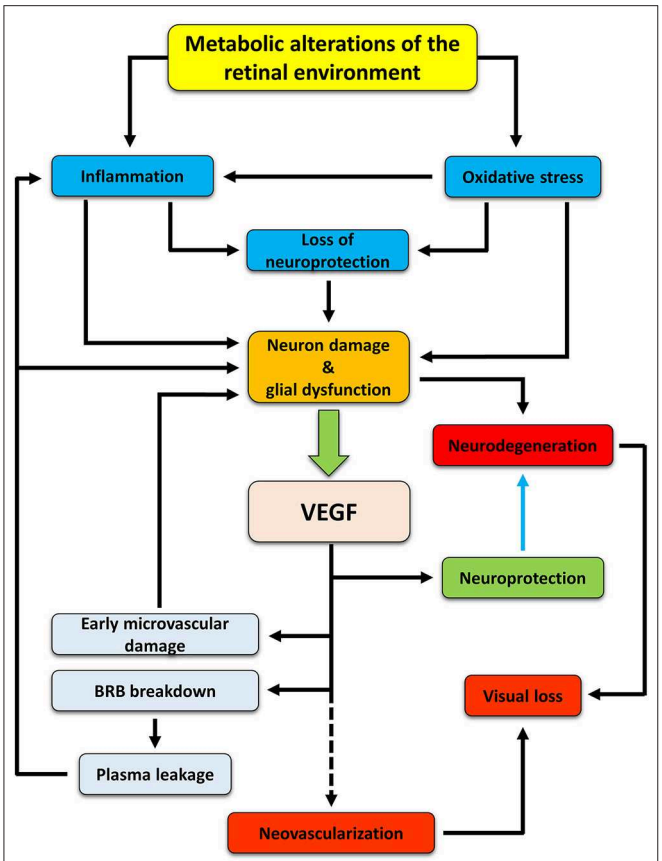

FIGURE 1 | Hypothetic cascade of events occurring in the retina during diabetes and leading to the development of DR. Hyperglycemia induces metabolic changes in the retinal milieu, leading to oxidative stress and inflammation. Oxidative and inflammatory processes cause damages to neuron and glial cells both directly and indirectly by inducing alterations in the production and release of neurotrophic factors. As a consequence, neurodegenerative processes are activated. In an attempt to protect themselves, suffering neurons would trigger production and release of VEGF, mainly by Müller cells, that may act as a neuroprotectant, thus counteracting neurodegeneration (blue arrow). However, if in the early phases of DR VEGF may act as a neuroprotective factor, its prolonged release triggers vascular damages (which, in turn, may reinforce in a different fashion inflammation and retinal damage), ultimately leading to new vessel proliferation. If untreated, neurodegenerative and neovascular processes concur to visual dysfunction, finally leading to vision loss.

Beazley-Long et al., 2013; Foxton et al., 2013; Casini et al., 2014; Hombrebueno et al., 2015; Amato et al., 2016). Consistent with this view, glutamate excitotoxicity, one of the major causes of retinal neuronal death in DR, has been reported to upregulate VEGF production in diabetic retinas (Cervantes-Villagrana et al., 2010), while inhibition of NMDA receptors resulted in decreased vitreoretinal VEGF in diabetic rats (Kusari et al., 2010). In general, it is interesting to note that in studies analyzing VEGF in DR models after treatment with neuroprotectants, a decrease in apoptotic markers is often associated with a decrease in VEGF expression and/or release (see for instance Amato et al., 2016, 2018b).

In summary, our hypothesis is that, in early DR, VEGF is expressed and released to protect retinal neurons. In this phase, VEGF would not act as a proangiogenic but as a prosurvival factor. Then, a prolonged upregulation of VEGF would lead to microvascular lesions and, further on, to the full manifestation of the pathology (**Figure 1**). If our hypothesis is correct, then any retinal stress causing neuronal damage should be accompanied by increased VEGF expression and/or release and by vascular changes. Similarly, any compound with neuroprotective properties should also induce VEGF downregulation and amelioration of the vascular lesions. The present review examined a variety of studies in models of DR and of other retinal diseases to highlight the co-occurrence of neuronal damage and VEGF upregulation (with the appearance of vascular lesions) as well as the concomitant neuroprotection and VEGF downregulation (with the amelioration of vascular lesions) in response to neuroprotective treatments.

METHODOLOGY AND DEFINITIONS

We considered different compounds belonging to different molecular classes but sharing the characteristic of protecting retinal neurons from a variety of stressing conditions. For each compound, a possible correlation between neuroprotective effects and the effects on VEGF expression/release or on vasculopathy has been considered. For the sake of simplicity, only *in vivo* and *ex vivo* studies have been reviewed. A compound was considered "neuroprotective" when it induced a decrease of oxidative stress, inflammation, or apoptotic markers or if it induced an amelioration of retinal function as evaluated, for instance, with electroretinogram (ERG). It was considered "vasoprotective" when it reduced VEGF expression/release, BRB leakage, or vascular lesions (including basement membrane thickening, leukocyte adhesion, occurrence of acellular capillaries, capillary degeneration, pericyte loss). For each compound, papers are first reviewed that documented either neuroprotective or vasoprotective effects of the compound. Then, we considered the papers in which both neuroprotective and vasoprotective effects were documented in the same experimental samples.

NUTRACEUTICALS

The term "nutraceutical" indicates a food (or part of a food) that can provide health benefits, including the prevention and/or treatment of a disease (Brower, 1998). Nutraceuticals are effective antioxidants since they may act as direct scavengers of reactive oxygen species or they may induce the expression of antioxidant enzymes (Milatovic et al., 2016). They may also exert anti-inflammatory effects by inhibiting pathways linked to the production of inflammatory mediators, including those activated by the nuclear factor kappa-light-chain-enhancer of activated B cells (NF-κB) (Aggarwal et al., 2009). These compounds can be used as natural dietary supplements and therefore can be easily administered, are readily available, and are not likely to induce collateral side effects (Chauhan et al., 2013). Nutraceuticals are

known to display neuroprotective effects due to their antioxidant and anti-inflammatory properties and to protect the retina from the vascular damage typical of DR (Rossino and Casini, 2019).

Curcumin

Curcumin is a yellowish polyphenolic substance constituting the major active compound of *Curcuma longa*. It is largely known for its antioxidant and anti-inflammatory properties (Hewlings and Kalman, 2017), and it may have therapeutic potential for retinal diseases (Wang et al., 2013).

Some studies reported beneficial effects of curcumin on the side of retinal neuroprotection. For instance, in rats with streptozotocin (STZ)-induced diabetes (a model of type 1 diabetes), curcumin inhibited retinal oxidative stress, protected Müller cells, and prevented the downregulation of glutamine synthetase, the enzyme involved in glutamate detoxification and recycling, thus protecting the retinal neurons from glutamate excitotoxicity (Zuo et al., 2013). On the other hand, there are data documenting an inhibitory effect of curcumin on diabetes-induced VEGF upregulation in diabetic rat retinas (Mrudula et al., 2007).

Other studies investigated the neuroprotective actions of curcumin together with its effects on VEGF expression and/or retinal vascular lesions. In particular, in STZ diabetic rats, oral curcumin administrations significantly reduced retinal oxidative stress, inflammation, thinning of the retina, and apoptosis, inhibiting, at the same time, VEGF upregulation and thickening of retinal capillary basement membrane (Kowluru and Kanwar, 2007; Gupta et al., 2011; Yang et al., 2018). Similarly, in a rat model of retinal ischemia-reperfusion, curcumin administered with the food inhibited NF-κB activation, with a consequent decrease of pro-inflammatory cytokines, and protected retinal neurons from apoptosis, while it also reduced the retinal capillary degeneration induced by the ischemic treatment (Wang L. et al., 2011).

Resveratrol

Resveratrol is a polyphenol found in different plants, such as grapes, peanuts, and berries. Similar to curcumin, it possesses important antioxidant properties (Gerszon et al., 2014).

There are studies reporting neuroprotective effects, while other investigations describe vasoprotective actions of resveratrol in retinal diseases. Indeed, orally administered resveratrol has been reported to decrease oxidative stress, NF-κB activation, and apoptosis in diabetic rat or mouse retinas (Kim et al., 2010; Soufi et al., 2012). On the other hand, additional studies in mice with STZ-induced diabetes documented the efficacy of resveratrol in decreasing diabetes-induced retinal VEGF upregulation, pericyte loss, and BRB breakdown (Kim et al., 2012).

Different studies have reported concomitant protective effects of resveratrol against diabetes-induced retinal inflammation or apoptosis of retinal cells on one side and VEGF overexpression, BRB leakage, or leukocyte adhesion on the other (Kubota et al., 2011; Sohn et al., 2016; Chen Y. et al., 2019). Similarly, in a mouse model of endotoxin-induced uveitis, resveratrol led to significant and dose-dependent suppression of oxidative stress, NF-κB activation, and leukocyte adhesion (Kubota et al., 2009).

Carotenoids

The carotenoids lutein and zeaxantin are the main constituents of oranges, yellow fruits, and dark green leafy vegetables. Together with meso-zeaxanthin, they form the macular pigment of primate eyes and prevent oxidative damage to the retina (Jia et al., 2017).

Likely due to its antioxidant properties, lutein is a recognized protective agent in the retina. In particular, in models of DR or of light-induced retinal degeneration, lutein was reported to preserve neurotrophin levels, protect retinal cells from apoptosis, and prevent both the oxidative stress and functional visual impairment caused by the disease (Sasaki et al., 2010, 2012; Hu et al., 2012; Ozawa et al., 2012).

Several papers have reported an effect of lutein and zeaxantin favoring both retinal cell protection and retinal function on one hand and inhibition of VEGF increase and vascular lesions on the other. Indeed, in retinas of STZ rats, zeaxantin inhibited the diabetes-induced oxidative stress as well as the upregulation of VEGF and intercellular adhesion molecule-1 (ICAM-1), an indicator of leukocyte adhesion (Kowluru et al., 2008). In addition, in the rat STZ model, a nutritional supplement containing lutein, zeaxantin, and other nutrients preserved retinal function, as evaluated with ERG, and at the same time reduced the diabetes-induced increase of NF-κB activation and interleukin-1β (IL-1β) expression, while it decreased VEGF and capillary degeneration (Kowluru et al., 2014). Similarly, in an obesity-induced high-fat diet rat model, lutein and zeaxantin, or meso-zeaxantin, reduced oxidative stress by promoting the expression of antioxidant enzymes and inhibited NF-κB activation, while they also inhibited VEGF and ICAM-1 upregulation and vascular pathology (Orhan et al., 2016; Tuzcu et al., 2017).

Catechins

Green tea is a popular beverage rich in catechin, epicatechin, epigallocatechin, epicatechin gallate, and epigallocatechin gallate. Among these, epigallocatechin gallate is the most abundant catechin in green tea and possesses antioxidant and anti-inflammatory activities (Chu et al., 2017).

Catechins have been shown to exert powerful anti-inflammatory effects in the retinas of STZ rats by decreasing NF-κB activation and the production of inflammatory factors, such as tumor necrosis factor α (TNFα), IL-6, and IL-1β (Wang N. et al., 2018). In addition, epicatechin has been shown to exert neuroprotective effects in retinas of diabetic rats likely by reducing the production of the precursor form of nerve growth factor (Al-Gayyar et al., 2011). On the vascular side, recent observations reported an effect of epigallocatechin-3-gallate in reducing vascular leakage and permeability in an *in vivo* model of VEGF-induced BRB breakdown (Lee et al., 2014).

There is evidence of concomitant neuroprotective and vasoprotective effects of catechins in rat models of DR. In particular, orally administered green tea was observed to protect the diabetic retina against oxidative stress and promote glutamate uptake by Müller cells. It also preserved retina functionality, as demonstrated by ERG responses, and reduced BRB permeability, as demonstrated by reduced downregulation of occludin, a tight junction protein of the BRB (Silva et al., 2013). In addition,

green tea was observed to prevent not only the diabetes-induced decrease of antioxidant enzymes and the increase of TNFα but also VEGF upregulation and the increase of retinal capillary basement membrane thickness (Kumar et al., 2012a).

Hesperetin

Hesperetin is a flavonoid polyphenol that is commonly present in citrus fruits and has been reported to exert antioxidant effects in diabetic retinas (Rossino and Casini, 2019).

In rodent models of retinal ischemia-reperfusion, hesperetin displayed potent neuroprotective actions as it prevented oxidative stress and apoptosis and preserved retinal layer thickness (Kara et al., 2014; Shimouchi et al., 2016). In addition, in retinas of STZ-treated rats, hesperetin administrations significantly reduced VEGF overexpression, BRB leakage, and pathologic vascular changes (Kumar et al., 2012b).

There is only one report in the literature concerning neuroprotective and vasoprotective effects of hesperetin in the same experimental material. In retinas of STZ-induced diabetic rats, orally administered hesperetin was effective in promoting antioxidant enzyme expression and preventing the increase of the pro-inflammatory cytokines TNFα and IL-1β and of apoptotic markers, while a protective effect of limiting the increase of basement membrane thickness was also reported (Kumar et al., 2013).

Other Nutraceuticals

There are a number of additional nutraceuticals that have been sporadically reported to exert both neuroprotective and vasoprotective effects, mostly in models of DR.

Quercetin, a common flavonoid polyphenol found in vegetables and fruits, has been reported to protect the diabetic retina from oxidative stress, inflammation, and histopathologic changes (Kumar et al., 2014; Ola et al., 2017) probably by promoting the expression of neurotrophic factors (Ola et al., 2017). Notably, quercetin has also been reported to prevent diabetes-induced retinal VEGF upregulation (Chen B. et al., 2017). Chrysin, another natural flavonoid, is found in herbs and honeycomb. It may exert neuroprotective effects since it has been shown recently to protect retinal photoreceptors by maintaining valid retinoid visual cycle-related components in the retinal pigment epithelium of diabetic rats (Kang et al., 2018). It has also been observed to inhibit VEGF upregulation, BRB leakage, and vascular lesions in the retinas of diabetic *db/db* mice (Kang et al., 2016). Anthocyanins constitute a further class of flavonoids, which are responsible for the red or blue color of plants, fruits, and flowers. Blueberry anthocyanins have been observed to protect diabetic rat retinas from oxidative stress and decrease VEGF levels in these same retinas (Song et al., 2016), while a *Vaccinium myrtillus* extract, containing large amounts of anthocyanins, reduced VEGF expression and preserved BRB integrity in retinas of STZ rats (Kim et al., 2015).

Different compounds have been described to exert at the same time neuroprotective and vasoprotective effects. For instance, eriodictyol, one of the most abundant dietary flavonoids, administered to STZ rats inhibited the retinal expression of the pro-inflammatory cytokine TNFα, while it also decreased the retinal levels of VEGF and of ICAM-1 and suppressed BRB breakdown (Bucolo et al., 2012). In both an *ex vivo* mouse model of retinal oxidative stress and the *in vivo* STZ rat model, Lisosan G, a fermented powder obtained from organic whole grains, has been described recently to exert powerful antioxidant, antiapoptotic, and anti-inflammatory actions. It also preserved retinal function, as evaluated with ERG. Concurrently, it inhibited upregulation of retinal VEGF and prevented BRB breakdown (Amato et al., 2018b). Similarly, an ethanolic extract of *Morus alba* leaves displaying high free radical scavenging activity reduced oxidative stress, inflammation, apoptosis, and VEGF expression in retinas of STZ rats (Mahmoud et al., 2017). Also, the traditional Chinese prescription *Tang Wang Ming Mu* granule has been found to protect diabetic rat retinas from oxidative stress and inflammation reducing at the same time retinal VEGF levels and vascular changes (Chen M. et al., 2017). Finally, kaempferol, a flavonol found in tea, broccoli, apples, strawberries, and beans, protected rat retinas from sodium iodate-induced retinal degeneration by reducing histopathologic changes and apoptosis, while it also reduced the upregulated VEGF protein expression (Du et al., 2018).

Taken together, these studies with nutraceuticals documented an action of these compounds that was at the same time both neuroprotective and vasoprotective. Indeed, the data, prevalently obtained in rodent models of DR, revealed that nutraceuticals, acting as antioxidant and/or as anti-inflammatory agents, not only are effective in reducing retinal neurodegeneration but also prevent the deleterious increase of VEGF levels and consequent vascular lesions.

ANTIOXIDANTS

The nutraceuticals discussed above display important antioxidant capabilities, but other antioxidant compounds have been also described, which may act in retinal diseases and protect both retinal neurons and vessels.

Calcium Dobesilate

Calcium dobesilate (CaD) is an oxygen free radical scavenger (Brunet et al., 1998; Szabo et al., 2001). It is considered a vasoprotective drug, and it has been approved for the treatment of DR in several countries for many years (Tejerina and Ruiz, 1998; Berthet et al., 1999); however, it has not been widely used in clinical practice. In effect, CaD exerts multifaceted actions contrasting neurovascular unit impairment, and therefore, it can be considered a good candidate drug for targeting the early stages of DR. In particular, the effects of CaD in DR have been recently reviewed, and they include (i) reduction of capillary permeability and consequent BRB leakage; (ii) inhibition of endothelial cell apoptosis; (iii) antioxidant activity and protection against reactive oxygen species; and (iv) inhibition of the expression of VEGF and ICAM-1 (Zhang et al., 2015).

In retinas of *db/db* mice (a model of type 2 diabetes) and in retinas of STZ rats, CaD significantly reduced biomarkers of oxidative stress and NF-κB activation with consequent decrease of pro-inflammatory cytokines, such as TNFα, IL-1β, IL-6, and IL-8 (Bogdanov et al., 2017; Voabil et al., 2017). In addition, in

STZ rats, CaD reduced vascular leakage and VEGF expression (Rota et al., 2004). Both neuroprotective and vasoprotective effects of CaD have been described in diabetic retinas. Indeed, in retinas of STZ rats, in addition to protective effects against oxidative stress, inflammation, and retinal thinning, CaD has been reported to exert inhibitory effects against diabetes-induced BRB breakdown, downregulation of tight junction protein expression, increased VEGF and ICAM-1 expression, and leukocyte adhesion (Leal et al., 2010). In retinas of *db/db* diabetic mice, CaD significantly decreased diabetes-induced oxidative stress and retinal cell apoptosis. In addition, it reduced glutamate extracellular concentration, by preventing glutamate transporter downregulation, and improved ERG responses. At the same time, CaD inhibited VEGF upregulation and vascular leakage (Sola-Adell et al., 2017).

Other Antioxidants

It is clear that suppression of antioxidant defenses is deleterious to the retina. For this reason, recent studies have focused on the ability of some antioxidant compounds to regulate antioxidant gene expression, such as the nuclear factor erythroid-2-related factor 2 (Nrf2) activator dh404 and a DNA methyltransferase (DNMT) inhibitor.

Nrf2 is a redox-sensitive transcription factor that is kept in a latent state until an increase in free radical concentration releases Nrf2, which enters the cell nucleus and initiates the transcription of antioxidant genes (Di Marco et al., 2015). Boosting Nrf2 with a specific activator increases the transcription of antioxidant genes and therefore may protect tissues from oxidative damage. In retinas of STZ rats, the Nrf2 activator dh404 has been reported not only to decrease oxidative stress and the expression of inflammatory mediators but also to prevent VEGF upregulation and vascular leakage (Deliyanti et al., 2018).

It has been observed that DNA methylation may be involved in the regulation of gene expression in the retina during the progression of DR (Kowluru et al., 2015; Mishra and Kowluru, 2016, 2019). In particular, DNMT inhibitors may favor the expression of antioxidant genes. Indeed, in diabetic rat retinas, DNMT inhibition restored antioxidant enzyme expression and, in parallel, also prevented the diabetes-induced increase of VEGF and of ICAM-1 expression (Xie et al., 2019).

These observations on the effects of antioxidant compounds in models of DR indicate that reduction of oxidative stress is accompanied by positive effects on the vascular pathology and therefore favors both neuroprotective and vasoprotective actions.

NEUROPEPTIDES

Neuropeptides are short to medium amino acid chains, which function primarily as complementary signals to "classic" neurotransmitters to fine-tune neurotransmission (Hokfelt et al., 2003). Some of them have been found to be important for the regulation of cell death/survival in different neuronal systems, where they express important neuroprotective properties (Catalani et al., 2017; Reglodi et al., 2017; Chen X.Y. et al., 2019). Neuropeptides and their receptors are widely expressed in mammalian retinas, where they exert multifaceted functions both during development and in the mature animal (Bagnoli et al., 2003). In particular, some of them may exert important roles in retinal diseases (Gabriel, 2013; Cervia et al., 2019).

Glucagon-Like Peptide-1

Glucagon-like peptide-1 (GLP-1) is known as a hormone secreted by the gastrointestinal tract in response to food, stimulating insulin and inhibiting glucagon secretion (Drucker and Nauck, 2006). GLP-1 has also been recognized as a neuropeptide. Indeed, GLP-1 and its receptor GLP-1R are expressed in the brain, where they influence multiple neural circuits modulating feeding behavior and reward (Smith et al., 2019). Both GLP-1 and GLP-1R are expressed in mammalian retinas (Zhang et al., 2009; Zhang Y. et al., 2011; Hernandez et al., 2016a; Cai et al., 2017; Hebsgaard et al., 2018).

Neuroprotective effects of GLP-1R activation have been demonstrated in a rat model of optic nerve crush, where intravitreal implants of beads with genetically modified cells producing GLP-1 decreased apoptosis and promoted survival of retinal ganglion cells (Zhang R. et al., 2011), and in diabetic rats, where exendin-4, an analog of GLP-1, protected from oxidative stress from apoptotic cell death and ameliorated retinal function as assessed with ERG (Zhang et al., 2009; Zhang Y. et al., 2011; Fan et al., 2014b; Zeng et al., 2016; Cai et al., 2017; Cervia et al., 2019). Most importantly, both neuroprotective and vasoprotective effects of GLP-1 agonists have been described in models of retinal diseases. For instance, in a rat model of retinal ischemia-reperfusion, exendin-4 suppressed inflammatory gene expression and reduced BRB permeability (Goncalves et al., 2016). Strong evidence for a double action of GLP-1 as a neuroprotectant and vasoprotectant also comes from studies in models of DR. Indeed, recent studies in rodent retinas have reported that GLP-1 or GLP-1R agonists may exert a neuroprotective action since they improved retinal function, as assessed with ERG, protected retinal cells from death, reduced oxidative stress and IL-1β expression, and inhibited the increase of extracellular glutamate. At the same time, these compounds induced vasoprotection since they decreased VEGF levels, preserved the expression of tight junction proteins of the BRB, reduced BRB leakage, and inhibited the increase of ICAM-1 levels (Fan et al., 2014a; Hernandez et al., 2016a; Sampedro et al., 2019).

Similar to GLP-1R agonists, inhibitors of dipeptidyl peptidase 4 (DPP4, the GLP-1 degrading enzyme) have been tested for their potential use in DR treatments. The data of different studies indicated that DPP4 inhibitors, such as linagliptin, saxagliptin, or sitagliptin, efficiently increase retinal GLP-1 levels and that this increase, in rodent models of DR, is correlated with reduced oxidative stress, inflammation (as assessed by IL-1β levels), extracellular glutamate levels and neuronal apoptosis and with preservation of retinal function. At the same time, DPP4 inhibitors induced amelioration of different vascular features, including diabetes-induced changes in the subcellular distribution of the tight junction proteins occludin, claudin-5, and zonula occludens-1; BRB breakdown; ICAM-1 upregulation; pericyte loss; and formation of acellular capillaries (Goncalves et al., 2012, 2014; Dietrich et al., 2016; Hernandez et al., 2017).

Somatostatin

Somatostatin (somatotropin release inhibiting factor, SRIF) is expressed in the retina, together with its five receptor subtypes (named sst1-5), where they express important physiological functions (Casini et al., 2005; Cervia et al., 2008a). Low vitreous levels and low intraocular production of SRIF have been found in patients with diabetic macular edema, chronic uveitis macular edema, and quiescent intraocular inflammation (Simo et al., 2007; Fonollosa et al., 2012), suggesting that SRIF alterations may be directly involved in the pathogenesis of these conditions. In addition, a variety of experimental observations suggested that SRIF may exert powerful neuroprotective effects in different retinal diseases (Cervia et al., 2008a; Cervia and Casini, 2013; Hernandez et al., 2014; Wang et al., 2017).

The SRIF analog pasireotide and SRIF receptor agonists targeting the sst2 or sst5 receptors were found to significantly protect rat retinal neurons in *in vivo* models of AMPA excitotoxicity (Kiagiadaki and Thermos, 2008; Kiagiadaki et al., 2010; Kokona et al., 2012). In addition, in a retinal ischemia-reperfusion mouse model, SRIF mediated the neuroprotective and anti-inflammatory effects of capsaicin, a selective agonist for transient receptor potential vanilloid type-1, a ligand-gated non-selective cation channel (Wang et al., 2017). Moreover, in retinas of STZ rats, topical SRIF administrations prevented glutamate accumulation, apoptosis, and ERG abnormalities (Hernandez et al., 2013). Similarly, studies in *ex vivo* ischemic retinas of mice or rats reported that SRIF, its analogs, or the constitutive activation of the sst2 receptor significantly preserved retinal neurons from ischemia-induced morphological changes and apoptosis (Catalani et al., 2007; Cervia et al., 2008b; Kokona et al., 2012). Moreover, in retinal explants in which hypoxic conditions induced the expression of apoptotic markers, the sst2-preferring SRIF analog octreotide reduced apoptotic signals (Dal Monte et al., 2012). Finally, in *ex vivo* explants of mouse retinas treated with high glucose, octreotide prevented apoptosis of retinal neurons, likely stimulating an increase of the autophagic flux (Amato et al., 2018a). Interestingly, a study in *ex vivo* ischemic mouse retinas reported that acute ischemia induces a sudden increase in VEGF release from neurons, suggesting that VEGF may represent a stress signal released by retinal neurons when their integrity is threatened. Supporting this view, the neuroprotective SRIF analog octreotide reduced VEGF release from ischemic retinas (Cervia et al., 2012).

Some studies reported concomitant effects of SRIF, or its analogs, on neuroprotection and vasoprotection. For instance, in a mouse model of retinal ischemia-reperfusion, octreotide has been reported to protect from oxidative stress, inflammation (as assessed by NF-κB activation), and neuronal death, while it also significantly reduced ICAM-1 expression, indicating decreased leukocyte adhesion (Wang et al., 2015). In *ex vivo* ischemic mouse retinas, octreotide inhibited the ischemia-induced increase of oxidative stress, glutamate levels, apoptosis, and VEGF expression (D'alessandro et al., 2014). Similar observations were reported in *ex vivo* mouse retinal explants challenged with high glucose, oxidative stress, or advanced glycation end products (AGE), toxic products that accumulate under hyperglycemic conditions and that are likely to play an important role in the pathogenesis of DR. In particular, these studies showed that protecting retinal neurons from diabetic stress also reduces VEGF expression and release, while inhibiting VEGF leads to exacerbation of apoptosis (Amato et al., 2016). Therefore, the retina in early DR may release VEGF as a prosurvival factor, and a neuroprotective agent such as octreotide may decrease the need of VEGF production by the retina, therefore limiting the vasculopathy associated with VEGF upregulation.

Angiotensin

The renin-angiotensin system (RAS) is involved in the regulation of blood pressure. Angiotensin I (AngI) is generated from the proteolytic cleavage of angiotensinogen, a reaction catalyzed by the enzyme renin. AngI is further processed by angiotensin-converting enzyme (ACE) and ACE2 to angiotensin II (AngII), the main effector of the RAS, acting at the angiotensin type 1 and type 2 receptors (AT1R and AT2R) (Fletcher et al., 2010). A local RAS is present in the retina, where RAS components have been localized to different retinal cell types, including retinal neurons and Müller cells (Wilkinson-Berka et al., 2012). A variety of studies have shown that reduction of AngII expression or blockade of AT1R on the one hand, or stimulation of ACE2 on the other, may reduce the retinal damage occurring in retinal pathologies, such as glaucoma, retinal ischemia, autoimmune uveitis, or DR (Cervia et al., 2019).

Several investigations have provided evidence for a neuroprotective role exerted by AT1R inhibitors in different models of retinal diseases. For instance, inhibitors like valsartan, losartan, or candesartan were effective in attenuating light-induced retinal damage in mice by reducing oxidative stress and improving ERG responses (Narimatsu et al., 2014). Similarly, candesartan prevented ganglion cell loss, thinning of the retina, and ERG deficits in a retinal excitotoxicity mouse model (Semba et al., 2014). In mice with increased intraocular pressure, used as models of glaucoma or ischemia-reperfusion, AT1R blockade reduced oxidative stress, inhibited the increase of extracellular glutamate, and mitigated ganglion cell loss (Yang et al., 2009; Fujita et al., 2012; Liu et al., 2012; Quigley et al., 2015). In rats or mice with STZ-induced diabetes, blockers of AT1R, in addition to protecting the retina from oxidative stress, apoptotic cell death, and histopathologic damage (Silva et al., 2009; Ola et al., 2013; Thangaraju et al., 2014), also preserved mitochondrial integrity, increased the expression of neurotrophic factors, and improved functional ERG responses (Silva et al., 2009; Ozawa et al., 2011; Ola et al., 2013). In experimental models of mouse autoimmune uveitis or endotoxin-induced uveitis, the delivery of different formulations of ACE2 and/or its product Ang(1-7) or the administration of an ACE2 activator reduced retinal inflammation (Qiu et al., 2014, 2016; Shil et al., 2014) and prevented histologic damage as well as ERG abnormalities (Qiu et al., 2016). Similarly, both in an experimental glaucoma model and in STZ rats, retinal ganglion cells were protected from apoptotic cell death by the administration of an ACE2 activator (Foureaux et al., 2013, 2015). On the vascular side, in retinas of STZ rats evidence was provided of an inhibitory effect on VEGF

expression and on leukocyte adhesion exerted by a prorenin receptor blocker (Satofuka et al., 2009).

There are a few studies documenting concomitant effects of the Ang system both on the side of neuroprotection and on that of vasoprotection. One study reported that in diabetic rats, increased plasma prorenin levels exacerbated the expression of inflammatory cytokines, retinal apoptotic cell death, as well as the formation of acellular capillaries, while a prorenin receptor blocker significantly reduced these effects (Batenburg et al., 2014). Similarly, adeno-associated virus-mediated gene delivery of ACE2 or Ang(1-7) significantly reduced diabetes-induced oxidative damage, inflammation, retinal vascular leakage, and formation of acellular capillaries in both diabetic mice and rats (Verma et al., 2012).

These data support the possibility that the documented neuroprotective actions of AngII blockade or ACE2 stimulation also influence the vascular pathology and induce an amelioration of the vascular traits (VEGF upregulation, acellular capillaries, leukocyte adhesion, BRB breakdown) especially in models of DR.

Pituitary Adenylate Cyclase-Activating Polypeptide and Vasoactive Intestinal Peptide

Pituitary adenylate cyclase-activating polypeptide (PACAP) and vasoactive intestinal peptide (VIP) belong to the same peptide superfamily, which also includes secretin and glucagon. The PACAP receptors can be classified into two groups: PACAP receptor 1 (PAC1), which binds PACAP with higher affinity than VIP, and vasoactive intestinal polypeptide receptors (VPAC1 and VPAC2), which bind PACAP and VIP with similar affinities (Vaudry et al., 2009).

PACAP and PAC1R have been detected in the retina, where they are involved in neurotransmission, neuromodulation, and, mostly, neuroprotective functions (Nakamachi et al., 2012). VPAC2 expression has also been reported in the mouse retina (Harmar et al., 2004). The retinoprotective effects of PACAP have been the subject of a variety of studies, and these data have been excellently reviewed (Atlasz et al., 2010; Nakamachi et al., 2012; Shioda et al., 2016). Further evidence has been provided by more recent studies. Indeed, PACAP has been shown to inhibit apoptosis and promote survival of retinal ganglion cells in different models of retinal injury (Lakk et al., 2015; Ye et al., 2019). In addition, intravitreal or topical administrations of PACAP or a PAC1 agonist to ischemic retinas *in vivo* ameliorated ERG responses, prevented inflammation, and reduced the thinning of retinal layers and the loss of cells in the ganglion cell layer (Danyadi et al., 2014; Vaczy et al., 2016; Werling et al., 2017; Atlasz et al., 2018). Similarly, PACAP intraocular delivery in rats with STZ-induced diabetes protected the retina from apoptosis and maintained retinal synaptic integrity (Szabadfi et al., 2014, 2016). PACAP was also demonstrated to contrast the diabetes-induced modifications of the expression of hypoxia-inducible factors (HIFs), among which HIF-1 is the main regulator of VEGF expression (D'amico et al., 2015).

Both neuroprotective and vasoprotective effects of PACAP have been documented in retinas of STZ rats and in ischemic retinas *in vivo*, where PACAP reduced thinning of retinal layers and prevented the expression of both inflammatory cytokines and VEGF (Werling et al., 2016; D'amico et al., 2017b). In addition, in an *ex vivo* model of retinal ischemia, PACAP effectively decreased oxidative stress, glutamate accumulation, inflammatory mediators, and apoptosis. At the same time, it also decreased VEGF expression, which was upregulated in the ischemic retina (D'alessandro et al., 2014). Finally, in *ex vivo* retinal explants stressed with high glucose, oxidative stress, or AGE, the strong PACAP antiapoptotic effects were paralleled by inhibition of the stress-induced increase of VEGF expression and release (Amato et al., 2016).

VIP is expressed in the retina in a population of amacrine cells (Perez De Sevilla Muller et al., 2019). It has been reported to reduce retinal neurodegeneration caused by ischemia-reperfusion injury, promoting an antioxidant effect (Tuncel et al., 1996). The neuroprotective effects of VIP may be mediated by activity-dependent neurotrophic protein (ADNP) (Bassan et al., 1999; Zusev and Gozes, 2004; Giladi et al., 2007). Indeed, both ADNP and an 8-amino acid peptide derived from ADNP (referred to as NAP) display important neuroprotective activities (Magen and Gozes, 2014). Interestingly, NAP seems to exert protective effects against both the neural and the vascular pathology induced by DR, as it reduced inflammation (D'amico et al., 2019) and apoptosis (Scuderi et al., 2014) as well as the levels of the α subunit of HIF-1 (HIF-1α) and VEGF in retinas of rats with STZ-induced diabetes (D'amico et al., 2017a).

Other Peptides

α-Melanocyte-stimulating hormone (α-MSH) is a widely-distributed 13-amino acid peptide derived from proteolytic cleavage of proopiomelanocortin (Wardlaw, 2011). It acts at five subtypes of G protein-coupled receptors designated MC1R to MC5R (Yang, 2011). α-MSH protected the rat retina from both functional and structural damage induced by ischemia-reperfusion (Varga et al., 2013), suppressed inflammation and maintained retinal structure in a mouse model of experimental autoimmune uveitis (Edling et al., 2011), and protected photoreceptors from degeneration in a rat model of retinal dystrophy (Naveh, 2003). In a rat model of STZ-induced diabetes, intravitreal injections of α-MSH reduced oxidative stress, inflammation, and apoptosis, while they also inhibited the expression of ICAM-1 (Zhang et al., 2014), indicating reduced leukostasis. In early diabetic retinas, α-MSH also reduced inflammation, ameliorated ERG responses, and reduced retinal thinning, while it inhibited BRB breakdown and vascular leakage, likely acting at MC4R (Cai et al., 2018).

Endothelin (ET) is a potent vasoconstrictor composed of three isoforms designated ET-1, ET-2, and ET-3, whose actions are mediated by the ET type A receptor (ETRA) and ET type B receptor (ETRB) (Davenport et al., 2016). There are indications that ET activity may be involved in DR, and evidence has been provided that ET inhibition may ameliorate the pathologic signs of DR. Indeed, an ETRA antagonist has been reported to block the diabetes-induced upregulation of both VEGF and ICAM-1 in retinas of STZ rats (Masuzawa et al., 2006), while other observations have described positive effects of ETR inhibition on

both neuronal and vascular changes seen in DR. For instance, ETRA and/or ETRB inhibitors reduced retinal thinning, the number of apoptotic cells, and the levels of the pro-inflammatory cytokine TNFα in diabetic rat retinas, and at the same time they also reduced pericyte loss, capillary degeneration, vascular leakage, and the levels of both VEGF and ICAM-1 (Chou et al., 2014; Alrashdi et al., 2018; Bogdanov et al., 2018).

Erythropoietin (EPO) stimulates erythroid progenitor cell and early erythroblast maturation and is mainly used in anemia treatment (Jelkmann, 2013). EPO is expressed in the retina (Hernandez et al., 2006; Fu et al., 2008), where it exerts well-documented neuroprotective functions (Kilic et al., 2005; Chung et al., 2009; Colella et al., 2011; Chang et al., 2013). Both neuroprotective and vasoprotective actions of EPO have been described. Indeed, in retinas of STZ rats, EPO was reported to significantly decrease oxidative stress, apoptotic neurodegeneration, and retinal thinning on one hand, and VEGF upregulation, BRB breakdown, and pericyte loss on the other (Zhang et al., 2008; Wang et al., 2010; Wang Q. et al., 2011). Similarly, carbamylated erythropoietin, an EPO derivative, protected diabetic rat retinas from retinal thinning, neuron apoptosis, and functional deficits as evaluated with ERG, while it also reduced VEGF upregulation and vascular leakage (Liu et al., 2015).

In addition to the peptides cited above, some evidence exists for an effect of a few other peptides that is both neuroprotective and vasoprotective. Indeed, antioxidative, anti-inflammatory, and/or antiapoptotic actions together with effects preventing VEGF upregulation and/or BRB breakdown have been described for the peptides growth hormone-releasing hormone (Thounaojam et al., 2017), insulin (Rong et al., 2018), melatonin (Djordjevic et al., 2018), substance P (D'alessandro et al., 2014), and vasoinhibins (Garcia et al., 2008; Arredondo Zamarripa et al., 2014).

Together, these data demonstrate that, similar to the nutraceuticals and antioxidants reviewed above, the powerful neuroprotective effects exerted by different classes of neuropeptides also result in VEGF downregulation and attenuation of the vascular damage in various models of retinal disease.

OTHER FACTORS

The urokinase-type plasminogen activator (uPA) receptor (uPAR) is a glycosylphosphatidylinositol-anchored receptor activated by uPA. uPAR lacks a transmembrane domain, however, it can activate intracellular signaling pathways through lateral interactions with other cell surface receptors, including integrins, G-protein–coupled receptors, and receptor tyrosine kinases, thus forming a system that is involved in many pathological processes, including retinal diseases (Cammalleri et al., 2019b). Recently, the inhibition of the uPAR system has been found to be effective in slowing down cone degeneration and visual dysfunction in a mouse model of retinitis pigmentosa (Cammalleri et al., 2019a). Of interest for this review, in two different models of DR, the STZ rat model mimicking type 1 diabetes (Navaratna et al., 2008; Cammalleri et al., 2017b) and the Torii rat model mimicking type 2 diabetes (Cammalleri et al., 2017a), inhibiting the uPAR system not only ameliorated diabetes-induced ERG dysfunction and reduced inflammation and apoptosis but also resulted in inhibition of VEGF upregulation and BRB breakdown.

Brimonidine is an α2 adrenergic agonist with extensively documented neuroprotective effects in a variety of models of retinal disease (see for instance Guo et al., 2015; Marangoz et al., 2018). In addition, in retinas of rats with STZ-induced diabetes, it has been reported to induce a significant decrease of VEGF expression and of BRB breakdown to levels similar to those observed in control rats (Kusari et al., 2010). Furthermore, in a mouse model of ischemic optic neuropathy, topically applied brimonidine not only reduced oxidative stress and ganglion cell loss but also decreased HIF-1α and VEGF expression (Goldenberg-Cohen et al., 2009).

Peroxisome proliferator-activated receptor α (PPARα), a hormone-activated nuclear receptor, is known as an important modulator of lipid metabolism (Pyper et al., 2010), which also possesses anti-inflammatory and antioxidant properties (Li et al., 2005; Simo and Hernandez, 2009). The PPARα agonist fenofibrate has been used clinically as a triglyceride-lowering drug. However, it seems that downregulation of PPARα in the retina plays a major role in the pathogenesis of DR (Hu et al., 2013), and two independent perspective clinical trials demonstrated that fenofibrate had unprecedented therapeutic effects in DR (Keech et al., 2007; Chew et al., 2010). Emerging evidence suggests that fenofibrate exerts a broad range of beneficial effects on diabetic complications acting against oxidative stress, inflammation, cell death, and angiogenesis (Noonan et al., 2013). In particular, in rodent models of DR, different studies documented the protective effects of fenofibrate or another PPARα agonist against oxidative stress, inflammation, retinal cell death, and decreased retinal function on one hand, and VEGF upregulation, vascular leakage, thickening of capillary basement membrane, ICAM-1 expression, and leukostasis on the other (Chen et al., 2013; Deng et al., 2017; Li et al., 2018; Liu et al., 2018, 2019; Wang N. et al., 2018; Qiu et al., 2019).

Acetaldehyde dehydrogenase 2 is a rate-limiting enzyme for alcohol metabolism, which has been shown to exert neuroprotective effects (Deza-Ponzio et al., 2018). In retinas of STZ rats, it has been reported to promote antioxidant enzyme activity, reduce the expression of proinflammatory cytokines, ameliorate ERG, and significantly reduce VEGF expression (He et al., 2018).

The last example, in this review, of a neuroprotective factor that also ameliorates vascular changes in retinal disease is not concerned with a compound but involves a procedure. Indeed, it is known that ischemic conditioning can be considered a form of protection against ischemic injury through the initiation of endogenous protective mechanisms (Heusch, 2013; Li et al., 2017). As expected, in retinas of STZ rats, ischemic conditioning produced anti-inflammatory and antioxidant effects, and it also protected ganglion cells from death. Interestingly, diabetic retinas treated with ischemic conditioning also showed a significantly downregulated VEGF protein expression (Ren et al., 2018).

TABLE 1 | Summary of the neuroprotective and vasoprotective effects of different compounds in models of retinal disease.

		Neuroprotection				Vasoprotection			References
	Compound	***OS****	***IF****	***APO****	***FUNC****	***VASC****	***BRB***	***VEGF***	
	Curcumin	○	○						Zuo et al., 2013
								○	Mrudula et al., 2007
		●	●					●	Kowluru and Kanwar, 2007
			●	●		●			Wang L. et al., 2011
		●	●					●	Gupta et al., 2011
		●		●		●		●	Yang et al., 2018
	Resveratrol			○					Kim et al., 2010
		○	○	○					Soufi et al., 2012
						○	○	○	Kim et al., 2012
		●	●			●			Kubota et al., 2009
			●			●		●	Kubota et al., 2011
			●				●		Sohn et al., 2016
			●	●			●	●	Chen Y. et al., 2019
	Carotenoids	○		○					Sasaki et al., 2010
					○				Hu et al., 2012
				○	○				Ozawa et al., 2012
				○					Sasaki et al., 2012
		●				●		●	Kowluru et al., 2008
			●		●	●		●	Kowluru et al., 2014
		●	●			●		●	Orhan et al., 2016; Tuzcu et al., 2017
	Catechins			○					Al-Gayyar et al., 2011
			○						Wang W. et al., 2018
							○		Lee et al., 2014
		●	●			●		●	Kumar et al., 2012a
		●			●		●		Silva et al., 2013
	Hesperetin			○					Kara et al., 2014
		○		○					Shimouchi et al., 2016
						○	○	○	Kumar et al., 2012b
		●	●	●		●			Kumar et al., 2013
	Quercetin	○	○	○					Kumar et al., 2014
				○					Ola et al., 2017
								○	Chen B. et al., 2017
	Chrysin				○				Kang et al., 2018
						○	○	○	Kang et al., 2016
	Anthocyanins						○	○	Kim et al., 2015
		●						●	Song et al., 2016
	Eriodictyol		●			●	●	●	Bucolo et al., 2012
	Lisosan G	●	●	●	●		●	●	Amato et al., 2018b
	Morus alba	●	●	●				●	Mahmoud et al., 2017
	Tang Wang Ming Mu	●	●			●		●	Chen M. et al., 2017
	Kaempferol			●				●	Du et al., 2018
Antioxidants	Calcium dobesilate	○	○						Bogdanov et al., 2017; Voabil et al., 2017
							○	○	Rota et al., 2004
		●	●	●		●	●		Leal et al., 2010
		●		●	●		●	●	Sola-Adell et al., 2017
	Nrf2 activator	●	●				●	●	Deliyanti et al., 2018

(Continued)

TABLE 1 | Continued

		Neuroprotection				Vasoprotection			References
	Compound	***OS****	***IF****	***APO****	***FUNC****	***VASC****	***BRB***	***VEGF***	
	DNMT inhibitor	●				●		●	Xie et al., 2019
Neuropeptides	GLP-1			○	○				Zhang et al., 2009; Zhang Y. et al., 2011; Fan et al., 2014b
				○					Zhang R. et al., 2011
		○		○	○				Zeng et al., 2016
		○		○					Cai et al., 2017
		●	●	●			●		Goncalves et al., 2012
		●	●		●	●	●	●	Fan et al., 2014a
			●	●			●		Goncalves et al., 2014
		●	●	●		●			Dietrich et al., 2016
			●				●		Goncalves et al., 2016
		●	●	●	●	●	●	●	Hernandez et al., 2016a
			●	●	●		●		Hernandez et al., 2017
			●	●	●		●	●	Sampedro et al., 2019
	SRIF			○					Catalani et al., 2007; Cervia et al., 2008b; Kiagiadaki and Thermos, 2008; Kiagiadaki et al., 2010; Dal Monte et al., 2012; Kokona et al., 2012; Amato et al., 2018a
				○	○				Hernandez et al., 2013
			○	○					Wang et al., 2017
								○	Cervia et al., 2012
		●		●				●	D'alessandro et al., 2014; Amato et al., 2016
		●	●	●		●			Wang et al., 2015
	Ang	○		○					Silva et al., 2009; Fujita et al., 2012; Ola et al., 2013
				○					Yang et al., 2009; Liu et al., 2012; Foureaux et al., 2013, 2015; Thangaraju et al., 2014; Quigley et al., 2015
		○		○	○				Narimatsu et al., 2014
				○	○				Semba et al., 2014
			○						Qiu et al., 2014; Shil et al., 2014
			○	○	○				Qiu et al., 2016
						○		○	Satofuka et al., 2009
		●	●			●	●		Verma et al., 2012
			●	●		●			Batenburg et al., 2014
	PACAP				○				Danyadi et al., 2014
					○				Szabadfi et al., 2014
			○	○					Vaczy et al., 2016
				○					Lakk et al., 2015; Szabadfi et al., 2016; Werling et al., 2017; Atlasz et al., 2018; Ye et al., 2019
		●		●				●	D'alessandro et al., 2014

(Continued)

TABLE 1 | Continued

		Neuroprotection				Vasoprotection			References
	Compound	***OS****	***IF****	***APO****	***FUNC****	***VASC****	***BRB***	***VEGF***	
				●				●	Amato et al., 2016; Werling et al., 2016
			●					●	D'amico et al., 2017b
	VIP			○					Tuncel et al., 1996
	VIP/NAP			○					Scuderi et al., 2014
			○						D'amico et al., 2019
								○	D'amico et al., 2017a
	α-MSH			○					Naveh, 2003
			○	○					Edling et al., 2011
		○		○	○				Varga et al., 2013
		●	●	●		●			Zhang et al., 2014
			●	●	●	●	●		Cai et al., 2018
	ET					○		○	Masuzawa et al., 2006
				●		●			Chou et al., 2014
			●				●	●	Alrashdi et al., 2018
			●	●				●	Bogdanov et al., 2018
	Erythropoietin			●			●		Zhang et al., 2008
		●				●			Wang et al., 2010
				●		●		●	Wang Q. et al., 2011
				●	●		●	●	Liu et al., 2015
	GHRH*	●	●	●			●	●	Thounaojam et al., 2017
	Insulin		●	●			●	●	Rong et al., 2018
	Melatonin	●						●	Djordjevic et al., 2018
	Substance P	●		●				●	D'alessandro et al., 2014
	Vasoinhibins						○		Garcia et al., 2008
		●					●		Arredondo Zamarripa et al., 2014
Other factors	uPAR		○	○	○				Cammalleri et al., 2019a
							○		Navaratna et al., 2008
			●	●	●		●	●	Cammalleri et al., 2017a
			●		●		●	●	Cammalleri et al., 2017b
	Brimonidine						○	○	Kusari et al., 2010
				○					Guo et al., 2015; Marangoz et al., 2018
		●		●				●	Goldenberg-Cohen et al., 2009
	PPARα agonists		●				●	●	Chen et al., 2013
				●	●	●	●		Deng et al., 2017
		●	●			●	●	●	Li et al., 2018
		●	●			●	●		Liu et al., 2018
			●	●				●	Wang N. et al., 2018
		●				●			Liu et al., 2019
			●		●	●		●	Qiu et al., 2019
	ALDH2*	●	●		●			●	He et al., 2018
	LRIC*	●	●	●				●	Ren et al., 2018

*The data indicated with "○" are from papers documenting either neuroprotective or vasoprotective effects; those indicated with "●" are from papers documenting both neuroprotective and vasoprotective effects in the same experimental samples. *ALDH2, acetaldehyde dehydrogenase 2; APO, apoptosis; FUNC, retinal function; GHRH, growth hormone-releasing hormone; IF, inflammation; LRIC, remote ischemic conditioning; OS, oxidative stress; VASC, vasculopathy. See "Abbreviations" for the other abbreviations.*

CONCLUSION

The experimental data summarized in this review of the literature clearly indicate that, in a variety of experimental models of retinal disease, a neuroprotective treatment is efficacious in preventing the vascular changes that are usually associated with the disease (see **Table 1** for a comprehensive summary of the data). Although the participation of VEGF is crucial in the early stages of DR, we cannot exclude the participation of some other important molecules, such as the neuronal guidance cues, including ephrins, netrin, and semaphorins, which are also released early by damaged neurons and may promote or attenuate the development of DR (Moran et al., 2016). These molecules are highly expressed in the retina and vitreous of patients with advanced DR (Umeda et al., 2004; Liu et al., 2011; Cerani et al., 2013; Dejda et al., 2014), and their inhibition, like that of VEGF, could reveal an efficient method to reduce aberrant growth of retinal vessels. The possibility exists that treatments with neuroprotectants, in addition to reducing VEGF expression/release, also limit the release of these molecules, thereby exerting a multitarget effect that results in efficient protection from microvascular damage and subsequent development of advanced stages of DR.

The fact that neuroprotection may limit vascular pathology could be explained assuming that the reviewed compounds may trigger two types of independent, parallel responses: one finalized to neuroprotection and the other affecting the mechanisms regulating VEGF expression and/or release. This might be the case, for instance, for SRIF. Indeed, for the SRIF analog octreotide, there is evidence of an effect, reducing oxidative stress and glutamate release (Dal Monte et al., 2003; D'alessandro et al., 2014), and of a regulatory action on the intracellular mechanisms for VEGF expression (Dal Monte et al., 2009, 2010; Mei et al., 2012). However, most compounds listed in this review are primarily antioxidant and anti-inflammatory substances, which are likely to exert their primary effects on retinal neurons. Therefore, it appears that protecting retinal neurons from stress reduces the probability of VEGF upregulation and the consequent vascular damage. This evidence indicates that treatments with natural substances (nutraceuticals or neuropeptides) during early phases of DR may represent the basis for efficacious therapies of DR that do not impact on the patients' quality of life and that may have only little or no side effects.

AUTHOR CONTRIBUTIONS

MR and GC collected the references. MR, MD, and GC organized the layout of the paper and wrote the manuscript.

FUNDING

This research was supported by the Italian Ministry of University and Research (FFABR 2017).

REFERENCES

Abcouwer, S. F., and Gardner, T. W. (2014). Diabetic retinopathy: loss of neuroretinal adaptation to the diabetic metabolic environment. *Ann. N. Y. Acad. Sci.* 1311, 174–190. doi: 10.1111/nyas.12412

Aggarwal, B. B., Van Kuiken, M. E., Iyer, L. H., Harikumar, K. B., and Sung, B. (2009). Molecular targets of nutraceuticals derived from dietary spices: potential role in suppression of inflammation and tumorigenesis. *Exp. Biol. Med.* 234, 825–849. doi: 10.3181/0902-MR-78

Al-Gayyar, M. M., Matragoon, S., Pillai, B. A., Ali, T. K., Abdelsaid, M. A., and El-Remessy, A. B. (2011). Epicatechin blocks pro-nerve growth factor (proNGF)-mediated retinal neurodegeneration via inhibition of p75 neurotrophin receptor expression in a rat model of diabetes [corrected]. *Diabetologia* 54, 669–680. doi: 10.1007/s00125-010-1994-3

Alrashdi, S. F., Deliyanti, D., and Wilkinson-Berka, J. L. (2018). Intravitreal administration of endothelin type A receptor or endothelin type B receptor antagonists attenuates hypertensive and diabetic retinopathy in rats. *Exp. Eye Res.* 176, 1–9. doi: 10.1016/j.exer.2018.06.025

Amato, R., Biagioni, M., Cammalleri, M., Dal Monte, M., and Casini, G. (2016). VEGF as a survival factor in *ex vivo* models of early diabetic retinopathy. *Invest. Ophthalmol. Vis. Sci.* 57, 3066–3076. doi: 10.1167/iovs.16-19285

Amato, R., Catalani, E., Dal Monte, M., Cammalleri, M., Di Renzo, I., Perrotta, C., et al. (2018a). Autophagy-mediated neuroprotection induced by octreotide in an *ex vivo* model of early diabetic retinopathy. *Pharmacol. Res.* 128, 167–178. doi: 10.1016/j.phrs.2017.09.022

Amato, R., Rossino, M. G., Cammalleri, M., Locri, F., Pucci, L., Dal Monte, M., et al. (2018b). Lisosan G protects the retina from neurovascular damage in experimental diabetic retinopathy. *Nutrients* 10:E1932. doi: 10.3390/nu10121932

Antonetti, D. A., Barber, A. J., Bronson, S. K., Freeman, W. M., Gardner, T. W., Jefferson, L. S., et al. (2006). Diabetic retinopathy: seeing beyond glucose-induced microvascular disease. *Diabetes* 55, 2401–2411. doi: 10.2337/db05-1635

Arredondo Zamarripa, D., Diaz-Lezama, N., Melendez Garcia, R., Chavez Balderas, J., Adan, N., Ledesma-Colunga, M. G., et al. (2014). Vasoinhibins regulate the inner and outer blood-retinal barrier and limit retinal oxidative stress. *Front. Cell Neurosci.* 8:333. doi: 10.3389/fncel.2014.00333

Atlasz, T., Szabadfi, K., Kiss, P., Racz, B., Gallyas, F., Tamas, A., et al. (2010). Pituitary adenylate cyclase activating polypeptide in the retina: focus on the retinoprotective effects. *Ann. N. Y. Acad. Sci.* 1200, 128–139. doi: 10.1111/j.1749-6632.2010.05512.x

Atlasz, T., Werling, D., Song, S., Szabo, E., Vaczy, A., Kovari, P., et al. (2018). Retinoprotective effects of TAT-bound vasoactive intestinal peptide and pituitary adenylate cyclase activating polypeptide. *J. Mol. Neurosci.* 68, 397–407. doi: 10.1007/s12031-018-1229-5

Azzouz, M., Ralph, G. S., Storkebaum, E., Walmsley, L. E., Mitrophanous, K. A., Kingsman, S. M., et al. (2004). VEGF delivery with retrogradely transported lentivector prolongs survival in a mouse ALS model. *Nature* 429, 413–417. doi: 10.1038/nature02544

Bagnoli, P., Dal Monte, M., and Casini, G. (2003). Expression of neuropeptides and their receptors in the developing retina of mammals. *Histol. Histopathol.* 18, 1219–1242. doi: 10.14670/HH-18.1219

Barber, A. J. (2003). A new view of diabetic retinopathy: a neurodegenerative disease of the eye. *Prog. Neuropsychopharmacol. Biol. Psychiatry* 27, 283–290. doi: 10.1016/S0278-5846(03)00023-X

Bassan, M., Zamostiano, R., Davidson, A., Pinhasov, A., Giladi, E., Perl, O., et al. (1999). Complete sequence of a novel protein containing a femtomolar-activity-dependent neuroprotective peptide. *J. Neurochem.* 72, 1283–1293. doi: 10.1046/j.1471-4159.1999.0721283.x

Batenburg, W. W., Verma, A., Wang, Y., Zhu, P., Van Den Heuvel, M., Van Veghel, R., et al. (2014). Combined renin inhibition/(pro)renin receptor blockade in diabetic retinopathy–a study in transgenic (mREN2)27 rats. *PLoS ONE* 9:e100954. doi: 10.1371/journal.pone.0100954

Beazley-Long, N., Hua, J., Jehle, T., Hulse, R. P., Dersch, R., Lehrling, C., et al. (2013). VEGF-A165b is an endogenous neuroprotective splice isoform of vascular endothelial growth factor A *in vivo* and *in vitro*. *Am. J. Pathol.* 183, 918–929. doi: 10.1016/j.ajpath.2013.05.031

Berthet, P., Farine, J. C., and Barras, J. P. (1999). Calcium dobesilate: pharmacological profile related to its use in diabetic retinopathy. *Int. J. Clin. Pract.* 53, 631–636.

Bogdanov, P., Simo-Servat, O., Sampedro, J., Sola-Adell, C., Garcia-Ramirez, M., Ramos, H., et al. (2018). Topical administration of bosentan prevents retinal neurodegeneration in experimental diabetes. *Int. J. Mol. Sci.* 19:E3578. doi: 10.3390/ijms19113578

Bogdanov, P., Sola-Adell, C., Hernandez, C., Garcia-Ramirez, M., Sampedro, J., Simo-Servat, O., et al. (2017). Calcium dobesilate prevents the oxidative stress and inflammation induced by diabetes in the retina of db/db mice. *J. Diabetes Complications* 31, 1481–1490. doi: 10.1016/j.jdiacomp.2017.07.009

Brower, V. (1998). Nutraceuticals: poised for a healthy slice of the healthcare market? *Nat. Biotechnol.* 16, 728–731. doi: 10.1038/nbt0898-728

Brunet, J., Farine, J. C., Garay, R. P., and Hannaert, P. (1998). Angioprotective action of calcium dobesilate against reactive oxygen species-induced capillary permeability in the rat. *Eur. J. Pharmacol.* 358, 213–220. doi: 10.1016/S0014-2999(98)00604-9

Bucolo, C., Leggio, G. M., Drago, F., and Salomone, S. (2012). Eriodictyol prevents early retinal and plasma abnormalities in streptozotocin-induced diabetic rats. *Biochem. Pharmacol.* 84, 88–92. doi: 10.1016/j.bcp.2012.03.019

Cai, S., Yang, Q., Hou, M., Han, Q., Zhang, H., Wang, J., et al. (2018). Alpha-melanocyte-stimulating hormone protects early diabetic retina from blood-retinal barrier breakdown and vascular leakage via MC4R. *Cell Physiol. Biochem.* 45, 505–522. doi: 10.1159/000487029

Cai, X., Li, J., Wang, M., She, M., Tang, Y., Li, H., et al. (2017). GLP-1 treatment improves diabetic retinopathy by alleviating autophagy through GLP-1R-ERK1/2-HDAC6 signaling pathway. *Int. J. Med. Sci.* 14, 1203–1212. doi: 10.7150/ijms.20962

Cammalleri, M., Dal Monte, M., Locri, F., Marsili, S., Lista, L., De Rosa, M., et al. (2017a). Diabetic retinopathy in the spontaneously diabetic torii rat: pathogenetic mechanisms and preventive efficacy of inhibiting the urokinase-type plasminogen activator receptor system. *J. Diabetes Res.* 2017:2904150. doi: 10.1155/2017/2904150

Cammalleri, M., Dal Monte, M., Locri, F., Pecci, V., De Rosa, M., Pavone, V., et al. (2019a). The urokinase-type plasminogen activator system as drug target in retinitis pigmentosa: new pre-clinical evidence in the rd10 mouse model. *J. Cell Mol. Med.* 23, 5176–5192. doi: 10.1111/jcmm.14391

Cammalleri, M., Dal Monte, M., Pavone, V., De Rosa, M., Rusciano, D., and Bagnoli, P. (2019b). The uPAR system as a potential therapeutic target in the diseased eye. *Cells* 8:E925. doi: 10.3390/cells8080925

Cammalleri, M., Locri, F., Marsili, S., Dal Monte, M., Pisano, C., Mancinelli, A., et al. (2017b). The urokinase receptor-derived peptide UPARANT recovers dysfunctional electroretinogram and blood-retinal barrier leakage in a rat model of diabetes. *Invest. Ophthalmol. Vis. Sci.* 58, 3138–3148. doi: 10.1167/iovs.17-21593

Casini, G., Catalani, E., Dal Monte, M., and Bagnoli, P. (2005). Functional aspects of the somatostatinergic system in the retina and the potential therapeutic role of somatostatin in retinal disease. *Histol. Histopathol.* 20, 615–632. doi: 10.14670/HH-20.615

Casini, G., Dal Monte, M., Fornaciari, I., Filippi, L., and Bagnoli, P. (2014). The beta-adrenergic system as a possible new target for pharmacologic treatment of neovascular retinal diseases. *Prog. Retin Eye Res.* 42, 103–129. doi: 10.1016/j.preteyeres.2014.06.001

Catalani, E., Cervia, D., Martini, D., Bagnoli, P., Simonetti, E., Timperio, A. M., et al. (2007). Changes in neuronal response to ischemia in retinas with genetic alterations of somatostatin receptor expression. *Eur. J. Neurosci.* 25, 1447–1459. doi: 10.1111/j.1460-9568.2007.05419.x

Catalani, E., De Palma, C., Perrotta, C., and Cervia, D. (2017). Current evidence for a role of neuropeptides in the regulation of autophagy. *Biomed. Res. Int.* 2017:5856071. doi: 10.1155/2017/5856071

Cerani, A., Tetreault, N., Menard, C., Lapalme, E., Patel, C., Sitaras, N., et al. (2013). Neuron-derived semaphorin 3A is an early inducer of vascular permeability in diabetic retinopathy via neuropilin-1. *Cell Metab.* 18, 505–518. doi: 10.1016/j.cmet.2013.09.003

Cervantes-Villagrana, A. R., Garcia-Roman, J., Gonzalez-Espinosa, C., and Lamas, M. (2010). Pharmacological inhibition of N-methyl d-aspartate receptor promotes secretion of vascular endothelial growth factor in muller cells: effects of hyperglycemia and hypoxia. *Curr. Eye Res.* 35, 733–741. doi: 10.3109/02713683.2010.483312

Cervia, D., and Casini, G. (2013). The Neuropeptide systems and their potential role in the treatment of mammalian retinal ischemia: a developing story. *Curr. Neuropharmacol.* 11, 95–101. doi: 10.2174/1570159X11311010011

Cervia, D., Casini, G., and Bagnoli, P. (2008a). Physiology and pathology of somatostatin in the mammalian retina: a current view. *Mol. Cell Endocrinol.* 286, 112–122. doi: 10.1016/j.mce.2007.12.009

Cervia, D., Catalani, E., and Casini, G. (2019). Neuroprotective peptides in retinal disease. *J. Clin. Med.* 8:E1146. doi: 10.3390/jcm8081146

Cervia, D., Catalani, E., Dal Monte, M., and Casini, G. (2012). Vascular endothelial growth factor in the ischemic retina and its regulation by somatostatin. *J. Neurochem.* 120, 818–829. doi: 10.1111/j.1471-4159.2011.07622.x

Cervia, D., Martini, D., Ristori, C., Catalani, E., Timperio, A. M., Bagnoli, P., et al. (2008b). Modulation of the neuronal response to ischaemia by somatostatin analogues in wild-type and knock-out mouse retinas. *J. Neurochem.* 106, 2224–2235. doi: 10.1111/j.1471-4159.2008.05556.x

Chang, Z. Y., Yeh, M. K., Chiang, C. H., Chen, Y. H., and Lu, D. W. (2013). Erythropoietin protects adult retinal ganglion cells against NMDA-, trophic factor withdrawal-, and TNF-alpha-induced damage. *PLoS ONE* 8:e55291. doi: 10.1371/journal.pone.0055291

Chauhan, B., Kumar, G., Kalam, N., and Ansari, S. H. (2013). Current concepts and prospects of herbal nutraceutical: a review. *J. Adv. Pharm. Technol. Res.* 4, 4–8. doi: 10.4103/2231-4040.107494

Chen, B., He, T., Xing, Y., and Cao, T. (2017). Effects of quercetin on the expression of MCP-1, MMP-9 and VEGF in rats with diabetic retinopathy. *Exp. Ther. Med.* 14, 6022–6026. doi: 10.3892/etm.2017.5275

Chen, M., Lv, H., Gan, J., Ren, J., and Liu, J. (2017). Tang Wang Ming Mu granule attenuates diabetic retinopathy in type 2 diabetes rats. *Front. Physiol.* 8:1065. doi: 10.3389/fphys.2017.01065

Chen, X. Y., Du, Y. F., and Chen, L. (2019). Neuropeptides exert neuroprotective effects in Alzheimer's disease. *Front. Mol. Neurosci.* 11:493. doi: 10.3389/fnmol.2018.00493

Chen, Y., Hu, Y., Lin, M., Jenkins, A. J., Keech, A. C., Mott, R., et al. (2013). Therapeutic effects of PPARalpha agonists on diabetic retinopathy in type 1 diabetes models. *Diabetes* 62, 261–272. doi: 10.2337/db11-0413

Chen, Y., Meng, J., Li, H., Wei, H., Bi, F., Liu, S., et al. (2019). Resveratrol exhibits an effect on attenuating retina inflammatory condition and damage of diabetic retinopathy via PON1. *Exp. Eye Res.* 181, 356–366. doi: 10.1016/j.exer.2018.11.023

Chew, E. Y., Ambrosius, W. T., Davis, M. D., Danis, R. P., Gangaputra, S., Greven, C. M., et al. (2010). Effects of medical therapies on retinopathy progression in type 2 diabetes. *N. Engl. J. Med.* 363, 233–244. doi: 10.1056/NEJMoa1001288

Cho, N. H., Shaw, J. E., Karuranga, S., Huang, Y., Da Rocha Fernandes, J. D., Ohlrogge, A. W., et al. (2018). IDF Diabetes Atlas: Global estimates of diabetes prevalence for 2017 and projections for 2045. *Diabetes Res. Clin. Pract.* 138, 271–281. doi: 10.1016/j.diabres.2018.02.023

Chou, J. C., Rollins, S. D., Ye, M., Batlle, D., and Fawzi, A. A. (2014). Endothelin receptor-A antagonist attenuates retinal vascular and neuroretinal pathology in diabetic mice. *Invest. Ophthalmol. Vis. Sci.* 55, 2516–2525. doi: 10.1167/iovs.13-13676

Chu, C., Deng, J., Man, Y., and Qu, Y. (2017). Green tea extracts epigallocatechin-3-gallate for different treatments. *Biomed. Res. Int.* 2017:5615647. doi: 10.1155/2017/5615647

Chung, H., Lee, H., Lamoke, F., Hrushesky, W. J., Wood, P. A., and Jahng, W. J. (2009). Neuroprotective role of erythropoietin by antiapoptosis in the retina. *J. Neurosci. Res.* 87, 2365–2374. doi: 10.1002/jnr.22046

Colella, P., Iodice, C., Di Vicino, U., Annunziata, I., Surace, E. M., and Auricchio, A. (2011). Non-erythropoietic erythropoietin derivatives protect from light-induced and genetic photoreceptor degeneration. *Hum. Mol. Genet.* 20, 2251–2262. doi: 10.1093/hmg/ddr115

Dal Monte, M., Latina, V., Cupisti, E., and Bagnoli, P. (2012). Protective role of somatostatin receptor 2 against retinal degeneration in response to hypoxia. *Naunyn Schmiedebergs Arch. Pharmacol.* 385, 481–494. doi: 10.1007/s00210-012-0735-1

Dal Monte, M., Petrucci, C., Cozzi, A., Allen, J. P., and Bagnoli, P. (2003). Somatostatin inhibits potassium-evoked glutamate release by activation of the sst(2) somatostatin receptor in the mouse retina. *Naunyn Schmiedebergs Arch. Pharmacol.* 367, 188–192. doi: 10.1007/s00210-002-0662-7

Dal Monte, M., Ristori, C., Cammalleri, M., and Bagnoli, P. (2009). Effects of somatostatin analogues on retinal angiogenesis in a mouse model of oxygen-induced retinopathy: involvement of the somatostatin receptor subtype 2. *Invest. Ophthalmol. Vis. Sci.* 50, 3596–3606. doi: 10.1167/iovs.09-3412

Dal Monte, M., Ristori, C., Videau, C., Loudes, C., Martini, D., Casini, G., et al. (2010). Expression, localization, and functional coupling of the somatostatin receptor subtype 2 in a mouse model of oxygen-induced retinopathy. *Invest. Ophthalmol. Vis. Sci.* 51, 1848–1856. doi: 10.1167/iovs.09-4472

D'alessandro, A., Cervia, D., Catalani, E., Gevi, F., Zolla, L., and Casini, G. (2014). Protective effects of the neuropeptides PACAP, substance P and the somatostatin analogue octreotide in retinal ischemia: a metabolomic analysis. *Mol. Biosyst.* 10, 1290–1304. doi: 10.1039/c3mb70362b

D'amico, A. G., Maugeri, G., Bucolo, C., Saccone, S., Federico, C., Cavallaro, S., et al. (2017a). Nap interferes with hypoxia-inducible factors and VEGF expression in retina of diabetic rats. *J. Mol. Neurosci.* 61, 256–266. doi: 10.1007/s12031-016-0869-6

D'amico, A. G., Maugeri, G., Rasa, D., Federico, C., Saccone, S., Lazzara, F., et al. (2019). NAP modulates hyperglycemic-inflammatory event of diabetic retina by counteracting outer blood retinal barrier damage. *J. Cell Physiol.* 234, 5230–5240. doi: 10.1002/jcp.27331

D'amico, A. G., Maugeri, G., Rasa, D. M., Bucolo, C., Saccone, S., Federico, C., et al. (2017b). Modulation of IL-1beta and VEGF expression in rat diabetic retinopathy after PACAP administration. *Peptides* 97, 64–69. doi: 10.1016/j.peptides.2017.09.014

D'amico, A. G., Maugeri, G., Reitano, R., Bucolo, C., Saccone, S., Drago, F., et al. (2015). PACAP modulates expression of hypoxia-inducible factors in streptozotocin-induced diabetic rat retina. *J. Mol. Neurosci.* 57, 501–509. doi: 10.1007/s12031-015-0621-7

Danyadi, B., Szabadfi, K., Reglodi, D., Mihalik, A., Danyadi, T., Kovacs, Z., et al. (2014). PACAP application improves functional outcome of chronic retinal ischemic injury in rats-evidence from electroretinographic measurements. *J. Mol. Neurosci.* 54, 293–299. doi: 10.1007/s12031-014-0296-5

Davenport, A. P., Hyndman, K. A., Dhaun, N., Southan, C., Kohan, D. E., Pollock, J. S., et al. (2016). Endothelin. *Pharmacol. Rev.* 68, 357–418. doi: 10.1124/pr.115.011833

Dejda, A., Mawambo, G., Cerani, A., Miloudi, K., Shao, Z., Daudelin, J. F., et al. (2014). Neuropilin-1 mediates myeloid cell chemoattraction and influences retinal neuroimmune crosstalk. *J. Clin. Invest.* 124, 4807–4822. doi: 10.1172/JCI76492

Deliyanti, D., Alrashdi, S. F., Tan, S. M., Meyer, C., Ward, K. W., De Haan, J. B., et al. (2018). Nrf2 activation is a potential therapeutic approach to attenuate diabetic retinopathy. *Invest. Ophthalmol. Vis. Sci.* 59, 815–825. doi: 10.1167/iovs.17-22920

Deng, G., Moran, E. P., Cheng, R., Matlock, G., Zhou, K., Moran, D., et al. (2017). Therapeutic effects of a novel agonist of peroxisome proliferator-activated receptor alpha for the treatment of diabetic retinopathy. *Invest. Ophthalmol. Vis. Sci.* 58, 5030–5042. doi: 10.1167/iovs.16-21402

Deza-Ponzio, R., Herrera, M. L., Bellini, M. J., Virgolini, M. B., and Herenu, C. B. (2018). Aldehyde dehydrogenase 2 in the spotlight: the link between mitochondria and neurodegeneration. *Neurotoxicology* 68, 19–24. doi: 10.1016/j.neuro.2018.06.005

Di Marco, E., Jha, J. C., Sharma, A., Wilkinson-Berka, J. L., Jandeleit-Dahm, K. A., and De Haan, J. B. (2015). Are reactive oxygen species still the basis for diabetic complications? *Clin. Sci.* 129, 199–216. doi: 10.1042/CS20150093

Dietrich, N., Kolibabka, M., Busch, S., Bugert, P., Kaiser, U., Lin, J., et al. (2016). The DPP4 inhibitor linagliptin protects from experimental diabetic retinopathy. *PLoS ONE* 11:e0167853. doi: 10.1371/journal.pone.0167853

Djordjevic, B., Cvetkovic, T., Stoimenov, T. J., Despotovic, M., Zivanovic, S., Basic, J., et al. (2018). Oral supplementation with melatonin reduces oxidative damage and concentrations of inducible nitric oxide synthase, VEGF and matrix metalloproteinase 9 in the retina of rats with streptozotocin/nicotinamide induced pre-diabetes. *Eur. J. Pharmacol.* 833, 290–297. doi: 10.1016/j.ejphar.2018.06.011

Drucker, D. J., and Nauck, M. A. (2006). The incretin system: glucagon-like peptide-1 receptor agonists and dipeptidyl peptidase-4 inhibitors in type 2 diabetes. *Lancet* 368, 1696–1705. doi: 10.1016/S0140-6736(06)69705-5

Du, W., An, Y., He, X., Zhang, D., and He, W. (2018). Protection of kaempferol on oxidative stress-induced retinal pigment epithelial cell damage. *Oxid. Med. Cell Longev.* 2018:1610751. doi: 10.1155/2018/1610751

Duh, E. J., Sun, J. K., and Stitt, A. W. (2017). Diabetic retinopathy: current understanding, mechanisms, and treatment strategies. *JCI Insight* 2:93751. doi: 10.1172/jci.insight.93751

Edling, A. E., Gomes, D., Weeden, T., Dzuris, J., Stefano, J., Pan, C., et al. (2011). Immunosuppressive activity of a novel peptide analog of alpha-melanocyte stimulating hormone (alpha-MSH) in experimental autoimmune uveitis. *J. Neuroimmunol.* 236, 1–9. doi: 10.1016/j.jneuroim.2011.04.015

Fan, Y., Liu, K., Wang, Q., Ruan, Y., Ye, W., and Zhang, Y. (2014a). Exendin-4 alleviates retinal vascular leakage by protecting the blood-retinal barrier and reducing retinal vascular permeability in diabetic Goto-Kakizaki rats. *Exp. Eye Res.* 127, 104–116. doi: 10.1016/j.exer.2014.05.004

Fan, Y., Liu, K., Wang, Q., Ruan, Y., Zhang, Y., and Ye, W. (2014b). Exendin-4 protects retinal cells from early diabetes in Goto-Kakizaki rats by increasing the Bcl-2/Bax and Bcl-xL/Bax ratios and reducing reactive gliosis. *Mol. Vis.* 20, 1557–1568.

Fletcher, E. L., Phipps, J. A., Ward, M. M., Vessey, K. A., and Wilkinson-Berka, J. L. (2010). The renin-angiotensin system in retinal health and disease: its influence on neurons, glia and the vasculature. *Prog. Retin. Eye Res.* 29, 284–311. doi: 10.1016/j.preteyeres.2010.03.003

Fonollosa, A., Coronado, E., Catalan, R., Gutierrez, M., Macia, C., Zapata, M. A., et al. (2012). Vitreous levels of somatostatin in patients with chronic uveitic macular oedema. *Eye* 26, 1378–1383. doi: 10.1038/eye.2012.161

Foureaux, G., Nogueira, B. S., Coutinho, D. C., Raizada, M. K., Nogueira, J. C., and Ferreira, A. J. (2015). Activation of endogenous angiotensin converting enzyme 2 prevents early injuries induced by hyperglycemia in rat retina. *Braz. J. Med. Biol. Res.* 48, 1109–1114. doi: 10.1590/1414-431x20154583

Foureaux, G., Nogueira, J. C., Nogueira, B. S., Fulgencio, G. O., Menezes, G. B., Fernandes, S. O., et al. (2013). Antiglaucomatous effects of the activation of intrinsic Angiotensin-converting enzyme 2. *Invest. Ophthalmol. Vis. Sci.* 54, 4296–4306. doi: 10.1167/iovs.12-11427

Foxton, R. H., Finkelstein, A., Vijay, S., Dahlmann-Noor, A., Khaw, P. T., Morgan, J. E., et al. (2013). VEGF-A is necessary and sufficient for retinal neuroprotection in models of experimental glaucoma. *Am. J. Pathol.* 182, 1379–1390. doi: 10.1016/j.ajpath.2012.12.032

Fu, Q. L., Wu, W., Wang, H., Li, X., Lee, V. W., and So, K. F. (2008). Up-regulated endogenous erythropoietin/erythropoietin receptor system and exogenous erythropoietin rescue retinal ganglion cells after chronic ocular hypertension. *Cell Mol. Neurobiol.* 28, 317–329. doi: 10.1007/s10571-007-9155-z

Fujita, T., Hirooka, K., Nakamura, T., Itano, T., Nishiyama, A., Nagai, Y., et al. (2012). Neuroprotective effects of angiotensin II type 1 receptor (AT1-R) blocker via modulating AT1-R signaling and decreased extracellular glutamate levels. *Invest. Ophthalmol. Vis. Sci.* 53, 4099–4110. doi: 10.1167/iovs.11-9167

Gabriel, R. (2013). Neuropeptides and diabetic retinopathy. *Br. J. Clin. Pharmacol.* 75, 1189–1201. doi: 10.1111/bcp.12003

Garcia, C., Aranda, J., Arnold, E., Thebault, S., Macotela, Y., Lopez-Casillas, F., et al. (2008). Vasoinhibins prevent retinal vasopermeability associated with diabetic retinopathy in rats via protein phosphatase 2A-dependent eNOS inactivation. *J. Clin. Invest.* 118, 2291–2300. doi: 10.1172/JCI34508

Gerszon, J., Rodacka, A., and Puchała, M. (2014). Antioxidant properties of resveratrol and its protective effects in neurodegenerative diseases. *Med. J. Cell Biol.* 4, 97–117. doi: 10.2478/acb-2014-0006

Giladi, E., Hill, J. M., Dresner, E., Stack, C. M., and Gozes, I. (2007). Vasoactive intestinal peptide (VIP) regulates activity-dependent neuroprotective protein (ADNP) expression *in vivo*. *J. Mol. Neurosci.* 33, 278–283. doi: 10.1007/s12031-007-9003-0

Goldenberg-Cohen, N., Dadon-Bar-El, S., Hasanreisoglu, M., Avraham-Lubin, B. C., Dratviman-Storobinsky, O., Cohen, Y., et al. (2009). Possible neuroprotective effect of brimonidine in a mouse model of ischaemic optic neuropathy. *Clin. Exp. Ophthalmol.* 37, 718–729. doi: 10.1111/j.1442-9071.2009.02108.x

Goncalves, A., Leal, E., Paiva, A., Teixeira Lemos, E., Teixeira, F., Ribeiro, C. F., et al. (2012). Protective effects of the dipeptidyl peptidase IV inhibitor

sitagliptin in the blood-retinal barrier in a type 2 diabetes animal model. *Diabetes Obes. Metab.* 14, 454–463. doi: 10.1111/j.1463-1326.2011.01548.x

Goncalves, A., Lin, C. M., Muthusamy, A., Fontes-Ribeiro, C., Ambrosio, A. F., Abcouwer, S. F., et al. (2016). Protective effect of a GLP-1 analog on ischemia-reperfusion induced blood-retinal barrier breakdown and inflammation. *Invest. Ophthalmol. Vis. Sci.* 57, 2584–2592. doi: 10.1167/iovs.15-19006

Goncalves, A., Marques, C., Leal, E., Ribeiro, C. F., Reis, F., Ambrosio, A. F., et al. (2014). Dipeptidyl peptidase-IV inhibition prevents blood-retinal barrier breakdown, inflammation and neuronal cell death in the retina of type 1 diabetic rats. *Biochim. Biophys. Acta* 9:25. doi: 10.1016/j.bbadis.2014.04.013

Guo, X., Namekata, K., Kimura, A., Noro, T., Azuchi, Y., Semba, K., et al. (2015). Brimonidine suppresses loss of retinal neurons and visual function in a murine model of optic neuritis. *Neurosci. Lett.* 592, 27–31. doi: 10.1016/j.neulet.2015.02.059

Gupta, S. K., Kumar, B., Nag, T. C., Agrawal, S. S., Agrawal, R., Agrawal, P., et al. (2011). Curcumin prevents experimental diabetic retinopathy in rats through its hypoglycemic, antioxidant, and anti-inflammatory mechanisms. *J. Ocul. Pharmacol. Ther.* 27, 123–130. doi: 10.1089/jop.2010.0123

Hammes, H. P. (2018). Diabetic retinopathy: hyperglycaemia, oxidative stress and beyond. *Diabetologia* 61, 29–38. doi: 10.1007/s00125-017-4435-8

Harmar, A. J., Sheward, W. J., Morrison, C. F., Waser, B., Gugger, M., and Reubi, J. C. (2004). Distribution of the VPAC2 receptor in peripheral tissues of the mouse. *Endocrinology* 145, 1203–1210. doi: 10.1210/en.2003-1058

He, M., Long, P., Yan, W., Chen, T., Guo, L., Zhang, Z., et al. (2018). ALDH2 attenuates early-stage STZ-induced aged diabetic rats retinas damage via Sirt1/Nrf2 pathway. *Life Sci.* 215, 227–235. doi: 10.1016/j.lfs.2018.10.019

Hebsgaard, J. B., Pyke, C., Yildirim, E., Knudsen, L. B., Heegaard, S., and Kvist, P. H. (2018). Glucagon-like peptide-1 receptor expression in the human eye. *Diabetes Obes. Metab.* 20, 2304–2308. doi: 10.1111/dom.13339

Hernandez, C., Bogdanov, P., Corraliza, L., Garcia-Ramirez, M., Sola-Adell, C., Arranz, J. A., et al. (2016a). Topical administration of GLP-1 receptor agonists prevents retinal neurodegeneration in experimental diabetes. *Diabetes* 65, 172–187. doi: 10.2337/db15-0443

Hernandez, C., Bogdanov, P., Sola-Adell, C., Sampedro, J., Valeri, M., Genis, X., et al. (2017). Topical administration of DPP-IV inhibitors prevents retinal neurodegeneration in experimental diabetes. *Diabetologia* 60, 2285–2298. doi: 10.1007/s00125-017-4388-y

Hernandez, C., Dal Monte, M., Simo, R., and Casini, G. (2016b). Neuroprotection as a therapeutic target for diabetic retinopathy. *J. Diabetes Res.* 2016:9508541. doi: 10.1155/2016/9508541

Hernandez, C., Fonollosa, A., Garcia-Ramirez, M., Higuera, M., Catalan, R., Miralles, A., et al. (2006). Erythropoietin is expressed in the human retina and it is highly elevated in the vitreous fluid of patients with diabetic macular edema. *Diabetes Care* 29, 2028–2033. doi: 10.2337/dc06-0556

Hernandez, C., Garcia-Ramirez, M., Corraliza, L., Fernandez-Carneado, J., Farrera-Sinfreu, J., Ponsati, B., et al. (2013). Topical administration of somatostatin prevents retinal neurodegeneration in experimental diabetes. *Diabetes* 62, 2569–2578. doi: 10.2337/db12-0926

Hernandez, C., and Simo, R. (2012). Neuroprotection in diabetic retinopathy. *Curr. Diab. Rep.* 12, 329–337. doi: 10.1007/s11892-012-0284-5

Hernandez, C., Simo-Servat, O., and Simo, R. (2014). Somatostatin and diabetic retinopathy: current concepts and new therapeutic perspectives. *Endocrine* 46, 209–214. doi: 10.1007/s12020-014-0232-z

Heusch, G. (2013). Cardioprotection: chances and challenges of its translation to the clinic. *Lancet* 381, 166–175. doi: 10.1016/S0140-6736(12)60916-7

Hewlings, S. J., and Kalman, D. S. (2017). Curcumin: a review of its' effects on human health. *Foods* 6:E92. doi: 10.3390/foods6100092

Hokfelt, T., Bartfai, T., and Bloom, F. (2003). Neuropeptides: opportunities for drug discovery. *Lancet Neurol.* 2, 463–472. doi: 10.1016/S1474-4422(03)00482-4

Hombrebueno, J. R., Ali, I. H., Xu, H., and Chen, M. (2015). Sustained intraocular VEGF neutralization results in retinal neurodegeneration in the Ins2(Akita) diabetic mouse. *Sci. Rep.* 5:18316. doi: 10.1038/srep18316

Hu, C. K., Lee, Y. J., Colitz, C. M., Chang, C. J., and Lin, C. T. (2012). The protective effects of Lycium barbarum and Chrysanthemum morifolum on diabetic retinopathies in rats. *Vet. Ophthalmol.* 2, 65–71. doi: 10.1111/j.1463-5224.2012.01018.x

Hu, Y., Chen, Y., Ding, L., He, X., Takahashi, Y., Gao, Y., et al. (2013). Pathogenic role of diabetes-induced PPAR-alpha down-regulation in microvascular dysfunction. *Proc. Natl. Acad. Sci. U.S.A.* 110, 15401–15406. doi: 10.1073/pnas.1307211110

Iadecola, C., and Anrather, J. (2011). Stroke research at a crossroad: asking the brain for directions. *Nat. Neurosci.* 14, 1363–1368. doi: 10.1038/nn.2953

Jelkmann, W. (2013). Physiology and pharmacology of erythropoietin. *Transfus Med. Hemother.* 40, 302–309. doi: 10.1159/000356193

Jia, Y. P., Sun, L., Yu, H. S., Liang, L. P., Li, W., Ding, H., et al. (2017). The pharmacological effects of lutein and zeaxanthin on visual disorders and cognition diseases. *Molecules* 22:E610. doi: 10.3390/molecules22040610

Jindal, V. (2015). Neurodegeneration as a primary change and role of neuroprotection in diabetic retinopathy. *Mol. Neurobiol.* 51, 878–884. doi: 10.1007/s12035-014-8732-7

Kang, M. K., Lee, E. J., Kim, Y. H., Kim, D. Y., Oh, H., Kim, S. I., et al. (2018). Chrysin ameliorates malfunction of retinoid visual cycle through blocking activation of AGE-RAGE-ER stress in glucose-stimulated retinal pigment epithelial cells and diabetic eyes. *Nutrients* 10:E1046. doi: 10.3390/nu10081046

Kang, M. K., Park, S. H., Kim, Y. H., Lee, E. J., Antika, L. D., Kim, D. Y., et al. (2016). Dietary compound chrysin inhibits retinal neovascularization with abnormal capillaries in db/db mice. *Nutrients* 8:782. doi: 10.3390/nu8120782

Kara, S., Gencer, B., Karaca, T., Tufan, H. A., Arikan, S., Ersan, I., et al. (2014). Protective effect of hesperetin and naringenin against apoptosis in ischemia/reperfusion-induced retinal injury in rats. *ScientificWorldJournal* 30:797824. doi: 10.1155/2014/797824

Keech, A. C., Mitchell, P., Summanen, P. A., O'day, J., Davis, T. M., Moffitt, M. S., et al. (2007). Effect of fenofibrate on the need for laser treatment for diabetic retinopathy (FIELD study): a randomised controlled trial. *Lancet* 370, 1687–1697. doi: 10.1016/S0140-6736(07)61607-9

Kiagiadaki, F., Savvaki, M., and Thermos, K. (2010). Activation of somatostatin receptor (sst 5) protects the rat retina from AMPA-induced neurotoxicity. *Neuropharmacology* 58, 297–303. doi: 10.1016/j.neuropharm.2009.06.028

Kiagiadaki, F., and Thermos, K. (2008). Effect of intravitreal administration of somatostatin and sst2 analogs on AMPA-induced neurotoxicity in rat retina. *Invest. Ophthalmol. Vis. Sci.* 49, 3080–3089. doi: 10.1167/iovs.07-1644

Kilic, U., Kilic, E., Soliz, J., Bassetti, C. I., Gassmann, M., and Hermann, D. M. (2005). Erythropoietin protects from axotomy-induced degeneration of retinal ganglion cells by activating ERK-1/-2. *FASEB J.* 19, 249–251. doi: 10.1096/fj.04-2493fje

Kim, J., Kim, C. S., Lee, Y. M., Sohn, E., Jo, K., and Kim, J. S. (2015). *Vaccinium myrtillus* extract prevents or delays the onset of diabetes–induced blood-retinal barrier breakdown. *Int. J. Food Sci. Nutr.* 66, 236–242. doi: 10.3109/09637486.2014.979319

Kim, Y. H., Kim, Y. S., Kang, S. S., Cho, G. J., and Choi, W. S. (2010). Resveratrol inhibits neuronal apoptosis and elevated Ca2+/calmodulin-dependent protein kinase II activity in diabetic mouse retina. *Diabetes* 59, 1825–1835. doi: 10.2337/db09-1431

Kim, Y. H., Kim, Y. S., Roh, G. S., Choi, W. S., and Cho, G. J. (2012). Resveratrol blocks diabetes-induced early vascular lesions and vascular endothelial growth factor induction in mouse retinas. *Acta Ophthalmol.* 90, 1755–3768. doi: 10.1111/j.1755-3768.2011.02243.x

Kokona, D., Mastrodimou, N., Pediaditakis, I., Charalampopoulos, I., Schmid, H. A., and Thermos, K. (2012). Pasireotide (SOM230) protects the retina in animal models of ischemia induced retinopathies. *Exp. Eye Res.* 103, 90–98. doi: 10.1016/j.exer.2012.08.005

Kowluru, R. A., and Kanwar, M. (2007). Effects of curcumin on retinal oxidative stress and inflammation in diabetes. *Nutr. Metab.* 4, 1743–7075. doi: 10.1186/1743-7075-4-8

Kowluru, R. A., Kowluru, A., Mishra, M., and Kumar, B. (2015). Oxidative stress and epigenetic modifications in the pathogenesis of diabetic retinopathy. *Prog. Retin. Eye Res.* 48, 40–61. doi: 10.1016/j.preteyeres.2015.05.001

Kowluru, R. A., Menon, B., and Gierhart, D. L. (2008). Beneficial effect of zeaxanthin on retinal metabolic abnormalities in diabetic rats. *Invest. Ophthalmol. Vis. Sci.* 49, 1645–1651. doi: 10.1167/iovs.07-0764

Kowluru, R. A., Zhong, Q., Santos, J. M., Thandampallayam, M., Putt, D., and Gierhart, D. L. (2014). Beneficial effects of the nutritional supplements on the development of diabetic retinopathy. *Nutr. Metab.* 11, 1743–7075. doi: 10.1186/1743-7075-11-8

Kubota, S., Kurihara, T., Mochimaru, H., Satofuka, S., Noda, K., Ozawa, Y., et al. (2009). Prevention of ocular inflammation in endotoxin-induced uveitis with resveratrol by inhibiting oxidative damage and nuclear factor-kappaB activation. *Invest. Ophthalmol. Vis. Sci.* 50, 3512–3519. doi: 10.1167/iovs.08-2666

Kubota, S., Ozawa, Y., Kurihara, T., Sasaki, M., Yuki, K., Miyake, S., et al. (2011). Roles of AMP-activated protein kinase in diabetes-induced retinal inflammation. *Invest. Ophthalmol. Vis. Sci.* 52, 9142–9148. doi: 10.1167/iovs.11-8041

Kumar, B., Gupta, S. K., Nag, T. C., Srivastava, S., and Saxena, R. (2012a). Green tea prevents hyperglycemia-induced retinal oxidative stress and inflammation in streptozotocin-induced diabetic rats. *Ophthalmic Res.* 47, 103–108. doi: 10.1159/000330051

Kumar, B., Gupta, S. K., Nag, T. C., Srivastava, S., Saxena, R., Jha, K. A., et al. (2014). Retinal neuroprotective effects of quercetin in streptozotocin-induced diabetic rats. *Exp. Eye Res.* 125, 193–202. doi: 10.1016/j.exer.2014.06.009

Kumar, B., Gupta, S. K., Srinivasan, B. P., Nag, T. C., Srivastava, S., and Saxena, R. (2012b). Hesperetin ameliorates hyperglycemia induced retinal vasculopathy via anti-angiogenic effects in experimental diabetic rats. *Vascul. Pharmacol.* 57, 201–207. doi: 10.1016/j.vph.2012.02.007

Kumar, B., Gupta, S. K., Srinivasan, B. P., Nag, T. C., Srivastava, S., Saxena, R., et al. (2013). Hesperetin rescues retinal oxidative stress, neuroinflammation and apoptosis in diabetic rats. *Microvasc. Res.* 87, 65–74. doi: 10.1016/j.mvr.2013.01.002

Kusari, J., Zhou, S. X., Padillo, E., Clarke, K. G., and Gil, D. W. (2010). Inhibition of vitreoretinal VEGF elevation and blood-retinal barrier breakdown in streptozotocin-induced diabetic rats by brimonidine. *Invest. Ophthalmol. Vis. Sci.* 51, 1044–1051. doi: 10.1167/iovs.08-3293

Lakk, M., Denes, V., and Gabriel, R. (2015). Pituitary adenylate cyclase-activating polypeptide receptors signal via phospholipase c pathway to block apoptosis in newborn rat retina. *Neurochem. Res.* 40, 1402–1409. doi: 10.1007/s11064-015-1607-0

Leal, E. C., Martins, J., Voabil, P., Liberal, J., Chiavaroli, C., Bauer, J., et al. (2010). Calcium dobesilate inhibits the alterations in tight junction proteins and leukocyte adhesion to retinal endothelial cells induced by diabetes. *Diabetes* 59, 2637–2645. doi: 10.2337/db09-1421

Leasher, J. L., Bourne, R. R., Flaxman, S. R., Jonas, J. B., Keeffe, J., Naidoo, K., et al. (2016). Global estimates on the number of people blind or visually impaired by diabetic retinopathy: a meta-analysis from 1990 to 2010. *Diabetes Care* 39, 1643–1649. doi: 10.2337/dc15-2171

Lee, H. S., Jun, J. H., Jung, E. H., Koo, B. A., and Kim, Y. S. (2014). Epigalloccatechin-3-gallate inhibits ocular neovascularization and vascular permeability in human retinal pigment epithelial and human retinal microvascular endothelial cells via suppression of MMP-9 and VEGF activation. *Molecules* 19, 12150–12172. doi: 10.3390/molecules190812150

Li, J., Wang, P., Chen, Z., Yu, S., and Xu, H. (2018). Fenofibrate ameliorates oxidative stress-induced retinal microvascular dysfunction in diabetic rats. *Curr. Eye Res.* 43, 1395–1403. doi: 10.1080/02713683.2018.1501072

Li, S., Gokden, N., Okusa, M. D., Bhatt, R., and Portilla, D. (2005). Anti-inflammatory effect of fibrate protects from cisplatin-induced ARF. *Am. J. Physiol. Renal Physiol.* 289, F469–F480. doi: 10.1152/ajprenal.00038.2005

Li, X., Ren, C., Li, S., Han, R., Gao, J., Huang, Q., et al. (2017). Limb remote ischemic conditioning promotes myelination by upregulating PTEN/Akt/mTOR signaling activities after chronic cerebral hypoperfusion. *Aging Dis.* 8, 392–401. doi: 10.14336/AD.2016.1227

Liu, J., Xia, X., Xiong, S., Le, Y., and Xu, H. (2011). Intravitreous high expression level of netrin-1 in patients with proliferative diabetic retinopathy. *Eye Sci.* 26, 85–90, 120. doi: 10.3969/j.issn.1000-4432.2011.02.017

Liu, Q., Zhang, F., Zhang, X., Cheng, R., Ma, J. X., Yi, J., et al. (2018). Fenofibrate ameliorates diabetic retinopathy by modulating Nrf2 signaling and NLRP3 inflammasome activation. *Mol Cell Biochem.* 445, 105–115. doi: 10.1007/s11010-017-3256-x

Liu, Q., Zhang, X., Cheng, R., Ma, J. X., Yi, J., and Li, J. (2019). Salutary effect of fenofibrate on type 1 diabetic retinopathy via inhibiting oxidative stress-mediated Wnt/beta-catenin pathway activation. *Cell Tissue Res.* 376, 165–177. doi: 10.1007/s00441-018-2974-z

Liu, X., Zhu, B., Zou, H., Hu, D., Gu, Q., Liu, K., et al. (2015). Carbamylated erythropoietin mediates retinal neuroprotection in streptozotocin-induced early-stage diabetic rats. *Graefes Arch. Clin. Exp. Ophthalmol.* 253, 1263–1272. doi: 10.1007/s00417-015-2969-3

Liu, Y., Hirooka, K., Nishiyama, A., Lei, B., Nakamura, T., Itano, T., et al. (2012). Activation of the aldosterone/mineralocorticoid receptor system and protective effects of mineralocorticoid receptor antagonism in retinal ischemia-reperfusion injury. *Exp. Eye Res.* 96, 116–123. doi: 10.1016/j.exer.2011.12.012

Magen, I., and Gozes, I. (2014). Davunetide: peptide therapeutic in neurological disorders. *Curr. Med. Chem.* 21, 2591–2598. doi: 10.2174/0929867321666140217124945

Mahmoud, A. M., Abd El-Twab, S. M., and Abdel-Reheim, E. S. (2017). Consumption of polyphenol-rich *Morus alba* leaves extract attenuates early diabetic retinopathy: the underlying mechanism. *Eur. J. Nutr.* 56, 1671–1684. doi: 10.1007/s00394-016-1214-0

Marangoz, D., Guzel, E., Eyuboglu, S., Gumusel, A., Seckin, I., Ciftci, F., et al. (2018). Comparison of the neuroprotective effects of brimonidine tartrate and melatonin on retinal ganglion cells. *Int. Ophthalmol.* 38, 2553–2562. doi: 10.1007/s10792-017-0768-z

Masuzawa, K., Goto, K., Jesmin, S., Maeda, S., Miyauchi, T., Kaji, Y., et al. (2006). An endothelin type A receptor antagonist reverses upregulated VEGF and ICAM-1 levels in streptozotocin-induced diabetic rat retina. *Curr. Eye Res.* 31, 79–89. doi: 10.1080/02713680500478923

Mei, S., Cammalleri, M., Azara, D., Casini, G., Bagnoli, P., and Dal Monte, M. (2012). Mechanisms underlying somatostatin receptor 2 down-regulation of vascular endothelial growth factor expression in response to hypoxia in mouse retinal explants. *J. Pathol.* 226, 519–533. doi: 10.1002/path.3006

Milatovic, D., Zaja-Milatovic, S., and Gupta, R. C. (2016). "Oxidative stress and excitotoxicity: antioxidants from nutraceuticals," in *Nutraceuticals*, ed R. C. Gupta (Amsterdam; Boston, MA; Heidelberg; London; New York, NY; Oxford; San Diego, CA; San Francisco, CA; Singapore; Sydney, NSW; Tokyo: Elsevier), 401–413. doi: 10.1016/B978-0-12-802147-7.00029-2

Mishra, M., and Kowluru, R. A. (2016). The role of DNA methylation in the metabolic memory phenomenon associated with the continued progression of diabetic retinopathy. *Invest Ophthalmol. Vis. Sci.* 57, 5748–5757. doi: 10.1167/iovs.16-19759

Mishra, M., and Kowluru, R. A. (2019). DNA methylation-a potential source of mitochondria DNA base mismatch in the development of diabetic retinopathy. *Mol. Neurobiol.* 56, 88–101. doi: 10.1007/s12035-018-1086-9

Moran, E. P., Wang, Z., Chen, J., Sapieha, P., Smith, L. E., and Ma, J. X. (2016). Neurovascular cross talk in diabetic retinopathy: pathophysiological roles and therapeutic implications. *Am. J. Physiol. Heart Circ. Physiol.* 311, H738–H749. doi: 10.1152/ajpheart.00005.2016

Mrudula, T., Suryanarayana, P., Srinivas, P. N., and Reddy, G. B. (2007). Effect of curcumin on hyperglycemia-induced vascular endothelial growth factor expression in streptozotocin-induced diabetic rat retina. *Biochem. Biophys. Res. Commun.* 361, 528–532. doi: 10.1016/j.bbrc.2007.07.059

Nakamachi, T., Matkovits, A., Seki, T., and Shioda, S. (2012). Distribution and protective function of pituitary adenylate cyclase-activating polypeptide in the retina. *Front. Endocrinol.* 3:145. doi: 10.3389/fendo.2012.00145

Narimatsu, T., Ozawa, Y., Miyake, S., Nagai, N., and Tsubota, K. (2014). Angiotensin II type 1 receptor blockade suppresses light-induced neural damage in the mouse retina. *Free Radic. Biol. Med.* 71, 176–185. doi: 10.1016/j.freeradbiomed.2014.03.020

Navaratna, D., Menicucci, G., Maestas, J., Srinivasan, R., Mcguire, P., and Das, A. (2008). A peptide inhibitor of the urokinase/urokinase receptor system inhibits alteration of the blood-retinal barrier in diabetes. *FASEB J.* 22, 3310–3317. doi: 10.1096/fj.08-110155

Naveh, N. (2003). Melanocortins applied intravitreally delay retinal dystrophy in Royal College of Surgeons rats. *Graefes Arch. Clin. Exp. Ophthalmol.* 241, 1044–1050. doi: 10.1007/s00417-003-0781-y

Noonan, J. E., Jenkins, A. J., Ma, J. X., Keech, A. C., Wang, J. J., and Lamoureux, E. L. (2013). An update on the molecular actions of fenofibrate and its clinical effects on diabetic retinopathy and other microvascular end points in patients with diabetes. *Diabetes* 62, 3968–3975. doi: 10.2337/db13-0800

Ola, M. S., Ahmed, M. M., Abuohashish, H. M., Al-Rejaie, S. S., and Alhomida, A. S. (2013). Telmisartan ameliorates neurotrophic support and oxidative stress in the retina of streptozotocin-induced diabetic rats. *Neurochem. Res.* 38, 1572–1579. doi: 10.1007/s11064-013-1058-4

Ola, M. S., Ahmed, M. M., Shams, S., and Al-Rejaie, S. S. (2017). Neuroprotective effects of quercetin in diabetic rat retina. *Saudi J. Biol. Sci.* 24, 1186–1194. doi: 10.1016/j.sjbs.2016.11.017

Ola, M. S., Nawaz, M. I., Siddiquei, M. M., Al-Amro, S., and Abu El-Asrar, A. M. (2012). Recent advances in understanding the biochemical and molecular mechanism of diabetic retinopathy. *J. Diabetes Complic.* 26, 56–64. doi: 10.1016/j.jdiacomp.2011.11.004

Orhan, C., Akdemir, F., Tuzcu, M., Sahin, N., Yilmaz, I., Deshpande, J., et al. (2016). Mesozeaxanthin protects retina from oxidative stress in a rat model. *J. Ocul. Pharmacol. Ther.* 32, 631–637. doi: 10.1089/jop.2015.0154

Ozawa, Y., Kurihara, T., Tsubota, K., and Okano, H. (2011). Regulation of posttranscriptional modification as a possible therapeutic approach for retinal neuroprotection. *J. Ophthalmol.* 2011:506137. doi: 10.1155/2011/506137

Ozawa, Y., Sasaki, M., Takahashi, N., Kamoshita, M., Miyake, S., and Tsubota, K. (2012). Neuroprotective effects of lutein in the retina. *Curr. Pharm. Des.* 18, 51–56. doi: 10.2174/138161212798919101

Pantalone, K. M., Hobbs, T. M., Wells, B. J., Kong, S. X., Kattan, M. W., Bouchard, J., et al. (2015). Clinical characteristics, complications, comorbidities and treatment patterns among patients with type 2 diabetes mellitus in a large integrated health system. *BMJ Open Diabetes Res. Care* 3:2015-000093. doi: 10.1136/bmjdrc-2015-000093

Perez De Sevilla Muller, L., Solomon, A., Sheets, K., Hapukino, H., Rodriguez, A. R., and Brecha, N. C. (2019). Multiple cell types form the VIP amacrine cell population. *J. Comp. Neurol.* 527, 133–158. doi: 10.1002/cne.24234

Pyper, S. R., Viswakarma, N., Yu, S., and Reddy, J. K. (2010). PPARalpha: energy combustion, hypolipidemia, inflammation and cancer. *Nucleic Recept. Signal.* 16:08002. doi: 10.1621/nrs.08002

Qian, H., and Ripps, H. (2011). Neurovascular interaction and the pathophysiology of diabetic retinopathy. *Exp. Diabetes Res.* 2011:693426. doi: 10.1155/2011/693426

Qiu, F., Meng, T., Chen, Q., Zhou, K., Shao, Y., Matlock, G., et al. (2019). Fenofibrate-loaded biodegradable nanoparticles for the treatment of experimental diabetic retinopathy and neovascular age-related macular degeneration. *Mol. Pharm.* 16, 1958–1970. doi: 10.1021/acs.molpharmaceut.8b01319

Qiu, Y., Shil, P. K., Zhu, P., Yang, H., Verma, A., Lei, B., et al. (2014). Angiotensin-converting enzyme 2 (ACE2) activator diminazene aceturate ameliorates endotoxin-induced uveitis in mice. *Invest. Ophthalmol. Vis. Sci.* 55, 3809–3818. doi: 10.1167/iovs.14-13883

Qiu, Y., Tao, L., Zheng, S., Lin, R., Fu, X., Chen, Z., et al. (2016). AAV8-mediated angiotensin-converting enzyme 2 gene delivery prevents experimental autoimmune uveitis by regulating MAPK, NF-kappaB and STAT3 pathways. *Sci. Rep.* 6:31912. doi: 10.1038/srep31912

Quigley, H. A., Pitha, I. F., Welsbie, D. S., Nguyen, C., Steinhart, M. R., Nguyen, T. D., et al. (2015). Losartan treatment protects retinal ganglion cells and alters scleral remodeling in experimental glaucoma. *PLoS ONE* 10:e0141137. doi: 10.1371/journal.pone.0141137

Reglodi, D., Renaud, J., Tamas, A., Tizabi, Y., Socias, S. B., Del-Bel, E., et al. (2017). Novel tactics for neuroprotection in Parkinson's disease: role of antibiotics, polyphenols and neuropeptides. *Prog. Neurobiol.* 155, 120–148. doi: 10.1016/j.pneurobio.2015.10.004

Ren, C., Wu, H., Li, D., Yang, Y., Gao, Y., Jizhang, Y., et al. (2018). Remote ischemic conditioning protects diabetic retinopathy in streptozotocin-induced diabetic rats via anti-inflammation and antioxidation. *Aging Dis.* 9, 1122–1133. doi: 10.14336/AD.2018.0711

Romano, M. R., Biagioni, F., Besozzi, G., Carrizzo, A., Vecchione, C., Fornai, F., et al. (2012). Effects of bevacizumab on neuronal viability of retinal ganglion cells in rats. *Brain Res.* 10, 55–63. doi: 10.1016/j.brainres.2012.08.014

Rong, X., Ji, Y., Zhu, X., Yang, J., Qian, D., Mo, X., et al. (2018). Neuroprotective effect of insulin-loaded chitosan nanoparticles/PLGA-PEG-PLGA hydrogel on diabetic retinopathy in rats. *Int. J. Nanomed.* 14, 45–55. doi: 10.2147/IJN.S184574

Rossino, M. G., and Casini, G. (2019). Nutraceuticals for the treatment of diabetic retinopathy. *Nutrients* 11:E771. doi: 10.3390/nu11040771

Rota, R., Chiavaroli, C., Garay, R. P., and Hannaert, P. (2004). Reduction of retinal albumin leakage by the antioxidant calcium dobesilate in streptozotocin-diabetic rats. *Eur. J. Pharmacol.* 495, 217–224. doi: 10.1016/j.ejphar.2004.05.019

Saint-Geniez, M., Maharaj, A. S., Walshe, T. E., Tucker, B. A., Sekiyama, E., Kurihara, T., et al. (2008). Endogenous VEGF is required for visual function: evidence for a survival role on muller cells and photoreceptors. *PLoS ONE* 3:e3554. doi: 10.1371/journal.pone.0003554

Sampedro, J., Bogdanov, P., Ramos, H., Sola-Adell, C., Turch, M., Valeri, M., et al. (2019). New insights into the mechanisms of action of topical administration of GLP-1 in an experimental model of diabetic retinopathy. *J. Clin. Med.* 8:E339. doi: 10.3390/jcm8030339

Sasaki, M., Ozawa, Y., Kurihara, T., Kubota, S., Yuki, K., Noda, K., et al. (2010). Neurodegenerative influence of oxidative stress in the retina of a murine model of diabetes. *Diabetologia* 53, 971–979. doi: 10.1007/s00125-009-1655-6

Sasaki, M., Yuki, K., Kurihara, T., Miyake, S., Noda, K., Kobayashi, S., et al. (2012). Biological role of lutein in the light-induced retinal degeneration. *J. Nutr. Biochem.* 23, 423–429. doi: 10.1016/j.jnutbio.2011.01.006

Satofuka, S., Ichihara, A., Nagai, N., Noda, K., Ozawa, Y., Fukamizu, A., et al. (2009). (Pro)renin receptor-mediated signal transduction and tissue renin-angiotensin system contribute to diabetes-induced retinal inflammation. *Diabetes* 58, 1625–1633. doi: 10.2337/db08-0254

Scuderi, S., D'amico, A. G., Castorina, A., Federico, C., Marrazzo, G., Drago, F., et al. (2014). Davunetide (NAP) protects the retina against early diabetic injury by reducing apoptotic death. *J. Mol. Neurosci.* 54, 395–404. doi: 10.1007/s12031-014-0244-4

Semba, K., Namekata, K., Guo, X., Harada, C., Harada, T., and Mitamura, Y. (2014). Renin-angiotensin system regulates neurodegeneration in a mouse model of normal tension glaucoma. *Cell Death Dis.* 17:296. doi: 10.1038/cddis.2014.296

Shil, P. K., Kwon, K. C., Zhu, P., Verma, A., Daniell, H., and Li, Q. (2014). Oral delivery of ACE2/Ang-(1-7) bioencapsulated in plant cells protects against experimental uveitis and autoimmune uveoretinitis. *Mol. Ther.* 22, 2069–2082. doi: 10.1038/mt.2014.179

Shimouchi, A., Yokota, H., Ono, S., Matsumoto, C., Tamai, T., Takumi, H., et al. (2016). Neuroprotective effect of water-dispersible hesperetin in retinal ischemia reperfusion injury. *Jpn. J. Ophthalmol.* 60, 51–61. doi: 10.1007/s10384-015-0415-z

Shioda, S., Takenoya, F., Wada, N., Hirabayashi, T., Seki, T., and Nakamachi, T. (2016). Pleiotropic and retinoprotective functions of PACAP. *Anat Sci. Int.* 91, 313–324. doi: 10.1007/s12565-016-0351-0

Silva, K. C., Rosales, M. A., Biswas, S. K., Lopes De Faria, J. B., and Lopes De Faria, J. M. (2009). Diabetic retinal neurodegeneration is associated with mitochondrial oxidative stress and is improved by an angiotensin receptor blocker in a model combining hypertension and diabetes. *Diabetes* 58, 1382–1390. doi: 10.2337/db09-0166

Silva, K. C., Rosales, M. A., Hamassaki, D. E., Saito, K. C., Faria, A. M., Ribeiro, P. A., et al. (2013). Green tea is neuroprotective in diabetic retinopathy. *Invest. Ophthalmol. Vis. Sci.* 54, 1325–1336. doi: 10.1167/iovs.12-10647

Simo, R., Carrasco, E., Fonollosa, A., Garcia-Arumi, J., Casamitjana, R., and Hernandez, C. (2007). Deficit of somatostatin in the vitreous fluid of patients with diabetic macular edema. *Diabetes Care* 30, 725–727. doi: 10.2337/dc06-1345

Simo, R., and Hernandez, C. (2009). Advances in the medical treatment of diabetic retinopathy. *Diabetes Care* 32, 1556–1562. doi: 10.2337/dc09-0565

Simo, R., and Hernandez, C. (2015). Novel approaches for treating diabetic retinopathy based on recent pathogenic evidence. *Prog. Retin Eye Res.* 48, 160–180. doi: 10.1016/j.preteyeres.2015.04.003

Simo, R., Stitt, A. W., and Gardner, T. W. (2018). Neurodegeneration in diabetic retinopathy: does it really matter? *Diabetologia* 61, 1902–1912. doi: 10.1007/s00125-018-4692-1

Simo, R., Sundstrom, J. M., and Antonetti, D. A. (2014). Ocular Anti-VEGF therapy for diabetic retinopathy: the role of VEGF in the pathogenesis of diabetic retinopathy. *Diabetes Care* 37, 893–899. doi: 10.2337/dc13-2002

Smith, N. K., Hackett, T. A., Galli, A., and Flynn, C. R. (2019). GLP-1: molecular mechanisms and outcomes of a complex signaling system. *Neurochem. Int.* 128, 94–105. doi: 10.1016/j.neuint.2019.04.010

Sohn, E., Kim, J., Kim, C. S., Lee, Y. M., and Kim, J. S. (2016). Extract of polygonum cuspidatum attenuates diabetic retinopathy by inhibiting the high-mobility group box-1 (HMGB1) signaling pathway in streptozotocin-induced diabetic rats. *Nutrients* 8:140. doi: 10.3390/nu8030140

Sola-Adell, C., Bogdanov, P., Hernandez, C., Sampedro, J., Valeri, M., Garcia-Ramirez, M., et al. (2017). Calcium dobesilate prevents neurodegeneration and vascular leakage in experimental diabetes. *Curr. Eye Res.* 42, 1273–1286. doi: 10.1080/02713683.2017.1302591

Solomon, S. D., Chew, E., Duh, E. J., Sobrin, L., Sun, J. K., Vanderbeek, B. L., et al. (2017). Diabetic retinopathy: a position statement by the American Diabetes Association. *Diabetes Care* 40, 412–418. doi: 10.2337/dc16-2641

Song, Y., Huang, L., and Yu, J. (2016). Effects of blueberry anthocyanins on retinal oxidative stress and inflammation in diabetes through Nrf2/HO-1 signaling. *J. Neuroimmunol.* 301, 1–6. doi: 10.1016/j.jneuroim.2016.11.001

Soufi, F. G., Mohammad-Nejad, D., and Ahmadieh, H. (2012). Resveratrol improves diabetic retinopathy possibly through oxidative stress - nuclear factor kappaB - apoptosis pathway. *Pharmacol. Rep.* 64, 1505–1514. doi: 10.1016/S1734-1140(12)70948-9

Stitt, A. W., Lois, N., Medina, R. J., Adamson, P., and Curtis, T. M. (2013). Advances in our understanding of diabetic retinopathy. *Clin. Sci.* 125, 1–17. doi: 10.1042/CS20120588

Szabadfi, K., Reglodi, D., Szabo, A., Szalontai, B., Valasek, A., Setalo, G. Jr., et al. (2016). Pituitary adenylate cyclase activating polypeptide, a potential therapeutic agent for diabetic retinopathy in rats: focus on the vertical information processing pathway. *Neurotox Res.* 29, 432–446. doi: 10.1007/s12640-015-9593-1

Szabadfi, K., Szabo, A., Kiss, P., Reglodi, D., Setalo, G. Jr., Kovacs, K., et al. (2014). PACAP promotes neuron survival in early experimental diabetic retinopathy. *Neurochem. Int.* 64, 84–91. doi: 10.1016/j.neuint.2013.11.005

Szabo, M. E., Haines, D., Garay, E., Chiavaroli, C., Farine, J. C., Hannaert, P., et al. (2001). Antioxidant properties of calcium dobesilate in ischemic/reperfused diabetic rat retina. *Eur. J. Pharmacol.* 428, 277–286. doi: 10.1016/S0014-2999(01)01196-7

Tarr, J. M., Kaul, K., Chopra, M., Kohner, E. M., and Chibber, R. (2013). Pathophysiology of diabetic retinopathy. *ISRN Ophthalmol.* 2013:343560. doi: 10.1155/2013/343560

Tejerina, T., and Ruiz, E. (1998). Calcium dobesilate: pharmacology and future approaches. *Gen. Pharmacol.* 31, 357–360. doi: 10.1016/S0306-3623(98)00040-8

Thangaraju, P., Chakrabarti, A., Banerjee, D., Hota, D., Tamilselvan, Bhatia, A., and Gupta, A. (2014). Dual blockade of Renin Angiotensin system in reducing the early changes of diabetic retinopathy and nephropathy in a diabetic rat model. *N. Am. J. Med. Sci.* 6, 625–632. doi: 10.4103/1947-2714.147978

Thounaojam, M. C., Powell, F. L., Patel, S., Gutsaeva, D. R., Tawfik, A., Smith, S. B., et al. (2017). Protective effects of agonists of growth hormone-releasing hormone (GHRH) in early experimental diabetic retinopathy. *Proc. Natl. Acad. Sci. U.S.A.* 114, 13248–13253. doi: 10.1073/pnas.1718592114

Tuncel, N., Basmak, H., Uzuner, K., Tuncel, M., Altiokka, G., Zaimoglu, V., et al. (1996). Protection of rat retina from ischemia-reperfusion injury by vasoactive intestinal peptide (VIP): the effect of VIP on lipid peroxidation and antioxidant enzyme activity of retina and choroid. *Ann. N.Y. Acad. Sci.* 805, 489–498. doi: 10.1111/j.1749-6632.1996.tb17509.x

Tuzcu, M., Orhan, C., Muz, O. E., Sahin, N., Juturu, V., and Sahin, K. (2017). Lutein and zeaxanthin isomers modulates lipid metabolism and the inflammatory state of retina in obesity-induced high-fat diet rodent model. *BMC Ophthalmol.* 17:129. doi: 10.1186/s12886-017-0524-1

Umeda, N., Ozaki, H., Hayashi, H., and Oshima, K. (2004). Expression of ephrinB2 and its receptors on fibroproliferative membranes in ocular angiogenic diseases. *Am. J. Ophthalmol.* 138, 270–279. doi: 10.1016/j.ajo.2004.04.006

Vaczy, A., Reglodi, D., Somoskeoy, T., Kovacs, K., Lokos, E., Szabo, E., et al. (2016). The protective role of PAC1-receptor agonist maxadilan in BCCAO-induced retinal degeneration. *J. Mol. Neurosci.* 60, 186–194. doi: 10.1007/s12031-016-0818-4

Varga, B., Gesztelyi, R., Bombicz, M., Haines, D., Szabo, A. M., Kemeny-Beke, A., et al. (2013). Protective effect of alpha-melanocyte-stimulating hormone (alpha-MSH) on the recovery of ischemia/reperfusion (I/R)-induced retinal damage in a rat model. *J. Mol. Neurosci.* 50, 558–570. doi: 10.1007/s12031-013-9998-3

Vaudry, D., Falluel-Morel, A., Bourgault, S., Basille, M., Burel, D., Wurtz, O., et al. (2009). Pituitary adenylate cyclase-activating polypeptide and its receptors: 20 years after the discovery. *Pharmacol. Rev.* 61, 283–357. doi: 10.1124/pr.109.001370

Verma, A., Shan, Z., Lei, B., Yuan, L., Liu, X., Nakagawa, T., et al. (2012). ACE2 and Ang-(1-7) confer protection against development of diabetic retinopathy. *Mol. Ther.* 20, 28–36. doi: 10.1038/mt.2011.155

Voabil, P., Liberal, J., Leal, E. C., Bauer, J., Cunha-Vaz, J., Santiago, A. R., et al. (2017). Calcium dobesilate is protective against inflammation and oxidative/nitrosative stress in the retina of a type 1 diabetic rat model. *Ophthalmic Res.* 58, 150–161. doi: 10.1159/000478784

Wang, J., Sun, Z., Shen, J., Wu, D., Liu, F., Yang, R., et al. (2015). Octreotide protects the mouse retina against ischemic reperfusion injury through regulation of antioxidation and activation of NF-kappaB. *Oxid. Med. Cell Longev.* 2015:970156. doi: 10.1155/2015/970156

Wang, J., Tian, W., Wang, S., Wei, W., Wu, D., Wang, H., et al. (2017). Anti-inflammatory and retinal protective effects of capsaicin on ischaemia-induced injuries through the release of endogenous somatostatin. *Clin. Exp. Pharmacol. Physiol.* 44, 803–814. doi: 10.1111/1440-1681.12769

Wang, L., Li, C., Guo, H., Kern, T. S., Huang, K., and Zheng, L. (2011). Curcumin inhibits neuronal and vascular degeneration in retina after ischemia and reperfusion injury. *PLoS ONE* 6:e23194. doi: 10.1371/journal.pone.0023194

Wang, L. L., Sun, Y., Huang, K., and Zheng, L. (2013). Curcumin, a potential therapeutic candidate for retinal diseases. *Mol. Nutr. Food Res.* 57, 1557–1568. doi: 10.1002/mnfr.201200718

Wang, N., Zou, C., Zhao, S., Wang, Y., Han, C., and Zheng, Z. (2018). Fenofibrate exerts protective effects in diabetic retinopathy via inhibition of the ANGPTL3 pathway. *Invest. Ophthalmol. Vis. Sci.* 59, 4210–4217. doi: 10.1167/iovs.18-24155

Wang, Q., Gorbey, S., Pfister, F., Hoger, S., Dorn-Beineke, A., Krugel, K., et al. (2011). Long-term treatment with suberythropoietic Epo is vaso- and neuroprotective in experimental diabetic retinopathy. *Cell Physiol. Biochem.* 27, 769–782. doi: 10.1159/000330085

Wang, Q., Pfister, F., Dorn-Beineke, A., Vom Hagen, F., Lin, J., Feng, Y., et al. (2010). Low-dose erythropoietin inhibits oxidative stress and early vascular changes in the experimental diabetic retina. *Diabetologia* 53, 1227–1238. doi: 10.1007/s00125-010-1727-7

Wang, W., Zhang, Y., Jin, W., Xing, Y., and Yang, A. (2018). Catechin weakens diabetic retinopathy by inhibiting the expression of NF-kappaB signaling pathway-mediated inflammatory factors. *Ann. Clin. Lab Sci.* 48, 594–600.

Wardlaw, S. L. (2011). Hypothalamic proopiomelanocortin processing and the regulation of energy balance. *Eur. J. Pharmacol.* 660, 213–219. doi: 10.1016/j.ejphar.2010.10.107

Werling, D., Banks, W. A., Salameh, T. S., Kvarik, T., Kovacs, L. A., Vaczy, A., et al. (2017). Passage through the ocular barriers and beneficial effects in retinal ischemia of topical application of PACAP1-38 in rodents. *Int. J. Mol. Sci.* 18:E675. doi: 10.3390/ijms18030675

Werling, D., Reglodi, D., Banks, W. A., Salameh, T. S., Kovacs, K., Kvarik, T., et al. (2016). Ocular delivery of PACAP1-27 protects the retina from ischemic damage in rodents. *Invest. Ophthalmol. Vis. Sci.* 57, 6683–6691. doi: 10.1167/iovs.16-20630

Wilkinson-Berka, J. L., Agrotis, A., and Deliyanti, D. (2012). The retinal renin-angiotensin system: roles of angiotensin II and aldosterone. *Peptides* 36, 142–150. doi: 10.1016/j.peptides.2012.04.008

Xie, M. Y., Yang, Y., Liu, P., Luo, Y., and Tang, S. B. (2019). 5-aza-2′-deoxycytidine in the regulation of antioxidant enzymes in retinal endothelial cells and rat diabetic retina. *Int. J. Ophthalmol.* 12, 1–7. doi: 10.18240/ijo.2019.01.01

Yang, F., Yu, J., Ke, F., Lan, M., Li, D., Tan, K., et al. (2018). Curcumin alleviates diabetic retinopathy in experimental diabetic rats. *Ophthalmic Res.* 60, 43–54. doi: 10.1159/000486574

Yang, H., Hirooka, K., Fukuda, K., and Shiraga, F. (2009). Neuroprotective effects of angiotensin II type 1 receptor blocker in a rat model of chronic glaucoma. *Invest. Ophthalmol. Vis. Sci.* 50, 5800–5804. doi: 10.1167/iovs.09-3678

Yang, Y. (2011). Structure, function and regulation of the melanocortin receptors. *Eur. J. Pharmacol.* 660, 125–130. doi: 10.1016/j.ejphar.2010.12.020

Ye, D., Shi, Y., Xu, Y., and Huang, J. (2019). PACAP attenuates optic nerve crush-induced retinal ganglion cell apoptosis via activation of the CREB-Bcl-2 pathway. *J. Mol. Neurosci.* 16, 019–01309. doi: 10.1007/s12031-019-01309-9

Zeng, Y., Yang, K., Wang, F., Zhou, L., Hu, Y., Tang, M., et al. (2016). The glucagon like peptide 1 analogue, exendin-4, attenuates oxidative stress-induced retinal cell death in early diabetic rats through promoting Sirt1 and Sirt3 expression. *Exp. Eye Res.* 151, 203–211. doi: 10.1016/j.exer.2016.05.002

Zhang, J., Wu, Y., Jin, Y., Ji, F., Sinclair, S. H., Luo, Y., et al. (2008). Intravitreal injection of erythropoietin protects both retinal vascular and neuronal cells in early diabetes. *Invest. Ophthalmol. Vis. Sci.* 49, 732–742. doi: 10.1167/iovs.07-0721

Zhang, L., Dong, L., Liu, X., Jiang, Y., Zhang, X., Li, X., et al. (2014). α-Melanocyte-stimulating hormone protects retinal vascular endothelial cells from oxidative stress and apoptosis in a rat model of diabetes. *PLoS ONE* 9:e93433. doi: 10.1371/journal.pone.0093433

Zhang, R., Zhang, H., Xu, L., Ma, K., Wallrapp, C., and Jonas, J. B. (2011). Neuroprotective effect of intravitreal cell-based glucagon-like peptide-1 production in the optic nerve crush model. *Acta Ophthalmol.* 89, 1755–3768. doi: 10.1111/j.1755-3768.2010.02044.x

Zhang, X., Liu, W., Wu, S., Jin, J., Li, W., and Wang, N. (2015). Calcium dobesilate for diabetic retinopathy: a systematic review and meta-analysis. *Sci. China Life Sci.* 58, 101–107. doi: 10.1007/s11427-014-4792-1

Zhang, X., Wang, N., Barile, G. R., Bao, S., and Gillies, M. (2013). Diabetic retinopathy: neuron protection as a therapeutic target. *Int. J. Biochem. Cell Biol.* 45, 1525–1529. doi: 10.1016/j.biocel.2013.03.002

Zhang, Y., Wang, Q., Zhang, J., Lei, X., Xu, G. T., and Ye, W. (2009). Protection of exendin-4 analogue in early experimental diabetic retinopathy. *Graefes Arch. Clin. Exp. Ophthalmol.* 247, 699–706. doi: 10.1007/s00417-008-1004-3

Zhang, Y., Zhang, J., Wang, Q., Lei, X., Chu, Q., Xu, G. T., et al. (2011). Intravitreal injection of exendin-4 analogue protects retinal cells in early diabetic rats. *Invest. Ophthalmol. Vis. Sci.* 52, 278–285. doi: 10.1167/iovs.09-4727

Zhao, Y., and Singh, R. P. (2018). The role of anti-vascular endothelial growth factor (anti-VEGF) in the management of proliferative diabetic retinopathy. *Drugs Context* 7:212532. doi: 10.7573/dic.212532

Zuo, Z. F., Zhang, Q., and Liu, X. Z. (2013). Protective effects of curcumin on retinal Muller cell in early diabetic rats. *Int. J. Ophthalmol.* 6, 422–424. doi: 10.3980/j.issn.2222-3959.2013.04.02

Zusev, M., and Gozes, I. (2004). Differential regulation of activity-dependent neuroprotective protein in rat astrocytes by VIP and PACAP. *Regul. Pept.* 123, 33–41. doi: 10.1016/j.regpep.2004.05.021

Conflict of Interest: The authors declare that the research was conducted in the absence of any commercial or financial relationships that could be construed as a potential conflict of interest.

frontiers in Neuroscience

ORIGINAL RESEARCH
published: 15 November 2019
doi: 10.3389/fnins.2019.01234

Investigations Into Bioenergetic Neuroprotection of Cone Photoreceptors: Relevance to Retinitis Pigmentosa

*Daniel S. Narayan, Glyn Chidlow, John P. M. Wood and Robert J. Casson**

Ophthalmic Research Laboratories, Discipline of Ophthalmology and Visual Sciences, University of Adelaide, Adelaide, SA, Australia

Recent studies suggest cone degeneration in retinitis pigmentosa (RP) may result from intracellular energy depletion. We tested the hypothesis that cones die when depleted of energy by examining the effect of two bioenergetic, nutraceutical agents on cone survival. The study had three specific aims: firstly, we, studied the neuroprotective efficacies of glucose and creatine in an *in vitro* model of RP. Next, we utilized a well-characterized mouse model of RP to examine whether surviving cones, devoid of their inner segments, continue to express genes vital for glucose, and creatine utilization. Finally, we analyzed the neuroprotective properties of glucose and creatine on cone photoreceptors in a mouse model of RP. Two different bioenergy-based therapies were tested in *rd1* mice: repeated local delivery of glucose and systemic creatine. Optomotor responses were tested and cone density was quantified on retinal wholemounts. The results showed that glucose supplementation increased survival of cones in culture subjected to mitochondrial stress or oxidative insult. Despite losing their inner segments, surviving cones in the *rd1* retina continued to express the various glycolytic enzymes. Following a single subconjunctival injection, the mean vitreous glucose concentration was significantly elevated at 1 and 8 h, but not at 16 h after injection; however, daily subconjunctival injection of glucose neither enhanced spatial visual performance nor slowed cone cell degeneration in *rd1* mice relative to isotonic saline. Creatine dose-dependently increased survival of cones in culture subjected to mitochondrial dysfunction, but not to oxidative stress. Despite the loss of their mitochondrial-rich inner segments, cone somas and axonal terminals in the *rd1* retina were strongly positive for both the mitochondrial and cytosolic forms of creatine kinase at each time point examined. Creatine-fed *rd1* mice displayed enhanced optomotor responses compared to mice fed normal chow. Moreover, cone density was significantly greater in creatine-treated mice compared to controls. The overall results of this study provide tentative support for the hypothesis that creatine supplementation may delay secondary degeneration of cones in individuals with RP.

Keywords: *rd1* mouse, retinitis pigmentosa, cone photoreceptor, bioenergetic neuroprotection, creatine, nutraceutical, S-opsin, M/L-opsin

OPEN ACCESS

Edited by:
Giovanni Casini,
University of Pisa, Italy

Reviewed by:
Lisa Nivison-Smith,
University of New South Wales, Australia
Claudio Punzo,
University of Massachusetts Medical School, United States
Francois Paquet-Durand,
University of Tübingen, Germany

****Correspondence:***
Robert J. Casson
robert.casson@adelaide.edu.au

Specialty section:
This article was submitted to Neurodegeneration, a section of the journal Frontiers in Neuroscience

Received: *10 July 2019*
Accepted: *31 October 2019*
Published: *15 November 2019*

Citation:
Narayan DS, Chidlow G, Wood JPM and Casson RJ (2019) Investigations Into Bioenergetic Neuroprotection of Cone Photoreceptors: Relevance to Retinitis Pigmentosa. Front. Neurosci. 13:1234. doi: 10.3389/fnins.2019.01234

INTRODUCTION

Human photoreceptors have a curious and incompletely understood energy metabolism. They derive their nutrient supply from the choriocapillaris, and recent evidence indicates that they are members of a "metabolic ecosystem" comprising the retinal pigment epithelium and adjacent Müller cells (Kanow et al., 2017). Oxidative phosphorylation is an important source of ATP for the retina (Anderson and Saltzman, 1964), and the region of greatest oxygen consumption is the mitochondrial-rich inner segments of the photoreceptors (Cringle et al., 2002). However, mammalian photoreceptors also display aerobic glycolysis (the Warburg effect), producing relatively large amounts of lactate despite the presence of abundant oxygen (Winkler, 1981; Wang et al., 1997; Chinchore et al., 2017; Narayan et al., 2017; Petit et al., 2018). The explanation for this unusual metabolism, which is reminiscent of cancer cells, is unclear, but it seems reasonable to infer that photoreceptors are promiscuous in terms of their energy supply.

Photoreceptors require large amounts of energy to maintain their resting potentials (Ames et al., 1992; Niven et al., 2007), with cones incurring an even greater energy expenditure than rods (Okawa et al., 2008). In the face of this relentless energy demand it seems likely that an impairment of energy metabolism would be detrimental to photoreceptor function with serious consequences for vision. Indeed, there is converging evidence that bioenergetic dysfunction is a key pathogenic factor in secondary cone degeneration in retinitis pigmentosa (RP) (Punzo et al., 2009; Ait-Ali et al., 2015; Narayan et al., 2016; Wang et al., 2016). In the majority of subtypes of RP, the genetic defect is expressed in the rods, but in most individuals the cones eventually degenerate resulting in loss of central vision. Therapeutic targeting of secondary cone degeneration in RP is a broad-spectrum strategy applicable to a large proportion of RP subtypes irrespective of the specific gene defect. Bioenergetic-based neuroprotection strategies, which include augmenting or conserving available energy supplies, boosting mitochondrial efficiency, and improving cellular energy-buffering, and offer great potential in RP. Nutraceutical approaches to bioenergetic neuroprotection gain further appeal by their relative safety and clinical translatability.

Recent studies in animal models of RP have demonstrated that high glucose is critical for cone survival and that reduced glucose entry into cones triggers their degeneration (Punzo et al., 2009; Ait-Ali et al., 2015; Venkatesh et al., 2016). Moreover, a single injection of glucose has been shown to cause a short-term improvement in cone morphology in a slow-progressing porcine model of RP (Wang et al., 2016). We have previously demonstrated that elevating the vitreal glucose level protects retinal ganglion cells against experimental ischemic injury (Casson et al., 2004; Shibeeb et al., 2016) and temporarily recovers contrast sensitivity in individuals with glaucoma (Casson et al., 2014; Shibeeb et al., 2016). Importantly, these effects can be achieved by local delivery of glucose. These insights provide considerable motivation to further investigate glucose energy supplementation as a potential therapy for RP.

A second bioenergetic approach with potential applicability to RP involves boosting levels of the nutraceutical creatine in cones. The creatine kinase/phosphocreatine system, plays an important role in mitochondrial energy metabolism (Wallimann et al., 2011), particularly in cells with high energetic demands such as photoreceptors (Linton et al., 2010). Functions ascribed to the creatine kinase/phosphocreatine kinase system include spatiotemporal buffering of ATP and improving the efficiency of oxidative phosphorylation. The creatine transporter, which is responsible for creatine uptake into cells, and creatine kinase, which catalyzes the reversible conversion of creatine into high energy phosphocreatine, are both expressed in photoreceptors (Acosta et al., 2005; Linton et al., 2010; Rueda et al., 2016; Chidlow et al., 2019); thus, supplementation with creatine is a neuroprotective strategy worthy of investigation.

The present study had three objectives: firstly, we, studied the neuroprotective efficacies of glucose and creatine in an *in vitro* model of RP. Next, we utilized a well-characterized mouse model of RP to examine whether surviving cones, devoid of their inner segments, continue to express genes vital for glucose and creatine utilization. Finally, we analyzed the neuroprotective properties of glucose and creatine on cone photoreceptors in the mouse model of RP.

MATERIALS AND METHODS

Retinal Cells *in vitro*: Establishment, Treatment, and Analysis of Cultures

Retinal cultures consisting of a mixed population of cell-types were established from 2 to 4 day old Sprague-Dawley rat pups via a combined enzymatic and mechanical dissociation procedure, as described previously (Wood et al., 2012). Dissociated cells were seeded on borosilicate glass coverslips pre-coated with poly-L-lysine (10 μg/ml; 15 min), at 0.5×10^6 cells/ml, in Minimal Essential Medium (Life Technologies Australia Pty Ltd, Mulgrave, VIC, Australia), containing 100 U/mL penicillin and streptomycin, 2 mM L-glutamine, 5 mM D-glucose and 10% (v/v) fetal bovine serum. Cultures were grown for 6 days *in vitro*, with no medium change during this time. Importantly, immunolabeling of cultures demonstrated the presence of S-opsin-expressing cone photoreceptors (**Figure 1**), enabling investigation of the responses of these cells to stressors and potential protectants *in vitro*.

Prior to experimental treatments, cultures were changed into an equivalent medium containing no glucose for 24 h; metabolic activity of cells was maintained by the presence of L-glutamine (Wood et al., 2005). For assessment of the potential protective effects of glucose (5 mM) or creatine (0.5 and 5 mM), cultures were pretreated for an additional 24 h with these compounds. To establish oxidative stress, tert-butyl hydroperoxide (tbH; 50 – 250 μM) was applied to cultures for 24 h. To induce metabolic stress, the mitochondrial Complex IV inhibitor sodium azide (250 μM – 1 mM) was applied for 24 h. All stressors and protectants were soluble in cell culture medium and hence, where applied, "vehicle" refers to an added equivalent volume of medium. After treatments, cultures were fixed in 10%

(w/v) neutral buffered formalin for 15 min and then processed for cone photoreceptor analysis via immunocytochemistry. A schematic representing the experimental timeline is provided in **Supplementary Figure S1**.

To assess if sodium azide increased aerobic glycolysis in mixed retinal cultures, cultures were changed into serum-free medium and incubated for 3 h in the presence or absence of sodium azide. Aliquots of medium were then analyzed using a lactate assay kit (BioVision Inc., Milpitas, CA, United States) and absorbances read with a microplate reader (Fluostar Optima; BMG Labtech, Mornington, VIC, Australia).

Survival of cones was assessed by immunocytochemical labeling of fixed cultures with S-opsin antibody (1:1000, see **Table 1**), as described in the immunohistochemistry methods section below. Nuclear counter-staining of cells was achieved with a final 5 min incubation of coverslips in 500 ng/ml 4′,6-diamidino-2-phenylindole (DAPI) before washing and mounting.

Animals and Procedures

This study was approved by the Animal Ethics Committees of SA Pathology/Central Adelaide Local Health Network (CALHN) and the University of Adelaide (Adelaide, SA, Australia) and conformed with the Australian Code of Practice for the Care and Use of Animals for Scientific Purposes, 2013, and with the ARVO Statement for the use of animals in vision and ophthalmic research. C3H/HeJArc (*rd1*) mice and C57BL/6J (wild-type, WT) mice were obtained from the Animal Resources Centre (Perth, WA, Australia). The C3H/HeJArc mouse is an inbred strain homozygous for the PDE6b mutation. *rd1* mice were inbred to produce offspring. All animals were housed in a temperature and humidity-controlled room with a 12-h light/dark cycle and provided with food and water *ad libitum*.

For detection of cone opsin proteins, creatine kinase isoforms, and glycolytic enzymes by immunohistochemistry, *rd1* mice at various postnatal day (P) time points [P7, P14, P21, P30, P45, and P60 (all $n = 3$) and WT mice (C57BL/6, $n = 3$)] were analyzed.

For the glucose neuroprotection study, *rd1* mice were randomly divided into experimental ($n = 13$) and control ($n = 11$) groups. At the starting age of P14, the right eyes of experimental mice were treated with an injection of 20 μl of 50% glucose into the subconjunctival space (see below). Injections were repeated at 24-hourly intervals. The left eye remained as an untreated control. Mice in the control group received a subconjunctival injection of osmotically matched 8.4% saline. Again, the fellow eye served as an untreated control. Injections were continued for 30 days in both groups. Optomotor testing was performed 10 days into the treatment regimen at P24. Mice were euthanized at P60.

For the creatine neuroprotection study, *rd1* mice were randomly divided into experimental ($n = 21$) and control ($n = 18$) groups. The experimental group was placed on a 2% oral creatine diet starting at the age of P21. Mice litters were weaned from their parents at P21 and this was the age oral treatment with creatine was commenced. Control animals were given an equicaloric standard mouse diet, without creatine. Mice were carefully observed to monitor their eating. Because the creatine was incorporated in the food, and mice were kept at 4 – 5 per cage, it was difficult to accurately assess how much food each mouse consumed. Daily weighing of mice was performed, and satisfactory weight gain was used as an indicator of appropriate food consumption. Optomotor testing was performed at P30. Mice in experimental and control groups continued their diet until they were euthanized at P60.

Tissue Processing and Immunohistochemistry

All mice were euthanized by transcardial perfusion with physiological saline under deep anesthesia. The superior aspect of each cornea was marked for orientation before globes were enucleated. For double labeling wholemount immunohistochemistry, eyes were fixed in 4% (w/v) neutral buffered formalin for 24 h and dissected into posterior eye-cups. Retinas were removed and prepared as flattened wholemounts by making another four radial cuts. Retinas were then incubated in phosphate buffered saline (PBS) containing 1% Triton X-100 detergent (PBS-T) for 1 h at room temperature. Next, retinas were incubated in PBS-T containing 3% normal horse serum (NHS-T) for 1 h at room temperature to block non-specific antibody binding. Retinas were then incubated overnight at 4°C with a combination of anti-S-opsin and anti-M/L-opsin antibodies diluted in NHS-T (see **Table 1**). On day 2, retinas were washed for 1 h at room temperature in PBS-T, then incubated overnight at 4°C with a combination of AlexaFluor-488 and -594 conjugated secondary antibodies (1:250; Invitrogen, Carlsbad,

TABLE 1 | Primary antibodies used in the study.

Protein	Source	Cat. No.	Species	Immunogen	Dilution
CK-B	Abcam	Ab125114	Mouse	Synthetic peptide SNSHNALKLRFPAEDEF, corresponding to N terminal amino acids 4–20 of human creatine kinase B type	1:1000
CK-MT1A	Proteintech	15346-1-AP	Rabbit	CKMT1A fusion protein Ag7583	1:5,000
Hexokinase II	Cell Signaling Technology	2867	Rabbit	Synthetic peptide corresponding to the sequence of human hexokinase II	1:500
LDH-A	Santa-Cruz	sc-27230	Goat	Epitope mapping at the N-terminus of LDH-A of human origin	1:1000
M/L-opsin	Merck-Millipore	AB5405	Rabbit	Recombinant human red/green opsin	1:1500
S-opsin	Santa-Cruz	sc-14363	Goat	Peptide mapping at the N-terminus of the opsin protein encoded by OPN1SW of human origin	1:1500

LDH-A, lactate dehydrogenase subunit A; CK-B, creatine kinase B-type; CK-MT1A, creatine kinase mitochondrial 1A.

CA, United States) diluted in NHS-T. Finally, retinas were washed in PBS for 1 h at room temperature prior to mounting with the photoreceptor side facing up using anti-fade mounting medium (Dako, CA, United States).

For immunohistochemistry on transverse sections, globes were immersion-fixed in Davidson's solution for 24 h and transferred to 70% ethanol until processing. Davidson's solution, which comprises 2 parts formaldehyde (37%), 3 parts 100% ethanol, 1 part glacial acetic acid and 3 parts water, is the preferred fixative for whole eyes as it provides optimal tissue morphology while avoiding retinal detachment. Globes were embedded sagittally and 4 μm serial sections were cut. For fluorescent double labeling immunohistochemistry, visualization of one antigen was achieved using a 3-step procedure, while the second antigen was labeled by a 2-step procedure, as previously described (Chidlow et al., 2011, 2016). In brief, tissue sections were deparaffinized and high-temperature antigen retrieval was performed. Subsequently, sections were incubated overnight in the appropriate combination of primary antibodies (**Table 1**). On the following day, sections were incubated with the appropriate biotinylated secondary antibody (1:250) for the 3-step procedure plus the correct secondary antibody conjugated to AlexaFluor 488 (1:250; Invitrogen) for the 2-step procedure for 30 min, followed by streptavidin-conjugated AlexaFluor 594 (1:500; Invitrogen) for 1 h. Sections were then mounted using anti-fade mounting medium.

Image Acquisition and Quantification

Confirmation of the specificity of antibody labeling was judged by the morphology and distribution of the labeled cells, by the absence of signal when the primary antibody was replaced by isotype/serum controls, and, by comparison with the expected staining pattern based on our own, and other, previously published results. Retinal wholemounts and transverse sections were examined under a fluorescence microscope (BX-61; Olympus, Mount Waverly, VIC, Australia) equipped with a scientific grade, cooled CCD camera.

Photomicrographs measuring 720 μm x 540 μm were taken using the fluorescence microscope on whole mounts retinas. Four photomicrographs of the central retina were taken directly superior, temporal, inferior, and nasal to the center of the optic nerve. Four photomicrographs of the peripheral retina were taken 1.5 mm superior, temporal, inferior, and nasal to the center of the optic nerve. This yielded a total of 16 photomicrographs per retina. Quantification of cone survival was performed using Image-J software (NIH, Bethesda, MD, United States). Initially, however, images were processed in Photoshop CS3 (Adobe, San Jose, CA, United States) for uneven lighting (using a flatten filter), sharpened, levels enhanced, and finally converted to 8-bit mode.

For the glucose experiment, three statistical comparisons were performed: glucose-injected vs. untreated contralateral eyes (Student's paired *t*-test); saline-injected vs. untreated contralateral eyes (Student's paired *t*-test); saline-injected eyes vs. glucose-injected eyes (Student's unpaired *t*-test). For the creatine experiment, statistical analysis was carried out by Student's unpaired *t*-test. The null hypothesis tested in each case was that cone density would be significantly higher in experimental vs. control eyes.

Measurement of Vitreal and Retinal Glucose After Subconjunctival Injection

Subconjunctival drug administration bypasses the conjunctival epithelial barrier, which is a rate-limiting factor for the permeation of water-soluble drugs (Gaudana et al., 2010); however, various dynamic, static, and metabolic barriers limit drug access to the posterior segment and retina. In order to establish whether subconjunctival glucose reaches the retina, a preliminary investigation was performed to measure the vitreous glucose concentration after subconjunctival injection. A single injection of 20 μl of 50% glucose was administered into the subconjunctival space in the right eyes of C57BL/6J mice. This procedure involved lifting the inside of the eyelid with fine forceps and delivering a subconjunctival injection using a 33G needle. Use of an operating microscope facilitated the procedure. Injections were performed under isoflurane sedation and topical amethocaine 0.5% anesthetic. During every injection, visualization of a subconjunctival bleb provided confirmation that the injection had been successfully administered. Left eyes were treated with an injection of osmotically matched 8.4% saline. Mice were euthanized after 1, 8, and 16 h ($n = 3$ per time point). Eyes were enucleated, the vitreous was removed as described previously (Skeie et al., 2011) and then sonicated. Vitreal samples (diluted to a final volume of 100 μl with distilled water) were then analyzed using a glucose hexokinase assay kit (Sigma-Aldrich Corp., St Louis, MO, United States) and absorbances read with a microplate reader (Fluostar Optima). The final vitreous glucose concentration (mmol/L) was determined by allowing for the 10-fold dilution factor, and comparing the absorbance with a previously constructed calibration curve. Statistical analysis was carried out by Student's paired *t*-test with Holm-Bonferroni correction. The null hypothesis tested was that the vitreous glucose concentration would be significantly higher in glucose- vs. saline-injected eyes.

A further experiment ($n = 3$) was carried out in which both the vitreal and retinal concentration of glucose was measured 30 min after a single subconjunctival injection of 20 μl of 50% glucose, using the method detailed above.

To analyze retinal uptake of 2-NBDG, mice underwent a single subconjunctival injection of 20 μl of 10 mM 2-NBDG (Invitrogen, Carlsbad, CA, United States) dissolved in water. After 30 min, mice were euthanized by exposure to a rising concentration of CO_2 and globes were enucleated under red light. They were then snap frozen in dry ice-cooled isopentane. Frozen, vertical sections (10 μm) were taken, mounted using anti-fade mounting medium, and examined under a fluorescence microscope.

Optomotor Testing

This test measures the tendency of an animal to follow a moving object using their head and eyes. Optomotor testing is an established method for quantifying visual function in mice (Prusky et al., 2004). The room was darkened for testing. The

only illumination came from the LED screens of the optomotor cage. However, animals were light adapted before starting the test, i.e., they were tested under photopic conditions. Mice were placed on a platform positioned in the middle of an arena created by a quad square of computer monitors. Vertical sine wave gratings (100% contrast) were projected on the computer monitors. The spatial frequencies tested were 0.05, 0.075, 0.1, 0.2, 0.3, 0.4, 0.5, and 0.6 cycles per degree, at a constant speed of 12 degrees/s. A camera was positioned directly above the platform in order to observe the animal's head movements. Mice were placed one at a time on the platform and allowed to move freely while the experimenter followed the mouse's head. When a grating perceptible to the mouse was projected on the cylinder wall and the cylinder was rotated (12 degrees/s), the mouse normally stopped moving its body and would begin to track the grating with reflexive head movements in concert with the rotation. A recorder assessed whether the mice tracked the cylinder by monitoring in the video window the image of the cylinder and the animal simultaneously. The spatial frequency of the grating was systematically increased the until the animal no longer responded. The process of incrementally changing the spatial frequency of the test grating was repeated until the highest spatial frequency that the mouse could track was identified as the threshold. A threshold for each direction of rotation was assessed this way, and the highest spatial frequency tracked in either direction was recorded as the threshold. Recorders were blinded to the treatment group and all mice were habituated before the outset of testing. For the glucose experiment, three statistical comparisons were performed: glucose-injected vs. untreated contralateral eyes (Student's paired *t*-test); saline-injected vs. untreated contralateral eyes (Student's paired *t*-test); saline-injected eyes vs. glucose-injected eyes (Student's unpaired *t*-test). For the creatine experiment, statistical analysis was carried out by Student's unpaired *t*-test. The null hypothesis tested in each

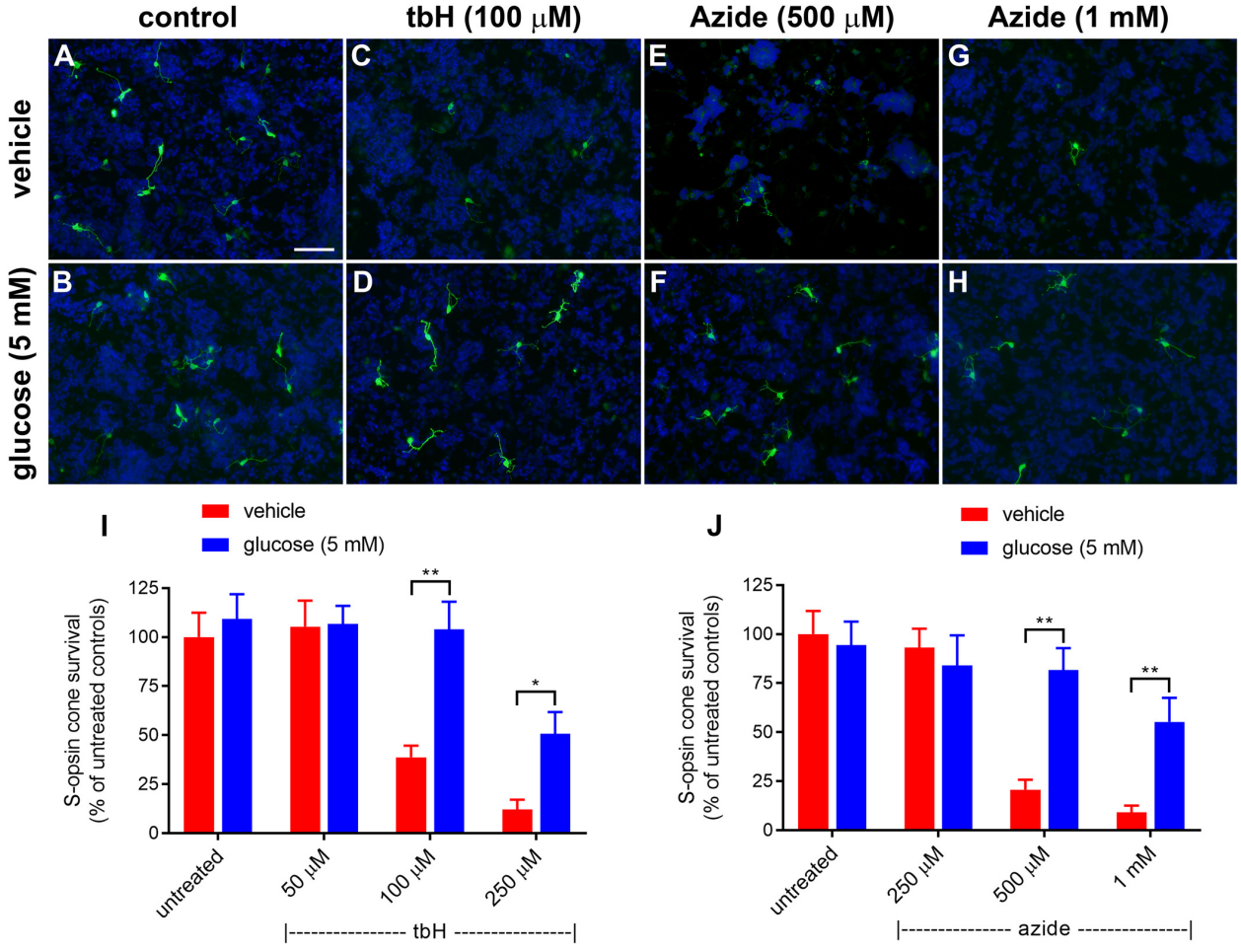

FIGURE 1 | Effect of glucose on stressor-induced S-opsin-labeled cone loss from mixed retinal cell cultures. Representative images from untreated **(A)**, vehicle-treated **(C,E,G)** or glucose (5 mM)-treated **(B,D,F,H)** cultures additionally exposed to **(C,D)**, 100 μM tbH **(E,F)**, 500 μM sodium azide **(G,H)**, 1 mM sodium azide. These data are followed by graphs quantifying the positive effect of glucose on tBH-induced **(I)** and sodium azide-induced **(J)** cone cell loss. It is evident that both tbH and sodium azide are markedly destructive to S-opsin labeled cones in culture and that glucose has clear protective influences on these cells in both cases. Values represent mean ± SEM, where $n = 8$ determinations from separate cultures. $^{**}P < 0.01$, and $^{*}P < 0.05$ by Student's paired *t*-test with Holm-Bonferroni correction. Scale bar, 50 μm.

case was that visual function would be significantly greater in experimental vs. control eyes.

RESULTS

Glucose Supplementation Protects Cones in Culture From Mitochondrial Dysfunction and Oxidative Injury

In order to investigate responses and potential protection of cone cells in culture, they were treated with one of two stressors: (1) sodium azide, which in inhibiting mitochondrial Complex IV causes metabolic compromise and (2) tbH, which induces intracellular oxidative stress. Both stressors mimic aspects of the pathology believed to be associated with RP (Narayan et al., 2016). Of note, sodium azide, by reducing mitochondrial activity, causes a compensatory increase in glycolysis, which is evidenced by increased lactate in the culture medium (**Supplementary Figure S1**).

Initially, we tested the protective effects of enriching the culture medium with 5 mM glucose; data are shown in **Figure 1**. Treatment with tbH caused a concentration-dependent loss of S-opsin cones with no observed decrease when 50 μM was applied, but with only 38.7 ± 5.9% or 12.0 ± 5.1% of cells remaining, respectively, when 100 μM or 250 μM tbH were applied. The presence of 5 mM glucose in the medium for 24 h prior to application of tbH was significantly protective: 104.0 ± 14.1% and 50.1 ± 11.1% of the control cell number

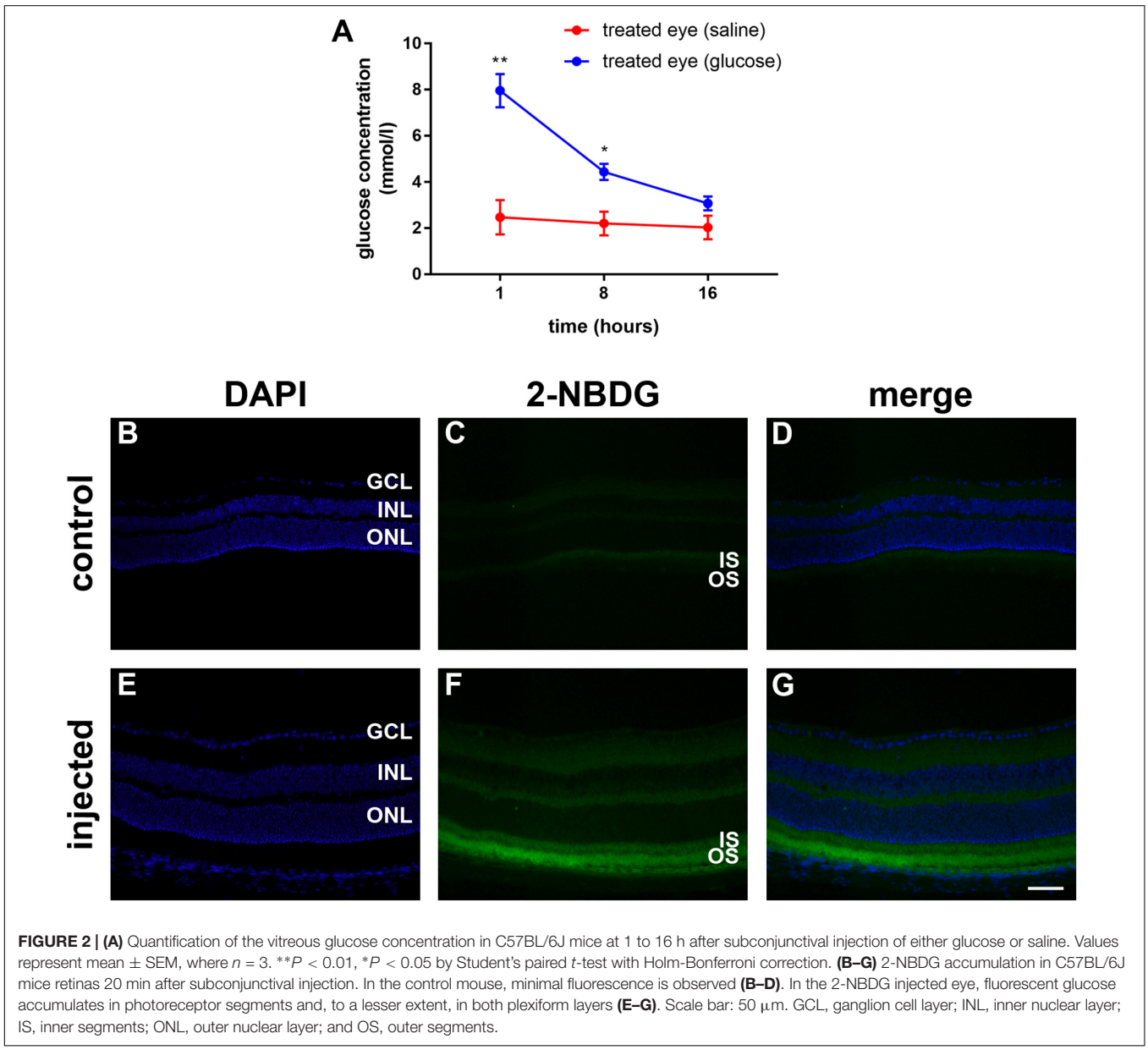

FIGURE 2 | (A) Quantification of the vitreous glucose concentration in C57BL/6J mice at 1 to 16 h after subconjunctival injection of either glucose or saline. Values represent mean ± SEM, where $n = 3$. $^{**}P < 0.01$, $^{*}P < 0.05$ by Student's paired t-test with Holm-Bonferroni correction. **(B–G)** 2-NBDG accumulation in C57BL/6J mice retinas 20 min after subconjunctival injection. In the control mouse, minimal fluorescence is observed **(B–D)**. In the 2-NBDG injected eye, fluorescent glucose accumulates in photoreceptor segments and, to a lesser extent, in both plexiform layers **(E–G)**. Scale bar: 50 μm. GCL, ganglion cell layer; INL, inner nuclear layer; IS, inner segments; ONL, outer nuclear layer; and OS, outer segments.

remained when cultures were treated with 100 μM and 250 μM tbH, respectively, in the presence of glucose (**Figure 1**).

Mitochondrial dysfunction, as induced by treatment of cultures with sodium azide for 24 h, caused a concentration-dependent loss of cones, with no significant loss when 250 μM was applied (93.1 ± 9.6% of control value), but significant decreases noted when 500 μM (20.7 ± 5.0% of control) or 1 mM (9.2 ± 4.0% of control) were applied (**Figure 1**). Pre-treatment with glucose significantly reduced the loss of cones with 81.6 ± 11.3% and 55.2 ± 12.3% of cones remaining after treatment with 500 μM and 1 mM azide, respectively.

Subconjunctival Delivery of Glucose Elevates the Vitreous Glucose Concentration

Prior to examining whether daily injections of glucose delay cone degeneration in a mouse model of RP, it was important to ascertain whether the delivery strategy resulted in a detectable increase in the level of glucose available to the retina. Thus, we measured the vitreous glucose concentration at time points after single subconjunctival injections of glucose or osmotically matched saline in WT mice. The results revealed statistically significant upregulations of glucose in the treated eye, compared to the saline-injected contralateral eye, at 1 h ($P < 0.01$, by paired Student's *t*-test) and 8 h ($P < 0.05$), but not 16 h, after injection (**Figure 2A**). Next, we part-repeated the experiment, except on this occasion we measured the retinal, as well as vitreal, glucose concentration at 1 h after injection, the time point of maximal elevation. In the vitreous, the glucose injected eye contained 9.8 ± 0.7 mmol/l glucose, which was significantly ($P < 0.01$ by Student's unpaired *t*-test) higher than the untreated contralateral eye (2.3 ± 0.2). In the retina, the glucose injected eye contained 38.3 ± 14.4 μg/retina glucose, whilst the untreated contralateral eye contained 16.0 ± 6.7 μg/retina glucose, a difference that did not reach statistical significance ($P > 0.1$). Of note, it is not possible for us to rule out that each retinal sample was contaminated by vitreous. In the mouse, the vitreous adheres to the retina tightly and this may have contributed to the trend of an elevated concentration in the retinal sample of the glucose injected eye.

In order to ascertain whether glucose reaches the photoreceptors after subconjunctival injection, we utilized 2-deoxy glucose (2-NDBG), a stable, fluorescent glucose derivative used for monitoring glucose uptake into living cells (Kanow et al., 2017). At 30 min after subconjunctival injection of 10 mM 2-NDBG, we harvested the retina for tissue sectioning and fluorescent imaging. **Figures 2B–G** reveals that 2-NBDG fluorescence was weakly localized to the inner and outer plexiform layers and was stronger in the photoreceptor inner and outer segments, confirming that glucose reaches the photoreceptor layer after subconjunctival injection.

Surviving Cones in the *rd1* Retina Express Glycolytic Enzymes

Photoreceptors have a high glycolytic flux and rate of lactate production even in the presence of oxygen, a phenomenon known as aerobic glycolysis. Accordingly, photoreceptors express glycolytic isoenzymes associated with aerobic glycolysis, including hexokinase II, pyruvate kinase M2 and lactate dehydrogenase (LDH). An increasing body of evidence suggests that energy starvation contributes to secondary degeneration of cones in RP (Punzo et al., 2009; Petit et al., 2018). Since glycolytic enzymes are concentrated in photoreceptor inner segments, and since loss of cone segments is an early pathological event in RP, we investigated whether surviving cones in the *rd1* retina continue to express genes vital for glucose utilization, including hexokinase II and lactate dehydrogenase subunit A (LDH-A).

In WT retinas, hexokinase II labeling was essentially restricted to rod and cone photoreceptor inner segments (**Figures 3A–C**). Despite the loss of inner segments, surviving cones in the *rd1* retina were strongly positive for hexokinase II at all time points examined, encompassing P7 to P60 (see **Figures 3D–L** for representative images).

In WT retinas, LDH-A was expressed by rod and cone photoreceptor somas, inner segments and axonal terminals, plus a limited number of cells in the inner retina (**Figures 4A–C**). In the *rd1* retina, LDH-A labeling was unequivocally expressed by surviving cones at each time point examined, encompassing P7 to P60 (see **Figures 4D–L** for representative images).

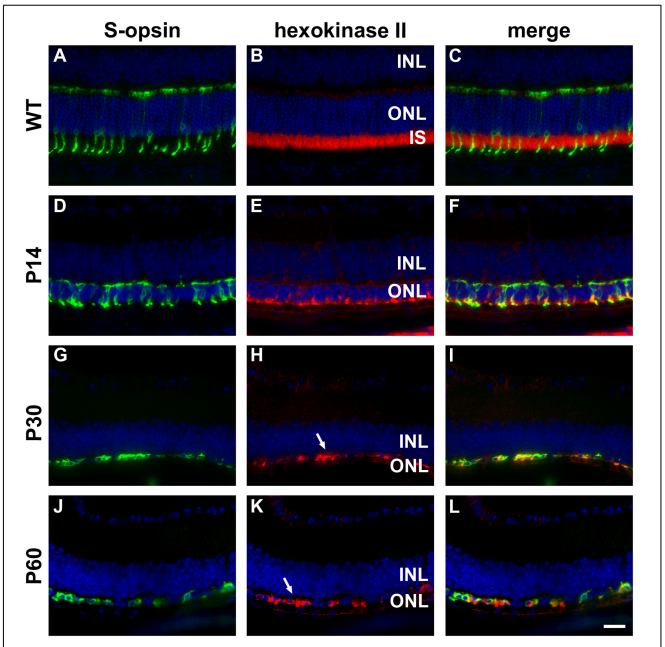

FIGURE 3 | Representative double labeling immunofluorescence images of hexokinase II with S-opsin in wild-type (WT) mouse retina and in *Rd1* mouse retinas from postnatal day (P) 14 to P60. **(A–C)** In WT retinas, hexokinase II is essentially restricted to rod and cone photoreceptor inner segments. **(D–F)** At P14, hexokinase II colocalizes with S-opsin in shrunken inner segments (arrow) and weakly labels occasional cone somas. **(G–L)** From P30 to P60, the ONL comprises a single layer of surviving cones largely devoid of segments. Hexokinase II colocalizes with S-opsin in cone somas (arrows). All images were captured from the inferior retina, which comprises primarily S-cones. INL, inner nuclear layer; IS, inner segments, ONL, outer nuclear layer; RPE, retinal pigment epithelium. Scale bar: 20 μm.

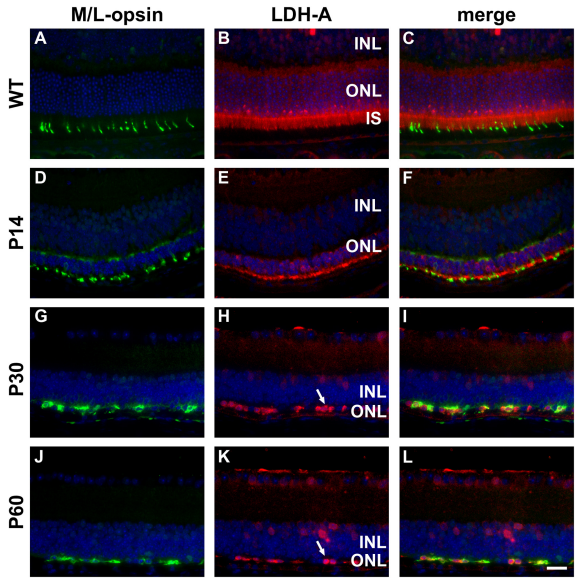

FIGURE 4 | Representative double labeling immunofluorescence images of LDH-A with M/L-opsin in wild-type (WT) mouse retina and in *Rd1* mouse retinas from postnatal day (P) 14 to P60. **(A–C)** In WT retinas, LDH-A is associated with rod and cone photoreceptor somas, inner segments and axonal terminals, together with cells in the inner retina. **(D–F)** At P14, hexokinase II colocalizes with M/L-opsin in shrunken inner segments (arrow) and weakly labels photoreceptor somas and axonal terminals. **(G–L)** From P30 to P60, the ONL comprises a single layer of surviving cones largely devoid of segments. LDH-A is observed in surviving cone somas (arrows). All images were captured from the superior retina, which comprises primarily M/L-cones. INL, inner nuclear layer; IS, inner segments, ONL, outer nuclear layer; RPE, retinal pigment epithelium. Scale bar: 20 μm.

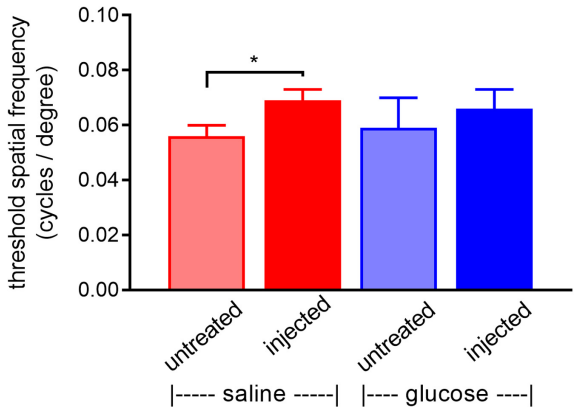

FIGURE 5 | Performance of *Rd1* mice in the optomotor tracking test undertaken at P24, following 10 days of treatment. *Rd1* mice received a daily unilateral subconjunctival injection of glucose or saline; the respective contralateral eyes were untreated. Values represent mean ± SEM, where $n = 11–13$. $^*P < 0.05$ by Student's paired *t*-test (saline-injected vs. untreated contralateral eyes). There were no significant differences between glucose-injected and untreated contralateral eyes (Student's paired *t*-test) or between saline-injected eyes and glucose-injected eyes (Student's unpaired *t*-test).

In addition to hexokinase II and LDH-A, surviving cones also displayed PKM2 and neuron-specific enolase immunoreactivities (data not shown). The overall data indicate that despite losing their inner segments, surviving cones in the *rd1* retina retain their complement of enzymes necessary to metabolize glucose.

Subconjunctival Delivery of Glucose Does Not Preserve Cones in *rd1* Retinas

rd1 mice received a daily unilateral injection of glucose or osmotically matched saline for 30 days. After 10 days of injections, their visual acuity was assessed using the optomotor reflex test. Both the saline-injected and glucose-injected groups displayed modestly enhanced optomotor responses compared to their respective contralateral eyes (**Figure 5**), although only the saline-injected group reached statistical significance ($P < 0.01$, by paired Student's *t*-test). Importantly, there was no difference between the glucose-injected and saline-injected groups ($P = 0.25$, by unpaired Student's *t*-test).

At P60, the number of surviving cones were quantified. Mouse retinas contain three types of cones, short wavelength light-responsive S-cones, medium to long wavelength light-responsive M/L-cones, and a majority of dual cones that express both opsins (Applebury et al., 2000; Haverkamp et al., 2005; Ortin-Martinez et al., 2014). In the *rd1* mouse, degeneration of cones is more rapid in the central than peripheral retina (Carter-Dawson et al., 1978; Lin et al., 2009). **Figures 6A–P**, **7A–P**, respectively, feature representative images of S-opsin$^+$ and M/L-opsin$^+$ cones from the different treatment groups. The photomicrographs highlight the central to peripheral divergence in cone survival in the *rd1* retina. The photomicrographs also reveal that, at P60, M/L-opsin$^+$ cones are more numerous in the superior retina relative to the inferior retina, whereas S-opsin$^+$ cones are far more numerous in the inferior retina. This hemispheric asymmetry in S-opsin$^+$ and M/L-opsin$^+$ cone expression is in agreement with earlier findings (Lin et al., 2009; Narayan et al., 2019). The very low numbers of M/L-opsin$^+$ cones in the inferior retina does not necessarily indicate that dual cones are preferentially lost in the inferior retina, instead it likely reflects the fact that M/L-opsin protein expression is intrinsically very much lower in cones in the inferior retina as compared to the superior retina (Applebury et al., 2000; Haverkamp et al., 2005). With the loss of their outer segments – which contain extraordinarily high levels of opsins – M/L-opsin is no longer detectable in dual cone somas and pedicles, which appear as apparent S-cones. The low numbers of S-opsin$^+$ cones in the superior retina simply reflects the fact that there are far fewer S-opsin$^+$ cones in the superior as compared to inferior retina. Quantification of the density of S-opsin$^+$ and M/L-opsin$^+$ cones in the whole retina showed a trend of higher counts of both cone types in each of the saline-injected and glucose-injected groups when compared to their respective, paired, contralateral eyes (**Figures 6Q**, **7Q**), although only the saline-injected group M/L-opsin$^+$ cone count reached statistical significance ($P < 0.05$, by paired Student's *t*-test). As for the optomotor testing, there was no significant difference between the number of S-opsin$^+$ cones or M/L-opsin$^+$ cones in the glucose-injected vs. saline-injected cohorts ($P = 0.25$, by unpaired Student's *t*-test). When

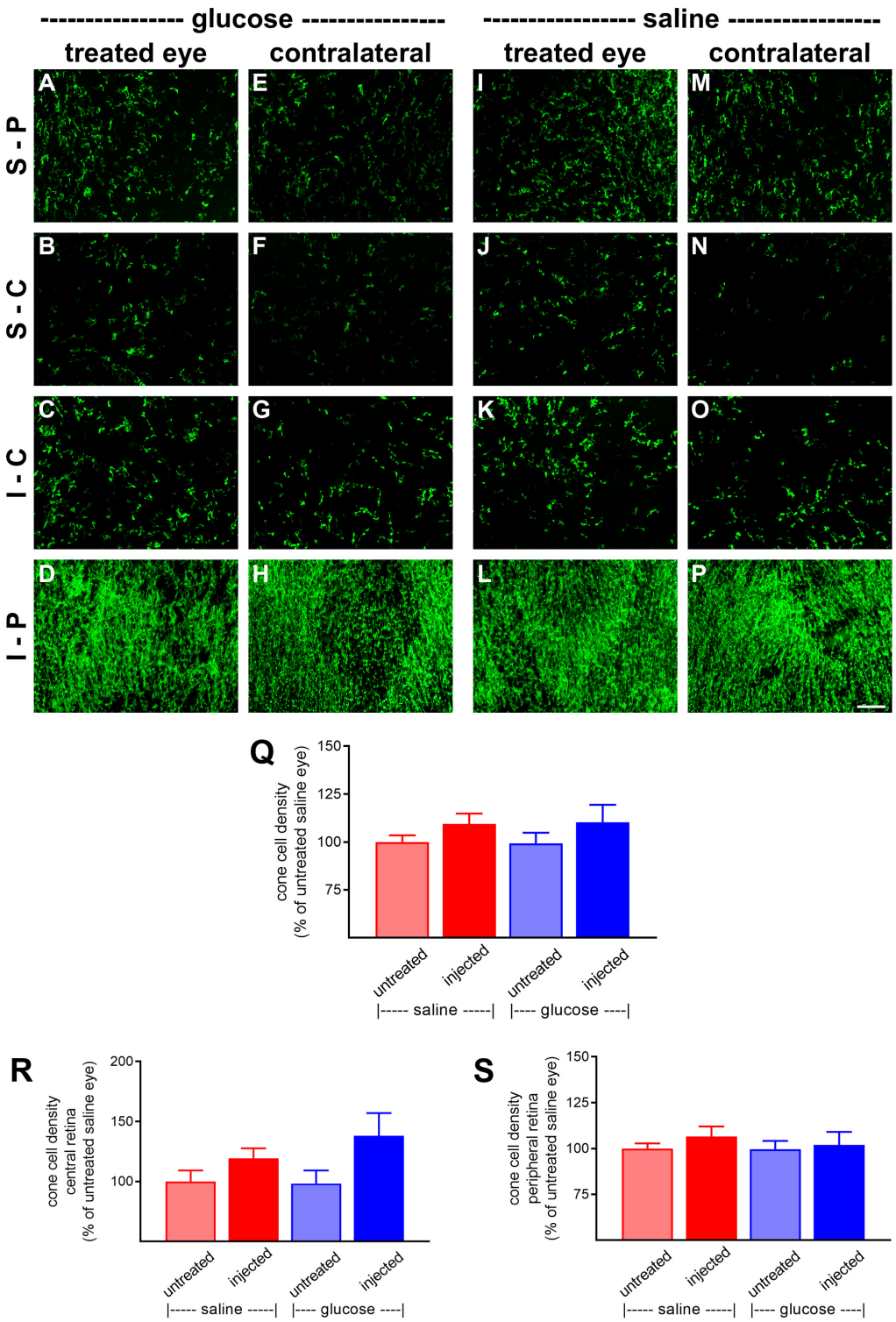

FIGURE 6 | Effect of daily glucose injections on S-opsin^{+}-cone survival. **(A–P)** Photomicrographs of wholemount *Rd1* retinas analyzed at postnatal day (P) 60 immunolabeled for S-opsin. Representative images from glucose-injected eyes **(A–D)** and the respective contralateral untreated eyes **(E–H)**, saline-injected eyes **(I–L),** and the respective contralateral untreated eyes **(M–P)** are shown. S-P, superior-peripheral retina; S-C, superior-central retina; I-C, inferior-central retina; I-P, inferior-peripheral retina. Scale bar 100 μm. **(Q–S)** Quantification of S-opsin-labeled cones in retinal wholemounts from *Rd1* mice treated with daily unilateral subconjunctival injections of glucose or saline, and in the respective untreated contralateral eyes. Data are shown for the whole retina **(Q)**, subdivided into central **(R)**, and peripheral **(S)** regions. Values, shown as % of the untreated saline group, represent mean ± SEM, where n = 11–13. There were no significant differences between glucose-injected and untreated contralateral eyes (Student's paired t-test), saline-injected vs. untreated contralateral eyes (Student's paired t-test), or between saline-injected eyes and glucose-injected eyes (Student's unpaired t-test).

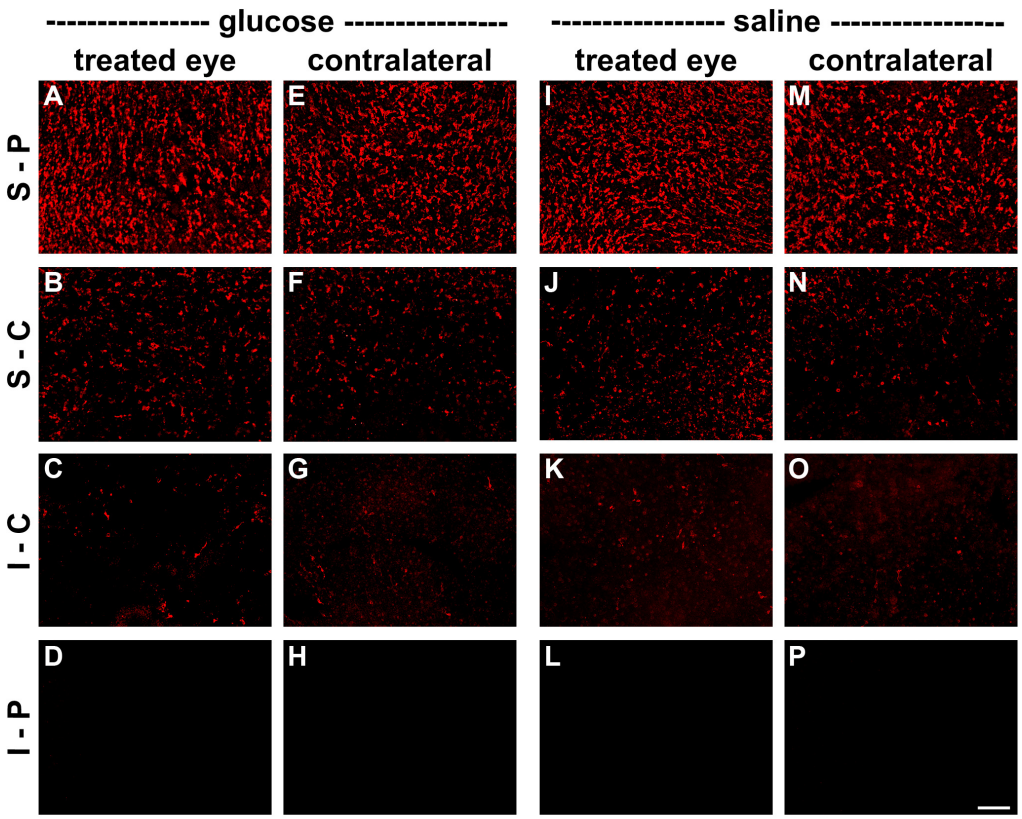

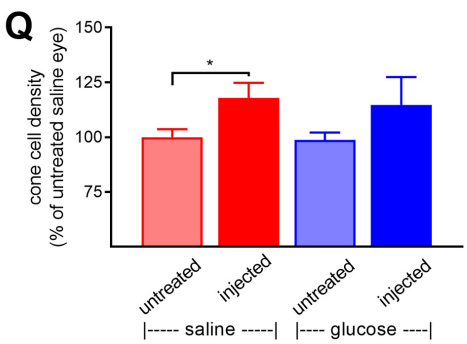

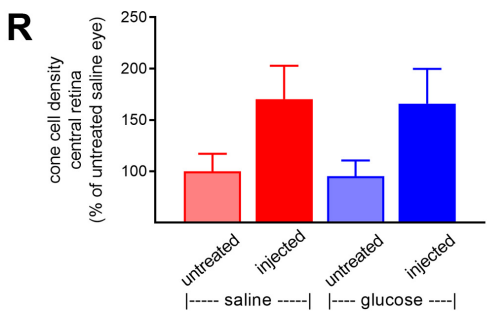

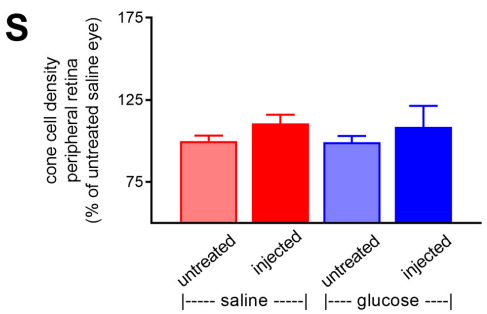

FIGURE 7 | Effect of daily glucose injections on M/L-opsin^{+}-cone survival. **(A–P)** Photomicrographs of wholemount *Rd1* retinas analyzed at postnatal day (P) 60 immunolabeled for M/L-opsin. Representative images from glucose-injected eyes **(A–D)** and the respective contralateral untreated eyes **(E–H)**, saline-injected eyes **(I–L)** and the respective contralateral untreated eyes **(M–P)** are shown. S-P, superior-peripheral retina; S-C, superior-central retina; I-C, inferior-central retina; I-P, inferior-peripheral retina. Scale bar 100 μm. **(Q–S)** Quantification of S-opsin-labeled cones in retinal wholemounts from *Rd1* mice treated with daily unilateral subconjunctival injections of glucose or saline, and in the respective untreated contralateral eyes. Data are shown for the whole retina **(Q),** subdivided into central **(R)**, and peripheral **(S)** regions. Values, shown as % of the untreated saline group, represent mean ± SEM, where n = 11–13. *$P < 0.05$ by Student's paired t-test (saline-injected vs. untreated contralateral eyes). There were no significant differences between glucose-injected and untreated contralateral eyes (Student's paired t-test) or between saline-injected eyes and glucose-injected eyes (Student's unpaired t-test).

the data were subdivided into central (**Figures 6R**, **7R**) and peripheral (**Figures 6S**, **7S**) regions, the same patterns of cone survival were evident, namely a non-significant trend of higher counts of both cone types in each of the saline-injected and glucose-injected groups when compared to their respective contralateral eyes. As for the pan retinal quantification, there was no significant difference between the glucose-injected vs. saline-injected cohorts in survival of either cone type in the central or peripheral retina regions of the retina.

Creatine Supplementation Protects Cones in Culture From Mitochondrial Dysfunction but Not Oxidative Injury

The effect of a creatine on survival of cones after induction of stress *in vitro* was assessed after a 24-h pre-treatment. Similar to the glucose experiments shown in **Figure 1**, tbH application caused a reduction to 37.9 ± 7.2% and 6.0 ± 3.0% of the control cell number when applied at 100 μM or 250 μM, respectively (**Figure 8**). Creatine pre-treatment (0.5 or 5 mM) had no significant effect on promoting additional survival of cells treated with tbH.

Sodium azide also caused a concentration-dependent loss of S-opsin-labeling cones from mixed retinal cell cultures: 44 ± 8.9% and 10.7 ± 2.7% of the control cell number of cones remained after application of 500 μM and 1 mM sodium azide, respectively (**Figure 8**). In this case, pre-treatment with creatine at the concentration of 0.5 mM was also not protective to cells, however, when applied at 5 mM, this compound did offer significant protection: there were 85.3 ± 11.0% and 56.0 ± 15.2% of the control number of cells remaining after treatment with 500 μM and 1 mM sodium azide, respectively (**Figure 8**).

Surviving Cones in the *rd1* Retina Express Creatine Kinase Isoenzymes

The creatine kinase/phosphocreatine system functions as a spatial and temporal energy buffer in cells, linking sites of

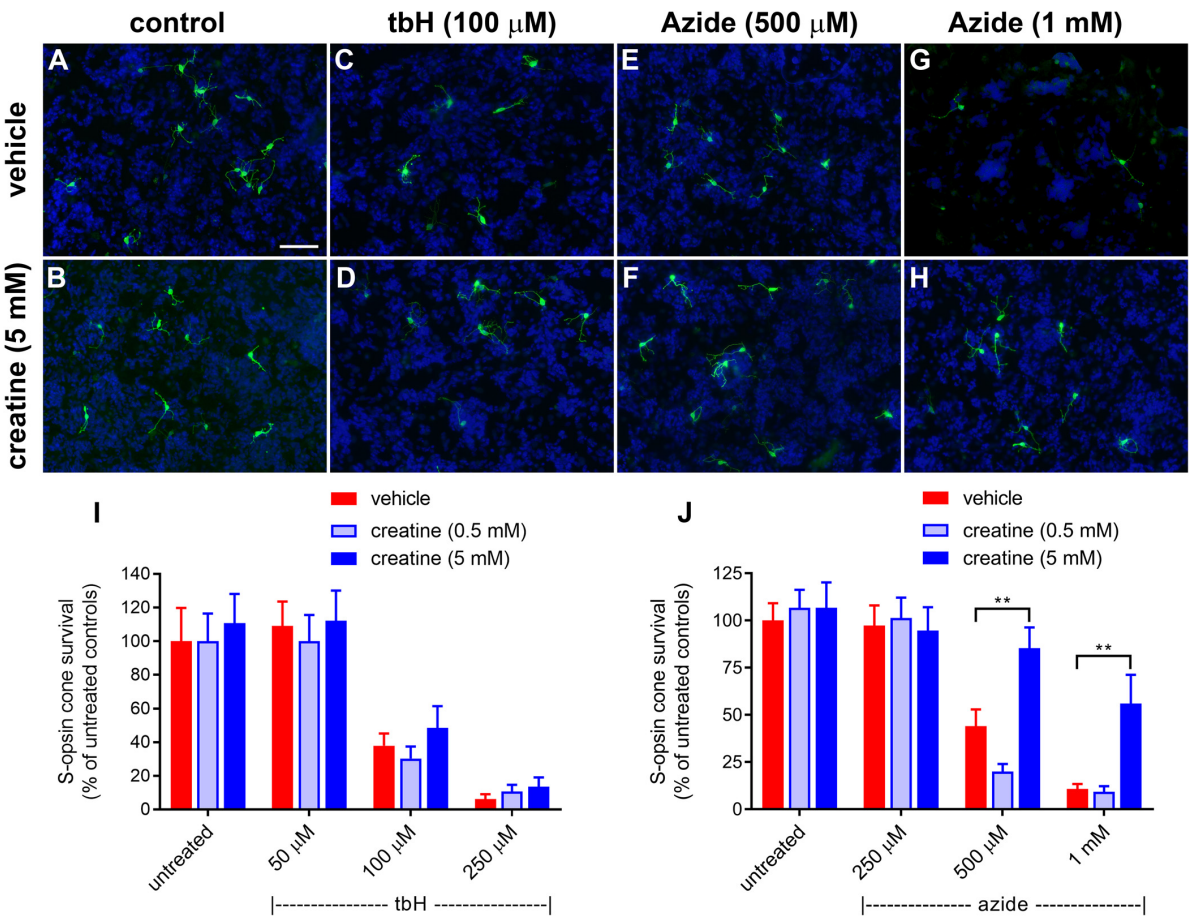

FIGURE 8 | Effect of creatine on stressor-induced S-opsin-labeled cone loss from mixed retinal cell cultures. Representative images from untreated **(A)**, vehicle-treated **(C,E,G)** or creatine (5 mM)-treated **(B,D,F,H)** cultures additionally exposed to **(C,D)**, 100 μM tbH **(E,F)**, 500 μM sodium azide **(G,H)**, 1 mM sodium azide. These data are followed by graphs quantifying the effect of creatine on tBH-induced **(I)** and sodium azide-induced **(J)** cone cell loss. It is evident that both tbH and sodium azide cause marked loss of S-opsin labeled cones in culture. It is further clear that although creatine has no effect on the cone loss induced by tbH, it is able to significantly protect these cells from sodium azide-induced toxicity. Values represent mean ± SEM, where $n = 8$ determinations from separate cultures. $^{**}P < 0.01$, by one way ANOVA, followed by Dunnett's multiple comparisons test. Scale bar, 50 μm.

energy production, and utilization. Typically, mitochondrial creatine kinase (MT-CK1A) converts creatine to high energy phosphocreatine at sites of ATP production, generating a diffusible energy substrate, whilst the cytoplasmic isoform (CK-B) catalyzes the reverse reaction at subcellular locations of energy usage (Wallimann et al., 2011). Before investigating whether augmenting retinal creatine delays cone loss in the *rd1* retina, it was important to ascertain whether the enzymes of the creatine-phosphocreatine system are preserved in surviving cones of the *rd1* retina during the period of cone degeneration. This is important since mitochondrial creatine kinase is principally localized in photoreceptor inner segments.

In WT mouse retina, CK-MT1A was present in rod and cone inner segments, in cone but not rod somas in the outer nuclear layer, and in photoreceptor terminals in the outer plexiform layer (**Figures 9A–C**). The pattern of expression at P7 was similar to WT (**Figures 9D–F**). By P14, rod death is quite advanced and CK-MT1A colocalizes with S-opsin in shrunken inner segments, cone somas and axonal terminals (**Figures 9G–I**). Despite the loss of inner segments from P21, surviving cone somas and axonal terminals in the *rd1* retina were strongly positive for CK-MT1A at all time points examined, encompassing P7 to P60 (**Figures 9J–R**). Labeling of cone cell bodies for CK-MT1A was considerably stronger than at P7 or in WT retinas.

In WT mouse retina, CK-B was present in cone but not rod inner segments and in terminals in the outer plexiform layer (**Figures 10A–C**). From these results, it might be inferred that creatine kinase plays a greater role in cones compared with rods. As for CK-MT1A, surviving cones in the *rd1* retina were positive for CK-B at all time points examined, encompassing P7 to P60 (see **Figures 10D–L**). Unlike the WT retina, in which cone somal labeling of CK-B was undetectable, from P21 onward cone cell bodies were clearly positive for CK-B.

Dietary Creatine Supplementation Augments Cone Survival in *Rd1* Retinas

rd1 mice received either normal chow or 2% oral creatine diet starting at P21. Optomotor testing was performed at P30, the results of which revealed that the creatine-enriched group exhibited approximately 4.5-fold greater visual acuity compared to the control diet cohort ($P < 0.01$, by unpaired Student's *t*-test; **Figure 11**). At P60, the number of surviving cones were quantified. **Figures 12A–P** shows representative photomicrographs of S-opsin$^+$ and M/L-opsin$^+$ cones from each treatment group. Quantification of the density of S-opsin$^+$ and M/L-opsin$^+$ cones in the whole retina revealed a modest, but statistically significant, protection of S-opsin$^+$ and M/L-opsin$^+$ cones in the creatine group compared to the normal diet cohort ($P < 0.05$; $P < 0.01$, respectively, by Student's unpaired *t*-test; **Figure 12Q**). When the data were subdivided into central (**Figure 12R**) and peripheral (**Figure 12S**) regions, the same patterns were evident, but the neuroprotective effect of creatine only reached significance in the peripheral retina for each cone type ($P < 0.01$, by Student's unpaired *t*-test).

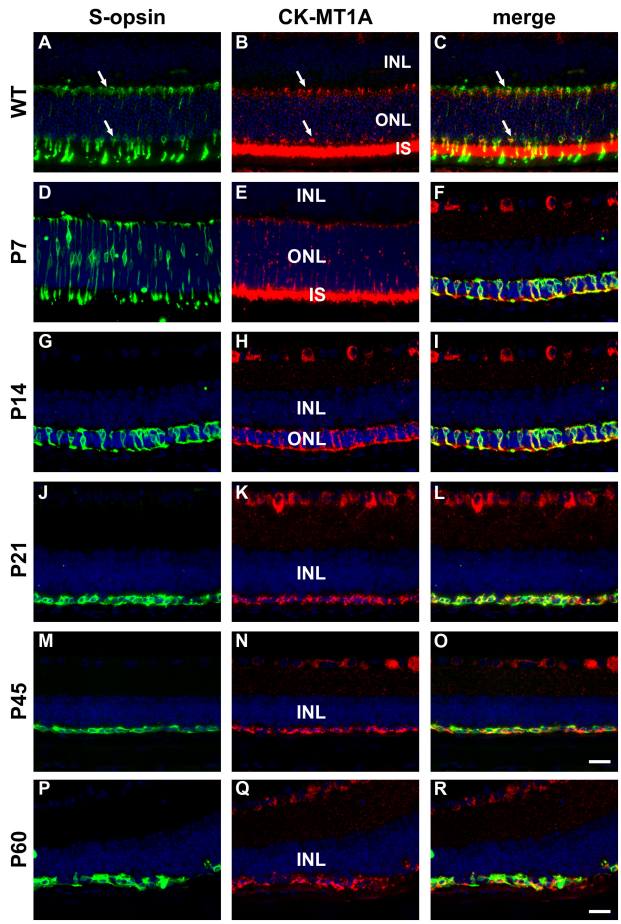

FIGURE 9 | Representative double labeling immunofluorescence images of ubiquitous mitochondrial creatine kinase (CK-MT1A) with S-opsin in wild-type mouse retina and *Rd1* mouse retinas from postnatal day (P) 7 to P60. In WT retinas **(A–C)** and at P7 **(D–F)**, CK-MT1A colocalizes with S-opsin in photoreceptor inner segments, cone somas, and axonal terminals. At P14, the ONL is dramatically reduced in thickness. CK-MT1A colocalizes with S-opsin in shrunken inner segments, cone somas, and axonal terminals **(G–I)**. From P21 onward, the ONL is reduced to a single layer of surviving cones largely devoid of segments. CK-MT1A expression within S-opsin-positive cone somas and axonal terminals persists at all time points **(J–R)**. All images were captured from the inferior retina, which comprises primarily S-cones. INL, inner nuclear layer; IS, inner segments; ONL, outer nuclear layer. Scale bar: 20 μm.

DISCUSSION

Targeting secondary cone degeneration is a broad-spectrum strategy applicable to a large proportion of RP subtypes irrespective of the primary gene defect. An increasing body of evidence has implicated energetic insufficiency as a key component of cone degeneration, and, in the present study, we utilized *in vitro* and *in vivo* models of RP to explore whether increasing the availability of two nutrients promotes cone survival. Our results showed that glucose improved cone survival in retinal cultures subjected to mitochondrial stress or oxidative insult; however, daily subconjunctival injections of

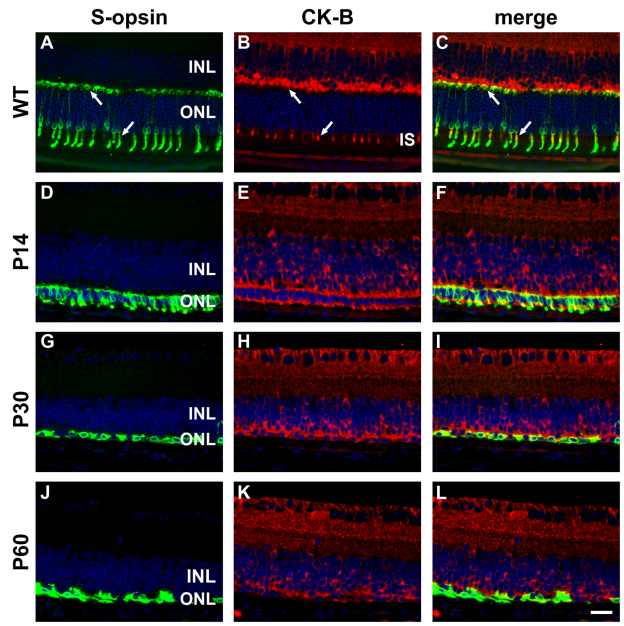

FIGURE 10 | Representative double labeling immunofluorescence images of cytosolic creatine kinase (CK-B) with S-opsin in wild-type (WT) mouse retina and in *Rd1* mouse retinas from postnatal day (P) 14 to P60. In WT retinas **(A–C)**, CK-B colocalizes with S-opsin in cone inner segments (arrows), and in axonal terminals in the outer plexiform layer (arrows). At P14, CK-B colocalizes with S-opsin in shrunken inner segments and axonal terminals, with weak CK-B labeling of somas **(D–F)**. From P30 to P60, the ONL comprises a single layer of surviving cones largely devoid of segments. CK-B colocalizes with S-opsin in cone somas and axonal terminals **(G–L)**. At all time points, CK-B is also expressed by inner retinal neurons and Müller cells. All images were captured from the inferior retina, which comprises primarily S-cones. INL, inner nuclear layer; IS, inner segments; ONL, outer nuclear layer. Scale bar: 20 μm.

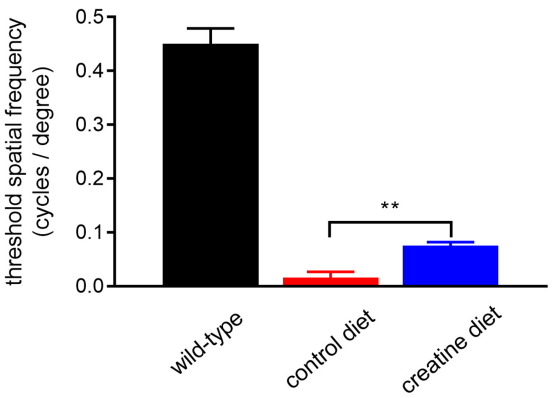

FIGURE 11 | Performance of *Rd1* mice in the optomotor tracking test undertaken at P30. Values represent mean ± SEM, where n = 18–21. $^{**}P < 0.01$ by Student's unpaired t-test (creatine-enriched diet vs. control diet eyes).

glucose neither enhanced spatial visual performance nor slowed cone cell degeneration in *rd1* mice relative to isotonic saline. In contrast, creatine not only promoted cone survival in retinal cultures, but also improved vision and reduced cone degeneration in *rd1* mice. The results of this study provide tentative support for the hypothesis that creatine supplementation may delay secondary degeneration of cones in individuals with RP.

Glucose Supplementation for Cone Survival

In order to mimic cone loss *in vitro* as a first step to understanding the potential role of nutraceutical protection of cones *in situ*, we established culture preparations in which cones were present. Immunocytochemical labeling of these cultures revealed a distinct population of small cells with dendrites, but no obvious segments. In fact, photoreceptors within the culture system employed lose their segments during the first 24 h *in vitro*. The absence of outer segments from otherwise viable photoreceptor cells in similar mixed cultures has been described previously (Gaudin et al., 1996). Our culture system can thus be used to assess the survival of cones whose segments have degenerated or are in the process of doing so. This model, therefore, is of direct relevance to RP, since degeneration of segments is an early pathological event in RP.

We subjected cultures to metabolic disturbance (sodium azide) and oxidative stress (tbH), each of which is implicated in the pathology of cone loss in RP. In both scenarios, concentration-dependent toxicity to S-opsin^{+}-cones was noted that was counteracted by pretreatment with glucose. Glucose has been shown to protect against retinal cell loss induced by azide in a previous *in vitro* study (Wood et al., 2012). Notably, however, protection was greater to glia than inner retinal neurons, a finding explained by the greater reliance of neurons on mitochondrial metabolism. The degree of cone protection was similar to that measured for inner retinal neurons previously, implying that the metabolism, and mitochondrial reliance of these cell types is analogous. It may seem that enhancing glycolysis by supplementation with glucose would inevitably counteract mitochondrial compromise, but this makes the assumption that cell metabolism is plastic and can respond rapidly and efficiently to altered energy demands and changing substrate supplies. In the present study, cells are maintained with pyruvate and glutamine, both of which are predominantly metabolized via mitochondria-based pathways. When mitochondria are made dysfunctional with azide, cells will die unless aerobic glycolysis can be alternatively promoted; the addition of glucose offers that possibility, but relies on the metabolic flexibility of the cells. Since aerobic glycolysis contributes to photoreceptor metabolism *in situ* (Chinchore et al., 2017), it is unsurprising that cones can respond to mitochondrial disturbance *in vitro*.

The protective effect of glucose against induced oxidative stress is highly unlikely to be mediated through a direct antioxidative action. Instead, glucose is able to counteract excessive oxidative stress by activation of the pentose phosphate pathway, which produces NADPH to maintain cellular glutathione levels (Ben-Yoseph et al., 1996). Glutathione is the major intracellular antioxidant and maintenance of its active reduced state occurs via the enzyme glutathione reductase. Expression of this enzyme has been demonstrated

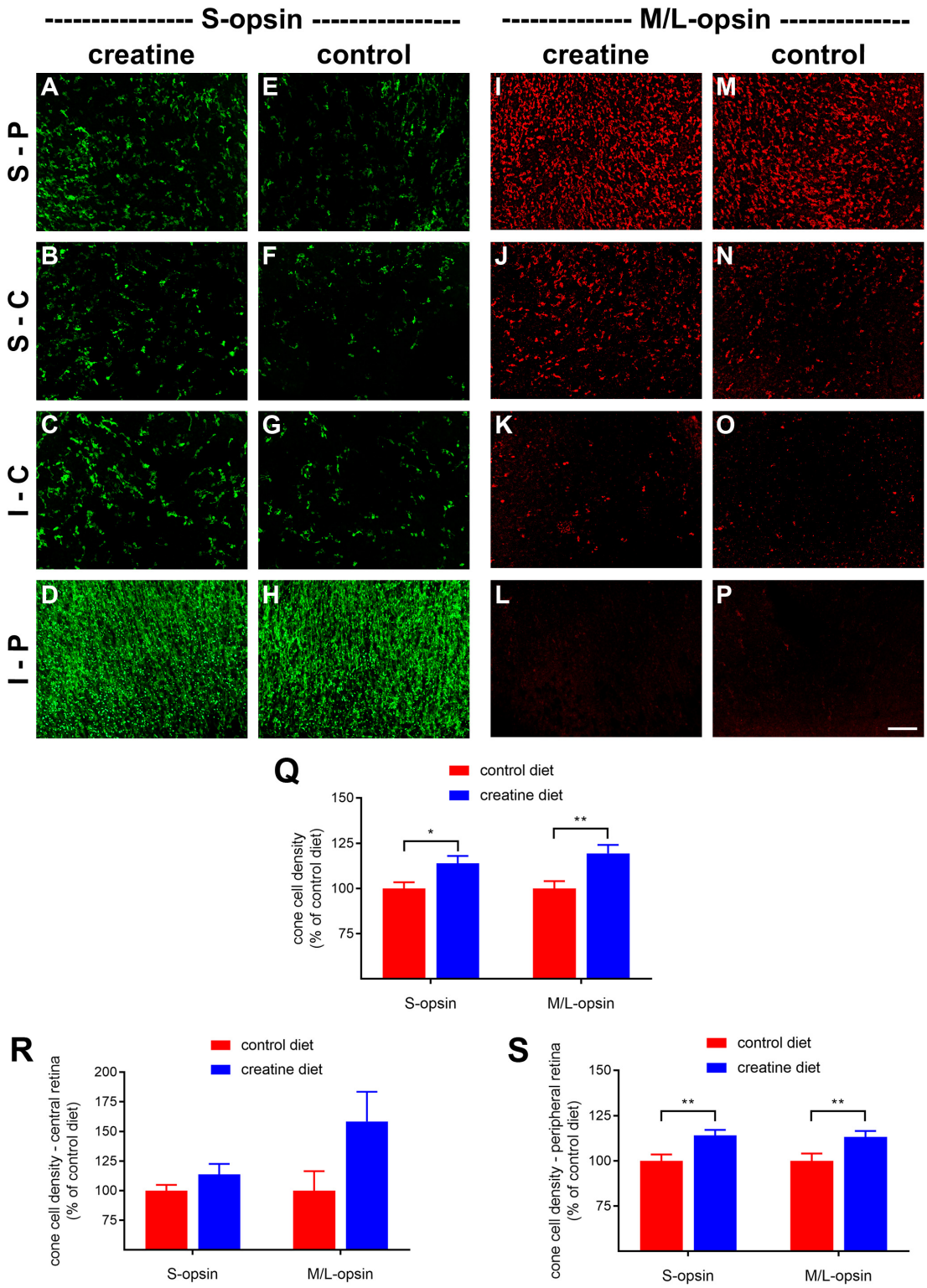

FIGURE 12 | Effect of creatine supplementation on cone survival. **(A–P)** Photomicrographs of wholemount *Rd1* retinas analyzed at postnatal day (P) 60 immunolabeled for S-opsin and M/L-opsin. Representative images from mice fed a creatine-enriched diet **(A–D,I–L)** or a normal diet **(E–H,M–P)** are shown. S-P, superior-peripheral retina; S-C, superior-central retina; I-C, inferior-central retina; I-P, inferior-peripheral retina. Scale bar 100 μm. **(Q–S)** Quantification of S-opsin-labeled cones and M/L-opsin-labeled cones in retinal wholemounts from *Rd1* mice fed a creatine-enriched diet or a standard diet. Data are shown for the whole retina **(Q),** subdivided into central **(R)**, and peripheral **(S)** regions. Values, shown as % of control diet, represent mean ± SEM, where $n = 18–21$. $^{*}P < 0.05$, $^{**}P < 0.01$ by Student's unpaired *t*-test (creatine vs. control eyes).

in photoreceptors *in situ* (Fujii et al., 2001). This, then, is a key action of glucose: maintaining control over oxidative attack via stimulation of additional or alternate metabolic pathways.

Healthy photoreceptors display a high rate of aerobic glycolysis (Chinchore et al., 2017). Accordingly, they express a specific complement of glycolytic isoenzymes, including hexokinase II, pyruvate kinase M2, and LDH-V, which are concentrated in their inner segments (Casson et al., 2016; Petit et al., 2018). The importance of hexokinase II for cone homeostasis has recently been established in a study by Petit et al. (2018), who showed that deletion of HK2 has minimal impact upon cone viability in normal conditions, but, that HK2 confers a survival advantage in cones under conditions of metabolic stress. Since loss of cone segments is an early pathological event in RP, we investigated whether surviving cones in the *Rd1* retina continue to express genes vital for aerobic glycolysis. The data showed that, at all ages analyzed, cone somas in the *Rd1* retina expressed hexokinase II and LDH-A (as well as PKM2 and neuron-specific enolase). The robust labeling of hexokinase II and LDH-A in surviving cones testifies to the fact that the biochemical machinery required for aerobic glycolysis persists despite the irrevocable disruption to their normal cellular architecture. Boosting energy supplies should allow cones to survive for longer and may even facilitate the process of segment regeneration, in an analogous manner to that observed in experimental retinal detachment following oxygen supplementation (Mervin et al., 1999).

The lack of protective effect of local glucose delivery in *Rd1* mice may be due to a number of factors. The first issue to consider is how much additional glucose is available for uptake by cones. Subconjunctival injection is considerably less invasive than intravitreal or subretinal injections, permitting daily administration, and resulting in higher bioavailability than other periocular injection sites; however, retinal bioavailability is lower than intravitreal injection owing to the various barriers between the sites of administration and the target (Del Amo et al., 2017). In previous work, we showed that subconjunctival injection of glucose elevated the vitreal glucose level and protected retinal ganglion cells from ischemia-reperfusion (Shibeeb et al., 2016), while in the present study, a single subconjunctival injection of glucose resulted in >threefold elevation of the vitreous glucose concentration. These data suggest that subconjunctivally administered glucose likely reaches the photoreceptor layer; however, it should be recognized that our earlier study featured target neurons that reside closest to the vitreous humor, as well as an acute, rather than chronic, model of injury. In the *Rd1* mouse, inner retinal neurons and glia would be exposed to the glucose before it reaches the cones, reducing the total amount delivered. To shed some light on this question, we analyzed tissue sections of retina from wild type mouse eyes that had undergone a subconjunctival injection of 2-NDBG, a stable, fluorescent glucose derivative used for monitoring glucose uptake into living cells. The data showed 2-NBDG fluorescence within photoreceptor inner and outer segments, confirming that at least some glucose reaches the photoreceptor layer after subconjunctival injection. The pattern of 2-NBDG fluorescence was similar to that reported after oral administration of the drug in mice (Kanow et al., 2017). While these qualitative data verify that glucose reaches cones after subconjunctival injection, they do not reveal the concentration.

A second issue relates to timing. Whilst there was a substantial increase in vitreal glucose after 1 h, the concentration decreased quite rapidly thereafter. In a chronic model of degeneration, controlled, slow release of drug is advantageous to ensure continued bioavailability. In contrast to the subconjunctival route, subretinal injection delivers glucose directly to cones, and excitingly this methodology has been shown to cause a short-term improvement in cone function as well as outer segment synthesis when tested in the early stages of cone pathology in the P23H porcine model of RP (Wang et al., 2016). Subretinal injection is, however, technically challenging and only suited to one-off applications such as delivery of genes or stem cells (Del Amo et al., 2017).

An additional explanation for the lack of efficacy of glucose on cone survival relates to reduced uptake of glucose into cones. Extracellular glucose is believed to enter cones primarily via GLUT1, although other uptake mechanisms may exist since GLUT1 expression in cones appears to be very modest given the extraordinarily high metabolic activity of these cells (Gospe et al., 2010; Ait-Ali et al., 2015; Swarup et al., 2019). The activity of GLUT1 is stimulated by a soluble factor released from rods (Ait-Ali et al., 2015). In *rd1* mice, rod death will result in less efficient uptake of glucose into cones and reduced aerobic glycolysis. In response, cones compensate by increasing synthesis of GLUT1 in a bid to increase intracellular glucose (Punzo et al., 2009; Venkatesh et al., 2015). Thus, although more glucose may be available for uptake after local delivery of glucose, this may not translate to a higher intracellular concentration. Therapies that target GLUT1 or its binding partner BSG-1 may need to be employed (Ait-Ali et al., 2015). A final point worth making is that, in our study, glucose supplementation began at P14 when rod photoreceptors would still be present. It is possible that any effects of glucose on cones were influenced by the presence of rods. Glucose may conceivably have influenced the time course of rod degeneration, but since retinas were not analyzed until P60, this data is not available.

The finding that saline injections had a small beneficial effect on visual function and cone survival was not entirely unexpected. It has been proven that saline or dry needle injections into the subretinal space provide a modest, but significant, boost to photoreceptor survival in inherited or induced models of degeneration via a mechanism of action hypothesized to involve the release of survival factors (Faktorovich et al., 1990, 1992; Silverman and Hughes, 1990). It is likely that repeated subconjunctival injections elicited an analogous response.

Creatine Supplementation for Cone Survival

Creatine supplementation has been shown to be support neuronal survival in a variety of animal models of neurodegenerative disease, including Alzheimer's disease (Brewer and Wallimann, 2000), Parkinson's disease (Matthews et al., 1999), amyotrophic lateral sclerosis (Klivenyi et al., 1999),

and Huntington's disease (Matthews et al., 1998; Ferrante et al., 2000; Andreassen et al., 2001). In the present study, creatine supplementation protected cones against mitochondrial compromise *in vitro*, and, improved visual function and cone survival in *rd1* mice.

The first important finding was that surviving cone photoreceptors in *rd1* mice continue to express creatine kinase. Despite the loss of their mitochondrial-rich inner segments, cone somas and axonal terminals in the *rd1* retina were strongly positive for both the mitochondrial and cytosolic forms of creatine kinase at each time point examined. The data reveal that the fundamental enzymes of the creatine-phosphocreatine system are preserved in surviving cones of the *rd1* retina and attest to the logic of the neuroprotective strategy.

The cone protection afforded by creatine has several possible mechanisms. Exogenous creatine supplementation has been shown to increase the total intracellular phosphocreatine level (Beal, 2011). Phosphocreatine provides energy to photoreceptor outer segments for phototransduction and to synaptic terminals for neurotransmission (Linton et al., 2010; Hurley et al., 2015). Hence, creatine-induced cone preservation may simply result from increasing the available phosphocreatine pool, thereby supporting overall cellular energy production. Secondly, and relatedly, mitochondrial creatine kinase is tightly coupled to ATP synthesis, respiratory chain activity and ATP export. This coupling improves the efficiency of oxidative phosphorylation, and the transport and utilization of intracellular energy. Creatine supplementation is believed to enhance these functions through the action of creatine kinase (see Wallimann et al., 2011). In the culture experiments outlined in the present study, creatine was clearly protective against cone loss induced by mitochondrial inhibition; this action could be explained by either of the above mechanisms. Thirdly, numerous studies have shown that exogenous creatine is highly effective at reducing cellular damage caused by oxidative stress (see Wallimann et al., 2011). This has been largely explained by the fact that creatine kinase stabilizes mitochondrial membranes, reducing the release of reactive oxygen species, although creatine is also a weak free radical scavenger itself and has been shown to protect against oxidative stress directly (Lawler et al., 2002). In the present study, however, creatine was not able to protect cones in culture from the effects of the tbH, thus dismissing the possibility of it having a direct antioxidant mode of action *in vitro*. This does not discount the possibility that creatine can act in an indirect antioxidant capacity *in situ*, however, via a reduction in mitochondrial release of free radicals. If this were the case, then this is highly relevant to RP since an increasing body of evidence implicates oxidative stress in the pathogenesis of cone degeneration in the disease (Shen et al., 2005; Komeima et al., 2006, 2007; Usui et al., 2009; Lee et al., 2011; Campochiaro et al., 2015). Finally, creatine displays anti-apoptotic properties, by virtue of inhibiting opening of the mitochondrial permeability transition pore, and induction of differential expression of pro-survival transcription factors and cell signaling pathways (see Wallimann et al., 2011). Further investigation is needed to definitively establish the precise mechanisms by which creatine enhances cone survival in the *rd1* mouse.

The major limitation of the present study is the early onset, and fast progression, of cone degeneration in the *rd1* model of RP. Creatine supplementation was initiated at the time of weaning, P21. By this age, however, all rod constituents and the majority of cone outer segments had degenerated. *rd1* mice do not produce a recordable electroretinogram for many days beyond P21 (Farber et al., 1994). The improvement observed in the optokinetic response in creatine-fed mice suggests that clinically useful visual function might be preserved even when cone degeneration has progressed to a late stage. Nevertheless, the use of a slower progressing model of degeneration, such as the *rd1*0 strain, would permit more expansive evaluation of cone structure and function, including quantification of the rate of cone segment loss, and measurement of the electroretinogram (Wang et al., 2014).

The results of randomized clinical trials with oral creatine supplementation for neurodegenerative diseases have largely been disheartening to date. A number of clinical trials investigating the efficacy of creatine in Parkinson's disease all failed to meet primary end points, despite some evidence of improvements in secondary outcomes (Bender and Klopstock, 2016). Likewise, clinical outcomes in trials of creatine in Huntingdon's disease and Amyotrophic lateral sclerosis have also been disappointing (Bender and Klopstock, 2016). Nevertheless, there are convincing reasons for further investigation of creatine in RP: firstly, creatine kinase is extremely abundant in mammalian photoreceptors and appears to play a pivotal role in vision (Linton et al., 2010); secondly, RP can be diagnosed prior to secondary cone degeneration. From the credible results of preclinical studies, it has been argued that prophylactic treatment with creatine to prevent neuronal degeneration is far more effective than treatment at later disease stages; thirdly, there are no current therapies for RP and any improvements in visual quality would be beneficial for individuals; fourthly, the safety and ease of delivery of creatine supplementation has been established and is clinically appealing, although it must be recognized that adverse effects such as gastrointestinal complaints, muscle cramps and an increase in body weight have been reported to occur occasionally after creatine supplementation (Andres et al., 2017). The development of a targeted ocular delivery system, which bypasses the systemic circulation, would potentially provide a safe, long-term route of administration of even higher doses of creatine, which has shown promise in individuals with premanifest Huntingdon's disease (Rosas et al., 2014).

DATA AVAILABILITY STATEMENT

The datasets generated for this study are available on request to the corresponding author.

ETHICS STATEMENT

The animal study was reviewed and approved by the Animal Ethics Committees of SA Pathology, Central Adelaide Local

Health Network (CALHN) and the University of Adelaide (Adelaide, SA, Australia) and conformed with the Australian Code of Practice for the Care and Use of Animals for Scientific Purposes, 2013, and with the ARVO Statement for the use of animals in vision and ophthalmic research.

AUTHOR CONTRIBUTIONS

All authors: full access to all the data in the study, take responsibility for the integrity of the data, and the accuracy of the data analysis. RC and GC: study concept and design. DN, GC, and JW: acquisition of data, and analysis and interpretation of data. DN, RC, and GC: drafting of the manuscript. JW: critical revision of the manuscript for important intellectual content. DN and RC: statistical analysis. RC: obtained funding, administrative, technical, and material support.

FUNDING

This research was supported by the National Health and Medical Research Council of Australia (APP1050982).

ACKNOWLEDGMENTS

The authors are indebted to Teresa Mammone for expert technical assistance.

SUPPLEMENTARY MATERIAL

The Supplementary Material for this article can be found online at: https://www.frontiersin.org/articles/10.3389/fnins.2019.01234/full#supplementary-material

REFERENCES

Acosta, M. L., Kalloniatis, M., and Christie, D. L. (2005). Creatine transporter localization in developing and adult retina: importance of creatine to retinal function. *Am. J. Physiol. Cell Physiol.* 289, C1015–C1023. doi: 10.1152/ajpcell.00137.2005

Ait-Ali, N., Fridlich, R., Millet-Puel, G., Clerin, E., Delalande, F., Jaillard, C., et al. (2015). Rod-derived cone viability factor promotes cone survival by stimulating aerobic glycolysis. *Cell* 161, 817–832. doi: 10.1016/j.cell.2015.03.023

Ames, A. III, Li, Y. Y., Heher, E. C., and Kimble, C. R. (1992). Energy metabolism of rabbit retina as related to function: high cost of Na+ transport. *J. Neurosci.* 12, 840–853. doi: 10.1523/jneurosci.12-03-00840.1992

Anderson, B. Jr., and Saltzman, H. A. (1964). Retinal oxygen utilization measured by hyperbaric blackout. *Arch. Ophthalmol.* 72, 792–795. doi: 10.1001/archopht.1964.00970020794009

Andreassen, O. A., Dedeoglu, A., Ferrante, R. J., Jenkins, B. G., Ferrante, K. L., Thomas, M., et al. (2001). Creatine increase survival and delays motor symptoms in a transgenic animal model of huntington's disease. *Neurobiol. Dis.* 8, 479–491. doi: 10.1006/nbdi.2001.0406

Andres, S., Ziegenhagen, R., Trefflich, I., Pevny, S., Schultrich, K., Braun, H., et al. (2017). Creatine and creatine forms intended for sports nutrition. *Mol. Nutr. Food Res.* 61:1600772. doi: 10.1002/mnfr.201600772

Applebury, M. L., Antoch, M. P., Baxter, L. C., Chun, L. L., Falk, J. D., Farhangfar, F., et al. (2000). The murine cone photoreceptor: a single cone type expresses both S and M opsins with retinal spatial patterning. *Neuron* 27, 513–523.

Beal, M. F. (2011). Neuroprotective effects of creatine. *Amino Acids* 40, 1305–1313. doi: 10.1007/s00726-011-0851-0

Bender, A., and Klopstock, T. (2016). Creatine for neuroprotection in neurodegenerative disease: end of story? *Amino Acids* 48, 1929–1940. doi: 10.1007/s00726-015-2165-0

Ben-Yoseph, O., Boxer, P. A., and Ross, B. D. (1996). Assessment of the role of the glutathione and pentose phosphate pathways in the protection of primary cerebrocortical cultures from oxidative stress. *J. Neurochem.* 66, 2329–2337. doi: 10.1046/j.1471-4159.1996.66062329.x

Brewer, G. J., and Wallimann, T. W. (2000). Protective effect of the energy precursor creatine against toxicity of glutamate and beta-amyloid in rat hippocampal neurons. *J. Neurochem.* 74, 1968–1978. doi: 10.1046/j.1471-4159.2000.0741968.x

Campochiaro, P. A., Strauss, R. W., Lu, L., Hafiz, G., Wolfson, Y., Shah, S. M., et al. (2015). Is there excess oxidative stress and damage in eyes of patients with retinitis pigmentosa? *Antioxid Redox Signal* 23, 643–648. doi: 10.1089/ars.2015.6327

Carter-Dawson, L. D., LaVail, M. M., and Sidman, R. L. (1978). Differential effect of the rd mutation on rods and cones in the mouse retina. *Invest Ophthalmol. Vis. Sci.* 17, 489–498.

Casson, R. J., Chidlow, G., Wood, J. P., and Osborne, N. N. (2004). The effect of hyperglycemia on experimental retinal ischemia. *Arch Ophthalmol.* 122, 361–366.

Casson, R. J., Han, G., Ebneter, A., Chidlow, G., Glihotra, J., Newland, H., et al. (2014). Glucose-induced temporary visual recovery in primary open-angle glaucoma: a double-blind, randomized study. *Ophthalmology* 121, 1203–1211. doi: 10.1016/j.ophtha.2013.12.011

Casson, R. J., Wood, J. P., Han, G., Kittipassorn, T., Peet, D. J., and Chidlow, G. (2016). M-type pyruvate kinase isoforms and lactate dehydrogenase a in the mammalian retina: metabolic implications. *Invest Ophthalmol. Vis. Sci.* 57, 66–80. doi: 10.1167/iovs.15-17962

Chidlow, G., Daymon, M., Wood, J. P., and Casson, R. J. (2011). Localization of a wide-ranging panel of antigens in the rat retina by immunohistochemistry: comparison of davidson's solution and formalin as fixatives. *J. Histochem. Cytochem.* 59, 884–898. doi: 10.1369/0022155411418115

Chidlow, G., Wood, J. P., Knoops, B., and Casson, R. J. (2016). Expression and distribution of peroxiredoxins in the retina and optic nerve. *Brain Struct. Funct.* 221, 3903–3925. doi: 10.1007/s00429-015-1135-3

Chidlow, G., Wood, J. P. M., Sia, P. I., and Casson, R. J. (2019). Distribution and activity of mitochondrial proteins in vascular and avascular retinas: implications for retinal metabolism. *Invest Ophthalmol. Vis. Sci.* 60, 331–344. doi: 10.1167/iovs.18-25536

Chinchore, Y., Begaj, T., Wu, D., Drokhlyansky, E., and Cepko, C. L. (2017). Glycolytic reliance promotes anabolism in photoreceptors. *eLife* 6:e25946. doi: 10.7554/eLife.25946

Cringle, S. J., Yu, D. Y., Yu, P. K., and Su, E. N. (2002). Intraretinal oxygen consumption in the rat *in vivo*. *Invest Ophthalmol. Vis. Sci.* 43, 1922–1927.

Del Amo, E. M., Rimpela, A. K., Heikkinen, E., Kari, O. K., Ramsay, E., Lajunen, T., et al. (2017). Pharmacokinetic aspects of retinal drug delivery. *Prog. Retin Eye Res.* 57, 134–185. doi: 10.1016/j.preteyeres.2016.12.001

Faktorovich, E. G., Steinberg, R. H., Yasumura, D., Matthes, M. T., and LaVail, M. M. (1990). Photoreceptor degeneration in inherited retinal dystrophy delayed by basic fibroblast growth factor. *Nature* 347, 83–86. doi: 10.1038/347083a0

Faktorovich, E. G., Steinberg, R. H., Yasumura, D., Matthes, M. T., and LaVail, M. M. (1992). Basic fibroblast growth factor and local injury protect photoreceptors from light damage in the rat. *J. Neurosci.* 12, 3554–3567. doi: 10.1523/jneurosci.12-09-03554.1992

Farber, D. B., Flannery, J. G., and Bowes-Rickman, C. (1994). The rd mouse story: seventy years of research on an animal model of inherited retinal degeneration. *Prog. Retin Eye Res.* 12, 31–64. doi: 10.1016/1350-9462(94)90004-3

Ferrante, R. J., Andreassen, O. A., Jenkins, B. G., Dedeoglu, A., Kuemmerle, S., Kubilus, J. K., et al. (2000). Neuroprotective effects of creatine in a transgenic mouse model of huntington's disease. *J. Neurosci.* 20, 4389–4397. doi: 10.1523/jneurosci.20-12-04389.2000

Fujii, T., Mori, K., Takahashi, Y., Taniguchi, N., Tonosaki, A., Yamashita, H., et al. (2001). Immunohistochemical study of glutathione reductase in rat ocular tissues at different developmental stages. *Histochem. J.* 33, 267–272.

Gaudana, R., Ananthula, H. K., Parenky, A., and Mitra, A. K. (2010). Ocular drug delivery. *AAPS J.* 12, 348–360. doi: 10.1208/s12248-010-9183-3

Gaudin, C., Forster, V., Sahel, J., Dreyfus, H., and Hicks, D. (1996). Survival and regeneration of adult human and other mammalian photoreceptors in culture. *Invest Ophthalmol. Vis. Sci.* 37, 2258–2268.

Gospe, S. M. III, Baker, S. A., and Arshavsky, V. Y. (2010). Facilitative glucose transporter Glut1 is actively excluded from rod outer segments. *J. Cell Sci.* 123, 3639–3644. doi: 10.1242/jcs.072389

Haverkamp, S., Wassle, H., Duebel, J., Kuner, T., Augustine, G. J., Feng, G., et al. (2005). The primordial, blue-cone color system of the mouse retina. *J. Neurosci.* 25, 5438–5445. doi: 10.1523/JNEUROSCI.1117-05.2005

Hurley, J. B., Lindsay, K. J., and Du, J. (2015). Glucose, lactate, and shuttling of metabolites in vertebrate retinas. *J. Neurosci. Res.* 93, 1079–1092. doi: 10.1002/jnr.23583

Kanow, M. A., Giarmarco, M. M., Jankowski, C. S., Tsantilas, K., Engel, A. L., Du, J., et al. (2017). Biochemical adaptations of the retina and retinal pigment epithelium support a metabolic ecosystem in the vertebrate eye. *eLife* 6, e28899. doi: 10.7554/eLife.28899

Klivenyi, P., Ferrante, R. J., Matthews, R. T., Bogdanov, M. B., Klein, A. M., Andreassen, O. A., et al. (1999). Neuroprotective effects of creatine in a transgenic animal model of amyotrophic lateral sclerosis. *Nat. Med.* 5, 347–350. doi: 10.1038/6568

Komeima, K., Rogers, B. S., and Campochiaro, P. A. (2007). Antioxidants slow photoreceptor cell death in mouse models of retinitis pigmentosa. *J. Cell Physiol.* 213, 809–815. doi: 10.1002/jcp.21152

Komeima, K., Rogers, B. S., Lu, L., and Campochiaro, P. A. (2006). Antioxidants reduce cone cell death in a model of retinitis pigmentosa. *Proc. Natl. Acad. Sci. U.S.A.* 103, 11300–11305. doi: 10.1073/pnas.0604056103

Lawler, J. M., Barnes, W. S., Wu, G., Song, W., and Demaree, S. (2002). Direct antioxidant properties of creatine. *Biochem. Biophys. Res. Commun.* 290, 47–52. doi: 10.1006/bbrc.2001.6164

Lee, S. Y., Usui, S., Zafar, A. B., Oveson, B. C., Jo, Y. J., Lu, L., et al. (2011). N-Acetylcysteine promotes long-term survival of cones in a model of retinitis pigmentosa. *J. Cell Physiol.* 226, 1843–1849. doi: 10.1002/jcp.22508

Lin, B., Masland, R. H., and Strettoi, E. (2009). Remodeling of cone photoreceptor cells after rod degeneration in rd mice. *Exp. Eye Res.* 88, 589–599. doi: 10.1016/j.exer.2008.11.022

Linton, J. D., Holzhausen, L. C., Babai, N., Song, H., Miyagishima, K. J., Stearns, G. W., et al. (2010). Flow of energy in the outer retina in darkness and in light. *Proc. Natl. Acad. Sci. U.S.A.* 107, 8599–8604. doi: 10.1073/pnas.1002471107

Matthews, R. T., Ferrante, R. J., Klivenyi, P., Yang, L., Klein, A. M., Mueller, G., et al. (1999). Creatine and cyclocreatine attenuate MPTP neurotoxicity. *Exp. Neurol.* 157, 142–149. doi: 10.1006/exnr.1999.7049

Matthews, R. T., Yang, L., Jenkins, B. G., Ferrante, R. J., Rosen, B. R., Kaddurah-Daouk, R., et al. (1998). Neuroprotective effects of creatine and cyclocreatine in animal models of Huntington's disease. *J. Neurosci.* 18, 156–163. doi: 10.1523/jneurosci.18-01-00156.1998

Mervin, K., Valter, K., Maslim, J., Lewis, G., Fisher, S., and Stone, J. (1999). Limiting photoreceptor death and deconstruction during experimental retinal detachment: the value of oxygen supplementation. *Am. J. Ophthalmol.* 128, 155–164. doi: 10.1016/s0002-9394(99)00104-x

Narayan, D. S., Ao, J., Wood, J. P. M., Casson, R. J., and Chidlow, G. (2019). Spatio-temporal characterization of S- and M/L-cone degeneration in the Rd1 mouse model of retinitis pigmentosa. *BMC Neurosci.* 20:46. doi: 10.1186/s12868-019-0528-2

Narayan, D. S., Chidlow, G., Wood, J. P., and Casson, R. J. (2017). Glucose metabolism in mammalian photoreceptor inner and outer segments. *Clin. Exp. Ophthalmol.* 45, 730–741. doi: 10.1111/ceo.12952

Narayan, D. S., Wood, J. P., Chidlow, G., and Casson, R. J. (2016). A review of the mechanisms of cone degeneration in retinitis pigmentosa. *Acta Ophthalmol.* 94, 748–754. doi: 10.1111/aos.13141

Niven, J. E., Anderson, J. C., and Laughlin, S. B. (2007). Fly photoreceptors demonstrate energy-information trade-offs in neural coding. *PLoS Biol.* 5:e116. doi: 10.1371/journal.pbio.0050116

Okawa, H., Sampath, A. P., Laughlin, S. B., and Fain, G. L. (2008). ATP consumption by mammalian rod photoreceptors in darkness and in light. *Curr. Biol.* 18, 1917–1921. doi: 10.1016/j.cub.2008.10.029

Ortin-Martinez, A., Nadal-Nicolas, F. M., Jimenez-Lopez, M., Alburquerque-Bejar, J. J., Nieto-Lopez, L., Garcia-Ayuso, D., et al. (2014). Number and distribution of mouse retinal cone photoreceptors: differences between an albino (Swiss) and a pigmented (C57/BL6) strain. *PLoS One* 9:e102392. doi: 10.1371/journal.pone.0102392

Petit, L., Ma, S., Cipi, J., Cheng, S. Y., Zieger, M., Hay, N., et al. (2018). Aerobic glycolysis is essential for normal rod function and controls secondary cone death in retinitis pigmentosa. *Cell Rep.* 23, 2629–2642. doi: 10.1016/j.celrep.2018.04.111

Prusky, G. T., Alam, N. M., Beekman, S., and Douglas, R. M. (2004). Rapid quantification of adult and developing mouse spatial vision using a virtual optomotor system. *Invest Ophthalmol. Vis. Sci.* 45, 4611–4616. doi: 10.1167/iovs.04-0541

Punzo, C., Kornacker, K., and Cepko, C. L. (2009). Stimulation of the insulin/mTOR pathway delays cone death in a mouse model of retinitis pigmentosa. *Nat. Neurosci.* 12, 44–52. doi: 10.1038/nn.2234

Rosas, H. D., Doros, G., Gevorkian, S., Malarick, K., Reuter, M., Coutu, J. P., et al. (2014). PRECREST: a phase II prevention and biomarker trial of creatine in at-risk Huntington disease. *Neurology* 82, 850–857. doi: 10.1212/WNL.0000000000000187

Rueda, E. M., Johnson, J. E. Jr., Giddabasappa, A., Swaroop, A., Brooks, M. J., Sigel, I., et al. (2016). The cellular and compartmental profile of mouse retinal glycolysis, tricarboxylic acid cycle, oxidative phosphorylation, and ˜P transferring kinases. *Mol. Vis.* 22, 847–885.

Shen, J., Yang, X., Dong, A., Petters, R., Peng, Y., Wong, F., et al. (2005). Oxidative damage is a potential cause of cone cell death in retinitis pigmentosa. *J. Cell Physiol.* 203, 457–464. doi: 10.1002/jcp.20346

Shibeeb, O., Chidlow, G., Han, G., Wood, J. P., and Casson, R. J. (2016). Effect of subconjunctival glucose on retinal ganglion cell survival in experimental retinal ischaemia and contrast sensitivity in human glaucoma. *Clin. Exp. Ophthalmol.* 44, 24–32. doi: 10.1111/ceo.12581

Silverman, M. S., and Hughes, S. E. (1990). Photoreceptor rescue in the RCS rat without pigment epithelium transplantation. *Curr. Eye Res.* 9, 183–191. doi: 10.3109/02713689008995205

Skeie, J. M., Tsang, S. H., and Mahajan, V. B. (2011). Evisceration of mouse vitreous and retina for proteomic analyses. *J. Vis. Exp.* 50:2795. doi: 10.3791/2795

Swarup, A., Samuels, I. S., Bell, B. A., Han, J. Y. S., Du, J., Massenzio, E., et al. (2019). Modulating GLUT1 expression in retinal pigment epithelium decreases glucose levels in the retina: impact on photoreceptors and muller glial cells. *Am. J. Physiol. Cell Physiol.* 316, C121–C133. doi: 10.1152/ajpcell.00410.2018

Usui, S., Komeima, K., Lee, S. Y., Jo, Y. J., Ueno, S., Rogers, B. S., et al. (2009). Increased expression of catalase and superoxide dismutase 2 reduces cone cell death in retinitis pigmentosa. *Mol. Ther.* 17, 778–786. doi: 10.1038/mt.2009.47

Venkatesh, A., Ma, S., Le, Y. Z., Hall, M. N., Ruegg, M. A., and Punzo, C. (2015). Activated mTORC1 promotes long-term cone survival in retinitis pigmentosa mice. *J. Clin. Invest* 125, 1446–1458. doi: 10.1172/JCI79766

Venkatesh, A., Ma, S., and Punzo, C. (2016). TSC but not PTEN loss in starving cones of retinitis pigmentosa mice leads to an autophagy defect and mTORC1 dissociation from the lysosome. *Cell Death Dis.* 7:e2279. doi: 10.1038/cddis.2016.182

Wallimann, T., Tokarska-Schlattner, M., and Schlattner, U. (2011). The creatine kinase system and pleiotropic effects of creatine. *Amino Acids* 40, 1271–1296. doi: 10.1007/s00726-011-0877-3

Wang, K., Xiao, J., Peng, B., Xing, F., So, K. F., Tipoe, G. L., et al. (2014). Retinal structure and function preservation by polysaccharides of wolfberry in a mouse model of retinal degeneration. *Sci. Rep.* 4:7601. doi: 10.1038/srep07601

Wang, L., Kondo, M., and Bill, A. (1997). Glucose metabolism in cat outer retina. Effects of light and hyperoxia. *Invest Ophthalmol. Vis. Sci.* 38, 48–55.

Wang, W., Lee, S. J., Scott, P. A., Lu, X., Emery, D., Liu, Y., et al. (2016). Two-step reactivation of dormant cones in retinitis pigmentosa. *Cell Rep.* 15, 372–385. doi: 10.1016/j.celrep.2016.03.022

Winkler, B. S. (1981). Glycolytic and oxidative metabolism in relation to retinal function. *J. Gen. Physiol.* 77, 667–692. doi: 10.1085/jgp.77.6.667

Wood, J. P., Chidlow, G., Graham, M., and Osborne, N. N. (2005). Energy substrate requirements for survival of rat retinal cells in culture: the importance of glucose and monocarboxylates. *J. Neurochem.* 93, 686–697. doi: 10.1111/j.1471-4159.2005.03059.x

Wood, J. P., Mammone, T., Chidlow, G., Greenwell, T., and Casson, R. J. (2012). Mitochondrial inhibition in rat retinal cell cultures as a model of metabolic compromise: mechanisms of injury and neuroprotection. *Invest Ophthalmol. Vis. Sci.* 53, 4897–4909. doi: 10.1167/iovs.11-9171

Conflict of Interest: The authors declare that the research was conducted in the absence of any commercial or financial relationships that could be construed as a potential conflict of interest.

frontiers in Neuroscience

ORIGINAL RESEARCH
published: 06 May 2020
doi: 10.3389/fnins.2020.00372

Myriocin Effect on Tvrm4 Retina, an Autosomal Dominant Pattern of Retinitis Pigmentosa

Ilaria Piano[1]†, Vanessa D'Antongiovanni[2]†, Elena Novelli[3], Martina Biagioni[3], Michele Dei Cas[4], Rita Clara Paroni[4], Riccardo Ghidoni[4,5], Enrica Strettoi[3] and Claudia Gargini[1]*

[1] Department of Pharmacy, University of Pisa, Pisa, Italy, [2] Department of Clinical and Experimental Medicine, University of Pisa, Pisa, Italy, [3] CNR Institute of Neuroscience, Pisa, Italy, [4] Department of Health Sciences, University of Milan, Milan, Italy, [5] Aldo Ravelli Center, University of Milan, Milan, Italy

Tvrm4 mice, a model of autosomal dominant retinitis pigmentosa (RP), carry a mutation of Rhodopsin gene that can be activated by brief exposure to very intense light. Here, we test the possibility of an anatomical, metabolic, and functional recovery by delivering to degenerating Tvrm4 animals, Myriocin, an inhibitor of ceramide *de novo* synthesis previously shown to effectively slow down retinal degeneration in rd10 mutants (Strettoi et al., 2010; Piano et al., 2013). Different routes and durations of Myriocin administration were attempted by using either single intravitreal (i.v.) or long-term, repeated intraperitoneal (i.p.) injections. The retinal function of treated and control animals was tested by ERG recordings. Retinas from ERG-recorded animals were studied histologically to reveal the extent of photoreceptor death. A correlation was observed between Myriocin administration, lowering of retinal ceramides, and preservation of ERG responses in i.v. injected cases. Noticeably, the i.p. treatment with Myriocin decreased the extension of the retinal-degenerating area, preserved the ERG response, and correlated with decreased levels of biochemical indicators of retinal oxidative damage. The results obtained in this study confirm the efficacy of Myriocin in slowing down retinal degeneration in genetic models of RP independently of the underlying mutation responsible for the disease, likely targeting ceramide-dependent, downstream pathways. Alleviation of retinal oxidative stress upon Myriocin treatment suggests that this molecule, or yet unidentified metabolites, act on cellular detoxification systems supporting cell survival. Altogether, the pharmacological approach chosen here meets the necessary pre-requisites for translation into human therapy to slow down RP.

Keywords: retinitis pigmentosa, photoreceptor rescue, oxidative stress, Myriocin, mutation-independent approach

OPEN ACCESS

Edited by:
Peter Koulen, University of Missouri System, United States

Reviewed by:
Melina A. Agosto, Baylor College of Medicine, United States
Benedetto Falsini, Università Cattolica del Sacro Cuore, Italy
Silvia Bisti, University of L'Aquila, Italy

***Correspondence:**
Ilaria Piano
ilaria.piano@unipi.it

† These authors have contributed equally to this work

Specialty section:
This article was submitted to Neurodegeneration, a section of the journal Frontiers in Neuroscience

Received: *30 July 2019*
Accepted: *26 March 2020*
Published: *06 May 2020*

Citation:
Piano I, D'Antongiovanni V, Novelli E, Biagioni M, Dei Cas M, Paroni RC, Ghidoni R, Strettoi E and Gargini C (2020) Myriocin Effect on Tvrm4 Retina, an Autosomal Dominant Pattern of Retinitis Pigmentosa. Front. Neurosci. 14:372. doi: 10.3389/fnins.2020.00372

INTRODUCTION

Recently, several experimental approaches have been proposed, aimed at recovering vision or preventing vision loss caused by retinal degeneration. Photoreceptor degeneration may be initiated by hundreds of different genetic mutations (RetNet, Retinal Information Network)[1] and visually impaired patients have reached an estimated number of over 20 million worldwide. Among

[1] http://www.sph.uth.tmc.edu/RetNet/

these, individuals with retinitis pigmentosa (RP) develop a typical phenotype characterized by rod degeneration with initial night blindness and loss of peripheral vision. Subsequently, cones also undergo degeneration, jeopardizing daytime vision and visual acuity, eventually leading to legal blindness. RP is a family of disorders typically caused by a single mutation in any of the numerous genes, approximately 70 of which have been identified so far. Thus, defining RP as a highly genetic heterogeneous disease is justified by a large number of underlying mutations, the different functions of the mutated genes, and the variable mode of inheritance (Wright et al., 2010). About 40% of RP cases show autosomal dominant inheritance and 25–30% of these are attributable to mutations in RHO, the gene that codes for rhodopsin, the photosensitive protein of rod photoreceptors.

A biochemical classification introduced in the 1990s (Sung et al., 1991; Sung et al., 1993) identifies two classes of mutations (I and II) on RHO. Class I mutations occur mainly near the C-terminal of the protein, which still retains the ability to bind to 11-*cis*-retinal and to form a functional chromophore but cannot be adequately transported to the outer segment and shows a constitutive activation or an increase in the transducin activation (Mendez et al., 2003). The most common class II mutations occur in the transmembrane or cytoplasmic domains of the protein, resulting in incorrect rhodopsin folding, retention in the endoplasmic reticulum, and inability to bind to 11-*cis*-retinal. Dominant (or dominant-negative) mutations are typically associated with a gain of function of the mutant protein, as observed in the highly studied, highly representative, P23H mutation, which causes retention of rhodopsin at the endoplasmic reticulum (ER) level. The consequent unfolded protein response (UPR) induction and proteosomal inhibition leads to aggregation of high-molecular-weight oligomers, which in turn form toxic intracellular inclusions (Lin et al., 2007; Mendes and Cheetham, 2008; Athanasiou et al., 2018). P23H and similar mutants are not easily approachable through gene therapy, because they require simultaneous suppression of native gene expression and supplementation with a wild-type (wt) version of the gene (MacLaren et al., 2016). Other forms of mutated rhodopsin (T4K, T4N, and T17M) show a lack of glycosylation of the residue N15, which leads to light-dependent retinal degeneration (Tam and Moritz, 2009).

The Tvrm4 mouse is an animal model particularly useful to study RHO mutations and the complex link between primary genetic defect and phenotype manifestation in order to develop appropriate approaches for preserving vision in humans with identical or similar genetic defects. The Tvrm4 strain constitutes an autosomal dominant RP model in which a missense mutation of RHO gene modifies the amino acid 307, isoleucine (ATC), in asparagine (AAC) (Budzynski et al., 2010). Peculiar characteristics of Tvrm4 mice are that they do not express the retinal pathological phenotype and exhibit normal rhodopsin levels if grown in normal housing conditions. However, these mice undergo RP-type retinal degeneration when exposed briefly (between 1 and 5 min) to strong white light (12,000 lux), however harmless to wt controls. The mutation leads to constitutively active mutated opsin (with prolonged dark adaptation times) and exposure to light causes an increase in the production of retinoid metabolites and intermediates of the phototransduction cascade, as well as an increase in mutant-free opsin levels that triggers processes leading to photoreceptor death (Budzynski et al., 2010). Light exposure for 1 to 5 min induces a massive photoreceptor death after 24 h; degeneration is mainly limited to the center of the retina while the peripheral area is less affected (effect probably due to the geometry of the eye) (Gargini et al., 2017). The peculiar features of Tvrm4 mutants, including the possibility of inducing retinal degeneration once neuronal development is completed, make them particularly useful for the study of autosomal dominant RP and retinal remodeling (Stefanov et al., 2019).

Using a widely exploited model of autosomal recessive RP, the rd10 mouse mutant of phosphodiesterase (Chang et al., 2002; Gargini et al., 2007), we have previously shown that long-term topical administration of Myriocin, an inhibitor of the enzyme serine-palmitoyl-CoA transferase involved in the first step of sphingolipids (i.e., ceramides) synthesis, is effective in slowing down the progression of the disease (Strettoi et al., 2010; Piano et al., 2013).

The involvement of sphingolipid metabolism, and in particular ceramide, in RP was first hypothesized in 2004. Tuson and collaborators showed that mutations of the ceramide kinase-like gene (CERKL) were associated with an autosomal recessive RP model (RP26) (Tuson et al., 2004); the role of CERKL in the retinal metabolism of sphingolipids was confirmed later (Garanto et al., 2013).

It is the purpose of the present study to show that Myriocin can be effective in more than one form of RP. To this aim, we administered Myriocin using two distinct protocols (local and systemic administration) immediately after light-induced retinal degeneration in Tvrm4 mice.

The results show that Myriocin is effective in slowing down retinal degeneration in this (fairly aggressive) model of autosomal dominant RP. Surprisingly, Myriocin, administered intraperitoneally for five consecutive days lowers apoptotic processes and increases the anti-oxidant defenses of the retinal cells.

MATERIALS AND METHODS

Animals

Animals were treated in accordance with Italian and European institutional guidelines, following experimental protocols approved by the Italian Ministry of Health (Protocol #14/D-2014, CNR Neuroscience Institute; Protocol #653/2017-PR, Department of Pharmacy, University of Pisa) and by the Ethical Committees of both Institutions. Protocols adhere to the Association for Research in Vision and Ophthalmology (ARVO) statement for the use of animals in research.

Heterozygous (±) Tvrm4 mice (RhoTvrm4/Rho+, from now on "Tvrm4 mice") with a I307N (near C-terminus) mutation of the rhodopsin gene (*Rho*) mice were used for this study (Budzynski et al., 2010). Tvrm4 mutants are on a C57Bl6/J background and exhibit no retinal phenotype unless exposed

to bright light stimuli. Genotyping was performed following Budzynski et al. (2010) and Jackson Laboratory's indications and only heterozygous mice were used for the experiments.

Induction of Retinal Degenerating Phenotype and Pharmacological Treatment

In this study we used young, adult mice aged 2–5 months, thus outside the time window of full retinal development (completed at around 30 days of age) and much younger than the manifestation of cellular aging (12 months). The age range chosen was already used in previous studies on Tvrm4 mutants, demonstrating that the light-induced damage is not influenced by the age of the animal (Budzynski et al., 2010; Gargini et al., 2017). Tvrm4 mice were dark adapted for 4 h and then given 1-μl eye drops of 0.5% atropine (Allergan); after 10 min, mice were placed in a black box and exposed to light pulses of 12,000 lux having durations of 2 min (for details, see Gargini et al., 2017). After light induction, the animals were assigned to one of the following experimental protocols:

Protocol I: Acute Administration of Myriocin by Intravitreal Injection (i.v.)

Mice were anesthetized with i.p. Avertin (0.5 g/mL 2,2,2-tribromoethanol in ter-amylic alcohol; 20 μl/g body weight). Using a surgical microscope, 1 μl of a 1.88 or 10 mM solution of Myriocin in DMSO was injected into the right vitreous body using a 30-gauge (0.3 × 8 mm) metal needle connected by a plastic tube to a 10-μl glass Hamilton syringe driven by an oil microinjector. The 7-fold dilution, considering the vitreous volume, leads to putative concentration of Myriocin of 0.27 and 1.43 mM, respectively. Left eyes were injected with an equal volume of DMSO. After 24 h, the retinas were isolated from animals under deep anesthesia. Retinas from n = 3 mice were fixed in 4% paraformaldehyde (PFA), rinsed in phosphate buffer (PB) 0.1 M, pH 7.4, and stained with ethidium homodimer to reveal cell nuclei. The outer nuclear layer (ONL) was imaged at a Leica TCS-SL confocal microscope using a 568 laser; 12 fields (250 μm × 250 μm) regularly distributed along the retinal surface were imaged and subsequently used to count the nuclei of pycnotic photoreceptors, corresponding to degenerating cells with highly condensed DNA. This method was used as in previous studies (Strettoi et al., 2010, PNAS) as it allows estimating the direct reduction effect of Myriocin on the rate of apoptotic cell death of photoreceptors. The average density of pycnotic cells per retina was calculated and the global average value was established for each experimental group (i.e., Myriocin and corresponding controls). Data were compared statistically using Sigmastat Software. Left and right retinas of n = 16 additional mice, injected with 10 mM Myriocin as above, were quickly isolated in cold ACSF and analyzed by HPCL-MS (n = 8 mice) and Western blot (WB) assay (n = 3) as described below. Animals were killed by cervical dislocation or anesthetic overdose immediately after eye removal.

Protocol II: Sub-Chronic Administration of Myriocin by Intraperitoneal Injection (i.p.)

Immediately after light induction, the animals were further subdivided randomly into two groups, a treatment group that received 1 mg/kg/day of Myriocin and a control group that received the vehicle (DMSO). In both cases, the animals were treated for 5 days and, at the end, used for functional analysis (ERG), biochemistry (WB), and immunohistochemistry. At the end of the experimental protocol, the animals were examined to exclude major adverse effects of the treatment (such as the presence of cataract, body weight loss, shaggy fur, or altered sensitivity to anesthesia).

Electroretinogram (ERG) Recordings

Animals were anesthetized with 20% Urethane (Sigma Aldrich, Milan, Italy), used at a concentration of 0.1 ml/10 g body weight. ERGs were recorded from dark-adapted mice using coiled gold electrodes making contact with the cornea moisturized by a thin layer of gel. Pupils were fully dilated by the application of a drop of 1% atropine (Farmigea, Pisa, Italy). Light stimulation and data analysis were as previously described in detail (Piano et al., 2016). Scotopic ERG recordings were average responses (n = 5) to flashes of increasing intensity (1.7×10^{-5} to 377 cd*s/m^2, 0.6 log units steps) presented with an inter-stimulus interval ranging from 20 s for dim flashes to 1 min for the brightest flashes. Isolated cone (photopic) components were obtained by superimposing the test flashes (0.016 to 377 cd*s/m^2) on a steady background of saturating intensity for rods (30 cd/m^2), after at least 15 min from background onset. The amplitude of the a-wave was measured at 7 ms after the onset of the light stimulus and the b-wave was measured from the peak of the a-wave to the peak of the b-wave.

The leading edge of the a-wave was fitted to the model of the activation phase of the rod G-protein transduction cascade (Lamb and Pugh, 1992) according to the following equation:

$$F(t) = exp[-1/2\Phi A(t - t_{eff})^2] \quad (1)$$

where $F(t)$ is the fraction of the circulating current normalized to its dark value, A is the amplification factor with the units of s^{-2}/Φ, expressed in terms of the gain parameters of the cascade stages, and t_{eff} is inclusive of any delay contained in both the response and the instrumentation. Further details for the application in the RP animal model are given in Gargini et al. (2007).

Oscillatory potentials (OPs) were also measured in both scotopic and photopic conditions. OPs were extracted digitally by using a fifth-order Butterworth filter as previously described (Hancock and Kraft, 2004; Lei et al., 2006). The peak amplitude of each OP (OP1–OP4) was measured. The ERG data for each condition of light induction were collected from at least six different animals.

Western Blot

Retinas from Tvrm4 mice were lysed in modified RIPA buffer as described before (Piano et al., 2019) and protein was quantified with the Bradford assay (Bio-Rad). For each experiment

performed, three different samples (each one composed of both retinas mixed together) for each experimental group were loaded on the gel, each from an animal previously used for ERG recordings. Proteins (25 μg) were separated onto a pre-cast 4–20% polyacrylamide gel (Mini-PROTEAN® TGX gel, BioRad) and transferred to PVDF membranes (*Trans*-Blot® Turbo™ PVDF Transfer packs, Bio-Rad). Membranes were blocked with 5% of non-fat dry milk (Bio-Rad) diluted in Tris-buffered saline (TBS, 20 mM Tris–HCl, pH 7.5, 150 mM NaCl) with 0.1% Tween 20. Primary antibodies against rhodopsin (cod. R5403, antibody concentration: ∼1 mg/ml, working dilution1:1000, Sigma Aldrich), cone-opsin blue and cone-opsin red/green incubated altogether (cod. AB5407 and AB5405, respectively antibodies concentration 1 mg/ml, working dilution 1:500, Millipore), caspase-3 (cod. sc-7272, antibody concentration: 200 μg/ml, working dilution 1:100, Santa Cruz Biotechnology), and Sod1 (cod. SAB5200083, antibody concentration 1 mg/ml, working dilution 1:500, Sigma Aldrich) were incubated overnight at 4°C. After performing three washings for 10 min each in T-TBS (TBS buffer with 0.1% of Tween-20), membranes were incubated with secondary antibodies (anti-mouse or anti-rabbit HRP conjugated, cod. AP308P or AP147P, respectively, antibodies concentration 1 mg/ml, working dilution 1:5000; Sigma Aldrich) for 2 h at room temperature. The immunoblot signal was visualized by using an enhanced chemiluminescence substrate detection system (Luminata™ Forte Western HRP Substrate, Millipore). The chemiluminescent images were acquired by Chemidoc XRS+ (Bio-Rad). Densitometry was undertaken using Bio-Rad ImageLab software.

Each protein of interest for the study was normalized for total protein content by using the Stain Free Technology (Bio-Rad) (Gürtler et al., 2013). To optimize the number of animals and the use of samples obtained, in some cases different proteins were analyzed on the same membrane following a stripping procedure preceded by three washings (10 min each) in glycine buffer, pH 2, followed by three washings in T-TBS and blocking in 5% of non-fat dry milk. The incubation of primary and secondary antibodies was performed with the same protocol described above.

Tissue Preparation, Histology, and Immunocytochemistry (IHC)

For retinal histological studies, mice were deeply anesthetized with intraperitoneal injections of 0.1 ml/5 g body weight Avertin as described above, their eyes quickly enucleated, and the animals killed by cervical dislocation. Eyes were labeled on the dorsal pole, the anterior segments were removed to obtain eye cups and fixed in 4% paraformaldehyde (PFA) in 0.1 M phosphate buffer, (PB), pH 7.4, for 30 min or 1 h, at room temperature. Eye cups were washed extensively in PB, infiltrated in 30% sucrose in PB at 4°C, frozen in Tissue-Tek O.C.T. compound (4583, Sakura Olympus, Italy) using cold isopentane and stored at −80°C until use. The eyes were used to prepare retinal whole mounts, in which the retina was separated from the pigment epithelium and flattened by making four radial cuts toward the head of the optic nerve, maintaining a reference on the dorsal pole. Areas of maximum photoreceptor loss were imaged on retinal whole mounts stained with 0.2 mM ethidium homodimer (Strettoi et al., 2010) and mounted with the photoreceptor side facing the coverslip. IHC on whole mounts was performed following Barone et al. (2012), by incubation in (a) block solution with 0.3% Triton X-100, 5% goat serum in 0.01 M phosphate buffer saline (PBS); (b) anti cone-arrestin (cod. AB15282, 1 mg/ml; working dilution 1:1000) primary antibody, overnight at 4°C; and (c) anti-rabbit 568-conjugated secondary antibody (cod. SAB4600310, 2 mg/ml, working dilution 1:5000). After rinsing in PBS, specimens were mounted in Vectashield (H-1000; Vector Laboratories, Burlingame, CA, United States) and coverslipped.

Ethidium-stained retinal whole mounts were examined with a Leica TCS SL confocal microscope equipped with a 568-nm laser using a 40×/1.25 oil objective. ONL series (n = 10 images along the z axis, encompassing the outermost 10 μm) and having a size of 250 × 250 μm were acquired for each retinal samples along the dorsoventral and peripheral axis (n = 12 fields/retina), using identical acquisition parameters for treated and control samples. Pycnotic profiles (corresponding to actively dying photoreceptors) were counted on projection images of each confocal series using the manual object counting tool of Metamorph. Counts were averaged and statistically compared using SigmaStat software.

Low-magnification images of retinal whole mount for cone-arrestin preparations were obtained with the Nikon Ni-E microscope using CFI plan fluor 10×/0.3 NA objective, with 16 mm working distance; images were tiled with Nis "Tiles and Positions" software to reconstruct the entire retinal surface. Areas of maximum photoreceptor loss were measured on full retinal montages saved as tiff files and transferred to an ImageJ analyzer. Images were homogeneously thresholded for brightness and the darkest, central region surrounding the optic nerve head (ONH) was automatically tracked and measured. This method was chosen as, at advanced stages of degeneration, cone-arrestin staining highlights clearly the dark, central area devoid of cones, allowing a quick and reproducible measurement of the extension of this zone in treated and control cases. This zone coincides with the central part of the retina where pycnotic (dying) photoreceptors are visible at early stages.

Ceramide Content

The third group of retinas from light-induced Tvrm4 mice, injected intravitreally with 10 mM Myriocin, as described in protocol 1, was used for paired ERG recordings and biochemical assessment of retinal ceramides. Freshly isolated retinas were rinsed in ACSF, placed in Eppendorf tubes and weighed on an analytical balance. The entire procedure took less than 2 min; samples were then snap frozen on dry ice stored at −80°C until use. Animals were killed by cervical dislocation immediately after eye removal.

The analysis and the extraction procedure from the retina sample for the determination of sphingolipids were carried out as already described (Platania et al., 2019). Briefly, retinas were homogenized in the TissueLyser (Qiagen, Hilden, Germany) and then aliquoted for the extraction of sphingolipids. Sphingolipids were extracted using a mixture of water/methanol/chloroform

(1:6:3, v/v/v). The analytical system consisted of a UPLC Dionex 3000 UltiMate (Thermo Fisher Scientific, United States) connected to an ABSciex 3200 QTRAP with electrospray ionization TurboIonSprayTM source (AB Sciex S.r.l., Milan, Italy). Quantitative sphingolipid determination was performed by multiple reaction monitoring (MRM) using as internal standard C12 ceramide. The separation was carried out on a reversed-phase BEH C-8 10 × 2.1 mm, 1.7 μm particle size (Waters, Milford, MA, United States) by mixing eluent A (water + 2 mM ammonium formate + 0.2% formic acid) and eluent B (methanol + 1 mM ammonium formate + 0.2% formic acid).

Statistical Analysis

Statistical comparisons for ERG and WB analysis were performed with analysis of variance (ANOVA) one- or two-way test followed by Bonferroni-corrected *t* test using Origin Lab 8.0 software (Microcal, Northampton, MA, United States).

RESULTS

Two studies previously published by the authors (Strettoi et al., 2010; Piano et al., 2013) showed that ocular administration of Myriocin, through instillation of nanosphere-based eye drops, was effective in slowing down the primary degeneration of rods as well as the degeneration of cones in rd10 mutants, mimicking typical, autosomal recessive RP. Current literature correlates the mechanism of action of Myriocin to the reduction of long-chain ceramides, mediated by the inhibition of the *de novo* synthesis of these important bioactive sphingolipids (Sanvicens and Cotter, 2006; German et al., 2006; Ranty et al., 2009; Kurek et al., 2017).

To verify whether this therapeutic approach can be considered mutation-independent, we administered Myriocin to the Tvrm4 mouse, which carries a different pathogenic mutation, with a different transmission modality compared to the rd10 mutant. Pilot experiments were done following the protocol previously used on rd10 mutants and based on a single intraocular administration of Myriocin, as this route was proven by us to produce readily-measurable retinal effects. Two-month aged animals were exposed to a strong white light for 2 min to trigger retinal degeneration; after 24 h, Myriocin was injected in the vitreous body of the right eye. The left eye, injected with vehicle, served as control. **Figure 1** illustrates whole-mount retinas stained with ethidium and imaged at the ONL (**Figures 1A,B**): the dark areas are zones of decreased fluorescence corresponding to thinning of the ONL and of lost missing photoreceptors. The extension of degenerated zones (circled in green) is visibly reduced in the retina treated with Myriocin with respect to the control side. Coherently, the number of pycnotic profiles (corresponding to condensed nuclei of actively dying photoreceptors) illustrated in **Figures 1C,D** is lower in retinas treated with Myriocin than in controls. The bar graph in **Figure 1E** shows an average decrement of over 1/3 dying photoreceptors in the retina of Myriocin-injected mice. As for the rd10 mutants used in the previous study (Strettoi et al., 2010), also in acutely treated Tvrm4 animals, the retinal function was tested by recording the ERG response. The experimental group shows a collective trend toward a higher conservation of the amplitude of the scotopic b-wave in Myriocin-injected mice, however, the difference with controls reaches statistical significance (**Figure 1F**).

To increase the chances of retinal rescue, we tested the effects of a single intraocular injection of 10 mM Myriocin by measuring in the same mice both retinal function by ERG recordings and total ceramide levels assessed by HPL-MS. **Figures 2A,B** illustrate the sensitivity curve of scotopic and photopic ERG, respectively, recorded from animals in which the right eye was injected with 10 mM Myriocin (red dots) and the left eye with vehicle (black dots); **Figure 2C** shows retinal ceramide levels measured in the same animals. Effective recovery of a retinal function cannot be demonstrated

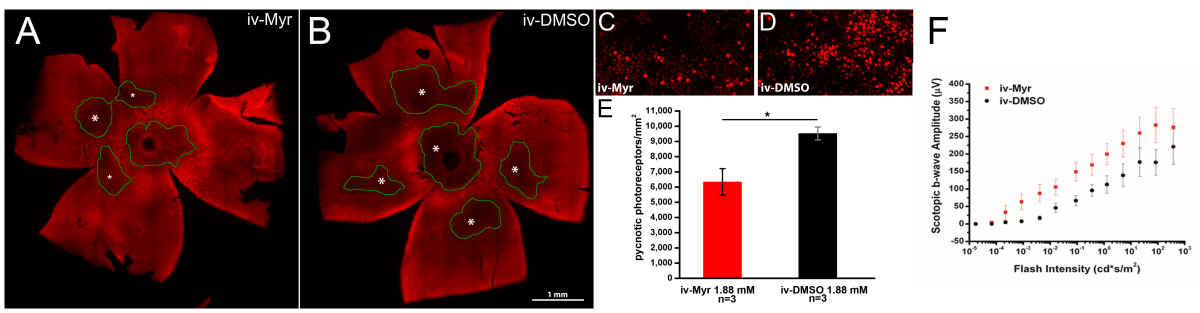

FIGURE 1 | Myriocin intravitreal injections in Tvrm4 mice. **(A,B)** Montages of images of whole-mount retinas stained with ethidium nuclear dye (red fluorescence). The focal plane is on the outer nuclear layer (ONL). Darker zones (green-encircled) indicate areas where photoreceptors have degenerated and their nuclei are missing. Larger degenerating zones are labeled with larger asterisks (*). The Myriocin-injected side shows dark zones that are visibly smaller (labeled with smaller asterisks) and less numerous compared to the control. **(C,D)** High magnification of the ONL of retinal whole mounts as those shown in A and B. Bright red nuclei belong to photoreceptors that entered in a stage of DNA condensation (pyknotic nuclei), visibly less numerous in the Myriocin-injected compared to the control eye. Imaged fields have consistent eccentricity and have been acquired with identical confocal microscope settings. **(E)** In the underlying bar graph, the average number of pyknotic nuclei is compared in retinas treated with Myriocin (red bars) and retinas treated with vehicle (black bars). Measurements are from three different mice ($n = 3$). **(F)** Sensitivity curve of the scotopic b-wave amplitude in Myriocin-treated (red squares) and vehicle-treated eyes (black circles) ($n = 3$). Bar values represent mean ± SEM.

(mainly due to the high variability encountered). Yet, an inverse correlation between the preservation of retinal light-responses and retinal ceramide content is observable (**Figure 2D**), albeit the finding does not reach statistical significance. The analysis of individual animals shows that when the amplitude of the ERG response in the eye treated with Myriocin is higher than in the eye injected with DMSO, ceramide levels are lower in Myriocin-treated eye than in the vehicle-treated one (sample no. 5). On the other hand, sample no. 9, in which the treatment was not effective, shows that the amplitude of the ERG is lower in the eye with higher ceramide levels. These data, showing a high individual variability, nevertheless indicate a direct correlation of retinal ceramide levels and degeneration and death of photoreceptors in Tvrm4 mutants (**Figure 2D**).

To test the possible therapeutic efficacy of Myriocin on a longer time scale, and considering (a) the impossibility to use repeated ocular administrations in mice and (b) the relatively quick rate of central retinal degeneration in Tvrm4 mutants (Gargini et al., 2017), we delivered Myriocin by intraperitoneal (i.p.) injections at the dose of 1 mg/kg/day for 5 days. The dose, route, and protocol of administration were based on existing literature (Glaros et al., 2007; Glaros et al., 2010; Lee et al., 2012).

The results obtained by recording the ERG in Tvrm4 animals exposed to light and treated via i.p. with Myriocin or vehicle, for 5 days, are shown in **Figure 3**. The bar graph shown in A compares the amplitude of the scotopic b-wave obtained from Tvrm4 animals where the degeneration was not induced (green bar—healthy control) with the two groups of animals exposed to light (pathological phenotype) treated with the vehicle (black bar) and with Myriocin (red bar). Figures A–C show that the treatment with Myriocin is effective in reducing retinal damage compared to animals treated with the vehicle alone, although photoreceptor preservation is not complete (Ctr vs. DMSO $p = 0.0008$; Ctr vs. Myr $p = 0.006$). **Figure 3B** shows that the amplitude of the b-wave is significantly larger ($p = 0.02112$; $p = 0.02744$; $p = 0.01$, respectively) in the group of animals treated with Myriocin ($n = 8$, red dots) compared

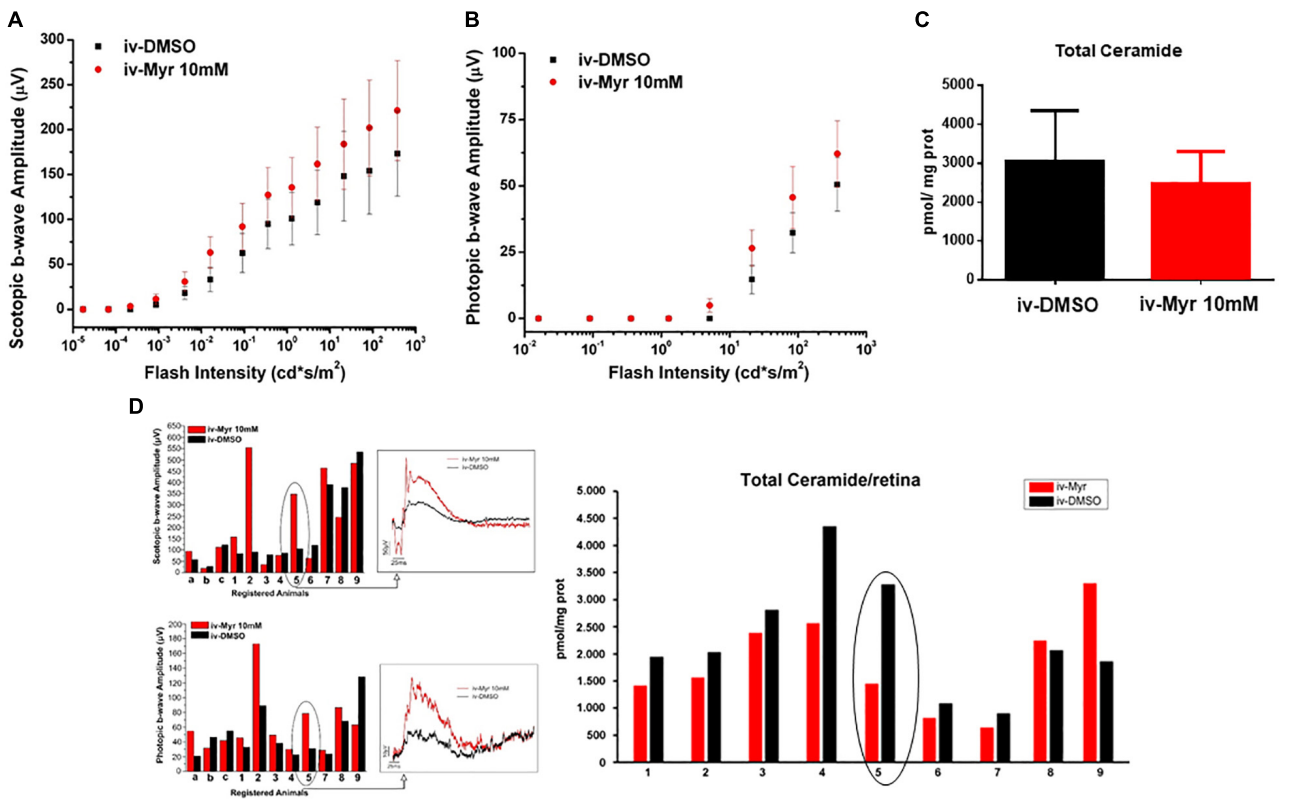

FIGURE 2 | Correlation between the decrease of ceramide content and functional recovery. **(A,B)** Sensitivity curve, respectively, of scotopic and photopic b-wave amplitude as a function of light flashes of increasing intensity. Although not significantly, the amplitude of the ERG response is increased in the eyes injected with Myriocin (red dots) compared to the eyes treated with the vehicle (black dots). Values represent mean ± SEM ($n = 12$; 11). **(C)** Bar graph showing quantification of Ceramide content in the same retinal samples used for ERG analysis. The value represents mean ± SEM ($n = 9$). **(D)** Correlation between retinal ceramide levels and functional activity. The bar graph on the left shows the scotopic and photopic b-wave amplitude recorded from Tvrm4 mice injected with 10 μM Myriocin in the right eye (red bars) and with vehicle in the left eye (black bars); representative (i.e., average-size) traces recorded at the highest luminance used (377 cd*s/m^2) are shown in the squared boxes on the right. The bar charts in the right of the panel show HPLC-MS quantification of ceramide content in the same retinas used for the ERG analysis. A correlation between the functionality of retinal neurons and ceramide levels is noted, even in cases when Myriocin does not show a protective effect: for instance, animal 5 has a larger ERG response of the eye treated with Myriocin, which corresponds to reduced levels of ceramide; animal 9 shows a smaller amplitude of the ERG in the Myriocin-treated eye, which, however has a higher ceramide content, possibly as a result of improper eye injection procedures.

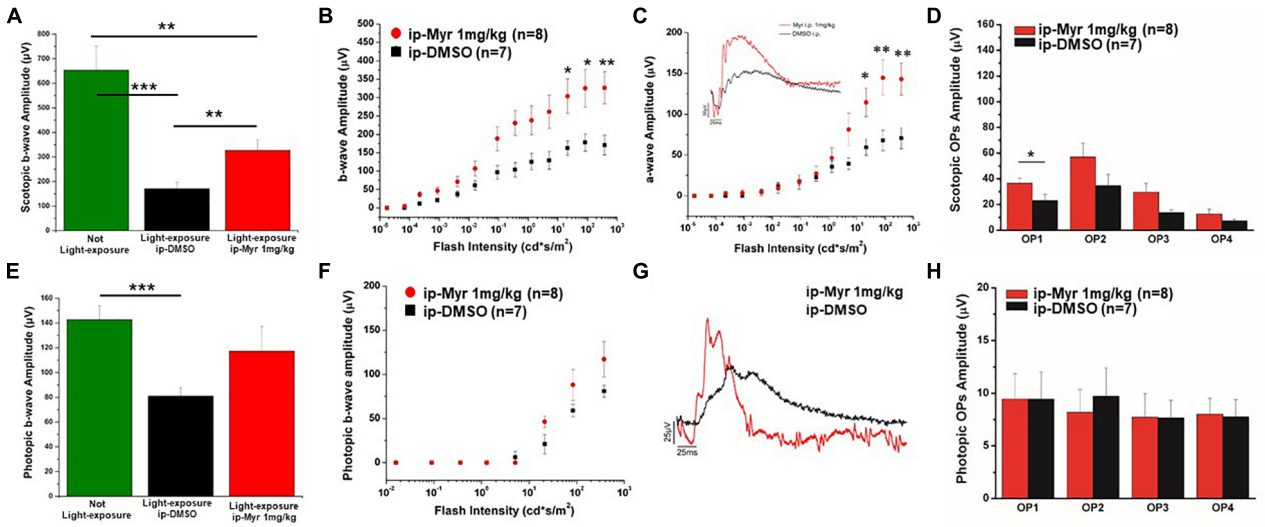

FIGURE 3 | Functional recovery in Tvrm4 mice after Myriocin intraperitoneal (i.p.) treatment. **(A)** The bar graph shows the scotopic b-wave amplitude measured at the highest luminance in non-induced control animals (green bar), in animals treated, after light induction, with vehicle (black bar), or with Myriocin (red bar). **(B)** The sensitivity curve of b-wave amplitude as a function of luminance shows a significant increase in Myriocin-treated versus control group. **(C)** The sensitivity curve of a-wave amplitude as a function of luminance shows a significant increase in Myriocin-treated versus control group. The inset represents an example of ERG traces recorded at the highest luminance used (377 cd*s/m^2). **(D)** Scotopic OPs obtained from ERG traces; the bar graph shows that only the OP1 relative to photoreceptor activity is significantly larger in Myriocin-treated mice with respect to the control mice. **(E)** Photopic ERG recordings from the not light-exposed Tvrm4 mice (green bar), vehicle-treated (black bar), and Myriocin-treated (red bar) mice. **(F)** The sensitivity curve of b-wave amplitude as a function of luminance shows a tendency to be larger in the Myriocin-treated group with respect to the control group. **(G)** Representative example of ERG traces recorded at the highest luminance used (377 cd*s/m^2) superimposed on a steady background (30 cd/m^2). **(H)** Photopic OPs obtained from ERG traces. The value represents mean ± SEM; $^*p \leq 0.05$, $^{**}p \leq 0.01$, $^{***}p \leq 0.001$.

to the group of animals treated with the vehicle ($n = 7$, black dots). Similarly, **Figure 3C** shows that also the amplitude of the a-wave is significantly higher in the animals treated with Myriocin with respect to the vehicle group ($p = 0.018$; $p = 0.0093$; $p = 0.01$, respectively); this effect is also confirmed by the a-wave analysis according to Lamb and Pugh (1992). The amplification parameter (A, s^{-2}/Φ) and the effective delay of the responses (t_{eff}) are shown in **Tables 1**, **2**. It can be observed that the amplification factor is significantly reduced and that the total delay is substantially increased in the group treated with the vehicle alone with respect to the Myriocin-treated group and also with respect to the healthy control; the analysis also shows that the injection of Myriocin is effective in restoring the A parameter near the physiological condition. **Figure 3D** shows that the OP amplitude shows a significant increase, mainly in the OP1 (directly correlated with the function of photoreceptors) in Myriocin-treated mice with respect to the vehicle group ($p = 0.048$).

Photopic ERG recordings are illustrated in **Figures 3E–H**; massive degeneration of the cones in the Tvrm4 mutant results in a significant reduction of the photopic b-wave amplitude with respect to the healthy control mice (Ctr vs. DMSO; $p = 0.00054$). The treatment with Myriocin shows a tendency, although not significant, to preserve the amplitude of the b-wave due to the activation of cone photoreceptors. The analysis of photopic OPs shows no differences between the two groups of mice.

The retinas obtained from the animals used for electrophysiological recordings were processed for immunohistochemistry and biochemistry experiments. **Figures 4A,B** show a retina obtained from an animal treated with Myriocin and one treated with the vehicle stained with cone-arrestin antibodies; the central area of degeneration (highlighted by the green outline) is largely reduced in the

TABLE 1 | Average value of amplification factor (A) of the a-wave measured at 14000. photoisomerization*rod^{-1} (Φ).

Experimental Group	A (s^{-2}/Φ) Mean ± St. Err.	*P* value (calculated respect to ip-DMSO)	*P* value (calculated respect to No light-exposure)
ip-DMSO	4.258 ± 0.45056		
ip- Myr	9.56067 ± 1.13184	0.0066**	N.S. ($P > 0.05$)
No light-exposure	9.7215 ± 0.97015	0.0092**	

TABLE 2 | Average value of effective delay (Teff) of the a-wave measured at 14000 photoisomerization*rod^{-1} (Φ).

Experimental Group	Teff (s) Mean ± St. Err.	*P* value (calculated respect to ip-DMSO)	*P* value (calculated respect to No light-exposure)
ip-DMSO	0.01097 ± 3.61E-4		
ip- Myr	0.00996 ± 2.27E-4	0.036*	0.00001***
No light-exposure	0.00772 ± 1.42E-4	0.00007***	

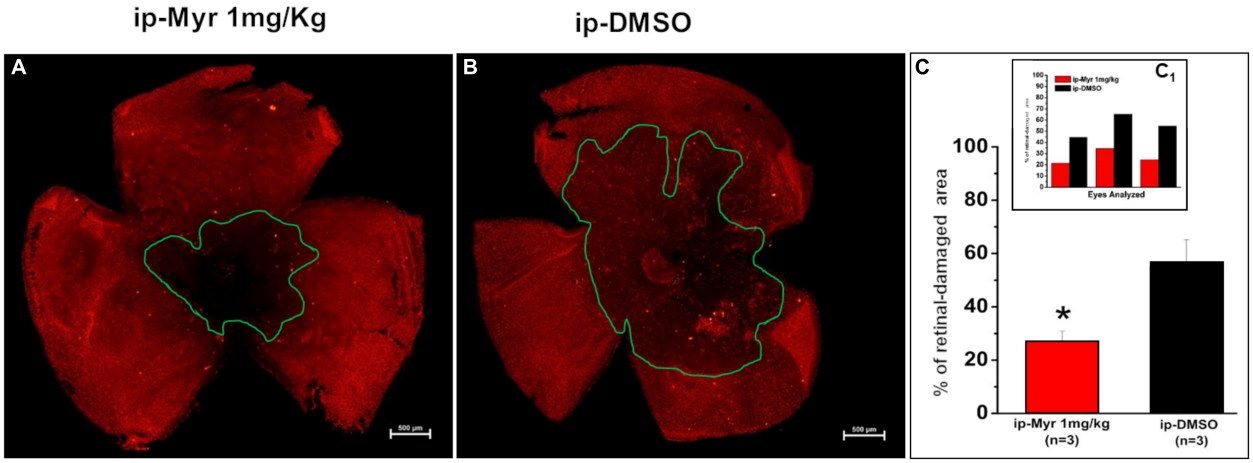

FIGURE 4 | Reduction of the photoreceptor-degeneration area after i.p. administration of Myriocin. **(A,B)** Representative images of retinal whole mounts obtained from control and Myriocin-treated mice obtained by anti-cone arrestin immunostaining (red fluorescence). The green lines surround the area affected upon the induction of the mutation by light exposure. **(C)** Quantification of the affected area calculated as a percentage of the total retinal area from three different experiments (shown in the insert bar graph, **C1**), showing a significant reduction in animals treated with Myriocin (red bars) compared to animals treated with vehicle (black bars). The values reported in the main bar graph represent global averages of all the experiments; Values are shown as mean ± SEM (n = 3, for each analyzed group); $^{*}p \leq 0.05$.

retina from the animal treated with Myriocin with respect to the control. Measurement of the degeneration zone with respect to the total retinal area, reported as a percentage, is shown in the bar graph of **Figure 4C**, proving how systemic administration of Myriocin for 5 days significantly reduces (p = 0.03471) the area of photoreceptor death. These data also indicate the ability of Myriocin or of an active metabolite to cross the blood–retinal barrier and reach the retina, which is known to weaken in neurodegenerations, thus allowing the passage of molecules useful for therapeutic treatment (Acharya et al., 2017).

In order to confirm the rescue effects described above, we measured the levels of rhodopsin and of blue and red/green cone-opsins by WB analysis (**Figures 5A–C**). The bar graph in **Figure 5B** shows that after induction of the mutation by light exposure, rhodopsin levels are significantly reduced

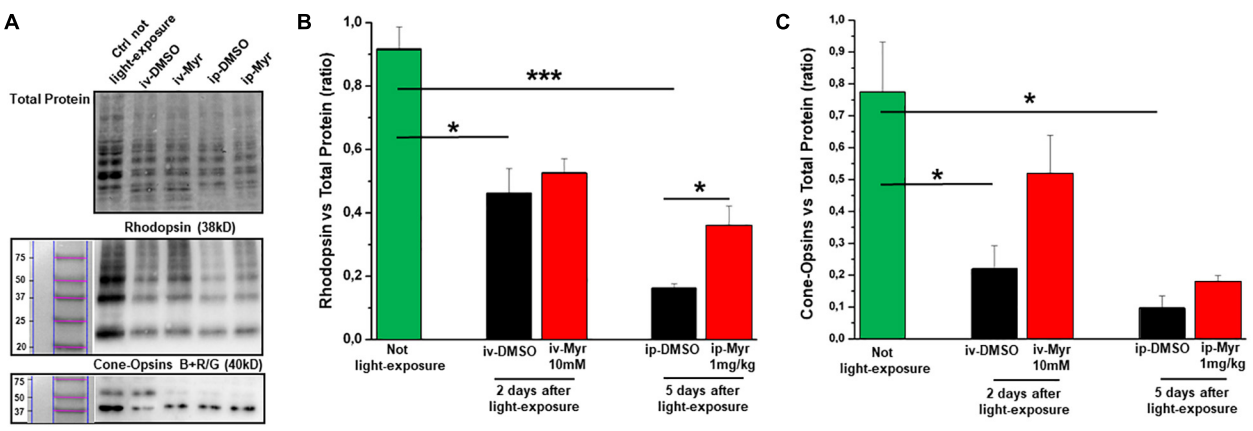

FIGURE 5 | Preservation of rhodopsin and cone-opsins level following treatment with Myriocin. **(A)** Representative example of WB experiment of rhodopsin and cone-opsins content. **(B)** Quantification by optical densitometry of rhodopsin levels in Tvrm4 animals not exposed (green bar) and treated with Myriocin (red bar) or with vehicle (black bar) by both intravitreal and intraperitoneal injection after light induction. The bar graph shows that the levels of rhodopsin are significantly reduced in the animals treated with DMSO with respect to the non-exposed controls; i.p. treatment with Myriocin results in a rhodopsin content significantly higher with respect to the group of animals treated with vehicle. **(C)** Quantification by optical densitometry of cone-opsins levels in Tvrm4 animals not exposed (green bar) and treated with Myriocin (red bar) or with vehicle (black bar) by both intravitreal and intraperitoneal injection after light induction. The bar graph shows that the levels of cone-opsins are significantly reduced in the animals treated with DMSO with respect to the non-exposed control. Treatment with Myriocin, by both routes of administration, leads to an increase in cone-opsins levels, although not statistically significant. Values are shown as mean ± SEM (n = 3, for each analyzed group); $^{*}p \leq 0.05$, $^{***}p \leq 0.001$.

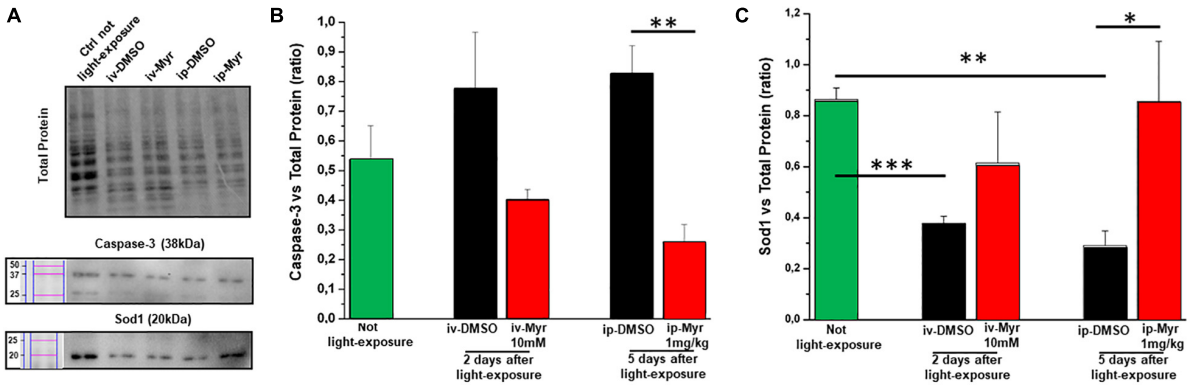

FIGURE 6 | Systemic Myriocin treatment increases the level of Sod1 protein. **(A)** Representative example of WB experiment of caspase-3 and Sod-1 content. **(B)** Quantification by optical densitometry of caspase-3 levels in Tvrm4 animals treated with Myriocin (red bar) or with vehicle (black bar) compared to the level in non-exposed mice (green bar). The bar graph shows that the levels of the pro-apoptotic marker caspase-3 are reduced in the group of animals treated with Myriocin. **(C)** Quantification by optical densitometry of Sod1 levels in Tvrm4 animals not light-induced (green bar), treated with vehicle (black bar), or treated with Myriocin (red bar). The bar graph shows that the levels of the anti-oxidant enzyme Sod1 are significantly increased in the group of mice treated with Myriocin, with respect to both the group of non-degenerate control animals and the group of mice treated with the vehicle alone. Values are shown as mean ± SEM (n = 4, for each analyzed group); *$p \leq 0.05$, **$p \leq 0.01$, ***$p \leq 0.001$. **(B)** Representative example of WB experiment.

compared to the levels measured in a healthy control animal (Ctr vs. i.v.-DMSO p = 0.012; Ctr vs. i.p.-DMSO p = 0.0004). The graph also shows that previously described i.v. treatment with Myriocin is not sufficient to preserve a number of rods such as to result in a significant increase in rhodopsin content; on the other hand, i.p. treatment with Myriocin is effective in saving a larger number of photoreceptors, resulting in a significant increase of this protein (i.p.-DMSO vs. i.p.-Myriocin p = 0.035). **Figure 5C** shows a similar trend also for the cone-opsins levels, which are significantly reduced in the induced animals treated with the vehicle alone with respect to healthy controls (Ctr vs. i.v.-DMSO p = 0.033; Ctr vs. i.p.-DMSO p = 0.014). Again, although not significantly, the treatment with Myriocin shows a trend toward cone preservation as shown in the bar graph of **Figure 5C**. These data are in agreement with ERG recordings that show a significant recovery only for the scotopic protocol.

The levels of caspase-3, a specific marker of apoptosis, were also measured by WB assay (**Figure 6A**), to confirm the reduction of common apoptotic pathway activation. **Figure 6B** shows how the levels of caspase-3 are increased in degenerating retina with respect to the control healthy group. Furthermore, i.p. treatment with Myriocin significantly reduces (p = 0.0057) the levels of caspase-3 compared to those obtained from control animals (n = 4/experimental group). This result confirms the anti-apoptotic effect of Myriocin, at the retinal level, also when administered systemically.

Finally, to assess whether Myriocin (or any derivative metabolites) could act via signaling pathways known to act in inherited retinal degeneration, we analyzed retinal protein levels of Sod1, one of the main enzymes of the physiological anti-oxidant system. **Figure 6C** shows how, in retinas obtained from light-induced Tvrm4 mice, the Sod1 content is significantly reduced with respect to the control healthy mice (Ctr vs. i.v.-DMSO; p = 0.0008; Ctr vs. i.p.-DMSO; p = 0.008). This result indicates a reduced ability of the damaged photoreceptors to remove ROS from the cellular environment. In both treatment protocols (i.v. and i.p.) with Myriocin, it is possible to note an increase in Sod1 levels toward physiological ones, although only in the case of i.p. administration is this increase significant (p = 0.035).

These results indicate that Myriocin, administered i.p., directly or by means of yet unknown metabolic derivatives, reaches the interior of the eye and exerts a protective effect on RP-like retinal degeneration. Besides the known activity as a suppressor of ceramide *de novo* synthesis and an anti-apoptotic agent, Myriocin could act, in medium and long-term treatments, on other cellular pathways, including induction of detoxifying anti-oxidant systems.

DISCUSSION

Previous studies have shown that increased ceramide levels in the rd10 animal model of autosomal recessive RP are in temporal association with the process of photoreceptor demise and that *in vivo* inhibition of *de novo* ceramide biosynthesis delays effectively this process (Strettoi et al., 2010; Piano et al., 2013). This observation supports the notion that this sphingolipid is involved in the neurodegenerative process taking place in RP. The results are in agreement with the increased ceramide levels found in tissues from individuals with other pathologies leading to apoptosis, such as brain tissue from Alzheimer's disease patients and thus provide additional evidence that elevated ceramide is a common pathogenic factor of a variety of neurodegenerative diseases (Han et al., 2002; He et al., 2009; Kurek et al., 2017). Both *in vitro* and *in vivo* studies on various animal models confirm that ceramide is involved in processes that trigger apoptotic death of photoreceptors and that treatments aiming at to reducing ceramide content are beneficial to cell viability and function

(Acharya, 2003; Acharya and Acharya, 2005; German et al., 2006; Sanvicens and Cotter, 2006; Rotstein et al., 2010).

The present study suggests that Myriocin, a selective inhibitor of SPT, the rate-limiting enzyme of ceramide biosynthesis, exerts rescue effects on the (rather acute) retinal degeneration process occurring in Tvrm4 mice, carrying a dominant mutation of rhodopsin inducible by light in adulthood and therefore completely different from the rd10 mutants previously employed.

We show that, similarly to rd10 mice, rescue effects obtained with a single intraocular injection of 1.88 mM Myriocin reduce the number of pycnotic photoreceptors, but this is not sufficient to efficiently rescue the ERG response (Strettoi et al., 2010) and does not change reproducibly ceramide levels (data not shown). Increasing the dose of Myriocin to 10 mM results in a similarly limited recovery of visual function and reveals single-case correlations between ERG amplitude and levels of retinal ceramide, without reducing it significantly on averaged data. WB analysis shows a Myriocin-related tendency to restore the levels of enzymes involved in apoptotic processes (caspase 3) and oxidative stress (Sod1) toward physiological values, indicating a reduction in the degenerative process. Most likely, the lack of functional effects after intravitreal treatment with Myriocin depends on the short duration of the treatment that fails to save a number of photoreceptors large enough to affect a mass-recording measurement such as the ERG. Moreover, the intrinsic variability in the size of the light-induced, degenerating area typical of the Tvrm4 phenotype makes the acutely induced and treated model quite complex for quantitative mass assays, despite the fact that we invariably use the contralateral, vehicle-treated eyes as controls. Conversely, a measurable decrement in the number of degenerating photoreceptor profiles (which are counted with single-cell resolution) is achieved with a single i.v. injection of 1.88 mM Myriocin, demonstrating efficacy in the acute phase of degeneration as already shown on the rd10 model (Strettoi et al., 2010).

To extend the time window of Myriocin treatment and appreciate the likely beneficial effects on the Tvrm4 retinal phenotype, we chose sustained (5-day) treatment achieved by the systemic administration of the drug by intraperitoneal injections (Osuchowski et al., 2004). Intraperitoneal treatment did not cause any adverse effect at general and ocular level although specific toxicity studies will be necessary in the future. Indeed, sustained, i.p. administration of Myriocin in Tvrm4 mice effectively reduces the size of the central-degenerating retina, rescues rhodopsin levels, and preserves the scotopic ERG. These results strongly suggest that Myriocin, or some active, yet unknown metabolite, are able to permeate the blood–retinal barrier, which, in these animals, could already be damaged due to the degenerative processes in progress and reduce the processes that lead to the death of photoreceptors. Indeed, levels of activated caspase-3 protein are reduced as well. Our experiment indications about levels of physiological defense pathways against the oxidative stress implicated in secondary cone degeneration (Usui et al., 2011) show that Myriocin i.p. treatment is associated with a significant increase in the content of the cytosolic isoform of retinal Sod1. Hence, Myriocin is not only an effective anti-apoptotic agent acting by inhibiting SPT and decreasing ceramide levels, in turn involved also in ROS generation (Sanvicens and Cotter, 2006) but is also capable of increasing the physiological anti-oxidant defenses by stimulating the synthesis of the key enzyme Sod1.

Although the efficacy of Myriocin as an anti-apoptotic and as a regulator of the cell cycle has already been proven in other tissues by means of either local (Reforgiato et al., 2016) and systemic administration to target cancer cells (Lee et al., 2012) or lipid metabolism in an animal model of type I diabetes (Kurek et al., 2017), our study is the first that demonstrates the ability of Myriocin, or of some active metabolite, to act effectively on the retina, an outpost of the brain, even when administered systemically, exerting a measurable anti-degenerative action and activating local anti-oxidant defenses. An anti-inflammatory benefit on retinal survival is not to be excluded, given the proven action of Myriocin as an immunosuppressant and anti-inflammatory agent (Caretti et al., 2014) and the increasing evidence of a contribution of inflammation-immune response on worsening of retinal phenotype in inherited photoreceptor degeneration (Zabel et al., 2016; Guadagni et al., 2019).

DATA AVAILABILITY STATEMENT

The datasets generated for this study are available on request to the corresponding author.

ETHICS STATEMENT

The animal study was reviewed and approved by Italian Ministry of Health and Ethical Committees of Department of Pharmacy, University of Pisa and CNR Neuroscience Institute.

AUTHOR CONTRIBUTIONS

IP, VD'A, and EN conceived and performed the experiments. MB contributed to the execution of the experiments. MD and RP performed the experiments on ceramide analysis. IP, VD'A, CG, and ES collected and critically analyzed the data. IP and CG wrote the manuscript. RG and ES critically reviewed the manuscript. All authors read, edited, and approved the final manuscript.

FUNDING

This study was funded and supported by Fondazione Roma, Italy, "Retinitis Pigmentosa Call". ES is an Italian beneficiary of a European Union's Horizon 2020 Research and Innovation Program, Marie Skłodowska-Curie Grant Agreement No. 674901.

ACKNOWLEDGMENTS

MD was supported by the Ph.D. program in Molecular and Translational Medicine of the University of Milan, Italy. We want to thank Luca Della Santina for the valuable advice.

REFERENCES

Acharya, N. K., Qi, X., Goldwaser, E. L., Godsey, G. A., Wu, H., Kosciuk, M. C., et al. (2017). Retinal pathology is associated with increased blood–retina barrier permeability in a diabetic and hypercholesterolaemic pig model: beneficial effects of the LpPLA $_2$ inhibitor darapladib. *Diab. Vasc. Dis. Res.* 14, 200–213. doi: 10.1177/1479164116683149

Acharya, U. (2003). Modulating sphingolipid biosynthetic pathway rescues photoreceptor degeneration. *Science* 299, 1740–1743. doi: 10.1126/science.1080549

Acharya, U., and Acharya, J. K. (2005). Enzymes of sphingolipid metabolism in *Drosophila melanogaster*. *CMLS Cell. Mol. Life Sci.* 62, 128–142. doi: 10.1007/s00018-004-4254-1

Athanasiou, D., Aguila, M., Bellingham, J., Li, W., McCulley, C., and Reeves, P. J. (2018). The molecular and cellular basis of rhodopsin retinitis pigmentosa reveals potential strategies for therapy. *Prog. Retin. Eye Res.* 62, 1–23. doi: 10.1016/j.preteyeres.2017.10.002

Barone, I., Novelli, E., Piano, I., Gargini, C., and Strettoi, E. (2012). Environmental enrichment extends photoreceptor survival and visual function in a mouse model of retinitis pigmentosa. *PLoS One* 7:e50726. doi: 10.1371/journal.pone.0050726

Budzynski, E., Gross, A. K., McAlear, S. D., Peachey, N. S., Shukla, M., He, F., et al. (2010). Mutations of the opsin gene (Y102H and I307N) lead to light-induced degeneration of photoreceptors and constitutive activation of phototransduction in mice. *J. Biol. Chem.* 285, 14521–14533. doi: 10.1074/jbc.M110.112409

Caretti, A., Bragonzi, A., Facchini, M., De Fino, I., Riva, C., Gasco, P., et al. (2014). Anti-inflammatory action of lipid nanocarrier-delivered myriocin: therapeutic potential in cystic fibrosis. *Biochim. Biophys. Acta* 1840, 586–594. doi: 10.1016/j.bbagen.2013.10.018

Chang, B., Hawes, N. L., Hurd, R. E., Davisson, M. T., Nusinowitz, S., and Heckenlively, J. R. (2002). Retinal degeneration Mutants in the Mouse. *Vis. Res.* 42, 517–525. doi: 10.1016/S0042-6989(01)00146-8

Garanto, A., Mandal, N. A., Egido-Gabás, M., Marfany, G., Fabriàs, G., Anderson, R. E., et al. (2013). Specific sphingolipid content decrease in cerkl knockdown mouse retinas. *Exp. Eye Res.* 110, 96–106. doi: 10.1016/j.exer.2013.03.003

Gargini, C., Novelli, E., Piano, I., Biagioni, M., and Strettoi, E. (2017). Pattern of retinal morphological and functional decay in a light-inducible, rhodopsin mutant mouse. *Sci. Rep.* 7:5730. doi: 10.1038/s41598-017-06045-x

Gargini, C., Terzibasi, E., Mazzoni, F., and Strettoi, E. (2007). Retinal organization in the retinal degeneration 10 (Rd10) mutant mouse: a morphological and ERG study. *J. Comp. Neurol.* 500, 222–238. doi: 10.1002/cne.21144

German, O. L., Miranda, G. E., Abrahan, C. E., and Rotstein, N. P. (2006). Ceramide is a mediator of apoptosis in retina photoreceptors. *Invest. Opthalmol. Vis. Sci.* 47, 1658. doi: 10.1167/iovs.05-1310

Glaros, E. N., Kim, W. S., Wu, B. J., Suarna, C., Quinn, C. M., Rye, K. A., et al. (2007). Inhibition of atherosclerosis by the serine palmitoyl transferase inhibitor myriocin is associated with reduced plasma glycosphingolipid concentration. *Biochem. Pharmacol.* 73, 1340–1346. doi: 10.1016/j.bcp.2006.12.023

Glaros, E. N., Kim, W. S., and Garner, B. (2010). Myriocin-mediated up-regulation of hepatocyte apoA-I synthesis is associated with ERK inhibition. *Clin. Sci.* 118, 727–736. doi: 10.1042/CS20090452

Guadagni, V., Biagioni, M., Novelli, E., Aretini, P., Mazzanti, C. M., and Strettoi, E. (2019). Rescuing cones and daylight vision in retinitis pigmentosa mice. *FASEB J.* 33, 10177–10192. doi: 10.1096/fj.201900414R

Gürtler, A., Kunz, N., Gomolka, M., Hornhardt, S., Friedl, A. A., McDonald, K., et al. (2013). Stain-free technology as a normalization tool in western blot analysis. *Anal. Biochem.* 433, 105–111. doi: 10.1016/j.ab.2012.10.010

Han, X., Holtzman, M. D., McKeel, D. W. Jr., Kelley, J., and Morris, J. C. (2002). Substantial sulfatide deficiency and ceramide elevation in very early Alzheimer's disease: potential role in disease pathogenesis: sulfatide deficiency and ceramide elevation in AD. *J. Neurochem.* 82, 809–818. doi: 10.1046/j.1471-4159.2002.00997.x

Hancock, H. A., and Kraft, T. W. (2004). Oscillatory potential analysis and ERGs of normal and diabetic rats. *Invest. Opthalmol. Vis. Sci.* 45:1002. doi: 10.1167/iovs.03-1080

He, B., Lu, N., and Zhou, Z. (2009). Cellular and nuclear degradation during apoptosis. *Curr. Opin. Cell Biol.* 21, 900–912. doi: 10.1016/j.ceb.2009.08.008

Kurek, K., Garbowska, M., Ziembicka, D. M., Łukaszuk, B., Rogowski, J., Chabowski, A., et al. (2017). Myriocin treatment affects lipid metabolism in skeletal muscles of rats with streptozotocin-induced type 1 diabetes. *Adv. Med. Sci.* 62, 65–73. doi: 10.1016/j.advms.2016.04.003

Lamb, T. D., and Pugh, E. N. Jr. (1992). A quantitative account of the activation steps involved in phototransduction in amphibian photoreceptors. *J. Physiol.* 449, 719–758. doi: 10.1113/jphysiol.1992.sp019111

Lee, Y. S., Choi, K. M., Lee, S., Sin, D. M., Lim, Y., Lee, Y. M., et al. (2012). Myriocin, a serine palmitoyltransferase inhibitor, suppresses tumor growth in a murine melanoma model by inhibiting de novo sphingolipid synthesis. *Cancer Biol. Ther.* 13, 92–100. doi: 10.4161/cbt.13.2.18870

Lei, B., Yao, G., Zhang, K., Hofeldt, K. J., and Chang, B. (2006). Study of rod- and cone-driven oscillatory potentials in mice. *Invest. Opthalmol. Vis. Sci.* 47:2732. doi: 10.1167/iovs.05-1461

Lin, J. H., Li, H., Yasumura, D., Cohen, H. R., Zhang, C., Panning, B., et al. (2007). IRE1 signaling affects cell fate during the unfolded protein response. *Science* 318, 944–949. doi: 10.1126/science.1146361

MacLaren, R. E., Bennett, J., and Schwartz, S. D. (2016). Gene therapy and stem cell transplantation in retinal disease: the new frontier. *Ophthalmology* 123, S98–S106. doi: 10.1016/j.ophtha.2016.06.041

Mendes, H. F., and Cheetham, M. E. (2008). Pharmacological manipulation of gain-of-function and dominant-negative mechanisms in rhodopsin retinitis pigmentosa. *Hum. Mol. Genet.* 17, 3043–3054. doi: 10.1093/hmg/ddn202

Mendez, A., Lem, J., Simon, M., and Chen, J. (2003). Light-dependent translocation of arrestin in the absence of rhodopsin phosphorylation and transducin signaling. *J. Neurosci.* 23, 3124–3129. doi: 10.1523/JNEUROSCI.23-08-03124.2003

Osuchowski, M. F., Johnson, V. J., He, Q., and Sharma, R. P. (2004). Myriocin, a serine palmitoyltransferase inhibitor, alters regional brain neurotransmitter levels without concurrent inhibition of the brain sphingolipid biosynthesis in mice. *Toxicol. Lett.* 147, 87–94. doi: 10.1016/j.toxlet.2003.10.016

Piano, I., D'Antongiovanni, V., Testai, L., Calderone, V., and Gargini, C. (2019). A nutraceutical strategy to slowing down the progression of cone death in an animal model of retinitis pigmentosa. *Front. Neurosci.* 13:461. doi: 10.3389/fnins.2019.00461

Piano, I., Novelli, E., Santina, L. D., Strettoi, E., Cervetto, L., and Gargini, C. (2016). Involvement of autophagic pathway in the progression of retinal degeneration in a mouse model of diabetes. *Front. Cell. Neurosci.* 10:42. doi: 10.3389/fncel.2016.00042

Piano, I., Novelli, E., Gasco, P., Ghidoni, R., Strettoi, E., and Gargini, C. (2013). Cone survival and preservation of visual acuity in an animal model of retinal degeneration. *Eur. J. Neurosci.* 37, 1853–1862. doi: 10.1111/ejn.12196

Platania, C. B. M., Cas, M. D., Cianciolo, S., Fidilio, A., Lazzara, F., Paroni, R., et al. (2019). Novel ophthalmic formulation of myriocin: implications in retinitis pigmentosa. *Drug Deliv.* 26, 237–243. doi: 10.1080/10717544.2019.1574936

Ranty, M. L., Carpentier, S., Cournot, M., Rico-Lattes, I., Malecaze, F., Levade, T., et al. (2009). Ceramide production associated with retinal apoptosis after retinal detachment. *Graefes Arch. Clin. Exp. Ophthalmol.* 247, 215–224. doi: 10.1007/s00417-008-0957-6

Reforgiato, M. R., Milano, G., Fabriàs, G., Casas, J., Gasco, P., Paroni, R., et al. (2016). Inhibition of ceramide de novo synthesis as a postischemic strategy to reduce myocardial reperfusion injury. *Basic Res. Cardiol.* 111:12. doi: 10.1007/s00395-016-0533-x

Rotstein, N. P., Miranda, G. E., Abrahan, C. E., and German, O. L. (2010). Regulating survival and development in the retina: key roles for simple sphingolipids. *J. Lipid Res.* 51, 1247–1262. doi: 10.1194/jlr.R003442

Sanvicens, N., and Cotter, T. G. (2006). Ceramide is the key mediator of oxidative stress-induced apoptosis in retinal photoreceptor cells. *J. Neurochem.* 98, 1432–1444. doi: 10.1111/j.1471-4159.2006.03977.x

Stefanov, A., Novelli, E., and Strettoi, E. (2019). Inner retinal preservation in the photoinducible I307N rhodopsin mutant mouse, a model of autosomal dominant retinitis pigmentosa. *J. Comp. Neurol.* 528, 1502-1522. doi: 10.1002/cne.24838

Strettoi, E., Gargini, C., Novelli, E., Sala, G., Piano, I., Gasco, P., et al. (2010). Inhibition of ceramide biosynthesis preserves photoreceptor structure and function in a mouse model of retinitis pigmentosa. *Proc. Natl. Acad. Sci. U.S.A.* 107, 18706–18711. doi: 10.1073/pnas.1007644107

Sung, C. H., Davenport, C. M., and Nathans, J. (1993). Rhodopsin mutations responsible for autosomal dominant retinitis pigmentosa. Clustering of functional classes along the polypeptide chain. *J. Biol. Chem.* 268, 26645–26649.

Sung, C. H., Schneider, B. G., Agarwal, N., Papermaster, D. S., and Nathans, J. (1991). Functional heterogeneity of mutant rhodopsins responsible for autosomal dominant retinitis pigmentosa. *Proc. Natl. Acad. Sci. U.S.A.* 88, 8840–8844. doi: 10.1073/pnas.88.19.8840

Tam, B. M., and Moritz, O. L. (2009). The role of rhodopsin glycosylation in protein folding, trafficking, and light-sensitive retinal degeneration. *J. Neurosci.* 29, 15145–15154. doi: 10.1523/JNEUROSCI.4259-09.2009

Tuson, M., Marfany, G., and Gonzàlez-Duarte, R. (2004). Mutation of CERKL, a novel human ceramide kinase gene, causes autosomal recessive retinitis pigmentosa (RP26). *Am. J. Hum. Genet.* 74, 128–138. doi: 10.1086/381055

Usui, S., Oveson, B. C., Iwase, T., Lu, L., Lee, S. Y., Jo, Y. J., et al. (2011). Overexpression of SOD in retina: need for increase in H2O2-detoxifying enzyme in same cellular compartment. *Free Radic. Biol. Med.* 51, 1347–1354. doi: 10.1016/j.freeradbiomed.2011.06.010

Wright, A. F., Chakarova, C. F., Abd El-Aziz, M. M., and Bhattacharya, S. S. (2010). Photoreceptor degeneration: genetic and mechanistic dissection of a complex trait. *Nat. Rev. Genet.* 11, 273–284. doi: 10.1038/nrg2717

Zabel, M. K., Zhao, L., Zhang, Y., Gonzalez, S. R., Ma, W., Wang, X., et al. (2016). Microglial phagocytosis and activation underlying photoreceptor degeneration is regulated by CX3CL1-CX3CR1 signaling in a mouse model of retinitis pigmentosa: CX3CR1 signaling in retinal degeneration. *Glia* 64, 1479–1491. doi: 10.1002/glia.23016 doi: 10.1002/glia.23016

Conflict of Interest: RG, ES, and CG have a patent for the employment of inhibitors of serine palmitoyltransferase for preventing and delaying retinitis pigmentosa (World Patent PCT/EP2010001119).

The remaining authors declare that the research was conducted in the absence of any commercial or financial relationships that could be construed as a potential conflict of interest.

Advantages of publishing in Frontiers

OPEN ACCESS
Articles are free to read for greatest visibility and readership

FAST PUBLICATION
Around 90 days from submission to decision

HIGH QUALITY PEER-REVIEW
Rigorous, collaborative, and constructive peer-review

TRANSPARENT PEER-REVIEW
Editors and reviewers acknowledged by name on published articles

Frontiers
Avenue du Tribunal-Fédéral 34
1005 Lausanne | Switzerland

Visit us: www.frontiersin.org
Contact us: info@frontiersin.org | +41 21 510 17 00

REPRODUCIBILITY OF RESEARCH
Support open data and methods to enhance research reproducibility

DIGITAL PUBLISHING
Articles designed for optimal readership across devices

FOLLOW US
@frontiersin

IMPACT METRICS
Advanced article metrics track visibility across digital media

EXTENSIVE PROMOTION
Marketing and promotion of impactful research

LOOP RESEARCH NETWORK
Our network increases your article's readership